

Manual Hydraulic Structures

Edition 2023

Delft University of Technology



Manual Hydraulic Structures

edition 2023

dr.ing. M.Z. Voorendt

PREFACE TO THE 2023 EDITION

The Manual is officially part of the lecture notes for the course “Hydraulic Structures 1” at Delft University of Technology (course code CTB3355 / CIE3330). It is the result of group work and origins in Dutch lecture notes that have been used since the execution of the Dutch Delta Works. Amongst the employees of the Hydraulic Engineering Department that contributed to this work are dr.ir. S. van Baars, ir. K.G. Bezuijen, ir. G.P. Bourguignon, prof. ir. A. Glerum, dr.ir. P.A. Kolkman, ir. H.K.T. Kuijper, dr.ir. H.G. Voortman, prof.drs.ir. J.K. Vrijling and ir. W.F. Molenaar. The latest years, this manual has been clarified, revised and expanded by me. We have received much feedback from students and got good input from our student-assistants, most recently from Jordi de Leau, Sjoerd van Til, Lodovico de Vito, Joris den Uijl and Ruben Frijns. All their help is highly appreciated and has been taken into account in this new edition.

The idea behind the Manual is to have only those tools together that are needed for a first conceptual design of a hydraulic structure: nothing more than a small collection of formulas, data, graphs, etc., just from the relevant civil engineering fields. The available tool in the box might not be the perfect tool for the job, but it will be something to push design of the hydraulic structure a bit further. Select what is needed, using a good understanding of basic physical laws.

It should be kept in mind that this Manual is intended as educational material, to teach students how make conceptual designs of hydraulic structures. For professional, detailed designs, more advanced methods will often be required that strictly comply with official standards, using the right safety approach.

It can be a bit of a challenge to quickly find what is needed in the Manual. An effort has been made to keep it as accessible as possible by dividing it into three parts: Loads, Materials and Structures. Some general information from structural mechanics and about the properties of standard structural profiles can be found in the appendices. Use the main structure and the table of contents to find faster what is needed.

In the 2023 edition, the original division of the Manual in three parts was restored by moving the first part of the 2022 edition to an appendix and to the General Lecture Notes for the explanation on structural safety. The appendix was extended with a few tables with profile characteristics. Table 2.1 with the Beaufort scale was added. Chapter 20 on earthquake loads was extended as well as Section 26.5 on liquefaction and Chapter 39 on ground anchors.

We keep on working on the Manual, because new insights and methods are being introduced, better ways to calculate loads etc. Suggestions and comments to improve this Manual are appreciated.

Mark Voorendt
Delft, February 2023

Part I: Loads

1.	WEIGHT	1
1.1	General.....	1
1.2	Design	1
2.	WIND	2
2.1	Theory	2
2.2	Wind loads for the preliminary design of structures.....	5
2.3	Wind loads according to Eurocode 1	9
2.4	Wind loads on vessels	17
2.5	Literature	18
3.	HYDROSTATIC PRESSURE	19
3.1	Theory	19
3.2	Water pressure on gates	20
4.	WATER, FLOW, THEORY	22
4.1	Conservation of mass	22
4.2	Conservation of energy	23
4.3	Flow in open water ways	27
4.4	Conservation of momentum	31
4.5	Literature	31
5.	WATER, FLOW, WIDE STRUCTURES	32
5.1	Flow across wide structures	32
5.2	Forces on wide structures	38
5.3	Potential flow and pressure distribution	39
5.4	Head losses in a culvert	40
5.5	Literature	40
6.	WATER, FLOW, SLENDER STRUCTURES.....	41
6.1	Drag and lift forces.....	41
6.2	Drag and lift forces, static part.....	41
6.3	Drag and lift forces, dynamic part (vibrations).....	44
7.	WATER, WATER LEVEL (TIDE, SET-UP, ETC.)	46
7.1	Astronomical tide	46
7.2	Wind set-up	48
7.3	Wave set-up	50
7.4	Other influences on the water level.....	50
7.5	Storm surge levels	52
8.	WATER, WAVES, THEORY.....	54
8.1	Translation waves.....	54
8.2	Wind waves	55

9.	WATER, WAVES, WAVE HEIGHTS	60
9.1	Wind-generated waves	60
9.2	Vessel-generated waves	64
9.3	Literature	66
10.	WATER, WAVES, SHALLOWS + BREAKING	67
10.1	Shallows: refraction	67
10.2	Shallows: shoaling (non-breaking waves)	69
10.3	Shallows: breaking waves.....	70
10.4	Obstacle: reflection.....	72
10.5	Obstacle: diffraction.....	73
11.	WATER, WAVES, RUN-UP + OVERTOPPING	75
11.1	Wave run-up.....	75
11.2	Wave overtopping	78
11.3	Literature.....	82
12.	WATER, WAVES, WALL, NON-BREAKING	83
12.1	Rule of thumb (hydrostatic pressure)	83
12.2	Linear wave theory	83
12.3	Sainflou method	84
12.4	Rundgren method.....	85
12.5	Goda method	85
13.	WATER, WAVES, WALL, BREAKING	87
13.1	Introduction	87
13.2	Minikin method	87
13.3	CERC 1984 method	88
13.4	Goda-Takahashi method	89
13.5	Comparison.....	90
14.	WATER, WAVES, SLENDER STRUCTURE, NON-BREAKING	93
14.1	Theory.....	93
14.2	(Preliminary) design.....	94
15.	WATER, WAVES, SLENDER STRUCTURE, BREAKING	100
16.	ICE.....	101
16.1	Thermal expansion.....	101
16.2	Ice accumulation	101
16.3	Collision	102
16.4	Ice attachment.....	102
16.5	Design rules	103
16.6	Literature.....	105
17.	TEMPERATURE	106
17.1	General	106
17.2	Unobstructed thermal deformation.....	107
17.3	Restrained thermal deformation.....	109

18.	SOIL - LOADING AND STRESSES	111
18.1	Vertical soil stress	111
18.2	Horizontal soil stress	115
19.	SOIL, SETTLEMENT	122
20.	SOIL, EARTHQUAKE	124
20.1	Relevancy and causes.....	124
20.2	The Richter scale	124
20.3	The Modified Mercalli scale	126
20.4	Earthquake design.....	127
20.5	Literature.....	130
21.	SOIL, GROUNDWATER	131
21.1	Groundwater pressure	131
21.2	Groundwater flow	132
21.3	Drainage	133
21.4	Influences on strength	133
21.5	Influence on stiffness.....	133
22.	SHIPPING, HYDRAULIC ASPECTS.....	134
23.	SHIPPING, BERTHING AND COLLISION.....	135
23.1	Introduction	135
23.2	Theory.....	135
23.3	Design rules for berthing and collision forces	136
23.4	Design of fenders	143
23.5	Literature.....	144
24.	SHIPPING - MOORING FORCES	145
24.1	Theory.....	145
24.2	Preliminary design.....	145

Part II: Materials

25.	SOIL - PROPERTIES	149
25.1	Purpose of determining soil types and characteristics	149
25.2	Determination of soil types.....	150
25.3	Determination of soil type characteristics	153
25.4	Soil parameters and models	156
25.5	Literature.....	158
26.	SOIL - STRENGTH (RESULTING IN BEARING CAPACITY)	159
26.1	Theory: strength schematization (Mohr-Coulomb).....	159
26.2	Vertical bearing capacity.....	160
26.3	Horizontal bearing capacity (resistance against sliding).....	165
26.4	Stability of slopes (Fellenius and Bishop).....	166
26.5	Liquefaction.....	169
26.6	References.....	174
27.	SOIL - STIFFNESS	175
27.1	Spring schematisation	175
27.2	Modulus of subgrade reaction.....	176
27.3	Vertical modulus of subgrade reaction (using Flamant).....	177
27.4	Horizontal modulus of subgrade reaction for (sheet piling) walls.....	178
27.5	Horizontal modulus of subgrade reactions for piles	179
28.	SOIL - SETTLEMENT	180
28.1	Consolidation	180
28.2	Primary settlement and creep	182
28.3	Soil relaxation.....	184
28.4	Literature.....	185
29.	CONCRETE.....	186
29.1	Properties of concrete	186
29.2	Properties of reinforcement steel	187
29.3	Properties of pre-stressed steel	188
29.4	Reinforced and pre-stressed concrete	189
29.5	Stiffness of the concrete structure.....	196
29.6	Concrete cover (Eurocode 2 method)	199
29.7	Crack width	201
29.8	Strut & tie modelling	208
29.9	Literature.....	216
30.	STEEL	217
30.1	General	217
30.2	Strength	219
30.3	Stability (buckling)	222
30.4	Welded connections	225
30.5	Bolt connections	229
30.6	Fatigue of welds	236
30.7	Literature.....	238

Part III: temporary and permanent structures

31.	STABILITY OF STRUCTURES ON SHALLOW FOUNDATIONS	241
31.1	Horizontal stability	241
31.2	Rotational stability	242
31.3	Vertical stability	243
31.4	Piping (internal backward erosion)	244
31.5	Scour protection	248
31.6	Literature.....	255
32.	PILE FOUNDATIONS: COMPRESSION PILES	256
32.1	Pile types	256
32.2	Bearing capacity of compression piles, general theory	259
32.3	Preliminary design: Pile resistance according to Prandtl and Meyerhof	259
32.4	Bearing capacity, method Koppejan.....	261
32.5	Stiffness	264
32.6	Pile plan	265
33.	PILE FOUNDATIONS: TENSION PILES	266
33.1	Bearing capacity of tension piles: comparison with compression piles.....	267
33.2	Bearing capacity: cone resistance method	268
33.3	Bearing capacity: clump criterion	274
33.4	Edge piles	276
33.5	Stiffness	276
33.6	Literature.....	276
34.	PILE FOUNDATIONS: LATERALLY LOADED PILES.....	277
34.1	Introduction	277
34.2	Blum: pile theory.....	277
34.3	Literature.....	281
35.	PILE FOUNDATIONS: PILE GROUPS.....	282
36.	STABILITY OF FLOATING STRUCTURES.....	283
36.1	Static stability	283
36.2	Dynamic stability	289
36.3	Literature.....	291
37.	RETAINING STRUCTURES.....	292
37.1	Gravity walls.....	292
37.2	Sheet piling	293
37.3	Combi-walls.....	321
37.4	Diaphragm walls.....	322
37.5	Literature.....	328

38.	CONSTRUCTION PITS: STRUTS AND WALES	329
38.1	Struts	329
38.2	Wales.....	332
38.3	Literature.....	333
39.	CONSTRUCTION PITS: ANCHORS.....	334
39.1	General	334
39.2	Tieback anchors.....	334
39.3	Screw anchors	338
39.4	Screw grout anchors.....	339
39.5	Grout anchors	341
39.6	Anchor piles	343
39.7	Literature.....	344
40.	CONSTRUCTION PITS: UNDERWATER CONCRETE FLOOR	345
40.1	General	345
40.2	Limit states.....	345
40.3	2-D Arch effect	346
40.4	3-D Dome effect	347
40.5	Transfer of forces to piles	348
41.	CONSTRUCTION PITS: DEWATERING	349
41.1	General	349
41.2	Design.....	352
42.	FLOOD DEFENCE DESIGN (EXCEEDANCE PROBABILITY).....	357
42.1	Flood defence height as the main property	357
42.2	Exceedance probability approach in general.....	357
42.3	Application of the exceedance probability approach in the Netherlands.....	359
42.4	Literature.....	364
43.	FLOOD DEFENCES: GATES	365
43.1	Flat gates	365
43.2	Mitre gates	367
43.3	Water pressure on radial gates.....	369
43.4	Water pressure on sector gates	373
43.5	Water pressure on arcs	373
APPENDICES		
	Appendix A Dutch translation of Hydraulic Structures keywords	375
	Appendix B Units and conventions.....	380
	Appendix C Trigonometric, cyclometric and hyperbolic functions	383
	Appendix D Structural mechanics.....	384
	Appendix E Natural oscillation frequencies.....	394
	Appendix F Properties of steel H- and I- profiles.....	395
	Appendix G Properties of steel pipes.....	397
	Appendix H Properties of sheetpile elements.....	400
	Appendix I Mechanical schematisations of connections	403

Manual Hydraulic Structures

Part I: Loads

1. Weight

1.1 General

Gravity is in many cases the most important load on a structure, because a structure's self-weight (a.k.a. 'dead load') usually constitutes the largest load by far. The weight sometimes works in favour of the structure:

- underwater concrete: to reduce the buoyancy (groundwater pressure)
- caisson: more weight means it can take more horizontal shear force
- immersed tunnel: weight is necessary to sink the tunnel to the bottom (of the river)

Sometimes the weight works to the disadvantage:

- bridges and gates: in every span, weight causes extra forces (and moments)
- shallow foundations: the larger the weight, the bigger and more expensive the footing

1.2 Design

The total weight of a structure can be calculated as follows:

$$G = \sum_i V_i \gamma_i$$

in which: G [kN] = weight of the structure
 V_i [m³] = volume of element i
 γ_i [kN/m³] = specific weight of element i

The specific weight, or unit weight, γ , is the force on an object due to gravity per unit volume of a material:

$$\gamma = \rho \cdot g$$

in which: ρ [kg/m³] = density (mass per unit of volume)
 g [m/s²] = acceleration due to gravity. $g \approx 9,81$ m/s² in the Netherlands, at sea level.

The following table gives rough estimates of the specific weights of the most important construction materials:

material	specific weight [kN/m ³]
Steel	78
Concrete (reinforced or prestressed)	25
Concrete (not reinforced)	24
Underwater concrete	23
Light-weight concrete	8 to 18
Bentonite slurry	11 to 13
Masonry, wet	23
Masonry, dry	20
Wood (soft)	6 to 7
Wood (hard)	8 to 10
Stone (excl. pores)	26
Gravel (dry)	16 to 17
Gravel (wet)	19 to 20
Sand (dry)	17 to 18
Sand (wet)	20 to 21
Clay	15 to 17
Peat	10 to 11

Table 1-1 Volumetric weights

For a more extensive overview of material and fluid densities, see for example <http://www.simetric.co.uk/>.

Note. Not only the structure's self-weight causes a load. Objects in the vicinity of the structure can also cause a (horizontal) load via the ground. This is why in calculations, one assumes a minimum evenly distributed vertical load (excluding the safety factor $\gamma = 1,5$) of $q_v = 20$ kPa next to a sheet pile or a retaining wall, unless it can be proved that no load (e.g., a concrete mixer truck) could ever reach the location.

2. Wind

revision: February 2008; Section 3 updated to Eurocode: February 2015; TGB-method included again (Section 2): 2018; Beaufort scale added in 2023

2.1 Theory

Wind is caused by uneven pressures in the atmosphere that exist in so-called high- and low-pressure areas. The wind climate is a stochastic process, which is described by a number of parameters, such as:

- wind direction
- wind velocity
- turbulence

The wind climate is determined by other factors besides the pressure differences, amongst which are the topography and the altitude. The parameters mentioned above are stochastic variables, which are estimated by statistically manipulating measured data concerning the wind climate. The data are gathered by meteorological institutes. Using a large number of meteorological stations, statistical data is collected for the description of the wind climate. The collection of data takes place at a set height: 10 m, above ground level and with a standardised terrain roughness (0,03 m).

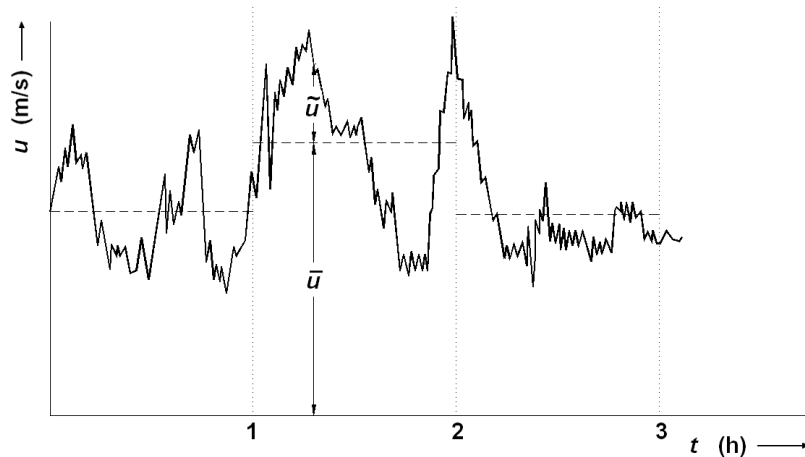


Figure 2-1 Wind velocity: one-hour average and fluctuation

The average wind velocity in an hour is described by the so-called long-term distribution (see Figure 2-1). The fluctuation of the wind velocity within the period of one hour is described by the short-term description, whereby an average value is distinguished from a value that fluctuates in the course of time:

$$\bar{\mathbf{u}}(t) = \begin{bmatrix} u_x(t) \\ u_y(t) \\ u_z(t) \end{bmatrix} = \begin{bmatrix} \bar{u}_x \\ \bar{u}_y \\ \bar{u}_z \end{bmatrix} + \begin{bmatrix} \tilde{u}_x(t) \\ \tilde{u}_y(t) \\ \tilde{u}_z(t) \end{bmatrix}$$

in which: $\bar{\mathbf{u}}(t)$ [m/s] = vector of the wind velocity in all three directions given as a function of time within an hour

\bar{u}_x [m/s] = average wind velocity in an hour in x-direction

$\tilde{u}_x(t)$ [m/s] = fluctuation of the wind velocity within an hour

The wind direction, wind velocity and turbulence in the lowest layers of the atmosphere play an important role in the design, realisation and use of hydraulic structures. The friction between the wind and the earth's surface is of large importance in this layer. Aspects such as the vegetation and buildings determine the friction.

In a neutrally stable atmosphere, the time-average wind velocity close to the surface follows a logarithmic profile (Figure 2-2):

$$\bar{u}(z) = \frac{u_*}{k} \ln\left(\frac{z}{z_0}\right)$$

where: $\bar{u}(z)$ [m/s] = average wind velocity in an hour at a height z

u_* [m/s] = friction velocity, which describes the amount of turbulence

$$u_* = \sqrt{\frac{\tau_w}{\rho}}, \text{ where } \tau_w = \text{surface shear stress and } \rho = \text{fluid (air) density}$$

k [-] = Von Kármán constant ($\approx 0,41$)

z [m] = height above the surface (normally this is the earth or marine surface, but in urban areas the average height of buildings should be taken as surface level)

z_0 [m] = roughness height of the surface, dependent on the nature of the terrain
The roughness height varies from 0,0002 m for water surfaces to 1,6 m for very large cities with tall buildings and skyscrapers.

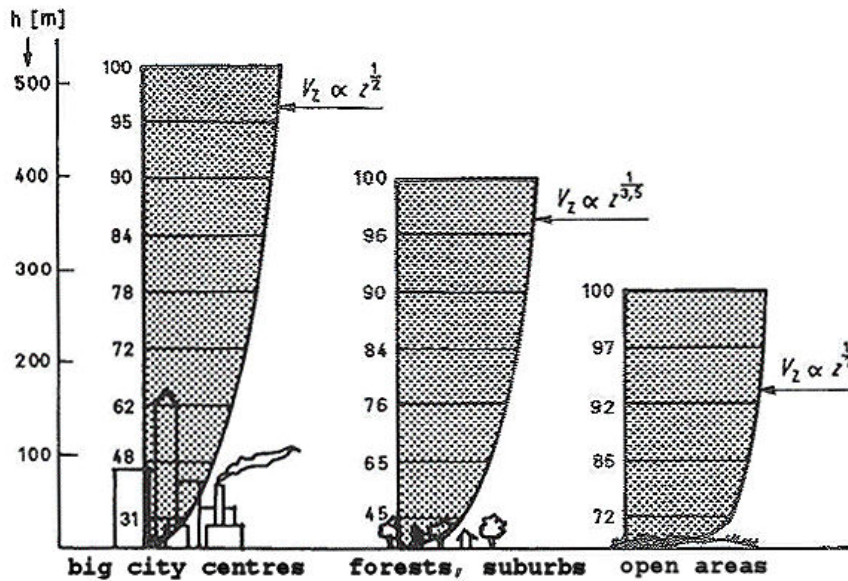


Figure 2-2 Logarithmic wind velocity profiles (adapted from 'De Ingenieur', 31 July 1970)

The wind fluctuation occurring within an hour can be expressed as a standard deviation from the average:

$$\sigma_u = \sqrt{\int_0^{1 \text{ hour}} (u(t) - \bar{u})^2 dt}$$

The coefficient of variation σ_u / \bar{u} is known as the turbulence intensity I , which at a height z above the ground surface can be approached by:

$$I(z) = \frac{k}{\ln\left(\frac{z}{z_0}\right)}$$

where k [-] = factor dependent on the surface. In rural area: $k = 1,0$; in built-up area: $k = 0,9$

From this, the standard deviation of the momentary wind velocity can be calculated with $\sigma_u = \bar{u} \cdot I$

The wind velocity is subject to fluctuations with maximum and minimum velocities. The maximums are known as wind gusts. The maximum momentary wind velocity in a gust can be described with a Rayleigh distribution:

$$P(\hat{u} > \xi) = \exp\left(-\frac{(\xi - \bar{u})^2}{2\sigma_n^2}\right)$$

The probability distribution of the maximum wind velocity in a period with n gusts can be determined with:

$$P(\hat{u}_n < \xi) = P(\hat{u} < \xi)^n = \left(1 - \exp\left(-\frac{(\xi - \bar{u})^2}{2\sigma_n^2}\right) \right)^n = \exp\left(-n \cdot \exp\left(-\frac{(\xi - \bar{u})^2}{2\sigma_n^2}\right)\right)$$

This probability distribution is a conditional probability distribution because \bar{u} must be known. For the determination of the unconditional probability distribution, one is referred to the course CIE4130, "Probabilistic design".

In meteorology, the scale of Beaufort is often used. Britain's admiral Sir Francis Beaufort (1774-1857) developed the scale in 1805 to help sailors estimate the winds via visual observations. See Table 2-1 for the corresponding wind velocities.

Beaufort 'force'	wind velocity				description for use at sea
	m/h	km/h	m/s	knots	
0 calm	0 - 1	< 1	< 0,3	0 - 1	Sea like a mirror.
1 light air	1 - 3	1 - 5	0,3 - 1,5	1 - 3	Ripples with the appearance of scales are formed, but without foam crests.
2 light breeze	4 - 7	6 - 11	1,5 - 3,3	4 - 6	Small wavelets, still short, but more pronounced. Crests have a glassy appearance and do not break.
3 gentle breeze	8 - 12	12 - 19	3,3 - 5,5	7 - 10	Large wavelets. Crests begin to break. Foam of glassy appearance. Perhaps scattered white horses.
4 moderate breeze	13 - 18	20 - 28	5,5 - 8,0	11 - 16	Small waves, becoming larger; fairly frequent white horses.
5 fresh breeze	19 - 24	29 - 38	8,0 - 10,8	17 - 21	Moderate waves, taking a more pronounced long form; many white horses are formed.
6 strong breeze	25 - 31	39 - 49	10,8 - 13,9	22 - 27	Large waves begin to form; the white foam crests are more extensive everywhere.
7 near gale	32 - 38	50 - 61	13,9 - 17,2	28 - 33	Sea heaps up and white foam from breaking waves begins to be blown in streaks along the direction of the wind.
8 gale	39 - 46	62 - 74	17,2 - 20,7	24 - 40	Moderately high waves of greater length; edges of crests begin to break into spindrift. The foam is blown in well-marked streaks along the direction of the wind.
9 severe gale	47 - 54	75 - 88	20,7 - 24,5	41 - 47	High waves. Dense streaks of foam along the direction of the wind. Crests of waves begin to topple, tumble and roll over. Spray may affect visibility.
10 storm	55 - 63	89 - 102	24,5 - 28,4	45 - 55	Very high waves with long overhanging crests. The resulting foam, in great patches, is blown in dense white streaks along the direction of the wind. On the whole, the surface of the sea takes on a white appearance. The tumbling of the sea becomes heavy and shock-like. Visibility affected.
11 violent storm	64 - 72	103 - 117	28,4 - 32,6	56 - 63	Exceptionally high waves (small and medium-size ships might be for a time lost to view behind the waves). The sea is completely covered with long white patches of foam lying along the direction of the wind. Everywhere the edges of the wave crests are blown into froth. Visibility affected.
12 hurricane	73 - 83	≥ 118	≥ 32,6	64 - 71	The air is filled with foam and spray. Sea completely white with driving spray; visibility very seriously affected.

Table 2-1 Beaufort scale of wind velocities (modified from sprayers101.com and www.weather.gov)

The load of the wind on an object is determined by the air flow around the object. This flow is an analogue of the flow around an object in a fluid flow (see Chapter 6).

The force on a structure in the wind direction (drag) and perpendicular to the wind direction (lift) is described by the following formulas:

$$F_D = \frac{1}{2} \rho u^2 C_D A \quad \text{and} \quad F_L = \frac{1}{2} \rho u^2 C_L A$$

The term $\frac{1}{2} \rho u^2$ is known as the dynamic pressure. A is the surface area, C_D and C_L are coefficients that depend on, amongst other things, the shape of the structure.

The wind velocity is a random variable. Because the dynamic pressure is a function of the wind velocity, the dynamic pressure is also a random variable. The following is valid for the average dynamic pressure and the variation coefficient of the dynamic pressure:

$$\bar{p}_w = \frac{1}{2} \rho \bar{u}^2 \quad V_{p_w} = \frac{\partial p_w}{\partial u} \frac{I \cdot \bar{u}}{\bar{p}_w} = 2 \cdot I$$

The design dynamic pressure at a height z above ground level can generally be described as:

$$p_w(z) = (1 + \alpha \cdot 2 \cdot I(z)) \cdot \frac{1}{2} \cdot \rho \cdot (u(z))^2$$

The old Dutch Technical Basic Rules for Structures ("Technische Grondslagen voor Bouwconstructies, TGB") use the value $\alpha = 3,5$. This value depends on the desired safety level and can be determined by a risk analysis.

Just like the wind velocity, the force on an object will be part constant and part variable. The variable part is caused by variations of the wind velocity, but also by possible separation vortices. The latter is particularly relevant in cases of relatively slender elements (round towers, suspension cables and so forth). The variable part of the load can cause vibrations of the structure or object. The same way as for an object in a stationary flow in a fluid, the sensitivity to vibrations can be analysed using the Strouhal value (see Section 6.3).

2.2 Wind loads for the preliminary design of structures

Former standard NEN 6702 'Loadings and deformations' (part of the *Technische Grondslagen voor Bouwconstructies*, TGB 1990) specified a relatively simple method to determine wind loads. This method, which could be used for the preliminary design of structures, is summarised below.

If the wind direction is perpendicular to a structure, the wind load can be calculated according to:

$$p_{rep} = C_{dim} \cdot C_{index} \cdot C_{eq} \cdot \phi_1 \cdot p_w \quad [\text{kN/m}^2],$$

in which:

p_{rep}	[kN/m ²]	= wind load as a result of wind pressure, suction, friction and over- or underpressure
p_w	[kN/m ²]	= peak velocity pressure (<i>stuwdruk</i>), depending on the height and location of the structure
C_{dim}	[-]	= factor for the dimensions of the structure
C_{index}	[-]	= wind type factor (<i>windvormfactor</i>)
C_{eq}	[-]	= pressure dissipation factor (<i>drukvereffeningsfactor</i>)
ϕ_1	[-]	= magnification factor for the dynamic wind component

In the case of most hydraulic structures ($h < 50$ m and $h/b < 5$), the wind load equation can be simplified to:

$$p_{rep} = C_{dim} \cdot C_{index} \cdot p_w \quad [\text{kN/m}^2]$$

Peak velocity pressure

The extreme value of the wind velocity pressure (dynamic wind load), working in the direction of the wind, can be estimated according to:

$$p_w = (1 + 7 \cdot I(z)) \cdot \frac{1}{2} \cdot \rho \cdot v_w^2(z) \quad [\text{N/m}^2],$$

in which:

$I(z)$ = turbulence-intensity at height z above the surrounding plane:

$$I(z) = \frac{k}{\ln\left(\frac{z-d}{z_0}\right)}$$

ρ [kg/m³] = mass density of air (1,25 kg/m³)

z_0 [m] = roughness length

d [m] = displacement height (reference level)

u^* [m/s] = friction velocity

k [-] = factor

$$v_w(z) = 2,5 u^* \ln\left(\frac{z-d}{z_0}\right) \quad (\text{wind velocity at height } z)$$

The values for z_0 , d , u^* and k are presented in Table 2-2. They depend on the openness of the field and the location of the structure in the Netherlands, indicated by the velocity pressure zone (I, II or III).

For the calculation of the wind velocity pressure, it should be noticed that for built-on areas, h should be not less than 9,0 m (even if it is in reality). If $h \leq 2,0$ m, the velocity pressure in open areas should be considered like in built-on areas.

factor	open area			built-on area		
	I	II	III	I	II	III
u^*	2,25	2,30	2,25	3,08	2,82	2,60
z_0	0,1	0,2	0,3	0,7	0,7	0,7
d	0,0	0,0	0,0	3,5	3,5	3,5
k	1,0	1,0	1,0	0,9	0,9	0,9

Table 2-2 Factors to calculate the peak velocity pressure

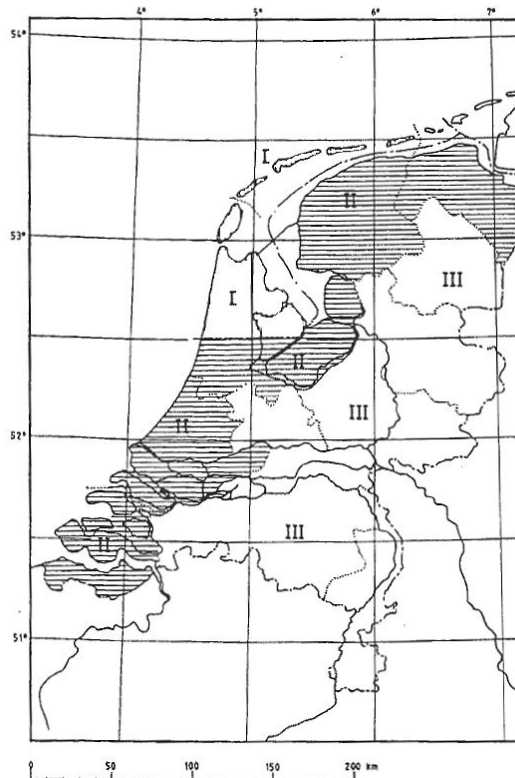


Figure 2-3 wind velocity pressure zones in the Netherlands (from: NEN 6702 / Eurocode 1)

Instead of using the equations above to calculate the peak velocity pressure, the values of Table 2-3 can be used.

h m	peak velocity pressure					
	zone I		zone II		zone III	
	open	built-on	open	built-on	open	built-on
≤ 2	0,64	0,64	0,54	0,54	0,46	0,46
3	0,70	0,64	0,54	0,54	0,46	0,46
4	0,78	0,64	0,62	0,54	0,49	0,46
5	0,84	0,64	0,68	0,54	0,55	0,46
6	0,90	0,64	0,73	0,54	0,59	0,46
7	0,95	0,64	0,78	0,54	0,63	0,46
8	0,99	0,64	0,81	0,54	0,67	0,46
9	1,02	0,64	0,85	0,54	0,70	0,46
10	1,06	0,70	0,88	0,59	0,73	0,50
11	1,09	0,76	0,91	0,64	0,76	0,54
12	1,12	0,81	0,94	0,68	0,78	0,58
13	1,14	0,86	0,96	0,72	0,80	0,61
14	1,17	0,90	0,99	0,76	0,82	0,64
15	1,19	0,94	1,01	0,79	0,84	0,67
16	1,21	0,98	1,03	0,82	0,86	0,70
17	1,23	1,02	1,05	0,85	0,88	0,72
18	1,25	1,05	1,07	0,88	0,90	0,75
19	1,27	1,08	1,09	0,90	0,91	0,77
20	1,29	1,11	1,10	0,93	0,93	0,79
25	1,37	1,23	1,18	1,03	1,00	0,88
30	1,43	1,34	1,24	1,12	1,06	0,95
35	1,49	1,43	1,30	1,20	1,11	1,02
40	1,54	1,50	1,35	1,26	1,15	1,07
45	1,58	1,57	1,39	1,32	1,19	1,12
50	1,62	1,62	1,43	1,37	1,23	1,16

Table 2-3 Peak velocity pressure values p_w or q_p [kN/m²] in the Netherlands as a function of the height above the surrounding level (from: NEN 6702 / Eurocode 1)

Factor for the dimensions of the structure C_{dim}

The dimensions of the structure should be taken into account, because wind gusts will not always affect the entire surface of the structure, depending on the proportion of height and width. The correcting factor for the dimensions C_{dim} is:

$$C_{dim} = \frac{1 + 7 \cdot I(h) \sqrt{B}}{1 + 7 \cdot I(h)} \quad (\leq 1)$$

where:

$$B = \frac{1}{0,4 + 0,021 h^{2/3} + 0,029 b^{2/3}} \quad \text{and} \quad I(h) = \frac{1}{\ln\left(\frac{h}{0,2}\right)}$$

h (height) and b (width) are the dimensions [m] in a plane perpendicular to the wind direction.

The value of C_{dim} can also be found in Table 2-4.

h m	b m							
	1	10	20	30	40	50	75	100
2	1.00	0.96	0.94	0.92	0.90	0.89	0.86	0.84
3	1.00	0.96	0.94	0.92	0.91	0.89	0.87	0.85
4	0.99	0.96	0.94	0.92	0.91	0.89	0.87	0.85
5	0.99	0.96	0.94	0.92	0.91	0.89	0.87	0.85
6	0.99	0.96	0.94	0.92	0.91	0.90	0.87	0.85
7	0.99	0.95	0.93	0.92	0.91	0.90	0.87	0.85
8	0.98	0.95	0.93	0.92	0.91	0.90	0.87	0.86
9	0.98	0.95	0.93	0.92	0.91	0.89	0.87	0.86
10	0.98	0.95	0.93	0.92	0.91	0.89	0.87	0.86
11	0.98	0.95	0.93	0.92	0.90	0.89	0.87	0.86
12	0.98	0.95	0.93	0.92	0.90	0.89	0.87	0.86
13	0.97	0.95	0.93	0.92	0.90	0.89	0.87	0.86
14	0.97	0.95	0.93	0.91	0.90	0.89	0.87	0.86
15	0.97	0.95	0.93	0.91	0.90	0.89	0.87	0.86
16	0.97	0.94	0.93	0.91	0.90	0.89	0.87	0.86
17	0.97	0.94	0.93	0.91	0.90	0.89	0.87	0.86
18	0.97	0.94	0.93	0.91	0.90	0.89	0.87	0.86
19	0.97	0.94	0.92	0.91	0.90	0.89	0.87	0.86
20	0.97	0.94	0.92	0.91	0.90	0.89	0.87	0.86
25	0.96	0.94	0.92	0.91	0.90	0.89	0.87	0.86
30	0.96	0.93	0.92	0.91	0.90	0.89	0.87	0.86
35	0.95	0.93	0.91	0.90	0.89	0.89	0.87	0.85
40	0.95	0.93	0.91	0.90	0.89	0.88	0.87	0.85
45	0.94	0.92	0.91	0.90	0.89	0.88	0.87	0.85
50	0.94	0.92	0.91	0.90	0.89	0.88	0.86	0.85

Table 2-4 Factor for the dimensions of the structure C_{dim} (from: NEN 6702)

Wind type factor C_{index}

Combinations of wind pressure, suction, friction and over- or under-pressure should be taken into account. For the values in case of wind pressure and suction on structural elements, see Figure 2-4.

For over- and under-pressure inside open buildings, a factor with value 0,3 should be applied. In the case of closed buildings, the factor for overpressure is 0,3 too, but for under-pressure it is:

$$C_{pi} = 1,0 - 0,1 \cdot \log\left(\frac{V}{A}\right) \quad (V = \text{volume of the building in m}^3; A = \text{total area of the openings in m}^2).$$

For walls parallel to the wind direction and roofs, different values apply (see NEN 6702). For the total load on a wall, the various combinations of wind types should be summarized, e.g., for a wall in a closed building with wind pressure on the outside and wind under-pressure on the inside, $C_{index} = 0,8 + 0,3 = 1,1$.

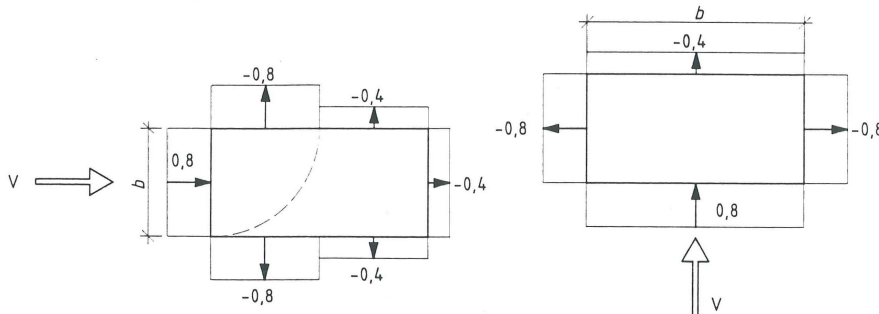


Figure 2-4 wind type factors on vertical walls (for structural elements > 10 m²) (from: NEN 6702)

Abroad

If the wind situation (and particularly the wind velocity) is not comparable to the coast or inland areas of the Netherlands, the dynamic pressure must be determined with the following formula:

$$q = \frac{1}{2} \rho u^2 C_D$$

In which: ρ [kg/m³] = air density (1,25 kg/m³)
 C_D [-] = drag coefficient, dependent on Reynolds value: $C_D \approx 0,7$

For a more accurate approximation of the drag coefficient C_D see §6 "Water, flow, slender structures". This C_D value depends on a number of different factors, including the shape and size of the structure or object. The factors are dealt with in larger detail in NEN 6702.

The average velocity is dependent on the altitude, the location and the measurement time according to the formula:

$$u = \beta_{\Delta T} \left(\frac{h}{10 \text{ m}} \right)^\alpha u_{1h,10m}$$

in which: $\beta_{\Delta T}$ [-] = correction factor for the duration of the gust
 h [m] = altitude of measurement
 α [-] = parameter for the roughness of the area
 ($\alpha = 0,13$ (coast), $\alpha = 0,19$ (inland))
 $u_{1h,10m}$ [m/s] = average wind velocity at an altitude of 10 m, during one hour

The wind velocity is given as an average for one hour. A gust of 3 seconds can reach a higher average velocity. The difference is indicated by the parameter $\beta_{\Delta T}$ (see following table).

The average wind velocity $u_{1h,10m}$ is dependent on both the location and the probability of exceedance T_{year} . According to the TGB, the following values are applicable in the Netherlands.

	$\beta_{\Delta T}$	$T_{year} = 1 \times \text{per } 5$ years	$T_{year} = 1 \times \text{per } 75$ years
Land	1,75	$u_{1h,10m} = 20,5 \text{ m/s}$	$u_{1h,10m} = 25,0 \text{ m/s}$
Coast	1,40	$u_{1h,10m} = 26,0 \text{ m/s}$	$u_{1h,10m} = 32,0 \text{ m/s}$

Table 2-5 Wind velocities according to TGB

For other exceedance frequencies $u_{1h,10m}$ may be linearly interpolated and extrapolated over $\log(T_{year})$. The given wind velocities apply to the Netherlands. These values must be measured again for other areas.

Notes

- For slender structures it is necessary to consider the load in transverse direction as well ($F_L = \frac{1}{2} \rho u^2 C_L$).
- For slender structures it is necessary to test the structure for vibrations caused by gusts.

(For this see the TGB 1972, or: Wind load, a commentary on the TGB ("Windbelasting, toelichting op de TGB") 1972).

2.3 Wind loads according to Eurocode 1

According to Eurocode 1991, part 1-4 'General actions - Wind actions', wind loads on structures (lower than 200 m) and structural elements shall be determined taking account of both external and internal wind pressures. This section of the Manual endeavours to present the main design procedure for wind loads, but especially the determination of the structural factor and the force coefficient is quite complex. For details and additional information, one is referred to the original text of Eurocode 1-4 (about 120 pages!). Furthermore, details can vary per country, so mind the National Annexes!

Important preliminary note

The Eurocode distinguishes between wind pressure, which is relevant for the design of cladding (*gevelbekleding*), fixings and structural parts (Section 2.2.1), and wind force, which should be used for overall wind effects (Section 2.2.2).

2.3.1 Wind pressure on surfaces

The net pressure on a wall, roof or element is the difference between the pressures on the opposite surfaces taking due account of their signs. Pressure, directed towards the surface is taken as positive, and suction, directed away from the surface as negative. See Figure 2-5 for some examples.

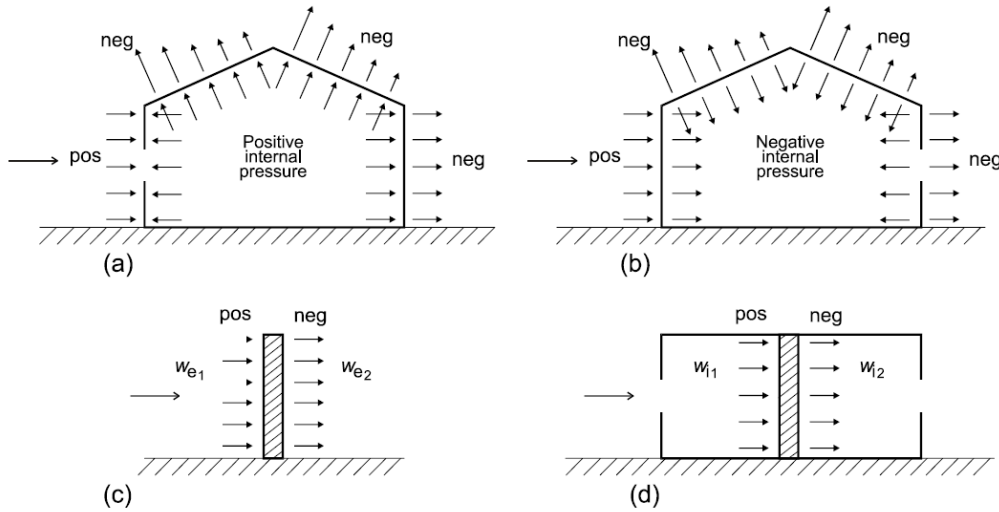


Figure 2-5 Pressure on surfaces (Eurocode 1)

The wind pressure acting on external surfaces w_e should be calculated according to:

$$w_e = q_p(z_e) \cdot c_{pe}$$

The wind pressure acting on the internal surfaces of a structure w_i should be obtained from:

$$w_i = q_p(z_i) \cdot c_{pi}$$

where: $q_p(z_x)$ [kN/m²] = peak velocity pressure (*extreme stuwdruk*) at reference height z_x
 z_x [m] = reference height for the external pressure z_e or internal pressure z_i
 c_{px} [-] = pressure coefficient for the external pressure c_{pe} or internal pressure c_{pi}

The value for the peak velocity pressure q_p can be calculated according to:

$$q_p(z) = [1 + 7 \cdot I_v(z)] \cdot \frac{1}{2} \cdot \rho \cdot v_m^2(z)$$

where: $I_v(z)$ [-] = wind turbulence intensity at height z
 ρ [kg/m³] = air density (recommended value is 1,25 kg/m³)
 $v_m(z)$ [m/s] = mean wind velocity at height z

The mean wind velocity $v_m(z)$ depends on the terrain roughness, orography (= topographic relief of the terrain) and the basic wind velocity, but for the Netherlands a table is available where the value for the peak velocity pressure q_p can easily be found (Table 2-3). The three pressure zones in the Netherlands can be found in Figure 2-3.

The external reference height z_e for windward walls of rectangular plan buildings depends on the aspect ratio h/b and is always the upper height of the different parts of the walls, see Figure 2-6. The recommended procedure is to take the height of the building as the reference height, but this can vary per national annex of the Eurocode.

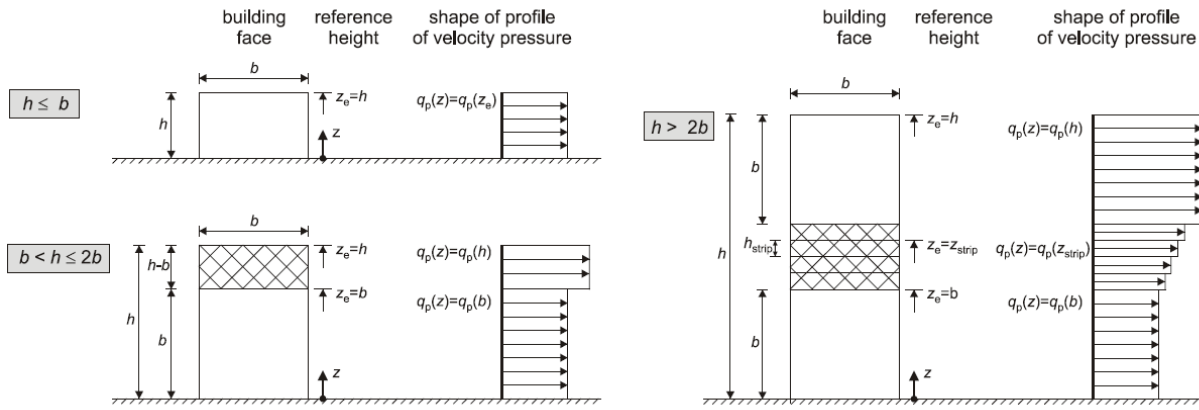


Figure 2-6 Reference height for wind loads (Eurocode 1)

The reference height z_i for the internal pressures should be equal to the reference height z_e for the external pressures on the faces which contribute by their openings to the creation of the internal pressure. If there are several openings, the largest value of z_e should be used to determine z_i .

External and internal pressures should be considered to act at the same time. For design conditions, the worst combination of external and internal pressures shall be considered. This has to be done for every combination of possible openings and other leakage paths.

The external pressure coefficient c_{pe} depends on the wind direction and on the size of the loaded area A that produces the wind action in the section to be calculated. The external pressure coefficients are given for loaded areas A of 1 m^2 (indicated with $C_{pe,1}$) and 10 m^2 ($C_{pe,10}$) in the tables. Values for $C_{pe,1}$ are intended for the design of small elements and fixings with an area of 1 m^2 or less, while values for $C_{pe,10}$ may be used for the design of the overall load bearing structure of buildings.

The different configurations are presented in Figure 2-7 and the corresponding external pressure coefficients in Table 2-6.

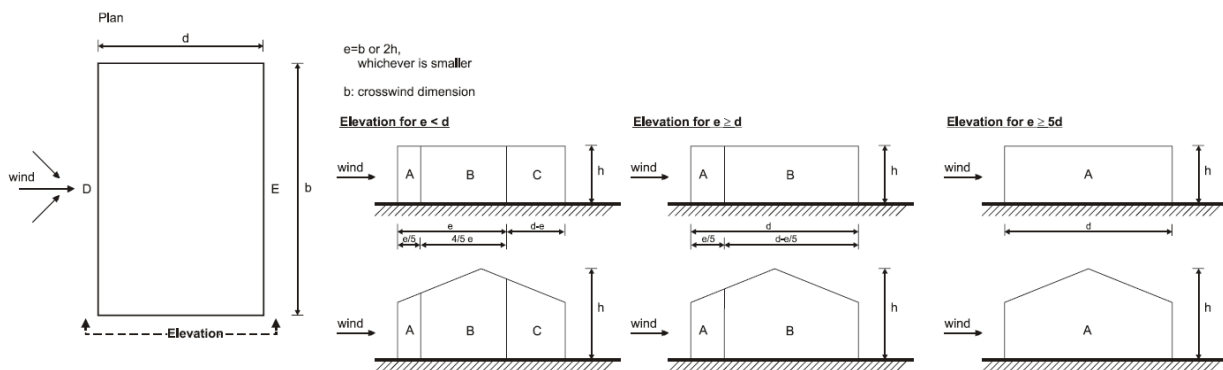


Figure 2-7 Key for vertical walls (Eurocode 1)

Zone	A		B		C		D		E	
h/d	$C_{pe,10}$	$C_{pe,1}$	$C_{pe,10}$	$C_{pe,1}$	$C_{pe,10}$	$C_{pe,1}$	$C_{pe,10}$	$C_{pe,1}$	$C_{pe,10}$	$C_{pe,1}$
5	-1,2	-1,4	-0,8	-1,1	-0,5		+0,8	+1,0	-0,7	
≤ 1	-1,2	-1,4	-0,8	-1,1	-0,5		+0,8	+1,0	-0,5	

Table 2-6 External pressure coefficients for the Netherlands (Eurocode 1 - Dutch national annex)

Reference is made to Eurocode 1 for the external pressure coefficients of all kinds of roofs and domes. Internal pressure does not only depend on the shape of the structure, but also on the number of openings and their location relative to the wind direction. For structures with a 'dominant face' the internal pressure should be taken as a fraction of the external pressure at the openings of the dominant face.

The following two equations can be used for internal pressure coefficient for faces with less than 30% openings:

- When the area of the openings at the dominant face is twice the area of the openings in the remaining faces,

$$c_{pi} = 0,75 \cdot c_{pe}$$

- When the area of the openings at the dominant face is at least 3 times the area of the openings in the remaining faces,

$$c_{pi} = 0,90 \cdot c_{pe}$$

The internal pressure coefficient of open silos and chimneys is $c_{pi} = -0,60$ and of vented tanks with small openings it should be based on $c_{pi} = -0,40$. In these cases the reference height z_i is equal to the height of the structure.

For free-standing walls and parapets, the values of the *resulting* pressure coefficients $c_{p,net}$ depend on the solidity ratio ϕ . For solid walls, $\phi = 1$, and for walls which are 80% solid (i.e. have 20 % openings) $\phi = 0,8$. The pressure coefficients $c_{p,net}$ mentioned in Table 2-7 should be used for the zones indicated in Figure 2-8. For porous walls and fences with a solidity ratio of less than 0,8 reference is made to Eurocode 1.

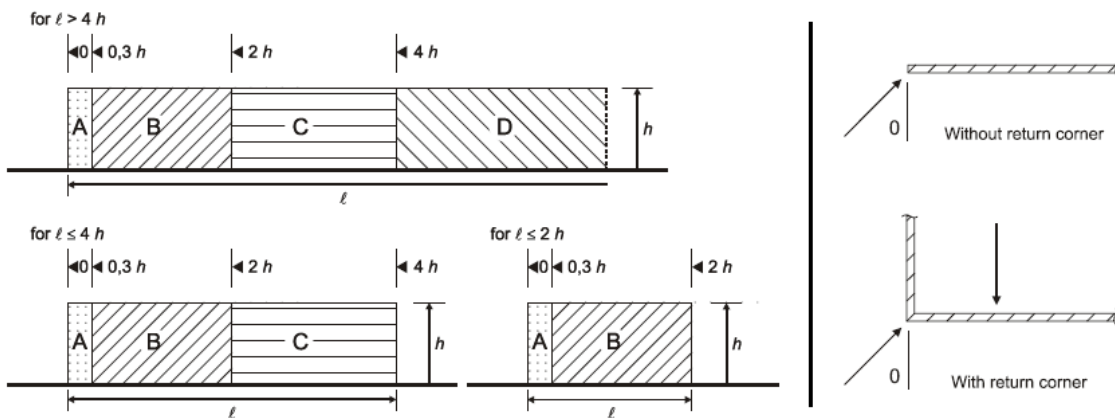


Figure 2-8 Key to zones of free-standing walls and parapets (Eurocode 1)

Solidity	Zone		A	B	C	D
$\phi = 1$	Without return corners	$l/h \leq 3$	2,3	1,4	1,2	1,2
		$l/h = 5$	2,9	1,8	1,4	1,2
		$l/h \geq 10$	3,4	2,1	1,7	1,2
	with return corners of length $\geq h^a$		2,1	1,8	1,4	1,2
$\phi = 0,8$			1,2	1,2	1,2	1,2

^a Linear interpolation may be used for return corner lengths between 0,0 and h

Table 2-7 Recommended pressure coefficients $c_{p,net}$ for free-standing walls and parapets (Eurocode 1)

For details and specific regulations per country, reference is made to Eurocode 1, part 1-4 and the national annexes to this standard.

2.3.2 Wind forces on whole structures

For the determination of wind forces on whole structures or structural components, the peak velocity pressure should be multiplied with the area of the wall and several coefficients:

$$F_w = c_s c_d \cdot c_f \cdot q_p(z_e) \cdot A_{ref}$$

where: F_w [kN] = wind force on a structure or structural component
 c_s [-] = coefficient that takes into account the effect on wind actions from the non-simultaneous occurrence of peak wind pressures on the surface
 c_d [-] = coefficient for the effect of vibrations of the structure due to turbulence
 c_f [-] = force coefficient
 $q_p(z_e)$ [kN/m²] = peak velocity pressure at reference height z_e (Table 2-3)
 A_{ref} [m²] = reference area of the surface

An alternative calculation method uses the wind pressures as calculated in the previous section:

- For external forces: $F_{w,e} = c_s c_d \cdot \sum_{surfaces} (w_e \cdot A_{ref})$
- For internal forces: $F_{w,i} = \sum_{surfaces} (w_i \cdot A_{ref})$
- For friction forces (on external surfaces A_{fr} parallel to the wind direction): $F_{fr} = c_{fr} \cdot q_p(z_e) \cdot A_{fr}$

where c_{fr} [-] = friction coefficient according to Table 2-8.

Surface	Friction coefficient c_{fr}
Smooth (i.e. steel, smooth concrete)	0,01
Rough (i.e. rough concrete, tar-boards)	0,02
very rough (i.e. ripples, ribs, folds)	0,04

Table 2-8 Wind friction coefficients c_{fr}

The force coefficient c_f of structural elements of rectangular section with the wind blowing normally to a face is determined by:

$$c_f = \psi_r \cdot \psi_\lambda \cdot c_{f,0}$$

where: ψ_r [-] = reduction factor for square sections with rounded corners. ψ_r depends on the Reynolds number and has a minimum value of 0,5.
 For sharp edges $\psi_r \approx 1,00$

ψ_λ [-] = end-effect factor for elements with free-end flow.
 ψ_λ depends on the effective slenderness λ and the solidity ratio ϕ of the structure.
 The effective slenderness λ of polygonal, rectangular and sharp-edged sections of structures is:

- for $\ell \geq 50$ m, $\lambda = 1,4 \cdot \ell/b$ or $\lambda = 70$, whichever is smaller
- for $\ell < 15$ m, $\lambda = 2,0 \cdot \ell/b$ or $\lambda = 70$, whichever is smaller
- for $15 \text{ m} \leq \ell < 50$ m: linear interpolation should be used

The solidity ratio ϕ is the ratio between the net area (= the area excluding openings) and the overall envelope area $A_c = \ell \cdot b$. For closed structures, $\phi = 1,0$.

The end-effect factor can be determined when λ and ϕ are known with help of Figure 2-13.

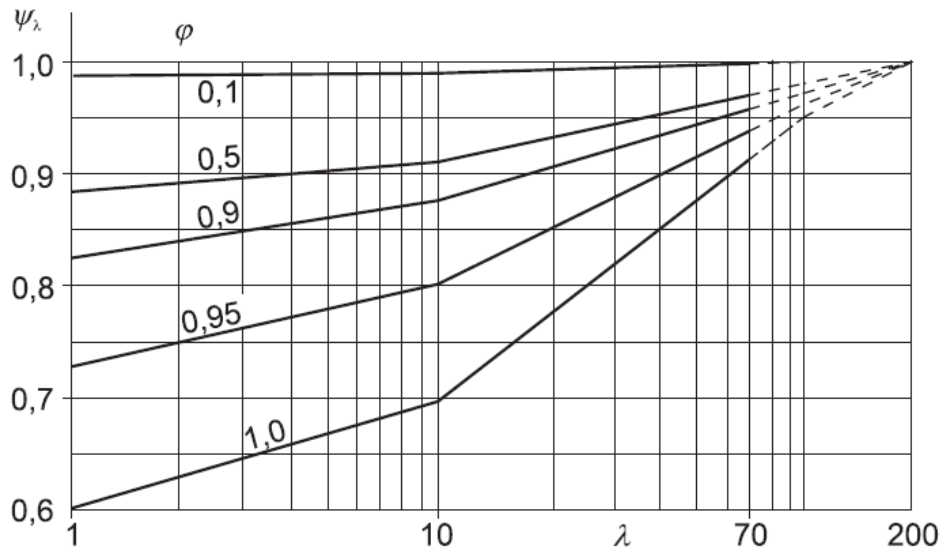


Figure 2-9 End-effect factor as a function of the effective slenderness (Eurocode 1)

$C_{f,0}$ [-] = force coefficient of rectangular sections with sharp corners and without free-end flow as given by Figure 2-10.

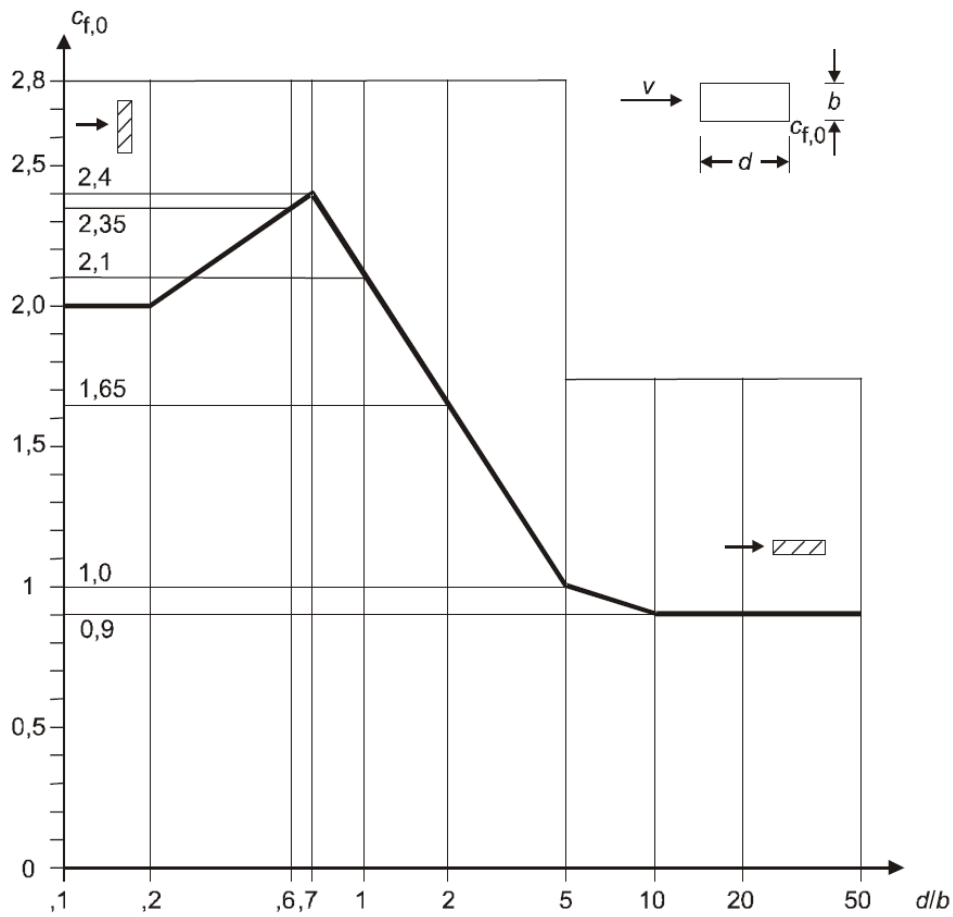


Figure 2-10 Force coefficient for rectangular sections with sharp corners and without free end flow

The coefficients c_s and c_d can be combined into one *structural factor* $c_s c_d$. For buildings with a height less than 15 m the value of $c_s c_d$ may be taken as 1. For (rectangular) civil engineering works (other than bridges) the structural factor should be calculated according to:

$$c_s c_d = \frac{1 + 2 \cdot k_p \cdot I_v \cdot \sqrt{B^2 + R^2}}{1 + 7 \cdot I_v(z_s)}$$

where: k_p [-] = peak factor defined as the ratio of the maximum value of the fluctuating part of the response to its standard deviation:

$$k_p = \sqrt{2 \cdot \ln(\nu \cdot T)} + \frac{0,6}{\sqrt{2 \cdot \ln(\nu \cdot T)}} \text{ with a minimum of } k_p = 3,0$$

T [s] = averaging time for the mean wind velocity ($T = 600$ s)

ν [Hz] = up-crossing frequency as given in:

$$\nu = n_{1,x} \cdot \sqrt{\frac{R^2}{B^2 + R^2}} \text{ and } \nu \geq 0,8$$

$n_{1,x}$ [Hz] = natural frequency of the structure. The limit of $\nu = 0,08$ Hz corresponds to a peak factor of 3,0.

I_v [-] = turbulence intensity = the standard deviation of the turbulence σ_v divided by the mean wind velocity $v_m(z)$:

$$I_v(z) = \frac{\sigma_v}{v_m(z)} = \frac{k_I}{c_o(z) \cdot \ln(z/z_0)} \text{ for } z_{\min} \leq z \leq z_{\max}$$

$$I_v(z) = I_v(z_{\min}) \text{ for } z < z_{\min}$$

k_I [-] = turbulence factor. The recommended value for k_I is 1,0.

c_o [-] = orography factor. Where orography (e.g. hills, cliffs etc.) increases wind velocities by more than 5% the effects should be taken into account using the orography factor c_o . Otherwise $c_o = 1,0$.

z_0 [m] = roughness length as given in Table 2-9

z_{\min} [m] = is the minimum height defined in Table 2-9.

z_{\max} [m] = is to be taken as 200 m

Terrain category		z_0 m	z_{\min} m
0	Sea or coastal area exposed to the open sea	0,003	1
I	Lakes or flat and horizontal area with negligible vegetation and without obstacles	0,01	1
II	Area with low vegetation such as grass and isolated obstacles (trees, buildings) with separations of at least 20 obstacle heights	0,05	2
III	Area with regular cover of vegetation or buildings or with isolated obstacles with separations of maximum 20 obstacle heights (such as villages, suburban terrain, permanent forest)	0,3	5
IV	Area in which at least 15 % of the surface is covered with buildings and their average height exceeds 15 m	1,0	10

Table 2-9 Roughness length z_0 and minimum height z_{\min} (Eurocode 1)

B^2 [-] = background factor, allowing for the lack of full correlation of the pressure on the structure surface:

$$B^2 = \frac{1}{1 + 0,9 \cdot \left(\frac{b+h}{L(z_s)} \right)^{0,63}}$$

$L(z_s)$ [m] = turbulent length scale

It is on the safe side to use $B^2 = 1,0$.

R^2 [-] = resonance response factor, allowing for turbulence in resonance with the vibration mode:

$$R^2 = \frac{\pi^2}{2 \cdot \delta} \cdot S_L(z_s, n_{1,x}) \cdot R_h(\eta_h) \cdot R_b(\eta_b)$$

δ [-] = total logarithmic decrement of damping:

$$\delta = \delta_s + \delta_a + \delta_d$$

δ_s = logarithmic decrement of structural damping, for some structural types indicated in Table 2-10, otherwise see Eurocode 1, Annex F.5

Structural type	structural damping, δ_s
reinforced concrete buildings	0,10
steel buildings	0,05
mixed structures concrete + steel	0,08

Table 2-10 logarithmic decrement of damping (Eurocode 1)

δ_a = logarithmic decrement of aerodynamic damping for the fundamental mode. If the modal deflections are constant over each height z , which is mostly the case, δ_a may be determined with:

$$\delta_a = \frac{c_f \cdot \rho \cdot b \cdot v_m(z_s)}{2 \cdot n_1 \cdot m_e}$$

n_1 [Hz] = fundamental flexural frequency of the structure

m_e [kg] = equivalent mass per unit length

ρ [kg/m³] = air density ($\approx 1,25$ kg/m³)

δ_d = logarithmic decrement of damping due to special devices (like tuned mass dampers and sloshing tanks etc.). If these special dissipative devices are added to the structure, δ_d should be calculated by suitable theoretical or experimental techniques.

S_L [m] = is the non-dimensional power spectral density function:

$$L(z) = L_t \cdot \left(\frac{z}{z_t}\right)^\alpha \quad \text{for } z \geq z_{min} \quad \text{and} \quad L(z) = L(z_{min}) \quad \text{for } z < z_{min}$$

z_t [m] = reference height = 200m

z_{min} [m] = minimum height (Table 2-9)

$\alpha = 0,69 + 0,05 \cdot \ln(z_0)$, where z_0 = roughness length (Table 2-9)

L_t [m] = reference length scale = 300 m

z_s [m] = reference height for determining the structural factor, see Figure 2-11

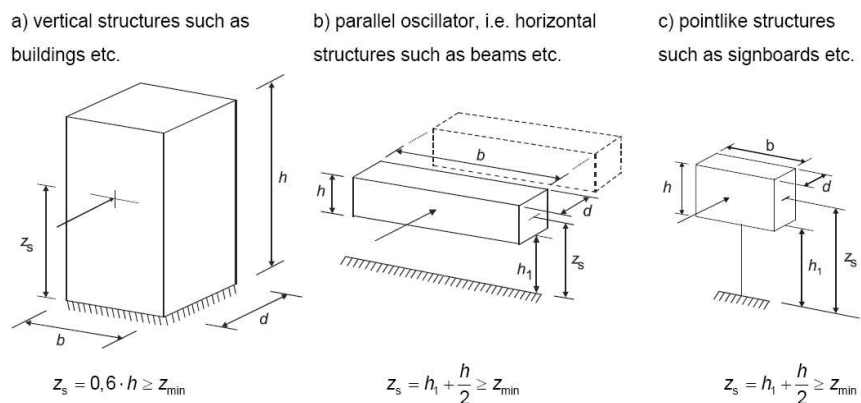


Figure 2-11 General shapes of structures and the reference height z_s

For a preliminary design one could consider to use $R^2 = 1$, which could result in a over-estimation of the structural factor $c_s c_d$ of up to 15% (the approved minimum value of $c_s c_d$ is 0,85).

2.4 Wind loads on vessels

The Oil Companies International Marine Forum (OCIMF) issued an information paper with coefficients and procedures for computing wind and current loads on oil tankers. According to this paper, the resultant wind force on a moored tanker (a very large crude carrier, i.e. 150 000 < DWT < 500 000) can be calculated using the following equations.

$$F_{Xw} = \frac{1}{2} C_{Xw} \rho_w v_{w,10}^2 A_T \text{ and } F_{Yw} = \frac{1}{2} C_{Yw} \rho_w v_{w,10}^2 A_L$$

in which:

- F_{Xw} [N] = longitudinal wind force (surge wind force)
- F_{Yw} [N] = lateral wind force (sway wind force)
- C_{Xw} [-] = longitudinal wind drag coefficient, see Figure 2-12
- C_{Yw} [-] = lateral wind force coefficient, see Figure 2-13
- ρ_w [kg/m³] = density of air ($\approx 1,28 \text{ kg/m}^3$)
- $v_{w,10}$ [m/s] = wind velocity at 10 m elevation
- A_T [m²] = transverse (head-on) wind area
- A_L [m²] = longitudinal (broadside) wind area

(Longitudinal and transverse directions are with respect to the vessel length axis)

The wind force coefficients depend on the wind angle of attack, the extent of loading by cargo (fully loaded or only ballasted) and the bow configuration.

If the wind velocity is known at a different elevation than 10 metres above water surface, the following equation can be used for conversion:

$$v_{w,10} = u_{w,h} \left(\frac{10}{h} \right)^{1/7}$$

where $u_{w,h}$ [m] = wind velocity at elevation h above ground/water surface.

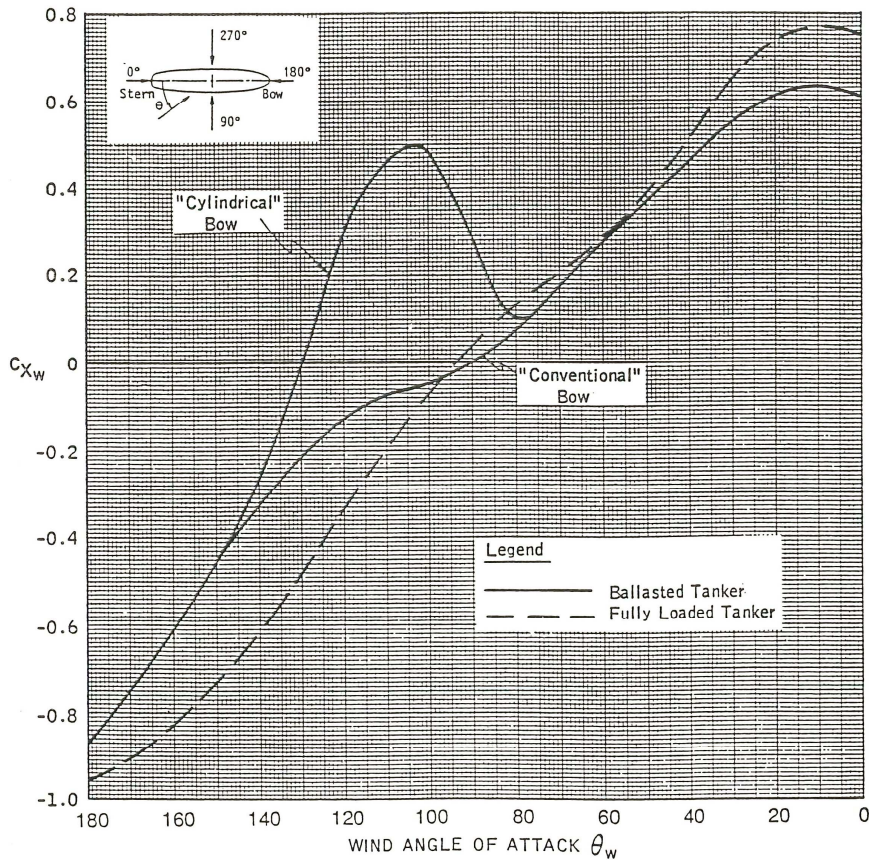


Figure 2-12 longitudinal wind drag coefficient for tankers

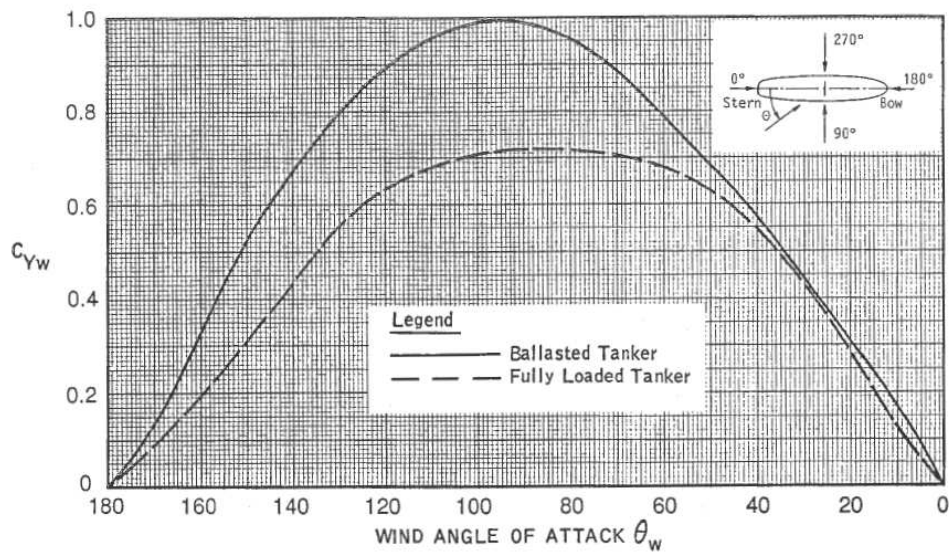


Figure 2-13 lateral wind force coefficient

2.5 Literature

- Nederlands Normalisatie-instituut: NEN 6702 "Technische Grondslagen voor Bouwconstructies", Belastingen en vervormingen, (TGB 1990), Delft 1990.
- Eurocode 1: Actions on structures - Part 1-4: General actions - Wind actions (NEN-EN 1991-1-4)
- Oil Companies International Marine Forum: Estimating the environmental loads on anchoring systems, first edition. Witherby & Co Ltd., London, 2010.

3. Hydrostatic pressure

3.1 Theory

Shear stresses only occur in fluids if there are velocity differences between the fluid particles. In a fluid at rest there is no shear stress and the pressures in one point are equal in all directions. This characteristic is known as Pascal's law. For flowing fluids, Pascal's law gives rather good approximations.

The hydrostatic (water) pressure in any given point under water is a function of the pressure head and the density of the water:

$$p = \rho_w g h$$

where: p [Pa] = water pressure
 h [m] = pressure head
 g [m/s²] = acceleration due to gravity
 ρ_w [kg/m³] = density of water ($\rho_{w,salt} = 1025$; $\rho_{w,fresh} = 1000$)

In water at rest or in a uniform flow (no acceleration or deceleration) in an open waterway, the pressure head is equal to the water depth at the point considered. Largely varying flow velocities in open waterways correspond to largely curved flow lines. In such cases, the pressure head is not equal to the water depth (see Chapter 5).

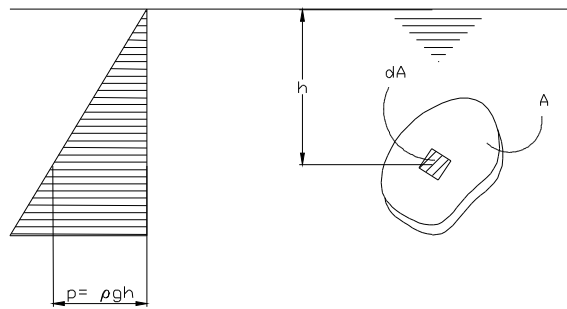


Figure 3-1 Water pressure

The force on a plain under water is calculated by integrating the pressure over the plain:

$$F = \int_A p \, dA$$

in which: F [N] = the force perpendicular to the plane
 dA [m²] = a small part of the area (see Figure 3-1)
 A [m²] = the total surface area

If the plane on which the force is working is straight, the force is equal to the product of the area of the plane and the water pressure in the mass centre of the plane. The components of the force in the x, y and z directions can be determined with:

$$F_x = \iint_A p \, dy \, dz \quad F_y = \iint_A p \, dx \, dz \quad F_z = \iint_A p \, dx \, dy$$

The co-ordinates of the line of action of the force in the x direction can be found with:

$$y_x = \frac{\iint_A p y \, dy \, dz}{F_x} \quad \text{and} \quad z_x = \frac{\iint_A p z \, dy \, dz}{F_x}$$

The lines of action of the forces F_y and F_z can be found in a similar manner.

The previous equations correspond exactly to the equations for the volumes and mass centres of the pressure diagrams. This makes it possible to determine the forces and their points of application for known shapes using relatively simple standard formulas.

3.2 Water pressure on gates

Water pressure has a linear relationship with the location beneath the water surface:

$$\sigma_w(z) = \rho_w g z$$

where:

- $\sigma_w(z)$ [N/m²] = water pressure at depth z
- ρ_w [kg/m³] = density of water (Notice that the densities of sea water and fresh water are different)
- g [m/s²] = gravity acceleration
- z [m] = depth below water surface

Water pressure is equal in all directions (Law of Pascal), so, the horizontal water pressure at a certain point equals the vertical pressure. The direction of the water pressure on a surface is perpendicular to that surface (a wall or a gate, for example) (Figure 3-2). The total water force on a straight surface can be calculated by multiplying the average pressure on the surface with the area of the surface:

$$F = \frac{\sigma_{min} + \sigma_{max}}{2} \cdot l_{gate} \cdot w_{gate}$$

where w_{gate} is the width of the gate.

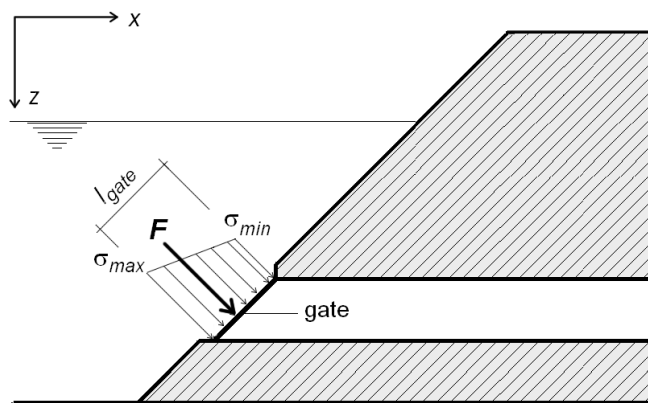


Figure 3-2 Determination of the force on a straight surface

In case of a circular gate, the principle is the same (Figure 3-3). For practical reasons, however, it could be more convenient to use a polar system of coordinates.

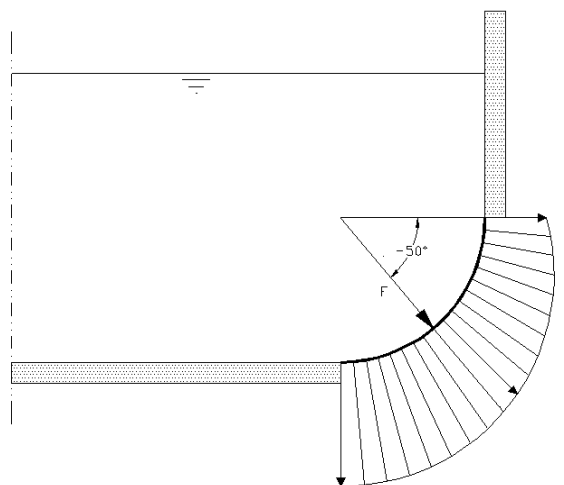


Figure 3-3 Determination of the force on a curved surface

In most cases, however, it is easier to consider the vertical and horizontal component of the water pressure on an object separately. The resulting force in x-direction, F_h , is equal to the summarized horizontal pressure on a projection of the gate to a vertical plane. The total force in z-direction, F_v , is equal to the weight of the water volume above the gate. This is indicated in Figure 3-4. The total force on the gate then is $F_{gate} = \sqrt{F_h^2 + F_v^2}$

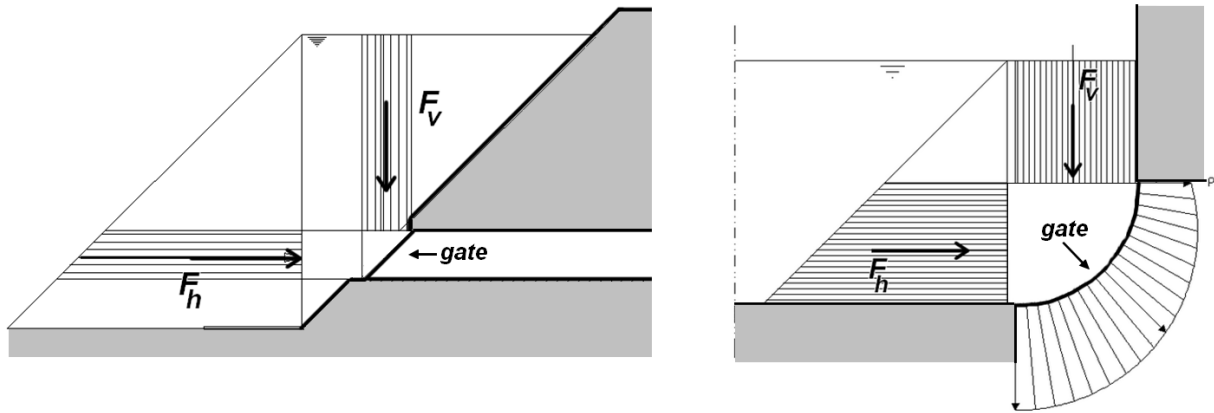


Figure 3-4 Simple determination of the water force on a straight gate (left) and a curved gate (right)

In the case of a radial gate with a vertical axis, the gate is curved in the horizontal plane to an arc with a centre that coincides with the position of the hinge. Thus, the resultant of the water pressure load goes precisely through the hinge in the horizontal plane. The direction of the resultant depends on the lengthwise profile of the gate. In the vertical plane, the direction and the position of the resultant of the water pressure depends on the shape of the gate in the vertical cross section. Figure 3-5 shows a number of possible cross sections and the forces on the gate per metre. The position of the seal with the bottom is an important detail which determines the size of the upward force.

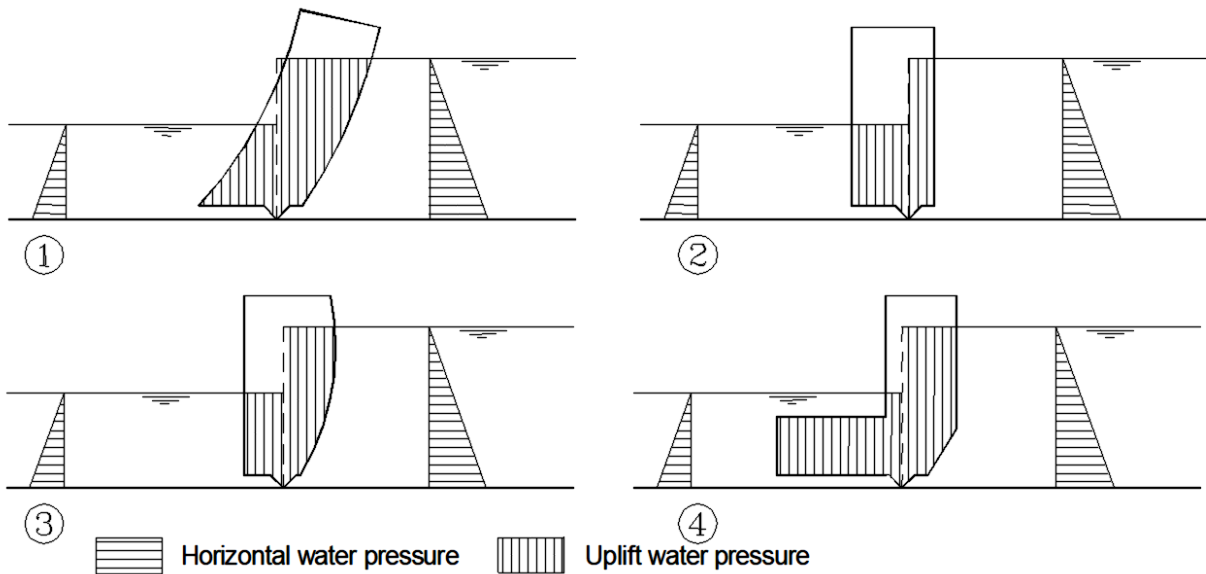


Figure 3-5 Loads dependent on the shape of the gate

For more information about the design of gates, see Chapter 43 of this manual (part III).

4. Water, flow, theory

revised: 2019

In hydraulic engineering the conservation of quantities is often used to deduce equations. Conservation of mass will be discussed first. After that, the conservation of energy will be dealt with, followed by the flow in open waterways which is related to that. Conservation of momentum is included in this chapter, which is useful for determining the flow across and forces on wide structures (walls), as explained in the next chapter.

4.1 Conservation of mass

In hydraulic engineering, the law of conservation of mass is used to determine the flow characteristics. Starting point is the choice of a control volume. The quantity mass within this control volume can change during a time interval by flow through the boundaries. The so-called continuity equation is the applied conservation law of mass:

$$\frac{d}{dt}m = \sum m_{in} - \sum m_{out}$$

The accumulated mass in the specified control volume can only change by in- and outflow through the boundaries, since mass cannot disappear or originate from nothing.

For water-related problems it is assumed that water is incompressible. In this case the mass balance and volume balance are equal. The in- and outflow of water is named discharge in hydraulic engineering. The continuity equation turns into:

$$\frac{d}{dt}V = Q_{in} - Q_{out}$$

This equation is even more simplified since many situations consist of steady conditions. Steady flow means that the flow at each location is constant in time. The flow conditions, including the water volume inside the control volume, do not change. Therefore, the discharge of the inflow and outflow should be equal.

$$\frac{d}{dt}V = 0 \Rightarrow Q_{in} = Q_{out} \Leftrightarrow A_{in} u_{in} = A_{out} u_{out}$$

in which: A [m²] = area
 u [m/s] = average flow velocity

For prismatic channels (having a constant width), the equation can be reduced to a 2D-situation, in which the area is replaced by the flow depth d .

Since the cross-sectional area at location 1 in Figure 4-1 is smaller than at location 2, the average flow velocity at location 2 is smaller than at location 1. The increase of the cross-section affects the flow velocity, not the discharge. This can be beneficial, as the narrowing reduces the friction of the flow, which prevents the erosion of river beds.

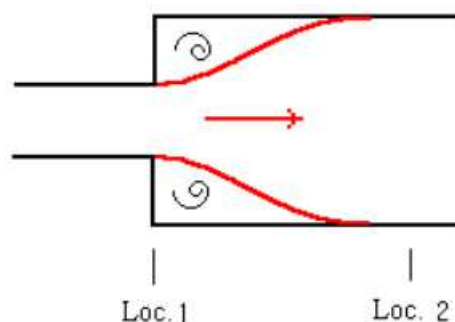


Figure 4-1 Widening of pipe flow (Engsoft Inc., n.d.)

The continuity equation can be used for small basins, like ports and creeks, and polder systems with pumping stations as well. In these unsteady situations, the in- and outflow of water results in a change of water level. For small systems, inertia can be neglected and the slope of the water level is negligible: the

water level will go up and down and is nearly horizontal all times, see Figure 4-2 for an example: a small basin with a wide gap (the water level will not be horizontal in case of a narrow gap). The associated equation is:

$$Q_{in} = A_b \frac{dh_b}{dt}$$

in which: Q_{in} [m³/s] = discharge (inflow is positive)
 A_b [m²] = surface area (of the basin)
 h_b [m] = water depth (in the basin)

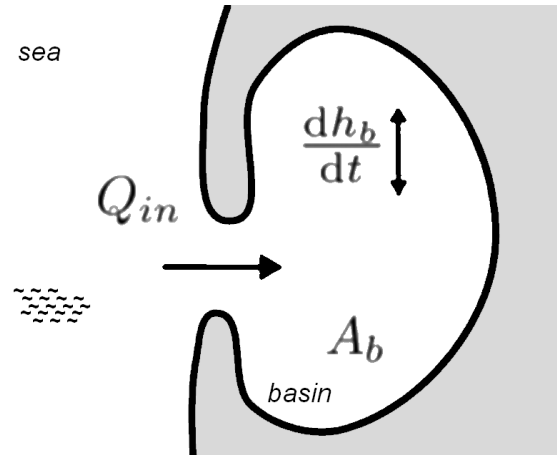


Figure 4-2 Small-basin approach (Battjes & Labeur, 2014, modified)

This equation assumes that the surface area is constant for every water depth. However, especially for creeks, estuaries and rivers this is not true, because the boundaries consist of sloped embankments and floodplains will flood during periods of higher water levels.

4.2 Conservation of energy

The concept for the conservation of energy is the same as for the conservation of mass. The conserved quantity is energy, which can be transported by the flow in and out of the control volume. Besides that, pumps add energy, turbines and friction lead to extraction or loss of energy.

$$\frac{dE}{dt} = \sum E_{in} - \sum E_{out} + E_{pump} - E_{turbine} - E_{loss}$$

Again, a steady situation is analyzed almost continuously, so the change of energy is zero. Furthermore, in hydraulic engineering, the amount of energy is expressed in a total head. This enables a graphical presentation of the energy head.

The next step is the definition of the in- and outflow. Fluid particles flowing through the boundaries of the control volume contain potential and kinetic energy. The well-known formulas for these types of energy are presented below.

$$E_{kin} = \frac{1}{2} mu^2$$

$$E_{pot} = mgz + \frac{m}{\rho} p$$

where: E_{kin} [J] = kinetic energy
 E_{pot} [J] = potential energy
 m [kg] = mass
 u [m/s] = velocity
 z [m] = height in reference system
 ρ [kg/m³] = density
 p [Pa] = pressure

The first term of the potential energy represents the height of the fluid particle, the second term is related to the work done by the pressure. The energy head is expressed in meters by summarizing the equations above and dividing by the term mg . The result is described by:

$$H = z + \frac{p}{\rho g} + \frac{u^2}{2g},$$

where H is the total energy head. This energy head consists of the piezometric head ($z + \frac{p}{\rho g}$) and the velocity head ($\frac{u^2}{2g}$).

These definitions are also indicated in Figure 4-3. The piezometric head is constant for a static body of fluid of constant density. At the bottom of the filter in Figure 4-3, the elevation head is quite small, but the pressure head is large, because there is a significant amount of water pressure acting on the bottom of the filter. At the level of the water table, the water pressure and thus the pressure head are nearly zero. However, the elevation head is large at this point by which the resulting piezometric head is the same. Therefore, no water will flow upwards or downwards.

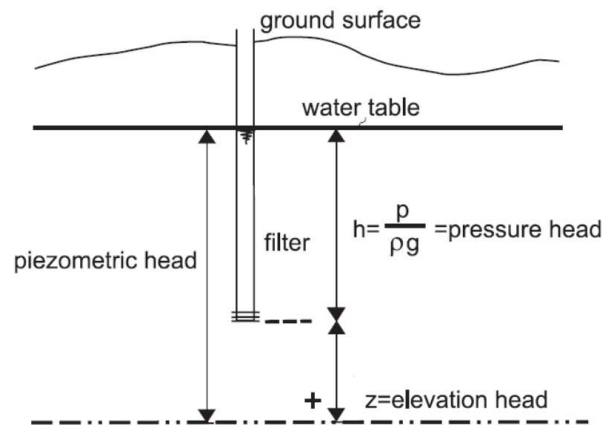


Figure 4-3 The components of the hydraulic head (Hendrayana, 2012)

The reference level can be chosen by the engineer; often the bottom of the water body is practical. With this choice, the piezometric head in a lake is equal to the water depth. The same applies to rivers, provided that the streamlines are straight and parallel.

In comparison to the mostly static conditions in lakes, the velocity head plays a more dominant role in pipe flow and rivers. In these situations, the energy conservation law for steady incompressible flow, as defined by Bernoulli, is frequently written as:

$$h_1 + \frac{u_1^2}{2g} + h_p = h_2 + \frac{u_2^2}{2g} + h_t + h_L$$

where:

h_1	[m]	=	piezometric head at boundary 1
h_2	[m]	=	piezometric head at boundary 2
h_p	[m]	=	head added by a pump
h_t	[m]	=	head extracted by a turbine
h_L	[m]	=	head loss
\bar{u}_1	[m/s]	=	average flow velocity through boundary 1
\bar{u}_2	[m/s]	=	average flow velocity through boundary 2

The energy equation for pipe flow is shown graphically in Figure 4-4. The energy at both boundaries is equal, because of the absence of pumps and turbines, and the neglect of the head losses. However, the composition of the total energy head changes: From the continuity equation, it follows that the velocity increases if the cross-sectional area decreases. The velocity head therefore increases and the piezometric head decreases, resulting in the same energy head at both boundaries.

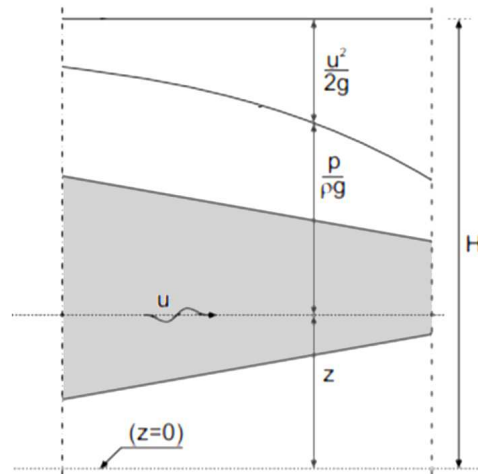


Figure 4-4 Energy balance for pipe flow (Zitman, 2017)

For the situation of Figure 4-4, head loss can be neglected, since turbulence is absent in the control volume and the control volume has a small length for which friction is negligible. Because there are no pumps and turbines, also these terms can be left out of the energy equation. One ends up with an equation similar to Bernoulli's equation:

$$h_1 + \frac{u_1^2}{2g} = h_2 + \frac{u_2^2}{2g}$$

This equation is still derived by using a control volume, therefore the average velocity through the boundaries has to be used. If the continuity equation is used to calculate the flow velocities, these can be used in the equation above. The Bernoulli equation is very similar, but it is derived by equating the energy terms at two points on a streamline: In this case, the flow velocities in these two points are filled in in the equation.

If turbulence is generated inside the control volume, Bernoulli's equation is not valid: a term for head loss has to be added. Head losses are associated with fast variations of flow patterns, for example at hydraulic jumps and overflow weirs. Widening, bifurcations and outflow of pipes into still water bodies, see also Figure 4-1, are called minor losses. Generally, these energy losses are expressed as a part of the velocity head:

$$\Delta H = K_L \frac{u^2}{2g}$$

in which: ΔH [m] = head loss
 K_L [-] = loss coefficient
 u [m/s] = flow velocity at the structure

The head losses of all components have to be summarized, each calculated with its own loss coefficient and flow velocity. For several components the loss coefficient is constant, like for the exit ($K_L=1,0$), but for others it is very dependent on the configuration. This can be seen in Figure 4-5 for the entrance losses.

For pipe flow components as contraction, expansion and bends are resulting in extra minor losses. These are not treated here; the loss coefficients can be found in other literature.

For long sections the major losses, caused by the friction along the riverbed and walls, comes into play. To determine the resulting head loss the well-known Darcy-Weisbach equation is used, comparable to the equation for minor losses:

$$\Delta H_f = f \frac{L}{D} \frac{u^2}{2g}$$

in which: ΔH_f [m] = head loss due to friction
 f [-] = friction factor
 L [m] = length of section
 D [m] = diameter

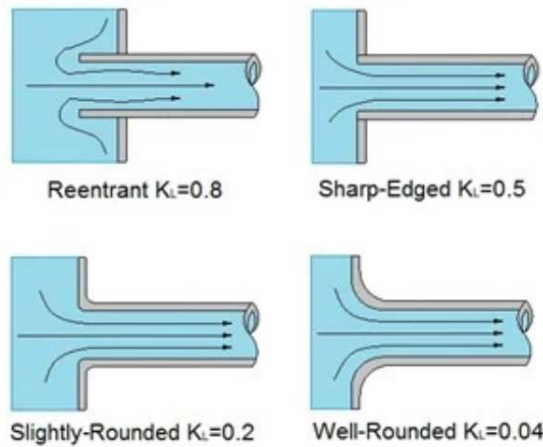


Figure 4-5 Entrance losses (Vano Engineering, 2012)

This equation should only be used for steady flows through conduits. The friction factor is depending on the Reynolds number and/or the relative pipe roughness. The Moody Diagram (see Figure 4-6) can be used to determine the friction factor.

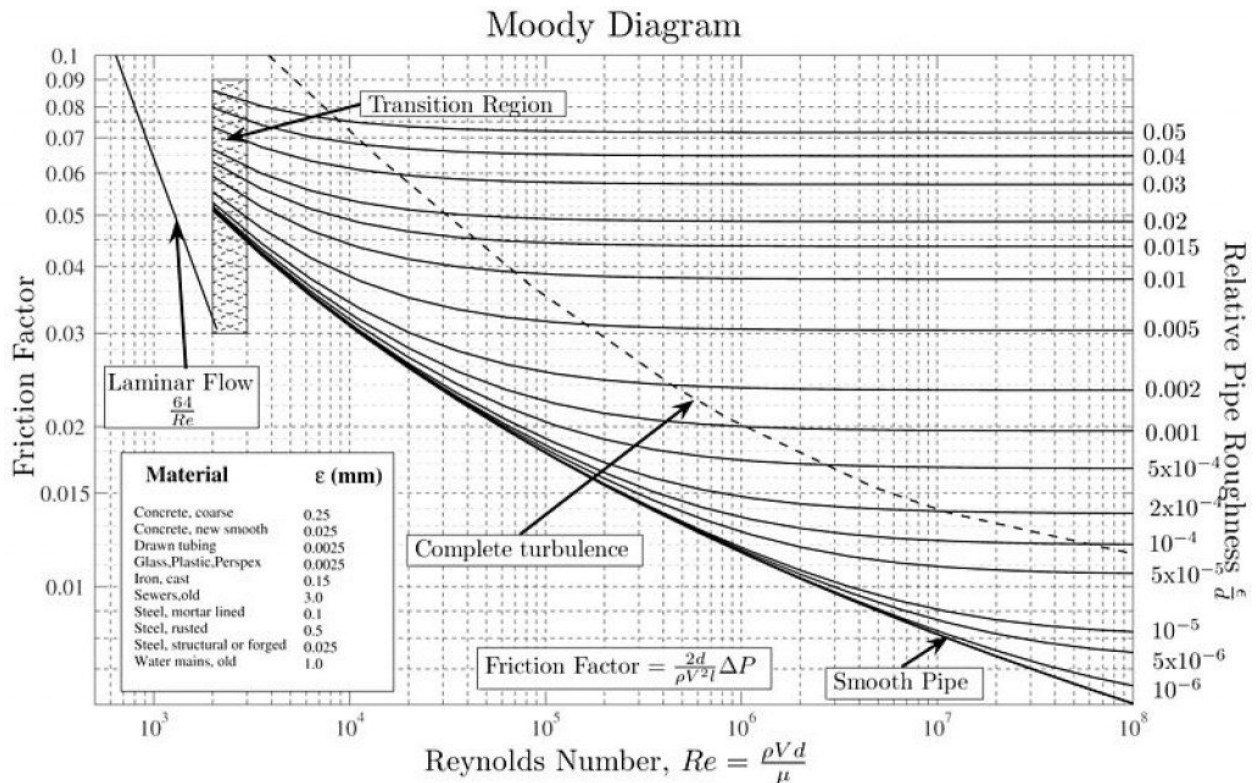


Figure 4-6 Moody diagram (STEM, 2017)

Procedure to use the Moody diagram:

1. Determine the Reynolds number of the flow.¹
2. Determine whether the Moody diagram can be used: If the Reynolds Number is in the laminar or transition range, use the appropriate equations. If, however, the flow is in the turbulent range, the Moody diagram can be used.
3. Compute the relative pipe roughness. This is the roughness of the pipe, divided by the diameter of the pipe. Ensure that the roughness and diameter are in matching units.
4. Find the line referring to the relative roughness on the right side of the diagram. If the value does not have a printed line, interpolate between two lines.
5. Follow this line to the left as it curves up until reach the vertical line is reached, corresponding to the flow's Reynolds Number.

¹ If you don't know the velocity by which to calculate the Reynolds Number, you will need to assume either a velocity, or an initial friction factor. If you assume an initial velocity, proceed as usual. If you assume a friction factor, jump to step 10. If done correctly, you will converge at the same answer.

6. Mark this point on the diagram.
7. Using a straight edge, follow the point straight left, parallel to the horizontal axis, until you reach the vertical axis.
8. Read the corresponding friction factor.
9. With this friction factor, calculate the energy losses.
10. Calculate a new velocity and Reynolds Number.
11. Compare your new Reynolds Number with the previous value. If the Reynolds number is considerably different from your previous value, repeat the calculations with this new Reynolds Value. If, however, it is close to your previous value, your answer has converged, and you are finished.

For rectangular instead of circular cross-sections, the pipe diameter d (to be used for the relative pipe roughness) can be assumed to be 4 times the hydraulic radius R_h .

4.3 Flow in open water ways

Water flows if there is a difference of piezometric head between two points. The flow velocity depends on the extent of the difference in piezometric head and the resistance encountered by the water. Friction and sudden changes of the flow profile cause the resistance encountered by the flowing water. The friction in open water ways can usually not be neglected because they commonly consist of long sections.

4.3.1 Bottom friction

Friction between water particles causes a logarithmical flow velocity change over the water depth. The average velocity can be calculated by using the traditional methods: the Chézy equation and the Manning equation. These equations relate the amount of bed and bank friction directly to the mean flow velocity. They are only valid for steady and uniform conditions.

The **Chézy** equation is:

$$u_m = C \sqrt{R \cdot i} \quad \text{with } C = 18 \cdot \log \frac{12R}{k_r}$$

where: u_m [m/s] = mean flow velocity

C [m^{1/2}/s] = Chézy's coefficient

R [m] = hydraulic radius of the flow profile $\approx \frac{Bd}{B+2d} \approx d$ (for: $B \gg d$)

d [m] = water depth

B [m] = flow width

i [-] = the slope of the river bed

k_r [m] = equivalent bed roughness:

$k_r \approx 2 D_{n50}$ for narrowly graded gravel and rock

$k_r \approx 3 D_{n90} \approx 6 D_{n50}$ for widely graded gravel and rock

$k_r \approx 10$ to 50 cm for sand, which is the height of the bed form (ripples or flow channels)

$k_r \approx 5$ cm for the bed form of river beds consisting of clay (ripples or flow channels)

D_{50} [m] = mass-median diameter of the sediment (= the diameter of the sieve openings through which 50 percent of the grains pass)

The disadvantage of the approximation of the flow velocity according to Chézy is that C isn't a constant. Therefore, internationally, Manning's equation is given preference.

Manning's equation is:

$$u_{gem} = \frac{1}{n} R^{2/3} \sqrt{i}$$

in which: n [-] = Manning's coefficient, dependent on the roughness of the riverbed [-].

This coefficient can easily be measured by determining the discharge Q , flow area A , slope i and water depth d . Henderson (1966) found the values given in Table 4-1.

Glass, smooth metal	$n = 0,010$
concrete made with wooden formwork (untreated)	$n = 0,014$
smooth earth, bare (no vegetation)	$n = 0,020$
river: clear and straight	$n = 0,025 - 0,030$
river: meandering and with shallows/ depths	$n = 0,033 - 0,040$
river: overgrown, meandering	$n = 0,075 - 0,150$

Table 4-1 Manning's coefficient (in $\text{m}^{-1/3} \text{s}$)

Chézy can be converted to Manning and vice versa, because:

$$C\sqrt{R \cdot i} = \frac{1}{n}R^{2/3}\sqrt{i} \Rightarrow C = \frac{1}{n}R^{1/6}$$

Notice that with increasing roughness of the bed, n , Chézy's coefficient decreases. Chézy's coefficient is therefore actually a smoothness coefficient. By approximating, among other things, the \log -term in the Chézy equation, the riverbed roughness parameters k and n can be converted into each other:

$$n^{-1} \approx 8,3 \cdot \sqrt{g} \cdot k^{-1/6}$$

Both equations can only be used for straight, prismatic channels. Bends and structural elements in the section result in more head loss, so the Chézy and Manning equation cannot be used in these cases, unless the coefficients include these local losses.

The bottom friction causes a decrease of the flow velocity over the water depth, see Figure 4-7.

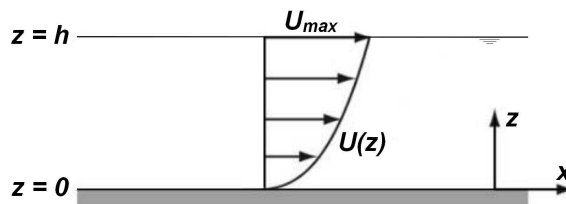


Figure 4-7 Flow velocity distribution over the water depth

The velocity distribution can be described by: $U(z) = U_{\max} \cdot \left(\frac{z}{h}\right)^{1/3}$

Geometrically, the average value will be at around 0,4 of the water depth h and for uniform flow, it is equal to: $\bar{U} = C\sqrt{R \cdot i}$ (as mentioned earlier).

4.3.2 Stage-discharge relation (Q - h relation)

The equilibrium flow depth in uniform, steady conditions is called the normal depth h . It depends on:

- the discharge Q [m^3/s]
- the channel slope i [m/m]
- the channel width b [m]
- the bed roughness k_r [m] ---> C [$\sqrt{\text{m}}/\text{s}$] (Chézy's constant)

The equilibrium flow depth can be found by using the Chézy equation and the continuity equation. This expression is known as the *stage-discharge* or the Q - h relation:

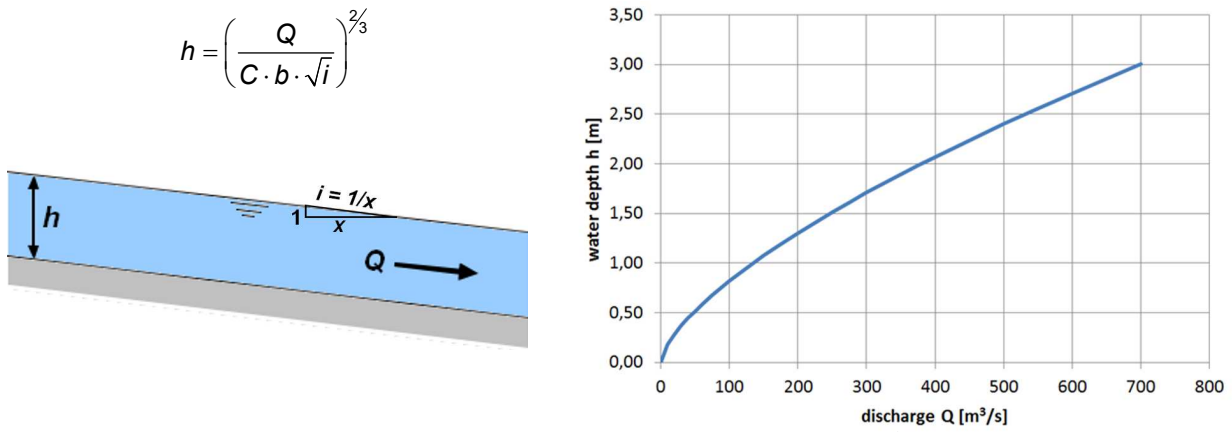


Figure 4-8 Explanatory sketch and an example of a Q-h curve (used parameters: $C = 56 \sqrt{m/s}$; $b = 240 \text{ m}$; $i = 1:10\,000$)

4.3.3 Backwater curves

The flow depth is not always equal to the normal depth. Spatial variations in friction and width and regulating structures in the river (like weirs) cause so-called quasi-uniform flow conditions. The effects of the variations and structures is noticeable over a large distance. From a spatial perspective, the flow adapts slowly to these conditions. The way of adaptation can be derived with help of the energy balance.

If the control volume includes a long river section, friction cannot be neglected. According to Figure 4-9, the slope of the total energy head H in downstream direction s is equal to i_w . For uniform conditions, the slope of the energy line is the same as the slope of the river bottom i_b , for non-uniform conditions it isn't.

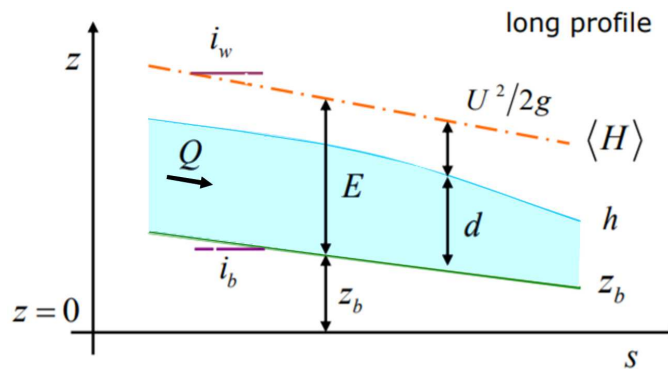


Figure 4-9 Energy balance for long sections (Blom, 2016)

For the derivation, the specific energy E is used:

$$E = d + \frac{u^2}{2g}$$

The gradient of the specific energy head is:

$$\frac{dE}{ds} = \frac{d}{ds} \left(d + \frac{Q^2}{2gA^2} \right) = i_b - i_w$$

If the discharge and width are constant, this reduces to the backwater equation, as found by Bélanger:

$$\frac{dd}{ds} = \frac{i_b - i_w}{1 - Fr^2}$$

in which: Fr [-] = Froude number ($= \frac{u}{\sqrt{gd}}$)

$$i_w$$
 [-] = friction slope ($= \frac{gFr^2}{C^2}$)

The Froude number correlates the kinetic force to the gravitational force. Due to the small slope of river beds in the Netherlands, the flow depth (and gravitation force) is large and therefore, the flow ($Fr \leq 1,0$) is most commonly subcritical. The velocity of subcritical flow is smaller than the wave celerity. Therefore, the flow conditions in a river are determined by the boundary conditions downstream.

Using the formula for the friction slope, the backwater equation can be written in a different form:

$$\frac{dd}{ds} = i_b \frac{d^3 - d_n^3}{d^3 - d_g^3}$$

in which: d_g [m] = critical depth = $\left(\frac{q^2}{g}\right)^{1/3}$ for rectangular cross-sections

At the critical depth, the Froude number is equal to 1,0. For flow depths very close to the critical depth, the backwater equation no longer holds.

As mentioned before, subcritical flow conditions are most common in the Netherlands. Under these conditions, the normal flow depth is larger than the critical depth, which means that the flow depths are determined by the downstream boundary conditions (for instance, the presence of a weir). Solving the backwater equation reveals that the flow depth approaches the normal flow depth exponentially with increasing distance from the boundary condition. Various types of backwater curves for subcritical flow/mild slopes are presented in Figure 4-10.

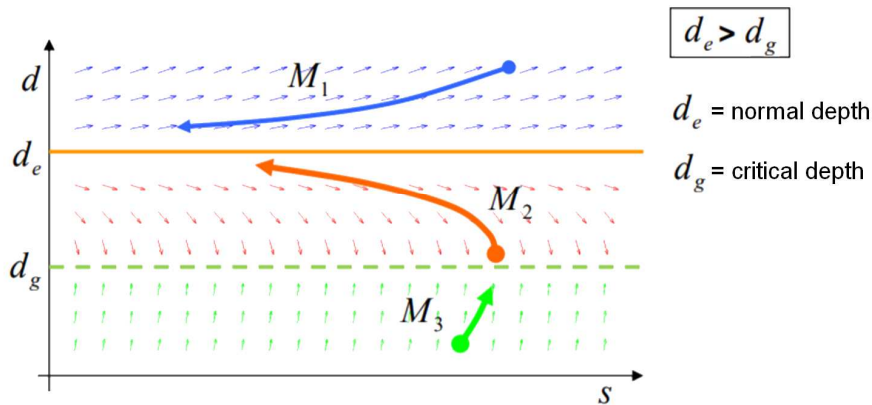


Figure 4-10 Theoretical types of backwater curves (Blom, 2016)

The water depth gradually approaches the normal depth more upstream of the boundary condition. The water depths in the influence area of the boundary condition can be calculated with the following formula (see Figure 4-11):

$$\Delta d(s) = \Delta d(0) \cdot e^{-\frac{(s-s_0)}{L}}$$

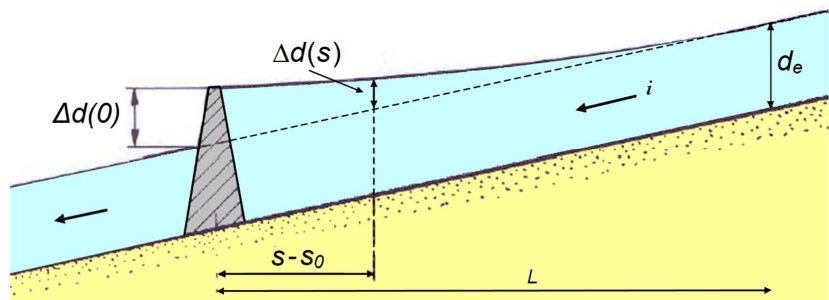


Figure 4-11 Backwater curve

- in which: $\Delta d(s)$ [m] = water depth difference with normal depth at point s .
- $\Delta d(0)$ [m] = water depth difference with normal depth at point $s = 0$.
- $s-s_0$ [m] = river length between boundary condition and point of interest.
- L [m] = adaptation length $\cong \frac{d_e}{3i_b}$
- d_e [m] = normal depth

Note. If the point of interest is more upstream than the boundary condition, the term $s-s_0$ is negative.

4.4 Conservation of momentum

Similar to the derivation of the mass and energy balance (see Sections 4.1 and 4.2), the derivation of the momentum balance (*impulsbalans*) starts with a control volume. The conserved quantity is momentum, the multiplication of mass and velocity. External forces can cause change of momentum, which has been introduced by Newton:

$$\sum F_{ext} = \frac{d(mu)}{dt}$$

in which: $\sum F_{ext}$ [N] = sum of external forces
 m [kg] = mass
 u [m/s] = velocity

Fluid particles contain mass and velocity, so the flow transports momentum. Momentum at the upstream boundary is transported inwards, at the downstream boundary outwards. Using the discharge instead of the mass, the momentum balance can be transformed into:

$$\sum F_{ext} = \rho Q(u_{in} - u_{out})$$

This simplification is only applicable for steady conditions, since the discharge is taken constant in time.

The potential external forces are very divergent. However, the pressure force at both boundaries is always part of the balance. Consequently, it is important to make a valid choice for the location of the boundaries. In case of parallel, straight flow lines at the boundary, the pressure force can be calculated as:

$$F_{h,in} = \frac{1}{2} \rho g B h_{in}^2 \text{ and } F_{h,out} = \frac{1}{2} \rho g B h_{out}^2$$

Where $F_{h,in}$ stands for the hydrostatic force at the inflowing boundary, $F_{h,out}$ for the one at the outflowing boundary.

4.5 Literature

- Battjes, J.A., & Labeur, R.J. (2014). *Open Channel Flow*. Delft: Lecture notes Delft University of Technology.
- Bezuyen, K.G., Stive, M.J.F., Vaes, G.J., Vrijling, J.K., & Zitman, T.J. (2012). *Inleiding Waterbouwkunde*. Delft: VSSD, Lecture notes Delft University of Technology.
- Blom, A. (2016). River Engineering. *Topic 3 - Steady flow II: Backwater curves*. Lecture notes Delft University of Technology.
- Elger, D.F., Williams, B.C., Crowe, C.T., & Roberson, J.A. (2014). *Engineering Fluid Mechanics*. Delft: VSSD.
- Engsoft Inc. (n.d.). *ES_CriFlow - Compressible Flow Analysis Engine of Steam, Rev. 1*. Retrieved from http://www.engsoft.co.kr/download_e/steam_flow_e.htm#TOC
- Hendrayana, H. (2012). *Introduction to groundwater modelling*. Yogyakarta: Lecture notes Gadjah Mada University.
- STEM. (2017, August 10). *How to Read a Moody Chart (Moody Diagram)*. Retrieved from Owlcation: <https://owlcation.com/stem/How-To-Read-a-Moody-Chart>
- Vano Engineering. (2012, December 30). *Head loss coefficients*. Retrieved from Vano Engineering: <https://vanoengineering.wordpress.com/2012/12/30/head-loss-coefficients/>
- Zitman, T.J. (2017). *Stationaire stroming*. Delft: Lecture notes Delft University of Technology.

5. Water, flow, wide structures

revised: 2019

There are two ways of determining the load caused by a flow against wide structures (walls):

1. Making use of the principle of conservation of momentum (*impulsbalans*);
2. Calculating the complete flow pattern along the wall, so that the pressure on the wall is known over the entire wall.

The advantage of the conservation of momentum is that it's easier much faster to elaborate. The disadvantage is that only the total force is calculated and not the distribution of pressure on the wall. To derive the latter, it is necessary to solve the entire flow pattern.

5.1 Flow across wide structures

Civil engineering works such as weirs, piers and sills, can influence the water level in a river. The extent of the influence is described by the discharge function of the structure. Hydraulic structures are constructed to change the flow conditions. For example, weirs provide sufficient water depth for ships during low river discharges. This effect is only noticeable in the river section near the weir due to the development of backwater curves. In Figure 5-1, the appearance of the theoretical curves around weirs are shown.

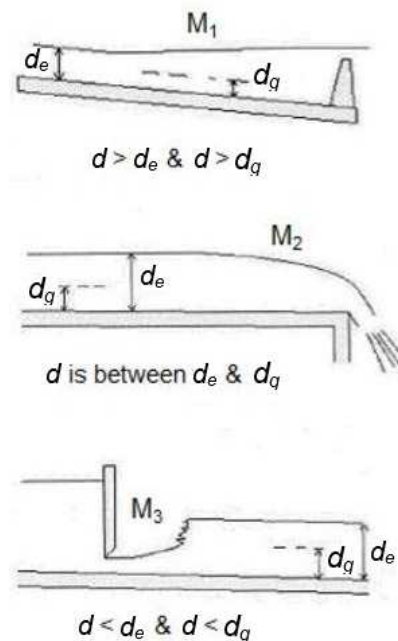


Figure 5-1 Backwater curves due to weirs (Bengston, 2012)

Two possible types of flow are distinguished for weirs, namely:

- overflow: the upstream water level is can be well controlled.
- underflow: in case of submerged underflow, the discharge through the structure is well-controlled.

The flow type depends on the situation and the desired result. Both types are explained in the following sections.

5.1.1 Overflow weirs

The overflow weirs can be divided into two categories: the broad-crested and the sharp-crested weirs. Weirs are classified as broad-crested if the streamlines above the weir itself are straight and parallel. Examples of broad-crested weirs are the sills of storm surge barriers. The streamlines on top of sharp-crested weirs are curved, which results in a different discharge function. Figure 5-2 can be used to determine the category of a particular structure.

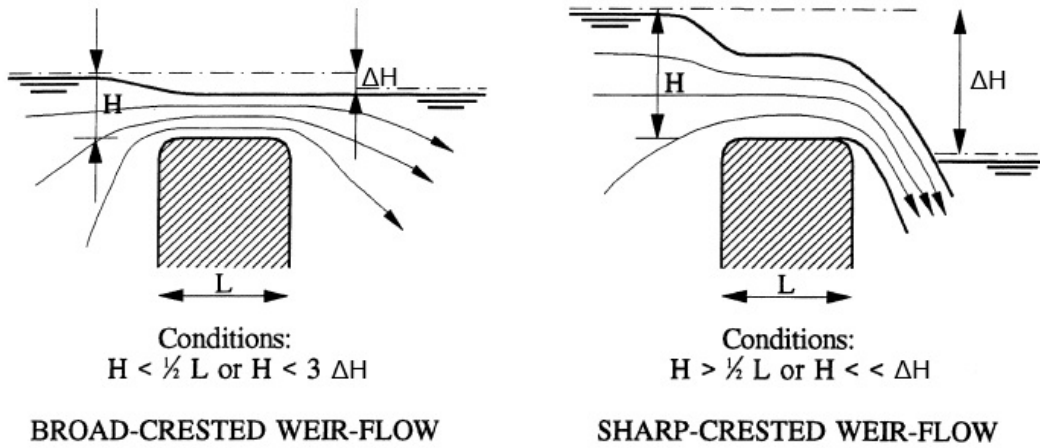


Figure 5-2 Broad-crested versus sharp-crested weirs (Ankum, 2002)

Broad-crested weirs

The discharge over a broad-crested weir mainly depends on the water levels upstream and downstream of the weir. Obviously, if there's no difference, there is no flow. If the downstream water level is slightly lower, the conditions occur as indicated in Figure 5-3, where water levels and energy heads are indicated. The top of the weir is chosen as reference level.

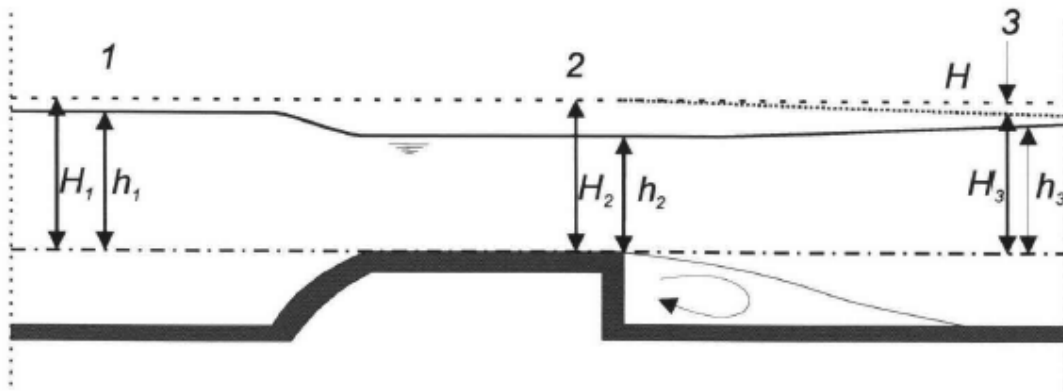


Figure 5-3 Flow conditions for broad-crested weir, submerged overflow (TU Delft Lecture notes 'Inleiding Waterbouwkunde,' 2012)

Application of Bernoulli's equation between points 1 and 2 results in:

$$u_2 = \sqrt{2g(H_1 - h_2)}$$

The energy head H_1 is difficult to measure. The use of water level h_1 is preferred, which is accompanied by the introduction of a discharge coefficient m_1 . Without this coefficient the calculated flow velocity would be too small. Furthermore, it is desired to relate the discharge over the weir to the water level difference over the weir, so h_3 is used instead of h_2 . The discharge coefficient is adapted to include the energy difference between point 1 and 3. The final result is:

$$Q = m_{sof} \cdot B \cdot h_3 \cdot \sqrt{2g(h_1 - h_3)}$$

in which: m_{sof} [-] = discharge coefficient for submerged overflow $\approx 1,1$
 B [m] = flow width

The formula above is only applicable when subcritical flow occurs above the weir. Similar to the mild slope conditions of the backwater curves, subcritical flow means that the upstream flow conditions determine the downstream boundary condition (in this case the water level h_3). By decrease of the downstream water level, the water depth on top of the sill decreases. Consequently, the Froude number and discharge over the structure increase, until critical flow occurs ($Fr = 1$). Figure 5-4 shows that, in this flow situation, the discharge is maximum for a given energy level.

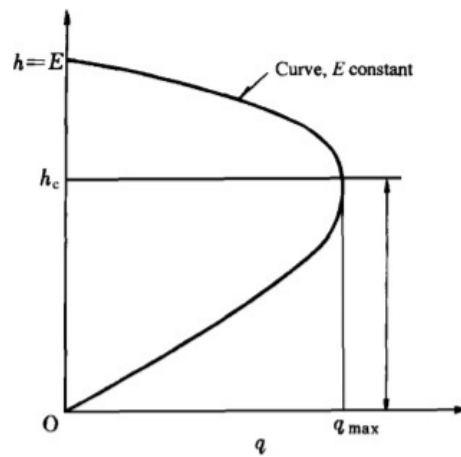


Figure 5-4 Discharge as a function of the water depth for a constant energy level (Nakayama & Boucher, 2000)

If the downstream water level decreases even more, the discharge over the weir doesn't increase further, because it is already maximum. The resulting changed flow condition can be seen in Figure 5-5. The flow situation has changed from submerged to free flow, with a different discharge function.

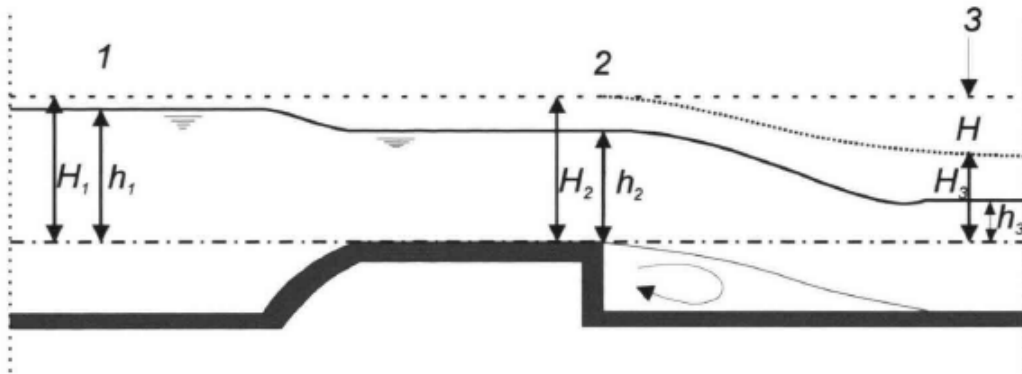


Figure 5-5 Flow conditions for broad crested-weir, free overflow (TU Delft Lecture notes 'Inleiding Waterbouwkunde,' 2012)

Again, Bernoulli's equation is used to obtain the discharge formula. assuming that critical conditions occur above the weir.

$$H_1 = h_2 + \frac{u_2^2}{2g} \quad \text{and} \quad Fr = \frac{u_2}{\sqrt{gh_2}} = 1,0$$

Combining these equations results in the discharge formula for free overflow of broad-crested weirs.

$$Q = \frac{2}{3} \cdot \sqrt{\frac{2}{3}g} \cdot m_{tof} \cdot B \cdot h_1^{3/2}$$

in which: m_{tof} [-] = discharge coefficient for free overflow $\approx 1,0$

The discharge coefficient considers the neglect of friction and the use of water level instead of energy level. The most important difference with the submerged overflow is that for free overflow only the upstream water level has influence. The downstream water level doesn't have any effect.

Sharp-crested weirs

Most weirs in the Netherlands are classified as sharp-crested weirs. These weirs are used to control the water levels in the polders and the rivers. The crest level of a sharp-crested weir is adapted in order that always a free flow situation is created. The flow situation for sharp-crested weirs is comparable with the free overflow situation for broad-crested weirs. The discharge formula for free flow can also be used for sharp-crested weirs albeit with a different discharge coefficient

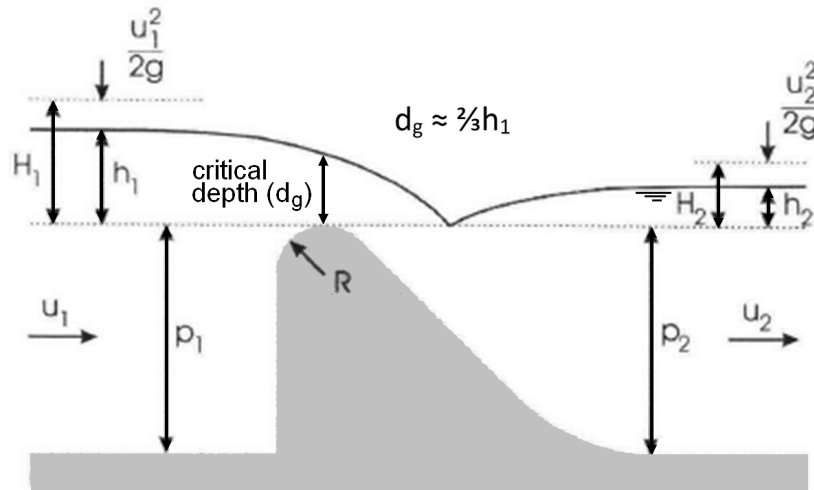


Figure 5-6 Flow conditions for sharp-crested weirs (TU Delft Lecture notes 'Inleiding Waterbouwkunde,' 2012)

$$Q = \frac{2}{3} \cdot \sqrt{\frac{2}{3}g} \cdot m_{sc} \cdot B \cdot h_1^{3/2}$$

in which: m_{sc} [-] = discharge coefficient for sharp-crested weirs

Due to the curved streamlines above the weir the flow velocity and discharge is larger than for broad-crested weirs. Therefore, the discharge coefficient for sharp-crested weirs is larger than 1,0. The radius of the crest R , the height of the crest p_1 and the upstream water level h_1 determine the discharge coefficient. Spillways of large dams make use of so-called ogee crests, which have a profile which maximizes the discharge coefficient ($m_{sc} \approx 1,35$).

By experimenting, Kindswater and Carter developed a more accurate formula than the standard weir equation. It only holds for rectangular sharp-crested weirs (ISO, 1980):

$$Q = \frac{2}{3} \cdot (B + K_B) \cdot \sqrt{2g} \cdot (h_1 + K_h)^{3/2} \cdot C_d$$

- in which: $B + K_B$ [m] = effective width
- $h_1 + K_h$ [m] = effective head
- K_B [m] = coefficient to account for the viscosity (see Figure 5-7)
- K_h [m] = coefficient to account for the surface tension = 0,001 m
- C_d [-] = discharge coefficient (see Figure 5-8)

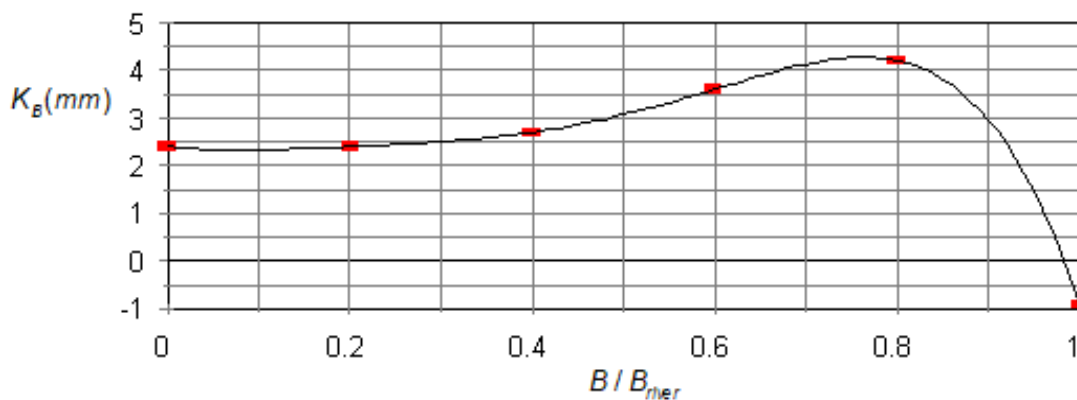


Figure 5-7 Determination coefficient K_B (LMNO Engineering)

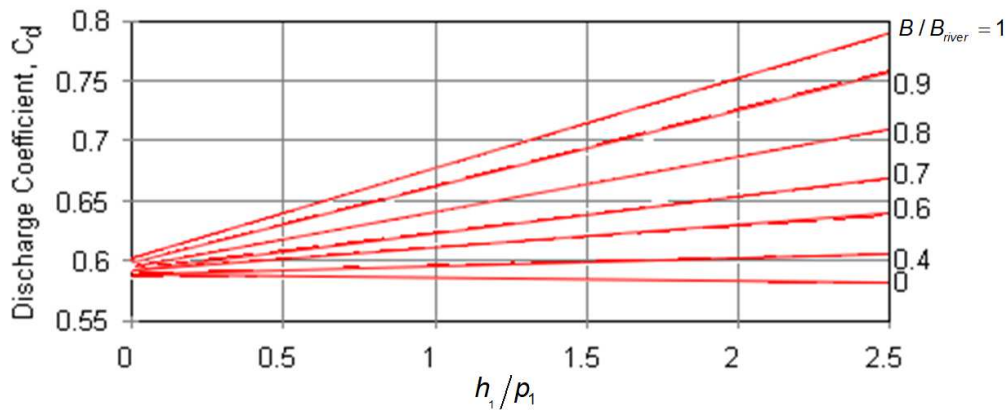


Figure 5-8 Discharge coefficient Kindsvater-Carter equation (ISO 1980)

In case of small discharge, often a triangular V-notch weir is applied. For example, in a fish trap all water flows through the v-shaped part and provides sufficient water depth for the migrating fish. Furthermore, discharge measurements are carried out often, because the discharge coefficient of V-notch weirs is known very accurate.

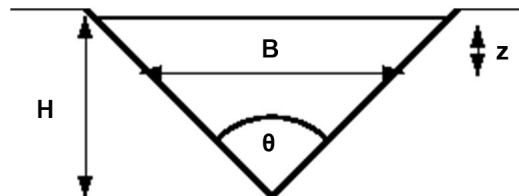


Figure 5-9 V-notch weir

The width, varying with the water depth, can be described with (see Figure 5-9):

$$B = 2(H - z) \cdot \tan\left(\frac{\theta}{2}\right)$$

The general equation for the theoretical discharge over a weir is applied to derive the discharge relation for a V-notch weir:

$$Q_{theory} = \int_{z=0}^H (u \cdot B) dz$$

By substituting u (critical flow conditions) and B , integrating and assuming that far upstream, the velocity head is negligible to the energy head, the discharge over the V-notch can be described as:

$$Q_{theory} = \frac{8}{15} \cdot \sqrt{2g} \cdot \tan\left(\frac{\theta}{2}\right) \cdot h^{5/2}$$

Losses occur for V-notched weirs due to the edges of the weir and contractions in the area of flow.

$$Q_{actual} = Q_{theory} \cdot C_d$$

The value of discharge coefficient C_d for a specifically shaped weir can be found experimentally. From dimensional analysis and experiments, the *average* value for V-notch weirs appeared to be 0,6.

5.1.2 Underflow weirs

Underflow weirs control the discharge by adjustment of the flow profile by tilting a gate vertically. In the Netherlands, several weirs are underflow weirs, like the ones near Driel and Hagestein. During opening of lifting gates of sluices the same flow patterns occurs, although the water level differences are small during these procedures. The flow conditions of underflow are separated into two categories: free flow and submerged flow.

Free underflow

The flow conditions for free flow are shown in Figure 5-10. Directly downstream of the weir, the flow is supercritical. More downstream a hydraulic jump (according to an M3 backwater curve) is located, which indicates the transition to subcritical flow.

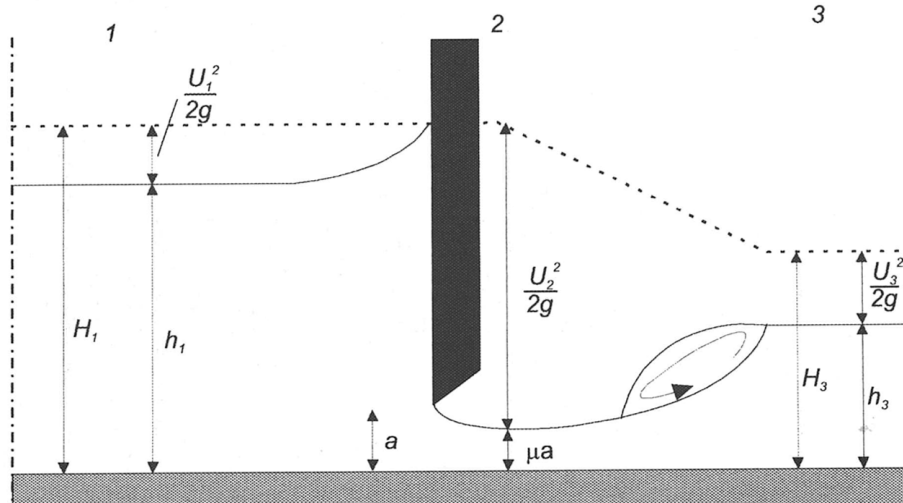


Figure 5-10 Flow conditions for free underflow (TU Delft Lecture notes 'Inleiding Waterbouwkunde,' 2012)

The discharge relation is obtained by applying Bernoulli's equation between point 1 and 2. Loss of energy is only significant more downstream of point 2. This results in the following:

$$Q = \mu \cdot B \cdot a \cdot \sqrt{2g(H_1 - \mu a)}$$

in which: μ [-] = contraction coefficient $\approx 0,6$
 a [m] = height of flow outlet

However, the contraction coefficient is dependent on the shape of the edge of the weir and cannot be calculated precisely. Besides that, the water level h_1 is rather used than the energy level H_1 . Again, a discharge coefficient is set, leading to the discharge equation for free underflow conditions:

$$Q = m_{fuf} \cdot B \cdot a \cdot \sqrt{2g(h_1 - a)}$$

in which: m_{fuf} [-] = discharge coefficient for free underflow

This discharge coefficient is variable, since it is dependent on the contraction coefficient, the upstream water level and the height of the flow outlet.

Free underflow only occurs when the downstream water level is low. Flow conditions will change from free to submerged underflow when the downstream water level rises. For preliminary design, it can be assumed that free underflow will occur when the following applies:

$$\frac{h_3}{a} \leq 1,42 \cdot \sqrt{\frac{h_1}{a}} - 0,3$$

Submerged underflow

In submerged flow conditions the hydraulic jump is located directly downstream of the weir, like in Figure 5-11. This is caused by a higher downstream water level, which is on its own caused by a downstream boundary condition.

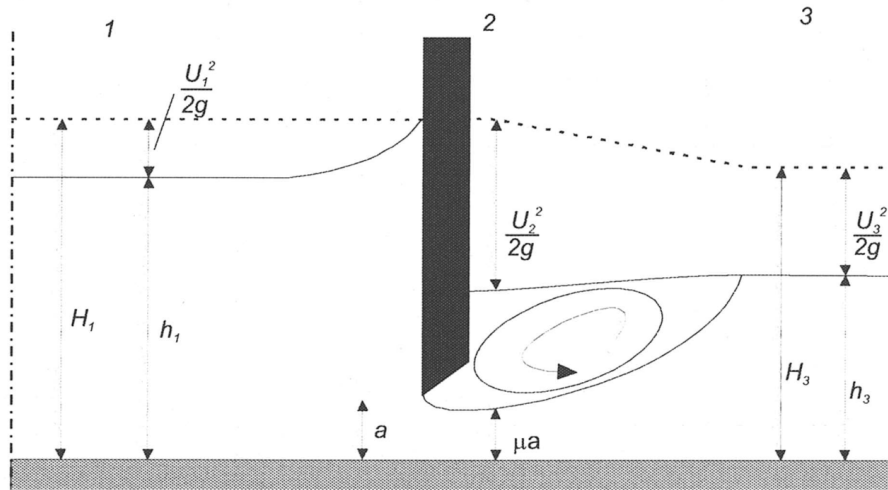


Figure 5-11 Flow conditions for submerged underflow (TU Delft Lecture notes 'Inleiding Waterbouwkunde,' 2012)

In this flow situation, energy is dissipated directly downstream of the weir. Therefore, preferably the downstream water level h_3 is linked to the discharge relation than h_2 . Consequently, the discharge coefficient for submerged underflow should take into account the considerably amount of energy loss. The resulting formula is:

$$Q = m_{suf} \cdot b \cdot a \cdot \sqrt{2g(h_1 - h_3)}$$

in which: m_{suf} [-] = discharge coefficient for submerged underflow $\approx 0,8$

Like all other discharge coefficients, the presented value is only useful for preliminary design. For more detailed design, experiments should give more accurate discharge coefficients.

5.2 Forces on wide structures

The forces on wide structures can be calculated if the flow conditions around the structure are known. Often these conditions are calculated with help of the mass and/or energy equation. Subsequently, the force can be calculated, since it is the only unknown in the momentum equation.

In Figure 5-12 the significant forces for a momentum balance of an underflow weir are shown. The example is based on two lakes with different water levels, which are connected by a canal with a sluice gate. For a rectangular channel and steady conditions, the specific discharge q is the same at locations 1 and 2.

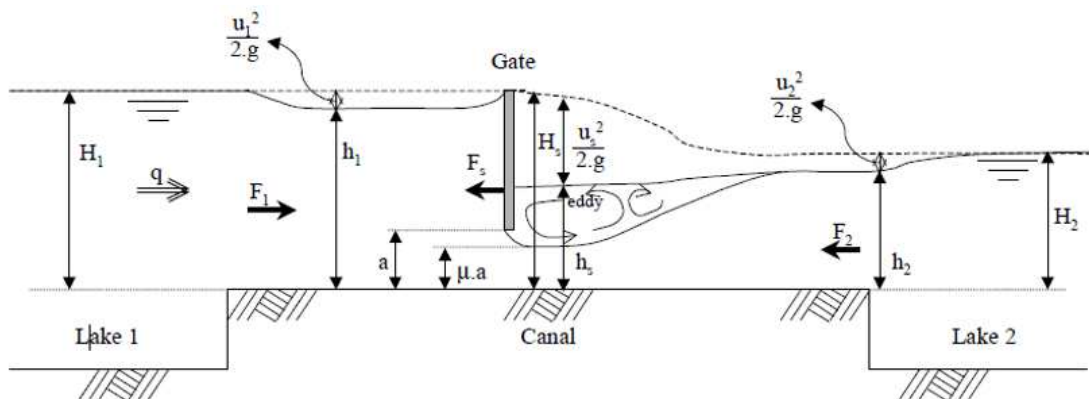


Figure 5-12 Flow around sluice gate in canal (TU Delft Lecture notes 'Inleiding Waterbouwkunde,' 2012)

When drawing up the balance of momentum, the balance area has to be selected very carefully. A good choice of the limits of the balance area can be deduced from the flow lines. To apply the balance equations correctly, it is necessary that the flow lines at the edges of the reference area are straight and parallel. Thus, the forces on the edges can be determined simply in accordance with the hydrostatic pressure distribution.

To solve the given balance of momentum, the water levels and flow velocities must first be solved. This can be done using a combination of the rules for “Preservation of discharge (volume and mass)” and “Preservation of energy (Bernoulli)”.

The following applies for the preservation of volume: $Q = u \cdot A = \text{constant}$

For the preservation of energy: $H = h + \frac{u^2}{2g} = \text{constant}$

Drawing up the momentum balance for this situation per unit width results in the following force on the gate F_s :

$$F_1 - F_2 - F_s - F_u = 0$$

$$\Rightarrow F_s = \frac{1}{2} \rho g h_2^2 - \frac{1}{2} \rho g h_1^2 - \rho q (u_1 - u_2)$$

If the velocities are not known, but the discharge and the water depths are, one could, knowing that $u = q/h$, rewrite this equation like:

$$F_s = \frac{1}{2} \rho g h_2^2 - \frac{1}{2} \rho g h_1^2 - \rho q^2 \left(\frac{1}{h_1} - \frac{1}{h_2} \right)$$

By vertical movement of the gate the flow conditions change and so does the force on the gate. It is good to realize that the largest force usually occurs while the gate is in closed position. In that case, the force simply is:

$$F_s = \frac{1}{2} \rho g (H_1^2 - H_2^2)$$

For other weirs the flow conditions are different, but the procedure is quite the same, so these are not addressed here. In the same way the forces on a culvert can be calculated.

The flow under the gate will cause resonance of the gate (with tidal movements, two directions of flow are involved!). The determination of the size and frequencies of dynamic forces is beyond the scope of this book.

5.3 Potential flow and pressure distribution

The pressure distribution on a structure in the flow, and thus also on the point of application, cannot be determined using the momentum balance. To do this, the potential flow theory may be used. However, one condition for the use of this theory is that the flow is free of rotations, which means that shear stresses are to be ignored. The potential flow theory will not be explained here, one is referred to the lecture notes “Open Channel Flow” (*Stroming in open waterlopen*), CTB3350 (Battjes & Labeur, 2014). An important property of a two-dimensional potential flow is that the flow lines and the equipotential lines are perpendicular to each other.

By drawing lines of equal potential at a distance $\Delta\phi$ of each other and flow lines at a distance $\Delta\psi$ of each other, $\Delta\phi$ being equal to $\Delta\psi$, one creates a flow net consisting of squares. Such a net can be drawn iteratively by using the above-mentioned properties. The diagonals of the flow net in turn form another square flow net with the same properties. This characteristic can be used as a visual test of the constructed flow net.

5.4 Head losses in a culvert

The head losses due to friction, entrance, and exit of the culvert (*duiker*) can be incorporated by using their respective reduction coefficients:

$$Q_d = \frac{Q_k}{\sqrt{\xi_{in} + \xi_{out} + \xi_f}}$$

in which: Q_k [m³/s] = discharge without losses

ξ_{in} [-] = entrance coefficient: $\xi_{in} = \left(1 - \frac{1}{\mu}\right)^2$

μ [-] = contraction coefficient

ξ_{out} [-] = exit coefficient

ξ_f [-] = friction coefficient

- To calculate the entrance coefficient ξ_{in} , the contraction coefficient μ is needed:
 $\mu \approx 0,6$ for rounded corners
 $\mu \approx 0,8$ for sharp corners
- For the exit coefficient ξ_{out} , usually a value of 1,0 applies
- The friction coefficient ξ_f depends on the geometry and material of the culvert, and is calculated as follows:

$$\xi_f = f \frac{L}{4R_h} \xi_f = f \frac{L}{4R_h}$$

in which: L [m] = culvert length

f [-] = friction factor

R_h [m] = hydraulic radius

The friction factor f can be derived from the Moody diagram (Section 4.2). In this diagram, for the relative pipe roughness, the diameter D is interchangeable with $4R_h$.

The reduced discharge will likely not satisfy the discharge requirement, which means that the geometry of the culvert should be changed one or two times until the solution satisfies the requested capacity (in other words, this is an iterative approach).

5.5 Literature

Ankum, P. (2002). *Design of Open-Channels and Hydraulic Structures*. Delft: Lecture notes Delft University of Technology.

Bengston, H. (2012, December 15). *Backwater Curve Calculations Spreadsheet*. Retrieved from Engineering Excel Spreadsheets:

<https://www.engineeringexcelspreadsheets.com/2012/12/backwater-curve-calculations-spreadsheet/>

Bezuyen, K. G., Stive, M. J., Vaes, G. J., Vrijling, J. K., & Zitman, T. J. (2012). *Inleiding Waterbouwkunde*. Delft: VSSD.

ISO (1980). International Organization of Standards. ISO 1438/1-1980(E). Water flow measurement in open channels using weirs and venturi flumes - Part 1: Thin plate weirs. 1980. Available from Global Engineering Documents at <http://global.ihs.com>

Kindsvater, C.E. and R.W. Carter. 1959. Discharge characteristics of rectangular thin-plate weirs. Transactions, American Society of Civil Engineers. v. 24. Paper No. 3001.

Nakayama, Y., & Boucher, R. (2000). *Introduction to Fluid Mechanics*. Oxford: Butterworth-Heinemann.

Pannekoek GWW B.V. (n.d.). *Foto's: Stuw 2 Burggenhoek*. Retrieved from Pannekoek GWW B.V.: <https://www.pannekoekgww.nl/projecten/detail/fotos-stuw-2-bruggenhoek>

Planthof, S. (2018). *Stuw Borgharen is open tijdens Monumentendag*. De Limburger, 4 September 2018 .

Rijkswaterstaat. (2018). '*Gelijk water*' bij stuw Driel. De Binnenvaartkrant, 18 October 2018.

6. Water, flow, slender structures

6.1 Drag and lift forces

An object, entirely in a uniform flow field, is subject to forces both in the direction of flow (drag force) and perpendicular to the flow (lift force). Drag and lift forces fluctuate in time. These forces cannot be determined theoretically with a linear flow theory such as Bernoulli's. The reason why the flow cannot be schematised as a potential flow is because of the occurrence of rotation: eddies behind the cylinder. A wake with a lower pressure is created directly behind the cylinder, which causes a resultant force in the direction of the wake. This turbulence also causes oscillations.

Experiments have shown that the resultant force on an object in the flow F [N] is reasonably proportional to the velocity head times the density of the fluid (compare this with Bernoulli's equation):

$$F \sim \rho g \frac{u^2}{2g} = \frac{1}{2} \rho u^2$$

in which: ρ [kg/m³] = density of water
 u [m/s] = de undisturbed flow velocity

The empirical formulas for drag and lift are:

$$F_D = \frac{1}{2} \rho u^2 (C_D + C'_D) A \quad \text{and} \quad F_L = \frac{1}{2} \rho u^2 (C_L + C'_L) A$$

in which: F_D [N] = drag force parallel to the flow direction
 F_L [N] = lift force perpendicular to the flow direction
 C_D [-] = drag coefficient (static)
 C_L [-] = lift coefficient (static)
 C'_D [-] = dynamic drag coefficient (time dependent)
 C'_L [-] = dynamic lift coefficient
 A [m²] = area facing flow, projected perpendicular to the flow direction

The fluctuation in time of the shapes of the wake and the eddies causes a fluctuation of the size and direction of the force, which, in turn, can cause oscillations. The drag force and lift force therefore consist of a static and a dynamic part. The corresponding coefficients are treated separately below.

Notes

- The drag force is parallel to the direction of flow (and not to the axis of the object!), the lift force is perpendicular to this.
- It is very important to notice that the turbulence of the water can wash out the soil behind a pile, thereby endangering the founding property of the pile. This erosion of the bed is called scour and is not discussed any further. When dimensioning a post, one must take this scour into account (less fixation and more effective pile length) or include bed protection measures. The scour behind a pile is 1.5 - 2 times the pile diameter in sandy soils.

6.2 Drag and lift forces, static part

The coefficients C_D and C_L are largely dependent on the shape of the structure and the flow around the structure, which are expressed in the Reynolds value, Re [-]:

$$Re = \frac{ud}{\nu}$$

in which: Re [-] = Reynolds value
 u [m/s] = flow velocity
 ν [m²/s] = kinematic viscosity = 10⁻⁶
 d [m] = measure of length dependent on geometry

In the field of hydraulic engineering, the flow is usually turbulent ($Re > 10^4$). The C_D coefficients for three different shapes (cylinder, plate and a streamlined wing) are given in Figure 6-1. This figure shows that the C_D coefficient of a cylinder (pile) in the area $10^5 < Re < 10^6$ is sensitive to fluctuations of Re . However, the C_D coefficients of angular objects, such as plates and beams, are barely dependent on Re in this turbulence area.

In the region $10^5 < Re < 10^6$, the wake behind a cylinder decreases for a larger Reynolds value, the separation points move further back. A smaller wake means a smaller resultant force. For objects with sharp edges, like flat plates and square piles, the separation points of the flow and thus the wake are more or less fixed. The resultant force on such objects is therefore less sensitive to fluctuations of Re .

shows that the shape of a pile is very important for the forces that result from flow against the pile.

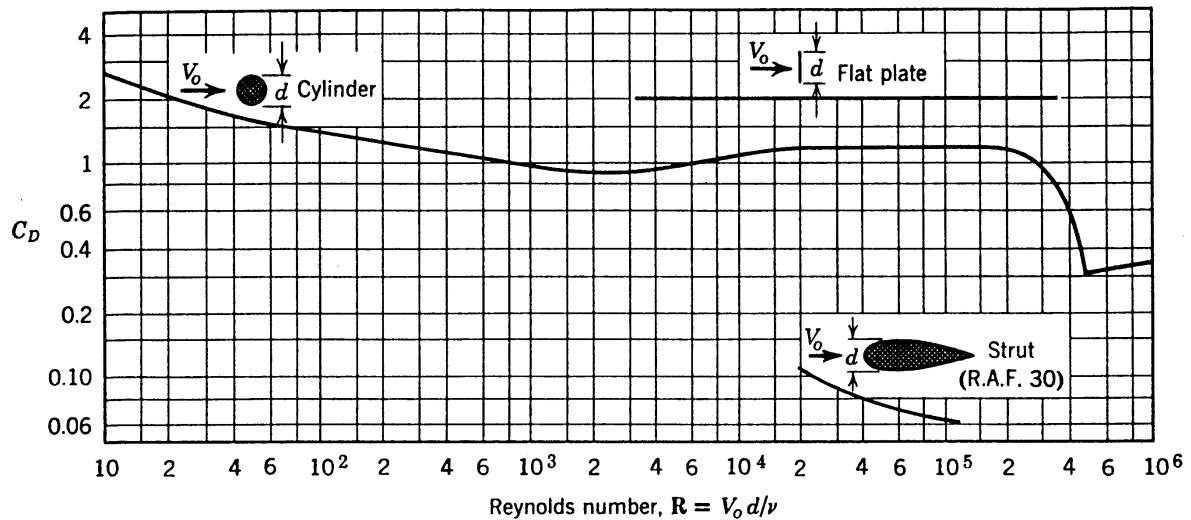


Figure 6-1 C_D value of a cylinder, plate and streamlined wing

The static lift coefficient (C_L) is zero for straight approaching flow.

The C_D and C_L coefficients of a bridge piers approached by flow at an angle are given in Figure 6-1. Three different shapes for the pier are indicated. The given coefficients are largest for the cylinder. However, this does not mean that the force on the cylinder is actually the largest, because the projected surface perpendicular to the flow is smaller for a cylinder than for the other given piers. The more the shape of the pier deviates from a cylinder, the larger the force on the pile if the flow approaches at an angle.

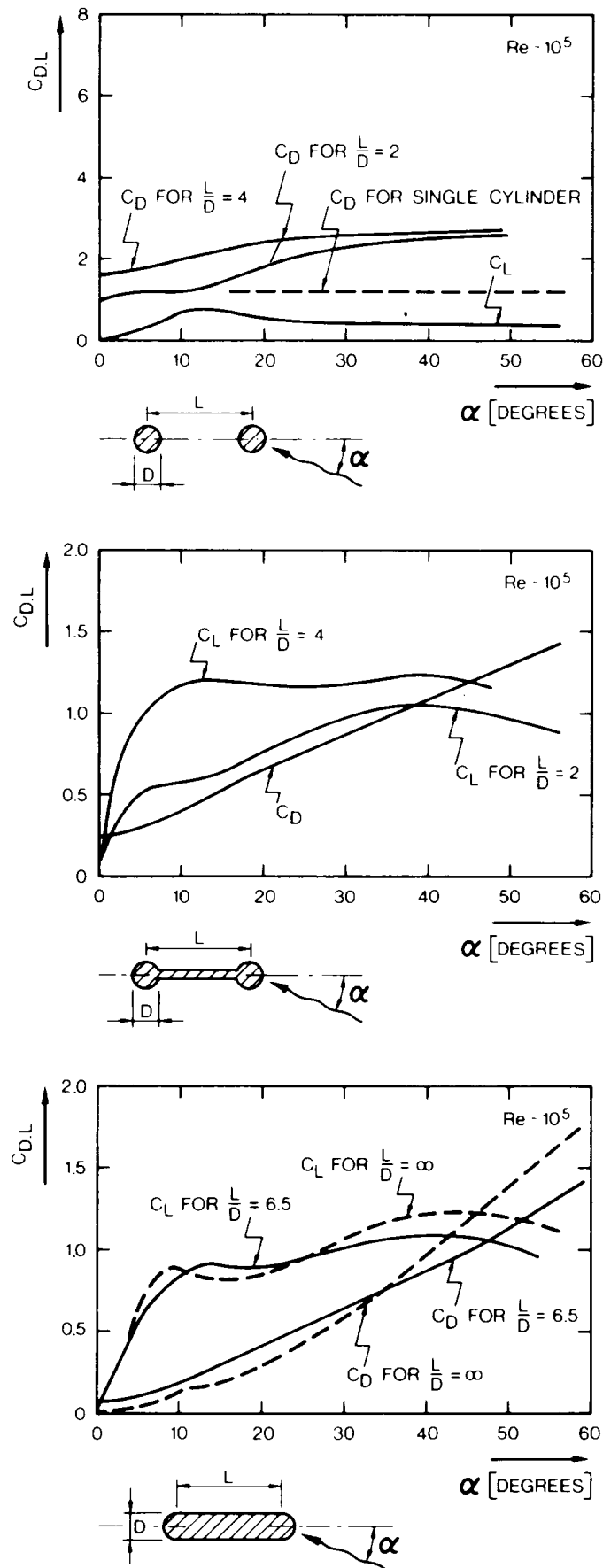


Figure 6-1 C_D and C_L coefficients of various pile shapes in the case of flow at an angle (Apetl and Isaacs, 1986)

6.3 Drag and lift forces, dynamic part (vibrations)

A structure that has been placed in a stationary flow can start to vibrate. These lecture notes only include an introduction to the phenomenon of vibrations as a result of stationary flow, as the complexity of the subject doesn't allow for a full description here.

The most important vibrations in a structure in a stationary flow are caused by instability of the wake and the vortices behind and alongside the structure or by hydrodynamic instability. Due to fluctuations in time of the vortices and the wake, the size and direction of the resultant force on an object in a stationary flow also fluctuates in time. Figure 6-2 indicates the pressure distribution around a cylinder due to changing vortices. This figure clearly shows that there is a dynamic resultant load.

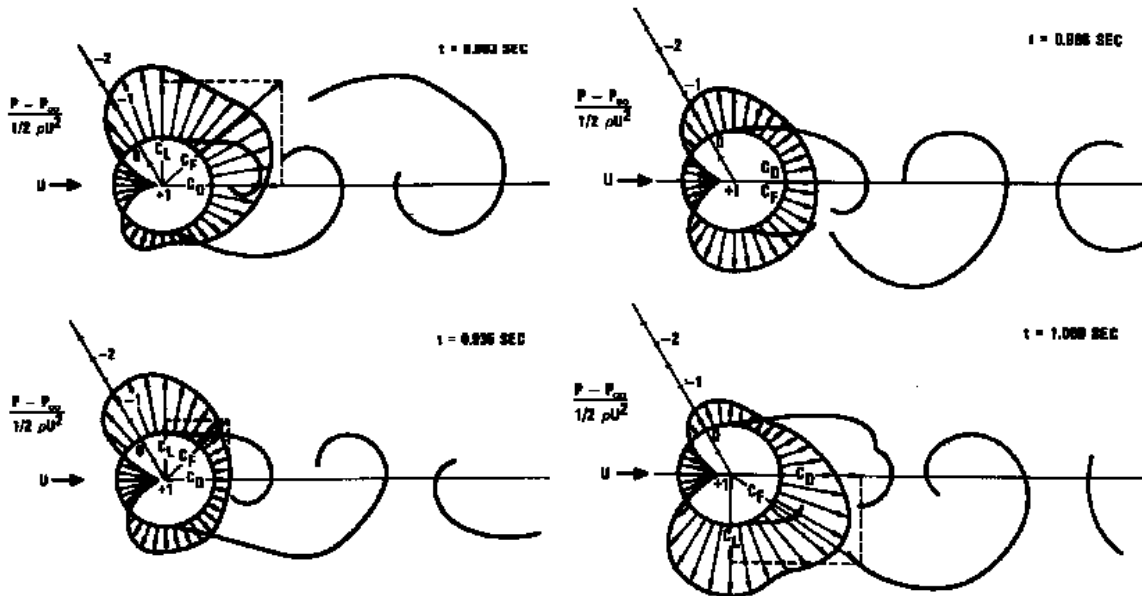


Figure 6-2 Fluctuation in time of the pressure and the wake with $Re=1.12 \cdot 10^5$ (Drescher 1956)

The frequency f_s of vortex shedding behind an object standing in the flow is given by:

$$f_s = \frac{uS}{D}$$

in which: u [m/s] = the flow velocity in an undisturbed flow
 S [-] = Strouhal number
 D [m] = the characteristic diameter perpendicular to the flow

The Strouhal number (S), named after the Czech physicist Vincenc Strouhal, is a dimensionless number describing oscillating flow mechanisms. For cylinders, this number is given as a function of the Reynolds number (Re) in Figure 6-3. For shapes with non-circular cross sections, reference is made to Figure 6-4.

Hydrodynamic instability occurs if a slight movement of an object is enforced by the flow, so that a small displacement can lead to vibrations with increasing amplitude. Depending on the stiffness of the structure hydrodynamic instability may occur. If $f_s > f_n$, no resonance will occur; here f_n is the natural oscillation frequency of the system (structure + water). This dynamic phenomenon is identical to a chimney swaying in the wind. Calculating the natural oscillation frequency is a study in its own right and is not covered in this course.

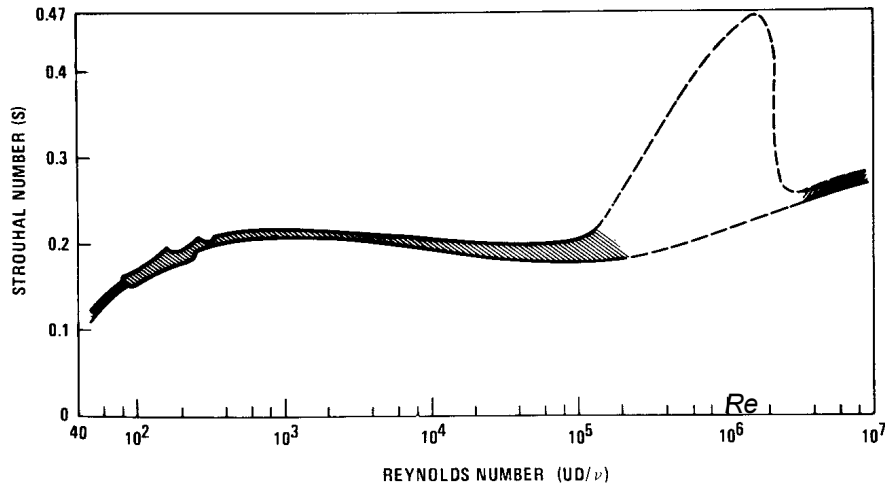


Figure 6-3 Strouhal number for cylinders

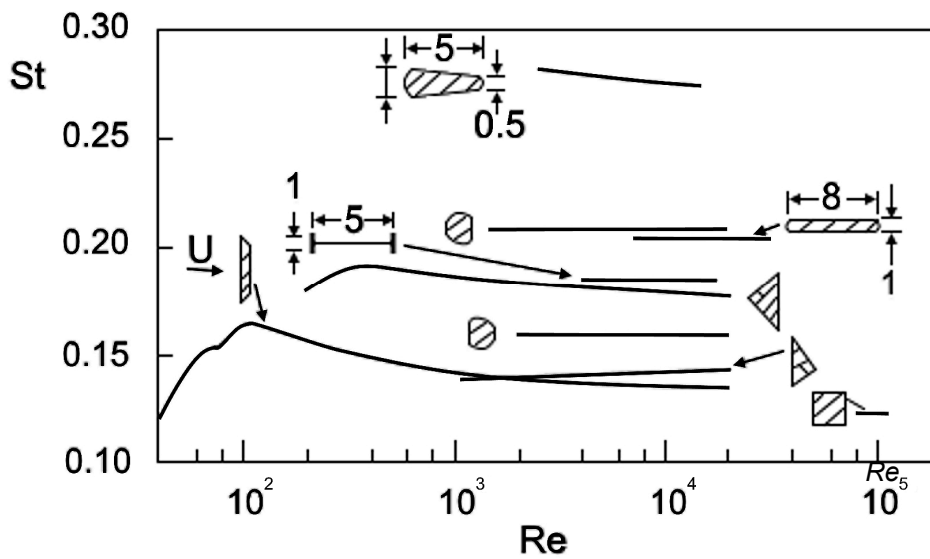


Figure 6-4 Strouhal number for non-circular cross sections

For the maximum dynamic drag coefficient (time dependent):

$$C'_D = 0,10 \text{ to } 0,5 \cdot C_D \quad \text{if: } f_s > f_n$$

$$C'_D = ? \text{ (danger of resonance)} \quad \text{if: } f_s < f_n$$

The static C_L coefficient is of course zero for a straight approaching flow ($\alpha = 0$). The dynamic C'_L coefficient is not zero due to the time dependent turbulent oscillations. The value of C'_L is strongly dependent on the ratio $\frac{f_s}{f_n}$ and increases largely near $\frac{f_s}{f_n} = 1$. Still no reasonably accurate expression is available for the value C'_L . For a preliminary design, one may therefore assume:

$$C'_L \approx C'_D.$$

7. Water, water level (tide, set-up, etc.)

Extended and updated: February 2015; wave set-up added: 2020

Water levels along the coast are mainly determined by the tide and by wind set-up. Furthermore, phenomena such as storm surges, shower oscillations, shower gusts and seiches are involved. These effects are explained in this chapter. The water level in rivers mainly depends on the discharge. Chapter 48 of this manual explains how these effects contribute to the design water level, needed for the evaluation of flood defences.

7.1 Astronomical tide

7.1.1 Theory

One of the most characteristic properties of coastal waters is the tidal movement. Different tides can be distinguished according to the water motion direction, namely:

- vertical tides: raising and falling of the water level
- horizontal tides: tidal flows in tidal inlets/ outlets and creeks and along the coast.

The tidal movements on earth are caused mainly by the following 5 factors:

1. The gravitational pull of the moon on the seawater.
2. The monthly rotation of earth around the shared earth-moon axis (centrifugal force).
3. The daily rotation of earth around its own axis.
4. The inclination of the earth's rotation axis.
5. The gravitational pull of the sun on the seawater.

1. The gravitational pull of the moon on seawater

The moon, and in lesser extent the sun, cause an uneven force distribution on the water due to the difference in distances between the points on earth and the moon, see Figure 7-1. The result is a semi-diurnal tide.

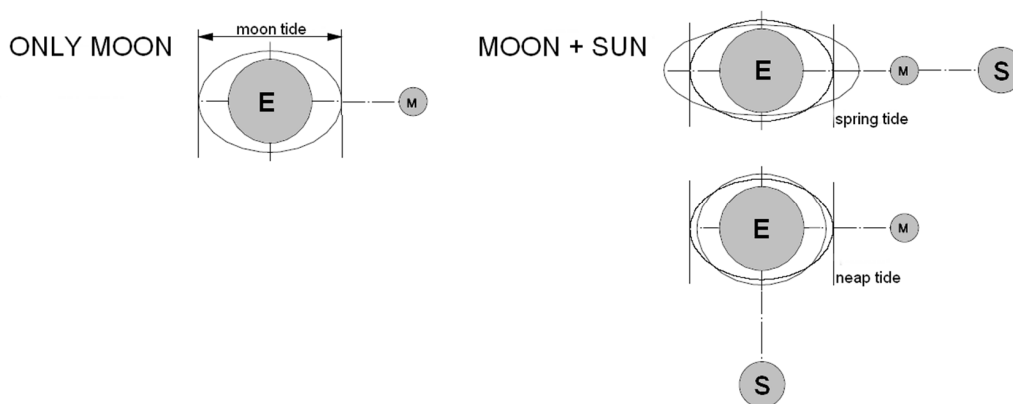


Figure 7-1 Pull of the moon and the sun

2. Rotation around the shared earth-moon axis

The earth has a monthly rotation around the shared earth-moon axis. This axis is approximately $0,6 r$ from the centre of earth. Because every point on earth covers the same distance for this rotation, the centrifugal force is the same everywhere on earth. (In this case one must not consider that the earth is rotating around its own axis, as this is taken into consideration in point 3.) Together these two forces form an elliptical force distribution around the earth. If the earth were covered entirely in water, the water mass would take the shape of an ellipsoid, as shown in Figure 7-2. This fictional situation is known as the equilibrium tide due to the moon.

3. Rotation around own axis

The earth spins as it were under the water mass, thus causing two high tides and two low tides a day (semi diurnal tide) in an arbitrary location. There are, however, places on earth where the tidal flow is influenced by the presence of a continent to such an extent that there is only one high tide per day (diurnal tide) in these locations.

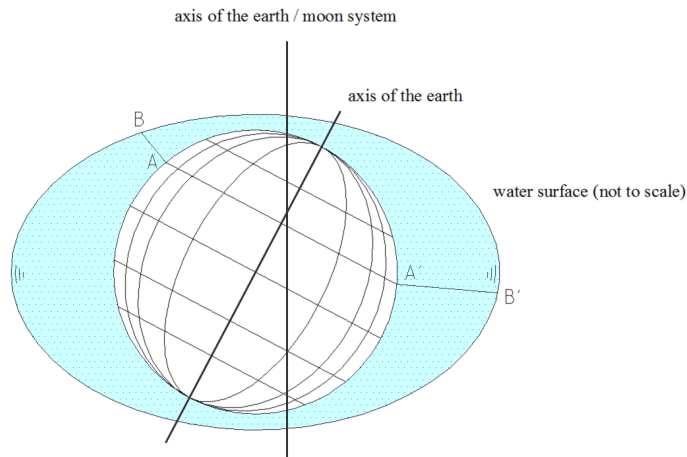


Figure 7-2 Two different high tides

4. Obliqueness rotation axis

Due to the obliqueness of the rotational axis of the earth, the tidal movement during a semi diurnal tide is AB one time and A'B' another. This causes a daily inequality of the maximum tide (see Figure 7-3). In winter, the high tide at daytime (AB) is generally smaller than the high tide at night (A'B'). In the summer, the opposite applies.

5. Gravitational pull of the sun on seawater

The influence of the sun is confined to reinforcing or weakening the moon tide. If the sun and the moon are on the same side of the earth, they reinforce each other. The resulting tide is known as spring tide, if they counteract each other it is called neap tide. Spring tide occurs at full and new moons; neap tide occurs in the first and last quarters.

In most seas, the semi-diurnal range (the difference in height between high and low waters over about half a day) varies in a two-week cycle. Approximately twice a month, the Sun, Moon, and Earth form a line and the tidal force due to the Sun reinforces that due to the Moon. The tide's range is then at its maximum. Figure 7-3 shows the tidal water level movements during a month in Vlissingen.

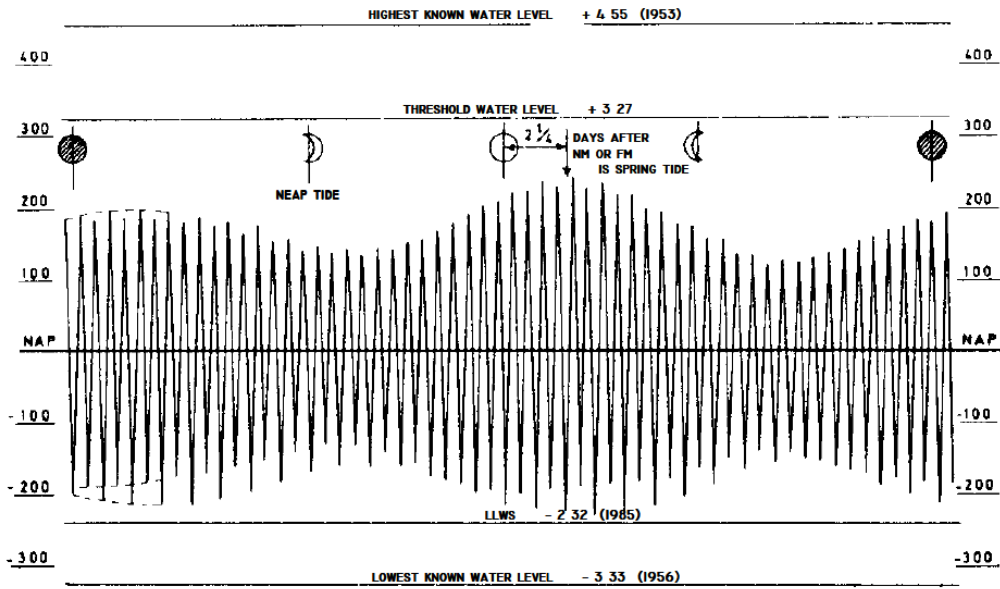


Figure 7-3 Water level in one month in Vlissingen

7.1.2 Design

In reality the astronomical tide bears little resemblance to the theoretical equilibrium tide. This is due to the presence of continents and the Coriolis effect, which causes the diversion of tidal flows. The true tidal water levels and the times of high and low tide can be predicted with a "harmonic analysis" or "Fourier analysis" of the data from measuring stations. These techniques are not discussed here.

Every year, the Dutch Institute for Public Works and Water Management, Rijkswaterstaat, publishes

forecasts made using these methods in the booklet Tide tables for the Netherlands ("Getijtafels voor Nederland"). For a number of measuring stations, the booklet lists when high and low tides will occur at and what their corresponding water levels are. Data on tides can be found at: www.rijkswaterstaat.nl/geotool/waterhoogte_tov_nap.aspx.

For design of hydraulic structures (lock gates for example), the extreme tidal levels are of importance:

The Lowest Astronomical Tide (LAT) is the lowest tide level that can be predicted to occur under average meteorological conditions and under any combination of astronomical conditions.

The **Highest Astronomical Tide (HAT)** is the highest level that can be predicted to occur under average meteorological conditions and under any combination of astronomical conditions.

Notice that these tidal levels are not the lowest or highest water levels that can occur, due to several other effects that are mentioned below.

7.2 Wind set-up

7.2.1 Theory

Wind set-up is the phenomenon of water being headed up by wind by means of the friction (shear stress) at the water surface. Wind set-up depends of many variables, such as the wave height and the temperature. The shear stress is defined by Vickers and Mahrt (1997) as:

$$\tau_w = \rho_{air} \cdot C_d \cdot u^2$$

where: τ_w [N/m²] = shear stress at the water surface
 C_d [-] = bulk drag coefficient
 ρ_{air} [kg/m³] = density of air
 u [m/s] = wind velocity at 10 m above the water surface

The bulk drag coefficient is not easy to determine, it is the constant of proportionality that marks the relationship between the wind speed and wind stress at the water surface. The coefficient mainly depends on the temperature, humidity, air stratification (*gelaagdheid*) and wave height (Smith, 1988).

Wind set-up has the character of a long wave (large wave length compared to the water depth), from which a continuity equation can be derived. If advective accelerations are neglected, the equation (Saathof, 1976) is:

$$\frac{\partial Q}{\partial T} + G \cdot a_c \frac{\partial h}{\partial s} + C_f \frac{|Q|Q}{A_c \cdot R} = C_w \frac{\tau_w \cdot \cos(\varphi) \cdot A_c}{h \cdot \rho_{water}}$$

Figure 7-4 shows a model to approximate the wind set-up (*opwaaiing*).

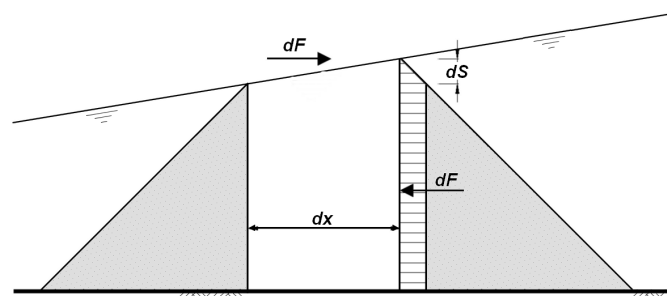


Figure 7-4 Balance of forces in case of wind set-up

The wind set-up per horizontal distance x in the equilibrium state is approximately:

$$\frac{\partial S}{\partial x} = C_2 \frac{u^2}{g \cdot d}$$

7.2.2 Design

Wind fields in shallow seas, deltas, closed-off creeks and lakes can lead to a considerable rise of the water surface near the water line. In the North Sea, the Wadden Sea and the IJsselmeer, the set-up can be as much as a couple of meters. In 1953 the rise in Vlissingen was 3,05 m.

If the wind set-up is small compared with the water depth, in an area with a horizontal bed, the slope $\frac{\partial S}{\partial x}$ is constant.

Usually, for designs, the following equation is used for the total set-up:

$$S = C_2 \cdot \frac{u^2}{g \cdot d} \cdot F$$

in which: S	[m]	= total wind set-up
x	[m]	= distance over which the set-up is considered
C_2	[-]	= coefficient taking into account various effects (like temperature, humidity)
F	[m]	= the total distance that contributes to the wind set-up, the 'fetch'
u	[m/s]	= wind velocity, at 10 m above the water surface
g	[m/s ²]	= gravitational acceleration
d	[m]	= average water depth over the fetch

The equation assumes that there is no in- or outflow in the water body. Furthermore, it assumes a stationary situation, where wind direction and wind velocity are constant over a sufficiently long period of time to develop an equilibrium between the acting wind force and the gravity that causes a slope of the water surface. The wind set-up increases with increasing wind velocity and fetch and decreasing water depth. The wind set-up is therefore of importance in river deltas, lakes and shallow seas. In coastal areas where the sea is deep, wind set-up hardly ever occurs. This implies that the effective fetch should not extend too far in sea, where the water depth is large (Figure 7-5).

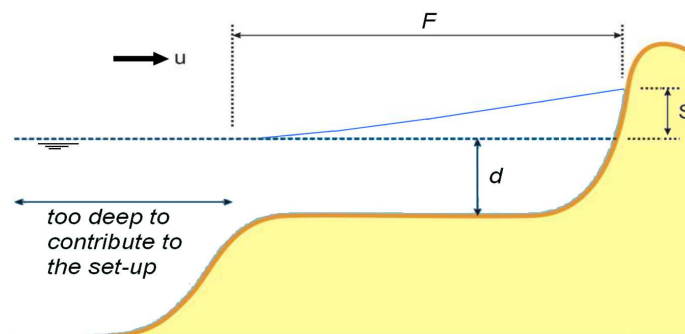


Figure 7-5 Relation between the wind set-up and the water depth

The coefficient C_2 in the equation has been determined empirically. Measurements of wind velocity and water levels in the Netherlands have led to a value of constant $\approx 3,5 \cdot 10^{-6}$ to $4,0 \cdot 10^{-6}$ which applies to Dutch circumstances (Deltarapport 1961).

Closed basins

In a closed basin or a lake, the total volume of water cannot change. This means that, provided that in a stationary state the inclination of the water surface may be assumed constant, the surface of the water (by approximation) will tilt around the basin gravity line perpendicular to the wind direction. The water in the area between the down-wind side and the gravity centre thus is subjected to wind set-down (Figure 7-6) and the set-up at the other side is less than in the case of an open water basin like a sea. This implies that the 'total wind set-up' S in the equation above comprises both the set-up as the set-down in the case of a closed basin!

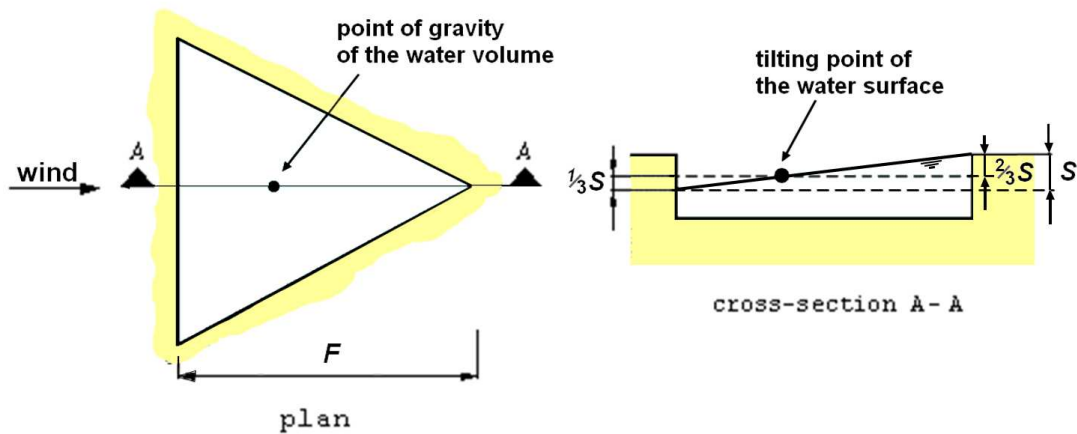


Figure 7-6 Wind set-up in a closed basin

7.3 Wave set-up

Wave set-up is the elevation of the time-averaged water level in the breaker zone, caused by the breaking of waves near a beach.

Sea and ocean waves transport energy and momentum (*impuls*) towards the coast. Breaking of the waves near the coast causes a force on the water because of the conservation of momentum. The component of this force parallel to the coast causes a surf current (*brandingsstroom*). The component of the force perpendicular to the coast pushes the water towards the coast, causing the elevation of the water level (wave set-up).

The water level elevates until the hydrostatic pressure equals the wave stress. From this equilibrium, the wave set-up can be calculated:

$$z = \frac{5}{16} \cdot \gamma \cdot H_b$$

where: z [m] = wave set-up

H_b [m] = wave height at the breaker line

γ [-] = breaker index: $\gamma = \frac{H_b}{d_b}$ (usually, $\gamma \approx 0,7$ to $0,8$)

d_b [-] = water depth at the breaker line

Wave set-down is a wave-induced decrease of the mean water level before the waves break (during the shoaling process). The set-down is in the order of magnitude of 20% of the wave set-up.

(Source: Bosboom and Stive, Coastal dynamics, Delft Academic Press, Delft, 2015, p 584. ISBN 9789065623720)

7.4 Other influences on the water level

Besides tides, wind and wave set-up, other factors can influence the water level, depending on local circumstances, such as:

7.4.1 Funnel-effect

If the wind blows in a direction where the water surface becomes narrower, the water level will be pushed up. This set-up is called the 'funnel effect' (*trechtereffect*). The funnel effect, as well as wind set-up, is comprised in the term 'storm set-up.'

7.4.2 Short-term atmospheric depressions

Short-term atmospheric depressions (*buistoten*) cause single elevations of the sea water level. These depressions are generated when a storm with low air pressure approaches the coast with the same velocity as the wave, thus building up an increasing large wave. A drop of 10 hPa (= 1000 Pa = 0,01 bar) more or less equals a water level elevation of 0,10 m (the exact value depends on the temperature of the water). The duration of a short-term atmospheric depression can vary between a couple of minutes and more than one hour.

The resulting water level elevation at the Dutch coast can be up to 0,50 to 1,00 m during storm conditions. However, it is not very likely that this coincides with extreme water levels, so usually only a reduced effect of atmospheric depressions is taken into account. This reduced value depends on the height needed to reduce wave run-up to acceptable amounts. The maximum value is 0,30 m along the Dutch coast, and only 0,05 m 20 km landward (TAW, 1989). The Dutch guide on lake and sea dikes (TAW, 1999) has adopted these values. During the passing of hurricane Hugo in Guadeloupe, a water level rise of 0,30 to 0,60 m was observed in deep water. In shallow water the rise was as much as 2,50 to 3,00 m.

If atmospheric depressions appear in a more or less regular series, the phenomenon is called oscillating depressions (*bui-oscillaties*). The period of an oscillating depression can vary from a couple of minutes to more than an hour; the amplitude in Dutch waters is usually about 0,20 to 0,30 m. In Dutch waters, the effect of short-term depressions dominates the effect of oscillating depressions; this is why it is assumed that the effect of the latter is discounted in the contribution of the short-term depressions (TAW, Grondslagen voor Waterkeren, 1989).

Because of the presence of the Hartelkering and the Maeslantkering, short-term atmospheric depressions have become much less relevant behind these barriers. The Dutch committee on flood defence (TAW) therefore recommended to neglect these effects behind the barriers, until further research will prove differently (TAW, TR Ontwerpbelastingen voor het Rivierengebied, 2007).

7.4.3 Seiches

Seiches (*'buihalingen'* = *staande golven in waterbasins*) are oscillatory elevations of the water level, or standing waves, in a water basin enclosed on three sides, for instance sheltered harbours and lakes. They are caused by oscillations of the (sea) water level outside the basin, particularly by shower oscillations with periods ranging from a couple of minutes to an hour. Typical periods of seiches are between 10 and 120 minutes.

Because of the presence of the Hartelkering and the Maeslantkering, the importance of shower gusts, shower oscillations and seiches has become much less relevant behind these barriers. The Dutch committee on flood defence (TAW) therefore recommended to neglect these effects behind the barriers, until further research will prove differently (*TAW Technisch Rapport Ontwerpbelastingen voor het rivierengebied*, 2007). Seiches in the IJsselmeer, with elevations up to 0,113 m, have been reported by Bottema, 2004.

7.4.4 Tidal resonance

Tidal waves in estuaries, bays or river mouths can possibly be reflected. Interference of the reflected wave with the incoming wave will then lead to an increase of the water level, which has to be taken into account when determining the height of a flood defence. This phenomenon is called tidal resonance (*getijresonantie*).

7.4.5 Tidal bores

A tidal bore (*vloedbranding*) is a natural phenomenon, where a tidal flood wave enters a river mouth in upstream direction, with a sudden elevation. Bores can only be observed in a few river mouths, as the flood wave should enter the river mouth at a certain moment with a large velocity. Furthermore, the river mouth should become narrow in such an extent, that the discharge capacity becomes too small to handle the flood wave in a normal way. The water level therefore suddenly elevates, showing kind of a steep wall of water, over which the water pours over, like in a high surf zone. Bores can be observed in several rivers in England and France. The bores in the Amazone and the T sien-tangKiang (China) are very impressive, reaching heights of up to 8 m.

7.4.6 Tsunamis

A tsunami is a series of waves in a water body caused by the displacement of a large volume of water, due to earthquakes, volcanic eruptions and other underwater explosions (including detonations, landslides, glacier calvings, meteorite impacts and other disturbances) above or below water. Tsunami waves differ from normal wind waves because their wavelength is far longer. Tsunamis generally consist of a series of waves, with periods ranging from minutes to hours, arriving in a so-called "wave train". Wave heights can be up to tens of metres in large events. Rather than appearing as a breaking wave, a tsunami may instead initially resemble a rapidly rising tide. This causes a water level elevation.

7.4.7 Climate change effects (sea level rise and increase of river discharges)

Water levels will in future be influenced by climate change effects. An increase of the average temperature causes thermal expansion of the ocean water, resulting in a water level elevation. The melting of ice masses on land (flowing into the oceans) has an additional effect on the sea water level. It is also forecasted that the rivers will be influenced by climate change, because the highest and lowest river discharges will become more extreme, due to more fluctuations of rainfall over land. In addition, climate change can influence wind set-up, atmospheric depressions, seiches and tidal resonance. Climate change effects should be considered over the design life time of hydraulic structures, in case of designs, or over the return period of the assessments, in case of assessments.

The magnitude of future sea level rise is still subject to research. The average trend of relative sea level rise observed in the Netherlands since 1900 is 0,19 m/century (Dillingh, 2008) and a deviation from this trend has not yet been observed. Forecast models, however, come with a wide range of results. A study in 1990 resulted in an estimate of the relative level rise of the North Sea is 0,40 to 0,80 m per century (Note on coastal defence 1990 – TR6 – Sea level rise, in Dutch: “Nota kustverdediging van 1990 - TR6 – Zeespiegelrijzing”). The Veerman Committee 2008 made a prognosis of 1,30 m in 100 year as a worst-case scenario, based on forecast models. Some newer models came up with values of 2,00 m and even more. It is the task of engineers to find a way to deal with these alternatives, ranging from adaptive to robust design strategies.

The combined effect of (absolute) sea level rise and land subsidence due to geological processes and gas and oil extraction is indicated as 'relative sea level rise'.

7.5 Storm surge levels

It is more or less possible to predict the timing and the water levels of a spring tide. The wind set-up near the coast line can be calculated with a given wind velocity. By analysing wind data, it is possible to calculate the probability of occurrence of a spring tide and a certain wind set-up. Such a combination is known as a storm surge (*stormvloed*).

Because the calculation model for wind set-up contains a number of uncertainties, a different approach can be used in practice. A statistical analysis of a few decades of water level measurements along the Dutch coast resulted in finding an exponential relation between storm surge levels and the frequency of exceedance of these levels². The normative water level (storm surge level) for a chosen small exceedance frequency was then determined by extrapolation of measuring points, see the high-water level measurements for Hoek van Holland in the following figure³ (measured at sea) (Wemelsfelder, 1939; Van Dantzig, 1956).

After a profound analysis of the available data, it was found that the frequency of exceedance of a certain water level h_0 can be described with an exponential function:

$$f(h > h_0) = e^{-\frac{h_0 - A}{B}}$$

where:

f	[year ⁻¹]	=	exceedance frequency
h	[m]	=	water level
h_0	[m]	=	reference level, for instance the height of structure
A, B	[m]	=	constants

² The total set of measurements includes the daily astronomical high-water levels, but these levels were filtered out by means of a peak-over-threshold method. In addition, succeeding measuring points belonging to one storm were reduced to one measurement point.

³ Notice that x- and y-axis are swapped in this figure, as usual with water levels, and the y-axis is plotted on a logarithmic scale. In addition, the direction of the y-axis deviates from the usual direction (y-values decrease towards the right of the graph).

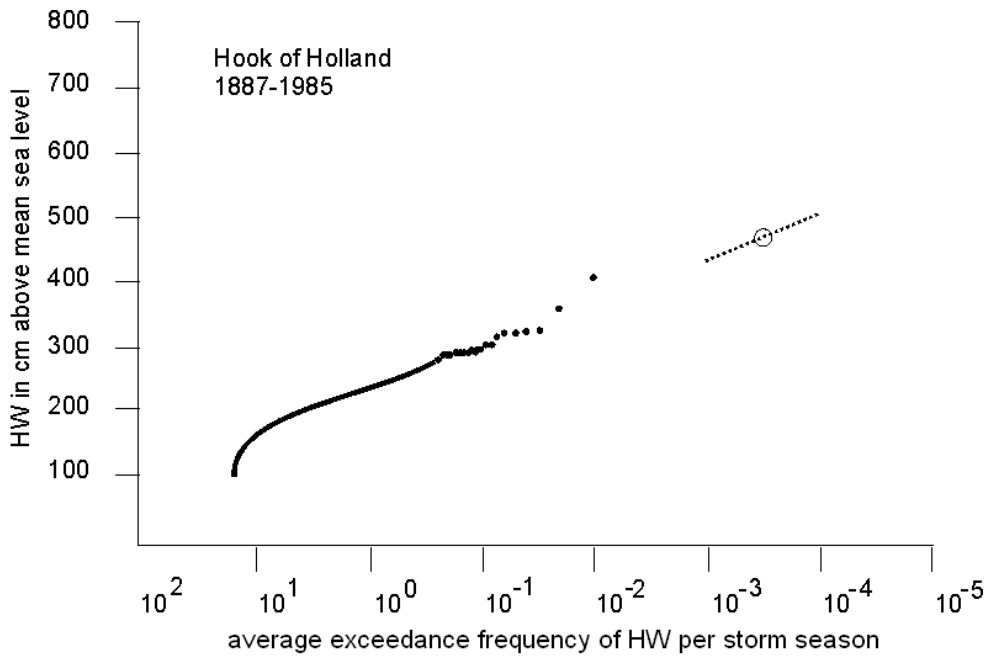


Figure 7-7 Water level exceedance frequencies at Hoek van Holland

The probability of exceedance is closely related to the frequency of exceedance. A difference is that a frequency can theoretically be more than 1,0, whereas a probability per definition cannot exceed this value. The relationship between exceedance probability and exceedance frequency is expressed as:

$$P(h > h_0) = 1 - e^{-f(h > h_0) \cdot n}$$

For exceedance probabilities frequencies of less than 0,1, the exceedance frequency has about the same magnitude, provided that the exceedance probability is considered over a period of one year ($n = 1$), which we usually do⁴. Figure 7-8 shows the difference between the exceedance frequency and the exceedance probability for a period of one year.

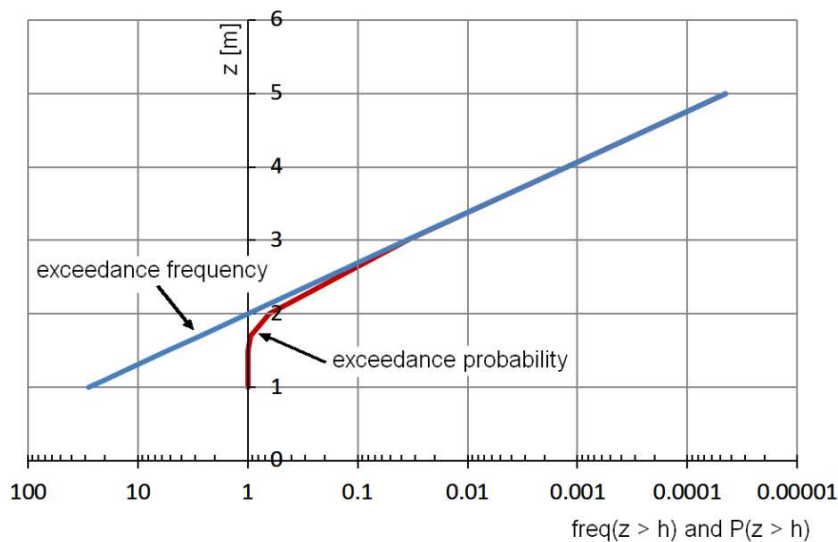


Figure 7-8 Comparison of the frequency and probability of exceedance for a theoretical case (z relative to NAP, $A = 2,0$; $B = 0,3$ and $t = 1,0$ year)

For foreign projects, however, there are often too few data to determine the design storm surge level on a statistical basis. In such cases the models for the tide and the wind set-up have to be used to estimate the storm surge level.

⁴ In practice, exceedance frequency and probability are therefore often confused and can easily lead to erroneous reasoning. It should also be noticed that the units are different: a frequency is expressed as a number of occurrences per year, and a probability is dimensionless.

8. Water, waves, theory

Section 2.3 on wave periods added in 2021

In hydraulic engineering, different types of waves can be distinguished, such as:

- Translation waves (sloping front!), caused for instance by:
 - quickly emptying or filling a lock chamber on or from a canal section
 - opening or closing a hydropower station
- wind waves, caused by the wind skimming large water surfaces
- tides, caused by the position and rotation of celestial bodies
- discharge waves caused by precipitation or thaw
- ships' waves
- pressure waves, which can be created in closed pipes by sudden discharge changes.

With the exception of pressure waves, all the above are waves which occur on the water surface. These waves are divided into short and long waves. Short waves, such as wind waves and ships' waves, cannot be disregarded in the vertical component of the wave velocity in relation to the horizontal component, as is the case with long waves, such as tide and translation waves.

This chapter briefly describes translation waves and wind waves. Tides are covered in Section 7.1. Discharge waves are discussed in Section 4.1. Pressure waves in closed pipes are not be treated in this Manual. When approaching shallows and obstacles, waves change their properties and can start to break. This is covered in Chapter 10 "Water, waves, shallows + breaking".

8.1 Translation waves

Translation waves can have different causes. One of the most common causes is emptying or filling a lock chamber. There are also natural processes that can cause a translation wave. Examples of these are dam breaches (of ice dams and natural soil dams) and tidal bores. Figure 8.1 gives a sketch of a translation wave. The propagation velocity of the wave is:

$$c = u \pm \sqrt{g \frac{(2d + \eta)(d + \eta)}{2d}}$$

in which: u [m/s] = the normal flow velocity
 d [m] = the water depth
 η [m] = the displacement of the water surface

For a relatively small η , the propagation velocity can be approached with:

$$c = u \pm \sqrt{gd}$$

The displacement of the water surface depends on the change of the discharge, the propagation velocity and the flow width:

$$\eta = \frac{\Delta Q}{Bc}$$

in which: ΔQ [m³/s] = the change of discharge
 B [m] = the flow width

In the translation wave the pressure is hydrostatic. The pressure under a translation wave with elevation η is:

$$p = \rho g(d + \eta)$$

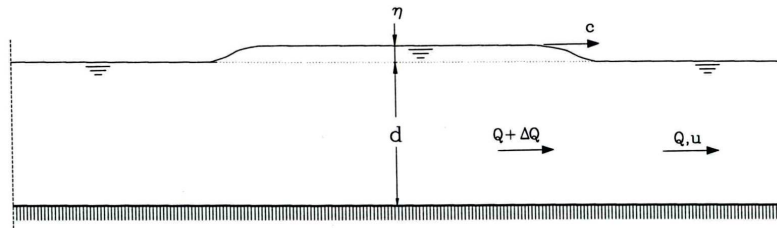


Figure 8-1 Translation wave

When the flow profile changes, a wave continues in the original direction and a wave reflects in the opposite direction. The same happens at the branching of a river.

When determining the displacement of the water surface with the continuing and reflected wave, the following applies, after the passing of the wave, at the point of profile adjustment:

- the water level to the left and the right of this point are equal
- the sum of the discharges equals zero.

8.2 Wind waves

8.2.1 Linear wave theory (regular waves)

This chapter briefly gives a number of characteristics of wind waves. For a more extensive explanation and the derivation of the equations one is referred to the course Ocean Waves (CT4325). The terms involved in wave theory can best be defined using a picture of a single wave.

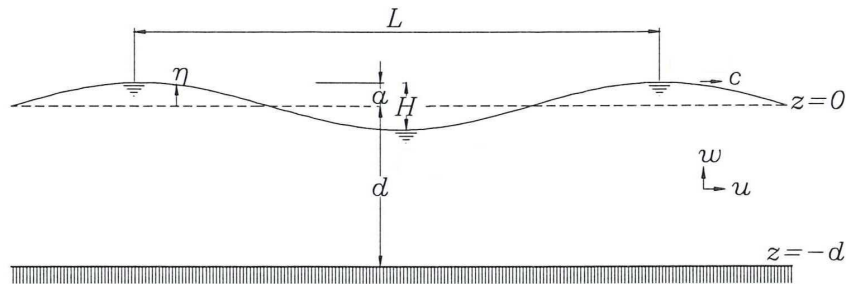


Figure 8-2 Sinusoidal wave shape

The most important terms are:

- L The wavelength is the horizontal distance between two successive wave crests (or troughs).
- T The period is the time, which passes at a certain fixed point between the passing of two consecutive wave crests
- f The frequency is defined as the number of waves per unit of time, which equals the inverse of the period ($= 1/T$)
- c The wave velocity (also known as the propagation velocity or phase velocity) with which the wave crest travels
- η The displacement of the water surface
- a The amplitude of the wave
- H The wave height is the difference in height between the highest and the lowest point of the wave profile ($H=2a$)
- H/L The steepness is the ratio wave height to wavelength
- u and w The velocity components of the orbital movement of the water particles
- p The water pressure
- d The water depth

Figure 8-2 shows a schematised, sinusoidal, vertical cross-section of the water surface, which is perpendicular to the direction of the wave crests. This schematisation is used in linear wave theory. The true shape of short waves is highly dependent on the steepness (H/L).

If $H/L \leq 1/40$, the shape of the wave is comparable to a sinusoid. For larger values of H/L , the shape will bear more resemblance to a trochoid.

The following applies in case of the sinusoidal approximation of the displacement of the water surface:

$$\eta(r,t) = a \sin\left(\frac{2\pi t}{T} - \frac{2\pi r}{L} + \alpha\right) \quad \text{or} \quad \eta(r,t) = a \sin(\omega t - k r + \alpha)$$

in which: $\omega = \frac{2\pi}{T}$ [rad/s] = angular frequency

$$k = \frac{2\pi}{L}$$
 [rad/m] = wave number

$$t$$
 [s] = point in time

$$r$$
 [m] = place measured in the wave direction

$$\alpha$$
 [rad] = phase

Note.

In American literature the following equation is used for the displacement of the surface:

$$\eta(r,t) = a \cos(k r - \omega t + \alpha). \text{ This means a phase shift of } \pi/2.$$

The wave velocity c , the wavelength L and the period T are related to each other according to the following equation:

$$c = \frac{L}{T} = \frac{\omega}{k}$$

From theoretical derivations, relations follow between the wave velocity, the wavelength and the water depth, such as:

$$c = \sqrt{\frac{g}{k} \tanh(kd)} \quad \text{or} \quad c = c_o \tanh(kd)$$

$$L = \frac{gT^2}{2\pi} \tanh(kd) \quad \text{or} \quad L = L_o \tanh(kd)$$

in which: $c_o = \frac{gT}{2\pi}$

$$L_o = \frac{gT^2}{2\pi}$$

In shallow water ($d \leq \frac{1}{25}L$), $\tanh(x) \approx x$. Therefore, the wave velocity in shallow water can be written as:

$$c = \sqrt{\frac{g}{k} \tanh(kd)} \approx \sqrt{gd}$$

When observing waves, it is noticeable that a wave group does not move at the same velocity as individual waves. A wave group propagates with a smaller velocity than the individual waves, whereby the waves overtake each other. The wave front moves at the so-called group velocity:

$$c_g = nc \quad \text{with} \quad n = \frac{1}{2} + \frac{kd}{\sinh(2kd)} \quad \text{for deep water:} \quad n = \frac{1}{2}$$

All water particles in a wave move in a more or less elliptic course. The movement of the particles decreases the deeper they are below the water surface. The elliptical movement of the water parts is known as orbital movement.

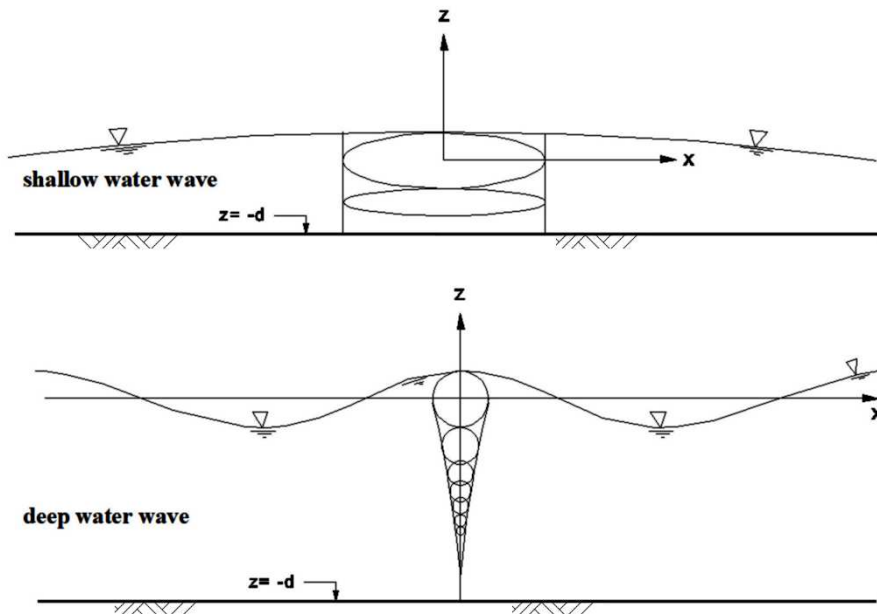


Figure 8-3 Orbital movement

The maximum horizontal and vertical components of the orbital velocity of a water particle are given by:

$$\hat{u} = \omega a \frac{\cosh(k(d+z))}{\sinh(kd)} \quad \text{and} \quad \hat{w} = \omega a \frac{\sinh(k(d+z))}{\sinh(kd)}$$

in which: \hat{u} [m/s] = maximal horizontal velocity
 \hat{w} [m/s] = maximal vertical velocity
 z [m] = co-ordinate of the considered depth relative to the average water surface

As is evident from the formula, the water velocity is largest at $z = 0$ and smallest at $z = -d$.

The pressure in a given point at a depth z below the average water line is:

$$p = -\rho g z + \rho g a \frac{\cosh(k(d+z))}{\cosh(kd)} \sin(\omega t - kr) \quad \text{for } z < 0$$

The pressure in a point above the average water line can be approximated by linear interpolation:

$$p = \rho g(\eta - z) \quad \text{for } z > 0$$

In the preceding, a possible flow velocity of the water was not taken into account. The given equations only apply for a co-ordinate system fixed to the undisturbed water surface. In a flow the equations are for a co-ordinate system that moves along with the flow. Relative to a fixed point, the propagation velocity and phase velocity are to be adjusted as follows:

$$c' = c + \bar{U} \bar{e}_r \quad \text{and} \quad \omega' = \omega + \bar{k} \cdot \bar{U} = \sqrt{gk \tanh(kd)} + \bar{k} \cdot \bar{U}$$

A wave has kinetic and potential energy. The potential energy is related to the displacement of the water surface and the kinetic energy is related to the orbital movement. The total mechanical energy of one wave is:

$$E = \frac{1}{8} \rho g H^2 L \quad (\text{per } m' \text{ wave crest})$$

The average energy per unit of surface area is thus:

$$E = \frac{1}{8} \rho g H^2$$

This energy plays an important part in the description of waves in a wave field.

A summary of linear wave theory is given in Table 8-1.

Relative depth Characteristics	Shallow Water $\frac{h}{L} < \frac{1}{20}$	Transitional water depth $\frac{1}{20} < \frac{h}{L} < \frac{1}{2}$	Deep Water $\frac{h}{L} > \frac{1}{2}$
Wave Celerity	$c = \frac{L}{T} = \sqrt{gh}$	$c = \frac{L}{T} = \frac{gT}{2\pi} \tanh kh$	$c = c_0 = \frac{L}{T} = \frac{gT}{2\pi}$
Wave Length	$L = T\sqrt{gh}$	$L = \frac{gT^2}{2\pi} \tanh kh$	$L = L_0 = \frac{gT^2}{2\pi}$
Group Velocity	$c_g = c = \sqrt{gh}$	$c_g = nc = \frac{1}{2} \left(1 + \frac{2kh}{\sinh 2kh} \right) \cdot c$	$c_g = \frac{1}{2} c_0 = \frac{gT}{4\pi}$
Energy Flux (per m width)	$F = Ec_g = \frac{1}{2} \rho g a^2 \sqrt{gh}$	$F = Ec_g = \frac{1}{2} \rho g a^2 n c$	$F = \frac{T}{8\pi} \rho g^2 a^2$
Particle velocity	Horizontal $u = a \sqrt{\frac{g}{h}} \sin \theta$ Vertical $w = \omega a \left(1 + \frac{z}{h} \right) \cos \theta$	Horizontal $u = \omega a \frac{\cosh k(h+z)}{\sinh kh} \sin \theta$ Vertical $w = \omega a \frac{\sinh k(h+z)}{\sinh kh} \cos \theta$	Horizontal $u = \omega a e^{kz} \sin \theta$ Vertical $w = \omega a e^{kz} \sin \theta$
Particle displacement	Horizontal $\xi = -\frac{a}{\omega} \sqrt{\frac{g}{h}} \cos \theta$ Vertical $\zeta = a e^{kz} \sin \theta$	Horizontal $\xi = -a \frac{\cosh k(h+z)}{\sinh kh} \cos \theta$ Vertical $\zeta = a \frac{\sinh k(h+z)}{\sinh kh} \sin \theta$	Horizontal $\xi = -a e^{kz} \cos \theta$ Vertical $\zeta = a e^{kz} \sin \theta$
Subsurface pressure	$p = -\rho g z + \rho g a \sin \theta$	$p = -\rho g z + \rho g a \frac{\cosh k(h+z)}{\cosh kh} \sin \theta$	$p = -\rho g z + \rho g a e^{kz} \sin \theta$
$a = \frac{H}{2} \quad \omega = \frac{2\pi}{T} \quad k = \frac{2\pi}{L} \quad \theta = \omega t - kx$			

Table 8-1 Summary of linear (Airy) wave theory - wave characteristics

8.2.2 Wave fields (irregular waves)

The previous section described the so-called regular wave. In a wave field generated by wind, there are many waves, with different periods, phases, wave heights and wave directions.

The water surface in a wave field is erratic and single waves cannot be distinguished. With a Fourier analysis, however, it is possible to describe this erratic surface as the sum of a large number of sinusoidal waves with different wave heights a , angular frequencies ω and phases α .

The movement of the water surface can be described as:

$$\eta(\vec{r}, t) = \sum_i \sum_j a_i \sin(\omega_i t - \vec{k}_{i,j} \cdot \vec{r} + \alpha_{i,j})$$

$$\text{in which: } \vec{k}_{i,j} = \begin{bmatrix} k_i \cos(\theta_j) \\ k_i \sin(\theta_j) \end{bmatrix}$$

$\theta_j =$ angle between the wave direction and the positive x-axis

If the consideration is limited to one point, the model becomes a one dimensional random-phase model:

$$\eta(t) = \sum_i a_i \sin(\omega_i t + \alpha_i)$$

The properties of a wave field are set in an energy spectrum. For the theoretical background and the formal definition of the energy spectrum, one is referred to the book used for the course on wind waves (*Waves in oceanic and coastal waters*, Holthuijsen, 2005).

Continuing with the one dimensional random-phase model, the energy spectrum is:

$$E_{\eta\eta}(f) \Delta f = \sum_{f_i=f}^{f+\Delta f} \frac{1}{2} a_i^2$$

A two-dimensional spectrum of frequency and direction is:

$$E_{\eta\eta}(f, \theta) \Delta f \Delta \theta = \sum_{f_i=f}^{f+\Delta f} \sum_{\theta_j=\theta}^{\theta+\Delta\theta} \frac{1}{2} a_{i,j}^2$$

A number of important characteristics of a wave field can be expressed in the moments of the spectrum. These moments are defined as:

$$m_n = \int_0^{\infty} f^n E_{\eta\eta}(f) df$$

One of the characteristics is the significant wave height. The significant wave height H_s is the average of the highest 1/3 of the waves. The relation between this wave height and the spectrum is:

$$H_s = 3,8 \sqrt{m_0}$$

The momentary wave height has a Rayleigh probability distribution. The exceedance probability of a given wave height within a given wave field is:

$$P(H > x) = \exp\left(-2\left(\frac{x}{H_s}\right)^2\right)$$

For the continuation of wave heights and exceedance probabilities, see the next chapter.

8.2.3 Wave periods

The mean wave period T_m is calculated as the average of all wave periods in a time-series representing a certain sea state at a specific location. The peak wave period T_p is defined as the wave period associated with the most energetic waves in the total wave spectrum at a specific location. Wave regimes that are dominated by wind waves tend to have smaller peak wave periods, and regimes that are dominated by swell have larger peak wave periods. The difference between peak and mean wave period is that only the most energetic component defines the T_p , but every single component contributes to the T_m .

The spectral wave period $T_{m-1,0}$ is commonly used as a characteristic period to describe the interaction between sea waves and coastal structures. This wave period is used for describing many processes like wave run-up, overtopping, reflection, and armour layer stability, especially when the structure has a shallow foreshore. The period can as well be used in situations characterized by a multi-modal wave spectrum.

The peak period is related to the significant wave height. For conceptual designs, it can be assumed that:

$$T_p \approx 5,3 \sqrt{H_{m0}} \quad (\text{DHI Shoreline Management Guidelines, 2017})$$

where: T_p [s] = peak wave period $\approx 1,11 T_{m-1,0}$
 H_{m0} [m] = significant wave height estimated from a wave spectrum $\approx H_s$

9. Water, waves, wave heights

updated: 2015; improved and expanded with vessel-generated waves in 2021

9.1 Wind-generated waves

9.1.1 Estimate of wave height and period if no measurements are available

The most important waves are waves generated by the wind. If a structure is to be dimensioned for a certain wave height, this wave height has to be known (measurements). If no measurements are available, the significant wave height and wave period can be estimated by using equations as proposed by Charles L. Bretschneider. These equations were later on improved by Young and Verhagen (1996) and Breugem and Holthuijsen (2006):

$$\tilde{H} = \tilde{H}_{\infty} \left\{ \tanh(0,343 \tilde{d}^{1,14}) \cdot \tanh \left(\frac{4,41 \cdot 10^{-4} \tilde{F}^{0,79}}{\tanh(0,343 \tilde{d}^{1,14})} \right) \right\}^{0,572}$$

$$\tilde{T} = \tilde{T}_{\infty} \left\{ \tanh(0,10 \tilde{d}^{2,01}) \cdot \tanh \left(\frac{2,77 \cdot 10^{-7} \tilde{F}^{1,45}}{\tanh(0,10 \tilde{d}^{2,01})} \right) \right\}^{0,187}$$

in which:

\tilde{H}	[-]	=	$\frac{g H_{m0}}{U_{10}^2}$	\tilde{T}	[-]	=	$\frac{g T_p}{U_{10}}$
\tilde{F}	[-]	=	$\frac{g F}{U_{10}^2}$	\tilde{d}	[-]	=	$\frac{g d}{U_{10}^2}$
F	[m]	=	fetch (<i>strijklengte</i>), the distance travelled by wind across open water				
d	[m]	=	average water depth over the fetch				
U_{10}	[m/s]	=	wind velocity at an altitude of 10 m				
T_p	[s]	=	peak wave period (see Section 8.2.2)				
\tilde{H}_{∞}	[-]	=	dimensionless wave height at deep water = 0,24				
\tilde{T}_{∞}	[-]	=	dimensionless wave period at deep water = 7,69				
H_{m0}	[m]	=	significant wave height, estimated from a wave spectrum ($H_{m0} \approx H_s$)				

An alternative for the improved Bretschneider formulas is provided by the nomograms of Groen and Dorrestein (Figure 9-1 and Figure 9-2). Figure 9-1 should be used for deep and transitional water ($d/L > 0,1$) and Figure 9-2 for shallow water ($d/L < 0,1$). One should use these nomograms cautiously: neither is dimensionless. Because Groen and Dorrestein used different data sets than Bretschneider, their findings are not identical.

For the water depth d it is recommended by the TAW to use one value, like the average depth of a lake or river, if suitable, or the water depth in a river-foreland (*uiterwaard*). The influence of local deep trenches is usually neglected.

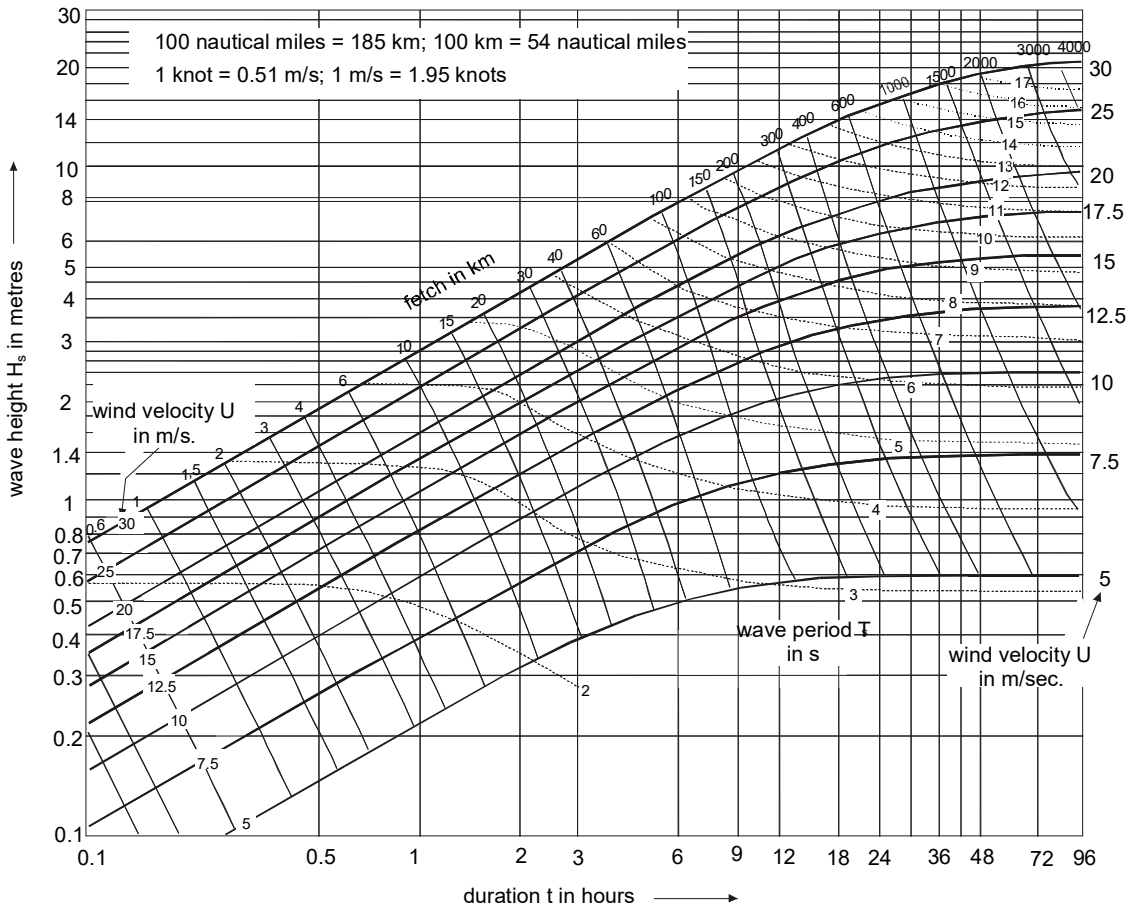


Figure 9-1 Nomogram, valid for deep and transitional water ($d/L > 0,1$) (Groen and Dorrestein, 1976)

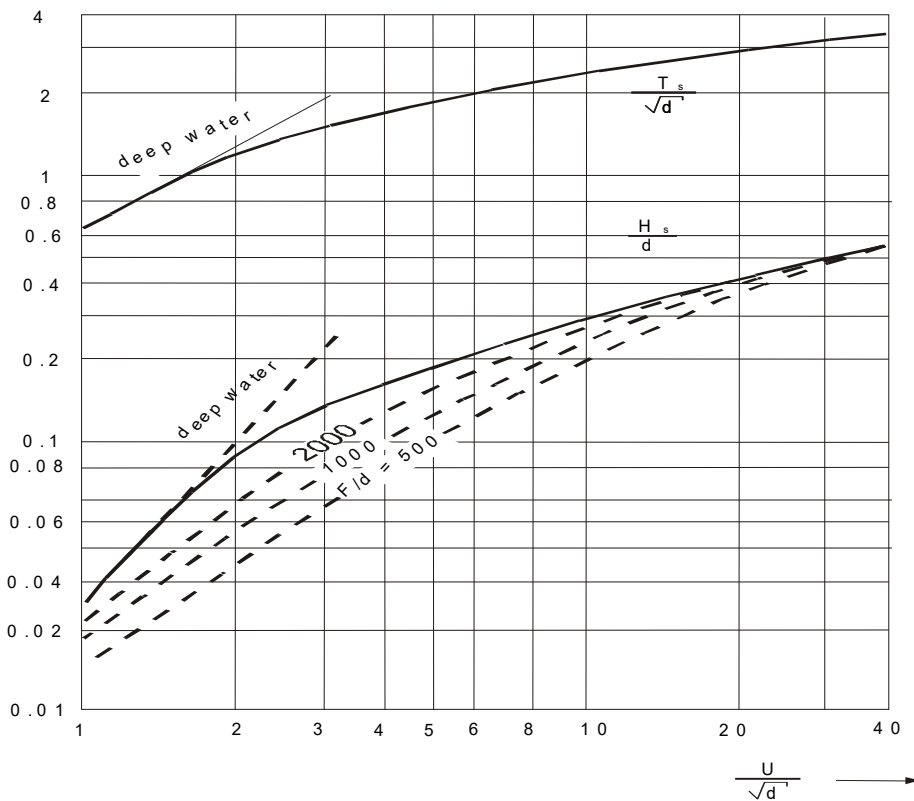


Figure 9-2 Nomogram, valid for shallow water ($d/L < 0,1$) (Groen and Dorrestein, 1976)

9.1.2 The effective fetch

The effective fetch in case of large (wide) waters

For the estimation of wave heights just in front of flood defences, it is recommended to use an effective fetch, which takes the shape of the water body into account. The effective fetch in a random situation is the weighted average of the projections $l(\alpha)$ on the wind direction of all fetches in all directions α (see Figure 9-3), according to:

$$F_e = \frac{\int_{-\alpha_m}^{\alpha_m} w(\alpha) \cdot l(\alpha) \cdot d\alpha}{\int_{-\alpha_m}^{\alpha_m} w(\alpha) \cdot d\alpha}$$

where: $w(\alpha)$ [-] = weight function. Recommended function is: $w(\alpha) = \cos(\alpha)$
 $l(\alpha)$ [m] = fetch in wind direction
 α [°] = deviation from the main wind direction in point of interest
 α_m [°] = boundary angle for wind directions that influence the effective fetch

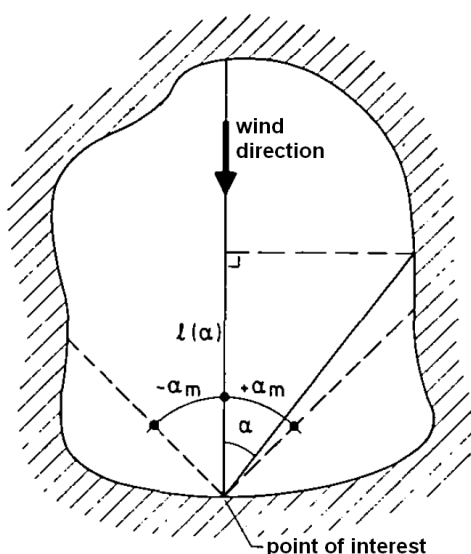


Figure 9-3 Definition sketch for determining the effective fetch (Holthuijsen, 1980)

The effective fetch in canals and other narrow waterways

Saville (1954) did a theoretical study of wind set-up for narrow fetches, based on the theory of Bretschneider. He made a considerable number of assumptions. Based on his findings and the resulting graph in the Shore Protection Manual 1974, Volume 1, Section 3.432, for conceptual designs, it can be assumed that, for canals and other narrow waterways with a width less than 10% of the length, the effective fetch should not be taken more than $3\frac{1}{3}$ to 5 times the width of the canal or waterway:

$$F_e < (3\frac{1}{3} \text{ to } 5) \cdot W_{canal} \quad \text{for } W_{canal} < 0,10 \cdot L_{canal}$$

9.1.3 The effective wind velocity in narrow waterways

If the wind direction is not coincident with the stream alignment, the effective wind velocity, u_e , can be approximated by the following relation (Carlson and Sayre, 1961):

$$u_e = u \cos(\alpha)$$

where α is the angle between the wind direction and the flow (Figure 9-4). The above relation is recommended for $\alpha < 45^\circ$.

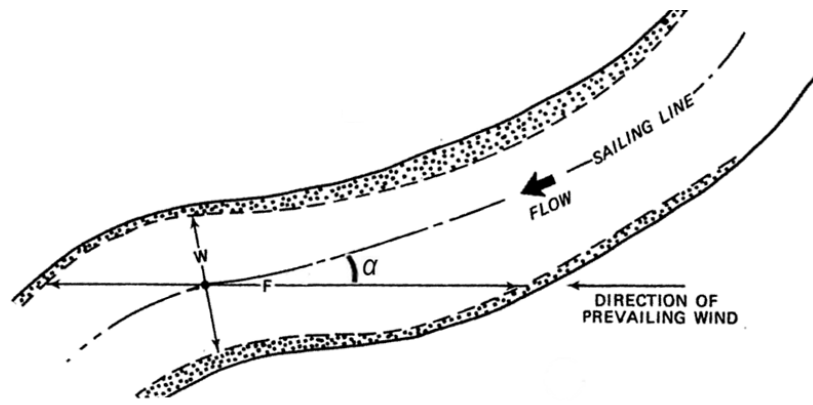


Figure 9-4 Fetch in a river bend (Bhowmik et al., 1982)

The effective wind velocity should also be corrected for stream velocity, as the wave generation depends on the wind velocity relative to the water surface. The effective wind velocity for streams can be modified similar to that of canals as suggested:

$$u_e = u \cos(\alpha) + v_{flow}$$

where v_{flow} is the flow velocity. v_{flow} is positive, if the wind is blowing in the general upstream direction, and is negative when the wind is blowing in the downstream direction. This correction should be applied, if α is less than 45° .

9.1.4 The design wave height

The significant wave height H_s is the average of the highest 1/3 of the waves. It is used to calculate wave overtopping, but for determination of the safety (integrity) of a structure, this significant wave is too low, because it is exceeded by many waves, which would lead to insufficient stability or strength. Therefore, the design wave height used for the calculation of the structural safety is higher than the significant wave height. If the effects of shallow water can be disregarded with a small wave height, a Rayleigh distribution can be assumed. The probability of exceedance of a given wave height within a given wave field is:

$$\Pr(H > x) = e^{-2\left(\frac{x}{H_s}\right)^2}$$

Therefore, the probability that the design wave height H_d is exceeded during a storm with N waves is:

$$\Pr(H > H_d) = 1 - e^{-N \cdot e^{-2(H_d/H_s)^2}}$$

The duration of a 'design storm' depends on local circumstances. For a storm on the Dutch North Sea coast, one can assume $T_{storm} = 35$ h, on the Wadden Sea, $T_{storm} = 45$ h, for Dutch lakes, $T_{storm} = 48$ h and for the lower rives (where there is influence from tides): $T_{storm} = 46$ h ('Handreiking voor het afleiden van ontwerpwaterstanden en golfcondities', 2015). However, the peak of a storm is much shorter, for instance 2 h along the coast and 4 h for rivers and the IJsselmeer. Assuming $T_{wave} = 3$ s, the number of waves N during the storm peak along the coast is:

$$N = \frac{T_{storm}}{T_{wave}} = \frac{2 \cdot 60 \cdot 60}{3} = 2400$$

If one allows an exceedance probability $P_r(H > H_d) = 0,01$, the design wave height H_d is:

$$H_d = \sqrt{\frac{1}{2} \ln\left(\frac{-\ln(1 - \Pr(H > H_d))}{N}\right)} \cdot H_s = \sqrt{\frac{1}{2} \ln\left(\frac{-\ln(1 - 0,01)}{2400}\right)} \cdot H_s = 2,5 \cdot H_s$$

To ascertain the design wave length one may assume that the shape of the energy spectrum essentially does not change for light and heavy storms, so $L_d \approx L_s$.

The wave can change shape if it reaches shallow water (refraction, shoaling and breaking) or obstacles (diffraction and reflection). This is treated in the next chapter.

9.2 Vessel-generated waves

(This section is largely based on Bhowmik et al., 1982)

9.2.1 Theory

The generation of waves by vessels

Vessels generate a disturbance in the flow field when moving on or near the free surface of a water body. The flow around the hull (*romp*) of the vessel accelerates due to changes both in magnitude and direction. The flow in front of the bow (*boeg*) decelerates until it reaches the stagnation point at the bow, where the velocity is zero because the vessel blocks the flow area. These accelerations and decelerations result in changes in pressure and thus in changes of the water level elevation. In areas with accelerated flow, the pressure and thus the water level elevation drops, and vice versa. Waves are generated at the bow, stern (*achterstevan*), and any points where there are abrupt changes in the vessel's hull geometry that cause disturbances in the flow field. As the vessel moves forward with respect to the water, the energy transferred from the vessel to the water is carried away laterally by a system of waves similar to that as shown in Figure 9-5 (Sorensen, 1973; Comstock, 1967).

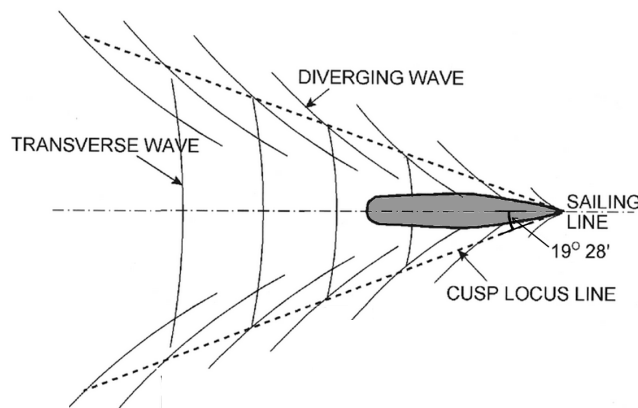


Figure 9-5 Wave pattern generated by a vessel in deep water, where the water depth has no influence of the flow field

In general, the system of vessel-generated waves consists of two sets of diverging waves and one set of transverse waves. The diverging waves move forward and out from the vessel, while the transverse waves move in the direction of the vessel. The transverse waves meet the diverging waves on both sides of the vessel along two sets of lines called the cusp lines, which form a 19°28' angle with the sailing line.

The waves that are generated both at the bow and stern of a vessel interact with each other at some distance from the vessel. If these waves are in phase, i.e., if the crest and trough of one set coincide with the other, they tend to reinforce each other, resulting in higher waves. If the waves are out of phase, they tend to cancel each other, resulting in relatively smaller waves. Whether the waves will reinforce or cancel each other depends on the length Froude number F_L , (Comstock, 1967; Sorensen, 1973):

$$F_L = \frac{V_{vessel}}{\sqrt{L_{vessel}}}$$

where V_{vessel} [m/s] = the vessel velocity
 L_{vessel} [m] = the vessel length

The wave heights in deep water generally increase with increasing velocity, except at certain velocities where the bow and stern waves tend to cancel each other out. The wave heights then decay with distance from the vessel as the total energy per wave is distributed over a larger area (Sorensen, 1973; Das, 1969; Bhowmik, 1976; Johnson, 1968; Das and Johnson, 1970).

In shallow water, the water particle motion generated by the waves will reach the bottom and the wave pattern will change significantly. The important parameter for shallow water waves is the depth Froude number:

$$F_d = \frac{V_{vessel}}{\sqrt{g \cdot d}}$$

where: V_{vessel} [m/s] = the vessel velocity
 g [m/s²] = gravitational acceleration
 d [m] = water depth

The waves will reach the bottom if $F_d >$ about 0,4. If F_d increases, with an increase in vessel velocity or a decrease in depth, the diverging waves rotate forward and finally make a right angle with the sailing line for $F_d = 1$. Therefore, at $F_d = 1$, both the diverging and transverse waves form a single wave, which travels with the same speed as the vessel. The limiting vessel velocity, determined at critical F_d , is given by $\sqrt{(g \cdot d)}$ (Sorensen, 1973).

Effects due to channel constriction

The depth restriction in shallow, narrow waters causes complex flow conditions and wave patterns. If the channel is so narrow that it affects the flow pattern around a vessel, the generated waves will be relatively higher than those generated in unrestricted waters by the same vessel moving at the same velocity. This is because of a significant reduction in the flow area and the associated higher accelerations of flow around the vessel. Higher acceleration results in lower pressures generating higher waves. If in addition to being narrow the channel is shallow, the combined effect will result in more complex flow conditions and much higher wave heights (Sorensen, 1973).

There has been very limited research in the area of waves generated by river traffic on restricted waterways. Most of the investigations concerned waves generated by vessels traveling in deep and unrestricted waters. The few investigations dealing with waves in restricted waterways were done mostly in Europe in relation to ship canal design, where wave heights were estimated in the vicinity of vessels.

Another effect of sailing vessels in a narrow water body is the drawdown of the water level (*spiegeldaling*) and the related squat of the vessel (*daling van het schip*). Schijf (1949) developed a method to calculate the squat, which was improved by empirical research later on, but this is outside the scope of this chapter.

9.2.2 Design

If no other source of information is available, the following rules of thumb can be considered for conceptual designs:

$H_s \approx 0,5$ m for inland waterways

$H_s \approx 1,0$ m for sea-going vessels (estuaries, Nieuwe Waterweg, etc.)

Based on laboratory and field observations, several researchers developed empirical equations for predicting wave heights based on channel and vessel parameters. Balanin and Bykov (1965) used the vessel velocity and a modified blockage factor as the primary variables to develop the following equation (transferred to SI units) for estimating the wave height in the vicinity of a vessel:

$$H = 8,2 \frac{v_{vessel}^2}{2g} \cdot \left[1 - \left(1 - \frac{1}{\left(4,2 + \frac{A_c}{A_m} \right)^{0,5}} \right) \cdot \left(\frac{\frac{A_c}{A_m} - 1}{\frac{A_c}{A_m}} \right)^2 \right]$$

where H [m] = wave height generated by a vessel
 v_{vessel} [m/s] = vessel velocity
 g [m/s²] = gravitational acceleration
 A_c [m²] = the cross-sectional area of the channel
 A_m [m²] = the submerged cross-sectional area of the vessel: $A_m \approx b \cdot D$
 b [m] = width of the vessel
 D [m] = draft of the vessel

Another equation for estimating maximum wave height, including the effect of the length of the vessel, was given by Hochstein (U.S. Army Corps of Engineers, 1980) as follows (also transferred to SI units):

$$H_{max} = 0,1470 \cdot v_{vessel}^2 \left(\frac{D}{L_{vessel}} \right)^{0,5} \cdot \left(1 - \frac{A_m}{A_c} \right)^{-2,5}$$

where H_{max} [m] = maximum wave height generated by a vessel
 L_{vessel} [m] = length of the vessel
 (other symbols as above)

9.3 Literature

- Bhowmik, N.G., Demissie, M., G. Chwen-Yuan Guo (1982). Waves generated by river traffic and wind on the Illinois and Mississippi rivers. Research report 167 (ISWS CR-293). Illinois State Water Survey.
- Bretschneider, C.I. (1958) *Revisions in wave forecasting: deep and shallow water*. Proceedings of the 6th Conference on Coastal Engineering, pp. 30-67
- Carlson, E.J., and W.W. Sayre (1961). *Canal bank erosion due to wind generated water waves*. U.S. Bureau of Reclamation Hydraulic Laboratory Report No. Hyd-465, Progress Report 1.
- Comstock, J. P., editor. (1967). *Principles of naval architecture*. Society of Naval Architects and Marine Engineers, New York, New York.
- Groen, P. and R. Dorrestein (1976) *Zeegolven. Opstellen op oceanografisch en maritiem meteorologisch gebied nr. 11*. Derde herziene druk. KNMI. Staatsdrukkerij- en uitgeverijbedrijf 's-Gravenhage
- Holthuijsen, L.H. (1980) *Methoden voor golfvoorspelling*. TAW.
- Holthuijsen, L.H. (2008) *Waves in oceanic and coastal waters*. Cambridge University Press, ISBN 978-0-521-86028-4
- Sorensen, R. M. (1973). *Ship generated waves*. Advances in Hydroscience, vol. 9, editor V.T. Chow, Academic press, New York and London.
- Young, I.R. and L.A. Verhagen (1996) *The growth of fetch-limited waves in water of finite depth. Part 1: Total energy and peak frequency*. Coastal Engineering 29, pp. 47-78

10. Water, waves, shallows + breaking

When waves approach the coast, a number of changes occur, caused by the change of water depth. Due to the smaller depth, the wave velocity decreases and the wave front turns so it runs increasingly parallel to the depth contours (refraction). As a result, the wave crests become narrower, the wave becomes more concentrated and the wave height increases. At the same time, the wave velocity decreases, thereby reducing the wavelength, causing a further increase of the wave height (shoaling). So, the wave height increases and the wave length reduces. At a certain point, the waves are so steep that they break. This section considers these three phenomena:

1. Refraction
2. Shoaling
3. Breaking of waves

Besides that, the effect of an obstacle is also discussed. The two most well-known consequences are:

1. Diffraction
2. Reflection

Unless stated otherwise, regular waves are assumed in this chapter.

10.1 Shallows: refraction

If a wave approaches a sloping coastline at an angle, the propagation velocity will vary along the wave crest due to the difference in water depth along the wave crest. After all:

$$c = \sqrt{\frac{g}{k} \tanh(kd)} = c_0 \cdot \tanh(kd)$$

In shallow water the propagation velocity is smaller. Therefore, with decreasing depth, the wavelength shortens. The wave front decelerates in the first part to reach shallow water. The wave front will thus turn. This causes a bend of the propagation velocity towards the coast. This phenomenon is known as refraction.

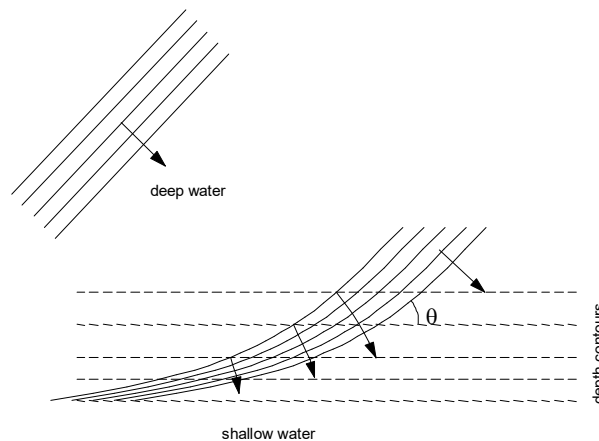


Figure 10-1 Refraction

In the case of a coast with straight parallel depth contours, the angle between the wave crest and a depth contour line can be derived directly from the local depth and the angle between the wave crests and a parallel contour line in deep water (Figure 10-1). This relation is called Snell's law and reads as follows:

$$\frac{\sin(\theta_1)}{\sin(\theta_0)} = \frac{c_1}{c_0} = \frac{c_0 \tanh(k_1 d_1)}{c_0} = \tanh(k_1 d_1) = \frac{L_1}{L_0}$$

in which: θ_0 = the angle between the wave crest and the depth contour line in deep sea

θ_1 = the angle between the wave crest and the depth contour line in shallow water

From shallow to deep

If one knows the angle of the wave ray, the wave height and wavelength in shallow water, one can calculate the wave ray angle in deep water using the above equation or the dotted line in Figure 10-2.

From deep to shallow

If the angle of the wave ray, the wave height and the wavelength in deep water are known, the angle of the wave ray in shallow water cannot be calculated using the equation above. The equation requires the wavelength in shallow water, for which the following applies:

$$L_1 = L_0 \tanh(k_1 d_1) \quad \text{met:} \quad k_1 = \frac{2\pi}{L_1}$$

So $\frac{\sin(\theta_1)}{\sin(\theta_0)}$ as a function of d/L_0 is an implicit function, which has to be solved iteratively. The inverse solution is given as a solid line in the graph below, plotted against the relative water depth d/L_0 (water depth d in shallow water, divided by the wavelength L_0 in deep water).

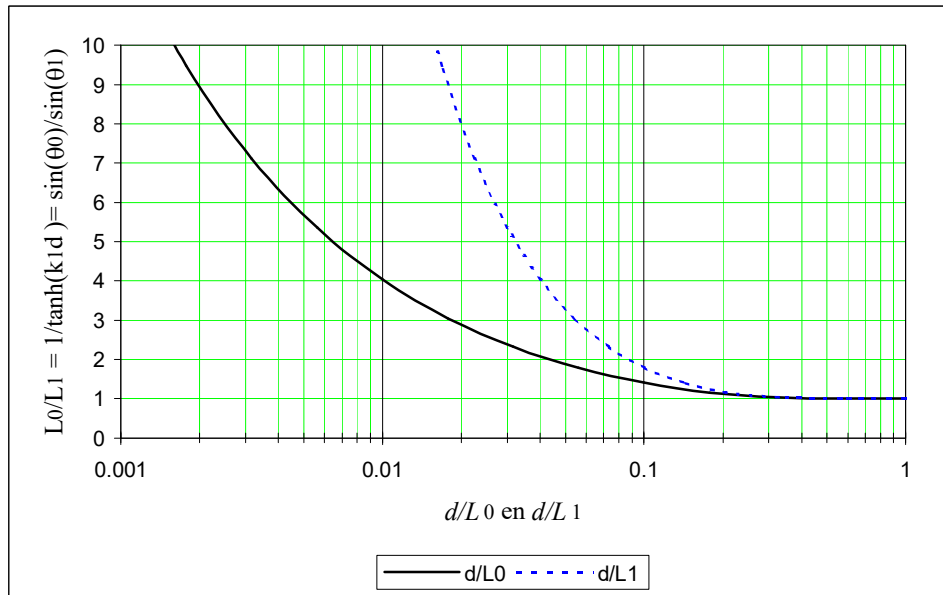


Figure 10-2 Relation between depth and wavelength (d = depth, L_1 = wavelength at considered depth, L_0 = wavelength in deep water)

Depending on the concentration or spread of wave rays, the wave height will increase or decrease. Generally, for the wave height in shallow water:

$$H = K_s K_r H_0$$

in which: K_r [-] = the refraction coefficient
 K_s [-] = the shoaling coefficient (see next section)

In the case of straight parallel depth contours, the wave height decreases with a factor:

$$K_r = \sqrt{\frac{b_0}{b_1}} = \sqrt{\frac{\cos(\theta_0)}{\cos(\theta_1)}}$$

with: b = the wave crest width

This is because the wave crest width b continues to increase while the wave crest turns, which causes a reduction of the energy density and thus also of the wave height. The change of wavelength in shallow water also leads to a change of the energy density and the wave height, but that phenomenon is called shoaling and is covered in the next section.

Refraction also occurs when a wave enters an area with a current (along the coast). In this case, the wave will turn more or less in the direction of the current.

10.2 Shallows: shoaling (non-breaking waves)

When the water depth decreases, the propagation velocity and the wavelength are reduced with a constant period. This influences the wave height.

10.2.1 Theory

Section 8.2 showed that the wave energy per unit of surface area equals:

$$E = \frac{1}{8} \rho g H^2$$

The group velocity is:

$$c_g = n c \quad \text{with} \quad n = \frac{1}{2} + \frac{kd}{\sinh(2kd)} \quad \text{and} \quad c = \sqrt{\frac{g}{k} \tanh(kd)} = c_0 \cdot \tanh(kd)$$

The energy flux is the amount of energy that passes a certain point per unit of width. This energy flux equals:

$$F = E \cdot c_g = \text{constant}$$

and is constant for non-breaking waves (no loss of energy) and straight approaching waves (no change of width).

The wave height is therefore:

$$H^2 = \frac{\text{constant}}{n \cdot c}$$

The wave height in a shallow area, H_1 , is therefore dependent on the wave height in deep water, H_0 , according to:

$$\frac{H_1}{H_0} = K_s = \sqrt{\frac{c_{g,0}}{c_{g,1}}} = \sqrt{\frac{c_0 n_0}{c_1 n_1}} = \sqrt{\frac{\frac{1}{2}}{\tanh(kd) n_1}} = \sqrt{\frac{1}{\tanh(kd) \left(1 + \frac{2kd}{\sinh(2kd)}\right)}}$$

The shoaling coefficient is therefore a function of the wave number k and the water depth d :

$$K_s = \frac{1}{\sqrt{\tanh(kd) \left(1 + \frac{2kd}{\sinh(2kd)}\right)}} \quad \text{with:} \quad kd = 2\pi \frac{d}{L}$$

This solution is represented by the dotted line in the figure below. If the wave height and wavelength are known in a certain shallow area, these can be used to calculate the wave height in deep water. The inverse, using this solution and a known wave height and a known wave length in deep water to calculate the wave height in shallow water is not possible. The problem is that L and thus also k are dependent on the depth d and on themselves, for:

$$L = L_0 \tanh(kd) = L_0 \tanh\left(\frac{2\pi d}{L}\right)$$

This is an implicit function. The shoaling coefficient, a function of the water depth d and wavelength in deep water L_0 , can therefore only be solved iteratively. This solution is represented by the solid line in Figure 10-3.

Besides shoaling, refraction also influences the wave height, for this see the previous section.

10.2.2 (Preliminary) design

The wave height H_1 of regular (non-breaking) waves in shallow water depends on the wave height in deep water H_0 , the refraction coefficient K_r , and on the shoaling coefficient K_s , according to:

$$H_1 = K_r K_s H_0$$

In Figure 10-4 the shoaling coefficient is given as a function of the relative water depth (water depth d in shallow water, divided by the wavelength L_0 in deep water).

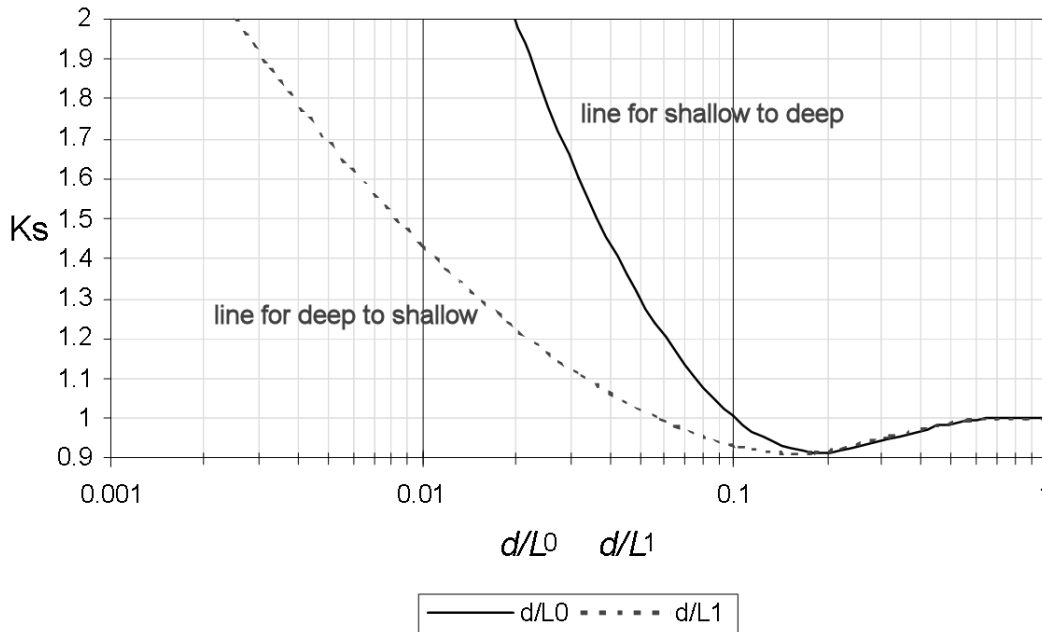


Figure 10-3 Relation between K_s and d/L (L = wavelength at considered depth, L_o = wavelength at deep sea)

For the refraction parameter, the following equation has been found:

$$K_r = \sqrt{\frac{\cos(\theta_o)}{\cos(\theta_1)}}$$

To calculate the refraction ($\theta_o \Rightarrow \theta_1$), see previous section.

The theory given above only applies for regular waves that don't break (or haven't yet broken).

10.3 Shallows: breaking waves

Distinction should be made between individual waves (for the calculation of loads on structures) and significant waves (for the calculation of run-up, overtopping, stability of stones).

Individual waves

Due to the decreasing wavelength and the increasing wave height in shallow areas, the steepness of the wave increases. Waves will theoretically break if they become too steep, or if the water depth becomes too small with respect to the wave height. Regular waves will generally break, if:

- $H \geq \frac{1}{7} \cdot L$

or:

- $H \geq 0,78 \cdot d$

where: H [m] = height of an individual regular wave
 L [m] = length of an individual regular wave
 d [m] = water depth (relative to still water)

There are also more complex formulas for the shallowness criterion, e.g. by Miche. In spite of the theoretically deduced criterion, individual non-breaking waves with a ratio of $H = 1,2 \cdot d$ have been observed under very specific circumstances.

Significant waves

When calculating breaking for a wave spectrum, the significant wave height H_s should be used. This is the average height of the 1/3 highest waves. For gentle bed slopes ($\leq 1/100$), it is often assumed that breaking occurs if:

- $\frac{H_s}{d} \geq 0,4$ to 0,5

The way in which a wave breaks on a smooth slope with a constant slope angle depends on the steepness of the wave and the slope of the bed. This is characterised with the breaker parameter, or Iribarren number, as proposed by Battjes (1974):

$$\xi = \frac{\tan \alpha}{\sqrt{H_s/L_0}}$$

in which: α [°] = angle of the slope
 H_s [m] = significant wave height
 L_0 [m] = wavelength in deep water

Depending on the value of the breaker parameter, different types of breaking occur, as is shown in Figure 10-4.

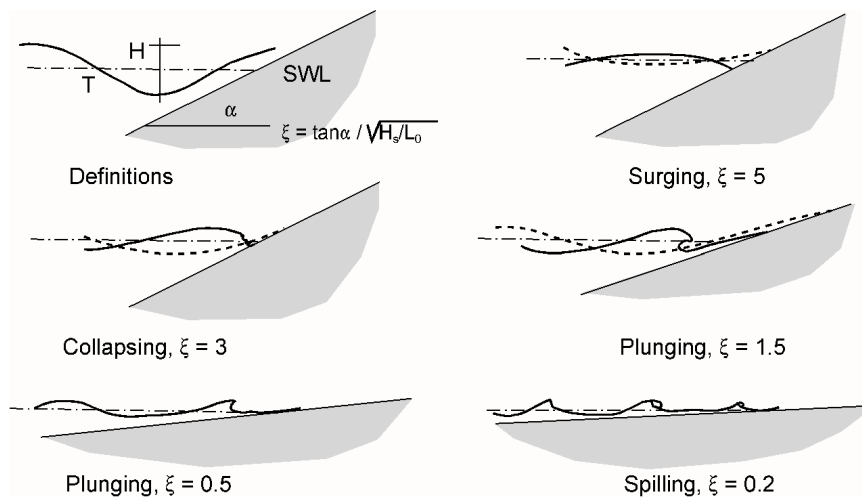


Figure 10-4 Types of breaking

Notes

- The depth profile need not be constant in time. Shallows can appear or disappear. It is therefore important to find out if the bed consists of rock or sand.
- The depth can depend on the tide and on the wind set-up (storm surge).
- Changes of depth also mean changes of refraction, shoaling and breaking.

The validity of wave theories is depicted in Figure 10-5.

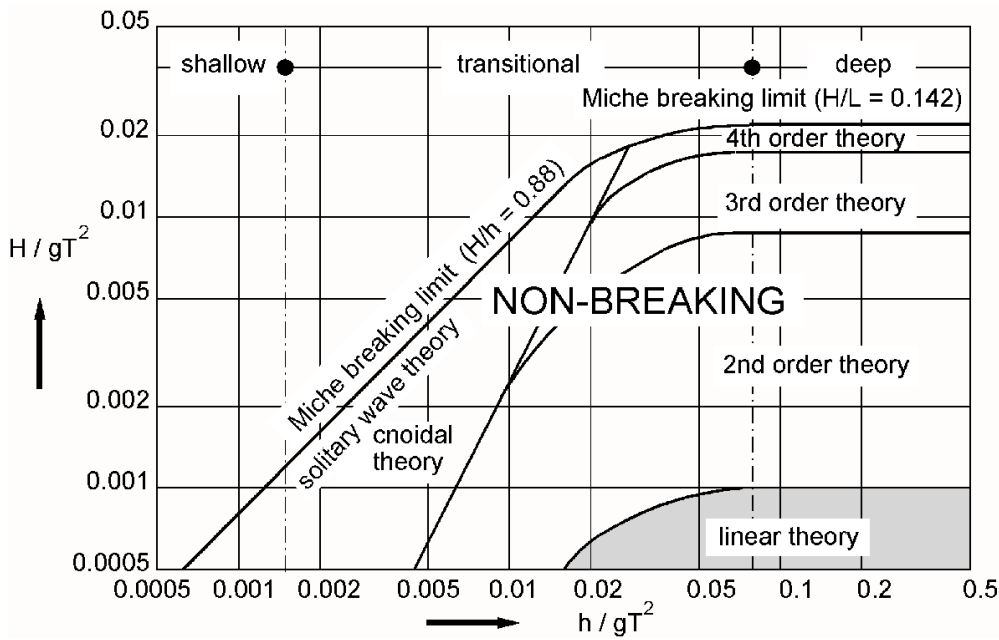


Figure 10-5 Validity of wave theories (Le Méhauté, 1976; Introduction to bed, bank and shore line protection, CIE4310)

10.4 Obstacle: reflection

If waves run into a structure they can break or reflect. The reflection can be partial or complete. Characteristics of completely reflected waves are:

- the energy of the reflected wave equals the energy of the incoming wave
- the period of the reflected wave equals the period of the incoming wave
- the reflected wave is in phase with the incoming wave.

The consequence of the above is that a standing wave with (in case of complete reflection) a wave height twice the size of an incoming wave is created in front of the structure. If the reflection is partial, the wave height of the standing wave will be less. In general, the following applies:

$$H = (1 + \chi) \cdot H_i$$

- in which: H [m] = the wave height of the standing wave
 H_i [m] = the wave height of the incoming wave
 χ [-] = the reflection coefficient ≤ 1

The value of χ depends on the permeability, roughness and slope of the structure and on the steepness of the incoming waves and the water depth in front of the structure.

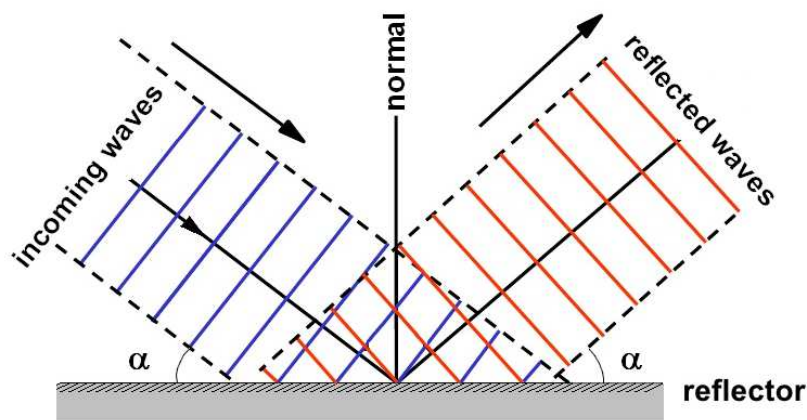


Figure 10-6 Reflection

The load on the wall can be calculated according to Chapter 12 of this Manual.

10.5 Obstacle: diffraction

If there's an obstacle in the course of a wave (e.g. a breakwater or an island), wave motion still occurs in the shadow zone behind the obstacle. The transfer of energy apparently not only takes place in the wave direction. The wave crests bend round the object shaped like circular arcs. This phenomenon is called diffraction.

The wave height changes due to diffraction, whereby the wave height on the lee side of the object is smaller than that of the incoming wave, whilst the wave height next to the object is often larger than that of the incoming wave.

Generally:

$$H = K_d H_o$$

where: K_d [-] = diffraction coefficient

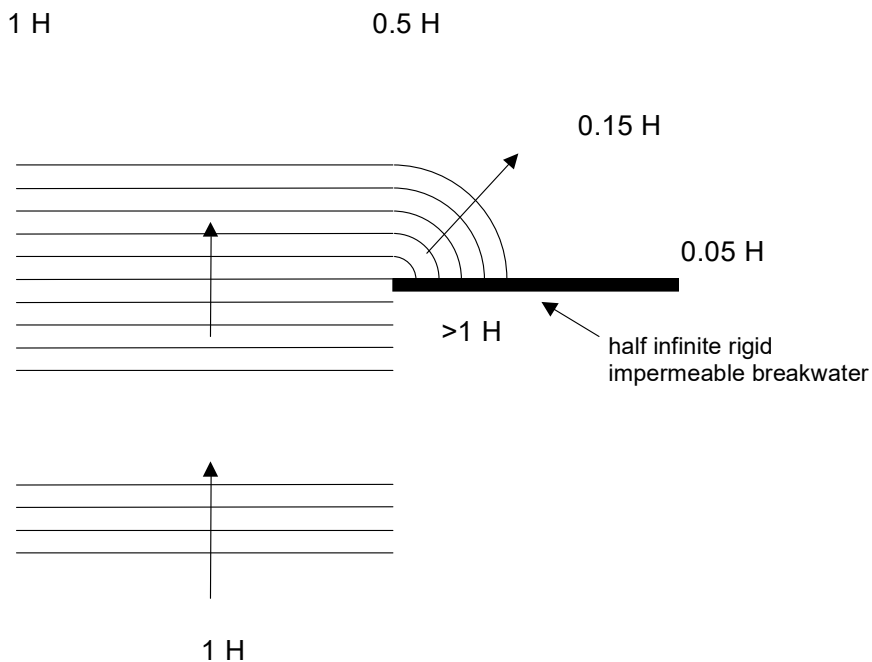


Figure 10-7 Diffraction

The "Shore Protection Manual" (CERC 1984) gives a large number of diagrams for the estimation of K_d with different wave directions. The Shore Protection Manual can be found on the internet on www.google.com with search request 'coastal engineering manual'. Figure 10-8 is taken from the book 'Oceanographical Engineering' by Robert Wiegel (1964). It shows the diagram for waves moving straight towards a breakwater. The distances in x- and z-direction are divided by the wavelength L .

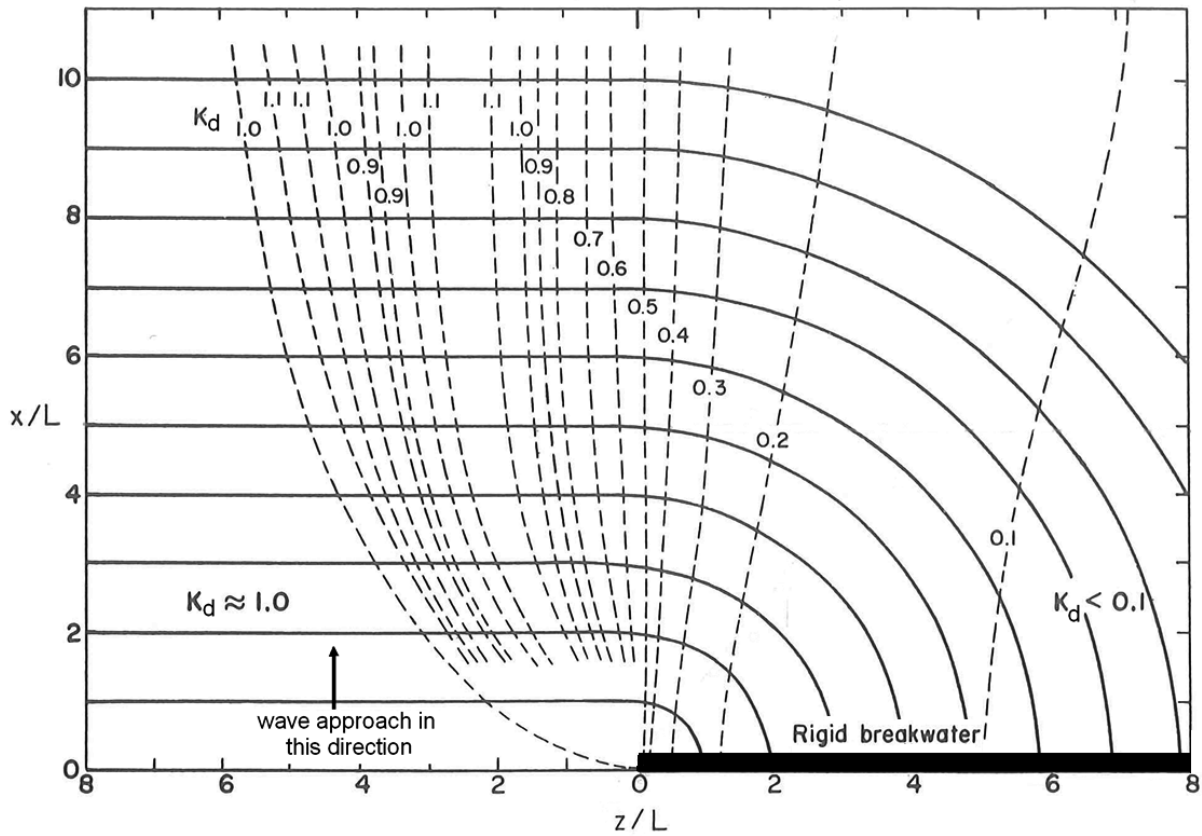


Figure 10-8 Diffraction coefficients for straight incoming waves (Wiegel, 1964)

For waves approaching from other directions relative to the breakwater, reference is made to literature, like *Diffraction of periodic sea waves along a vertical breakwater* by Penny and Price (1952).

11. Water, waves, run-up + overtopping

References to the European Overtopping Manual 2007 removed in February 2022

For the design of slanting structures (a slope or a wall) it is important to know how far a wave can run up the slope, or how much water can go over the structure. In the first place, this depends on the average water level (= highest astronomical tide + storm set-up, or the highest river level during a peak discharge) and in the second place on the height of the waves attacking the structure.

This chapter covers the following two phenomena:

1. Wave run-up (*golfofloop*)
2. Wave overtopping (*golfoverslag*)

These phenomena play a role in determining the crest height of flood defences and the top of structure level of other hydraulic structures, see Chapter 42. The 2%-run-up calculation for the determination of dike heights was used in the Netherlands and Germany until the end of the twentieth century, but has been replaced by the more universal calculation of critical overtopping discharges⁵.

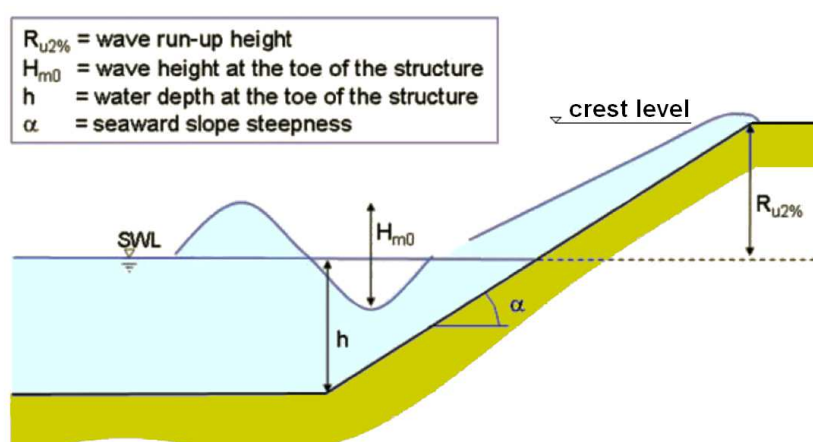


Figure 11-1 Principle sketch for the 2% run-up height

11.1 Wave run-up

The wave run-up R is the difference between the average water level and the highest point on a slope that is reached by water running up the slope. This applies to both breaking and non-breaking waves.

The wave run-up depends on:

- The wave field
- The geometry of the flood defence
- The roughness of the slope surface

As a rule of thumb, the following 'old Delft formula' could be used to calculate the run-up height (sometimes called the 'crest freeboard') related to an acceptable amount of run-up on dikes:

$$R_{2\%} = 8 \cdot H_s \cdot \tan(\alpha)$$

where:

$R_{2\%}$	[m]	= the value of run-up exceeded by 2% of the waves
H_s	[m]	= the significant wave height
α	[°]	= the angle of the outer dike slope with the horizontal

This 'old Delft formula' is valid for the Dutch coast under storm conditions and:

- relatively gentle slopes (1:3)
- "normal" wave steepness (between 4 and 5%)

⁵ The 2% run-up requirement was introduced for the design of the 32 km long Afsluitdijk. It was assumed that the inner slope of a dike would fail after 40 to 60 overtopping waves, which equals about 2% of the waves in a 'typical' Dutch storm), but since 1999 this has been replaced with an overtopping criterion (TAW- Leidraad Zee- en Meerdijken, 1999).

With help of several extra parameters, the old Delft formula becomes more sophisticated:

$$R_{2\%} = 8 \cdot H_s \cdot \tan(\alpha) \cdot \gamma_f \cdot \gamma_b \cdot \gamma_\beta$$

where:

γ_f [-] = factor taking the slope roughness into account

γ_b [-] = berm influence factor

γ_β [-] = influence factor for oblique wave attack

See below for an explanation of these factors.

I.A. Hunt found out that the factor of '8' in the old Delft formula actually is related to the wave steepness, which can be represented by the breaker parameter (Iribarren parameter) ξ (see section 10.3):

$$R_u = f(\xi) \cdot H_s,$$

or to be more precise:

$$R_{u2\%} = 1,5 \cdot \gamma_f \cdot \gamma_b \cdot \gamma_\beta \cdot H_s \cdot \xi_p$$

where the maximum of $R_{u2\% \max} = 3 \cdot H_s$

J.W. van der Meer fine-tuned Hunt's equation. For design and assessment calculations, using a partial safety factor of one standard deviation, it reads:

$$R_{2\%} = 1,75 \cdot \gamma_b \cdot \gamma_f \cdot \gamma_\beta \cdot \xi_{m-1,0} \cdot H_{m0} \quad \text{with a maximum of: } R_{2\%, \max} = 1,07 \cdot \gamma_f \cdot \gamma_\beta \cdot \left(4,0 - \frac{1,5}{\sqrt{\gamma_b \cdot \xi_{m-1,0}}} \right) \cdot H_{m0}$$

where the breaker parameter (Iribarren parameter) is defined by:

$$\xi_{m-1,0} = \frac{\tan \alpha}{\sqrt{H_{m0} / L_0}} = \frac{\tan \alpha}{\sqrt{H_s / (1,56 \cdot T_{m-1,0}^2)}}$$

H_{m0} = estimate of the significant wave height from spectral analysis = $4\sqrt{m_0}$. $H_{m0} \approx H_s$ (Holthuijsen, 2007)

$T_{m-1,0}$ is a calculated wave period that follows from the wave spectrum. In about 80% of the cases,

$$T_{m-1,0} \approx 0,9 \cdot T_p$$

The Van der Meer equation has been adopted by the CUR-TAW-guidelines and the European Overtopping Manuals of 2007 and 2018. The equation is not very reliable for an overall influence factor $\gamma_b \cdot \gamma_f \cdot \gamma_\beta$ lower than 0,4.

Roughness (factor γ_f)

The reduction factor γ_f that takes the roughness and the permeability of the surface of the outer slope into account is:

- 1,00 for asphalt, concrete with a smooth surface
- 0,95 for concrete blocks, block mats
- 0,70 for gravel, gabions
- 0,60 for quarry stone (rip-rap)
- 0,50 for cubes (random positioning)
- < 0,50 for X-blocs, tetrapods, dolosses (see European Overtopping Manual for more data)

Berm influence (factor γ_b)

A berm reduces the wave run-up and its influence can be taken into account by using a berm influence factor γ_b (also known as the *shoulder reduction factor*). The magnitude of the berm influence factor depends on the length of the berm B_b and the water depth above the berm h_B .

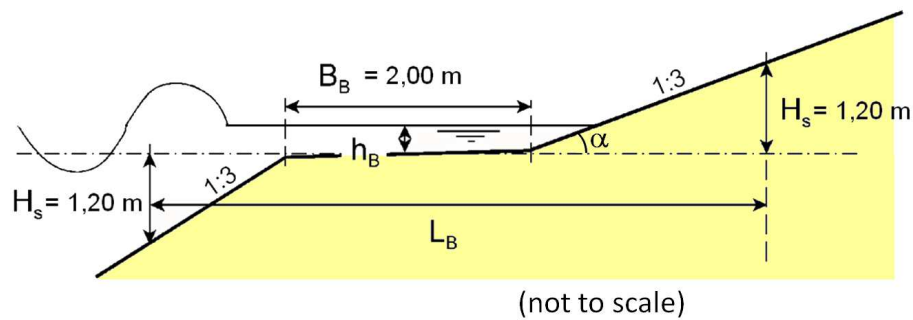


Figure 11-2 Definitions berm reduction

At both sides of the berm, the slope is intersected at a vertical distance H_s from the horizontal centre plane of the berm, giving a length L_B . h_B is the distance between SWL and the berm level (can be negative or positive). γ_b finally becomes:

$$\gamma_b = 1 - \frac{B_B}{L_B} \left[0,5 + 0,5 \cos \left(\pi \frac{h_B}{x} \right) \right]$$

where:

B_B	[m]	=	berm width
L_B	[m]	=	influence length of the berm
h_B	[m]	=	water depth above the berm
x	[m]	=	influence height of the berm:
			$x = R_{2\%}$ if the berm is above SWL
			$x = 2H_s$ if the berm is at or below SWL

With limits: $0,6 \leq \gamma_b \leq 1$. The equation above shows that a berm at storm surge level is most efficient. In that case, the optimal width of the berm is $B_B \approx 0,4 L_B$, (see Figure 11-2 for an explanation of L_B) and the maximum berm width is 25% of the wave length: $B_B < 0,25 L_{wave}$. The slope of the berm is 1:15 at steepest, otherwise it should be considered as a slope rather than a berm. For more information, see TAW Technisch Rapport Golfoploop en Golfoverslag bij Dijken (2002).

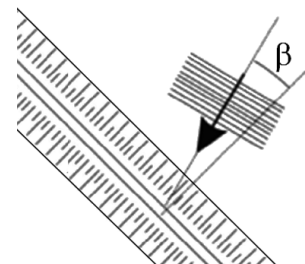
If there is no berm, no berm influence factor should be used in overtopping or run-up calculations.

Angle of incidence (factor γ_β)

For oblique waves the angle of wave attack is defined as the angle between the direction of propagation of waves and the axis perpendicular to the structure (for perpendicular wave attack: $\beta = 0^\circ$). For short-crested waves:

$$\begin{aligned} \gamma_\beta &= 1 - 0,0022 \beta \text{ for } : 0^\circ \leq \beta \leq 80^\circ \\ \gamma_\beta &= 0,824 \text{ for } \beta > 80^\circ \end{aligned}$$

So, at an angle of 80° (fetch waves) the reduction is only 18%, compared to perpendicular wave attack.



Foreshore reduction

On very shallow foreshores waves will break; the wave spectrum transforms and is flattened, and the waves are no longer Rayleigh-distributed. According to TAW (2002) one should use for the calculation of ξ not the T_{m0} , but the $T_{m-1,0}$, which is m_1/m_0 (the first negative moment of the spectrum divided by the zero-order moment of the spectrum). In case no detailed spectrum information is available, one may use $T_{m-1,0} \approx 0,9 T_p$. For the wave height on the shallow foreshore one should use the H_{m0} on the foreshore.

11.2 Wave overtopping

Overtopping waves can jeopardise a civil engineering work if they cause erosion or softening of the foundations. Wave overtopping can also cause a nuisance for the surroundings. To prevent severe wave overtopping, the design of the structure should therefore include a sufficient freeboard above the design water level.

For wave overtopping considerations, the wave run-up R_n simply exceeds the crest height z . The wave overtopping is usually characterised by an overtopping discharge q per metre of the water defence, averaged over time. This discharge depends on the wave height, the wave steepness, the slope and the existing freeboard. This concerns overtopping discharges averaged over time. In reality, a far larger discharge can occur for a short time, depending on the percentage of overtopping waves. With the results of several investigations, a global relationship between all of these factors can be derived.

11.2.1 Allowable overtopping discharges

In August 2007, the EurOtop team released the "Wave Overtopping of Sea Defences and Related Structures: Assessment Manual", in short: "European Overtopping Manual" (EurOtop team 2007). That manual gives "guidance on analysis and/or prediction of wave overtopping for flood defences attacked by wave action." It replaces the older Dutch "Technical Report Wave Run-up and Wave Overtopping at Dikes" of TAW, Technical Advisory Committee on Flood Defences, author: J.W. van der Meer, and two other (foreign) reports.

In general, three types of overtopping requirements can be distinguished, of which the strictest (lowest allowable overtopping discharge) should be considered governing for the design:

1. Storage capacity of the area behind the structure

Next to these ULS and SLS requirements, the storage capacity of the water system behind the defence could restrict the allowable overtopping volume. This could become critical if the water system behind the structure won't be able to handle the overtopping quantities and causes flooding of the area. In case of overtopping of lock gates (*sluisdeuren*), it should be considered how much overtopping can be allowed in the lock chamber (*sluiskolk*). Along the coast, sea water will overtop into a fresh water basin or lake, causing salt intrusion. No generic quantities can be given for the storage capacity of areas behind water-retaining structures, because the characteristics of these areas vary too much.

2. Ultimate limit state (ULS), regarding the structure itself

The European Overtopping Manual 2007 gives maximum allowable overtopping discharges, to be used for the design of hydraulic structures where waves could overtop. ULS requirements concern the structural integrity (structural safety) of the hydraulic structure itself. Maximum overtopping discharges and volumes are given in Table 11-1. The requirements in the European Overtopping Manual 2018 differ a bit from the old version and are made dependant on the significant wave height.

Hazard type and reason	mean discharge q (l/s/m)
Embankment seawalls / sea dikes	
No damage if crest and rear slope are well protected	50-200
No damage to crest and rear face of grass covered embankment of clay	1-10
No damage to crest and rear face of embankment if not protected	0,1
Promenade or revetment seawalls	
Damage to paved or armoured promenade behind seawall	200
Damage to grassed or lightly protected promenade or reclamation cover	50

Table 11-1 ULS requirements for overtopping (European Overtopping Manual 2007)

3. Serviceability limit state (SLS), regarding use of the structure

The European Overtopping Manual 2007 gives maximum allowable overtopping discharges, related to the direct impact on pedestrians, vehicles and property behind the defence, see Table 11-2. The requirements in the European Overtopping Manual 2018 differ a bit from the old version and are made dependant on the significant wave height.

Hazard type and reason	mean discharge q (ℓ/s/m)	max. volume V_{max} (ℓ/m)
For pedestrians		
Trained staff, well shod and protected, expecting to get wet; overtopping flows at lower levels only, no falling jet, low danger of fall from walkway	1 - 10	500 at low level
Aware pedestrian, clear view of the sea, not easily upset or frightened, able to tolerate getting wet, wider walkway	0,1	20 - 50 at high level or velocity
For vehicles		
Driving at low speed, overtopping by pulsating flows at low flow depths, no falling jets, vehicle not immersed	10 - 50	100 - 1000
Driving at moderate or high speed, impulsive overtopping giving falling or high velocity jets	0,01 - 0,05	5 - 50 at high level or velocity
For property behind the defence		
significant damage or sinking of larger yachts	50	5000 - 50 000
sinking small boats set 5 - 10 m from wall; damage to larger yachts	10	1000 - 10 000
Building structure elements	1	-
Damage to equipment set back 5 - 10 m	0,4	-

Table 11-2 SLS requirements for overtopping (European Overtopping Manual 2007)

11.2.2 Overtopping of structures with a slope

The principal equation used for wave overtopping, given in the European Overtopping Manual 2018, is:

$$\frac{q}{\sqrt{g \cdot H_{m0}^3}} = a \cdot e^{-\left(\frac{b R_c}{H_{m0}}\right)^{1,3}}$$

where:

$$\begin{aligned} \frac{q}{\sqrt{g \cdot H_{m0}^3}} \quad [-] &= \text{dimensionless overtopping discharge} \\ q \quad [m^3/s/m] &= \text{overtopping discharge} \\ \frac{R_c}{H_{m0}} \quad [-] &= \text{the relative overtopping height (also called the 'relative crest freeboard')} \\ R_c \quad [m] &= \text{overtopping height (also called the 'crest freeboard')} \\ H_{m0} \quad [m] &= \text{estimate of significant wave height from spectral analysis} = 4\sqrt{m_0} \approx H_s \end{aligned}$$

(See Figure 11-1 for a definition sketch, but instead of $R_{2\%}$ read R_c)

Further needed parameters, according to the Overtopping Manual 2018, for the design or assessment of structures with an outer slope less steep than 1:2 and not too shallow foreshores ($h/H_{m0,deep} > 1$):

$$\begin{aligned} a \quad [-] &= \frac{0,026}{\sqrt{\tan \alpha}} \gamma_b \cdot \xi_{m-1,0} \\ b \quad [-] &= \frac{2,5}{\xi_{m-1,0} \cdot \gamma_b \cdot \gamma_f \cdot \gamma_\beta \cdot \gamma_v} \\ \xi_{m-1,0} \quad [-] &= \text{breaker parameter (see previous section)} \\ \gamma_b \quad [-] &= \text{influence factor of a berm (see previous section)} \\ \gamma_f \quad [-] &= \text{influence factor for the permeability and roughness of the slope, sometimes written as } \gamma_R \text{ (see previous section)} \end{aligned}$$

- γ_β [-] = factor for oblique wave attack (notice that γ_β differs from γ_β for wave run-up)
 $\gamma_\beta = 1 - 0,0033|\beta|$ for $0^\circ \leq \beta \leq 80^\circ$
 $\gamma_\beta = 0,736$ for $\beta > 80^\circ$
- β [°] = the angle between the direction of propagation of waves and the axis perpendicular to the structure
- γ_v [-] = influence factor for a vertical wall on top of the crest (see section below)

The breaker parameter also referred to as surf similarity or Iribarren number is defined as:

$$\xi_{m-1,0} = \frac{\tan \alpha}{\sqrt{H_{m0} / L_{m-1,0}}}$$

where $\tan \alpha$ is the slope of the front face of the structure and $L_{m-1,0}$ being the deep water wave length:

$$L_{m-1,0} = \frac{g \cdot T_{m-1,0}^2}{2 \cdot \pi} \text{ [m]}$$

The European Overtopping Manual 2018 gives a maximum value for the validity of the equation:

$$\frac{q}{\sqrt{g \cdot H_{m0}^3}} = 0,1035 \cdot e^{-\left(\frac{1,35 \cdot R_c}{H_{m0} \cdot \gamma_f \cdot \gamma_\beta \cdot \gamma^*}\right)^{1,3}}$$

The wave steepness $s_0 (= H_{m0} / L_{m-1,0})$ can vary from 0,04 (steep storm waves) and 0,01 (long waves due to swell or wave breaking).

The equations above translate to the following design equation for the overtopping height:

$$R_c = \frac{\xi_{m-1,0} \cdot H_{m0} \cdot \gamma_b \cdot \gamma_f \cdot \gamma_\beta \cdot \gamma_v}{2,5} \cdot \left\{ -\ln \left(\frac{q \sqrt{\tan \alpha}}{\sqrt{g \cdot H_{m0}^3} \cdot 0,026 \cdot \gamma_b \cdot \xi_{m-1,0}} \right) \right\}^{1/1,3}$$

and a minimum of:

$$R_c > \frac{H_{m0} \cdot \gamma_f \cdot \gamma_\beta \cdot \gamma^*}{1,35} \cdot \left\{ -\ln \left(\frac{q}{0,1035 \cdot \sqrt{g \cdot H_{m0}^3}} \right) \right\}^{1/1,3}$$

where γ^* can be the same as γ_v , but it can include several other effects, like the presence of a promenade, a smooth slope or a parapet ('bull nose').

Influence of wave walls on top of a slope (factor γ_v)

A vertical wave wall on top of a slope can reduce the overtopping considerably. For the case of a smooth dike where a vertical wall is built on the top of the slope of the dike, the influence factor $\gamma^* = \gamma_v$ is defined as follows:

$$\gamma_v = e^{-0,56 \cdot \frac{h_{wall}}{R_c}}$$

The height of the storm wall h_{wall} is included in the crest freeboard.

The range of application of this equation can be given as follows:

- the foot of the storm wall is above the still water level
- $\cot(\alpha) = 2$ to 3 (this could also be an average slope)
- $s_{m-1,0} = 0,01$ to 0,05
- $\xi_{m-1,0} = 2,2$ to 4,8 (based on the seaward slope only, this means non-breaking waves)
- $R_c / H_{m0} > 0,6$

If there is no vertical wall on top of a slope, of course no correction factor γ_v should be used in the overtopping calculation.

11.2.3 Overtopping of vertical walls

Method Franco 1994

This section deals with wave overtopping over entire vertical walls, so not with (relatively small) vertical walls on top of a slope. To calculate the amount of wave overtopping over vertical walls or vertical structures like caisson breakwaters and navigation locks (including the gates), Franco and colleagues proposed the following equation for non-impulsive waves (Franco et. al., 1994):

$$\frac{q}{\sqrt{g \cdot H_s^3}} = a \cdot e^{-b \frac{R_c}{\gamma \cdot H_s}}$$

where:

R_c	[m]	=	overtopping height
q	[m ³ /m/s]	=	specific discharge
a, b	[-]	=	empirical coefficients
γ	[-]	=	geometrical parameter
H_s	[m]	=	significant wave height
g	[m/s ²]	=	gravity acceleration

For rectangular shapes: $a = 0,192$, $b = 4,3$, $\gamma = 1$.

Method European Overtopping Manual 2018

The European Overtopping Manual 2018 distinguishes two types of wave conditions in front of the vertical wall: If the waves are relatively small compared to the local water depth, or in case of gentle wave steepnesses, they will not critically be influenced by the toe or approach slope of the structure. The resulting loads on the structure are rather smooth-varying. These conditions are called 'non-impulsive'. The other type of conditions, the 'impulsive' conditions, occurs if the waves are larger in relation to the local water depth. Several waves will break violently against the wall with forces up to 40 times more than under non-impulsive conditions. This also leads to higher overtopping volumes.

Whether or not the wave conditions are impulsive, can be determined with help of the following equations.

non-impulsive conditions, if: $\frac{h^2}{H_{m0} \cdot L_{m-1,0}} > 0,23$

impulsive conditions, if: $\frac{h^2}{H_{m0} \cdot L_{m-1,0}} \leq 0,23$

where:

h	[m]	=	water depth at the toe of the structure
H_{m0}	[m]	=	estimate of significant wave height from spectral analysis $\approx H_s$
$L_{m-1,0}$	[s]	=	spectral wave length in deep water

The overtopping volumes for deterministic design and assessment can then be calculated, according to:

for non-impulsive conditions:

$$\frac{q}{\sqrt{g \cdot H_{m0}^3}} = 0,062 \cdot e^{-2,61 \cdot \frac{R_c}{H_{m0}}}$$

for impulsive conditions:

$$\frac{q}{\sqrt{g \cdot H_{m0}^3}} = 0,0155 \cdot \left(\frac{H_{m0}}{h \cdot s_{m-1,0}} \right)^{0,5} \cdot e^{-2,2 \frac{R_c}{H_{m0}}} \text{ valid for } 0,1 < \frac{R_c}{H_{m0}} < 1,35$$

and

$$\frac{q}{\sqrt{g \cdot H_{m0}^3}} = 0,0020 \cdot \left(\frac{H_{m0}}{h \cdot s_{m-1,0}} \right)^{0,5} \cdot \left(\frac{R_c}{H_{m0}} \right)^{-3} \text{ valid for } \frac{R_c}{H_{m0}} \geq 1,35$$

where $s_{m-1,0}$ [-] = wave steepness with L_0 , based on $T_{m-1,0} = H_{m0}/L_{m-1,0} = 2\pi \cdot H_{m0}/(gT_{m-1,0}^2)$
(other symbols: see above)

These equations assume no influence of the foreshore (like shoaling, steepening and breaking) and no presence of a significant mound.

For equations for probabilistic design, battered walls and vertical walls with parapets, composite walls and other shapes, the reader is referred to the European Overtopping Manual 2018.

Note

If non-breaking waves are reflected by a vertical structure, interference of incoming and reflecting waves will occur. This will result in a standing wave with a height twice as much as the incoming wave. In the overtopping volume equation, however, the wave height of the incoming wave, not the standing wave, should be used, because the parameters in the equations already include this effect.

11.3 Literature

Franco, L., Gerloni, M. de, Meer, J.W. van der (1994). *Wave overtopping on vertical and composite breakwaters*. Proceedings of the 24th International Conference on Coastal Engineering. Kobe, pp 1030-1044

EurOtop (2018). Manual on wave overtopping of sea defences and related structures. An overtopping manual largely based on European research, but for worldwide application. Van der Meer, J.W., Allsop, N.W.H., Bruce, T., De Rouck, J., Kortenhaus, A., Pullen, T., Schüttrumpf, H., Troch, P. and Zanuttigh, B., www.overtopping-manual.com.

12. Water, waves, wall, non-breaking

Updated: February 2015

Civil engineering works located at the sea side of a breaker zone, can be subjected to loads by non-breaking waves. Non-breaking waves also occur in waterways and lakes in which the wave height is limited. Unlike around slender structures, the wave pattern is influenced by a wall. The wave height in front of the wall is determined by refraction and diffraction (see Sections 10.1 and 10.5).

There are five methods to calculate the load on a wall due to non-breaking waves. They are given in the table below with a description of when they are applied.

No	Method	Design phase	Notes
1	Rule of thumb	preliminary estimate	conservative
2	Linear theory	preliminary (and final) design	-
3	Sainflou	preliminary design	simple!
4	Rundgren	final design	not in this handbook
5	Goda	final design	also for sills!

Table 12-1 Summary of methods

12.1 Rule of thumb (hydrostatic pressure)

According to linear wave theory for non-breaking waves against a vertical wall, the wave height H in front of the wall is double the incoming wave height H_i , in the case of total reflection. In short:

$$H = 2H_i \quad \text{and with} \quad H = 2a: \quad a = H_i$$

The wave force is maximum when the wave in front of the wall reaches its highest level (wave top). If this is considered as a stationary load, the following rule of thumb can be applied to calculate the maximum wave force F_{max} [N/m] against a wall (per metre width):

$$F_{max} = \frac{1}{2}\rho g H_i^2 + d \rho g H_i$$

in which: ρ [kg/m³] = density of water
 g [m/s²] = gravity acceleration
 H_i [m] = the wave height of an incoming wave (= $2 a_i$)
 a [m] = amplitude of the wave (half the wave height)
 d [m] = depth of the breakwater

This can be used for a quick estimate of the upper boundary value of the wave load.

12.2 Linear wave theory

For non-breaking waves against a vertical wall, the force on a wall can be determined using the pressure distribution in a vertical, taken from wave theory. As mentioned before, according to linear wave theory, the wave height H in front of the wall:

$$H = 2H_i \quad \text{and with} \quad H = 2a: \quad a = H_i \quad \text{is valid.}$$

The maximum pressure against a wall in case of reflection is then:

$$p = \rho g H_i \frac{\cosh(k(d+z))}{\cosh(kd)} \quad \text{for} \quad -d < z < 0$$

$$p = \left(1 - \frac{z}{H_i}\right) \rho g H_i \quad \text{for} \quad 0 < z < H_i$$

in which: H_i [m] = wave height of an incoming wave
 k [m⁻¹] = the wave number of the incoming wave (= $2\pi/L$)

The force per metre follows from integration over the water depth:

$$F = \int_{-d}^0 \rho g H_i \frac{\cosh(k(d+z))}{\cosh(kd)} dz + \int_0^{H_i} \left(1 - \frac{z}{H_i}\right) \rho g H_i dz$$

$$= \rho g H_i \left(\frac{(\exp(kd) - \exp(-kd))}{2k \cosh(kd)} + \frac{H_i}{2} \right)$$

In the case of a large wavelength, the wave pressure approaches the hydrostatic pressure (= rule of thumb). Figure 12-1 gives an example of this. The figure illustrates the wave pressures for different wavelengths, which are to be added to the hydrostatic pressure corresponding to the still water level.

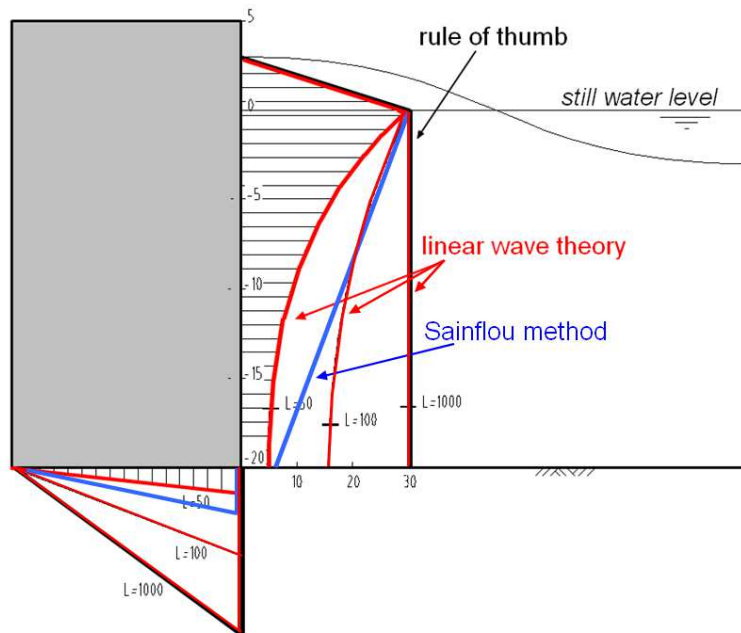


Figure 12-1 Rule of thumb, linear wave theory, and Sainflou method: wave pressure

12.3 Sainflou method

In practice another simple approximation is often used for the calculation of the total force on a wall. This method is known as Sainflou's method. This approach is shown schematically in Figure 12-2 and only applies to non-breaking waves. The approach is based on Stokes' second order wave theory. The incoming waves have the shape of a trochoid and complete reflection ($\chi = 1$) is assumed. Due to interference of reflected waves with incoming waves, peaks in front of the wall will reach an amplitude with the magnitude of the incoming wave height.

The still water level in front of the vertical wall will increase with h_0 [m]:

$$h_0 = \frac{1}{2} \cdot k \cdot H_{in}^2 \cdot \coth(k \cdot d)$$

where:

- h_0 [m] = increase of the mean water level in front of the structure
- H_{in} [m] = height of the incoming wave; not influenced by the presence of the wall
- d [m] = water depth in front of the sill, 2 or 3 wave lengths away from the wall
- k [m^{-1}] = wave number of the incoming wave:

$$k = \frac{2\pi}{L_0} \quad \text{or} \quad k = \frac{2\pi}{L}$$
- L [m] = wave length

For 100% reflection: $H_{refl} = 2 \cdot H_{in}$, where H_{refl} is the height of the wave that originates from the interference of the incoming and the reflected wave.

Sainflou and Stokes's second order wave theory lead to the same maximum pressures at mean water level and near the bed as the linear theory; viz.:

$$p_1 = \rho \cdot g \cdot (H_{in} + h_0)$$

$$p_0 = \frac{\rho \cdot g \cdot H_{in}}{\cosh(k \cdot d')}$$

where:

d' [m] = water depth above foundation level of the structure.

The pressure between p_0 and p_1 is assumed to be linear. Therefore, Sainflou leads to an overestimation of the load for steep waves.

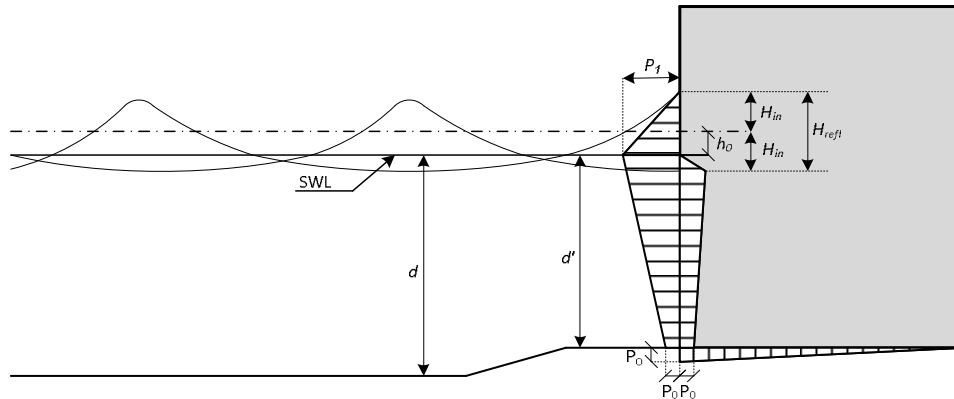


Figure 12-2 Sainflou: wave pressure

12.4 Rundgren method

Based on adapted higher order wave theory, Rundgren adapted Sainflou's formulas. The adapted formulas were used to make the graphs in the Shore Protection Manual (CERC, 1984). In these graphs, overtopping and oblique approach are taken into account, which reduces the load. Rundgren's wave theory is not covered in this manual.

12.5 Goda method

Goda (1985, 1992) found a general expression for the wave pressure on caissons, placed on a rockfill sills. This expression can also be used for broken and breaking waves. Worldwide Goda's equations are used often for the design of vertical breakwaters, see Figure 12-3. Goda's equations don't have an analytical base but rather an empirically foundation.

For the determination of the design wave height H_D and the design wavelength L_D , see the methods in Chapters 9 and 10. Goda proposed his own formula for H_D and L_D , however, these are not dealt with in this manual.

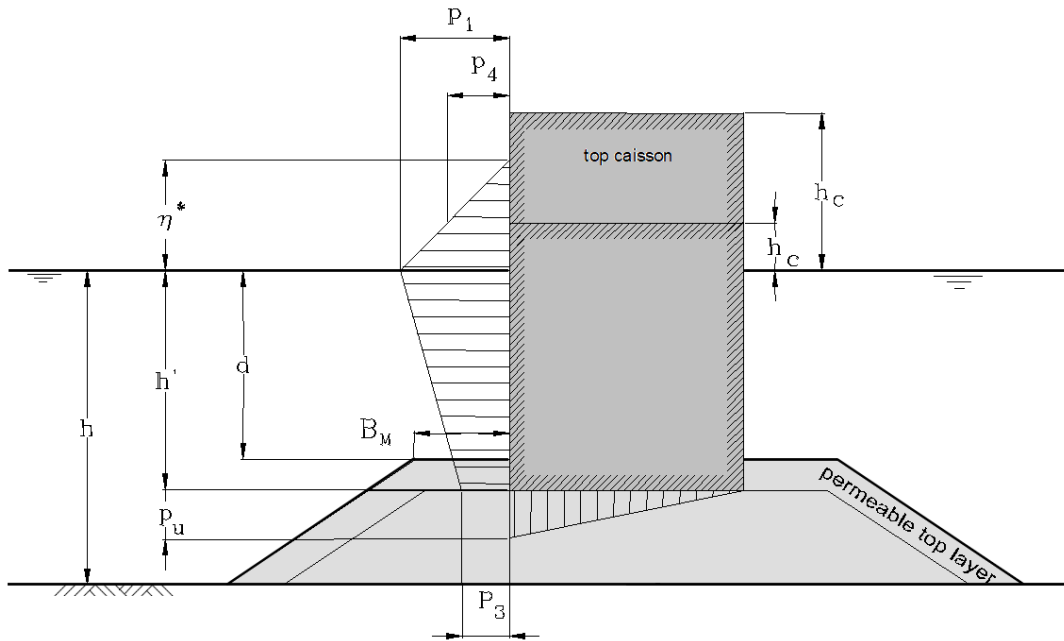


Figure 12-3 Goda (modified by Tanimoto): wave pressure

The sill height is $h - d$.

The sill width is B_m .

The maximum wave pressures are:

$$p_1 = 0,5 (1 + \cos(\beta)) (\lambda_1 \alpha_1 + \lambda_2 \alpha_2 \cos^2(\beta)) \rho g H_D$$

$$p_3 = \alpha_3 p_1$$

$$p_4 = \alpha_4 p_1$$

$$p_u = 0,5 (1 + \cos(\beta)) \lambda_3 \alpha_1 \alpha_3 \rho g H_D$$

in which: β = the angle of the incoming wave

$$\eta^* = 0,75 (1 + \cos(\beta)) \lambda_1 H_D$$

$$\alpha_1 = 0,6 + 0,5 \left(\frac{4\pi h / L_D}{\sinh(4\pi h / L_D)} \right)^2$$

$$\alpha_2 = \min \left(\frac{(1 - d/h_b)(H_D/d)^2}{3}, \frac{2d}{H_D} \right)$$

$$\alpha_3 = 1 - (h'/h) \left(1 - \frac{1}{\cosh(2\pi h / L_D)} \right)$$

$$\approx \frac{1}{\cosh(kd)} \quad (\text{without sill})$$

$$\alpha_4 = 1 - \frac{h_c^*}{\eta^*}$$

$$h_c^* = \min(\eta^*, h_c)$$

$\lambda_1, \lambda_2, \lambda_3$ = factors dependent on the shape of the structure and on wave conditions;

(vertical wall and non-breaking waves: $\lambda_1 = \lambda_2 = \lambda_3 = 1$)

h_b = water depth at a distance $5H_D$ from the wall

H_D = design wave height (see Chapters 9 and 10)

L_D = design wavelength (see Chapters 9 and 10)

d = water depth above the top of the sill

h' = water depth above the wall foundations plane

h = water depth in front of the sill.

13. Water, waves, wall, breaking

13.1 Introduction

For the description of conditions in which a wave breaks, see Section 10.3 "Shallows: breaking".

For unbroken waves, the pressure distribution in the wave is a measure for the force on the wall. In the case of breaking waves this is not so. For those waves it is mainly the velocity with which the water particles hit the wall that is of importance. The shape of the breaking wave and possible air that is caught between the structure and the breaking wave largely influence the maximum wave shock and the course of the pressure distribution in time. The load due to breaking waves is still a point of research. The dynamic character of the load is an essential facet of breaking waves. Due to the collision between the wave and the structure a transfer of impulse takes place. At the moment of impact, a relatively high pressure occurs, which only lasts a very short time (in the order of 0,01 s). Because of the short time span, this pressure is not representative for the stability of a structure (due to the inertia of mass). This pressure can be of importance for the strength of the structure (partial collapse).

If possible, it is better to prevent waves to break before they hit the structure, so that the shock will be less. In most cases it is therefore more economical not to place too high a sill in front of a straight wall, so that the waves won't break and the load of the non-breaking waves is governing (*maatgevend*).

The sections below describe three models for breaking and broken waves. These models are:

- Minikin
- CERC 1984, broken waves
- Goda-Takahashi

These models are no more than rough estimates.

13.2 Minikin method

Minikin's model is based on both laboratory tests and on prototype measurements. Figure 13-1 gives a diagram of the model. It is based on a maximum dynamic pressure at the still water level and on a parabolic decline to zero over the distance $H_b/2$ above and below the still water level plus an increase of the hydrostatic pressure as a result of the displacement of the water surface.

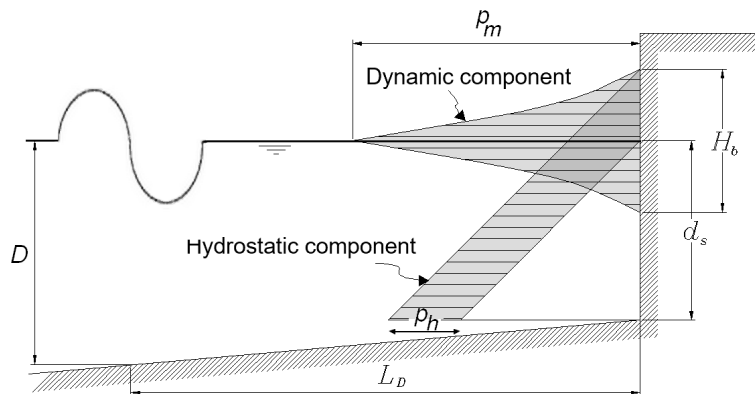


Figure 13-1 Minikin: broken wave pressure

The maximum pressure of the dynamic component is:

$$p_m = \frac{1}{2} C_{mk} \pi \rho g \frac{H_b}{L_D} \frac{d_s}{D} (D + d_s)$$

The maximum pressure of the hydrostatic component is:

$$p_h = \rho \cdot g \cdot \frac{1}{2} H_b$$

where: C_{mk} [-] = coefficient of the impact. Minikin found $C_{mk} \approx 2$.
 H_b [m] = height of the breaking wave
 d_s [m] = depth in front of the wall
 D [m] = depth at one wavelength in front of the wall
 L_D [m] = wavelength at depth D

The resultant wave force according to Minikin is:

$$F = F_{dyn} + F_{hydr} = \frac{\rho_m H_b}{3} + \frac{\rho g H_b}{2} \left(\frac{H_b}{4} + d_s \right)$$

Note

Minikin's method is unfortunately described incorrectly in CERC (1984). In the original publication by Minikin (1963), the pressure on the wall was expressed in tonnes per square foot. This is not correct. It should be ton force per square foot. This mistake was overseen in conversion to SI units for the CERC 1984 and has led to a formula for p_m which gives values that are far too large. This is why many publications warn against Minikin's method, mentioning that the equation gives values that are 10 to 15 times too large, whilst the original method actually gave far lower values. One is advised not to use equations derived from Minikin (except for the corrected equations given above).

13.3 CERC 1984 method

The model of CERC (United States Army Coastal Engineering Research Center) 1984, for broken waves, merely gives an indication of the load. If accurate estimates are needed of the maximum load on a structure due to breaking waves, more thorough research must be carried out for the specific situation. Like Minikin's model, the model assumes a dynamic and a hydrostatic component of the water pressure on the structure.

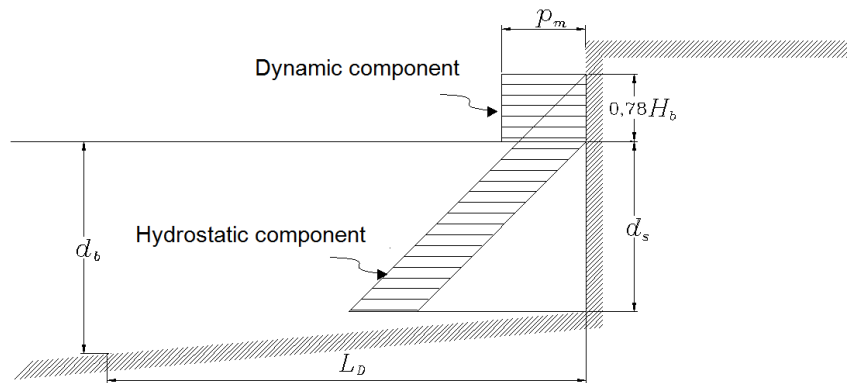


Figure 13-2 CERC 1984: broken wave pressure

The dynamic component is derived from the wave propagation velocity c at the moment the waves started to break. The broken wave is considered a translation wave with the propagation velocity:

$$c = \sqrt{gd_b} .$$

The dynamic pressure is:

$$p_m = \rho g \frac{c^2}{2g} = \frac{\rho g d_b}{2}$$

where: d_b [m] = the water depth where the wave broke

As in Minikin's model, the hydrostatic component of the load is caused by the displacement of the water surface. The total load as a result of the broken wave is therefore:

$$F = \rho g h_c \left(\frac{d_b}{2} + \frac{h_c}{2} + d_s \right)$$

in which: h_c [m] = the height of the broken wave (translation wave) = $0,78 H_b$

13.4 Goda-Takahashi method

Goda's model was already given in the previous chapter. According to Takahashi and others (1994), a couple of factors need to be adjusted for waves that break on the berm of the sill on top of which a caisson has been placed:

$$\lambda_1 = \lambda_3 = 1$$

$$\lambda_2 = \max\left(1, \frac{\alpha_1}{\alpha_2}\right)$$

where: α_1 = impulse coefficient

The impulse coefficient is determined with the following equations:

$$\alpha_1 = \alpha_n \alpha_m$$

$$\alpha_m = \min\left(\frac{H_D}{d}, 2\right)$$

$$\alpha_n = \frac{\cos(\delta_2)}{\cosh(\delta_1)} \quad \text{if } \delta_2 \leq 0$$

$$\alpha_n = \frac{1}{\cos(\delta_1) \sqrt{\cosh(\delta_2)}} \quad \text{if } \delta_2 > 0$$

$$\delta_1 = 20 \delta_{11} \quad \text{if } \delta_{11} \leq 0$$

$$\delta_1 = 15 \delta_{11} \quad \text{if } \delta_{11} > 0$$

$$\delta_2 = 4,9 \delta_{22} \quad \text{if } \delta_{22} \leq 0$$

$$\delta_2 = 3,0 \delta_{22} \quad \text{if } \delta_{22} > 0$$

$$\delta_{11} = 0,93 \left(\frac{B_M}{L_D} - 0,12 \right) + 0,36 \left(\frac{h-d}{h} - 0,6 \right)$$

$$\delta_{22} = -0,36 \left(\frac{B_M}{L_D} - 0,12 \right) + 0,93 \left(\frac{h-d}{h} - 0,6 \right)$$

where: B_M [m] = width of the berm in front of the wall (see Figure 12-3)

The dimensions of the berm have an important influence on the extent of the load. Figure 13-3 shows this influence for an example.

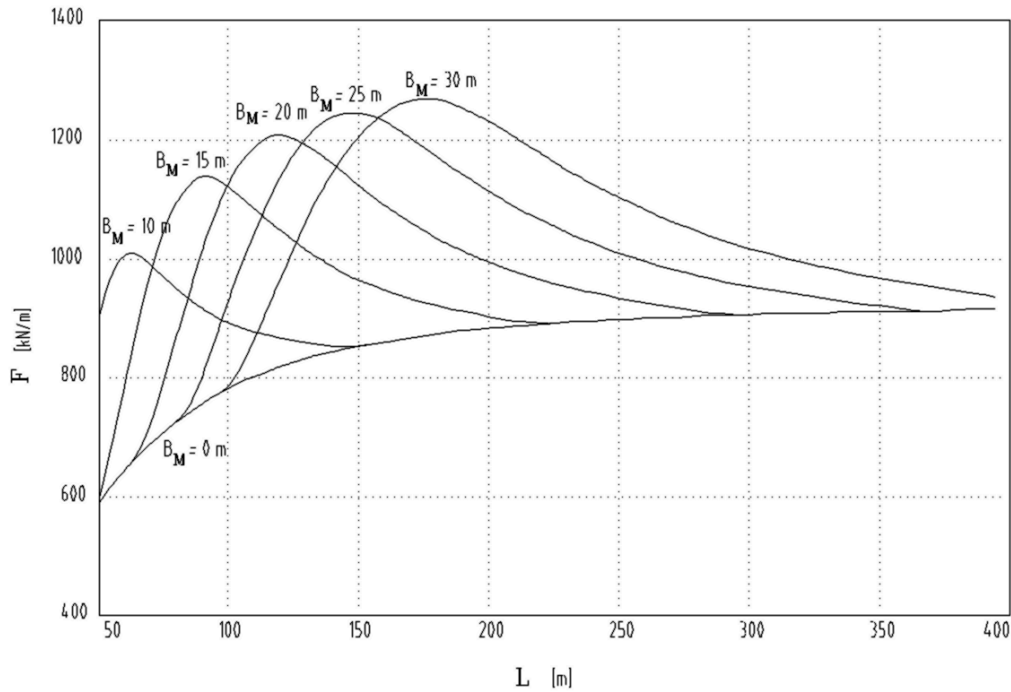


Figure 13-3 Influence of a berm on the wave load ($H_D = 6 \text{ m}$, $h = 9 \text{ m}$, $h' = 7 \text{ m}$, $d = 5 \text{ m}$, $h_c = \infty$)

13.5 Comparison

Figure 13-4 shows a comparison of the different models. The wave load was calculated for various different wave periods, for a given configuration (a caisson on a quarry stone sill).

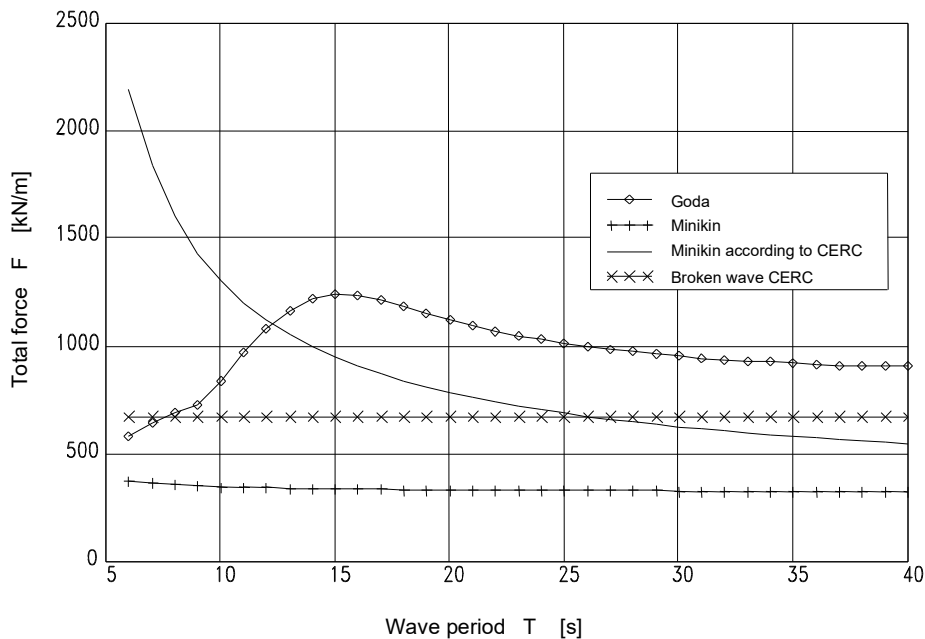


Figure 13-4 Comparison of Minikin, Goda and broken waves according to CERC 1984 ($H_D = 6 \text{ m}$, $h = 9 \text{ m}$, $h' = 7 \text{ m}$, $d = 5 \text{ m}$, $h_c = \infty$)

The comparison of the different calculation models revealed that there are considerable differences between the results of the models, particularly when waves with periods between 6 and 15 seconds are considered. When applying the models, one could consider upper and lower boundaries, where Minikin's model is clearly a lower boundary for the above-mentioned periods.

One reason for the deviation between the models could be the different researchers' ways of measuring the wave load. The wave force of a breaking wave varies in time. The moment the wave breaks against the structure, the largest impact occurs during a very short time span, when the pressure against the wall is extremely high. Directly after the impact, the pressure decreases very quickly and stays constant a

while at a certain level of pressure. This is shown schematically in Figure 13-5. This schematisation is known as the “church roof” load. The response of the structure under a “church roof” load depends on the stiffness and on the inertia of the structure. These determine the speed of reaction of the structure. A structure with little inertia (mass) and a large stiffness will be more sensitive to short impulse loads than a structure with a larger inertia.

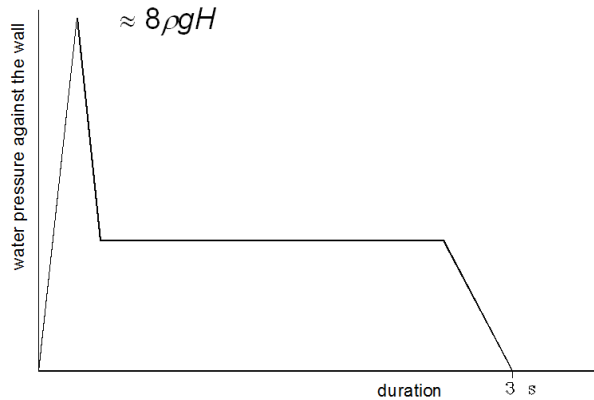


Figure 13-5 Course of the load in time

The wave load and the response of the structure are still subject to research.

Figure 13-6 shows the force F on a smooth wall for different wave steepnesses ($s = H / L$), according to the four given methods. Here, the sill height in the Goda formulas is kept equal to zero, even though, the Goda formulas were derived for a caisson on a sill.

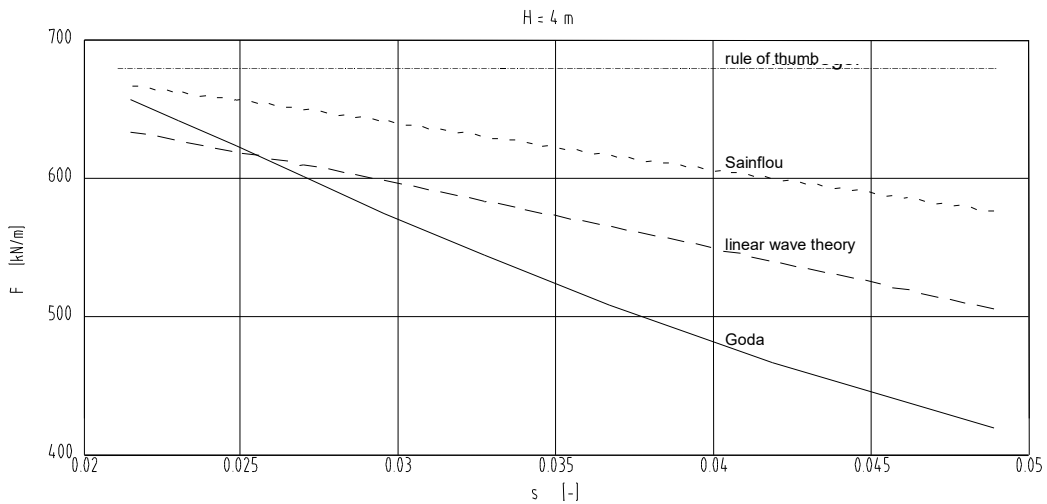


Figure 13-6 Wave load F of non-breaking waves ($H = 4 \text{ m}$) as a function of the steepness s ($h = h' = d = h_0 = 15\text{m}$)

The wave load of a four-metre high wave on the same wall is plotted as a function of the wave period in Figure 13-7.

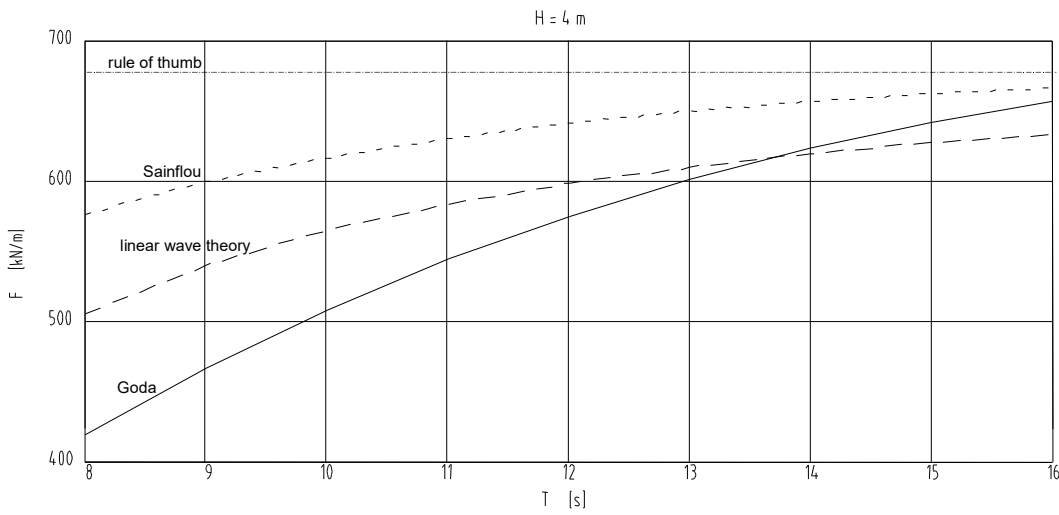


Figure 13-7 Wave load F of non-breaking waves ($H = 4$ m) as a function of the period T ($h = h' = d = h_b = 15$ m)

Notice that the graphs do not begin at “zero”, so the graphs give a distorted view. The differences between the linear wave theory and Sainflou or Goda are no more than 10% or 20%. Particularly for long waves (hence not very steep), the rule of thumb has a small error.

14. Water, waves, slender structure, non-breaking

Analogous to the formulation of the force on an object in a stationary flow, Morison et al (1950) found a relation between the force on a vertical pile as a function of the velocity and the acceleration of water particles in a wave. The part of the force that is caused by the flow velocity is the drag force and the part that is caused by the acceleration of the water particles is the inertia force.

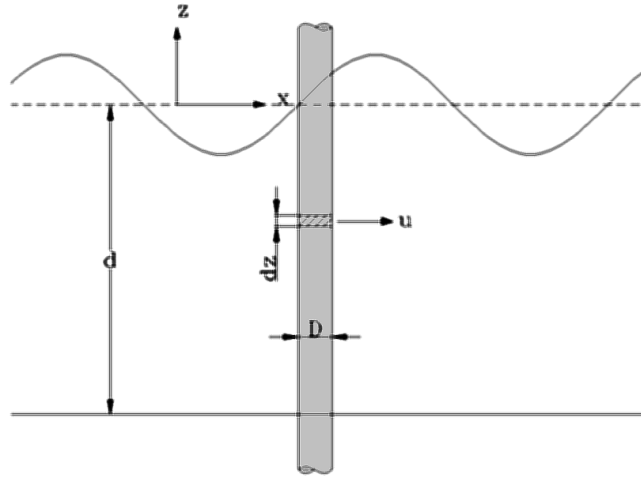


Figure 14-1 Wave load on a slender structure

14.1 Theory

Morison's formula for a fixed body in an oscillatory flow includes an inertia part and a drag part:

$$\frac{dF}{dz} = p(t, z) = p_i + p_D = C_I \rho \frac{\pi D^2}{4} \frac{du}{dt} + C_D \frac{1}{2} \rho D u |u|$$

where:	$p(t, z)$	[N/m]	=	pile force per unit of length of the pile at time t and in position z [N/m]
	p_i	[N/m]	=	inertia force (per unit of length of the pile)
	p_D	[N/m]	=	drag force (per unit of length of the pile)
	C_I	[-]	=	inertia coefficient $\approx 2,0$
	C_D	[-]	=	drag coefficient (for low flow velocities $C_D \approx 1,2$, see Figure 14-1)
	ρ	[kg/m ³]	=	density of the water
	D	[m]	=	diameter of the pile
	u	[m/s]	=	horizontal velocity of the water particles: $u = \omega a \frac{\cosh(k(d+z))}{\sinh(kd)} \sin(\omega t)$
	$\frac{du}{dt}$	[m/s ²]	=	horizontal acceleration of the water: $\frac{du}{dt} = \omega^2 a \frac{\cosh(k(d+z))}{\sinh(kd)} \cos(\omega t)$
	ω	[rad/s]	=	angular frequency ($2\pi/T$)
	k	[rad/m]	=	wave number ($2\pi/L$)
	d	[m]	=	depth

Because the velocity and the acceleration of the water particles are not in phase, the maximum total force is smaller than the sum of the maximum drag force and the maximum inertia force.

The force on the pile over time is found by integration:

$$F(t) = \int_{-d}^{\eta} p(t, z) dz = \int_{-d}^{\eta} p_i dz + \int_{-d}^{\eta} p_D dz = C_I \rho \frac{\pi D^2}{4} \int_{-d}^{\eta} \frac{du}{dt} dz + C_D \frac{1}{2} \rho D \int_{-d}^{\eta} u |u| dz$$

The moment on the pile relative to the bed is found by integrating the wave pressure multiplied by the height on the pile:

$$M(t) = \int_{-d}^{\eta} p(t, z)(z + d) dz = \int_{-d}^{\eta} p_i(z + d) dz + \int_{-d}^{\eta} p_D(z + d) dz$$

14.2 (Preliminary) design

The maximum force and the maximum moment in the above integrals are generally solved as follows:

$$F_{\max} = F_i + F_D = C_i K_i H \rho g \frac{\pi D^2}{4} + C_D K_D H^2 \frac{1}{2} \rho g D$$

$$M_{\max} = F_i d S_i + F_D d S_D$$

where: C_i [-] = inertia coefficient $\approx 2,0$
 C_D [-] = drag coefficient (for small flow velocities $C_D \approx 1,2$, see Figure 14-1)
 K_i [-] = correction for extent of inertia force (Figure 14-2)
 K_D [-] = correction for extent of drag force (Figure 14-3)
 S_i [-] = correction for position of resultant inertia force (Figure 14-4)
 S_D [-] = correction for position of resultant drag force (Figure 14-5)
 H [m] = wave height
 D [m] = diameter pile
 d [m] = depth

The "Shore Protection Manual" (CERC 1984) gives graphs with the maximum values of the coefficients C_D , K_i , K_D , S_i , S_D . These graphs are also included in the following sections. The values of the coefficients depend on the wave period, the phase, the water depth and the applicable wave theory for the determination of the velocity of the water particles.

The graphs show various different curves. These depend on the ratio:

$$\frac{H}{H_b}$$

in which: H_b [m] = wave height when breaking (see Section 10.3)

Just like a body in a constant flow, a pile in a wave is subjected to a lifting force perpendicular to the direction of the wave and the axis of the pole. This force is caused by fluctuations of the vortices next to and behind the pile. Due to resonance of the pile, these forces have been known to be 4,5 times larger than the drag force. In most cases, the lift force is of the same order of magnitude as the drag force.

For a preliminary design, the maximum lift force can be approximated by:

$$F_{L,\max} = C_L \frac{1}{2} \rho g D H^2 K_{D,\max}$$

in which: C_L [-] = lift coefficient
 $K_{D,\max}$ [-] = maximum value of K_D

The lift coefficient C_L is unknown, but in most cases:

$$0 < C_L < C_D$$

is valid. This can be used to determine a safe upper bound.

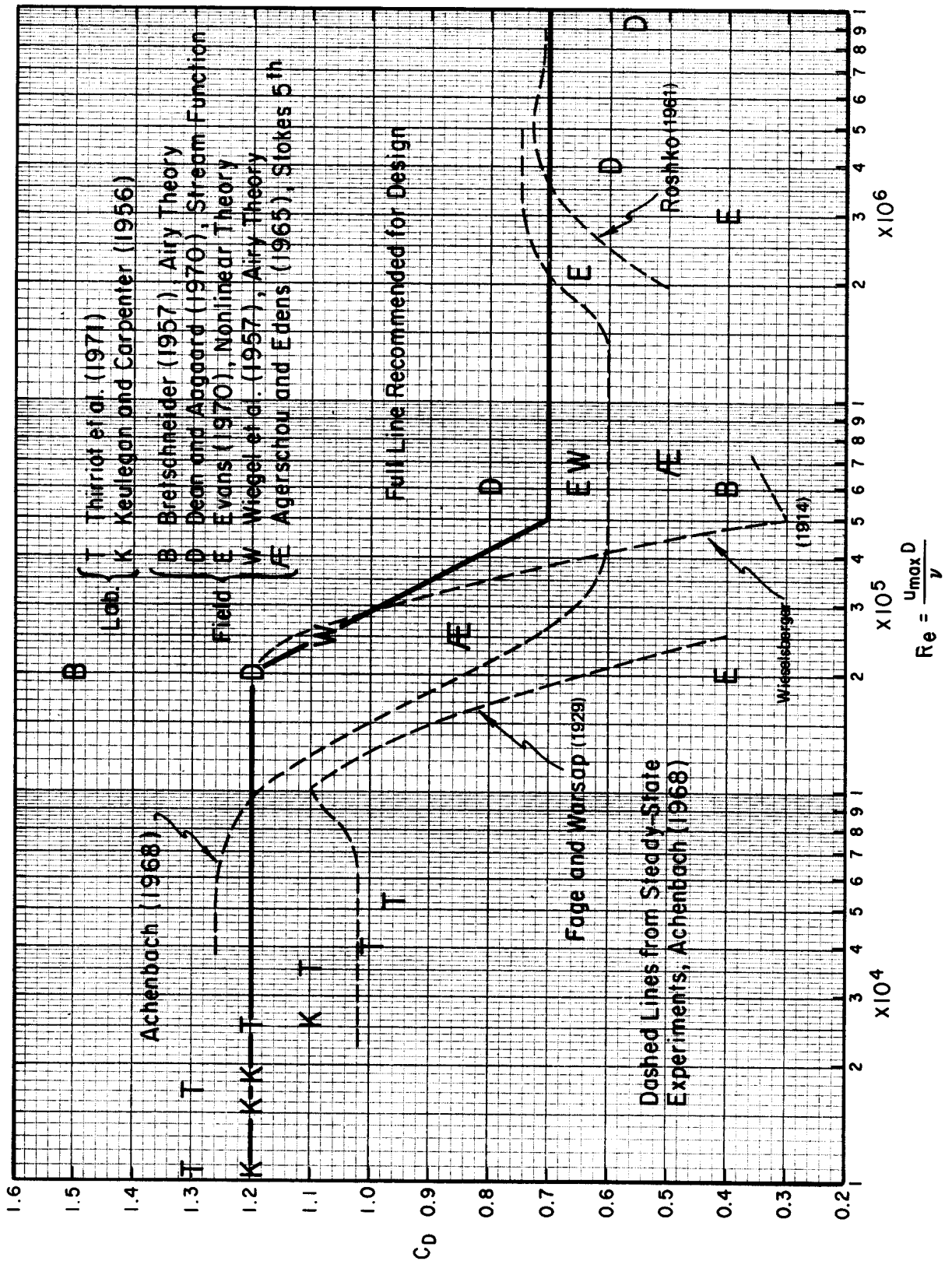


Figure 14-1 C_D coefficient (Shore Protection Manual 1984)

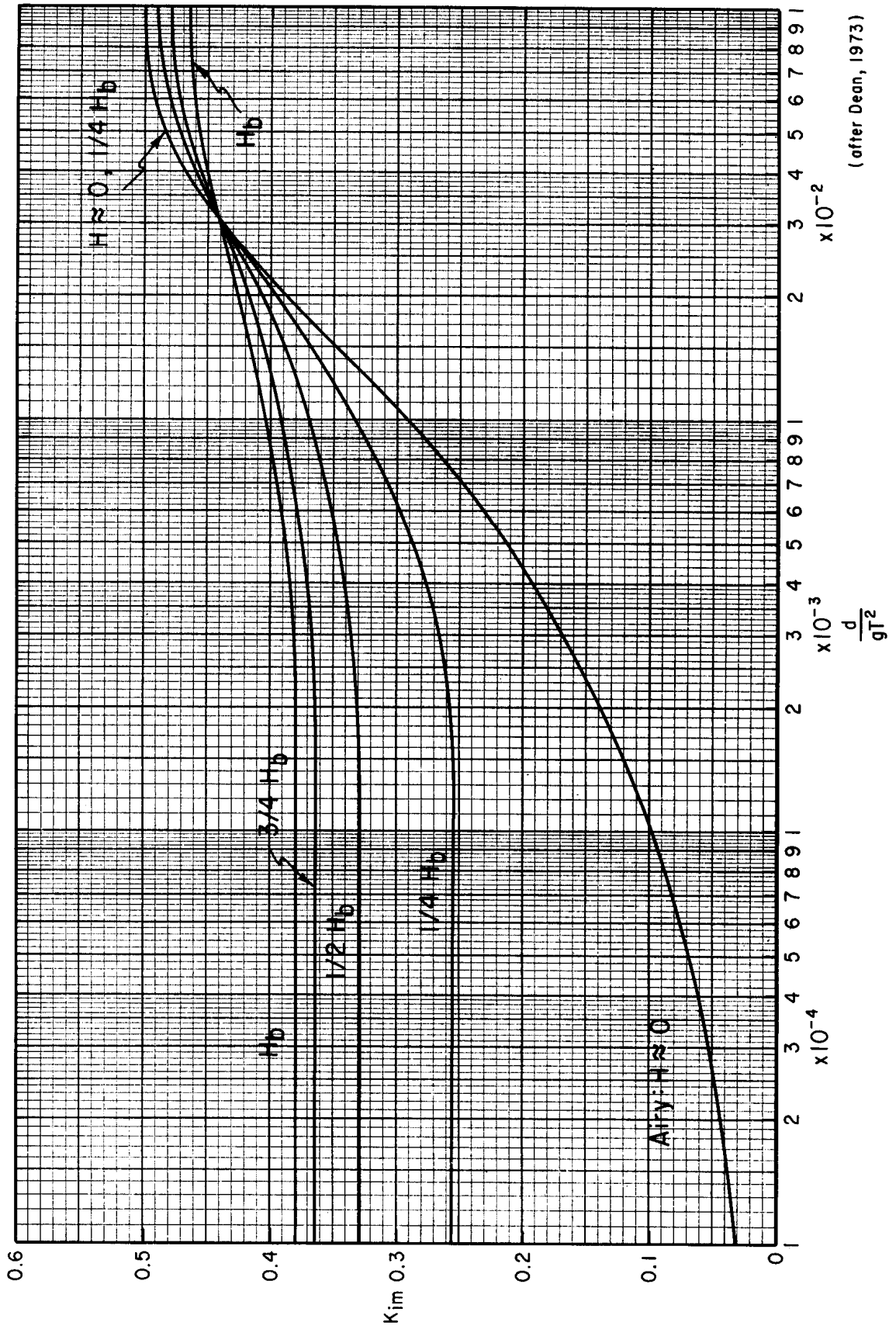


Figure 14-2 K_i coefficient (Shore Protection Manual 1984)

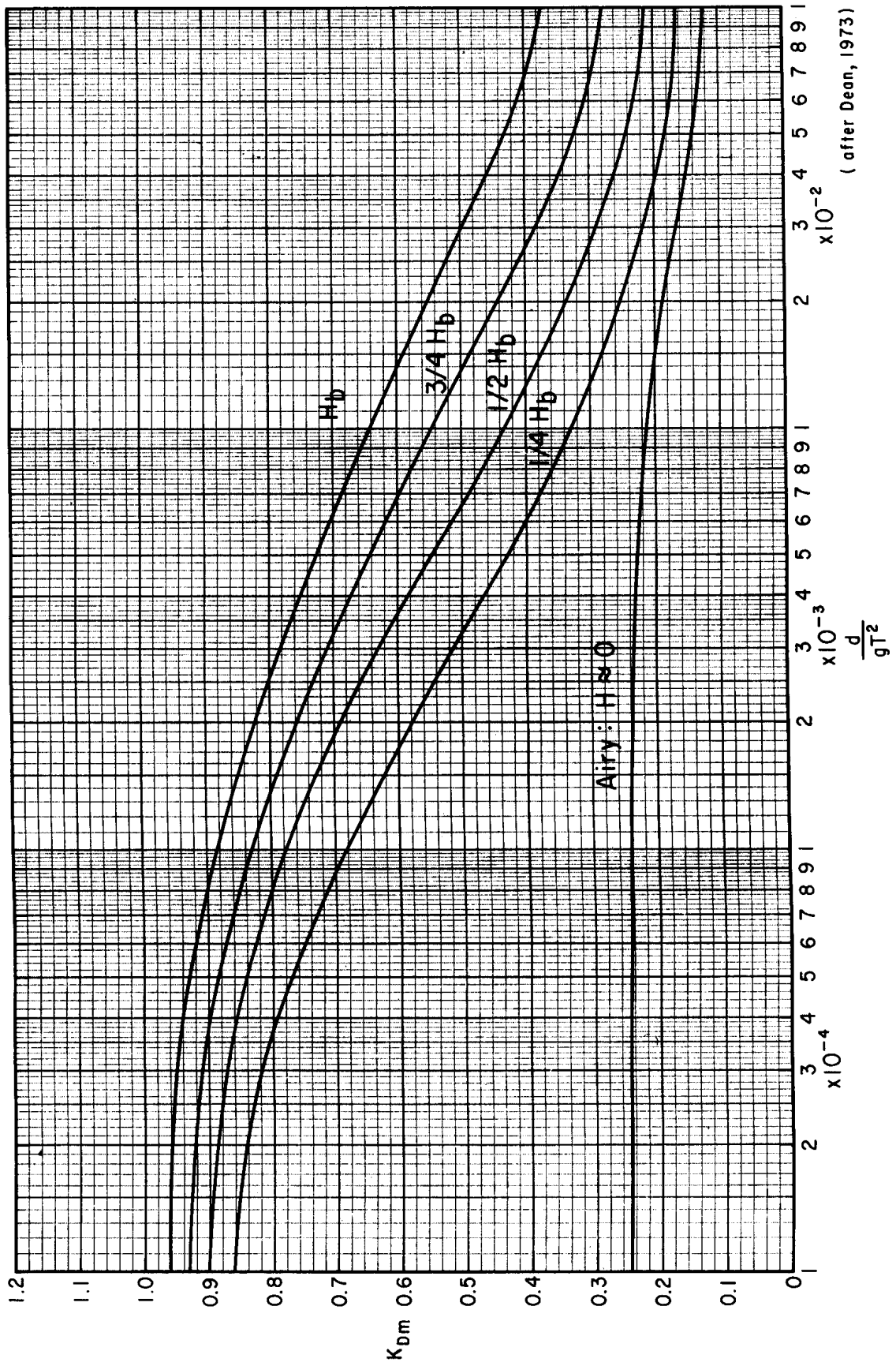


Figure 14-3 K_D coefficient (Shore Protection Manual 1984)

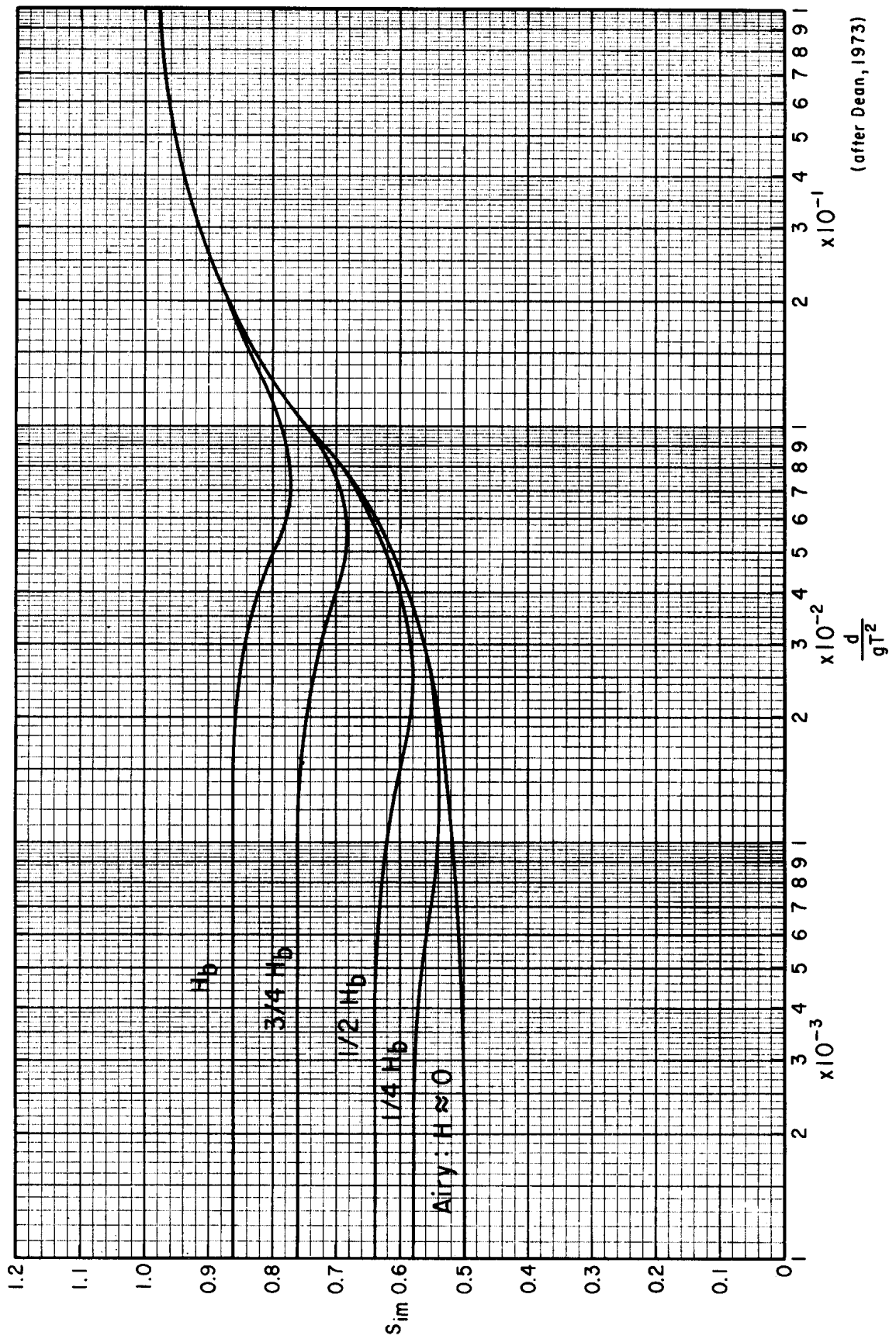


Figure 14-4 S_i coefficient (Shore Protection Manual 1984)

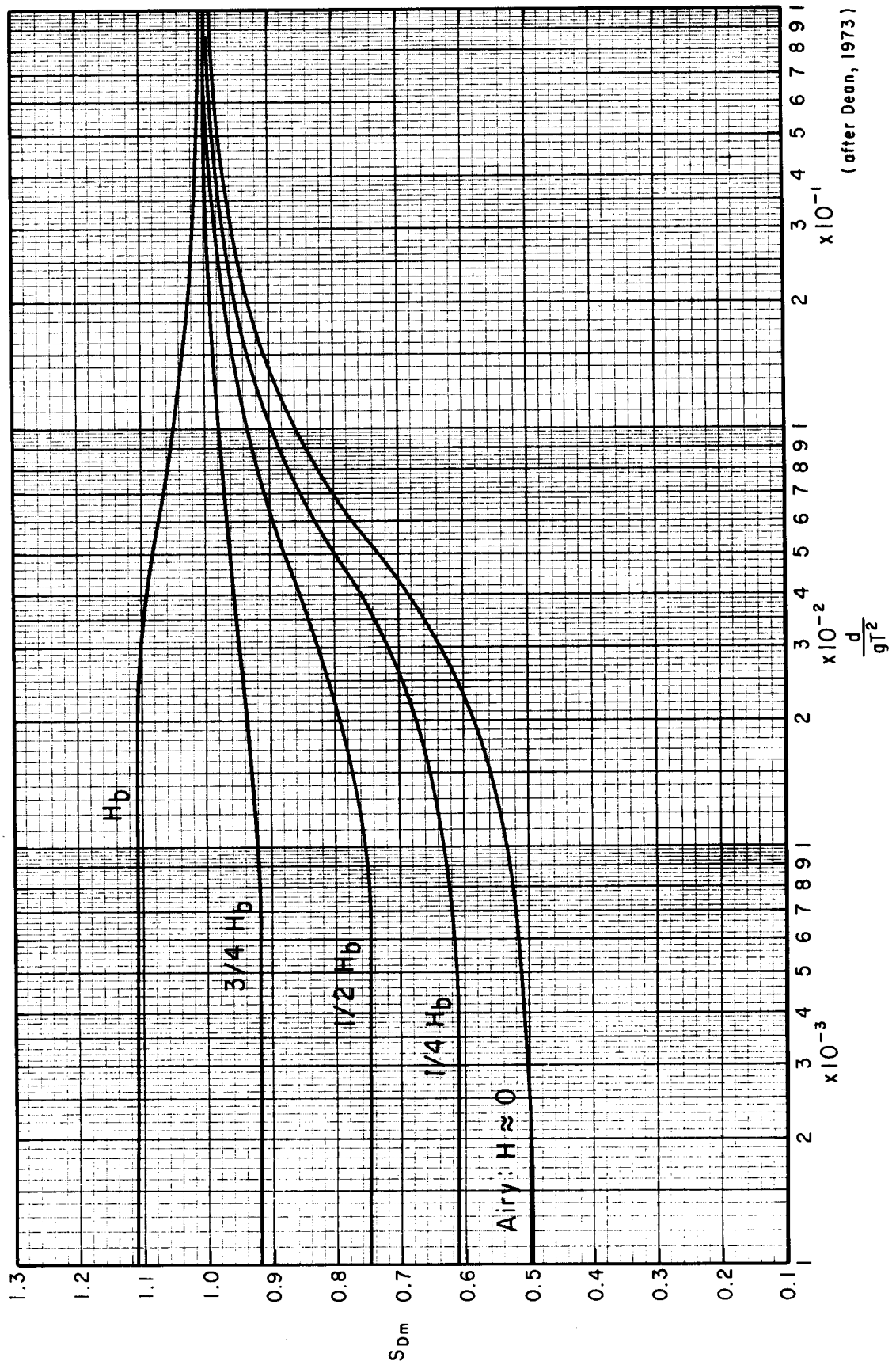


Figure 14-5 S_D coefficient (Shore Protection Manual 1984)

15. Water, waves, slender structure, breaking

The water particles in breaking waves have large horizontal velocities, but the accelerations are small compared to the velocity of the water. Consequently, the inertia force on a slender structure is negligible relative to the drag force. The maximum force on a pile can therefore be approximated using the reduced formula:

$$F_{\max} = F_D = C_D^* K_D H^2 \frac{1}{2} \rho g D$$

In this case, the maximum moment on the pile is:

$$M_{\max} = F_D d S_D$$

Observations revealed that the value of C_D^* in breaking waves is 2,5 times larger than in non-breaking waves:

$$C_D^* \approx 2,5 \cdot C_D$$

Thus, the known values of C_D for non-breaking waves can be used (see Section 14 "Water, waves, slender structures").

Breaking waves in shallow water involve super-critical flow ($C_D = 0,7$). In these conditions, one can assume the following for the preliminary design of cylindrical piles:

$$C_D^* \approx 2,5 \cdot 0,7 \approx 1,75$$

$$K_D \approx 1,0$$

$$S_D \approx 1,11$$

$$H = H_b \quad [-] = \text{height of the breaking wave}$$

$$d = d_b \quad [-] = \text{depth at which the wave breaks}$$

Section 10.3 "Shallows: breaking" mentions the following about breaking:

Theoretically the wave breaks at a steepness of $H/L = 1/7$. The depth also limits the wave height. It has been theoretically deduced that an individual wave will break when $\frac{H}{d} \geq 0,78$ (there are also more complex formulas e.g. by Miche). However, individual waves with a ratio of $\frac{H}{d} = 1,2$ have been observed.

When calculating breaking for a wave spectrum:

$$\frac{H_s}{d} = 0,4 \sim 0,5$$

16. Ice

extended with design rules: February 2015; improved: February 2017

One distinguishes four ways in which ice can exert a load on a hydraulic engineering work. These are:

- Thermal expansion.
- Ice accumulation.
- Collision.
- Ice attachment.

16.1 Thermal expansion

During the freezing process of a layer of ice on water, the thickness of the ice increases without an increase of the ice area. There is hardly any expansion perpendicular to the direction of growth of the ice. Therefore, the freezing process itself does not generate any loads.

After the freezing process, changes of the ice temperature can cause loads. This thermal expansion of the ice can sometimes cause static horizontal loads. This only applies if the ice is restricted in its expansion. Examples of this are the forces on structures on the banks of frozen lakes and the forces on the piles of berths as a result of the expansion of the ice between the piles.

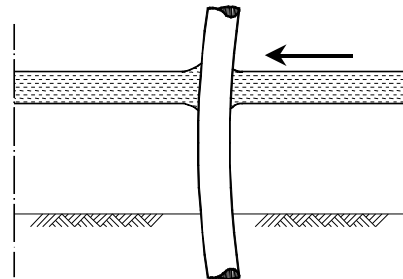


Figure 16-1 Thermal expansion

The thermal expansion of ice is comparable to the temperature load as described in Chapter 17 "Temperature". On average, the coefficient of thermal expansion is about $\alpha = 5,5 \cdot 10^{-5} \text{ }^\circ\text{C}^{-1}$.

The expansion causes stresses both in the structure loaded by the ice and in the ice itself. These stresses create equilibrium in the interface between the structure and the ice. The upper limit of these stresses is the yield stress of the structure or of the ice.

The yield stress of the ice largely depends on the density and the composition of the ice. The salinity (salt concentration), the extent of water pollution and the temperature are hence important factors involved. It is therefore not possible to give a general yield stress of ice. It is very much linked to the location where the ice was formed and also the temperature history of the ice.

Research into the yield stress of ice has been carried out in several different locations. The yield stress varies between 20 and 300 kN/m². The large spread of the values of the strength show that knowledge of the local ice strength is of large importance.

An important phenomenon associated with thermal expansion is the buckling of the ice surface in places where the ice shows irregularities. Thus, a completely new situation is created with respect to thermal expansion.

16.2 Ice accumulation

As a result of a slight current, ice can accumulate against a structure. A current beneath the ice causes a shear force along the ice, which is in equilibrium with forces on the structure. Due to the accumulation of ice against the structure in slowly flowing water, a static horizontal load is created.

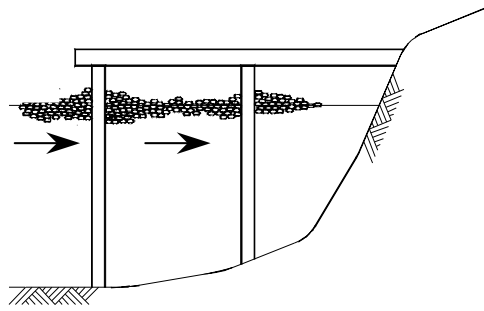


Figure 16-2 Accumulation of ice

16.3 Collision

The dynamic horizontal load on a structure is caused by colliding blocks of ice, which were carried along by the wind and the current. This is particularly of importance for structures in rivers and along coasts with a considerable current.

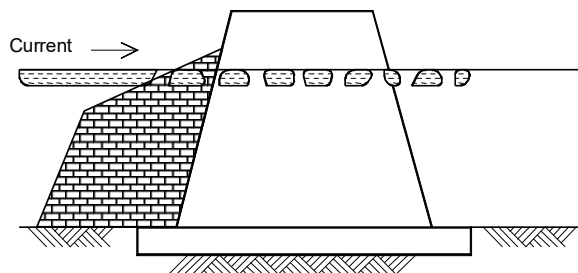


Figure 16-3 Collision of ice floes and breaking on an ice breaker

The impact of large ice sheets that collide against a structure can be compared with the impact of ships that run into a structure. The fact that the mass and particularly the velocity of the colliding ice sheet determine the load on a structure follows from the equations in Chapter 23 "Shipping, berthing". Here, too, the stresses are in equilibrium in the interface between the structure and the ice. If the maximum yield stress of the ice is exceeded, it will collapse. It is known that the stresses are maximal in the outer fibres, as a result of bending. Therefore, collapse of the ice takes place sooner in a case of bending than in case of a uniformly distributed normal force. This knowledge can be used to reduce or prevent forces on structures. An angled slope or an oblique edge in front of a structure can make the ice buckle and thus prevents the ice sheet from sliding into the structure.

16.4 Ice attachment

The static vertical load on a structure as a result of the attachment of ice onto a structure is of particular importance when water levels vary. Ice attachment can occur anywhere between the high and the low water levels. Under water this mass causes an upward force and above water it results in a downward load on the structure.

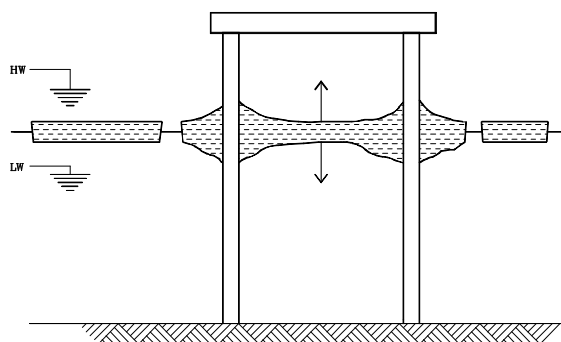


Figure 16-4 Ice attachment

16.5 Design rules

It should be judged per situation whether ice loading is relevant for the design of hydraulic structures. For example, there can be ice loading from frozen surface water acting on a quay wall, but at the same time the ground water on the other side of the wall can be frozen too, mainly or partly eliminating the outer ice load.

The Dutch Guidelines Design Hydraulic Structures (*Richtlijnen Ontwerp Kunstwerken, ROK, 2013*) of Rijkswaterstaat prescribe an ice load of 400 kN/m¹ on the walls of lock chambers, at the expected water level during ice conditions. ROK also specifies the directions and locations of ice loads on gates:

- For thermal expansion: in length direction of lock chambers, 0,20 m below the upstream water level;
- For accumulating ice: perpendicular to gates, at upstream water level;
- For attached ice: in vertical direction, equally distributed over horizontal beams (*regels*) that are located under water.

16.5.1 General design rules for determining horizontal ice loads

The Dutch Manual Sheetpile Walls (*Handboek Damwandconstructies, CUR-publication 166*⁶) states that in most cases, ice loads will appear not to be critical for the design of sheet pile walls. For retaining walls adjacent to open water, the combination of ice load, ship impact and wave load should not be considered. Either the ice load or the combination of ship impact and wave load is governing. For the estimation of horizontal ice loads on sheetpile walls, it can generally be assumed that the ice layer has a thickness of 0,50 m and a compressive strength of 1,5 MPa for sea water and 2,5 MPa for fresh water. Because this load will vary over the contact surface from 0 to the compressive strength of ice, a levelling coefficient of 0,33 may be applied. This leads to the following design values for corresponding line loads, acting at the most unfavourable water level: 250 kN/m for sea water and 400 kN/m for fresh water (corresponding with the value mentioned in the ROK).

For the strength calculation of structural members also a concentrated load of 1500 kN should be considered according to CUR 166, if ice could affect these members⁷. In intertidal areas, where ice floes (*schotsen*) can origin, a horizontal line load of 100 kN/m can be used and possibly also vertical loads (not quantified in CUR 166, but below there a design rule is given).

The Ice Handbook for Engineers gives the following equation for static ice load:

$$F_{static} = k_c \cdot \sigma_c \cdot D \cdot h$$

where	F_{static} [kN]	= static ice load
	k_c [-]	= degree of confinement (<i>opsluiting</i>) of the ice in front of the structure, varying from 1 to 3
	σ_c [kN/m ²]	= average uniaxial compressive strength of the total ice thickness
	D [m]	= width of the structure
	h [m]	= ice thickness

⁶ Reference is made to Section 3.2.5 of part 2 of the 5th edition of this publication.

⁷ This seems a very high value, so for the dimensioning of specific structural members one should judge whether situations can occur that can indeed inflict such a force.

16.5.2 Horizontal loads caused by thermal expansion of ice

According to Korzhavin (1962), if an ice cover is prevented from expanding (e.g. ice between two bridge piers) ice will exert a maximal horizontal linear load of:

$$F_{\max} = 54,13 \cdot \psi \cdot \frac{h^2}{h + 9,1 \cdot h_s} \cdot \frac{(0,35 \cdot T_i + 1)^{5/3}}{T_i^{0,22}} \cdot \left(\frac{\Delta T_i}{\Delta t} \right)^{1/3}$$

where:

F_{\max}	[kN/m]	= maximum force per running metre of ice cover (linear loading)
h	[m]	= ice thickness
h_s	[m]	= thickness of snow layer on the ice
T_i	[°C]	= average air temperature of the previous 24 hours
ΔT_i	[°C]	= maximum rise in air temperature within a given period Δt within the preceding 24 hours
Δt	[h]	= period during which the temperature is rising
ψ	[-]	= coefficient to include the effect of the length (L) of the ice-cover: $\psi = 1,0$ for $L < 50$ m $\psi = 0,9$ for $50 < L < 75$ m $\psi = 0,8$ for $75 < L < 100$ m $\psi = 0,7$ for $100 < L < 150$ m $\psi = 0,6$ for $L > 150$ m

CUR 166 mentions line loads coming from thermal expansion of enclosed ice. The magnitude of these loads depends on the initial temperature of the ice, the temperature gradient and the thickness of the ice [m], see Figure 16-5.

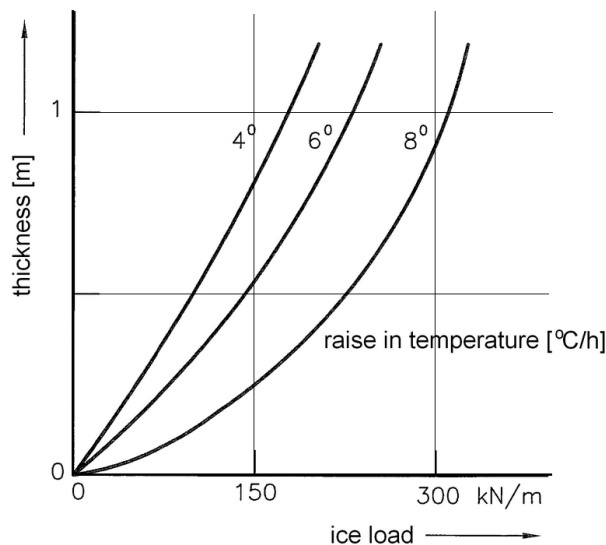


Figure 16-5 Loads caused by thermal expansion of ice (CUR 166)

It should additionally be checked whether this force F_{\max} does not exceed the failure compressive strength of the ice (see below for the compressive strength of ice).

16.5.3 Compressive strength of ice

The German manual on quay walls, the *Empfehlungen des Arbeitsausschusses "Ufereinfassungen"* (EAU, 2012) gives rules to calculate the compressive strength of ice and measured maximum thickness of ice layers (in Germany, varying from 0,35 to 0,80 m).

According to the EAU 2012, concentrated ice loads on vertical piles can be calculated with:

$$P_p = k \cdot \sigma_0 \cdot \sqrt{d} \cdot h^{1,1}$$

where: P_p [kN] = concentrated ice load (force)
 σ_0 [kN/m²] = uniaxial compressive strength of ice related to a specific expansion rate $\varepsilon = 0,001 \text{ s}^{-1}$
 d [m] = width of the pile
 h [m] = thickness of the ice
 k [m^{0,4}] = empirical coefficient; for floating ice: $k = 0,564$; for ice frozen onto the pile: $k = 0,793$

The horizontal uniaxial compressive strength of ice, σ_0 , can be calculated according to empirical equations as found by Austin Kovacs (1996) (adopted by the EAU 2012):

$$\sigma_0 = \frac{2,7 \cdot 10^6 \cdot \varepsilon^{0,33}}{\varphi_B}$$

and

$$\varphi_B = 19,37 + 36,18 \cdot S_B^{0,91} \cdot |g_m|^{-0,69}$$

where σ_0 [kN/m²] = uniaxial compressive strength of ice
 φ_B [m‰] = porosity of the ice layer
 ε [s⁻¹] = specific expansion rate = 0,001 s⁻¹
 S_B [m‰] = salinity of the ice
 (usual values are: < 1 ‰ for fresh water, and 35 ‰ for sea water)
 g_m [°C] = temperature in the middle of the ice layer

16.5.4 Vertical ice loads

Vertical loads on single piles due to attached ice on rising or falling water levels can be calculated according to the Russian national standard SNiP 2.06.04.82 (1995):

$$A_V = \left(0,6 + \frac{0,15 \cdot D}{h} \right) \cdot 0,4 \cdot \sigma_0 \cdot h^2$$

where: A_V [kN] = vertical ice load on a pile
 h [m] = thickness of the ice layer
 D [m] = diagonal of the pile
 σ_0 [kN/m²] = compressive strength of the ice layer

For piles being part of a pile group, or piles next to fixed structures, a geometrical reduction factor f_g may be applied to A_V (see the EAU or SNiP for details).

16.6 Literature

- CUR 166: Handboek Damwandconstructies, CUR, 2012
- EAU, Empfehlungen des Arbeitsausschusses "Ufereinfassungen", Springer Verlag, 2012
- Ice handbook for engineers, version 1.2. Luleå Tekniska Universitet - Institutionen för samhällsbyggnad. Luleå, 2009
- Korzhavin, K.N. Action of ice on engineering structures, Novosibirsk, Akad. Nauk. USSR 1962. (Translation: TL 260 of CRREL Hanover, New Hampshire, 1971)
- ROK, Richtlijnen voor het Ontwerp van Kunstwerken. Rijkswaterstaat 2013
- SNiP 2.06.04.82 Наррузки и воздействия на гидротехнические сооружения (волновые, ледовые и от судов). Russian standard 'Loads and actions on hydraulic engineering structures (wave and ice generated and from ships). Moscow, 1995.

17. Temperature

17.1 General

Temperature changes of structures and parts of structures usually lead to deformations and stresses. The cause of the temperature change can be both internal and external. Examples of external causes are:

- accumulation of warmth due to solar rays (daytime)
- loss of heat due to warmth emission (night time)
- adaptation to a changing air temperature
- cooling due to wind
- cooling due to precipitation
- cooling due to the evaporation of water in or on the structure
- warming or cooling due to activities in the structure (heating, air conditioning)

An internal cause of temperature change is the development of heat during the setting and hardening of concrete (hydration heat).

The temperature spread in a cross section of a structure element depends on the heat flow through the element. Some examples of possible temperature profiles are shown in Figure 17-1.

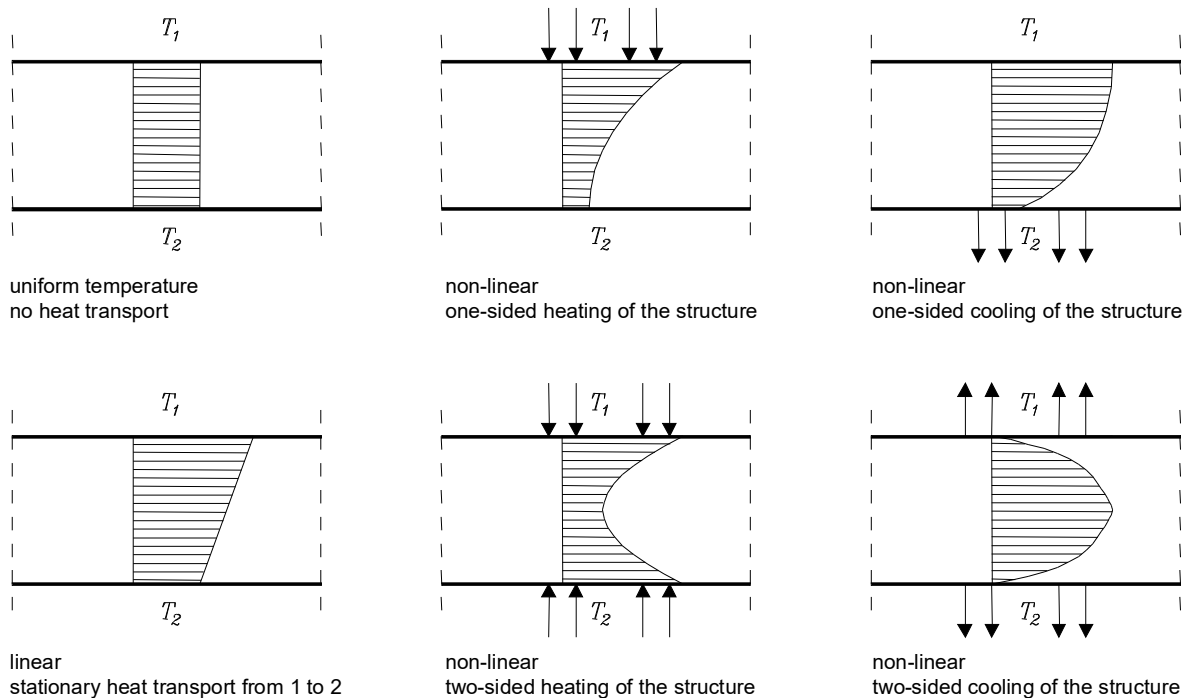


Figure 17-1 Temperature profiles

17.2 Unobstructed thermal deformation

17.2.1 Temperature change

When the temperature of an unobstructed object changes its length increases or decreases linearly according to:

$$\varepsilon = \frac{\Delta \ell}{\ell} = \alpha \Delta T$$

in which: ε [-] = the strain (*rek*)
 $\Delta \ell$ [m] = the change in length
 ℓ [m] = the length at the reference temperature
 α [°C⁻¹] = the linear expansion coefficient
 ΔT [°C] = the change in temperature

The linear expansion coefficients of a number of materials are given below:

Concrete	$1,0 \cdot 10^{-5} \text{ } ^\circ\text{C}^{-1}$
Steel	$1,2 \cdot 10^{-5} \text{ } ^\circ\text{C}^{-1}$
Ice	$5,5 \cdot 10^{-5} \text{ } ^\circ\text{C}^{-1}$

Table 17-1 Linear coefficients of expansion

It is noticeable that the linear expansion coefficients of concrete and steel are almost equal. This is useful because otherwise temperature fluctuations in reinforced concrete would create more problems. Figure 17-2 shows an example of the elongation of a simple beam due to a temperature increase. The shape of the beam is not relevant for the linear expansion.



Figure 17-2 Increase in the length of a beam due to a total rise in temperature

After a temperature change, one can determine the position of all points on an arbitrary object relative to a fixed point because the shape of an object is not of importance. An example is given in Figure 17-3.

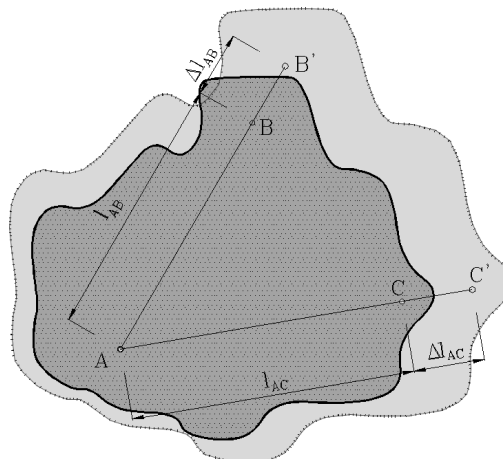


Figure 17-3 Change of the area of a sheet due to a total rise in temperature

17.2.2 Temperature gradient

The preceding applies for a total temperature change (of the entire body). However, it is also possible that a temperature gradient occurs in the body. Figure 17-4 shows an example of this. There is a temperature rise on the underside and a temperature decrease on top. The consequence is a shortening on the upper side and a lengthening at the bottom of the beam, causing a curvature of the beam.

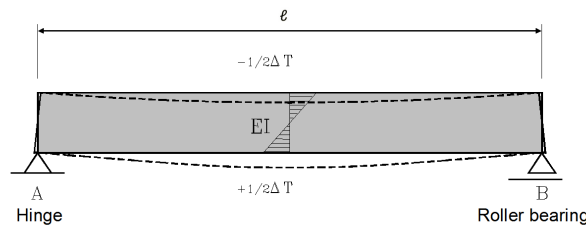


Figure 17-4 Temperature gradient in a beam

The curvature of the beam is equal in all places along the beam and amounts to:

$$\kappa = \frac{\varepsilon_b - \varepsilon_o}{h} = -\frac{\alpha \Delta T}{h}$$

The angle of rotation of the beam is found by integrating the curvature over the length:

$$\varphi_B = \varphi_A + \int_0^x \kappa dx = \varphi_A + \kappa x$$

The deflection is found by integrating the angle of rotation:

$$f_x = \int_0^x \left(\varphi_A + \int_0^x \kappa dx \right) dx = \varphi_A x + \frac{1}{2} \kappa x^2$$

Using the boundary conditions at the two supports one finds:

$$\varphi_A = -\frac{1}{2} \kappa l = \frac{\alpha \Delta T l}{2h}$$

The deflection in the middle is therefore:

$$f_m = -\frac{1}{4} \kappa l^2 + \frac{1}{8} \kappa l^2 = -\frac{1}{8} \kappa l^2 = \frac{\alpha \Delta T l^2}{8h}$$

In the case of a plate instead of a beam, the deflection must be considered in two directions. If the plate can deform unrestrainedly, it will rest on the corners if it bulges out.

For a temperature change of the beam, in which the temperature change is in the same direction both on top and in the bottom, one can distinguish an average temperature change and a temperature gradient. The change in length and the deflection can be calculated using the equations derived for the deformations.

The preceding, assumed a linear course of the temperature over the height of the structure. In reality, the course of the temperature is often not linear but curved. In such a case, the temperature course is divided into an average temperature, a linear temperature gradient and a so-called characteristic temperature. The linear temperature gradient is chosen such that the remaining characteristic temperature does not cause any deformations. An example is given in Figure 17-5. As regards the characteristic temperature, the following applies:

$$\int_0^h (T_e - T_0) dz = 0 \quad \text{and} \quad \int_0^h (T_e - T_0) z dz = 0$$

in which: h [m] = height of the structure
 T_e [°C] = characteristic temperature
 T_0 [°C] = reference temperature

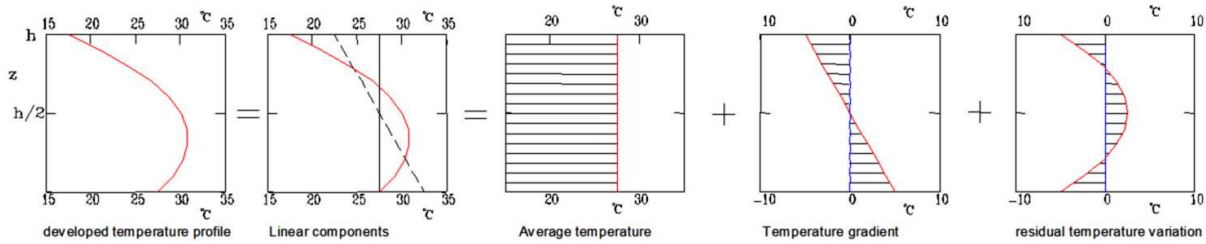


Figure 17-5 Arbitrary temperature distribution

The characteristic temperature does not cause any resulting deformations, but it does cause stresses. For a construction material such as concrete, one must take these stresses into account. This is of particular importance for the two-sided cooling of a thick structure during and after the setting of the concrete (hydration heat), causing tensile stress in the concrete.

17.3 Restrained thermal deformation

17.3.1 Temperature change

If the deformations of a structure due to temperature changes can take place without restraints, no stresses occur in the material. Generally, however, the deformation is restrained. This is usually the result of the boundary conditions of the supports, which in turn are determined by possible adjoining structure elements and the surroundings. As an example, consider a structure buried in the ground. In the case of restrained deformation, the total deformation equals the unrestrained temperature deformation minus the deformation resulting from the stress increase.

The restriction of the linear expansion of a beam can be schematised as a beam with a spring in the roller bearing (see Figure 17-6).

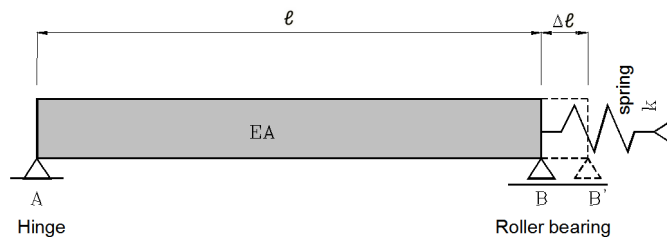


Figure 17-6 Restrained deformation due to temperature change

The elongation of the beam results in a force in the spring equal to:

$$F = k \Delta l$$

where: k [kN/m] = the stiffness of the spring

The occurring deformation is equal to the unrestrained temperature deformation minus the linear elastic deformation:

$$\Delta l = \alpha \Delta T \ell - \frac{F \ell}{EA}$$

This leads to the force F :

$$\frac{F}{k} = \alpha \Delta T \ell - \frac{F \ell}{EA} \Rightarrow F = \frac{\alpha \Delta T \ell}{\frac{1}{k} + \frac{\ell}{EA}}$$

If $k = EA$, 50% of the unrestrained deformation occurs. If $k > 100 \cdot EA$, a fully restrained deformation is involved.

17.3.2 Temperature gradient

The restraint of the rotation of a beam due to the supports can be schematised by a rotation spring (see Figure 17-7). The moment in the bearing then equals $M = c \cdot \varphi$

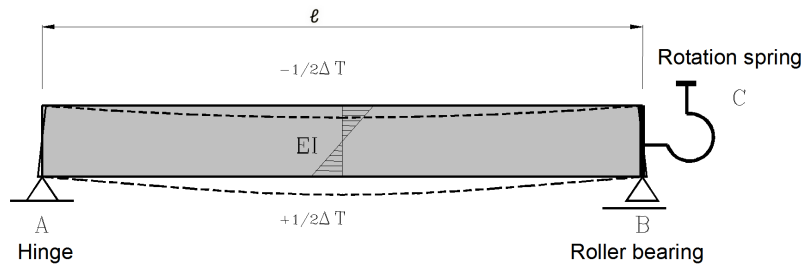


Figure 17-7 Restrained rotation

The rotation in the bearing equals the unrestrained temperature deformation minus the linear elastic deformation:

$$\varphi = \frac{\alpha \Delta T \ell}{2h} - \frac{M \ell}{3EI}$$

where: α [$^{\circ}\text{C}^{-1}$] = linear expansion coefficient
 h [m] = height of the beam

The moment is therefore:

$$\frac{M}{c} = \frac{\alpha \Delta T \ell}{2h} - \frac{M \ell}{3EI} \Rightarrow M = \frac{\alpha \Delta T \ell}{2h \left(\frac{1}{c} + \frac{\ell}{3EI} \right)}$$

17.3.3 Longitudinal direction

If the deformations of a plate are restrained, one must take the deformation in all directions into account. Close to the supports of the plate, where the deformation is restrained, shrinkage can cause a considerable tensile stress. This tensile stress is parallel to the supports. This is why concrete slabs should contain sufficient reinforcement in the direction perpendicular to the span (longitudinal reinforcement). The tensile stress will propagate further into the field as the slab is wider (see Figure 23-8).

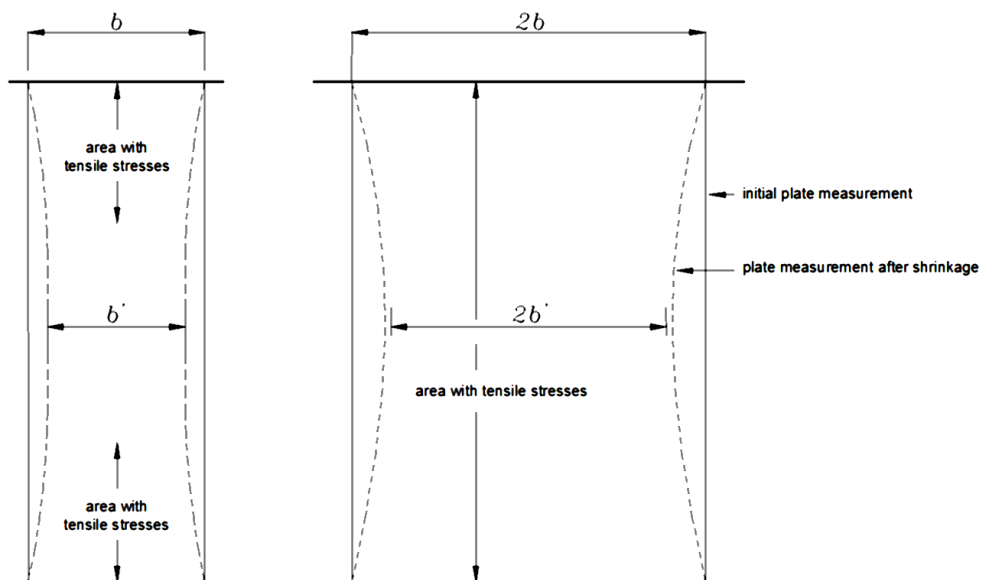


Figure 17-8 Effect of the width of a slab

Note

For compound structures one has to take in account that different temperatures create different expansions. For example, an oil pipe with warm oil on a (cold) jetty needs an expansion loop.

18. Soil - loading and stresses

The effective soil stress is often the most important load on a structure, next to water pressure. After all, the effective soil stress is the only load on the entire structure that adjusts itself (up to a certain point) to the other loads: It resists the forces acting on the soil, creating equilibrium. Unless the ground collapses (actively or passively), the ground pushes back, both in normal direction and in shear direction, as much as the structure pushes the ground.

The effective stress load caused by the loads on the structure is calculated by calculating all other loads and considering the effective stress as the *balancing item*. One should not forget to check whether this load will ever exceed the maximum compression stress and the maximum shear stress of the soil during any construction or operational phases. For the maximum soliciting stresses, see Chapter 31 and for the bearing capacity of the soil see Chapter 26.

One must also remember to check that this load never causes the maximum displacement (and particularly the displacement difference) to be exceeded during any construction or operational phases.

If the maximum forces or displacements are likely to be exceeded, the design of the structure should be adjusted. The calculations of the loads then start anew and the design is therefore an iterative process.

This chapter describes the distribution of loads in soil in vertical and horizontal direction. The resistance, or strength, of soil against loads is described in Chapter 26.

18.1 Vertical soil stress

18.1.1 General

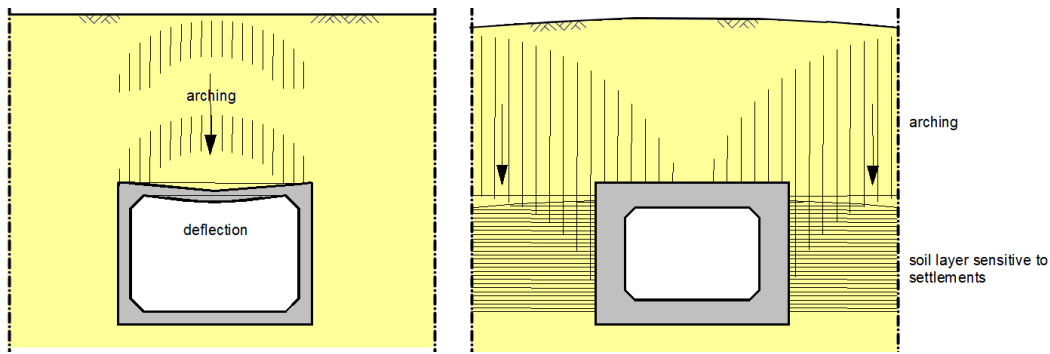
The exception to the rule given above, which states that the effective pressure can only be calculated as a balancing item of the other loads, is the vertical effective pressure on top of a structure. The vertical loads occur on horizontal and diagonal planes of structures in the ground, e.g. cellars and tunnels. The total load corresponds to the weight of the ground. One has to divide total stresses into inter-granular stresses and water pressures (see Chapter 21 "Soil, groundwater").

The vertical effective pressure (load) for a soil system with n dry layers and m wet layers can be determined according to:

$$\sigma_v' = \sigma_v - p \quad \text{i.e.:} \quad \sigma_v' = \sum_{i=1}^n \gamma_{d,i} d_i + \sum_{j=1}^m \gamma_{n,j} d_j - p$$

in which:	σ_v'	[kN/m ²]	= vertical inter-granular stress (= effective pressure)
	σ_v	[kN/m ²]	= total vertical stress
	$\gamma_{d,i}$	[kN/m ³]	= dry volumetric weight of soil layer i : $\gamma_{d,i} = \rho_{d,i}g$
	$\gamma_{n,j}$	[kN/m ³]	= wet volumetric weight of soil layer j : $\gamma_{n,j} = \rho_{n,j}g$
	σ	[kg/m ³]	= volumetric mass of a soil layer
	d_i	[m]	= thickness of soil layer i above the considered plane
	n	[-]	= number of dry layers above the considered plane
	m	[-]	= number of wet layers above the considered plane
	p	[kN/m ²]	= water pressure in the considered plane

The interaction between the structure and the ground is different from the interaction between the structure and the groundwater. The groundwater does not have any shear stiffness and the groundwater pressures do not depend on possible deformations of the structure. This is different for the soil. In soil it is possible that deformations of a structure or the surrounding ground cause a redistribution of the total stresses. For instance, in a tunnel of limited dimensions arching can occur in transverse direction, thereby more or less relieving the roof of the tunnel of stresses. A stiff structure can also be subjected to a larger load if there are settlements of the surrounding ground, because the surrounding ground is "suspended" from the structure.

Figure 18-1 Arching (Left $K_a < 1$, right $K_p > 1$)

18.1.2 Pressure under a structure / surcharge

Loads on ground level result in a change of the stresses in the subsoil. The horizontal and vertical earth pressures on a structure will consequently increase. There are various models to calculate the increase of the earth pressure as a result of a load on ground level. The best known are models by Boussinesq, Flamant and Newmark. For these methods the reader is referred to the lecture notes Soil Mechanics (Verruijt and Van Baars).

The ratio between the stiffness of the structure and the stiffness of the soil has an important influence on the soil pressure distribution under the structure. There are several models or schematisations in use for soil stiffness. Depending on the model, the influence on soil pressure distribution, especially the spreading of pressure, is either less or more significant, see below in this section under 'stress distribution'. Generally, the Winkler model is used for soil stiffness, which models the soil as a system of mutually independent vertical springs with stiffness k .

Considering the stiffness ratio soil-structure, an extreme case is to assume an infinitely stiff structure. This assumption implies that the foundation surface remains level. In combination with the Winkler soil stiffness model the calculation of the soil pressure distribution is analogous to the calculation of a cross-section of a beam with normal and shear forces, and bending moments (For a foundation ΣV and ΣH are the equivalent of normal and shear force respectively; the resulting overturning moment ΣM is the equivalent of the bending moment). Therefore the stress in point (x,y) under an infinitely stiff structure, the whole contact surface remains under pressure, is:

$$\sigma_{x,y} = \frac{V}{A} + \frac{M_y}{I_y} x + \frac{M_x}{I_x} y$$

- in which:
- I_y = the moment of inertia of the foundation around the y -axis
 - I_x = the moment of inertia of the foundation around the x -axis
 - A = the area of the foundation = $b \cdot h$
 - V = the vertical load
 - M_y = moment in y direction relative to the centre of mass of the foundation
 $M_y = V \cdot e_x$
 - M_x = moment in x direction relative to the centre of mass of the foundation
 $M_x = V \cdot e_y$

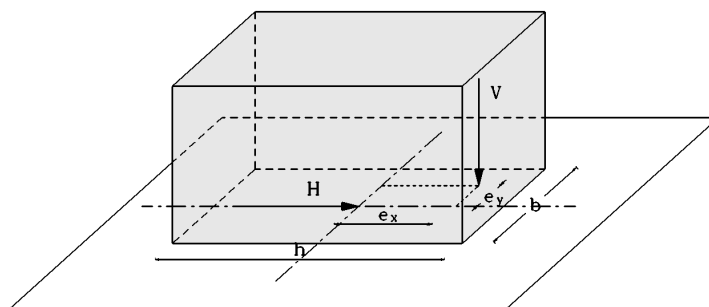


Figure 18-2 Stiff structure on a shallow foundation

Since the entire foundation surface remains under pressure, the working line of the resulting force lies within the core of the foundation surface. The dimensions of the core of the surface can easily be determined using:

$$e_b = \frac{W_b}{A} ; e_o = \frac{W_o}{A} ; e_l = \frac{W_l}{A} ; e_r = \frac{W_r}{A}$$

in which: e_b, e_o, e_l, e_r : dimensions of the core according to Figure 18-3.

$$W_b = \text{section modulus } \frac{I_x}{y_b} \qquad W_l = \text{section modulus } \frac{I_y}{x_l}$$

$$W_o = \text{section modulus } \frac{I_x}{y_o} \qquad W_r = \text{section modulus } \frac{I_y}{x_r}$$

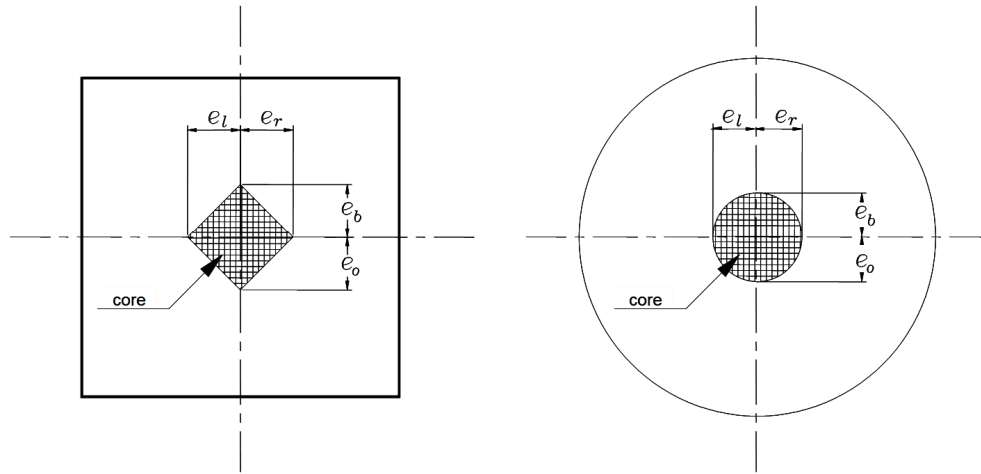
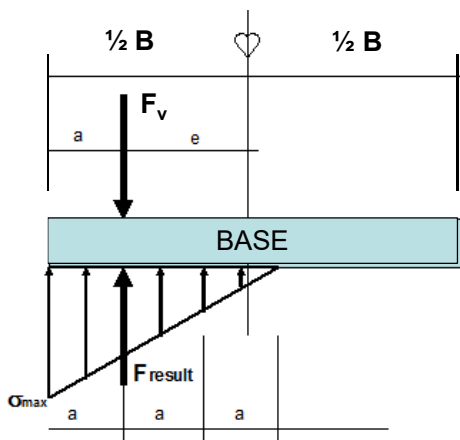


Figure 18-3 The cores of a square and a circular cross-section

If the resultant of the loads lies outside the core of the foundation surface, the previous equations for the stresses in the foundation plane do not apply.

Large eccentricities, the resulting force has a working line outside the core of the foundation surface, considerably complicate the calculation of soil pressure distributions under the foundation.

A well-known solution for a rectangular foundation assumes a triangular soil pressure distribution for the part of the base that remains in contact with the soil. For equilibrium of forces ($\Sigma V = \Sigma H = \Sigma M = 0$) the working line of the resultant of the soil pressure should be the same line as the one for the resultant of the loads. Using the position of the centre of gravity for a triangle, one-third of the base, the maximum (required) soil pressure can be determined easily (see Figure 18-4).



$$F_v = F_{result} = \frac{1}{2} \cdot \sigma'_{max,soil} \cdot 3a \quad \Rightarrow$$

$$\sigma'_{max,soil} = \frac{2 \cdot F_v}{3a}$$

Figure 18-4 Pressures in the case of a very eccentric load

If the structure is not infinitely stiff relative to the soil, use of the Winkler model for the soil stiffness only yields approximate results. For finite stiffness of the structure, relative to the soil stiffness, the way to determine the soil pressure distribution more accurately is to use the theories on elastic or elasto-plastic half spaces. Reference is made to the work of Hetenyi – “Beams on elastic foundation” (1946).

Vertical stress distribution under a structure or top load

A stress at ground level will spread in depth due to the shear stresses in the soil. The course of the stresses was solved by Flamant. The spread of the stress somewhat resembles a Gaussian curve. Because this is difficult in calculations, for a preliminary design one can spread the stress under an angle of 1:1 for stiff soil layers (as shown in the figure below), 2:1 (vertical : horizontal) for medium stiff layers and 1:2 (vertical : horizontal) for stony materials and granulates (Figure 18-5).

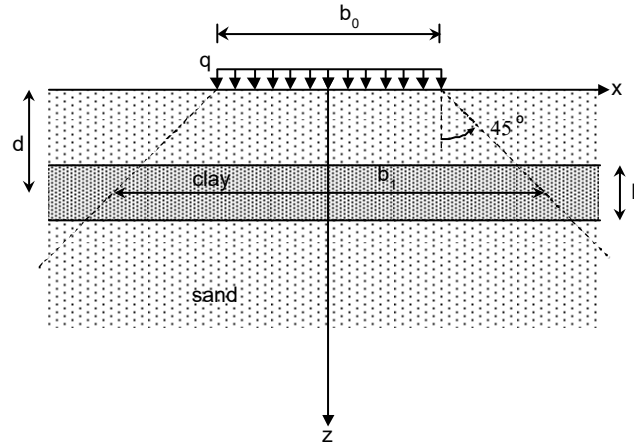


Figure 18-5 Simplified stress spread in depth

The contributing width b_1 and length l_1 in case of a spread of 1:1 then are:

$$b_1 = b_0 + 2d \quad \text{and:} \quad l_1 = l_0 + 2d$$

The average increase in stress in the clay layer due to the load is then:

$$\Delta \bar{\sigma}' = \frac{b_0 l_0}{b_1 l_1} q$$

The strain in the clay layer is subsequently calculated with: $\Delta \sigma' = E_{oed} \Delta \varepsilon$ (Hooke) or, even better, with the theory developed by Koppejan.

The total settlement u then follows from:

$$u = h \Delta \varepsilon$$

Note

- Computer programmes are faster at calculations than man and therefore do not use this simplified stress spreading method, but methods such as Flamant.

Flamant's solution is based on one of Boussinesq's solutions (point force on an infinite half space⁸); which is why computer programmes often state the stress spreading method is based on Boussinesq. Flamant (1892) found a solution for the stresses in an infinite half-space subjected to a line load (Figure 18-6). On the basis of superposition, this solution can be transformed to a solution for a strip-shaped load.

⁸ A half-space is either of the two parts into which a plane divides the three-dimensional (Euclidean) space

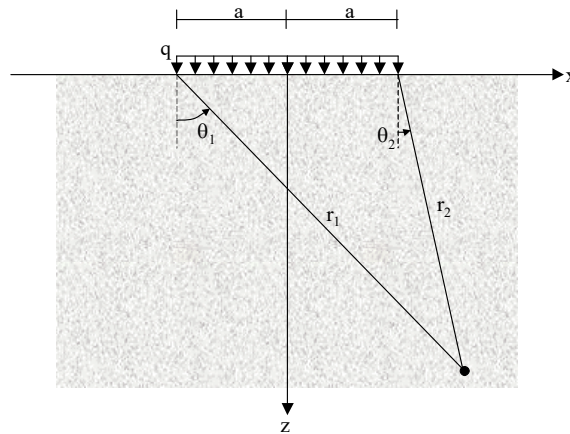


Figure 18-6 Strip load (Flamant)

The stresses in an arbitrary point in this homogenous half-space are:

$$\sigma'_{zz} = \frac{q_v}{\pi} [(\theta_1 - \theta_2) + \sin \theta_1 \cos \theta_1 - \sin \theta_2 \cos \theta_2]$$

$$\sigma'_{xx} = \frac{q_v}{\pi} [(\theta_1 - \theta_2) - \sin \theta_1 \cos \theta_1 + \sin \theta_2 \cos \theta_2]$$

$$\sigma'_{xz} = \frac{q_v}{\pi} [\cos^2 \theta_2 - \cos^2 \theta_1]$$

18.2 Horizontal soil stress

When determining the total horizontal soil stress acting on a structure, the (ground)water pressure (p) and the effective vertical soil pressure (σ') should be considered separately:

$$\sigma_{\text{soil},h} = \sigma_h' + p$$

The reason for this is that the magnitude of water pressure at a certain depth is the same in all directions (law of Pascal), but this does not apply to soil pressure:

The horizontal water pressure p at a certain depth is equal (in magnitude, not in direction) to the vertical groundwater pressure at that same depth. It can be calculated according to Section 21.1.

The relation between the horizontal and the vertical effective pressure is usually assumed to be constant:

$$\sigma_h' = K \cdot \sigma_v'$$

There are three types of soil behaviour under stress. The first type occurs when soil is at rest, so when it does not deform due to deflection or sliding aside of a structure. This state of stress is called 'neutral stress'. The second type of soil behaviour under stress occurs when the soil becomes less compacted than at rest, due to, e.g., deflection of a sheetpile wall, or the sliding aside of a gravity structure away from the soil body. This is called 'active soil stress'. The third type of soil stress, the 'passive stress', occurs when the soil is compressed due to movement of a wall in the direction of the soil.

Bear in mind that if the soil retaining structure cannot deform or displace, or if displacements are not tolerable, neutral stresses should be used in design calculations. If displacements will not or cannot be calculated, it cannot be checked whether these displacements would be acceptable. In that case neutral stresses should be used as well, leading to conservative designs.

The three types of soil behaviour are explained in the following sections.

18.2.1 Neutral soil stress (Jáky's theory)

Hungarian geotechnologist József Jáky studied the relation between vertical and horizontal soil at rest. He assumed a constant relation between the horizontal and the vertical effective soil pressure. The coefficient expressing this relation is unknown and difficult to measure. However, for soil at rest (= without deformation) one often uses Jáky's formula to simplify reality:

$$\sigma'_h = K_0 \cdot \sigma'_v \quad \text{with: } K_0 = 1 - \sin(\phi)$$

where:

σ'_h	[Pa]	=	horizontal soil pressure
σ'_v	[Pa]	=	vertical soil pressure
K_0	[-]	=	neutral soil pressure coefficient
ϕ	[°]	=	angle of internal friction

This formula was first published in 1944 and still seems to be relatively accurate for the limit values. It works well for water ($\phi = 0^\circ$, so $K_0 = 1,0$) and seems to work fairly well for sand ($\phi = 30^\circ$, so $K_0 = 0,5$). This formula is very popular, for want of anything better, but not very scientific. Overloaded soil generally shows a far higher value. However, the accuracy of Jáky's neutral soil pressure coefficient is often disputed, but at least it gives values between 0 and 1, and leads to conservative results, so it is still being used. A study in 2005 even led to the conclusion that it is surprising that the equation is a good representation of the true stress ratio in soils at rest (Michalowski, 2005 Journal of Geotechnical and Geo-environmental engineering ASCE).

Large shallow foundations expand due to temperature changes, so in these cases one must take a larger pressure on the vertical walls into account than predicted by Jáky. In this case:

$$\sigma'_{h,n} = K_0 \cdot \sigma'_v \quad \text{with: } K_0 \approx 1$$

Eurocode 7 also takes the over-consolidation ratio (OCR) into account for the horizontal soil pressure. The over-consolidation ratio is the relation between the original effective vertical soil pressure and the actual effective vertical soil pressure at the same depth. The neutral soil pressure coefficient should then be calculated according to:

$$K_0 = (1 - \sin \phi) \cdot \sqrt{OCR}$$

This equation should not be used for 'very high values of OCR'.

Notes

- *If a structure is sensitive to seasonal temperature changes (resulting in stress increment in the structure), a soil pressure coefficient of $K = 1,0$ should be used under the following two conditions:*
 - *The horizontal effective pressure on the wall of a tunnel or open excavation acts unfavourably;*
 - *The bottom of the structure is wider than 15 m.*
- *For the variable load at ground level next to an open excavation or an excavated building site, an evenly distributed surface load of at least 20 kN/m² or VOSB class 45 should be used.*

18.2.2 Active and passive soil stress (Rankine's theory)

Soil under active stress develops less horizontal soil pressure than soil under passive stress. In principle, the horizontal soil pressure is undetermined; only a lower and an upper limit can be given, corresponding to two types of ground collapse: active or passive deformation. Figure 18-7 shows the various types of soil deformation due to movement of walls or structures.

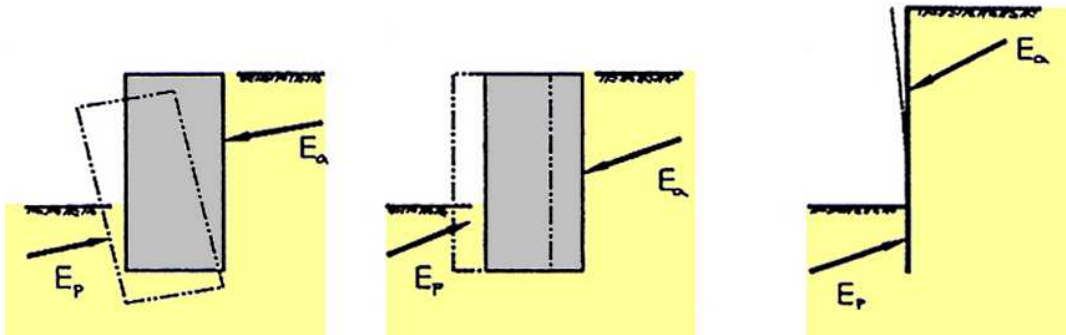


Figure 18-7 Soil deformation due to rotation, displacement or deflection of a wall or structure

Using Mohr's circle, William Rankine, a Scottish civil engineer, found a definition for the maximum and minimum horizontal effective stresses with a given vertical pressure. When a straight wall without shear stress collapses, a straight slip plane develops, see Figure 18-8.

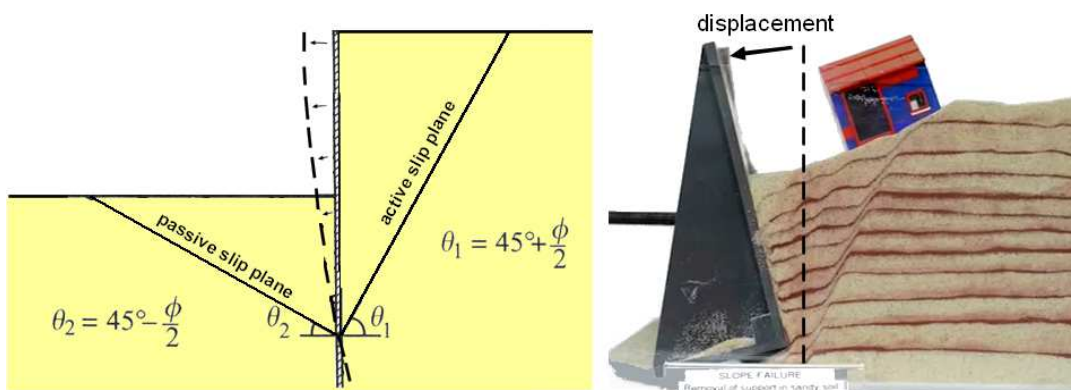


Figure 18-8 Slip planes caused by displacement of a retaining wall (left: theoretical; right: empirical)

According to Rankine (based on Mohr-Coulomb and smooth horizontal walls) the lower and upper pressure limits are as follows:

$$\sigma'_{h,min} = K_a \sigma'_v - 2c\sqrt{K_a} \quad \text{with} \quad K_a = \frac{1 - \sin \phi'}{1 + \sin \phi'} \quad \text{coefficient of active soil pressure [-]}$$

$$\sigma'_{h,max} = K_p \sigma'_v + 2c\sqrt{K_p} \quad \text{with} \quad K_p = \frac{1 + \sin \phi'}{1 - \sin \phi'} \quad \text{coefficient of passive soil pressure [-]}$$

and c = cohesion

If the soil is non-cohesive (like sand), $c = 0$, which simplifies the equation.

The value of the real horizontal effective soil pressure lies somewhere between the maximum and minimum pressure and depends mainly on the horizontal displacement of the wall. The horizontal soil pressure develops gradually between the two limit states, see Figure 18-9.

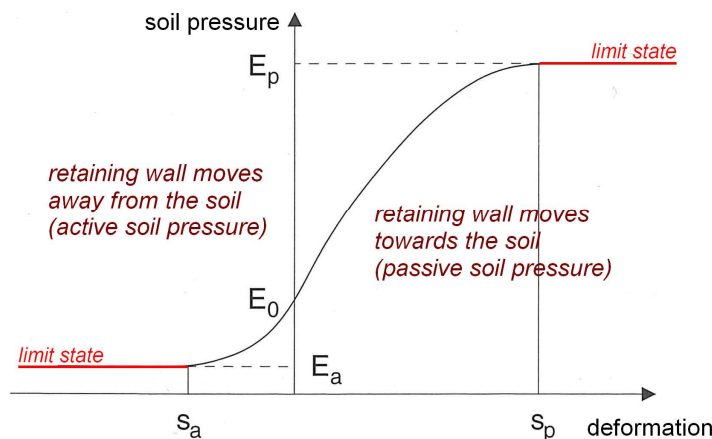


Figure 18-9 Horizontal soil pressure versus deformation of the soil

The horizontal soil pressure can be influenced by cold flow, temperature changes and the loading history. Please bear in mind that in reality, K_p is limited to a maximum value of about 7. More accurate, especially for K_p , are the equations of Fritz Kötter, who assumed curved slip planes. These equations can be found in the user manual of D-Sheetpiling, or in the original publication of Kötter (1903).

18.2.3 Horizontal soil pressure on a vertical wall including friction

To include the effect of friction at the soil/wall interface, the equations for the active and passive soil coefficients can be extended according to Heinrich Müller-Breslau:

$$K_a = \left(\frac{\cos \varphi}{1 + \sqrt{\frac{\sin(\varphi + \delta_a) \cdot \sin \varphi}{\cos \delta_a}}} \right)^2 \quad \text{and} \quad K_p = \left(\frac{\cos \varphi}{1 - \sqrt{\frac{\sin(\varphi - \delta_p) \cdot \sin \varphi}{\cos \delta_p}}} \right)^2,$$

where δ represents the angle of wall friction, normally $\frac{1}{2}\varphi < \delta < \varphi$ and δ_a taken positive and δ_p negative. These equations apply to horizontal ground surfaces and a vertical wall.

18.2.4 Horizontal pressure on an oblique wall (*hellende wand*) and wall friction

If the ground level behind the wall deviates from the horizontal plain with an angle β , the horizontal soil coefficient for soil at rest may be calculated according to Eurocode 7:

$$K_{0,\beta} = K_0 \cdot (1 + \sin \beta)$$

Müller-Breslau found the following equations for active and passive horizontal soil stresses for inclined walls, inclined ground levels and wall friction:

$$K_{a,h,\sigma} = \frac{\cos^2(\phi + \alpha)}{\cos^2(\alpha) \left(1 + \sqrt{\frac{\sin(\phi + \delta) \sin(\phi - \beta)}{\cos(\alpha - \delta) \cos(\alpha + \beta)}} \right)^2}$$

$$K_{p,h,\sigma} = \frac{\cos^2(\phi - \alpha)}{\cos^2(\alpha) \left(1 - \sqrt{\frac{\sin(\phi - \delta) \sin(\phi + \beta)}{\cos(\alpha - \delta) \cos(\alpha + \beta)}} \right)^2}$$

$$K_{a,h,c} = -\frac{2 \cos(\phi) \cos(\beta) (1 - \tan(\alpha) \tan(\beta)) \cos(\alpha - \delta)}{1 + \sin(\phi + \delta - \alpha - \beta)}$$

$$K_{p,h,c} = \frac{2 \cos(\phi) \cos(\beta) (1 - \tan(\alpha) \tan(\beta)) \cos(\alpha - \delta)}{1 - \sin(\phi - \delta + \alpha + \beta)}$$

in which: α = the obliqueness of the structure (see Figure 18-10)

β = the angle of the ground level (see Figure 18-10)

φ = angle of internal friction

δ = the angle between the resultant force exerted on the soil retaining wall and the normal to this wall (see Figure 18-10) (assumption $\delta \approx 0,8$ to $0,9 \cdot \varphi$)

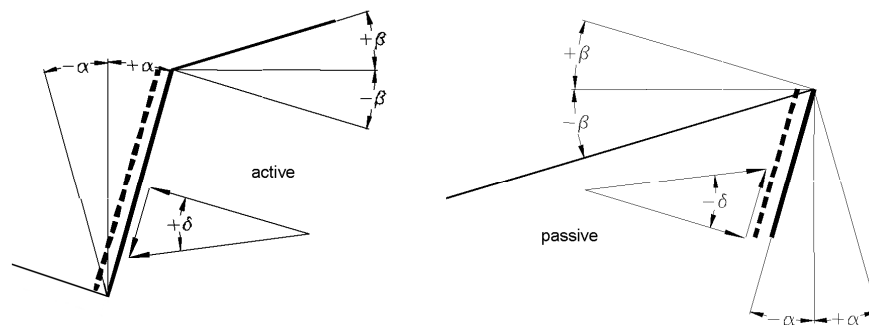


Figure 18-10 Definition of angles (be careful: in some literature these angles are defined differently in combination with also differing equations. The combination leads to the same results, just don't mix up the combination of angle definitions and equations!)

The aforementioned formulas assume straight slip planes. For angles of internal friction (φ) higher than 30° , curved slip planes are more realistic (the theory of curved slip plane is not discussed in this manual). If nevertheless the Müller-Breslau equations are used for these higher values of φ , the resulting values for $K_{p,h,c}$ are unrealistically high. In reality, $K_{p,h,c}$ is limited to a maximum value of about 7. This also applies to the simplified equations.

18.2.5 Horizontal soil pressure an oblique wall, wall friction and cohesion

In case of cohesive soil types, the horizontal soil pressures can be calculated according to:

$$\sigma'_{h,\min} = K_{a,h,\sigma} \sigma'_v + K_{a,h,c} c$$

$$\sigma'_{h,\max} = K_{p,h,\sigma} \sigma'_v + K_{p,h,c} c$$

in which: $K_{a,h,\sigma}$ = active coefficient for the effective stress
 $K_{a,h,c}$ = active coefficient for the cohesion
 $K_{p,h,\sigma}$ = passive coefficient for the effective stress
 $K_{p,h,c}$ = passive coefficient for the cohesion
 c = cohesion

These equations are the most generic form of the horizontal soil pressure coefficients, as they can include (but not necessarily) inclined planes, wall friction and cohesion.

18.2.6 Infinite surface load next to a wall

In the case of a surface load q that reaches infinitely far in two directions, the additional horizontal load on an oblique wall is:

$$\Delta\sigma'_{h,\min} = K_{a,h,\sigma} q \frac{\cos(\alpha)\cos(\beta)}{\cos(\alpha + \beta)} \quad \Delta\sigma'_{h,\max} = K_{p,h,\sigma} q \frac{\cos(\alpha)\cos(\beta)}{\cos(\alpha + \beta)}$$

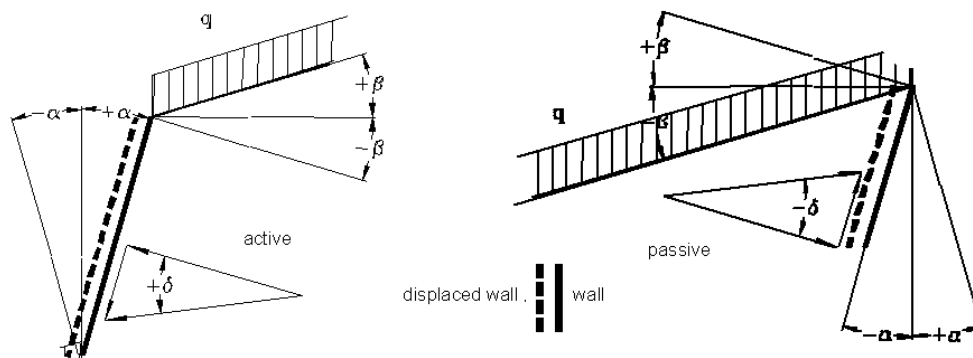


Figure 18-11 Infinitely extended surface load

For vertical walls, where $\alpha = \beta = 0^\circ$, these equations reduce to:

$$\Delta\sigma'_{h,\min} = K_{a,h,\sigma} q \quad \Delta\sigma'_{h,\max} = K_{p,h,\sigma} q$$

18.2.7 Finite surface load next to a wall

If the load is merely exerted on a strip along the side of the soil retaining structure, the horizontal load on the structure is smaller at the bottom of the wall. An approximation of the horizontal load on the soil-retaining structure is given in Figure 18-12. In this case one assumes that the surface loads spreads to a depth b that is determined by the active slip plane that could occur behind the surface load. It is also assumed that the load reduces to zero over a height of $\frac{1}{2}b$.

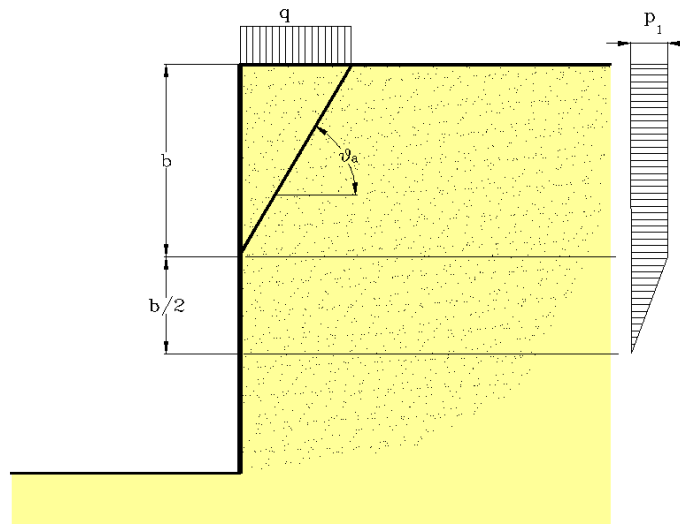


Figure 18-12 Load on a strip next to the soil retaining structure

The influence at a depth b is calculated using angle θ_a for active soil and θ_b for passive soil:

$$\tan \theta_a = \tan \phi + \sqrt{\frac{(1 + \tan^2 \phi) \cdot \tan \phi}{\tan \phi + \tan \delta}} \quad \text{and} \quad \tan \theta_p = -\tan \phi + \sqrt{\frac{(1 + \tan^2 \phi) \cdot (-\tan \phi)}{-\tan \phi + \tan \delta}}$$

By approximation the additional horizontal load $\Delta \sigma'_h$ is $\Delta \sigma'_h = p_1 = q K_{a,h,\sigma}$

18.2.8 Infinite surface load at a distance of a wall

In the case of a very extensive load at some distance from the soil retaining structure, the top of the structure will have a smaller load. An approximation of the horizontal load on the structure is given in Figure 18-13.

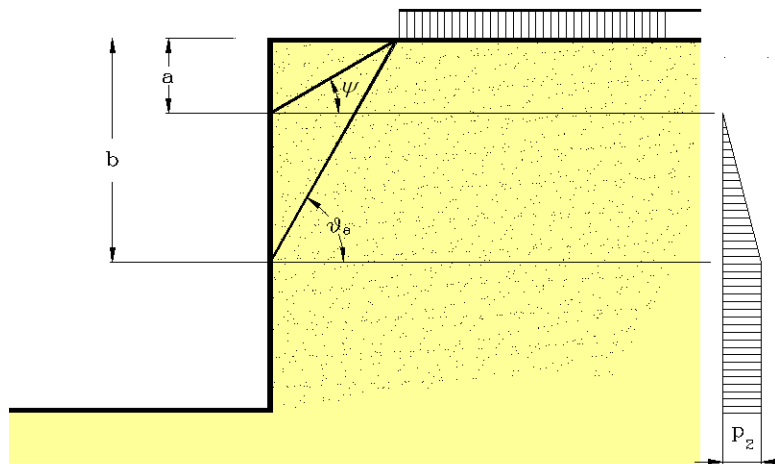


Figure 18-13 Extensive load at a distance from the structure

In this case, too, the maximum horizontal soil pressure is: $p_2 = q K_{a,h,\sigma}$. As a rule-of-thumb, the following angles could be assumed: $\psi = 45^\circ$ and $\theta_a = 45^\circ + \frac{1}{2}\phi$.

18.2.9 Finite surcharge load at a distance of a wall

One can approximate the horizontal load due to a uniformly distributed vertical load at some distance from the soil retaining structure according to Figure 18-14.

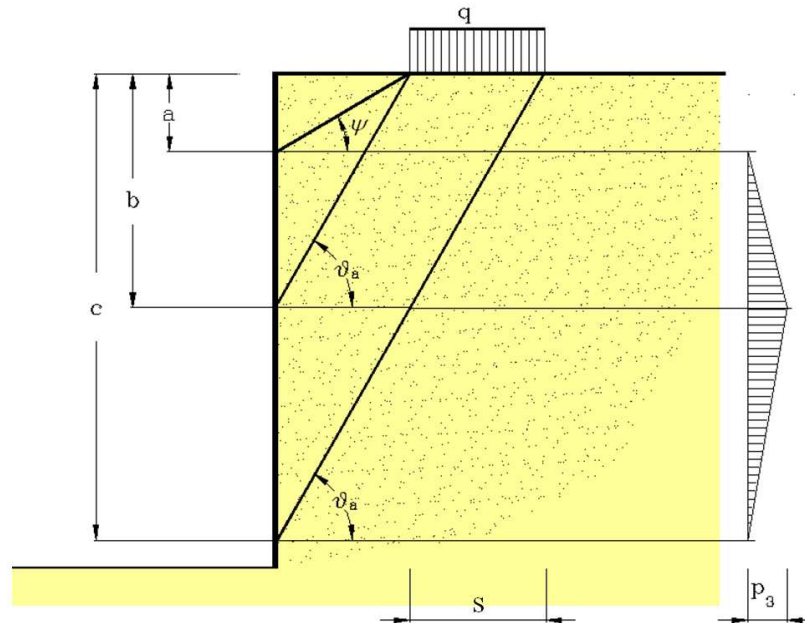


Figure 18-14 Strip load at some distance from the structure

In this case, the maximum horizontal earth pressure caused by the surface load is $p_3 = \frac{2qs\theta}{c-a}$

where: $\theta = \frac{\sin(\vartheta_a - \psi)\cos(\delta)}{\cos(\vartheta_a - \psi - \delta)}$

s = the width of strip on which the load is acting

a, c = see Figure 18-14

δ = the angle between the resultant force exerted on the soil retaining wall and the normal to this wall (see Figure 18-11)

18.2.10 Horizontal stress distribution next to a finite surface load

The stress on a retaining wall next to a surface load at a certain distance of that wall may be assumed to vary over angles of $\pm 45^\circ$, like depicted in Figure 18-15. It gradually decreases further aside, until the retaining wall does not experience any influence of the surface load any more.

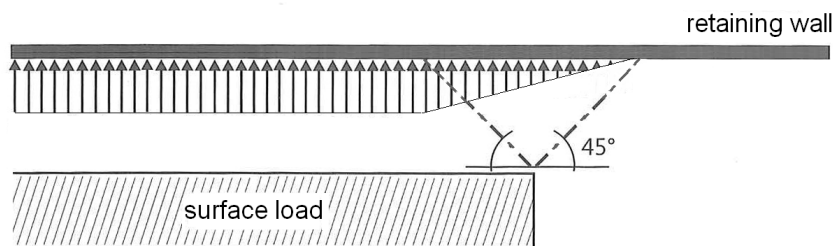


Figure 18-15 Top view of a situation with horizontal stress distribution next to a finite surface load (adapted from EAU 2012)

18.2.11 Horizontal soil pressure on piles

For a three-dimensional situation, as for piles, one can increase K_p and the cohesion to include the effect of shell behaviour. The Danish structural engineer Jørgen Brinch Hansen, who was specialised in soil mechanics, developed one method for this in his book "The ultimate resistance of rigid piles against transversal forces". The 3-D values for the coefficient of passive earth pressure and the cohesion as a result of shell behaviour is included in the computer program D-sheetpiling. The calculation is too complicated to discuss in this Manual.

19. Soil, settlement

Settlements (*zettingen*) occur as a result of raising the effective stresses in the subsoil. For instance, this could be by placing a foundation or by lowering the groundwater level. Settlements as such are usually not a problem for a structure, as long as the settlements are even. Only for flood defences the lowering of the crest due to settlements should be taken into account (regarding critical overtopping discharges), also when the settlement is even.

Uneven settlements can create large stresses in a structure. There are several causes for this:

- Uneven foundation pressure
- Different sized foundation elements (even if the pressure is equal!). Wide elements will settle more than narrow elements with an equal foundation pressure because the stress in the heart of the structure is spread out less and thus works to a larger depth.
- Local deviations from the soil properties. Locally the soil may be stiffer or less stiff, which causes uneven settlements for even loads.
- Changes of the horizontal stresses due to a nearby structure excavation or a (bored) tunnel.

According to NEN 6740, article 5.2.2.2, no span (foundation beams!) may undergo a rotation due to settlement differences larger than:

$$\frac{\Delta z}{\ell} = \theta = 1/300$$

For shallow foundations, the settlement can be calculated according to Chapter 28 (Part II). For pile foundations, the above requirement is usually met. To check the design of pile foundations, see Chapter 32 (compression piles).

For excavations (building site) the consequences of the swell of weaker soil layers located at a larger depth must also be taken into account. For excavations (building site), a pipe located nearby could undergo a rotation (see figure below). This can also be tested using the rotation condition given above.

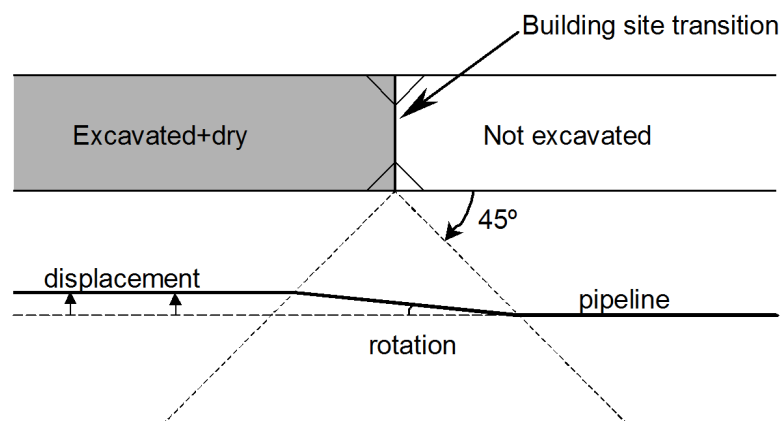


Figure 19-1 Displacement and rotation of a pipe near a building site excavation (top view)

If one expects problems due to excessive settlement differences, one can take the following measures:

- Using equal foundation pressures.
- Using equal-sized foundation elements.
- Applying soil improvement measures.
- Demanding stricter requirements for the structure excavation or (bore) tunnel.
- Applying pile foundations.
- Introducing movement joints.
- Reducing the distance between joints.
- Changing the statically indeterminate structure into a statically determinate structure.

Figure 19-2 indicates the difference between a statically determinate beam (two supports) and a statically indeterminate beam (three supports). In the first case the forces and moments are not influenced by the settlement of a support. In the second case the moment above the settled middle support decreases and the moment in the field thus increases.

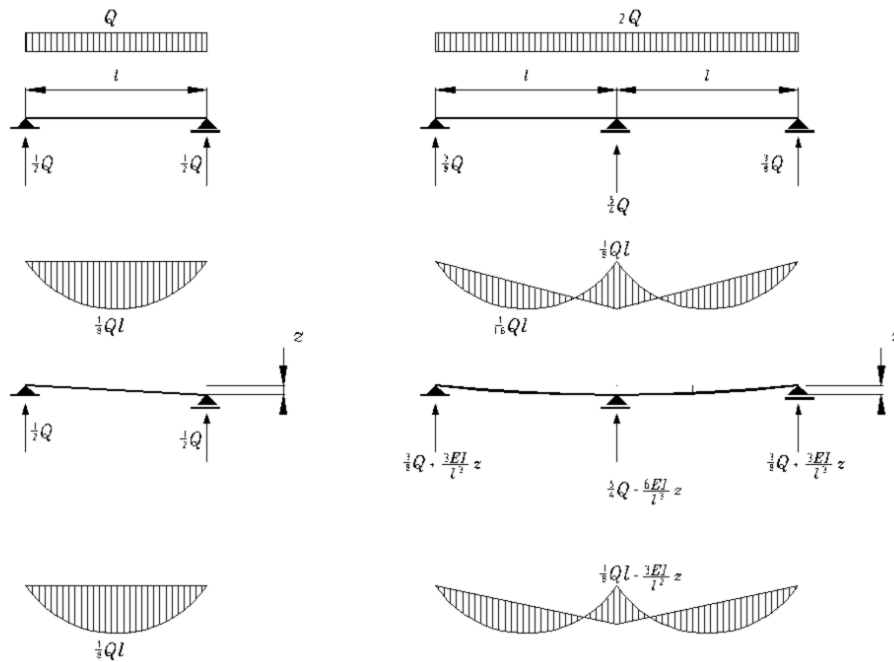


Figure 19-2 Forces and moments as a result of the settlement of a support

Settlements can be taken into account in the structural calculations in two ways, namely:

- Taking an imposed deformation into account
- Schematising the ground as a spring

The schematisation of the ground as a spring is not an accurate method because the ground does not behave like a spring. It is preferable to take the settlements into account as imposed deformations, whereby the settlements are determined using the distribution of forces in the structure initially neglecting the settlements. In this way, the settlements are overestimated and the calculated load is conservative. It is possible to carry out the calculations a number of times, thus iterating, to estimate the loads more accurately. For both methods of calculation, see Chapters 26 and 27 (Part II).

20. Soil, earthquake

Extended: 2023

20.1 Relevancy and causes

The theory of the generation of tectonic earthquakes assumes that the earth's crust consists of plates that move very slowly relative to each other. At the interface between the plates (the fault line), elastic deformation takes place until a maximum shear stress is exceeded. At that moment the earth's crust deforms plastically and the potential energy of the elastic deformation is released. This occurs as a jerky deformation (waves and vibrations). Earthquakes can as well be caused by deformations in the earth's crust, like earthquakes due to gas and oil extraction.

Earthquakes can have two main effects on structures:

1. They can cause a peak loading on the foundation of structures. The peak loading is caused by the transfer of the acceleration from the soil via the foundation towards the structure and transformed to a reaction force by the mass of the structure.
2. They can lead to a decrease of the bearing capacity of the subsoil due to the cyclic character of loading. This can lead to liquefaction (*zettingsvloeiing*) in sandy soils and softening of clay layers.

Obviously, both effects should be considered in the designs of structures in earthquake-sensitive areas.

20.2 The Richter scale

The Richter scale is mostly used to register and classify earthquakes. It is based on the magnitude of the earthquake: the maximum registered amplitude of the earthquake at its epicentre. The epicentre is the projection of the point of origin of the earthquake on the Earth's surface. The magnitude is independent of the location of the measurement of the amplitude. The logarithmic basis of the scale implies that each whole number increase in magnitude represents a tenfold increase in measured amplitude. As an estimate of energy, each whole number step in the magnitude scale corresponds to the release of about 31 times more energy than the amount associated with the preceding whole number value.

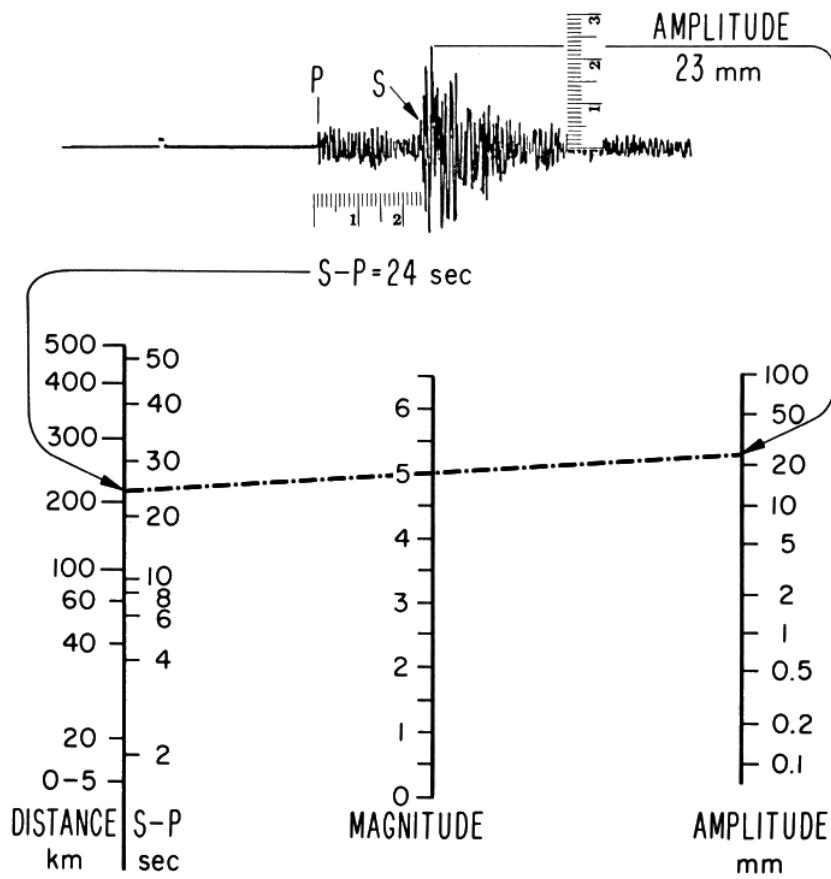
Although every earthquake has a unique magnitude that is the same in all locations on earth, the effect of the earthquake is not the same everywhere. Therefore, the magnitude of an earthquake cannot be used for a good estimation of the amount of damage to or load on a structure. The table below, however, can be used to give a global indication of the effects.

Earthquake severity	
Richter Magnitudes	Earthquake effects
less than 3,5	Generally not felt, but recorded
3,5 - 5,4	Often felt, but rarely causes damage.
under 6,0	At most slight damage to well-designed buildings. Can cause major damage to poorly constructed buildings over small regions.
6,1 - 6,9	Can be destructive in areas up to about 100 kilometres across where people live.
7,0 - 7,9	Major earthquake. Can cause serious damage over larger areas.
8,0 or larger	Large earthquake. Can cause serious damage in areas several hundred kilometres across.

Table 20-1 Effects related to the Richter scale

Another indication is that the energy related to magnitude 1 corresponds to a car (1000 kg) falling to the ground from a height of 100 metres. For every single increase of magnitude, the number of cars can be multiplied by thirty. Hence, for magnitude 8, one would have to drop 22 billion cars from the Dom tower in Utrecht.

To determine the Richter scale, a nomogram can be used that requires the distance to the epicentre and the maximum amplitude as input. An example of such a nomogram is given in Figure 20-1.



TO DETERMINE THE MAGNITUDE OF AN EARTHQUAKE WE CONNECT ON THE CHART
 A. THE MAXIMUM AMPLITUDE RECORDED BY A STANDARD SEISMOMETER, AND
 B. THE DISTANCE OF THAT SEISMOMETER FROM THE EPICENTER OF THE
 EARTHQUAKE (OR THE DIFFERENCE IN TIMES OF ARRIVAL OF THE P AND S WAVES)
 BY A STRAIGHT LINE, WHICH CROSSES THE CENTER SCALE AT THE MAGNITUDE

Figure 20-1 Determination of the magnitude of an earthquake on the Richter scale (Richter, 1958)

Figure 20-2 shows the areas where earthquakes of magnitude IV or larger were registered in 1996.

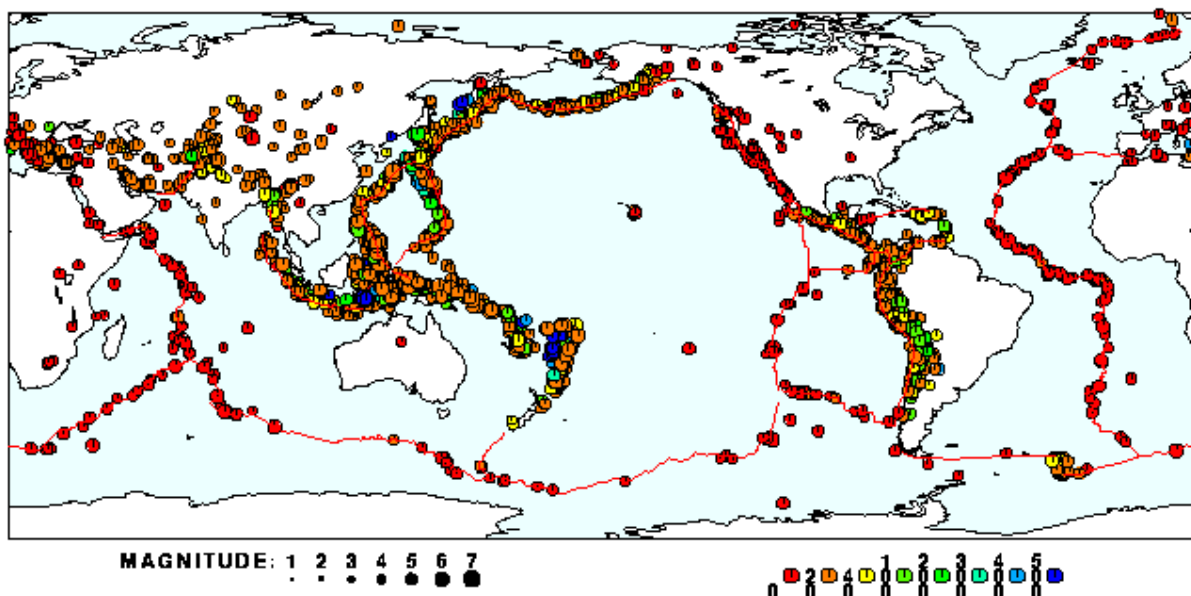


Figure 20-2 Observed earthquakes of 1996 ($M \geq 4$)

20.3 The Modified Mercalli scale

For the determination of earthquake loads on structures, the Modified Mercalli scale is more useful than the scale of Richter. The modified Mercalli scale is based on earthquake intensities, taking the effects of earthquakes into account rather than their amplitude. It does not have a mathematical basis; instead it is an arbitrary ranking based on observed effects. Amongst other factors, the intensity depends on the distance to the epicentre and the structure of the earth's crust. Figure 20-3 can be used for the estimation of earthquake intensities in the Netherlands. Notice that the gas-mining induced earthquakes in the northern part of the Netherlands are not included in this graph.

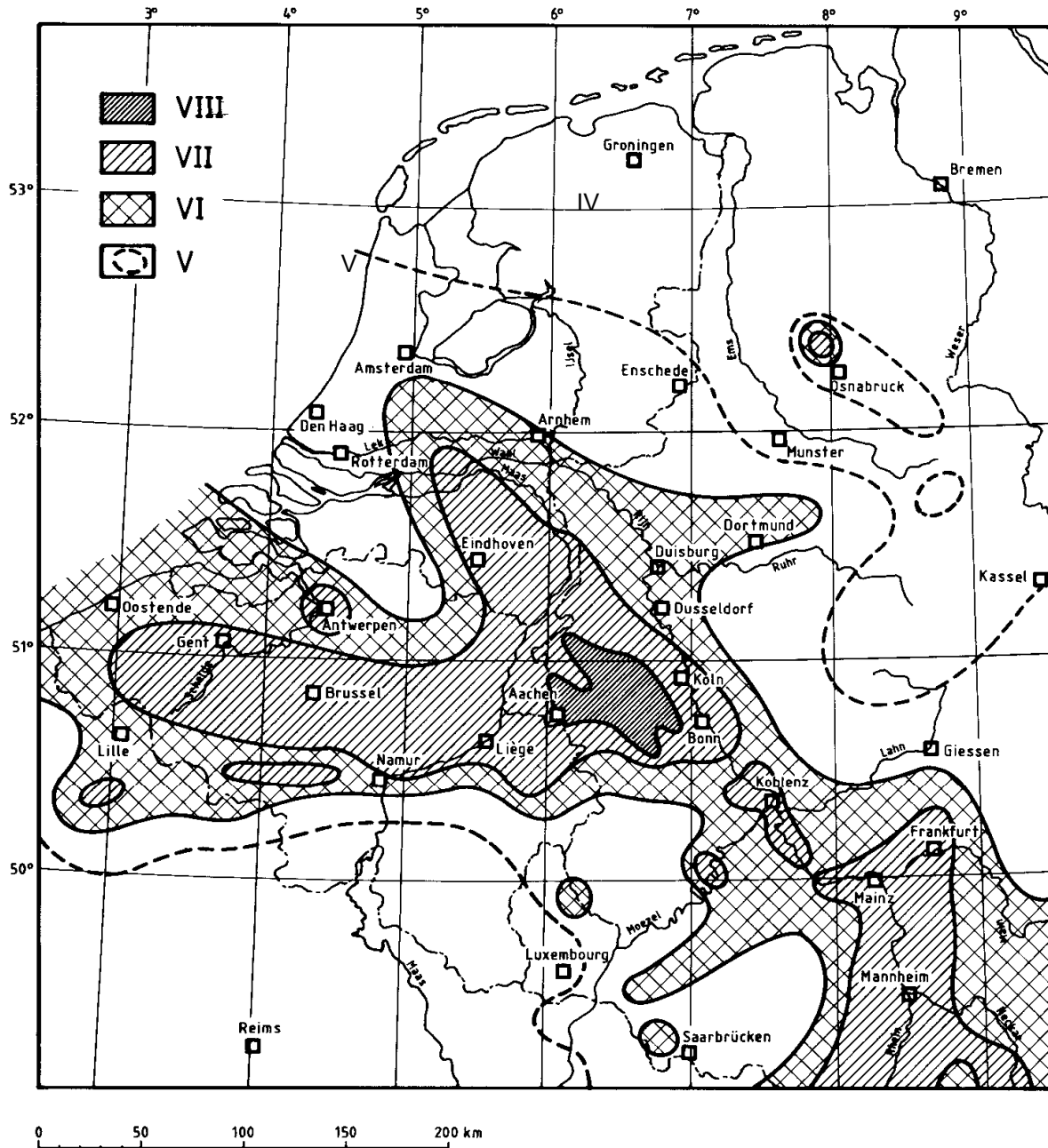


Figure 20-3 Earthquake intensities in and around the Netherlands (Modified Mercalli Scale)

20.4 Earthquake design

20.4.1 Horizontal acceleration

The magnitude of the horizontal acceleration of the soil and structures founded in this soil is related to the earthquake intensity. For the estimation of the horizontal acceleration at a certain intensity, the classification of Table 20-2 can be helpful. Notice that these values are not design values.

Intensity	Description	Acc. [m/s ²]
I	Only registered by seismographs	0,01
II	Very weak; only felt in favourable circumstances	0,02
III	Weak; felt by a few people; vibrations similar to those of passing traffic	0,05
IV	Moderate; felt by many; tremors as vibrations cause by heavy traffic; doors and windows rattle	0,1
V	Fairly strong; generally felt by everybody; hanging objects sway; clocks stop running	0,2
VI	Strong; shock reactions; objects in houses fall over; trees move; insufficiently solid houses are damaged	0,5
VII	Very strong; many buildings are damaged; chimneys break; waves in ponds; church bells ring	1,0
VIII	Destructive; panic; general damage to buildings; weak buildings are partially destroyed	2,0

Table 20-2 Horizontal acceleration per earthquake intensity (modified Mercalli scale) (1931)

A graph indicating the relationship between the horizontal acceleration and the return period of the earthquake, like in Figure 20-1, can be helpful when deciding the maximum acceptable acceleration.

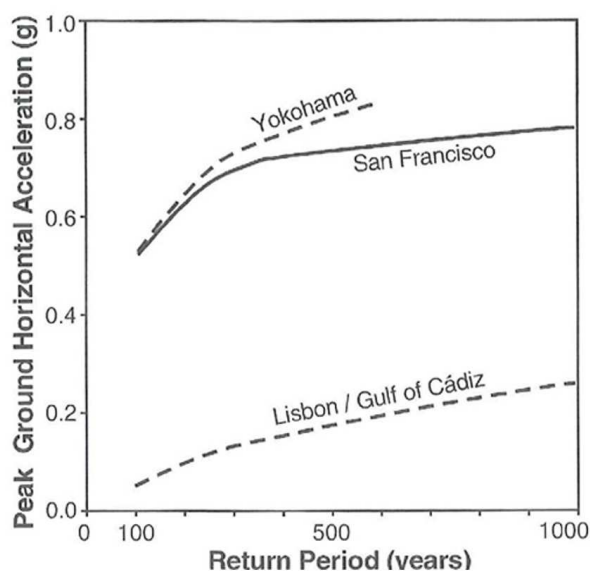


Figure 20-1 Relationship between horizontal acceleration during an earthquake and the return period of occurrence

20.4.2 Earthquake forces on structures

In the Netherlands, designs rarely take earthquakes into account, unless large consequences (and thus large risks) are involved, for instance for nuclear power plants. Even the storm surge barriers in the Delta Works were not dimensioned for earthquakes. The probability that (serious) damage is caused by an earthquake was considered very small and the probability that it happens during a storm surge is negligible. However, in the southern part of the Netherlands there is some minor tectonic activity, and in the northern part of the Netherlands, the damage due to natural gas extraction has become an increasing point of concern.

Buildings

For buildings, the accelerations in all directions of the earth's surface are of particular importance. These accelerations cause dynamic loads. The dynamic character of the loads does not always stand out equally well in different structure regulations and norms. In the various regulations the earthquake load is often calculated as a static load, a function of the mass of the elements of the structure, in all directions. The stiffness of the elements of the structure is not always taken into account.

The equivalent static method (ESM) approaches the dynamic behaviour of the structure by also relating the size of the load to the structure's lowest natural frequency. This and other methods to determine the earthquake load are described in specialised literature on seismic design of reinforced concrete structures. The essence of most of these methods is that the structure is schematised as a mass-spring system with freedom of movement in all directions.

For a description of earthquakes as a statistic process, one is referred to the lecture notes *Statistic vibrations* (in Dutch: "Stochastische trillingen") (Vrouwenvelder, 1997).

Soil-retaining structures

For soil retaining structures, it is unusual to schematise the structure as a mass-spring system. The difficulty with such a schematisation is estimating the mass of the soil to be retained in earthquake conditions.

The German manual on quay walls, the EAU (*Empfehlungen des Arbeitsausschusses Uferneufassungen*, Wilhelm Ernst & Sohn, München), gives an approximation method that is simple in application. This approach considers the maximum horizontal acceleration constant and assumes that the maximum horizontal and vertical accelerations do not occur simultaneously (the fact that this assumption is not always correct, was shown in Kobé, Japan). With these assumptions, the resultant acceleration can be found by vectorial addition of gravity and the horizontal acceleration caused by the earthquake. The calculation is based on a fictitious rotation of the system, such that the resultant acceleration coincides with the gravitational acceleration. This means that both the sheet piling and the ground level in front of and behind the retention structure are given a rotation according to Figure 20-4.

The rotation amounts to $\tan\left(\frac{a}{g}\right)$.

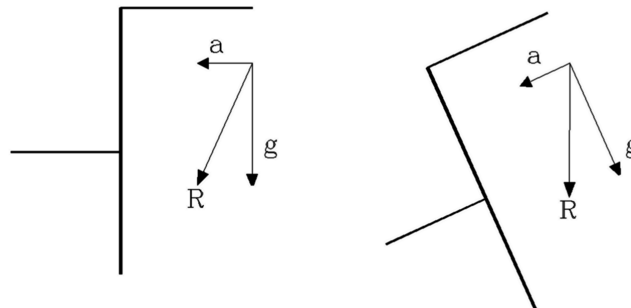


Figure 20-4 Fictitious rotation of the soil retaining structure and the ground level as a result of horizontal accelerations

Using the general horizontal ground pressure coefficients K_a and K_p , as given in Chapter 18, the horizontal ground pressure can be determined for a rotated schematisation. The real horizontal load is found by resolving the force into its true horizontal and vertical components.

For the soil below the groundwater level, the mass of the water must be taken into account as well. This is done by correcting the rotation, for this one is referred to the German guidelines on quay wall design, the EAU 2012.

Hydraulic structures

Westergaard (1931) was the first to find an expression for the hydrodynamic pressures on dams due to earthquakes. He based his method on the 2D wave equation for compressible fluids and made a few assumptions:

- the pressure at water surface is zero, so no vertical movements of water particles at the surface (hence, no surface waves)
- the dam is infinitely long, is rigid and has a vertical face
- the reservoir is infinitely long as well.

Westergaard simplified the pressure distribution to the shape of a parabola (Figure 20-2):

$$p_{dyn}(z) = \frac{7}{8} \rho \cdot k_h \cdot g \sqrt{d \cdot z}$$

where: $p_{dyn}(z)$ [Pa] = hydrodynamic pressure at depth z
 ρ [kg/m³] = density of water
 k_h [-] = horizontal seismic coefficient, the maximum horizontal component of the acceleration of the foundation divided by g . See Table 20-2 for the values of seismic acceleration per earthquake intensity
 g [m/s²] = gravitational acceleration
 d [m] = water depth
 z [m] = vertical coordinate ($z = 0$ at water surface, $z = d$ at bottom level)

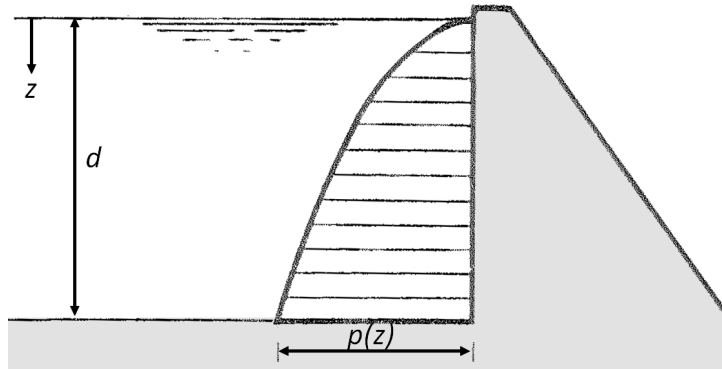


Figure 20-2 Distribution of hydrodynamic pressure on a dam due to an earthquake (Westergaard, 1931)

To find the total pressure on a dam during an earthquake, the hydrostatic pressure shall be added to the hydrodynamic pressure.

Westergaard's method is only valid, if the period of excitation is larger than the fundamental resonance period for water pressure as defined by Chopra (1966):

$$T_{excitation} > T_1, \text{ where } T_1 = \frac{4d}{c_p}$$

and: T_1 [s] = fundamental eigenperiod
 d [m] = water depth
 c_p [m/s] = celerity of pressure waves in water (equal to the speed of sound ≈ 343 m/s)

The negligence of surface waves introduces an error, especially for low head dams. Bustamante et al. found the following errors when ignoring surface waves when including the compressibility of water:

$$\text{error} < 0,05 \text{ if } \frac{d}{T_e} > 4,2\sqrt{d}$$

$$0,05 < \text{error} < 0,20 \text{ if } 2,6\sqrt{d} < \frac{d}{T_e} < 4,2\sqrt{d}$$

$$\text{error} > 0,20 \text{ if } \frac{d}{T_e} < 2,6\sqrt{d}$$

To compensate for the absence of the effect of the reservoir length, Brahtz and Heilbron (1933) introduced a correction factor on Westergaard's equation to take this effect into account. See Figure 20-3

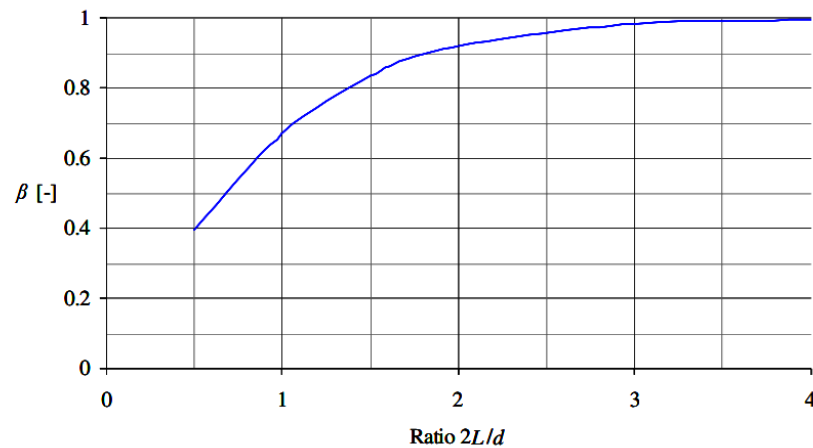


Figure 20-3 Correction factor β to include the reservoir length in the hydrodynamic pressure according to Westergaard
 $2L$ = the reservoir length; d = the water depth (Versluis, 2010)

When designing a structure in such a way that it will resist earthquakes, it should be considered per failure mechanism what load combination is most critical, see Figure 20-4 for an example. The water pressure is a combination of hydrostatic, hydrodynamic and surface wave pressures

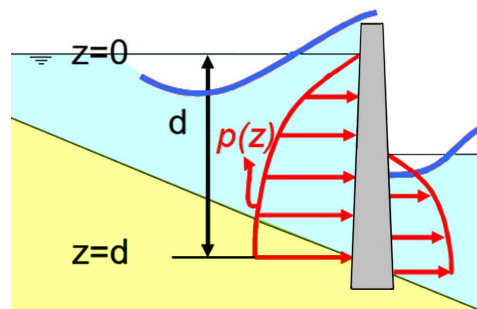


Figure 20-4 Potential load situation to be taken into account in a design (excl. hydrostatic pressure) (modified from Molenaar, 2020)

Another widely used method to calculate hydrodynamic pressures was proposed by Housner (1954). He made a distinction between pressure caused by the added mass and the convective pressures, for example caused by sloshing (*klotsen*). Instead of assuming an infinitely long basin, Housner uses a coordinate system. The method of Housner is adequately described by Versluis (2010).

20.4.3 Loss of bearing capacity due to liquefaction

The cyclic character of the horizontal acceleration of the ground is a key characteristic for the occurrence of liquefaction. Liquefaction (*zettingsvloeiing*) is the phenomenon of a (partially) saturated granular soil that substantially loses strength and stiffness in response to an applied cyclic stress, causing it to behave like a liquid and losing its bearing capacity. The horizontal acceleration is related to the earthquake intensity. Section 26.5 of this Manual (part II) explains how it can be determined whether liquefaction can occur.

20.5 Literature

Brahtz, J.H.A. and C.H. Heilbron (1933). Discussion on "Water Pressures on Dams During Earthquakes" by H.M. Westergaard. Transactions, American Society of Civil Engineers (ASCE), Vol. 98, Paper No. 1835, New York City, NY, pp. 452–454

Chopra, A.K. (1966). Hydrodynamic Pressures on Dams During Earthquakes. Report No. 66-2, Department of Civil Engineering, University of California, Berkeley, CA, pp. 1–14

Housner, G.W. (1954). Earthquake Pressures on Fluid Containers. Eight Technical Report under Office of Naval Research, California Institute of Technology, Pasadena, CA, pp. 1-13

Versluis, M. (2010). Hydrodynamic pressures on large lock structures. MSc-thesis, Delft University of Technology

Westergaard, H.M. (2031). Water pressures on dams during earthquakes. Paper no. 1835, Proceedings ASCE, pp 448-472.

21. Soil, groundwater

An important aspect of the soil is the presence of groundwater. Groundwater largely influences both the strength and the stiffness behaviour of the ground. Furthermore, groundwater is also responsible for a large load on the structure.

Sometimes the load of the groundwater is only temporarily undesirable. If that is the case, one can opt for drainage. That is why this chapter also considers groundwater flow and drainage. Groundwater flow can cause erosion, this is known as pipng (*zanduitspoeling*).

These six facets of groundwater are discussed below in the following order:

- Load
- Groundwater flow
- Piping
- Drainage
- Influencing strength
- Influencing stiffness

21.1 Groundwater pressure

In the Netherlands, many structures placed in the ground are also found to be in the groundwater, due to the high groundwater level. The structure therefore undergoes an upward load. If there is no groundwater flow (e.g. seepage or consolidation), this load is identical to that of a floating object:

$$p = \rho \cdot g \cdot h$$

where: p	[Pa]	=	(ground)water pressure
ρ	[kg/m ³]	=	the density of the water (salt = 1025 kg/m ³ ; fresh = 1000 kg/m ³)
g	[m/s ²]	=	the gravitational acceleration
h	[m]	=	the piezometric head or piezometric height

For excavations, one must always check if this load on the bottom of a clay layer, building site floor or cellar floor won't allow the structure to burst open. There should be a sufficient safety margin between the upward groundwater load and the downward load of the weight of the clay layer or structure ($\gamma_{m,g} = 1,1$) or the tensile force of the tension piles ($\gamma_{m,b4} = 1,4$).

Loading a layer of little permeable soil (clay or peat) leads to a temporary increase of the piezometric head. Consolidation then gradually reduces the piezometric head back to its initial value (see Part II, Section 28.1).

Soil layers (particularly the deeper Pleistocene sand layers) can have a different piezometric head due to ground water flow, which can cause seepage. The piezometric head in sand layers in the vicinity of rivers is closely related to the river water level (see note).

The water level can easily be measured with a piezometer. Groundwater stresses in deeper layers are therefore always measured using a piezometer. For soil layers close to ground level the water levels in ditches are conveniently assumed. Due to run-off ground level is often considered a maximum piezometric head in polders.

Naturally, groundwater flow occurs around a water retaining structure and thus the groundwater pressure is not constant. This is described in the next section.

Note

Before the fall of the Berlin Wall, the German government built a new 100 million Euro parliament building (Reichstag) in Bonn, beside a river. Once the car park in the basement had been completed, high water levels were encountered in the river. The levels above ground had not yet been constructed and thus did not provide compensatory weight. The company that had to place sheet piling around the excavated building site had experienced delays, leaving the groundwater and river water free reign to destroy the structure, which consequently happened. Nobody dared to implement the only alternative (flooding the car park to provide additional weight) to save the Reichstag for fear of water damage to the basement.

21.2 Groundwater flow

21.2.1 Theory

In many cases of groundwater flow one can assume that the specific discharge is linearly proportional to the hydraulic gradient:

$$q = -k \cdot i$$

in which: q [m/s] = specific discharge (= Q/A)
 k [m/s] = permeability coefficient
 i [-] = hydraulic gradient: $i = \frac{dh}{ds}$
 h [m] = potential, piezometric head
 s [m] = distance along a fictitious flow line

This is called Darcy's law. This law only applies if the potential flow is laminar. Thereto the following applies:

$$Re = \frac{u d}{\nu} < 1$$

in which: Re [-] = the Reynolds value
 u [m/s] = the fluid's filtration velocity
 d [m] = diameter of the soil particles
 ν [m²/s] = kinematic viscosity

$Re > 1$ occurs for soil particles with large diameters (stone) and for large flow velocities, which don't usually occur in groundwater flow.

A rough indication of the permeability of various types of soil is given below:

Soil type	k [m/s]
Gravel	10^{-2}
Coarse sand	10^{-3}
Moderately coarse to moderately fine sand	10^{-3} to 10^{-4}
Fine sand	10^{-4} to 10^{-5}
Clay	10^{-9} to 10^{-11}

Table 21-1 Permeability versus soil type

Groundwater flow can thus be described using the theory of potential flow. This means that a two-dimensional groundwater flow can be analysed using a flow net (see Example).

The following applies between the flow lines:

$$q da = -k \frac{dh}{ds} da = \text{constant}$$

in which da [m] = distance between two successive flow lines

Because the successive flow lines and equipotential lines create a square, the following applies:

$\frac{da}{ds} = \text{constant}$. Because k is a constant, the potential difference between two successive equipotential lines is constant.

With a given potential in two locations, the course of the potential and the specific discharge along a flow line are fixed in a flow net.

Erosion below structures due to groundwater flow ('piping') is treated in section 31.4 (part III of this manual).

21.3 Drainage

The groundwater flow in a drained area is usually 3-dimensional, so a 2-dimensional flow net method cannot be used. For calculations involving drainage, the water levels and the groundwater pressures, see Chapter 41 (in part III of this manual).

21.4 Influences on strength

The soil's shear strength depends on the cohesion, the angle of internal friction and the so-called inter-granular stress (also known as effective stress). The inter-granular stress, also known as effective soil stress (σ') depends on the total stress and the water pressure:

$$\sigma' = \sigma - \rho$$

in which: σ [Pa] = total stress
 ρ [Pa] = water pressure (also denoted as σ_w)

This shows that the presence of groundwater reduces the effective stress and thus the shear stress of the soil, as:

$$\tau = c' + \sigma'_n \cdot \tan(\varphi)$$

As regards the shear stress τ , it is therefore important to keep the water pressure under the structure as low as possible. That is why the seepage screens (sheetpile walls that increase the length of seepage paths to prevent piping) are usually installed on the upstream side under the bottom slab of the structure. A separate chapter is dedicated to loads caused by inter-granular stress σ' (Chapter 18).

21.5 Influence on stiffness

Another soil property that is largely influenced by the presence of groundwater is the course of the compaction of the soil as a result of an increase of the ground pressure. In the case of impermeable soil (clay, peat), an increase of the total stress often causes a proportional increase of the water pressure. This is because water cannot flow out of the pores quickly enough when the soil is compressed. The water can be considered incompressible and accounts for the entire increase of pressure. The result is a high total stress and water pressure and a relatively low effective stress. As a consequence of the increase of the water pressure, groundwater will flow to a place with a lower potential. This way, the water pressure and the effective stress adjust to the load.

In this case, the compression process depends on the speed with which the groundwater can flow out of the pores. This process of reducing the water pressure and increasing the effective stress is called the consolidation process. The presence of groundwater therefore causes a temporary increase of stiffness in compressible, impermeable soil.

For this see also in part II, Chapters 27 ('Stiffness') and 28 ('Settlement').

22. Shipping, hydraulic aspects

Water movements created by sailing and manoeuvring ships can be of importance for structures in ports and shipping lanes. These water movements are:

- Return current
- Water level depression
- Ships wakes
- Propeller wash

Generally, these hydraulic loads on a structure are inferior to the other loads. However, the hydraulic loads are of large importance to the stability of flexible structures adjoining the hydraulic engineering work. For the design of such structures one is referred to the book for course CIE4310: "Introduction to Bed, bank and Shore protection" (Schierck & Verhagen, 2016).

23. Shipping, berthing and collision

Extended: 2018, 2022

23.1 Introduction

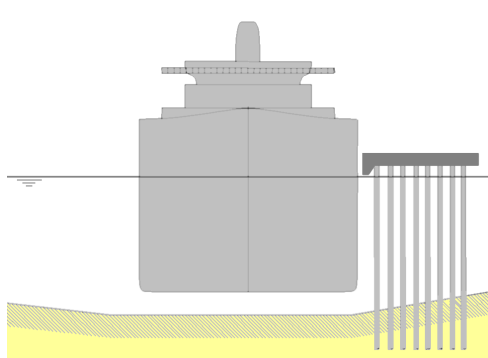
Berthing a ship (*aanleggen van een schip*) to a structure and collision of a ship against a structure are, theoretically, the same process. The only differences are the velocity and the extent of control of the process.

A number of aspects are of importance in relation to the load of a berthing ship on a structure. These aspects are:

- dimensions of the ship
- mass of the ship
- velocity of the ship
- stiffness of the ship's hull
- mass of the water moving along with the ship, known as the hydrodynamic or added mass
- approach angle
- stiffness of the mooring structure
- geometry of the mooring structure
- place where the ship hits the structure
- current
- wind

23.2 Theory

A schematic representation of a berthing vessel including the main parameters relevant to calculating the berthing impact is depicted in Figure 23-1.



k_{ship} = stiffness of the ship's hull

k_{water} = hydrodynamic stiffness

$k_{structure}$ = stiffness of the structure

m_{ship} = mass of the ship

m_{water} = hydrodynamic-, added mass

$m_{structure}$ = mass of the structure

c_{ship} = damping of the ship's hull

c_{water} = hydrodynamic damping

$c_{structure}$ = damping of the structure

Figure 23-1 A berthing vessel and main parameters related to berthing impact

Together with the water that moves along, the ship to be moored has the following amount of kinetic energy:

$$E_{kin} = \frac{1}{2}(m_s + m_w)v_s^2$$

in which: E_{kin} [Nm] = kinetic energy

m_s [kg] = mass of the ship

m_w [kg] = mass of the water moving with the ship; additional mass

v_s [m/s] = velocity of the ship and water (\perp structure)

The kinetic energy has to be absorbed by the berthing structure and it is a measure of the load on a structure. The maximum force that develops between the ship and the berthing structure largely depends on the stiffness of the whole ship-water-structure system. This system can be schematised as a mass-spring-dashpot system (*massa-veer-dempersysteem*).

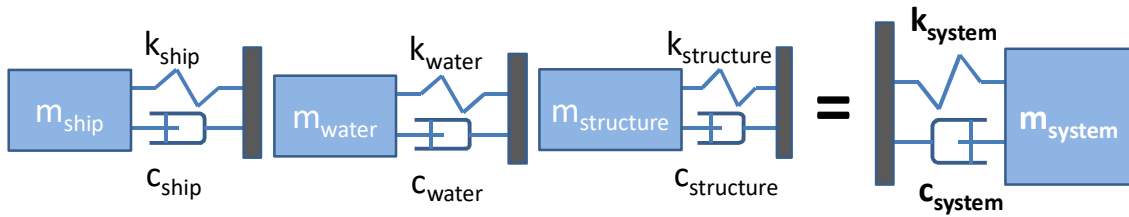


Figure 23-2 Schematisation of a berthing vessel as a mass-spring-dashpot system

In a preliminary design damping will be neglected, which results in a conservative calculation of the berthing load on the structure. Without damping, which dissipates energy, all of the kinetic energy is transformed into potential energy. The potential energy in a spring is:

$$E_{pot} = \int_0^{\Delta x} k(x) x dx \quad \text{for a linear spring system:} \quad E_{pot} = \int_0^{\Delta x} k x dx = \frac{1}{2} k \Delta x^2$$

where

$$\begin{aligned} \Delta x \text{ [m]} &= \text{displacement of the spring} \\ k \text{ [Pa]} &= \text{spring stiffness of the total system} \end{aligned}$$

In general, $k = \frac{F}{\Delta x}$. For the spring stiffness of the berthing system, the combination of the structure and the ship should be considered and the water stiffness can be neglected. The stiffness of the total system is:

$$\frac{1}{k_{system}} = \frac{1}{k_{structure}} + \frac{1}{k_{fender}}.$$

Usually $k_{fender} \ll k_{structure}$.

Compared to the mass of the ship plus added water mass, the mass of the structure (the part that would move) is negligible. Hence, the maximum potential energy in the spring equals the maximum kinetic energy of the ship and the water. For a linear elastic structure, equating potential and kinetic energy

$$\text{gives: } E_{pot,max} = E_{kin,max} \Leftrightarrow \frac{1}{2} k \Delta x^2 = E_{kin,max} \Leftrightarrow \Delta x = \sqrt{\frac{2 E_{kin,max}}{k}}$$

23.3 Design rules for berthing and collision forces

23.3.1 Berthing energy

The current practice in the design calculations and dimensioning of fendering systems and flexible structures is based on energy considerations. In these, it is assumed that the loss of kinetic energy of the ship is transformed into an equal amount of energy absorbed by the fender or the structure. The basic principle was first developed by Gottfried Leibniz and Johann Bernoulli:

$$E_{kin} = \frac{1}{2} m v^2 \quad [\text{J} = \text{Nm}]$$

Including the effects of added water mass, eccentricity and structural deformation, the equation, according to F. Vasco Costa (1973), transforms into:

$$E_{kin} = \frac{1}{2} m_s v_s^2 C_H C_E C_S$$

CETMEF, a French research institute, recommended to include the effect of the water that is confined in between the ship and the structure:

$$E_{kin} = \frac{1}{2} m_s v_s^2 C_H C_E C_S C_C \quad \text{or:} \quad E_{kin} = \frac{1}{2} (m_s + m_w) v_s^2 C_E C_S C_C$$

where: C_H [-] = hydrodynamic coefficient = $\frac{m_s + m_w}{m_s}$
 C_E [-] = eccentricity coefficient
 C_S [-] = ship coefficient
 C_C [-] = confinement coefficient
 m_s [kg] = mass of the ship
 v_s [m/s] = velocity of the ship (component \perp structure)

This approach is globally used and accepted, e.g. prescribed in the BS6349 (British Standard) and mentioned in PIANC report 151.

The parameters to calculate the kinetic energy are explained below.

Mass of the vessel m_s

The mass of a vessel depends on the type of vessel and should be increased with its dead load.

Velocity of the vessel v_s

The velocity with which a vessel berths is an important factor, after all, the kinetic energy is proportional to the square of the velocity. A large number of measurements revealed that the berthing speed depends on the ship's dimensions, the type of load (cargo) and the berthing conditions.

In good berthing conditions, one could use Table 23-1 for mooring speeds.

ship [ton]	Observed velocity [m/s]	Design velocity [m/s]
<10 000	0,10 ~ 0,30	0,20
10 000 ~ 50 000	0,10 ~ 0,20	0,15
>50 000	0,10 ~ 0,15	0,15

Table 23-1 Berthing speeds in good conditions (velocity component $v_s \perp$ structure)

As the observed velocities exceed these design velocities, one can conclude that the design velocities are too low. One is therefore advised to assume the maximum observed velocities instead.

The design velocity as given in Figure 23-3 is as a function of both the ship's dimensions and the berthing conditions. As the velocities in this figure are sometimes lower than the observed velocities, one is advised not to assume velocities lower than the maximum observed velocities given in the table above.

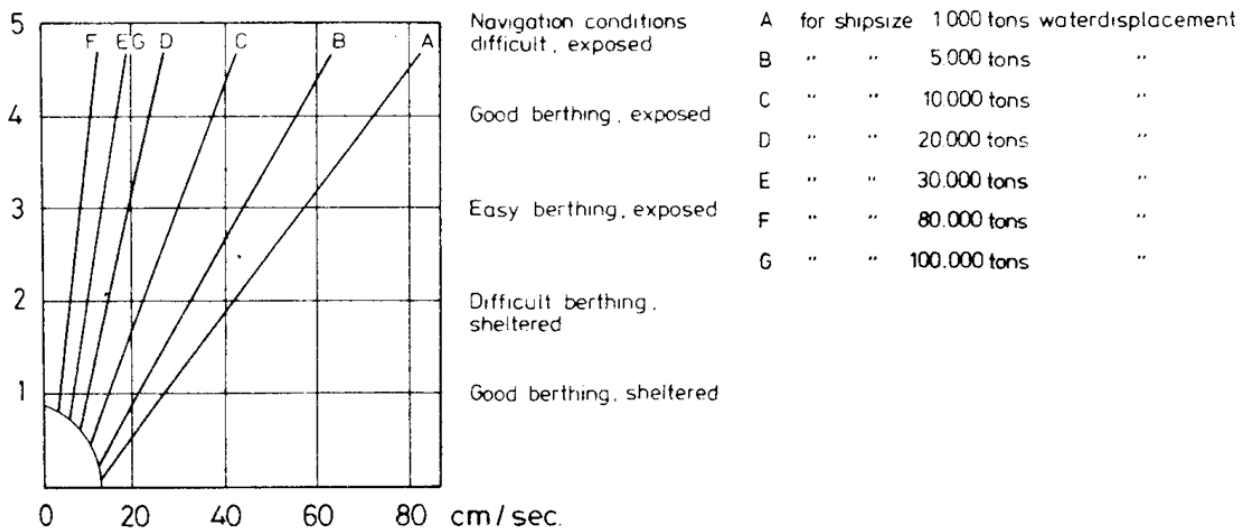


Figure 23-3 Design velocity

ROK (2017) gives maximum velocities per type of inland waterway, see Table 23-3. These velocities can be used to calculate collision forces.

Klasse	I	II	III	IV	Va	Vb t/m VII
velocity [m/s]	4,1	4,8	5,1	5,3	5,5	4,5

Table 23-2 Maximum vessel velocities per type of inland waterway (ROK, 217)

Hydrodynamic coefficient C_H

The hydrodynamic coefficient is in fact simply the ratio between the mass of the ship plus the water moving with the ship and the mass of the ship:

$$C_H = \frac{m_s + m_w}{m_s}$$

The mass of the ship that should be used to calculate the hydrodynamic coefficient is the total water displacement of the loaded ship (FLD = full load displacement). The additional mass of the water depends on, amongst other factors, the movement of the ship in three-dimensional space. Several models have been developed to determine the hydrodynamic additional mass. They are based on the potential theory or on the theory regarding the preservation of impulse. However, here a simple approximation that can be used for a preliminary design suffices. This approximation is based on the potential theory and is known as Stelson Mavils' equation:

$$m_w = \rho L \frac{1}{4} \pi D^2$$

in which: ρ [kg/m³] = density of (sea)water
 L [m] = length of the ship
 D [m] = draught of the ship

(To compare this formula with Morison's formula, see Chapter 14 "Water, waves, slender structure")

The equation for the hydrodynamic coefficient can be simplified further with an assumption for the block coefficient C_b :

$$C_b \approx \frac{\pi}{4}$$

$$m_s = \rho L B D C_b$$

$$C_H = \frac{m_s + m_w}{m_s} \approx 1 + \frac{D}{B}$$

For head-on collisions, it is of current practice to take $C_H = 1,2$ (PIANC report 151, 2014), but it is clear that this hydrodynamic aspect is directly influenced by the shape of the striking bow.

Note: Vasco-Costa formula reads as follows $C_H = 1 + \frac{2D}{B}$ use of this well-known formula is wide spread. Engineering judgement is required!

ROK 2017 gives the following values for the added water mass per class of inland waterway:

CEMT class waterway	added water mass [tonnes]
I	400
II	650
III	1000
IV	1500
Va	3000
Vb	3000
Vla	3000
Vlb	6000
Vlc	9000
VII	15000

Table 23-3 Added water mass per class of inland waterway (ROK, 2017)

Coefficient of eccentricity C_E

The coefficient of eccentricity takes into account the energy dissipation caused by the yawing (*bijdraaien*) of the ship when it moors eccentrically against the structure. This yawing is shown in Figure 23-4.

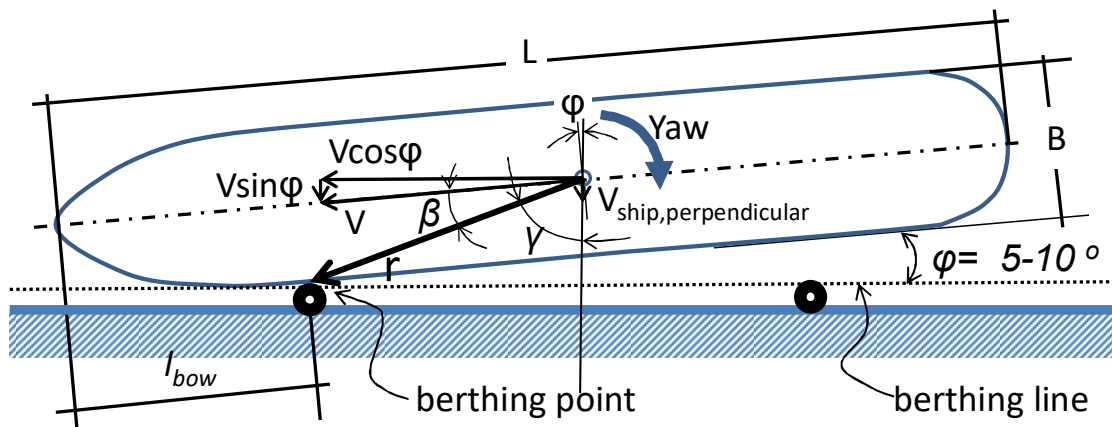


Figure 23-4 Eccentric berthing

If the movement of the ship at time of impact with the structure can be described solely as a translation of the centre of gravity, the coefficient of eccentricity is:

$$C_E = \frac{k^2 + r^2 \cos^2(\gamma)}{k^2 + r^2} \quad \gamma = 90^\circ - \beta - \varphi \quad r = \sqrt{\left(\frac{1}{2}L - \ell_{bow}\right)^2 + \frac{1}{4}B^2}$$

in which:

- k [m] = radius of gyration (*traagheidsstraal*) of the ship
- r [m] = the radius between the gravity centre of the ship and the berthing point
- β [°] = the angle between radius r and the ship's velocity along the axis of the ship
- γ [°] = the angle between radius r and the ship's velocity perpendicular to the berthing line
- φ [°] = the berthing angle; the angle between the ship's axis and the berthing line
- ℓ_{bow} [m] = distance between the bow tip and the point where the straight part of the hull starts to curve to the bow

The radius of gyration of the ship can be approximated by:

$$k = (0,19C_b + 0,11)L$$

in which: C_b [-] = block coefficient = $C_b = \frac{V}{L \cdot B \cdot D}$

- L [m] = length of the ship
- B [m] = width of the ship
- D [m] = draught of the ship
- V [m³] = (volumetric) water displacement of the ship

The smaller the value of C_b , the larger the load F . Therefore, a small C_b is governing.

The following approximation applies: $0,6$ (slender ships) $\leq C_b \leq 0,95$ (container ships)

Ship coefficient C_S

The ship coefficient takes the elasticity of the ship's side into account. This coefficient depends on the stiffness of the structure and that of the ship's shell and takes into account the part that is taken on by the structure. In the case of weak structures, such as, for instance, a wooden pier with fenders, nearly all of the energy is absorbed by the structure because the deflection of the ship's shell is negligible. In this case, $C_S = 1$.

For a relatively stiff structure, such as a quay with wooden support beams and car tyres, the deflection of the ship's shell will not be entirely negligible compared to the deflection of the structure. In this case, $C_S = 0,9$ can be used for design purposes.

Confinement coefficient C_c

The confinement coefficient, or cushion factor, takes the dissipation of energy into account, caused by the fact that water has to be squeezed away from the space between the ship and quay structure. If the structure is closed, e.g. a straight vertical sheetpile wall, a cushion of water between the structure and ship will slow down the ship. For a closed quay and parallel mooring ($\theta = 0^\circ$) this can lead to a 20% reduction of the amount of energy to be absorbed. If there is a small angle between the ship and the quay ($\theta = 5^\circ$) this reduction can disappear almost entirely because the water can simply flow away. If the structure is open, e.g. a jetty, no hydrodynamic damping will occur.

Therefore, the limit values of the confinement coefficient are: $0,8 \leq C_c \leq 1,0$ (PIANC report 151, 2014). For safety reasons, one can assume $C_c = 1,0$ for a preliminary design.

23.3.2 Collision forces

Calculation using the stiffness

Because the stiffness of the structure is unknown until after the design phase, the load of a ship on a structure is not given as a force, but as an amount of kinetic energy that needs to be absorbed. Besides the amount of kinetic energy to be absorbed during mooring, other forces on the ship must also be taken into account, such as wind and current. These forces are transferred to the structure via the ship.

If the kinetic energy of the vessel is known, the collision force F_{coll} on the (linear elastic) structure can be computed with:

$$F = k \Delta x = \sqrt{2k E_{kin}}$$

where: k [N/m] = total stiffness of the structure (combined stiffness of fender plus quay wall)
 Δx [m] = deformation of the structure
 E_{kin} [Nm] = kinetic energy of the vessel (see previous section)

This formula shows the influence of the stiffness of the structure on the resultant force of the ship on the structure and therefore also of the structure on the ship. The total stiffness of the system is determined by both the structure (including the foundation) and the used fenders. In very stiff structures, the fenders are governing for the design. Assuming a cell-fender with the spring characteristics given below and a diameter of 0,80 m, one finds a fender stiffness of:

$$k_{fender} = \frac{F}{\Delta x} \approx \frac{1100 \text{ kN}}{10\% \cdot 0,80 \text{ m}} \approx 14\,000 \text{ kN/m}$$

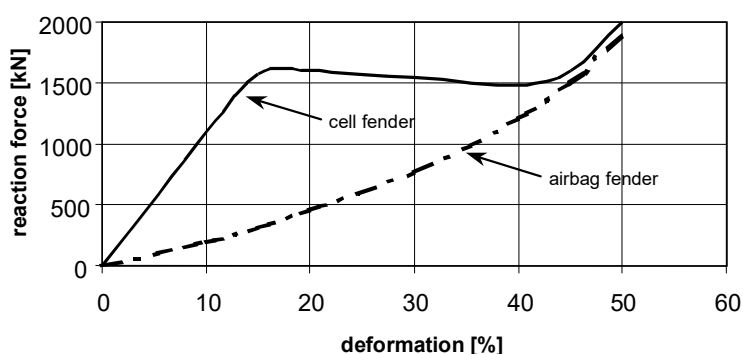


Figure 23-5 Force versus deformation of a cell-fender and an airbag fender

This stiffness of the cell-fender only applies up to a deformation of 15%. After that, the behaviour is no longer linear and the reaction force remains fairly constant at 1,5 MN. The advantage of the cell-fender is that it absorbs a lot of energy by means of a relatively large deformation, without increasing force (rectangular shaped area under the curve). The disadvantage is that the mooring force is very large for possible small boats; during the first initial deformation, the force rapidly increases to a first maximum (triangular shaped area under the curve). Airbag fenders deform more than cell-fenders, but also cause smaller mooring forces for small boats.

Calculation of forces according to the ROK rule-of-thumb

The Richtlijnen voor het Ontwerp van Kunstwerken (ROK) of Rijkswaterstaat (2017) gives the following equation for calculating the collision force F for inland vessels, without using the structural stiffness:

$$F_{coll} = 3,3\sqrt{E_{kin}} + 5,6$$

where: F_{coll} [MN] = collision force
 E_{kin} [MNm] = kinetic energy of the vessel (see previous section)

This equation (mind the units!) applies to structures that are not intended to be hit by vessels and are 'vessel-unfriendly'. It assumes a collision against a rigid structure and the energy is fully absorbed by the vessel, which will thereby be heavily damaged. The damage zone is such, that the plastic deformation of the structure is negligible.

If the vessel hits the structure not in a perpendicular way, the collision force can be decomposed in a force perpendicular to the structure, F_{\perp} and a force parallel to the structure F_{\parallel} :

$$F_{\perp} = F_{coll} \cdot \sin \alpha$$

$$F_{\parallel} = F_{coll} \cdot \cos \alpha$$

where α = the 'collision angle' between the vessel direction and the structure (90° is perpendicular).

This equation applies to collision angles between 63° and 90° (assuming a friction coefficient of 0,5). For smaller angles, the kinetic energy will not be entirely be absorbed by the vessel. For collision angles smaller than 63° , the following equations should be used:

$$F_{\perp} = \delta \cdot F_{coll} \cdot \sin \alpha$$

$$F_{\parallel} = 0,5 \cdot F_{\perp}$$

where δ = a reduction factor according to Table 23-4.

α°	60	50	40	30	20	10	5
δ	0.98	0.91	0.82	0.73	0.64	0.48	0.34

Table 23-4 Reduction factor for the perpendicular collision force component for collision angles $\alpha < 63^{\circ}$ (ROK, 2017)

23.3.3 Design according to Eurocode 1

For preliminary designs, Eurocode 1, part 1-7 (NEN-EN 1991-1-7+C1+A1, 2015), distinguishes between a frontal impact force F_{dx} , in the normal sailing direction, and a lateral force F_{dy} , perpendicular to the sailing direction. Two tables are given with indicative values for the dynamic collision forces, including the effect of the hydrodynamic mass. One table is for inland ships (Table 23-5 in this manual) and the other one is for sea-going vessels (Table 23-6). These tables should not be used for berthing structures that resist the impact load of ships under normal conditions, like quay walls and breasting dolphins.

CEMT ^a class	reference type of ship	length ℓ (m)	mass m (ton) ^a	force F_{dx} ^b (kN)	force F_{dy} ^b (kN)
I		30 – 50	200 – 400	2 000	1 000
II		50 – 60	400 – 650	3 000	1 500
III	'Gustav König'	60 – 80	650 – 1 000	4 000	2 000
IV	Klasse 'Europe'	80 – 90	1 000 – 1 500	5 000	2 500
Va	Groot Rijnschip	0 – 110	1 500 – 3 000	8 000	3 500
Vb	Duwboot + 2 bakken (lang)	110 – 180	3 000 – 6 000	10 000	4 000
Vla	Duwboot + 2 bakken (breed)	110 – 180	3 000 – 6 000	10 000	4 000
Vlb	Duwboot + 4 bakken	110 – 190	6 000 – 12 000	14 000	5 000
Vlc	Duwboot + 6 bakken	190 – 280	10 000 – 18 000	17 000	8 000
VII	Duwboot + 9 bakken	300	14 000 – 27 000	20 000	10 000

^a the mass (1 ton = 1 000 kg) is the total mass of the ship, including ship structure, load and fuel.
^b the forces include the effect of the hydrodynamic mass, and is based on calculations that include the expected circumstances per class of waterway.

Table 23-5 Berthing forces per inland ship class, according to Eurocode 1 (NEN-EN 1991-1-7+C1+A1)

vessel type	length ℓ (m)	mass m ^a (ton)	force F_{dx} ^{b,c} (kN)	force F_{dy} ^{b,c} (kN)
small	50	3 000	30 000	15 000
average	100	10 000	80 000	40 000
large	200	40 000	240 000	120 000
very large	300	100 000	460 000	230 000

^a the mass (1 ton = 1 000 kg) is the total mass of the ship, including the ship structure, load and fuel.
^b the given values are related to a velocity of about 5 m/s and include the effects of additional hydraulic mass.
^c if relevant, the effect of a ram bow (*bulbsteven*) should have been taken into account

Table 23-6 Berthing forces per sea-going vessel class, according to Eurocode 1 (NEN-EN 1991-1-7+C1+A1)

It is recommended to adjust the indicative values given in Table 23-5 and Table 23-6, depending on the consequences of the structural failure due to a ship collision. In case of small consequences, the forces may be reduced. In case of large consequences, the values should be increased. Eurocode 1 recommends a factor of 1,3 for a frontal collision and 1,7 for a lateral collision. In ports and harbours, the values in the tables may be reduced by a factor 0,5.

In case of non-frontal impacts, an additional friction force F_R acts in the same direction as F_{dx} , and can be calculated with:

$$F_R = \mu \cdot F_{dy}$$

where μ represents a friction coefficient [-], for which usually a value of 0,4 is used.

Advanced methods for calculating the collision forces are given in appendix C of Eurocode 1-7 (NEN-EN 1991-1-7+C1+A1).

23.3.4 Design according to AASHTO

The USA standard for bridge design, AASHTO LRFD Bridge Design Specifications (2013) gives the following equation to calculate the kinetic energy of a vessel:

$$E_{kin} = 500 C_H m_s v_s^2 \quad [\text{kJ} = \text{kNm}]$$

where:

- C_H [-] = hydrodynamic coefficient
- m_s [ton] = weight of the vessel displacement
- v_s [m/s] = velocity of the vessel

The value of the hydrodynamic coefficient depends on the keel clearance and the draught of the vessel:

- $C_H = 1,05$ if the keel clearance $> 0,5$ x draught
- $C_H = 1,25$ if the keel clearance $< 0,1$ x draught

Values in between should be interpolated.

The hydrodynamic coefficient for berthing ships is higher than for colliding vessels, because of the larger mass of water that is affected if a quay is approached in parallel direction.

AASHTO gives the following equation for the static impact force of a frontal collision:

$$F_s = 1,2 \cdot 10^5 v_s \sqrt{DWT} \quad [\text{N}]$$

where:

- v_s [m/s] = velocity of the vessel
- DWT [ton] = deadweight tonnage of the vessel

The static force in lateral direction is 50% of the frontal force F_s .

23.4 Design of fenders

Fenders absorb kinetic energy of mooring ships in such a way, that the force on the structure (thereby also the force on the ship) remains below an acceptable limit. The amount of energy that needs to be

absorbed is $E = \int_0^{u, \max} F(u) \delta u$, in which $F(u)$ is the force and u, \max is the entire displacement. This leads

to the conclusion that for a given amount of energy, the force is determined by the total displacement and therefore the stiffness of the structure. In principle, the more flexible the structure is, the smaller the force is and the larger the displacement. The relationship between the force and the displacement is determined by the spring characteristics of the structure. The spring characteristics of a linearly elastic structure are linear. In the case of rubber fenders, the spring characteristics are generally not linear. An example for a rubber cell fender is given in Figure 29-6.

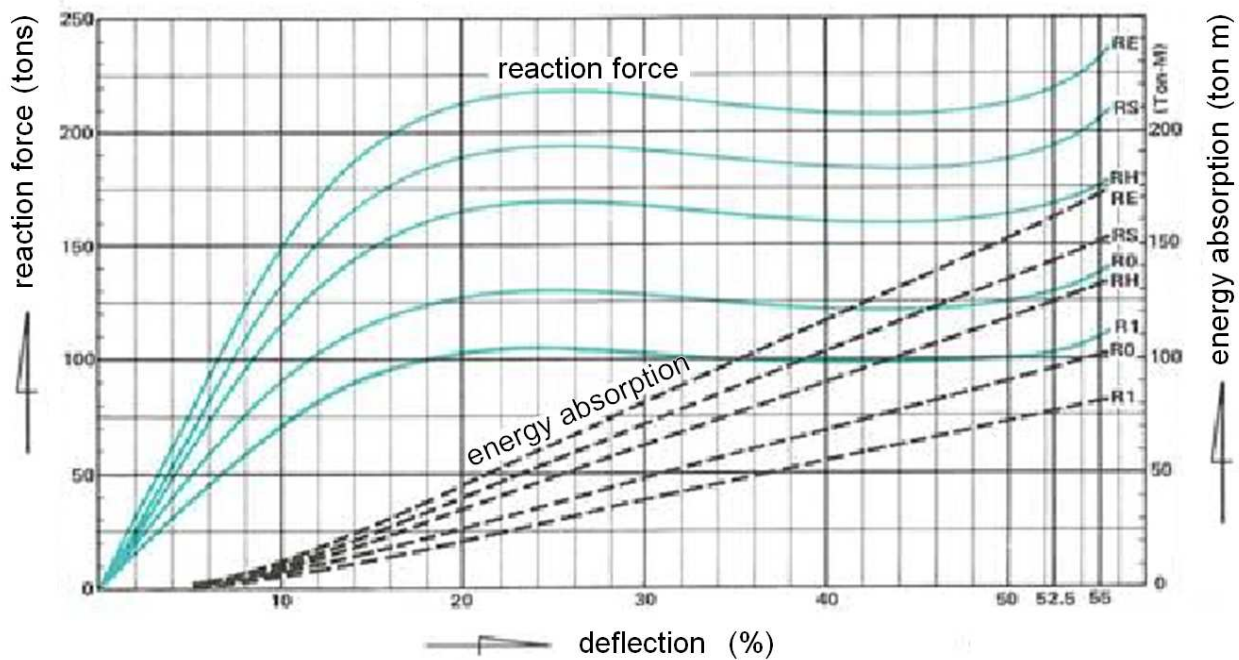


Figure 23-6 Spring characteristics of Cell-fenders with different rubber compound (source unknown)

Fender panels are used to spread the concentrated force of the fender over a larger part of the ship's hull. The distributed load on the ship should not exceed 400 kN/m^2 to prevent damage to tankers. It is important to take the kind of ship and its cargo into account when selecting a fender type. For instance, at mooring places for Nafta tankers, it is important to keep the forces on the ship small, resulting in soft fenders. A disadvantage of such soft fenders is that the movements of the moored ship will be larger.

Guidelines for the design of fender systems are given in PIANC report 33 (2002).

23.5 Literature

AASHTO LRFD Bridge Design Specifications - SI Units (8th Edition). American Association of State Highway and Transportation Officials (AASHTO), Washington, DC, 4th ed. edition, 2017. ISBN 9781560516545.

Eurocode 1: Actions on structures, Part 1-7: General actions - Accidental actions. NEN-EN 1991-1-7+C1+A1, 2015.

PIANC (2002). Guidelines for the design of fender systems. Report 33. Brussels, Belgium.

PIANC (2014). Design of lock gates for ship collision. Report 151. Brussels, Belgium.

Rijkswaterstaat (2017). Richtlijnen Ontwerp Kunstwerken (ROK). Technisch document.RWS, dienst GPO.

Vasco Costa, F. (1973). Dynamics of berthing impacts. NATO Advanced Study Institute on Analytical Treatment of Problems in the Berthing and Mooring of Ships. Wallingford, England.

24. Shipping - mooring forces

24.1 Theory

Mooring forces are relevant for the design of bollards (*bolders*) on quays, and quay walls, for the design of ships and for the choice of suitable mooring ropes, also called 'hawsers' (*trossen*).

Forces in mooring ropes can be caused by:

- Loads on the ship such as wind, current and water level differences (filling a lock!)
- Movements of the ship, the mass of the ship and the stiffness of the mooring cables are of importance in this respect.
- Pre-stressing forces in the mooring cables

Pre-stressing forces in the cables are generated during the hauling in and after mooring. The fracturing force of the cables and the number of cables limit the mooring force. Increasingly, modern quays and mooring structures are equipped with "quick release hooks". These release the mooring cables automatically if a maximum force is exceeded. So-called yielding bolts are used to connect the structure with conventional bollards and mooring bits, which are still used often in heavy quay structures and sluices. The yielding bolts yield when the maximum acceptable force is exceeded.

24.2 Preliminary design

For a preliminary design one can assume the mooring forces for seagoing vessels, self-propelled barges (for inland waterways) (*binnenvaartschepen*) and yachts (*plezierjachten*) as specified in the tables below, as can be found in several standards, like the German EAU 2012 and British Standard 6394 (part 4), with more or less similar values.

Seagoing vessels	
water displacement of ship [ton] ⁹⁾	mooring force
	[kN]
< 2 000	0 - 100
2 000 ~ 10 000	100 - 300
10 000 ~ 20 000	300 - 600
20 000 ~ 50 000	600 - 800
50 000 ~ 100 000	800 - 1000
100 000 ~ 200 000	1000 - 1500
> 200 000	1500 - 2000

Table 24-1 Mooring forces of sea going ships per bolder

Inland barges	
class of ship ¹⁰⁾	mooring force [kN]
CEMT Class I + II	150
CEMT Class III + IV	200
CEMT Class V	250
CEMT Class VIa	300
CEMT Class VIb	350

Table 24-2 Mooring forces of inland barges per bolder (RVW 2017)

Yachts	
class of ship	mooring force [kN]
Yachts	55

Table 24-3 Mooring forces of yachts per bolder

Guidelines for mooring systems can be found in PIANC reports 168 (Single point yacht mooring design and 186 (Mooring of large ships at quay walls) and RecCom report 10 (Mooring systems for recreational crafts, 2005).

⁹ Example: Water displacement of a seagoing ship = 70 000 tonnes: Mooring force = $800 + 200 \cdot (70-50) / (100-50) = 880$ kN.

¹⁰ The CEMT barge class definitions can be found in the 'Richtlijnen Vaarwegen 2017' of *Rijkswaterstaat* (downloadable from internet).

Manual Hydraulic Structures

Part II: Materials

25. Soil - properties

Section 25.5 extended: 2015. Chapter re-arranged and expanded: 2021

25.1 Purpose of determining soil types and characteristics

Stiffness and strength of soils

Before collecting or calculating soil parameters, one must be aware of whether the type of problem that has to be dealt with is:

- a strength problem (e.g., the stability of a dike),
- a stiffness problem (e.g., the settlement of a road) or
- a mixed problem (e.g., the foundation of a structure).

Specific tests exist to determine the strength parameters (e.g., the direct shear test) and the stiffness parameters (e.g., the oedometer test). Tests to determine both types of parameters also exist (e.g., tri-axial compression test).

Most calculations also distinguish between problems of strength and stiffness. Koppejan's settlement calculation, for example, is a stiffness calculation. Prandtl and Brinch Hansen's bearing capacity calculation is a strength calculation and the spring model used to calculate sheet piling (like D-Sheet Piling) is a mixed model; the model produces estimates of both strength and displacement(s). The problem, the parameters and the calculation must correspond.

Soil investigation

Loads on hydraulic engineering works are transferred to the subsoil. The properties of the soil are therefore of great importance for the design and the dimensioning of a structure. The nature of the loads on the structure and the properties of the subsoil determines the choice of the type of foundation.

A number of techniques are available to investigate the subsoil. This includes:

- soundings
- borings
- water pressure measurements
- vane shear tests (determination of c_u)
- pump tests
- (seismic research)
- (nuclear research)

These research methods are suitable to investigate the layered composition of the soil and to estimate some soil parameters. The subsoil is usually composed of different types of soil layers. First, an attempt is made at establishing the structure of the soil layers. For this, see Section 25.3. After that, the necessary soil parameters are determined for every soil layer. Fieldwork provides all the required information, but to determine the soil parameters more accurately laboratory tests are needed. It is best to obtain soil samples by boring; these samples can then subsequently be tested in a laboratory.

The most important laboratory tests for alluvial soil types (sand and clay) are:

- consolidation test (= oedometer test) (determination of stiffness and permeability)
- triaxial compression test (determination of stiffness and strength)
- (permeability test)
- (direct shear test)
- (Cassagrande's test)

For rock and stony materials, other parameters are relevant, such as the compression strength, the splitting strength, the density and the permeability. Tests mentioned above can be used to calculate the representative parameters of a given soil layer. For this see Section 0 "Determination of soil parameters from laboratory tests".

If no laboratory tests are available, a few soil parameters one can be estimated empirically, using the q_c values of the soundings. For this refer to Section 0 "Determination of soil parameters from cone penetration tests values". Alternatively, values coming from Dutch practice can be used. Table 25-6 of Section 0 gives the representative low values of several important soil parameters for a number of soil types. Besides the aforementioned parameters the table mentions the following parameters: volumetric

weight (γ), sounding value (q_c), swelling coefficient (C_{sw} , to be used instead of C_c in case of pressure reduction), Young's modulus (E), and the undrained shear strength ($f_{undr} = c_u$).

25.2 Determination of soil types

Soil type determination based on particle diameter

ISO 14688-1:2002, establishes the basic principles for the identification and classification of soils on the basis of those material and mass characteristics most commonly used for soils for engineering purposes. Table 25-1 is applicable to natural soils in situ, similar man-made materials in situ and soils redeposited by people.

ϕ scale	Size range (metric)	Aggregate name (Wentworth class)	Other names
<-8	>256 mm	Boulder	
-6 to -8	64-256 mm	Cobble	
-5 to -6	32-64 mm	Very coarse gravel	Pebble
-4 to -5	16-32 mm	Coarse gravel	Pebble
-3 to -4	8-16 mm	Medium gravel	Pebble
-2 to -3	4-8 mm	Fine gravel	Pebble
-1 to -2	2-4 mm	Very fine gravel	Granule
0 to -1	1-2 mm	Very coarse sand	
1 to 0	0.5-1 mm	Coarse sand	
2 to 1	0.25-0.5 mm	Medium sand	
3 to 2	125-250 μm	Fine sand	
4 to 3	62.5-125 μm	Very fine sand	
8 to 4	3.9-62.5 μm	Silt	Mud
10 to 8	0.98-3.9 μm	Clay	Mud
20 to 10	0.95-977 nm	Colloid	Mud

Table 25-1 ISO 14688-1:2002 classification for sediments (ISO, 2002)

Dutch standard NEN 5104 uses a slightly different classification, see Table 25-2.

particle size		fraction
from	to	
-	2 μm	lutum
2 μm	63 μm	silt
63 μm	105 μm	very fine sand
105 μm	150 μm	fine sand
150 μm	210 μm	medium fine sand
210 μm	300 μm	medium coarse sand
300 μm	420 μm	coarse sand
420 μm	2,0 mm	very coarse sand
2,0 mm	5,6 mm	fine gravel
5,6 mm	16 mm	medium course gravel
16 mm	63 mm	course gravel
63 mm	200 mm	pebbles / cobbles ¹
200 mm	630 mm	boulders
630 mm	-	blocks

Table 25-2 Classification of soil types per particle size (NEN 5104)

¹ Cobbles are larger than pebbles, but they resort under one category, different from 'gravel', according to NEN 5104.

Soil type determination based on cone penetration tests

Soil type determination, based on cone resistance and friction ratio

A CPT including local friction measurement clearly shows which soil layers are present and is therefore used most often. There is a strong correlation between the soil type and the friction ratio, see Table 25-3. The friction ratio is the sleeve friction divided by the cone resistance and is therefore dimensionless. Nowadays, the cylindrical electronic penetrometer with friction sleeve is often used for soundings.

soil type	cone resistance [MPa]	friction ratio [-]
gravel	> 4 - 10	0,2 - 0,5
coarse sand	> 2 - 10	0,4 - 0,6
fine sand	> 1 - 10	0,9 - 1,0
silty sand	1,5 - 4	0,8 - 1,4
clayey sand	1 - 2	1,0 - 2,0
loam	1 - 3	2,0 - 4,0
clay, stiff	2 - 4	2,0 - 4,0
clay, medium	1 - 2	3,0 - 5,0
clay, soft	0,5 - 1,0	4,0 - 6,0
clayey peat	0,1 - 0,5	5,0 - 8,0
peat	0,1 - 2,0	5,0 - 10,0

Table 25-3 Indicative values of cone resistance and friction ratio per soil type (Reader Geotechniek, 2014)

Notes

- It is advisable to always carry out a couple of borings; firstly, because the percentages in the table above are not always correct; secondly, because a boring provides a lot of visual information and thirdly because a boring is necessary to obtain soil samples for laboratory tests.
- It is important that one first compares the table above with the values found by borings. One should therefore always carry out a sounding near a boring.
- If weak soil layers are present (especially for an excavation (building site)), it is sensible to have a couple of CPTs that include water pressure measurements carried out, because these measurements distinguish well between permeable and non-permeable soil layers.

Method Robertson

Peter Robertson developed a more sophisticated classification chart that is used for the determination of soil (behaviour) types. The simplest version of this chart, which was published by Robertson in 1986 and updated in 2010, uses the CPT-values of the cone resistance and the friction ratio, see Figure 25-1. The cone resistance is made dimensionless by dividing it with the atmospheric pressure p_a (0,1 MPa).

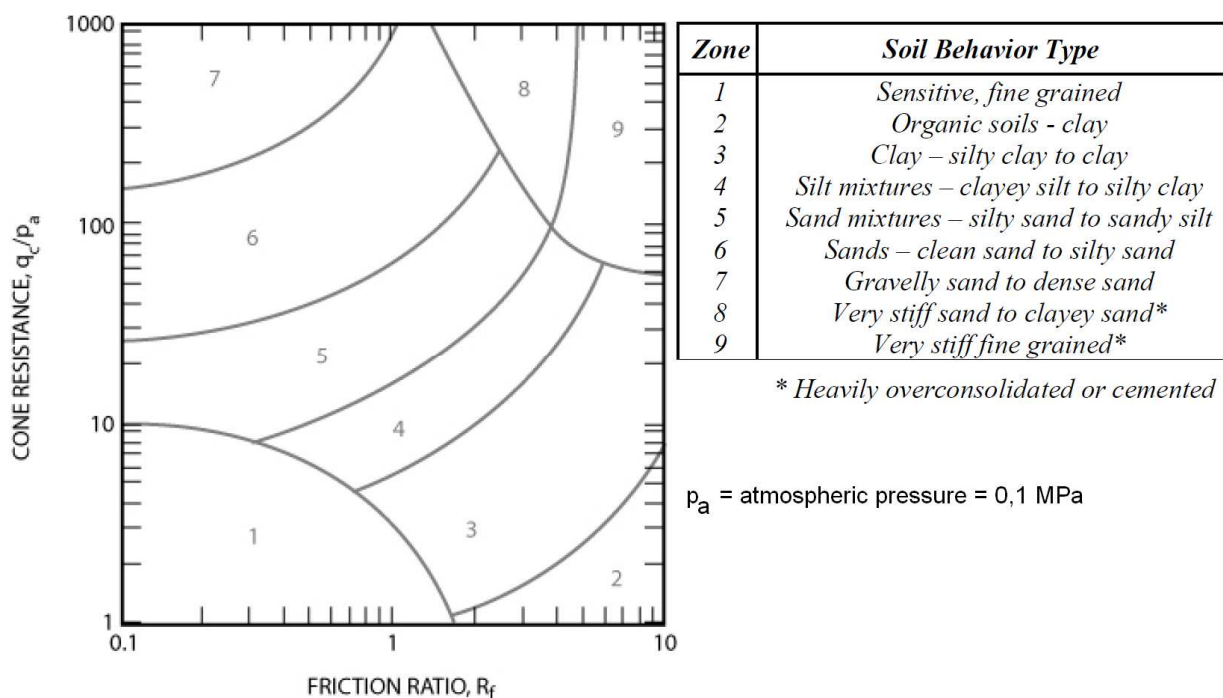


Figure 25-1 Soil classification chart based on CPT cone resistance and friction ratio (Robertson 1986, 2010)

The chart is global in nature and can provide reasonable predictions of soil behaviour type for CPT soundings up to about 20 m in depth. Overlap in some zones should be expected and the zones should be adjusted somewhat based on local experience.

Robertson improved this chart by using a normalized cone resistance Q_t and a normalized friction ratio F_R :

$$Q_t = \frac{q_t - \sigma_{vo}}{\sigma'_{vo}} \tag{31.1}$$

$$F_R = \frac{f_s}{q_t - \sigma_{vo}} \cdot 100 \tag{31.2}$$

- where: Q_t [-] = normalized cone resistance
 F_R [%] = normalized friction ratio
 q_t [MPa] = measured CPT cone resistance, corrected for pore pressure:
 $q_t = q_c + (1 - \alpha) \cdot u_2$ if the pore pressure filter is directly behind the cone tip
 $q_t = q_c + (1 - \alpha) \cdot \{\beta(u_1 - u_0) + u_0\}$ if the filter is situated in the cone tip
 $q_t = q_c$ in sandy soils, or if pore pressures were not measured
 u_0 = hydrostatic water pressure
 u_1 = water pressure if the pore pressure filter is situated in the cone tip
 u_2 = water pressure if the pore pressure filter is situated behind the cone tip
 α = net area ratio of the cone because of the slit behind the cone tip
 α is usually determined from laboratory calibration, with typical values between 0,70 and 0,85
 β = factor for the differing soil types for the conversion of u_1 to u_2
 mostly $\beta = 0,8$ is used
 σ_{vo} [MPa] = total vertical soil stress determined using the specific weight per soil layer
 σ'_{vo} [MPa] = effective vertical soil stress determined using the specific weight per soil layer
 f_s [MPa] = measured CPT cone resistance (not corrected)

The normalized chart is shown in Figure 25-2.

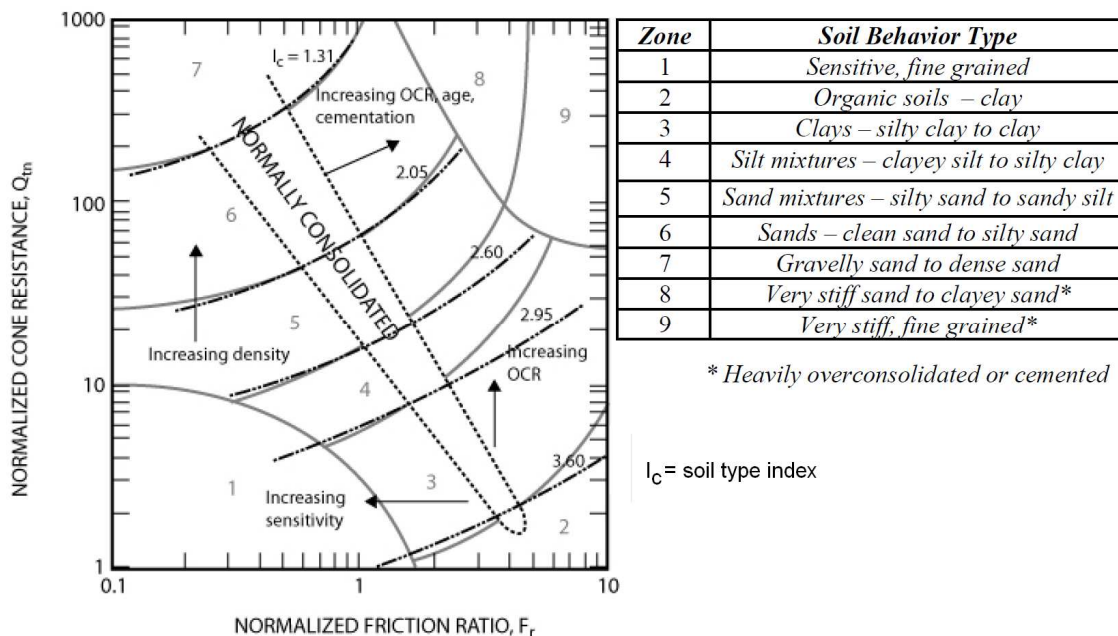


Figure 25-2 Normalized chart for the classification of soil types on basis of SPT (Robertson 1990, 2010)

This normalized chart corrects for unequal cone end area effects and some other effects related to specific characteristics of the CPT. The normalized chart in general provides more reliable identification of soil types than the non-normalized chart, although when the in-situ vertical effective stress is between 50 and 150 kPa, there is often little difference between the two charts. The advantage of the non-normalized chart is that it can be used in real-time to evaluate the soil type during and immediately after the CPT. The normalized chart can only be used after the CPT during post-processing, because it requires information on soil specific weights and groundwater conditions that are not available during the CPT.

In this double-logarithmic chart, the boundaries between the soil types can be approximated by concentric circles. A soil type index, describing these circles, can be defined by:

$$I_c = \sqrt{\left(3,47 - \log\left(\frac{q_c}{p_a}\right)\right)^2 + \left(\log R_f + 1,22\right)^2} \quad (31.3)$$

(use the basic CPT-values for the non-normalized chart)

Instead of the charts, Table 25-4 can be used now to identify soil types (which is very suitable for automated identification of soil types).

Zone	Soil Behavior Type	I_c
1	Sensitive, fine grained	N/A
2	Organic soils – clay	> 3.6
3	Clays – silty clay to clay	2.95 – 3.6
4	Silt mixtures – clayey silt to silty clay	2.60 – 2.95
5	Sand mixtures – silty sand to sandy silt	2.05 – 2.6
6	Sands – clean sand to silty sand	1.31 – 2.05
7	Gravelly sand to dense sand	< 1.31
8	Very stiff sand to clayey sand*	N/A
9	Very stiff, fine grained*	N/A

Table 25-4 Soil types related to soil type index I_c

25.3 Determination of soil type characteristics

Determination of soil parameters from laboratory tests

For the weak soil layers compression test are usually carried out in case of settlement questions, for strength questions triaxial test are usual. For stronger soil layers (sand and gravel), usually only triaxial tests are performed. From these tests one can determine the strength and stiffness parameters for a certain soil layer.

In calculations the 5% upper or lower limit values are to be used. For soil both the real average value x_{avg} and the real average spread σ are unknown. That is why an average value x_{avg} and the standard deviation σ are first determined with tests. Subsequently, the student- t method can be used to calculate the representative upper or lower limits of the average x_{rep} :

$$x_{rep} = x_{avg,5\%char} = x_{avg} \pm t_{5\%} \cdot \sigma \cdot \frac{1}{\sqrt{n}} \quad (31.4)$$

in which n is the number of tests.

The value of $t_{5\%}$ depends on the number of samples n :

n	2	3	4	5	6	7	8	9	10	11	21	∞
$t_{5\%}$	6,31	2,92	2,35	2,13	2,01	1,94	1,89	1,86	1,83	1,81	1,72	1,64

Table 25-5 Student- t distribution

Determination of soil parameters from cone penetration tests

If no laboratory tests have been carried out, one can estimate the stiffness and strength parameters of the soil layers for a preliminary design with rules of thumb using the sounding values (q_c). Electric Cone penetration tests (CPTs) provide a fast, repeatable and economical way to determine soil stratigraphy and soil types. There are various ways to determine soil types from these tests, using the measured cone resistance q_c , the sleeve friction f_s and, if available, the pore pressure u . Instead of the sleeve friction, the friction ratio R_f is often used:

$$R_f = \frac{f_s}{q_c} \cdot 100 \quad (31.5)$$

where R_f [%] = friction ratio
 f_s [MPa] = CPT sleeve friction
 q_c [MPa] = CPT cone resistance

The best way to determine what soil type a soil layer consists of is to carry out borings in different locations and to analyse the samples in a laboratory. Usually, one opts for a cheaper alternative. In this case only a few borings and a (much) larger number of cone penetration tests (CPT) are carried out (e.g. every 25 metres). The cheaper CPT's (*sonderingen*) are then linked to the more expensive boring samples, to determine the soil profile and the soil characteristics of every layer that has been distinguished.

There are two types of CPT's, related to the type of cone being used. One measures both the cone resistance and the local friction and one measures the cone resistance and the (pore) water pressure.

The CPT including water pressure measurements clearly shows:

- where the impermeable layers (clay and peat) are.
- how well the layer seals off water.
- what the water pressure is at a greater depth, in the permeable layers (sand and gravel).

Sand (rules of thumb)

The Young's modulus E results from:

$$E_{oed} = \frac{(1-\nu)}{(1+\nu)(1-2\nu)} E \quad (31.6)$$

with:

E_{oed} = constrained modulus (*modulus bij zijdelingse opsluiting*):

$$\begin{aligned} E_{oed} &= 4 q_c && 0 < q_c < 10 \text{ MPa} \\ &= 2 q_c + 20 \text{ MPa} && \text{for: } 10 < q_c < 50 \text{ MPa} \\ &= 120 \text{ MPa} && 50 \text{ MPa} < q_c \end{aligned}$$

$$\nu \quad [-] = \text{Poisson's ratio (dwarscontractiecoëfficiënt): } \nu = 0,3$$

Other parameters for sand: $c' = 0$ and $\phi' = 29^\circ + \frac{q_c}{4 \text{ MPa/}^\circ}$

For sand calculations assume the drained values (so the parameters with an \times' , instead of \times_u).

If there are no known values of q_c or if these values vary too much, one can use the following as a rough estimate for clean sand: $E = 250 \sigma_v'$ and $\phi = 32^\circ$.

For unloading and reloading, the following applies (for sand, clay and peat): $E_{unload/reload} \approx (3 \sim 5) \cdot E'$

Clay, peat and loam (rules of thumb)

$$c_u = f_{undr} = \frac{q_c}{20} \quad (\text{clay/loam})$$

$$c_u = f_{undr} = \frac{q_c}{30} \quad (\text{peat, humous clay})$$

$$E_u \approx E = 100 \cdot f_{undr} \quad (\text{clay/peat})$$

$$E_u \approx E = 40 \cdot f_{undr} \quad (\text{loam})$$

$$\nu = 0,4$$

$$\nu_u = 0,5$$

For clay, peat and loam one must distinguish between a short-term load (undrained, so parameters with an \times_u) and a long-term load (drained, so parameters with an \times'). For the drained stiffness E' the assumption $E_u \approx E'$ does not take creep into account. For calculations concerning the stiffness of drained soil, it is preferable to use the primary and secondary settlement constants C_p and C_s .

The following applies for unloading and reloading (for sand, clay and peat): $E_{unload/reload} \approx (3 \sim 5) \cdot E$

Determination of soil parameters with the Eurocode table

The table on the next page is table 1 from Eurocode 7. It shows the representative values X_{rep} for different soil types. The table is based on values found in practice in the Netherlands. These values can be used in the Netherlands as an estimate if no laboratory research is available.

Soil type		Representative value ^{a)} of the soil property															
Main type	consistency ^{b)}	γ	γ_{sat}	q_c	C_p	C'_s	$C_c / (1+e_0)$	C_a	η	$C_{sw} / (1+e_0)$	E_{100}	ϕ	c'	c_u ($= f_{und}$)			
		kN/m ³	kN/m ³	Mpa							Mpa	°	kPa	kPa			
gravel	slightly silty	17	19	15	500	∞	0,0046	0		0,0015	45	32,5	0	-			
	moderate	18	20	25	1000	∞	0,0023	0		0,0008	75	35	0	-			
	solid	19	20	30	1200	1400	0,0019	0,0016		0,0006	90	37,5	40	0			
sand	loose	18	20	10	400	∞	0,0058	0		0,0019	30	30	0	-			
	moderate	19	21	15	600	∞	0,0038	0		0,0013	45	32,5	0	-			
	solid	20	21	22,5	1000	1500	0,0023	0,0015		0,0008	75	35	40	0			
loam ^{a)}	loose	17	19	5	200	∞	0,0115	0		0,0038	15	30	0	-			
	moderate	18	20	15	600	∞	0,0038	0		0,0013	45	32,5	0	-			
	solid	19	20	25	1000	1500	0,0023	0,0015		0,0008	75	35	40	0			
clay	slightly silty clayey	18	19	12	450	650	0,0051	0,0035		0,0017	35	30	27	32,5	0		
	greatly silty clayey	18	19	8	200	400	0,0115	0,0038		0,0038	15	30	25	30	0		
	slightly sandy	19	19	1	25	650	0,0920	0,0037		0,0307	2	27,5	30	0	50		
clay	moderate	20	20	2	45	1300	0,0511	0,0020		0,0170	3	27,5	32,5	1	100		
	solid	21	22	3	70	1900	0,0329	0,0230		0,0013	0,0009	5	7	2,5	3,8	200	
	greatly sandy	19	20	2	45	70	0,0511	0,0329		0,0170	0,0110	3	5	27,5	35	0	1
clay	weak	14	14	0,5	7	80	0,3286	0,0131		0,1095	1	17,5	0	25			
	moderate	17	17	1	15	160	0,1533	0,0061		0,0311	2	17,5	5	50			
	solid	19	20	2	25	320	0,0920	0,0767		0,0307	0,0256	4	10	13	15	100	
clay	weak	15	15	0,7	10	110	0,2300	0,0092		0,0767	1,5	22,5	0	40			
	moderate	18	18	1,5	20	240	0,1150	0,0046		0,0383	3	22,5	5	80			
	solid	20	21	2,5	30	500	0,0767	0,0460		0,0256	0,0153	5	10	13	15	120	
peat	greatly sandy	18	20	1	25	50	0,0920	0,0164		0,0037	0,0007	2	5	27,5	32,5	0	1
	organic	13	13	0,2	7,5	30	0,3067	0,0153		0,1022	0,5	15	0	1	10		
	moderate	15	16	0,5	10	40	0,2300	0,1533		0,0115	0,0077	1	2	0	1	25	
peat	weak	10	12	0,1	5	20	0,4600	0,3067		0,0230	0,0153	0,2	0,5	1	2,5	10	
	moderately preloaded	12	13	0,2	7,5	10	0,3067	0,2300		0,0153	0,0115	0,5	1,0	2,5	5	20	
	variation coefficient	0,05	0,05	-	-	-	0,23	0,23		0,1022	0,0767	0,5	1,0	2,5	5	20	

Table 25-6 Indicative soil properties according to Eurocode 7 NEN-EN9997 (to be verified by on-site soil investigation!)

^{a)} The table gives the low and the high characteristic value of the average of the soil type concerned. If an increase of the characteristic value of a soil property would lead to a situation that is more unfavourable than the given low value for that property, the value on the right should be used. If there is no value mentioned on the right side of a cell, then the value just below it should be used. This is, for example, the case for negative friction on a pile where a higher value for ϕ' , c' and c_u also results in a high value of the negative friction. The table gives the high characteristic average values for $C_c / (1+e_0)$, C_a and $C_{sw} / (1+e_0)$.

^{b)} Loose: $0 < R_n < 0,33$; moderate: $0,33 < R_n < 0,67$; solid: $0,67 < R_n < 1,00$.

^{c)} The γ -values are applicable to a natural moisture content

^{d)} The values for α_c (cone resistance) given in this table should be considered as entry values for use of the table and should not be used in calculations.

^{e)} The values concern saturated loam

^{f)} The C_a -values are valid for a trajectory of stress increase of at least 100%.

^{g)} For gravel, sand and to a lesser extent also for loam and sandy clay, α_c , E_{100} , ϕ' and the compressibility coefficients C_p , $C_c / (1+e_0)$ and $C_{sw} / (1+e_0)$ are normalised for an effective soil stress σ'_v of 100 kPa. In that sense the equation $q_{c,meas} = q_c \cdot \text{meas} \cdot C_{cp}$ should be used, where $C_{cp} = (100 / \sigma'_v)^{0,67}$. For an angle of internal friction ϕ' and cohesion c' it applies that these are dependent on the consistency of the soil. This implies that this conversion is also needed for ϕ' and c' . If $q_{c,meas}$ would become larger than the value given in the table, the value given in the lowest row of the concerning soil type should be used.

^{h)} The Youngs' modulus in case of recurrent stress can be considered to be three times the given value.

Example: In clean sand at a depth of 5 m below water it is measured that $q_{c,meas} = 9$ MPa and $\sigma'_v = 50$ kPa. C_{cp} then is $2^{0,67} \approx 1,6$ and $q_{c,meas} = 9 \cdot 1,6 = 14,4$ MPa. This means that $E = 45$ MPa, $\phi' = 32,5^\circ$, $C_p = 600$, $C_c / (1+e_0) = 0,0038$ and $C_{sw} / (1+e_0) = 0,0013$.

25.4 Soil parameters and models

In all engineering sciences an effort is made to link analytical, numerical and physical models. Below the analytical Mohr-Coulomb model and some numerical models are linked, by means of the soil properties, to soil investigation results (= 'real' physical model).

Mohr-Coulomb (general)

Strength:

In the Mohr-Coulomb model the following expressions are derived for drained and undrained shear strengths respectively:

$$\text{Drained: } \tau_{\max} = c' \cdot \cos(\phi) + \frac{1}{2}(\sigma_h' + \sigma_v') \cdot \sin(\phi) \quad (31.7)$$

$$\text{Undrained: } f_{undr} = c_u = \tau_{\max} = c' \cdot \cos(\phi) + \frac{1}{2}(\sigma_h' + \sigma_v') \cdot \sin(\phi) \quad (31.8)$$

The stresses σ_v' and σ_h' can be assumed equal to the stresses before loading because during the quick loading the normal effective stresses and thus the strength of the undrained soil does not change.

The difference between the above-mentioned Mohr-Coulomb strength and the Coulomb strength is quite significant:

$$\tau_{\max} = c' + \sigma_n' \cdot \tan(\phi) \quad (\text{Coulomb}) \quad (31.9)$$

Stiffness:

$$E_{oed} = \frac{(1-\nu)}{(1+\nu)(1-2\nu)} E \quad (31.10)$$

$$K = \frac{E}{3(1-2\nu)} \quad (31.11)$$

$$G = \frac{E}{2(1+\nu)} \quad (\tau = G\gamma) \quad (31.12)$$

$$\sigma_h' = K_0 \cdot \sigma_v' \quad \text{with: } K_0 = \frac{\nu}{1-\nu} \quad (\text{which differs from Jáký's formula: } K_0 = 1 - \sin\phi) \quad (31.13)$$

According to Mohr-Coulomb, the difference between the stiffness to be taken into account for drained or undrained loading of clay is merely a factor:

$$\frac{E_u}{E'} = \frac{1+\nu_u}{1+\nu'} \quad \text{with: } \nu_u = 0,5 \quad \text{and} \quad \nu' = 0,3 \quad \Rightarrow \quad \frac{E_u}{E'} = 1,15 \quad (31.14)$$

In reality the difference is bigger because Mohr-Coulomb does not take creep into account. For clay and peat, it is better to assume:

$$\frac{E_u}{E'} \approx 2 \text{ to } 3 \quad (31.15)$$

It is even better to use Koppejan's settlement formulas (Section 28.2) and the primary and secondary settlement constants C_P and C_S in calculations.

In the case of unloading and reloading one can assume that a little creep occurs, thus one can presume:

$$E_{\text{relief / reapplication}} \approx (3 \sim 5) \cdot E' \quad (31.16)$$

Winkler

Soil is often modelled as a set of uncoupled linear springs, known as the Winkler model. See Chapter 27 for a further description of spring schematisations.

D-sheet Piling (spring model)

D-Sheet Piling (named Msheet in earlier days) is a computer programme for the calculation of (mostly) sheet pile walls and laterally loaded piles. It is based on Winkler's spring model. When using the programme, a choice has to be made between the use of either straight or curved slip planes in the soil. The physical reality is such that the friction between the sheet piling or pile and the soil results in curved slip planes instead of straight planes. For hand calculations curved slip planes are far too difficult to calculate. For convenience, one uses straight slip planes instead. However, the straight slip planes model calculates a strength that is too optimistic, hence less safe. To arrive at a more conservative, safe, strength the wall friction angle δ should be reduced more in straight than in the curved slip planes model. Using D-Sheet Piling, or similar computer programmes, it is anyway better to choose for curved slip planes, because it is more accurate (the computer does the extra/more difficult computation).

For the calculation of slip planes with wall friction angle δ Eurocode 7, NEN 9997-1+C1:2012 applies:

Qualitative description wall surface	More specific definition Roughness wall surface	Wall friction angle δ	
		Straight slip surface	Curved slip surface
Toothed	$> 10 d_{50}$	$2/3 \varphi'_k$	$\leq \varphi'_k$
Rough	$0.5 d_{50} - 10 d_{50}$	$2/3 \varphi'_k$	$\leq \varphi'_k - 2.5^\circ$ with a maximum of 27.5°
Half rough	$0.1 d_{50} - 0.5 d_{50}$	$2/3 \varphi'_k$	$2/3 \varphi'_k$
Smooth	$0.1 < d_{50}$	0°	0°

* For clay, loam, sand and pebbles

** For diaphragm walls the wall friction angle has to be reduced more than for steel walls

The stiffness (modulus of sub grade reactions for the springs) is discussed in Section 27.2 "Modulus of subgrade reaction". The strength of the soil is covered in Chapter 26.

Plaxis (finite elements model)

Plaxis can calculate using several soil models. All models require a reduction of the friction at the soil-structure interfaces.

For vertical interfaces one can assume: $R_{\text{interface}} \approx 0,8$ so: $\tan(\delta) \approx 0,8 \cdot \tan(\phi)$

For horizontal interfaces one can assume: $R_{\text{interface}} \approx 0,67$ so: $\tan(\delta) \approx \frac{2}{3} \cdot \tan(\phi)$

For this see Section 26.3 "Soil - strength, Horizontal bearing capacity (resistance against sliding)".

If the Soft-Soil (Creep) Model is used in Plaxis, the following applies for clay and peat:

$$\lambda^* = \frac{1}{C'_p} \quad (31.17)$$

$$\kappa^* \approx \frac{1 - \nu_{\text{unloading}}}{1 + \nu_{\text{unloading}}} \cdot \frac{1 + 2K_0}{C_p} \quad \text{with: } \nu_{\text{unloading}} \approx 0,15 \quad \text{and: } K_0 \approx 0,60 \quad (31.18)$$

$$\mu^* \approx \frac{1}{\ln(10)} \cdot \frac{1}{C'_s} \quad (31.19)$$

25.5 Literature

Paul W. Mayne, Matthew R. Coop, Sarah M. Springman, An-Bin Huang and Jorge G. Zornberg. *Geomaterial behavior and testing*. Proceedings of the 17th International Conference on Soil Mechanics and Geotechnical Engineering, 2009.

Peter K. Robertson. *Soil classification using the cone penetration test*. Canadian Geotechnical Journal, NRC Research Press, 1990

Peter K. Robertson. *Soil behaviour type from the CPT: an update*. 2nd International symposium on Cone Penetration Testing. 2010

Peter K. Robertson and K.L. Cabal (Robertson). *Guide to Cone Penetration Testing for Geotechnical Engineering*. Gregg Drilling & Testing, Inc. 5th Edition, November 2012

A. Verruijt. *Soil mechanics*. Delft University of Technology, 2001, 2012

26. Soil - strength (resulting in bearing capacity)

(improved: February 2017, liquefaction added in 2023)

In general, the bearing capacity of a soil should be sufficient to resist the acting loads:

$$S < R \rightarrow \sigma'_{k,max} < p'_{max}$$

The maximum value of the resulting vertical pressure applied by a structure, $\sigma'_{k,max}$, can be calculated according to Section 37.3 of this Manual. The present chapter covers some of the classic methods concerning the bearing capacity of soil, p'_{max} :

- Mohr-Coulomb (general strength theory)
- Prandtl and Brinch Hansen (vertical bearing capacity)
- Horizontal bearing capacity
- Fellenius and Bishop (stability of a slope, including reinforced earth)

26.1 Theory: strength schematization (Mohr-Coulomb)

Various models are available to schematise the strength of soil. The most important models are the Mohr-Coulomb model and the Cam Clay model. This manual only discusses the Mohr-Coulomb model. Mohr's circle of stress shows all stress combinations possible in the soil. Coulomb's line of collapse shows which combination leads to collapse and when. These two parts together form the Mohr-Coulomb model.

Mohr

Mohr's circle of stress shows all stress combinations in a two-dimensional space, given that there are two planes with zero shear stress, in which only a normal stress acts. The directions of the normal stresses in these two planes are called the principal directions. If the stresses in two planes are known, all states of stress are defined by Mohr's circle (Figure 26-1).

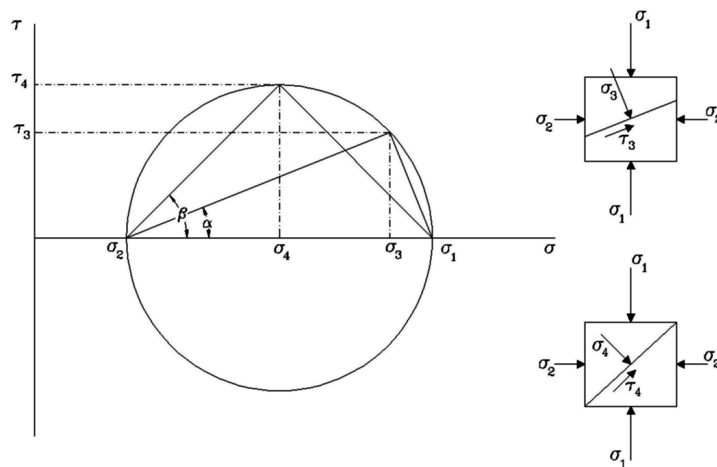


Figure 26-1 Mohr's circle

Coulomb

Coulomb assumes a strength that is expressed by the shear resistance. If this resistance to shear is exceeded a plane of slip is created. The maximum shear resistance is:

$$\tau_{max} = c' + \sigma'_n \tan(\delta)$$

in which:

τ_{max}	[kPa]	= max shear stress on a given plane
c'	[kPa]	= cohesion
δ	[°]	= angle of internal friction
σ'_n	[kPa]	= the effective normal stress in a given plane

As long as the shear stress $|\tau|$ is smaller than $c' + \sigma'_n \tan(\delta)$, no sliding will occur.

Mohr-Coulomb

Contrary to Coulomb's collapse, the Mohr-Coulomb model assumes that not one (σ_n') but two stresses (σ_v' and σ_h') determine the maximum failure value of the shear stress (or shear resistance) τ . After all, Mohr's circle considers whether collapse is possible in all directions. Figure 26-2 shows the maximum absorbable shear stress in the σ, τ -plane.

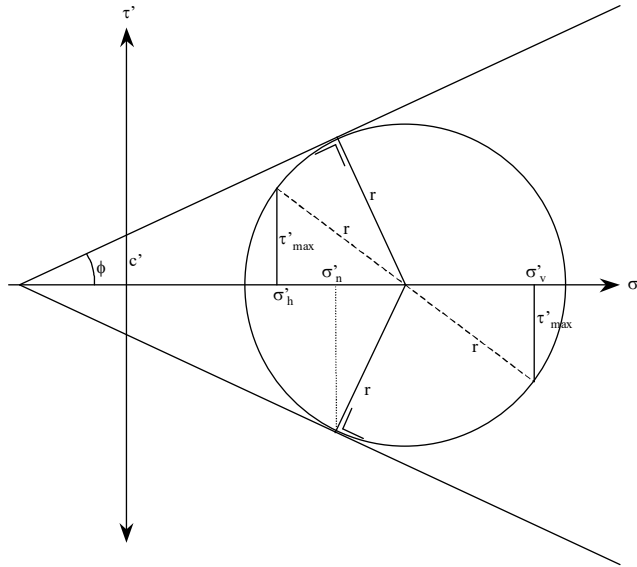


Figure 26-2 Maximum absorbable shear stress according to Mohr-Coulomb

According to Mohr-Coulomb the following applies: $\tau_{\max} = c' \cdot \cos(\varphi) + \frac{1}{2}(\sigma_h' + \sigma_v') \cdot \sin(\varphi)$

Therefore, for undrained materials (clay and peat): $c_u = \tau_{\max} = c' \cdot \cos(\varphi) + \frac{1}{2}(\sigma_h' + \sigma_v') \cdot \sin(\varphi)$

For this the stresses σ_v' and σ_h' before the application of the load can be assumed because the water pressure absorbs all normal stresses during the application of the load. Consequently, the shear stress remains constant.

26.2 Vertical bearing capacity

Rule-of-thumb

Only for very preliminary designs, it could be considered to use some standard values for the vertical bearing capacity under static loading, as given by British Standard 8004 (not prevailing any more), see Table 26-1.

Category	Type of soil	Presumed allowable bearing value (kN/m ²)	Remarks
Non-cohesive soils	Dense gravel, or dense sand and gravel	> 600	Width of foundation not less than 1 m. Groundwater level assumed to be below the base of the foundation
	Medium dense gravel, or medium dense sand and gravel	< 200 to 600	
	Loose gravel, or loose sand and gravel	< 200	
	Compact sand	> 300	
	Medium dense sand	100 to 300	
	Loose sand	< 100	
Cohesive soils	Very stiff boulder clay and hard clay	300 to 600	Susceptible to long-term consolidation settlement
	Stiff clay	150 to 300	
	Firm clay	75 to 150	
	Soft clay and silt	<75	
	Very soft clay and silt	Not applicable	

Table 26-1 Presumed allowable bearing values under static loading (from former BS 8004)

In the Netherlands, the bearing capacity for vertically loaded structures, used for preliminary designs, should not exceed 500 kPa (the design value should not exceed 400 kPa), according to CUR Handboek Funderingen.

Prandtl & Brinch Hansen

The Brinch Hansen method is often used for determining the maximum bearing capacity of the soil under a foundation. This method is based on Prandtl's theoretical slip surfaces (Figure 26-3).

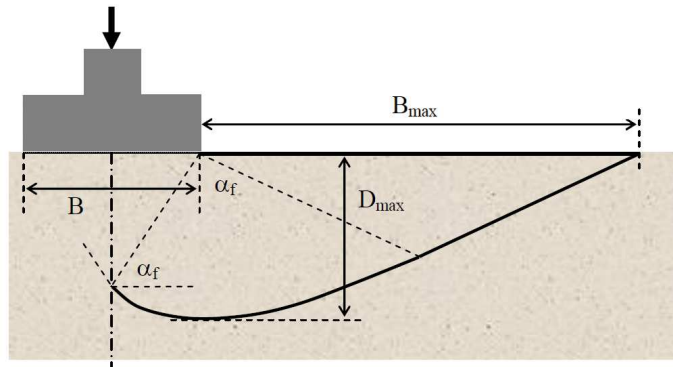


Figure 26-3 Slip surface according to Prandtl and maximum depth and width of the slip body according to Buisman (De Smedt, 2013)

Buisman found equations for the maximum depth (D_{max}) and width (B_{max}) of the slip body (Figure 26-3).

$$D_{max} = \frac{B \cdot \cos \varphi}{2 \cdot \cos \alpha_f} e^{\alpha_f \cdot \tan \varphi} \quad \text{and} \quad B_{max} = B \cdot \tan \alpha_f \cdot e^{\left(\frac{\pi}{2} \cdot \tan \varphi\right)} = B \cdot \sqrt{N_q}$$

where:

φ = angle of internal friction,

α_f = angle as depicted in Figure 26-3: $\alpha_f = \frac{\pi}{4} + \frac{\varphi}{2}$ (α and φ in radians)

N_q = bearing capacity factor (see next page)

These equations apply to homogeneous soil, but they could give an indication of the maximum dimensions of the slip body in layered soil. The depth D_{max} of the slip body is restricted to $3B$ and the horizontal dimension B_{max} to $10B$. For undrained soil, the angle of internal friction φ is zero, in which case $D_{max} = B/\sqrt{2}$ en $B_{max} = B$.

NEN 9997-1+C1, article 6.5.2.2, relates D_{max} and B_{max} to the angle of internal friction, φ' , see Figure 26-4.

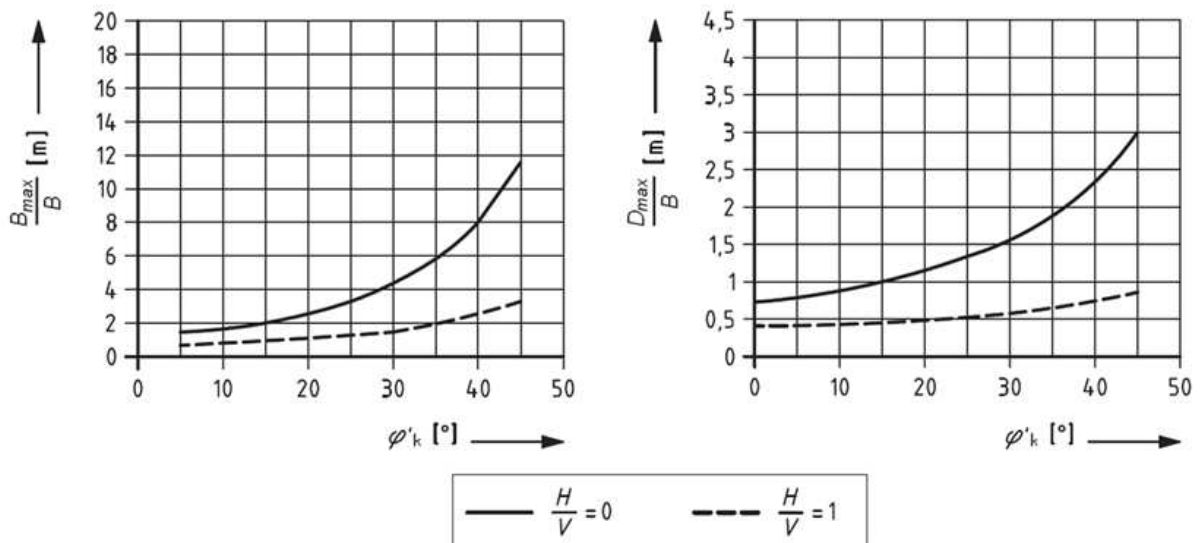


Figure 26-4 Maximum depth and width of the slip body as a function of the angle of internal friction (NEN9997-1+C1)

The maximum bearing force that a soil can resist can be calculated with:

$$V_{\max} = p'_{\max} \cdot A_{\text{eff}}$$

where:

$$p'_{\max} \quad [\text{kPa}] = \text{bearing capacity of the soil, see the equations below for drained and undrained conditions}$$

$$A_{\text{eff}} \quad [\text{m}^2] = \text{effective foundation area} = L \cdot B, \text{ see explanation at the end of this Section}$$

The bearing capacity p'_{\max} depends on the condition of the soil, which can be drained or undrained.

The *drained condition* indicates a soil state in which any excess pore water pressure has fully dissipated. This does not mean that all the water has flowed out of the pores, but it means that there is no stress-induced pressure in the pore water. Granular soils drain very quickly, and hence they are always treated as drained and analysed in terms of effective stresses using φ' ($c'=0$). Also the bearing capacity of clay and peat, exposed to long-term loads (months or years), should be calculated as under drained condition.

The *undrained condition* occurs in cohesive impermeable soils, in which pore water pressures increase directly after the load is applied. In undrained soil, an undrained shear strength, the shear strength c_u ($=s_u$) is used instead of the effective cohesion c' , which is used for drained soil conditions. For undrained conditions, an internal friction angle of $\varphi' = 0$ is used.

Both conditions should be checked in a bearing capacity calculation. In addition, punching through a possible lower soft layer should be checked for the drained condition (not explained in this Manual).

Drained conditions

The soil bearing capacity in drained materials is usually expressed by:

$$p'_{\max, \text{drained}} = c' N_c s_c i_c + \sigma'_q N_q s_q i_q + 0,5 \gamma' B \cdot N_\gamma s_\gamma i_\gamma$$

which consists of contributions from cohesion (index c), surcharge including soil coverage (q) and the specific weight of the soil below the foundation (γ) (Figure 26-5). There are multiple theories and equations to include these contributions and the effects of horizontal loads and the shape of the structure. The coefficients in this Manual come from Craig's Soil Mechanics, 8th edition (2012).

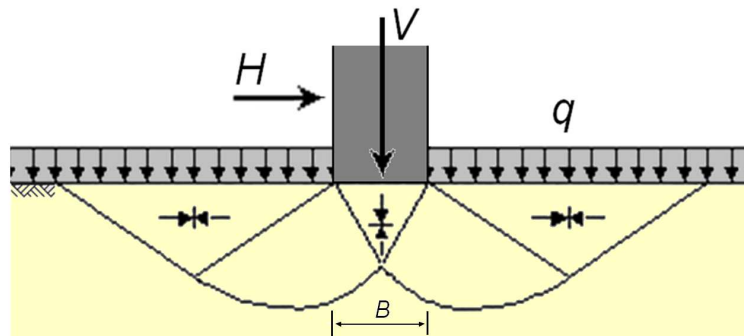


Figure 26-5 Collapse of soil under a structure according to Prandtl and Brinch Hansen

The main bearing capacity factors can be calculated with:

$$N_c = (N_q - 1) \cdot \cot \varphi' \quad N_q = \frac{1 + \sin \varphi'}{1 - \sin \varphi'} \cdot e^{\pi \tan \varphi'} \quad N_\gamma = (N_q - 1) \cdot \tan(1,32 \cdot \varphi')$$

Shape factors ($B \leq L \leq \infty$) bring the effect of possible 3D-slip bodies into account. Rectangular foundation strips mainly fail in two directions, whereas square footings cause sliding planes in all directions. Therefore, the contribution of the cohesion and surcharge increase, if the foundation slab becomes more square-shaped. However, the resistance of the soil under the slab decreases, if the slab becomes more square-shaped, because the slip planes tend to become less deep in case of 3D slip planes:

$$s_c = \frac{s_q N_q - 1}{N_q - 1} \quad s_q = 1 + \frac{B}{L} \sin \varphi' \quad s_\gamma = 1 - 0,3 \frac{B}{L}$$

The presence of an inclined load, implying a horizontal component, considerably reduces the bearing capacity. The factors to deal with an inclined direction of the resulting force ($B \leq L \leq \infty$) are:

$$\text{If } H \text{ parallel to } L \text{ and } L/B \geq 2: i_c = \frac{i_q N_q - 1}{N_q - 1}; \quad i_q = i_\gamma = 1 - \frac{H}{V + A c' \cot \varphi'}$$

$$\text{If } H \text{ parallel to } B: i_c = \frac{i_q N_q - 1}{N_q - 1}; \quad i_q = \left(1 - \frac{0,70 \cdot H}{V + A \cdot c' \cdot \cot \varphi'}\right)^3; \quad i_\gamma = \left(1 - \frac{H}{V + A \cdot c' \cdot \cot \varphi'}\right)^3$$

Only the part of the foundation slab which has effective stresses underneath is included in the effective width B . The factors for the bearing force are also given in Figure 26-6.

φ'	N_c	N_q	N_γ
0,0	5,0	1,0	0,0
5,0	6,5	1,6	0,1
10,0	8,3	2,5	0,3
15,0	11,0	3,9	1,1
20,0	14,8	6,4	2,7
22,5	17,5	8,2	4,1
25,0	20,7	10,7	6,3
27,5	24,9	13,9	9,5
30,0	30,1	18,4	14,4
32,5	37,0	24,6	21,9
35,0	46,1	33,3	33,7
37,5	58,4	45,8	52,5
40,0	75,3	64,2	83,3
42,5	99,2	91,9	135,3

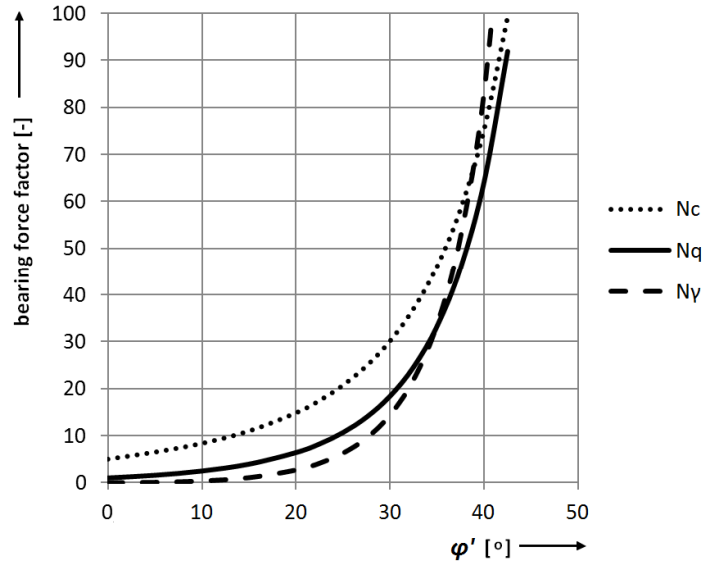


Figure 26-6 Bearing force factors as function of the angle of internal friction

Undrained conditions

The bearing capacity for undrained can basically be calculated according to the equation for drained conditions, but now the angle of internal friction, φ , equals zero, which implies that $N_\gamma = 0$ and $N_q = 1,0$. Instead of the cohesion c' , the undrained shear strength c_u should be used.

The equation for the bearing capacity thus modifies into:

$$p'_{\max, \text{undrained}} = c_u N_c s_c i_c + \sigma'_q$$

where:

$$N_c = (2 + \pi) \left(1 + 0,27 \sqrt{\frac{d}{B}}\right)$$

$$s_c = 1 + 0,2 \frac{B}{L}$$

$$i_c = 0,5 \cdot \left(1 + \sqrt{1 - \frac{H}{A \cdot c_u}}\right)$$

d [m] = foundation depth

for the rest, see above, under 'drained conditions'

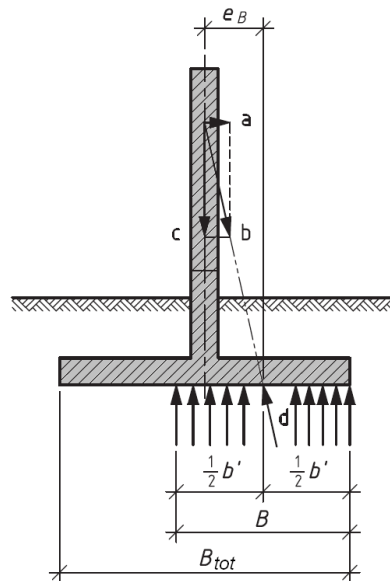
Clarification of the symbols used in this Section:

p'_{max}	[kPa]	= bearing capacity of the soil
c'	[kPa]	= (weighted) cohesion
c_u	[kPa]	= design value of the undrained shear strength (= s_u)
σ'_q	[kPa]	= effective surcharge pressure surrounding a foundation element at construction

level: $\sigma'_q = q' + \sum_{i=1}^{i=n} (d_i \cdot \gamma'_{soil,i})$, where:

q'	[kPa]	= effective surcharge acting on the ground surface
n	[-]	= number of horizontal soil layers between the construction level and the ground surface
d_i	[m]	= thickness of soil layer i
$\gamma'_{soil,i}$	[kN/m ³]	= effective volumetric weight of soil layer i
γ'_{soil}	[kN/m ³]	= (weighted) effective volumetric weight of the soil below construction level
x_c	[-]	= factor for the influence of cohesion
x_q	[-]	= factor for the influence of the soil cover
x_γ	[-]	= factor for the influence of the effective volumetric weight of the soil
ϕ'	[°]	= (weighted) angle of internal friction
H	[kN]	= horizontal component of the resulting force acting on the soil
V	[kN]	= vertical component of the resulting force acting on the soil
A	[m ²]	= effective foundation area: $A = B \cdot L$
L	[m]	= length of the effective foundation area, for circular slabs: $L = B$
B	[m]	= width of the effective foundation area, for circular slabs: $L = B$

For an eccentrically loaded foundation, B is approximated by $B_{tot} - 2e_B$ and L by $L_{tot} - 2e_B$, see the following figure from NEN9997-1+C1:



Notes

- The factors for the bearing force are too conservative. This is because it is assumed that the factors do not influence each other, which is incorrect.
- The factors for the shape of the foundation and particularly for the horizontal load are not substantiated scientifically but they are based on empirical relations, experiments, calculations, etc.
- For a horizontal load H one not only has to apply a reduction in the calculation of the vertical bearing force F , but one also has to check if sliding can occur (e.g. using Coulomb).
- The reduction of the vertical bearing force V as a result of the horizontal load H is considerable. Assuming $H/V = 0,30$ results in $i_q = 0,50$!

Layered soil

If the foundation's subsoil is layered, one can fill in the weighted soil properties in the previous equations according to the following equations and Figure 26-7:

$$\varphi' = \frac{\sum_{i=1}^{i=n} h_i X_i \varphi_i}{\sum_{i=1}^{i=n} h_i X_i} \quad c' = \frac{\sum_{i=1}^{i=n} h_i X_i c_i}{\sum_{i=1}^{i=n} h_i X_i} \quad \gamma' = \frac{\sum_{i=1}^{i=n} h_i X_i \gamma_i'}{\sum_{i=1}^{i=n} h_i X_i}$$

in which:

φ_i	[°]	= angle of internal friction for layer i
c_i	[kPa]	= cohesion of layer i
γ_i'	[kN/m ³]	= effective specific weight of layer i
n	[-]	= the number of horizontal layers between the influence depth D_{max} and the construction level
h_i	[m]	= thickness of layer i (within the influence depth D_{max})
X_i	[m]	= distance between the centre of layer i to the influence depth D_{max}
D_{max}	[m]	= the influence depth

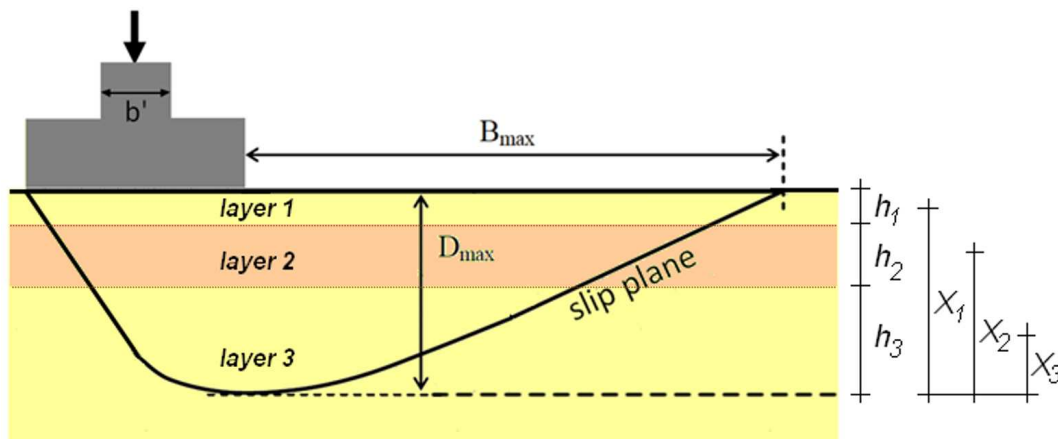


Figure 26-7 Principle sketch for the calculation of equivalent soil properties of layered subsoil

The previous equations can be used to determine the dimensions of a foundation in an iterative way. As a first estimate, one often uses a rule of thumb which assumes that the soil under and next to the foundation does not collapse if the work-line of resultant force intersects with the core of the foundation surface (see Section 37.2).

26.3 Horizontal bearing capacity (resistance against sliding)

Theory

Horizontally loaded foundations transfer their load to the subsoil by means of friction in the foundation plane and possibly passive earth pressure behind the foundation. To calculate the maximum friction against the foundation surface one normally uses Coulomb's formula:

$$\tau_{max} = f \cdot \sigma_n'$$

where:	τ_{max}	[kPa]	= maximum shear stress in the foundation surface
	f	[-]	= coefficient of friction = $\tan(\delta)$
	δ	[°]	= angle of friction between foundation slab and soil
	σ_n'	[kPa]	= the effective normal (vertical) stress under the foundation

One might wonder whether the cohesion of a soil layer should also be included in the formula above, but on grounds that are sensitive to settlements, foundations are never situated directly on cohesive materials but always on sand or gravel, which makes this question irrelevant.

The coefficient of friction between concrete and sand is usually in the order of 40% to 50%. For the coefficient of friction between steel and sand, roughly the same values are found.

The angle of friction parameter δ is a parameter that belongs to Coulomb's model of friction. The angle of internal friction ϕ is a parameter that corresponds to Mohr-Coulomb's model of friction. These are different models. Coulomb's model of friction is based on one stress: the normal stress σ_n' , whilst Mohr-Coulomb's model of friction is based on two stresses: σ_v' and σ_h' .

Assuming the normal stress σ_n' and the stress perpendicular to this σ_{\perp}' it is possible to work ϕ into δ :

$$\tan(\delta) = \frac{1}{2} \sqrt{(1+K)^2 \cdot \sin^2(\phi) - (1-K)^2} \quad \text{with: } K = \frac{\sigma_{\perp}'}{\sigma_n'}$$

If $K = 1$ then: $\tan(\delta) = \sin(\phi)$

Design

Usually, $\sigma_h' < \sigma_v'$ is valid for soil layers, because $K_0 < 1$.

For horizontal surfaces the normal stress (vertical) is therefore greater than the stress perpendicular to this (horizontal):

$$\sigma_n' > \sigma_{\perp}'$$

By approximation one can assume:

$$\tau_{\max} = \tan(\delta) \sigma_n' \quad \text{with: } \delta \approx \frac{2}{3} \phi$$

For vertical surfaces the normal stress (horizontal) is therefore smaller than the vertical stress perpendicular to this:

$$\sigma_n' < \sigma_{\perp}'$$

By approximation one can assume:

$$\tau_{\max} = \tan(\delta) \cdot \sigma_n' \quad \text{with: } \delta \approx (0,8 \text{ to } 0,9) \cdot \phi$$

The values given above can be derived theoretically. Furthermore, these values are also found experimentally.

26.4 Stability of slopes (Fellenius and Bishop)

Many methods for checking the stability of slopes are based on circular slip surfaces. The earth mass above the failure arc is divided into slices, of which one, with a width b and (average) height h , has been drawn. If one considers the moments relative to the centre of the circle, the following applies for the driving moment:

$$M_a = \sum \gamma \cdot b \cdot h \cdot R \cdot \sin(\alpha)$$

which considers the sum of the contributions of all slices and where γ is the volumetric weight of soil. If the ground mass is composed of several layers, one may have to deal with different volumetric weights over the height h . If the water table is found above the slip plane one must take into account the volumetric weight of wet soil below the water table and the weight of dry soil above it (unless there is also capillary rise, as tends to be the case particularly for clay and peat). Possible water above ground level should also be taken into account.

The resisting moment is:

$$M_w = \sum \tau \cdot \frac{b}{\cos(\alpha)} \cdot R$$

in which $b/\cos(\alpha)$ approximates the length of the circumference over the slice width b .

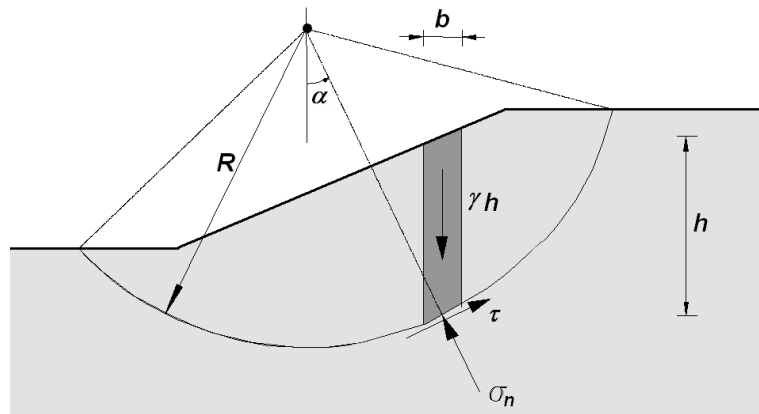


Figure 26-8 The principle of a slip surface calculation

Fellenius assumes that the shear stress τ along the whole circumference is a factor F smaller than the maximum shear stress that can be developed. This factor is also called the stability factor and it can be considered a type of safety coefficient.

Therefore, the shear stress can be denoted as:

$$\tau = \frac{1}{F} (c' + \sigma_n' \cdot \tan(\varphi'))$$

in which: c' [kPa] = cohesion
 σ_n' [kPa] = normal effective stress, with $\sigma_n' = \sigma_n - p$
 φ' [-] = angle of internal friction
 p [kPa] = water pressure

Fellenius

Fellenius assumes that the slices do not exert any force on each other. The balance of forces along the radial leads to:

$$\sigma_n' \cdot b \frac{1}{\cos \alpha} = \gamma b h \cos(\alpha) \Leftrightarrow \sigma_n' = \gamma h \cos^2(\alpha)$$

Inserting the normal stress produces:

$$\tau = \frac{1}{F} (c' + (\gamma h \cos^2(\alpha) - p) \tan(\varphi'))$$

A balance of moments around the centre of the circle means that the driving moment M_a equals the resisting moment M_r . Together this results in the following formula by Fellenius for safety:

$$F = \frac{\sum \{ [c' + (\gamma h \cos^2 \alpha - p) \tan \varphi'] / \cos \alpha \}}{\sum \gamma h \sin \alpha}$$

Bishop

Due to the shear force that is created under a slice, the vertical balance should be corrected, so that:

$$\gamma h = \sigma_n' + p + \tau \cdot \frac{\sin \alpha}{\cos \alpha}$$

Inserting this in the driving moment M_d leads to Bishop's iterative formula:

$$F = \frac{\sum \frac{c' + (\gamma h - p) \tan \varphi'}{\cos \alpha (1 + \tan \alpha \cdot \tan \varphi' / F)}}{\sum \gamma h \sin \alpha}$$

The stability check consists of dividing the soil, for instance into 10 slices of equal width, measuring α and h for each slice and then determining the safety factor F . The verification is carried out for several slip planes (different centre points and radii). The smallest value of F (corresponding to the most critical slip plane) has to be greater than 1,2 for temporary building works (e.g., excavated building sites) or 1,3 for permanent works. The aforementioned method of calculation entails a lot of work. Particularly if one considers that several slope angles have to be investigated in order to find the steepest possible slope. This is why the calculations are always carried out by a computer programme (e.g., D-Geo Stability).

For an infinite slope of dry, non-cohesive material, one finds: $F = \frac{\tan \phi'}{\tan \alpha}$

Note:

One should not value the calculated safety factor too much, because the entire method is questionable. Some of the flaws are:

- *the circular slip plane is not entirely correct because the soil can deform.*
- *the calculations only include the balance of moment and not the complete balance of force.*
- *the transfer of forces between the slices is not taken into account.*

The groundwater pressures are not always well known, but they are very important. A high groundwater pressure reduces the safety factor. In little permeable soil types, the water pressure certainly needs (a lot of) time to adjust to the drainage and to the dewatering of an excavated building site. Using values for the water pressure that are too optimistic in calculations has led to the collapse of slopes (sliding) in many cases. Measures against this include:

- *designing with more realistic values (and thus shallower slopes).*
- *dewatering the area earlier.*
- *draining the excavated building site slowly.*
- *applying sand drains or geo-drains for faster drainage of little permeable soil layers in places where slip planes can be expected.*

Reinforced earth (Terre Armée)

A reinforced earth wall is a wall consisting of prefab slabs piled on top of each other. Two strips of geo-textile (or zinc-coated steel), which disappear horizontally in the soil behind the wall, are attached to each slab. Due to the weight of the soil, the strips can absorb a tensile force and hold the individual wall elements in place. The collapse mechanism of the entire wall can be solved with Fellenius and Bishop but that requires calculating the extra tensile force of the strips correctly. The part of the strip outside of the slip circle (see Figure 26-9) can absorb an additional force in the order of:

$$F_{strip} = 2bl_{eff}\sigma'_v \tan \delta$$

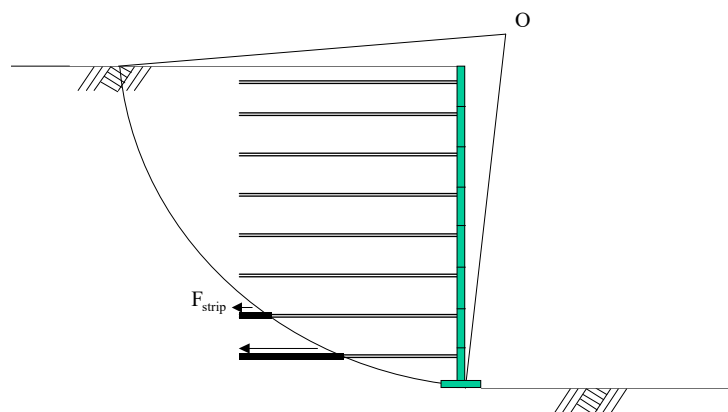


Figure 26-9 Extra stability due to reinforced earth

Note

Next to no computer programmes can calculate reinforced earth. The programmes that do calculations with geo-textiles (nearly) never include the correct effective length in calculations (including Mstab). Plaxis, however, does calculate this length properly.

26.5 Liquefaction

Theory

Liquefaction (*zettingsvloeiing*) is the phenomenon of a (partially) saturated granular soil that substantially loses strength and stiffness in response to an applied cyclic stress, causing it to behave like a liquid. It mostly occurs in saturated, loose (i.e., not compacted, with low density) sandy soils with poor drainage. There are mainly two types of liquefaction:

- Liquefaction under non-cyclic loading, by sudden changes in stress conditions. Dikes with over-steepened slopes can liquefy if loose saturated cohesionless soils are loaded rapidly.
- Liquefaction under cyclic loading, for instance caused by earthquake shaking, storm wave loading, pile driving.

Loose sand in general has a tendency to compress if a load is applied. This results in an increase of pore water pressure and the water attempts to flow out from the soil to zones of low pressure (usually upward towards the ground surface). However, if the loading is rapidly applied and large enough, or is repeated many times in such a way that the water does not flow out before the next cycle of load is applied, the water pressures may build up to the extent that it exceeds contact stresses between the grains of soil that keep them in contact. These contacts between grains are the means by which the weight of structures and overlying soil layers is transferred from the ground surface to layers of soil or rock at greater depths (Wikipedia, 2022). The principle is explained in Figure 26-10, for an earthquake load.

Figure 26-10a shows the situation before an earthquake: sand particles maintain contact with each other. During the earthquake, Figure 26-10b, the pore water increases and the contacts between the particles are lost. After liquefaction, Figure 26-10c, the contacts between the particles are recovered. A decrease of volume, causing settlement, can occur because of water drained from the liquefaction deposit.

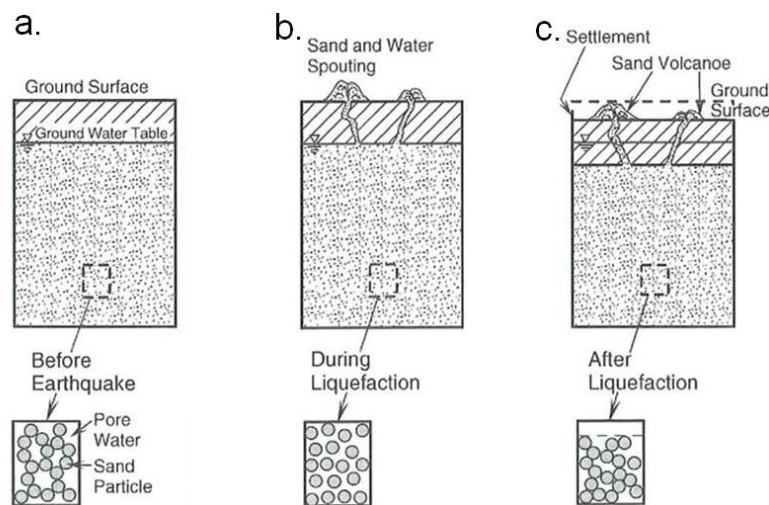


Figure 26-10 The principle of liquefaction

The cyclic loading causes a reduction of the effective soil stress to zero and a complete loss of shear strength. Liquefaction can therefore lead to insufficient bearing capacity of a structure. "Structures whose foundations bear directly on liquefying sand will experience a sudden loss of support, resulting in drastic and irregular settlement. This will cause structural damage, including cracking of foundations and damage to the building structure, or leave the structure unserviceable, even without structural damage. Where a thin crust of non-liquefied soil exists between building foundation and liquefied soil, a 'punching shear' type foundation failure may occur. Irregular settlement may break underground utility lines. The upward pressure applied by the movement of liquefied soil through the crust layer can crack weak foundation slabs and enter buildings through service ducts, and may allow water to damage building contents and electrical services. Bridges and large buildings constructed on pile foundations may lose support from the adjacent soil and buckle, or come to rest at a tilt (Wikipedia, 2022).

Sloping ground and ground next to rivers and lakes may slide on a liquefied soil layer (termed 'lateral spreading'), opening large ground fissures, and can cause significant damage to buildings, bridges, roads and services such as water, natural gas, sewerage, power and telecommunications installed in the

affected ground. Buried tanks and manholes may float in the liquefied soil due to buoyancy. Earth embankments such as flood levees and earth dams may lose stability or collapse if the material comprising the embankment or its foundation liquefies (Wikipedia, 2022).

Figure 26-11 shows various ways in which quay walls can deform by liquefaction due to earthquake loading.

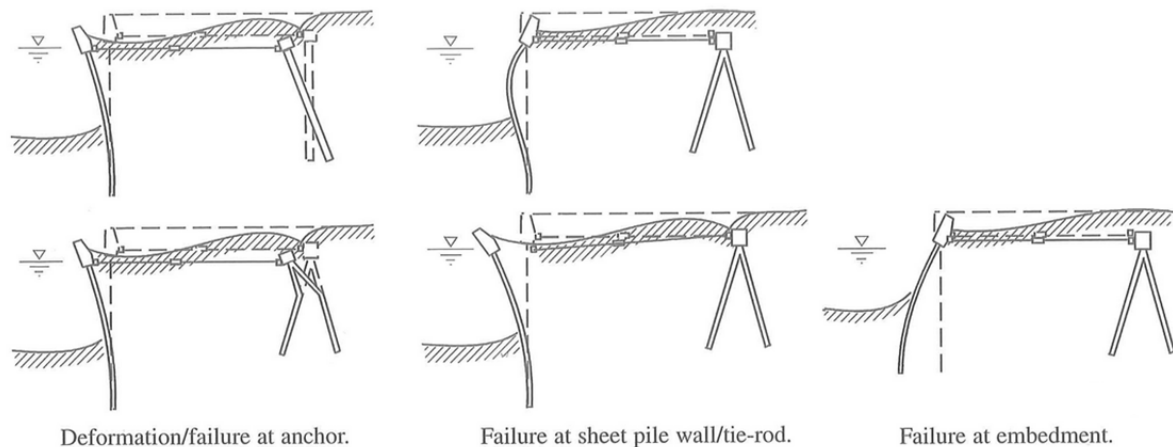


Figure 26-11 Potential ways of deformation of sheet-pile quay walls by liquefaction caused by earthquakes (from: Quay Walls, 2013)

Design for cyclic loading

In general, for structural designs that take earthquakes into account, the main principle is that the cyclic stress ratio (*CSR*) does not exceed the cyclic resistance ratio (*CRR*), otherwise there will be liquefaction:

$$\text{if } CSR > CRR \Rightarrow \text{liquefaction}$$

The cyclic stress ratio CSR

There are several ways to define the cyclic stress ratio. The most common expression, applicable for tectonic earthquakes, is given by Seed and Idriss (1971) and adopted in NEN-EN 1998-5²:

$$CSR = 0,65 \cdot \frac{a_{max}}{g} \cdot \frac{\sigma_{v0}}{\sigma'_{v0}} \cdot r_d$$

where: <i>CSR</i> [-]	= cyclic stress ratio
<i>a_{max}</i> [m/s ²]	= peak horizontal acceleration of the subsoil (see below)
<i>g</i> [m/s ²]	= acceleration of gravity
<i>σ_{v0}</i> [Pa]	= total vertical overburden stress
<i>σ'_{v0}</i> [Pa]	= effective vertical overburden stress
<i>r_d</i> [-]	= stress reduction coefficient (see below)

These parameters are most critical at the ground surface, as they will lead to a maximum value for *CSR* in an area where structures are founded. This 'simplified procedure' has not been validated for depths of more than 23 m.

The peak horizontal acceleration *a_{max}*

The horizontal acceleration is a measure for the severity of the cyclic loading. The horizontal acceleration is related to earthquake intensities. Chapter 20 includes a few graphs that show where what intensity and related horizontal acceleration can be expected. Depending on the expected damage due to an earthquake and the likelihood of occurrence, together they form the earthquake risk, it can be decided what earthquake intensity should be resisted by the structure under design.

The stress reduction by depth coefficient *r_d*

For earthquakes, the stress caused by the horizontal acceleration will decrease with the depth. The cyclic stress ratio *CSR* shall therefore be corrected for the depth. Figure 26-12 shows a graph with depth-related values for the reduction coefficient.

² For induced earthquakes, the method of Idriss Boulanger (2008) is better suitable to predict liquefaction. For a description of that method see Geotechniek, 2014 Funderingsdag special 'Verweking, funderingen en grond-constructie interactie bij aardbevingen' by M. Korff and P. Meijers.

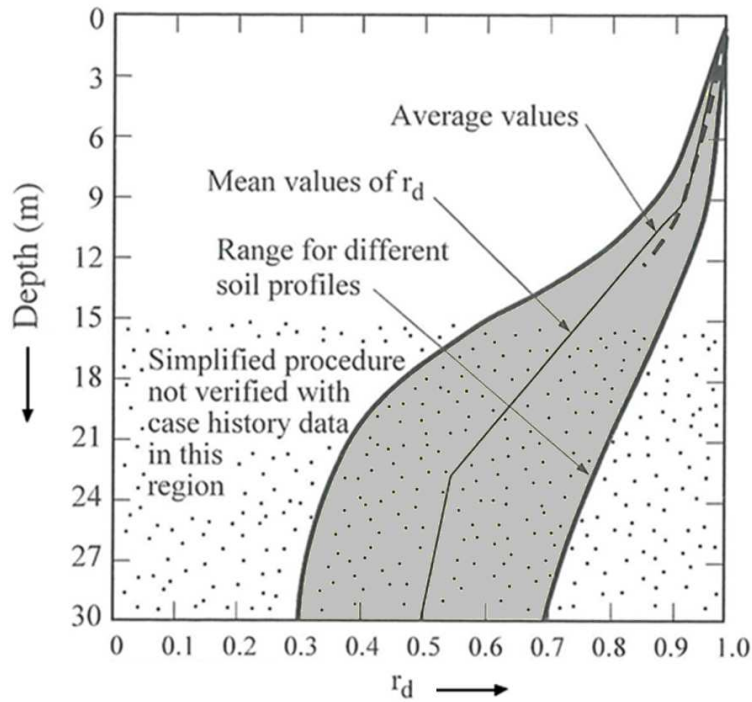


Figure 26-12 Reduction coefficient for the cyclic stress ratio, depending on the depth (after Seed and Idriss (1971))

For routine practice and non-critical projects, the following equations may be used:

$$r_d = 1,0 - 0,00765 \cdot z \quad \text{for } z \leq 9,15 \text{ m}$$

$$r_d = 1,174 - 0,0267 \cdot z \quad \text{for } 9,15 \text{ m} < z \leq 23 \text{ m}$$

where z [m] = depth below the ground surface.

The cyclic resistance ratio CRR

The cyclic resistance ratio, CRR, is dependent on the soil properties. Robertson and Wride (1998) found a relation between the cyclic resistance ratio and the cone tip resistance, obtained by a cone penetration test, see Figure 26-13.

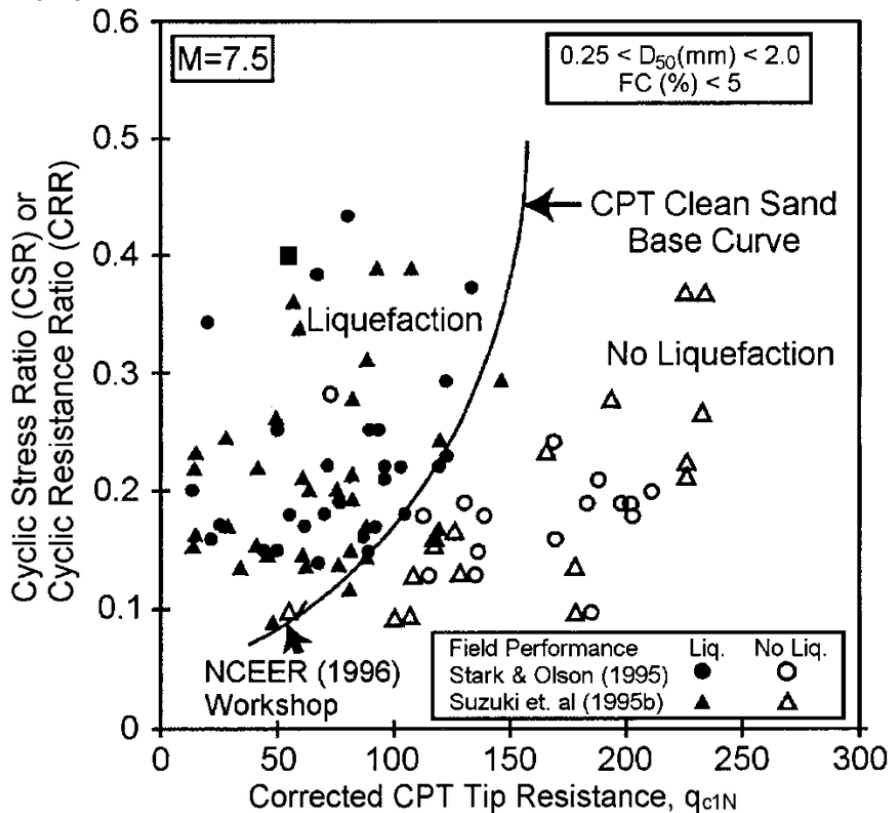


Figure 26-13 The cyclic resistance ratio $CRR_{7,5}$ as a function of the cone penetration tip resistance

This graph is validated for earthquake magnitude 7,5 (scale of Richter) and clean, course sands (content of fines < 5% and $0,25 \text{ mm} < D_{50} < 2,0 \text{ mm}$). The corrected tip resistance is calculated by:

$$q_{c1N} = C_q \cdot \frac{q_c}{P_a}$$

$$C_q = \left(\frac{P_a}{\sigma'_{vo}} \right)^n$$

where: q_{c1N} [Pa] = corrected tip resistance
 C_q [-] = normalising factor for cone penetration resistance
 q_c [Pa] = tip resistance value according to a cone penetration test
 P_a [Pa] = atmospheric pressure ($\approx 0,1 \text{ MPa}$)
 σ'_{vo} [Pa] = effective vertical soil stress
 n [-] = exponent, depending on the soil type (0,5 for clean sands to 1,0 for clayey soils)

The normalising factor C_q becomes large at shallow depths because of low overburden pressure, however, values larger than 1,7 should not be applied.

The graph in Figure 26-13 has been derived for course, clean sand and therefore needs to be corrected for silty sands into an equivalent clean sand value:

$$(q_{c1N})_{cs} = K \cdot q_{c1N}$$

where K [-] is the correction factor for grain characteristics and depends on the soil behaviour type index I_c :

$$\text{for } I_c \leq 1,64 : K = 1,0$$

$$\text{for } I_c > 1,64 : K = -0,403 \cdot I_c^4 + 5,581 \cdot I_c^3 - 21,63 \cdot I_c^2 + 33,75 \cdot I_c - 17,88$$

in which $I_c = \sqrt{(3,47 - \log Q)^2 + (1,22 + \log F)^2}$

$$Q \text{ [-]} = \text{normalised cone resistance: } Q = \frac{q_c - \sigma_{vo}}{\sigma'_{vo}}$$

$$F \text{ [-]} = \text{normalised friction ratio: } F = \frac{f_s}{q_t - \sigma_{vo}} \cdot 100\%$$

where f_s = the sleeve resistance and q_t = cone resistance, corrected for pore pressure, see Section 25.2 and other symbols as above.

For earthquake magnitudes other than 7,5, a magnitude scaling factor, MSF , should be used for the cyclic resistance ratio. The cyclic resistance ratio then is:

$$CRR = CRR_{7,5} \cdot MSF$$

Multiple studies have suggested values for this magnitude scaling factor. The results are summarised by Youd and Noble (1997a) in Table 26-2. The choice for the scaling factor should be based on engineering judgement.

Magnitude, M (1)	Seed and Idriss (1982) (2)	Idriss ^a (3)	Ambraseys (1988) (4)	Arango (1996)		Andrus and Stokoe (1997) (7)	Youd and Noble (1997b)		
				Distance based (5)	Energy based (6)		$P_L < 20\%$ (8)	$P_L < 32\%$ (9)	$P_L < 50\%$ (10)
5.5	1.43	2.20	2.86	3.00	2.20	2.8	2.86	3.42	4.44
6.0	1.32	1.76	2.20	2.00	1.65	2.1	1.93	2.35	2.92
6.5	1.19	1.44	1.69	1.60	1.40	1.6	1.34	1.66	1.99
7.0	1.08	1.19	1.30	1.25	1.10	1.25	1.00	1.20	1.39
7.5	1.00	1.00	1.00	1.00	1.00	1.00	—	—	1.00
8.0	0.94	0.84	0.67	0.75	0.85	0.8?	—	—	0.73?
8.5	0.89	0.72	0.44	—	—	0.65?	—	—	0.56?

Table 26-2 Magnitude scaling factors (MCF) for the cyclic resistance ratio CRR for earthquake magnitudes other than 7,5 on the scale of Richter. (from: Youd and Noble (1997a))

Additional corrections can be made for the nonlinear relation of the cyclic resistance ratio with the vertical soil stress, for sloping ground surfaces and thin soil layers.

Liquefaction can be prevented by applying soil improvement:

- replacement of the soil
- compaction of the soil

Design for non-cyclic loading

Methods to check the occurrence (or the likelihood of occurrence) of static liquefaction are still in development.

CPT-based liquefaction potential of dikes

De Gast et al. (2022) studied the relationship between the liquefaction behaviour of Dutch dikes and the soil type derived from cone penetration tests. Starting point for their method is the relative density of sand as an indicator of contractive/dilative behaviour. They based their method on the soil classification chart developed by Robertson (see Section 25.2).

Liquefaction is likely, in case two conditions apply:

- contractive sands and contractive transitional soils
This is the case if the soil type resides under the contractive dilative boundary line in Robertson's chart. For this line, it applies that

$$CD = (Q_{tn} - 11)(1 + 0,06F_r) = 70$$

where F_r [-] = normalised friction ratio

Q_{tn} [-] = normalised cone resistance including a stress exponent:

$$Q_{tn} = \left(\frac{q_t - \sigma_{v0}}{p_a} \right) \left(\frac{p_a}{\sigma'_{v0}} \right)^n$$

q_t [MPa] = cone resistance

σ_{v0} [MPa] = total vertical soil stress

σ'_{v0} [MPa] = effective vertical soil stress

p_a [MPa] = atmospheric reference pressure

n [-] = stress exponent: $n = 0,381 \cdot I_c + 0,05 \cdot \frac{\sigma'_{v0}}{p_a} - 0,15$

I_c [-] = soil behaviour index: $I_c = \left((3,74 - \log Q_t)^2 + (\log F_r + 1,22)^2 \right)^{0,5}$

Q_t [-] = normalised cone resistance: $Q_t = \frac{q_t - \sigma_{v0}}{\sigma'_{v0}}$ (see also Section 25.2)

The $CD = 70$ line is indicated in Figure 26-14 Robertson's chart with the contractive dilative boundary CD .

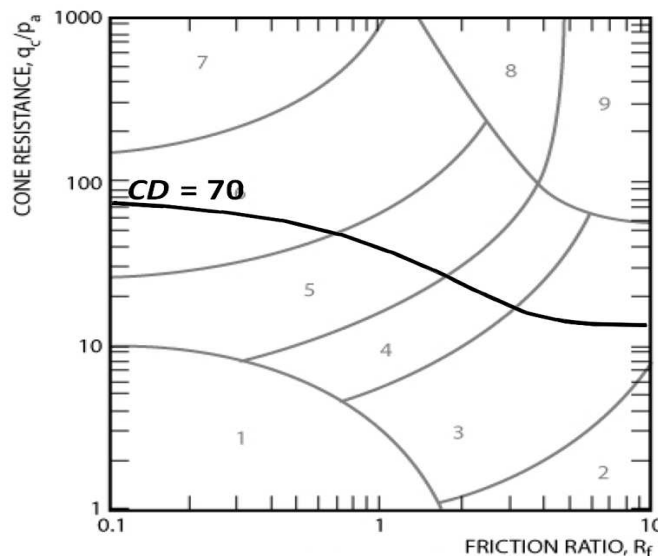


Figure 26-14 Robertson's chart with the contractive dilative boundary CD

- sands and transitional soils with a relative density D_r below 66%

$$D_r = \sqrt{\frac{Q_{tn}}{350}} < 66\%$$

26.6 References

For more information on liquefaction design, one is referred to:

Eurocode 8, NEN-EN 1998-5 (2xxx) Design of structures for earthquake resistance - foundations, retaining structures and geotechnical aspects.

Gast, T. de, K.G. Gavin, P.D. Notenboom, R. Abraimi and C. Reale (2022). CPT based liquefaction potential of flood defences in the Netherlands. In: Cone penetration testing, pp 889-893 Taylor Francis.

Groot, M.B. de, M. van der Ruyt, D.R. van Mastbergen and G.A. van der Ham (2009). Brevloeiing in zand. In: Geotechniek, July 2009.

Groot, M.B. de, T.P. Stoutjesdijk, P. Meijers and T. Schweckendiek. Verwekingsvloeiing in zand. In: Geotechniek, October 2007.

Korff, M. and Meijers, P. (2014). Verweking, funderingen en grond-constructie interactie bij aardbevingen. In: Geotechniek, Funderingsdag 2014 special.

PIANC-report 'Seismic design guidelines for port structures', 2001. Report of working group 34, MARCOM.

Youd, Idriss et al. (2001) 'Liquefaction resistance of soils: Summary report from the 1996 NCEER and 1998 NCEER/NSF workshops on evaluation of liquefaction resistance of soils. Journal of Geotechnical and Geoenvironmental Engineering, April 2001.

27. Soil - stiffness

Schematizations of soil stiffness are used for determining the flow of forces through the structure and for estimates of the displacement of the structure. The two most frequently used models:

1. Winkler model, based on the schematization of the soil into a set of uncoupled linear springs.
2. Elastic solid foundation model. This model is based on the relation between stress, strain and the Young's modulus.

For conceptual design the use of the Winkler model is often more convenient, therefore the Elastic solid foundation model will not be elaborated here.

27.1 Spring schematisation

For design calculations involving the stiffness properties of soil, the soil is often modelled as a set of uncoupled linear springs, known as the Winkler model. This is a popular schematization because it is a simple model, easy to use.

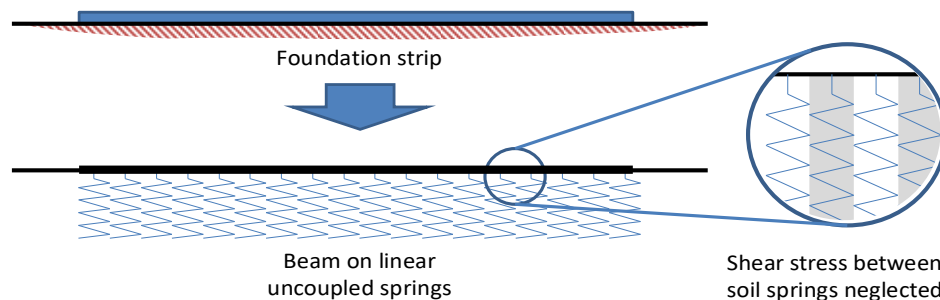


Figure 27-1 Winkler foundation model

Since a linear relationship between the action on the foundation, suppose pressure p , and the deflection w is assumed:

$$p = k_o \cdot w$$

where k_o [N/m²/m] = foundation modulus

For beams with width b , we use $p = k \cdot w = k_o \cdot b \cdot w$ (unit of k : N/m/m).

If the foundation is infinitely stiff the foundation modulus k_o is in fact fully determined by the soil characteristics. For the infinite stiff foundation, k_o is better known as the modulus of subgrade reaction k (*beddingsconstante*).

Note: the modulus of subgrade reaction is in fact not a soil parameter; i.e., not only soil parameters influence its value but the geometry of the structure as well.

As downside of the simple Winkler model the following can be mentioned:

- The springs are not linked or coupled to each other (see Figure 27-1), while in reality the soil elements are linked by means of shear stresses.
- The spread of stress in the subsoil is not really included in the schematisation because of the independent, uncoupled behaviour of every spring.
- The soil is not a spring and definitely does not behave as a linear one.
- Springs have a spring constant k (generally $k = EA/l$). The schematisation as spring therefore requires a "contributing depth", to account for l , which is unknown.

Figure 27-2 shows the real and the calculated pressure distributions under a very stiff foundation, using the linear spring model for soil. The biggest difference is the soil pressure near the edges of the foundation.

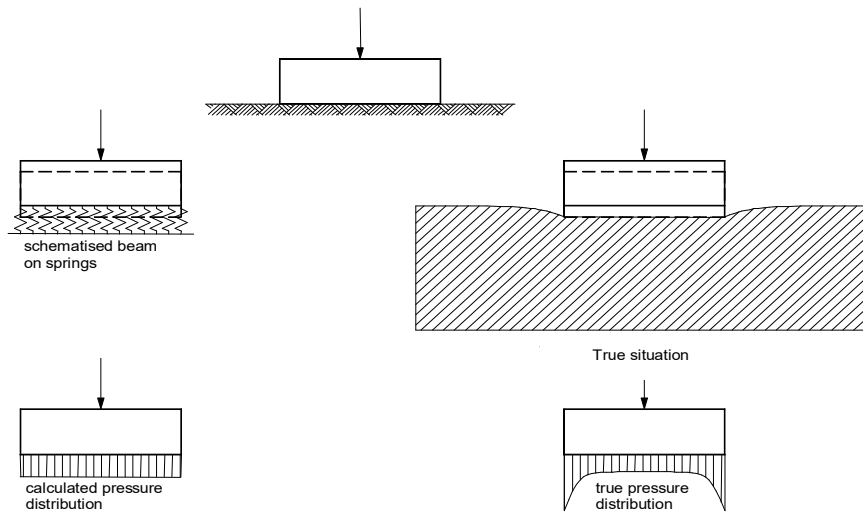


Figure 27-2 Calculated versus true pressures

In the case of an infinitely stiff plate, the foundation pressure is, neither in reality nor according the continuum theory, constant. The pressure along the edge is, after all, higher than in the middle. According to the “spring” method, the pressure is the same everywhere.

For foundations of limited dimensions, settlements not only depend on the stiffness of the soil and the stresses in the foundation plane, but also on the dimensions of the structure. Figure 27-3 shows the settlements for a foundation slab of ϕ 75 cm and for a slab of ϕ 150 cm. In both cases, the settlement of the largest foundation slab is bigger than the settlement of the smaller plate, for the same soil stiffness and equal pressures on the foundation surface.

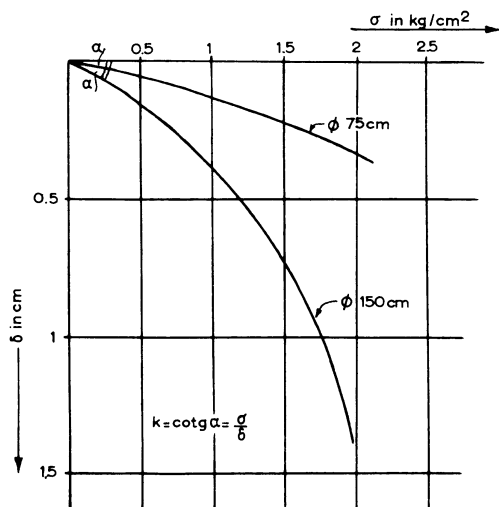


Figure 27-3 measured settlements for two foundation slabs

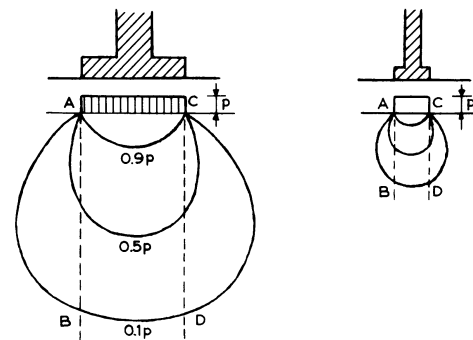


Figure 27-4 Influence depth of a foundation strip

This can be explained by the spread of the load in subsoil. Figure 27-4 shows the influence of the size of the foundation slab on the spread of the load in the subsoil. By approximation the depth of influence of the foundation is directly proportional to the dimensions of the foundation area. The area of the foundation should therefore be taken into account in the calculation of the modulus of sub grade reaction.

27.2 Modulus of subgrade reaction

Estimating the stiffness of a structure is usually relatively easy. The bending stiffness (or flexural rigidity) of a beam is characterised by its EI value. Estimating the stiffness of soil, however, is more difficult. The modulus, or coefficient, of subgrade reaction (*beddingsconstante*) is a spring constant for soil and is defined as:

$$k = \frac{\sigma}{\delta}$$

in which: k [Pa/m] = modulus of subgrade reaction
 σ [Pa] = the (effective) stress at the bottom of, under the foundation surface
 δ [m] = the displacement of the foundation surface

This section discusses three different types of modulus of sub grade reactions:

- Vertical modulus of subgrade reactions
- Horizontal modulus of subgrade reactions for (sheet pile) walls
- Horizontal modulus of subgrade reactions for piles

Often estimates are made from global tables, like Table 27-1. However, it is best to obtain estimates based on in-situ testing.

Soil type	Subgrade reaction (kN/m ³)
Loose sand	5,000 – 16,000
Medium dense sand	10,000 – 80,000
Dense sand	60,000 – 125,000
Clayey sand	30,000 – 80,000
Silty sand	20,000 – 50,000
Clayey soil $s_u < 50$ kPa	10,000 – 20,000
50kPa $< s_u < 100$ kPa	20,000 – 50,000
100 kPa $< s_u$	>50,000

Table 27-1 Modulus of subgrade reaction according to Terzaghi (1955)
 s_u is the undrained shear strength

27.3 Vertical modulus of subgrade reaction (using Flamant)

The solution for surface loads was already treated in Section 24.1. The stresses in an arbitrary point in a homogenous half space are:

$$\sigma'_{zz} = \frac{q_v}{\pi} [(\theta_1 - \theta_2) + \sin \theta_1 \cos \theta_1 - \sin \theta_2 \cos \theta_2] \quad \sigma'_{xz} = \frac{q_v}{\pi} [\cos^2 \theta_2 - \cos^2 \theta_1]$$

$$\sigma'_{xx} = \frac{q_v}{\pi} [(\theta_1 - \theta_2) - \sin \theta_1 \cos \theta_1 + \sin \theta_2 \cos \theta_2]$$

Because all stresses have been solved, all strains and therefore also all displacements can be solved. The following is valid for the z-axis:

$$\varepsilon_{zz(x=0)} = \frac{2q_v}{\pi E} [\theta_1(1-2\nu) + \sin \theta_1 \cos \theta_1(1+\nu)] \Rightarrow$$

$$u_{z(x=0)} = \int_{z=0}^{z=\infty} \varepsilon_{zz(x=0)} \delta z \approx \frac{2aq_v}{E}(1+\nu)[1,762 \cdot (1-2\nu) + 1,443]$$

where ν = poisson's ratio of the soil [-].

The modulus of subgrade reaction for the z-axis is then:

$$k_{(x=0)} = \frac{q_v}{u_{z(x=0)}} \approx \frac{E}{2a} \cdot \frac{1}{(1+\nu) \cdot (1,762 \cdot (1-2\nu) + 1,443)}$$

A reasonable estimate for the modulus of subgrade reaction of drained soil is:

$$k \approx 0,31 \cdot \frac{E}{2a} \quad (\nu = 0,3)$$

A reasonable estimate for the modulus of subgrade reaction of undrained soil is:

$$k \approx 0,53 \cdot \frac{E}{2a} \quad (v_u \stackrel{def}{=} 0,5 \quad \text{and} \quad E_u \stackrel{def}{=} \frac{1+v_u}{1-\nu} E)$$

The geometry (width of the load: $2a$) is clearly present in the modulus of sub grade reaction, which proves that the value of k depends on the geometry of the structure.

For line loads one does not use the modulus of subgrade reaction per area unit, but per length unit of the line load. This modulus of subgrade reaction k' has a different dimension ($[\text{kN}/\text{m}^2]$ instead of $[\text{kN}/\text{m}^3]$) and is independent of the width of the line load, because:

$$k' = \frac{k}{2a} \approx 0,31 \cdot E \quad (\nu = 0,3)$$

27.4 Horizontal modulus of subgrade reaction for (sheet piling) walls

This section explains what modulus of subgrade reaction should be used according to CUR 166 (Sheet pile walls) to calculate a sheet pile wall with a spring model. The figure below is used to calculate the horizontal stress-displacement relationship.

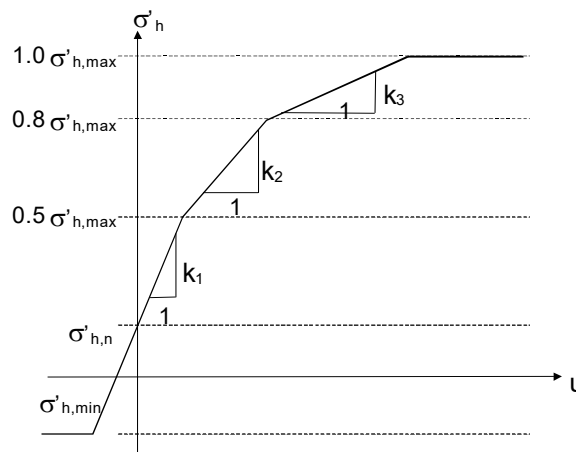


Figure 27-5 Horizontal stress-displacement relationship

In the figure the following applies:

$$\begin{aligned} \sigma'_{h,min} &= K_a \sigma'_v - 2c \sqrt{K_a} \\ \sigma'_{h,max} &= K_p \sigma'_v + 2c \sqrt{K_p} \\ \sigma'_{h,n} &= K_0 \sigma'_v \end{aligned}$$

where:

K_0 , K_a and K_p are the neutral, active and passive soil pressure coefficients (see Section 24.2).

The stress-displacement relationship is split into three branches. The moduli of subgrade reaction for these three branches are given in a table of CUR-report 166 (Table 27-1), which is based on measurement data obtained in the Netherlands.

$$\begin{aligned} k_1 &\text{ applies to } \sigma'_{0,h} < \sigma'_h < 0,5 \sigma'_{h,max} \\ k_2 &\text{ applies to } 0,5 \sigma'_{h,max} \leq \sigma'_h \leq 0,8 \sigma'_{h,max} \\ k_3 &\text{ applies to } 0,8 \sigma'_{h,max} < \sigma'_h < 1,0 \sigma'_{h,max} \end{aligned}$$

where $\sigma'_{0,h}$ [kPa] = neutral soil pressure
 σ'_h [kPa] = max. horizontal soil pressure for the concerning part of the modulus of subgrade reaction
 $\sigma'_{h,max}$ [kPa] = representative value of the max. horizontal soil pressure (passive) after increase of the pressure

		k_1 [kN/m ³]		k_2 [kN/m ³]		k_3 [kN/m ³]	
		k_{low}	k_{high}	k_{low}	k_{high}	k_{low}	k_{high}
sand	q_c [MPa]						
loose	5	12 000	27 000	6000	13 500	3000	6750
moderate	15	20 000	45 000	10 000	22 500	5000	11 250
firm	25	40 000	90 000	20 000	45 000	10 000	22 500
clay	f_{undr} [kPa]						
weak	25	2000	4500	800	1800	500	1125
moderate	50	4000	9000	2000	4500	800	1800
firm	200	6000	13 500	4000	9000	2000	4500
peat	f_{undr} [kPa]						
weak	10	1000	2250	500	1125	250	560
moderate	30	2000	4500	800	1800	500	1125

Table 27-1 Representative values of the horizontal moduli of sub grade reaction (CUR 166, 5th edition)

Note

- To calculate the displacement normative k -values are used, i.e.: k_{low} .
- To calculate the forces and moments, two calculations are carried out. One with $k_{low}/1,3$ and a second with k_{high} . It is impossible to tell which of the two is normative in advance, although in most cases the calculation with the low modulus of sub grade reactions is normative.

27.5 Horizontal modulus of subgrade reactions for piles

For horizontally loaded piles horizontal modulus of subgrade reactions are used. The pressure distribution around a pile is completely different to the distribution around a wall. This also means different modulus of subgrade reactions are to be used. According to Menard these constants can best be based on the radial elasticity modulus E_{menard} . According to Menard, the following relationship between the modulus of subgrade reaction and the radial elasticity modulus is valid for piles:

$$\frac{1}{K_h} = \frac{1}{3 \cdot E_{menard}} \left(4,0 \cdot \left(2,65 \cdot \frac{D}{0,60\text{m}} \right)^\alpha + \alpha \cdot \frac{D}{2} \right) \quad (D \geq 0,60 \text{ m})$$

$$\frac{1}{K_h} = \frac{D}{E_{menard}} \cdot \frac{4,0 \cdot (2,65)^\alpha + 3\alpha}{18} \quad (D < 0,60 \text{ m})$$

One can measure E_{menard} by blowing up a balloon in a boring hole and by measuring which radial deformation occurs at a given pressure. In most cases, however, E_{menard} is not measured. Usually the cone resistance q_c has been found from soundings. In that case the following empirical relationship between Menard's elasticity modulus and the cone resistance can be used:

$$E_{menard} = q_c \cdot f$$

Type of soil	f	α
gravel	-	1.4
sand	0,8 to 1,0	1/3
silt	2,0 to 3,0	1/2
clay	3,0	2/3
peat	3,0 to 4,0	1.0

Table 27-2 Empirical relationships

One can calculate using the dynamic stiffness for short-term loads, such as a collision against a bridge piling. The dynamic stiffness is greater than the static stiffness, for instance:

$$E_{dynamic} = 3 \cdot E_{static}$$

This linear stiffness behaviour is limited by the strength behaviour of piles. The derivation of the three-dimensional K_p values (with shell behaviour) is complex and goes beyond the scope of this manual. See the publication "The ultimate resistance of rigid piles against transversal forces" by Brinch Hansen (1961). This is a standard part of the single pile module of the computer programme D-Sheet Piling.

28. Soil - settlement

slightly improved: February 2011; revised: February 2015; slightly improved: February 2017

Settlement is the process of soil compression. It is an important phenomenon for hydraulic engineering because it results in a decrease of the ground level including all structures resting on shallow foundations. Especially for flood defences this is relevant because settlement will reduce their water retaining height, which immediately affects their primary function if the design does not sufficiently take this effect into account. Furthermore, uneven settlements should be avoided or compensated for, in order to prevent structural failure due to too high stresses in the structure.

Settlement can take place in the subsoil (*zetting*) or in an embankment (*klink*). Land subsidence, by the way, also causes a drop in ground level, but this takes place at another geological scale and should be taken into account when designing flood defences.

Settlement can mainly be caused by two different natural phenomena. It can be caused by expulsion of water out of the pores between the soil particles due to an increase in vertical loading, which is called 'consolidation'. It can also be the result of an ongoing, slower, densification process during which the soil properties gradually change, which is called 'creep' (*kruip*), 'secondary settlement' or 'secular effect'.

These phenomena and the opposite effect of compression (relaxation of soil) are described in the following sections, starting with consolidation.

28.1 Consolidation

Theory

Consolidation is the process that involves a decrease in the water content of a saturated soil due to loading, without replacement of water by air. Especially long-term static loads cause expulsion of water, resulting in a reduction in volume without changing its shape. The degree of consolidation, U , indicates how much water (pressure) has already dissipated. The following applies for one-dimensional (= vertical) consolidation (Verruijt, 2012, Chapter 16):

$$U = 1 - \frac{8}{\pi^2} \sum_{j=1}^{\infty} \frac{1}{(2j-1)^2} \cdot e^{\left(-\frac{(2j-1)^2 \cdot \pi^2 \cdot c_v t}{4 \cdot d_c^2} \right)},$$

or by approximation:

$$U \approx \frac{2}{\sqrt{\pi}} \cdot \sqrt{\frac{c_v \cdot t}{d_c^2}} \quad \text{if } (U \leq 0,5) \quad \text{and} \quad U \approx 1 - \frac{8}{\pi^2} \cdot e^{\left(-\frac{\pi^2}{4} \cdot \frac{c_v t}{d_c^2} \right)} \quad \text{if } (U > 0,5)$$

in which: c_v [m²/s] = coefficient of consolidation (oedometer test)
 d_c [m] = drainage path length (drainage height). If a soil layer is drained on the top and from below, the drainage path length is half the height of the soil layer.
 t [s] = duration

The consolidation "constant" c_v can be derived from Darcy's law:

$$c_v = \frac{k_v}{\gamma_w m_v}$$

No sensible estimates can be made for general values of c_v , as both the vertical permeability k_v [m/s] and the vertical soil stiffness m_v [m²/kN] vary too much per soil layer. Furthermore, k_v and m_v decrease during consolidation due to their dependence on the stresses! The only reasonable solution is to do oedometer tests for the correct stress path. To have an idea of the order of magnitude, the value of c_v of clay can have values of 0,5 to 10 m²/year and for organic silt it can be 1,6 to 50 m²/year.

According to Terzaghi (1943), the duration of one-dimensional consolidation until $U = 1$ (= hydrodynamic duration) can be computed with:

$$t_h = \frac{d_c^2 \cdot T_v}{c_v}$$

where: t_h [s] = hydrodynamic duration
 d_c [m] = (vertical) consolidation path length
 c_v [m²/s] = coefficient of consolidation

$$T_v \text{ [-]} = \text{dimensionless time factor: } T_v = \frac{\pi}{4} U^2 \quad \text{for } U < 0,6$$

$$T_v = -0,933 \cdot \log(1-U) - 0,085 \quad \text{for } U > 0,6$$

At the end of the hydrodynamic period, $U=1$ and $T_v = 2$.

Note

Depending on how the excess pore-water is dissipated, two or three-dimensional consolidation is involved. In literature one can find equations for the adjustment of the water pressure in time for both two and three-dimensional consolidation (Lambe and Whitman, 1969). Theoretically, in the case of one-dimensional loading (oedometer test, horizontal strain is zero), 100% of the load goes to the water pressure and 0% to the effective stress (so: $U_o = 0$). In the case of plain stress loading (triaxial test, horizontal stress is constant), 33% goes to the water pressure and 67% to the vertical effective stress ($U_o = 0,67$). In a combination, plain-strain loading (biaxial test) 50% goes to the water pressure and 50% to the effective stress ($U_o = 0,50$). In reality, most loads are in principle something in between a one-dimensional load and a plain-strain load. That is why it would be better to use $U_o \approx 0,25$. The total consolidation process goes therefore much faster than the equation of the degree of consolidation suggests. More information on this topic can be found in other literature (A.Verruijt, 1987).

Vertical drainage

The best-known vertical drainage systems are sand drains and synthetic geo-drains. Vertical drainage is applied to accelerate the consolidation process. The most important reason for accelerating the consolidation process is the problem that one starts construction too late. An additional matter is that the drainage costs can sometimes be earned back by interest savings by being able to purchase the land later.

Drawbacks of vertical drainage are:

- the extra costs,
- the environmental drawbacks (plastic in the soil),
- the degradation of the seal against vertical water transport ("piercing the polder").

One must realise that the vertical drainage does not accelerate the secondary settlement (creep). If one doesn't satisfy a certain residual settlement requirement, vertical drainage is not a solution in all cases. Preferably one should consider working with a longer settlement period or with temporary embankments.

In the case of vertical drainage, there is a constant horizontal drainage distance for all soil layers. This makes calculating the degree of consolidation per layer easier:

$$U_h = 1 - e^{-\frac{8T_h}{\mu}}$$

where:

U_h [-] = horizontal degree of consolidation (for vertical drainage)
 T_h [-] = time factor for horizontal flow:

$$T_h = \frac{c_h \cdot t}{D^2}, \text{ where:}$$

c_h [m²/s] = horizontal consolidation coefficient (oedometer test)

D [m] = equivalent drain distance:

$$D = 1,05 \cdot \ell \text{ (for triangular pattern of drainage)}$$

$$= 113 \cdot \ell \text{ (for square pattern of drainage)}$$

ℓ [m] = distance between two vertical drains

$$c_h = \frac{k_h}{m_v \cdot \gamma_w}$$

μ [-] = a function mainly related to drain spacing and size and the extent of soil disturbance due to drain installation (smear effect). The basic form of μ for ideal drain with no smear effect can be expressed as follows:

$$\mu = \frac{n^2}{n^2 - 1} \left[\ln(n) - \frac{3}{4} + \frac{1}{n^2} \left(1 - \frac{1}{4n^2} \right) \right], \text{ where:}$$

$$n [-] = \frac{D}{d}$$

$$d \text{ [m]} = \text{equivalent drain thickness: } d = \frac{2(b+t)}{\pi}$$

Notes

- In some literature 'consolidation' has the meaning of the primary settlement. In this Manual 'consolidation' is considered as the cause of primary settlement.
- Densification of an embankment ('klink' in Dutch) can consist of three effects: primary settlement, secondary (creep) settlement and lateral deformation. Lateral, or horizontal, deformation (expansion) does not influence the total volume, so it results in a decreased embankment height.
- The horizontal permeability of a soil layer can be greater (or smaller) than the vertical permeability.
- The distance ℓ between two drains is generally between 1 and 3 m.
- A triangular pattern is always more economical than a square pattern.
- The cross-section of narrow synthetic drains is $b \times t = 100 \times 4 \text{ mm}^2$. The cross-section of wide synthetic drains is $b \times t = 300 \times 4 \text{ mm}^2$.

28.2 Primary settlement and creep

In practice, the compressibility of soil is an important property regarding settlement problems. Compression is the decrease in volume without the change of shape.

Soil is not a linearly elastic material. Generally, the stiffness increases with an increase of the average compressive stress (σ'_o) caused by higher loading. Due to this increase in loading the soil particles will come closer together (the porosity decreases), increasing the number of contact points and enlarging the areas of contact. As a result, water residing in the pores will be expelled. This phenomenon is called 'primary settlement'.

A related phenomenon is secondary settlement, also called 'creep' or 'secular effect'. Creep is the ongoing compression under a constant load, where the soil properties gradually change. Also here water is expelled out of the pores. This compaction goes on practically forever, also if the pore pressures have been long reduced to zero. Internationally, the Anglo-Saxon method is often used to determine soil settlement. This method comprises primary and secondary settlement and is expressed by the symbol ε that represents the relative settlement, so the reduction of the height of a soil layer (ΔH) divided by the initial layer height (H):

$$\varepsilon = \varepsilon_p + \varepsilon_s ,$$

and $\Delta H = \varepsilon \cdot H$. The total settlement of n soil layers thus is $\Delta H_{total} = \sum_{i=1}^n \Delta H_i$.

A well-known equation for the primary compression comes from Karl von Terzaghi:

$$\varepsilon_p = \frac{C_c}{1+e_0} \log\left(\frac{\sigma'_{v,i} + \Delta\sigma'_v}{\sigma'_{v,i}}\right)$$

in which: ε_p [-] = relative primary settlement = $\Delta H_p / H_p$
 C_c [-] = primary compression coefficient
 e_0 [-] = initial void ratio (*poriëngetal*) (see Section 28.3)
 $\sigma'_{v,i}$ [kPa] = initial vertical effective stress
 σ'_v [kPa] = (new) vertical effective stress = $\sigma'_{v,i} + \Delta\sigma'_v$

The following equation for creep has been developed by prof. Keverling Buisman:

$$\varepsilon_s = C_\alpha \log\left(\frac{\Delta t}{t_{ref}}\right)$$

in which: ε_s [-] = relative secondary settlement (= creep) = $\Delta H_s / H_s$
 C_α [-] = secondary compression coefficient
 Δt [day] = duration of the secondary settlement
 t_{ref} [day] = reference duration (one day)

This formula has no advantages, but it does have three disadvantages:

- The initial pore value e_0 is unknown and difficult to estimate.
- The formula for secondary compression is not intended for weak soil.
- The formula for secondary compression is nonsense. The value of the pressure difference $\Delta\sigma'$ is not even included in the formula!

The equation according to linear elasticity is also used:

$$\varepsilon = m_v \Delta\sigma$$

in which: m_v = (vertical) compression constant = $1 / E_{oed}$

As soil is not a linear elastic material, this formula has limited applicability. The constant m_v depends on the state of stress and can only be assumed constant in a limited stress course. The most used method for determination of the compressibility in the Netherlands is proposed by Koppejan. The following equation is based on Koppejan's original formula from 1948, but includes the degree of consolidation:

$$\varepsilon = \left(\frac{U}{C'_p} + \frac{1}{C'_s} \log\left(\frac{\Delta t}{t_{ref}}\right) \right) \cdot \ln\left(\frac{\sigma'_{v,i} + \Delta\sigma'_v}{\sigma'_{v,i}}\right)$$

in which: ε [-] = relative compression = $\Delta H / H$
 H [m] = layer thickness
 U [-] = degree of consolidation (see Section 28.1)
 C'_p [-] = primary compression coefficient
 C'_s [-] = secondary compression coefficient
 t [day] = duration after the application of the additional loading
 t_{ref} [day] = reference duration (one day)
 $\Delta\sigma'_v$ [kPa] = increase of the vertical effective stress in the weak layer
 $\sigma'_{v,i}$ [kPa] = initial vertical effective pressure

This equation comprises both primary settlement and creep, taking the degree of consolidation into account.

Notes

- Be aware that the formula is confusing. It contains both an e-log and a 10-log.
- Usually, $t_{\infty} = 10\ 000$ days (= 30 years) is considered the maximum settlement time.
- On completion of a structure, the usual requirement is that the total settlement $< 0,30$ m, provided that the settlement is even and resulting level differences are dealt with in an appropriate way (for instance by applying concrete slabs (rijplaten) at the interface of an abutment and an embankment).
- If both sand layers and clay or peat layers are present, the compression of the sand layers is usually negligible.
- Take spreading of the load in the soil into account. A spread of the stress under an angle of 45 degrees is customary (for slabs both in lengthways and widthways directions: For a square slab with length = D , $\Delta\sigma'$ is reduced to $1/9^{\text{th}}$ at a depth D (see Section 24.1).
- The parameters C'_p and C'_s follow from oedometer tests on samples obtained by (tube sample) borings. For a preliminary design the values in Table 31-4 (the Eurocode table with soil properties) would suffice.
- After a situation of preloading, the soil will behave much stiffer (approximately a factor 3 to 5) as long as the maximum effective vertical stress that has acted on the soil in the past is not exceeded. This maximum stress is referred to as the pre-consolidation pressure, σ'_{max} (grensspanning). Compression will be usually be small, if the vertical effective stress remains below σ'_{max} . This implies that the settlement of preloaded soil will be smaller than of non-preloaded soil. For detailed designs, it is better to divide the settlement calculation into a stiff part before the vertical effective soil pressure reaches σ'_{max} and a weak part thereafter. In that case,

$$\varepsilon = \left(\frac{U}{C'_p} + \frac{1}{C'_s} \log(t) \right) \cdot \ln \left(\frac{\sigma'_{max}}{\sigma'_{v,i}} \right) + \left(\frac{U}{C'_p} + \frac{1}{C'_s} \log(t) \right) \cdot \ln \left(\frac{\sigma'_v}{\sigma'_{max}} \right)$$

where:

- C_p [-] = primary compression coefficient below pre-consolidation pressure ($\sigma'_v < \sigma'_{max}$)
 C_s [-] = secondary compression coefficient below pre-consolidation pressure ($\sigma'_v < \sigma'_{max}$)
 C'_p [-] = primary compression coefficient above pre-consolidation pressure ($\sigma'_v > \sigma'_{max}$)
 C'_s [-] = secondary compression coefficient above pre-consolidation pressure ($\sigma'_v > \sigma'_{max}$)
 σ'_{max} [kPa] = pre-consolidation pressure of the soil

Reference is made to specialised readers on soil mechanics for more details on this calculation method.

28.3 Soil relaxation**Free relaxation**

Excavations (e.g., for a construction site) relieve the soil situated at a greater depth. This causes relaxation (= swell) of the soil. In turn this causes the excavate ground surface to rise in time.

To determine the total relaxation Δh_{total} the following formula is used:

$$\frac{\Delta h_{total}}{h} = \frac{C_{sw}}{(1+e_0)} \cdot \log \left(\frac{\sigma'_i + \Delta\sigma}{\sigma'_i} \right)$$

in which:

- h [m] = initial thickness of the relaxing layer
 C_{sw} [-] = swell or relaxation coefficient (zwellcoëfficiënt, or zwellingsmodulus) (see Table 25-6)
 e_0 [-] = initial void ratio (poriëngetal)
 σ'_i [N/m²] = initial effective stress
 $\Delta\sigma$ [N/m²] = reduction of the effective stress due to the excavation

The void ratio is defined with:

$$e = \frac{V_{pores}}{V_{grains}}$$

in which:

- V_{pores} [m³] = volume of the pores, which is the volume of water if the soil is completely saturated
 V_{grains} [m³] = volume of the solid material (sediment grains)

Restricted relaxation

If the relaxation is restricted, for instance by the presence of a submerged concrete floor with tensile piles, relaxation cannot lead to an elevation of the excavated ground surface. Instead, it leads to an increase of the effective stress under the floor. A secondary effect (creep) is not taken into account in relaxation calculations, so the extent of the effective stress against the floor depends on the degree of consolidation of the swelling layer and on the extent of the change of the effective stress due to the excavation.

If the stiffness of the soil is linear when it is relieved of its load, one can pose:

$$\sigma'_{relaxation} = (1-U) \cdot \Delta\sigma'_{excavate}$$

The calculation of the degree of consolidation U , the moment the floor is constructed is carried out according to Section 28.1 "Consolidation". For this one can assume that:

$$c_{v,relaxation} \approx 4 \cdot c_v,$$

because the stiffness ($1/m_v$) is far greater when being relieved of pressure, which has consequences for c_v according to:

$$c_v = \frac{k_v}{\gamma_w m_v}$$

If the excavation takes place in fully consolidated soil ($U = 1$), there will be no relaxation stress $\sigma'_{relaxation}$ under the underwater concrete floor, as $(1-U)$ will equal 0.

28.4 Literature

Barron, R.A. (1948) *Consolidation of fine-grained soils by drain wells*. Transactions of American Society for Civil Engineers, Vol. 113, No. 2346, pp. 718-724.

Knappet, J.A. and R.F. Graig (2012). *Craig's soil mechanics* (8th edition). Spon Press, London.

Terzaghi, K. (1943) *Theoretical soil mechanics*. John Wiley & Sons, New York.

Verruijt, A. and S. van Baars (2005). *Soil mechanics*. VSSD, Delft, 2005.

29. Concrete

major revision: February 2011
crack width and strut & tie modelling added: February 2018 and improved: 2020

Concrete is a commonly used and very suitable construction material, particularly for non-moving parts of hydraulic structures. The design of concrete structures is a profession in itself. It should be realised that the theory of concrete for hydraulic engineering purposes has other emphases than the theory for the more common non-residential building (*utiliteitsbouw*) branch, because of the following reasons:

1. In non-residential building, structural elements can often be schematised as bending beams. Hydraulic structures are usually not slender and have complex 3-D shapes.
2. In hydraulic structures, the concrete parts below the water surface are under pressure. A pre-tensile stress is present on all sides. This circumstance differs from non-residential building.
3. The reinforcement steel in hydraulic structures in sea water must be well protected from corrosion. This is why often pre-stressed reinforcement is used to reduce the crack width to zero.

29.1 Properties of concrete

For design calculations European standards should be used: for concrete NEN-EN 1992-1-1:2005 (Eurocode 2: Design of concrete structures). For the theory about this subject, the course of CT2051 and CT3051 is recommended. The prescribed characteristics for concrete classes currently available in the Netherlands are presented in Table 29-1 (EN 206-1 Table 7 and EN 1992-1-1 Table 3.1).

concrete class (old)	strength class	f_{ck} (MPa)	$f_{c\ cub\ k}$ (MPa)	f_{cm} (MPa)	f_{ctm} (MPa)	$f_{ctk, 0,05}$ (MPa)	$f_{ctk, 0,95}$ (MPa)	E_{cm} (GPa)
B15	C12/15	12	15	20	1,6	1,1	2,0	27
B25	C20/25	20	25	28	2,2	1,5	2,9	30
B35	C30/37	30	35	38	2,9	2,0	3,8	33
B45	C35/45	35	45	43	3,2	2,2	4,2	34
B55	C45/55	45	55	53	3,8	2,7	4,9	36
B65	C53/65	53	67	63	4,2	3,0	5,5	38
B75	C60/75	60	75	68	4,4	3,1	5,7	39
B85	C70/85	70	85	78	4,6	3,2	6,0	41

Table 29-1 Characteristics of concrete classes

f_{ck}	[MPa]	= characteristic compressive cylinder strength of concrete at 28 days
$f_{c\ cub\ k}$	[MPa]	= characteristic compressive cube strength of concrete at 28 days
f_{cm}	[MPa]	= mean value of concrete cylinder compressive strength after 28 days ($f_{cm} = f_{ck} + 8$)
f_{ctm}	[MPa]	= mean value of axial tensile strength of concrete: $f_{ctm} = 0,30 \cdot f_{ck}^{(2/3)}$ for qualities \leq C50/60; $f_{ctm} = 2,12 \cdot \ln(1 + (f_{ck}/10))$ for qualities $>$ C50/60
$f_{ctk, 0,05}$	[MPa]	= characteristic axial tensile strength of concrete ($f_{ctk, 0,05} = 0,7 f_{ctm}$ 5% fractile)
$f_{ctk, 0,95}$	[MPa]	= characteristic axial tensile strength of concrete ($f_{ctk, 0,95} = 1,3 f_{ctm}$ 95% fractile)
E_{cm}	[GPa]	= secant modulus of elasticity of concrete ($E_{cm} = 22 (f_{cm}/10)^{0,3}$) (f_{cm} in MPa)

The strength class, or concrete quality, is indicated by the letter C (from **C**oncrete), followed by the characteristic compressive cylinder strength and the characteristic compressive cube strength at 28 days. The choice for a certain strength class depends on the design, the way of construction, and the costs. The lowest quality, C12/15 is not very suitable as a construction material. For in situ cast concrete, qualities C20/25, C25/30, C30/37 are very common, because they provide sufficient strength and stiffness for non-residential building and can be handled very well during construction. The strength of prefabricated concrete elements is usually higher than in situ cast concrete, because manufacturing circumstances can be better controlled and quick hardening is required for mass production: C35/45 is the minimum, but more common are C45/55 and C50/60.

The design value for concrete compressive strength can be computed as follows:

$$f_{cd} = \frac{\alpha_{cc} \cdot f_{ck}}{\gamma_c} \quad (35.1)$$

The design value for concrete tensile strength can be computed as follows:

$$f_{ctd} = \frac{\alpha_{ct} \cdot f_{ctk,0.05}}{\gamma_C} \quad (35.2)$$

where:

f_{cd}	[MPa]	= design value of concrete compressive strength
f_{ctd}	[MPa]	= design value of concrete tensile strength
α_{cc}	[-]	= coefficient taking account of long-term effects on the compressive strength and of unfavourable effects resulting from the way the load is applied ($\alpha_{cc} = 1,0$)
α_{tc}	[-]	= coefficient taking account of long-term effects on the compressive strength and of unfavourable effects resulting from the way the load is applied ($\alpha_{tc} = 1,0$)
f_{ck}	[MPa]	= characteristic compressive cylinder strength of concrete at 28 days
$f_{ctk,0.05}$	[MPa]	= characteristic axial tensile strength of concrete (5% fractile)
γ_C	[-]	= partial safety factor for concrete

An overview of the partial safety factors for materials for ultimate limit states for concrete (γ_C) and steel (γ_S) is given in Table 29-2.

Design situations	γ_C for concrete	γ_S for reinforcement steel	γ_S for prestressing steel
Persistent & Transient loads	1,5	1,15	1,1
Accidental loads	1,2	1,0	1,0

Table 29-2 Partial safety factors for material

29.2 Properties of reinforcement steel

For reinforcement steel TGB 1990 gives material properties for some steel classes:

Steel type		f_{yk} [N/mm ²]	f_{yd} [N/mm ²]	ϵ_{uk} [N/mm ²]
Bars	FeB 220 HWL	220	190	5,00
	FeB 400 HWL, HK	400	350	4,00
	FeB 500 HWL, HK	500	435	3,25
	FeB 500 HKN	500	435	2,75
Wire fabrics (wapeningsnetten)	FeB 500 HKN, HWN	500	435	2,75

Table 29-3 Characteristics of reinforcement steel classes according to the old TGB 1990 standard

where:

f_{yk}	[N/mm ²]	= characteristic yield strength of reinforcement
f_{yd}	[N/mm ²]	= design yield strength of reinforcement
ϵ_{uk}	[-]	= characteristic strain (<i>rek</i>) of reinforcement or pre-stressing steel at maximum load

The TGB 1990 standard has been replaced by a NEN standard that shows some differences regarding the characteristic values of reinforcement steel classes. The NEN standard (NEN 6008) applies only in a limited part of Europe. The most frequently used reinforcement steel class is B500B.

Reinforcement steel classes	\varnothing [mm]	R_e [MPa]	R_m / R_e [-]	A_{gt} [%]
B500A	4-16	500	1,05 (1,03 for $\varnothing \leq 5.5\text{mm}$)	3,0 (2,0 for $\varnothing \leq 5.5\text{mm}$)
B500B	6-50	500	1,08	5,0
B500C	6-50	500	1,15 (1,13 for $\varnothing \leq 12\text{mm}$)	7,5 (7,0 for $\varnothing \leq 12\text{mm}$)

Table 29-4 Characteristics of reinforcement steel classes according to the NEN 6008 standard

where:

\varnothing	[mm]	=	nominal diameter
R_e	[MPa]	=	characteristic yield strength of reinforcement (f_{yk})
R_m	[MPa]	=	characteristic tensile strength of reinforcement (f_{tk})
R_m/R_e	[-]	=	minimum ratio tensile strength/yield strength (f_{tk}/f_{yk})
A_{gt}	[-]	=	minimum percentage total elongation at maximum force
A	[-]	=	indicates a smooth, dented or ribbed profile
B	[-]	=	indicates a dented or ribbed profile
C	[-]	=	indicates a ribbed profile

Commonly used reinforcement bar diameters in Hydraulic Engineering are \varnothing 12, 16, 20, 25 and 32 mm.

The Young's modulus of reinforcement steel (E_s) is $2,0 \cdot 10^5$ N/mm²

29.3 Properties of pre-stressed steel

In principle the function of pre-stressing is to prevent the occurrence of cracks in the concrete structure by creating compressive stresses in a structural member where one normally would expect tensile stresses. The elimination of tensile stresses does not only result in the prevention of cracks in the concrete, but also in a more economical use of materials (slender structures). In Figure 29-1 the principle of pre-stressing is visualized for a simply supported beam (*vrij opgelegde balk*) on two supports. The load on the beam results in compressive stresses above the centroid (*neutrale lijn*) and tensile stresses below the centroid as indicated in the left stress diagram. As the result of pre-stressing a normal force is exerted, resulting in an evenly distributed compressive stress over the whole cross-section of the beam (middle stress diagram). This compressive stress eliminates the tensile stress at the underside of the beam and reinforces the compressive stress at the topside, resulting in compressive stresses over the whole cross-section (right stress diagram).

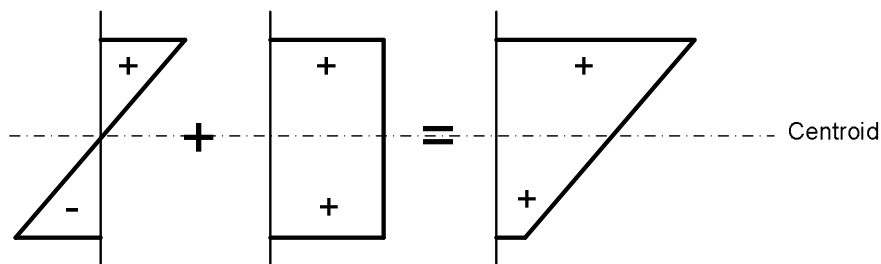


Figure 29-1 the principle of pre-stressing.

The following methods for pre-stressing concrete are used:

- 1) Pre-tensioning (*voorspanning met aanhechting, VMA*): This principle is mainly used in the prefabrication of concrete members. In the factory the tendons (*voorspanwapening*) are pre-stretched before the concrete is poured. After the concrete has hardened enough the tendons are released. The force present in the tendons is absorbed via adhesion (friction) between the steel and the concrete.
- 2) Post-tensioning (*voorspanning zonder aanhechting, VZA*): Here the tendons are situated in a protective tube. After pouring the concrete they are slightly tensioned in order to prevent attachment with the cement water. After a certain period, when the concrete has reached a strength determined by the structural engineer, the tendons are pre-stressed to approximately 20% of their capacity. This is called pre-stressing the self-weight (*eigen gewicht aanspannen*). When the concrete has reached its ultimate strength, the tendons are pre-stressed to 100% of their capacity.

There are three types of pre-stressing steels, namely: wire (*voerspandraad*), strands (*voorspanstreng*) and bars (*voorspanstaven*). The properties of these three types are described in the following standards, NEN-EN 10138-2 (draft) "wire", NEN-EN 10138-3 (draft) "strand" and NEN-EN 10138-4 (draft) "bars". Furthermore, the NEN-EN 10138-1 (draft) "general requirements" and NEN-EN 1992-1 are applicable. In Table 29-5 the characteristic values for certain diameters of all three types of pre-stressing steel are presented, for information regarding other available diameters the reader is referred to the standards mentioned above.

Steel type	d [mm]	S_n [mm ²]	f_{pk} [N/mm ²]	$f_{p0.1k}$ [N/mm ²]	ϵ_{uk} [-]
Wire					
Y1860C	4,0	12,57	1860	1599	0,035
Y1770C	6,0	28,27	1770	1521	0,035
Y1670C	8,0	38,48	1670	1437	0,035
Y1570C	10,0	78,54	1570	1299	0,035
Strand					
Y1860S3 class A	6,5	23,40	1860	1598	0,035
Y1770S7 class A	16,0	150,00	1770	1587	0,035
Y1960S3 class B	6,5	21,10	1960	1687	0,035
Y1960S7 class B	9,0	50,00	1960	1680	0,035
Bar					
Y1030H	26,0	531	1030	834	0,035
Y1030H	40,0	1257	1030	835	0,035
Y1230H	26,0	531	1230	1079	0,035
Y1230H	40,0	1257	1230	1080	0,035

Table 29-5 Characteristic values for pre-stressing steels.

where:

- d : nominal diameter
 S_n : nominal cross-sectional area
 f_{pk} : characteristic value for the tensile strength of pre-stressing steel
 $f_{p0.1pk}$: characteristic 0,1% yield boundary for pre-stressing steel
 ϵ_{uk} : characteristic strain (*rek*) of reinforcement or pre-stressing steel at maximum load

The design value for the tensile strength is equal to: $f_{pd} = \frac{f_{p0.1k}}{\gamma_s}$

The design value for the characteristic yield boundary can be computed as follows: $\epsilon_{ud} = 0,9 \cdot \epsilon_{uk}$.

The Young's modulus for pre-stressed steel (E_p) is $2,05 \cdot 10^5$ N/mm² for wire and bars and $1,95 \cdot 10^5$ N/mm² for strands.

29.4 Reinforced and pre-stressed concrete

To design reinforced or pre-stressed concrete structures the following limit states have to be considered:

- 1) Ultimate limit states, leading to failure of the structure;
- 2) Serviceability limit states; leading to restriction of use of the structure.

ultimate limit state:

- fracture due to bending and / or normal force
- fracture due to shear force
- fracture due to punching
- fracture due to torsion

serviceability limit state:

- unacceptable deformation
- unacceptable cracking (*scheuren*)

For a more elaborate consideration of the limit states, reference is made to the Eurocode 0, Section 3. Bending and shear force are discussed briefly here because they are of importance in a preliminary design.

Bending and/or normal force

The limit state involving bending and normal force is:

$$M_{Ed} = M_{Rd} \quad \text{and} \quad N_{Ed} = N_{Rd}$$

- in which:
- M_{Ed} [Nm] = design value of the maximum occurring bending moment
 - M_{Rd} [Nm] = maximum allowable bending moment
 - N_{Ed} [Nm] = design value of the normal force
 - N_{Rd} [Nm] = maximum allowable normal force

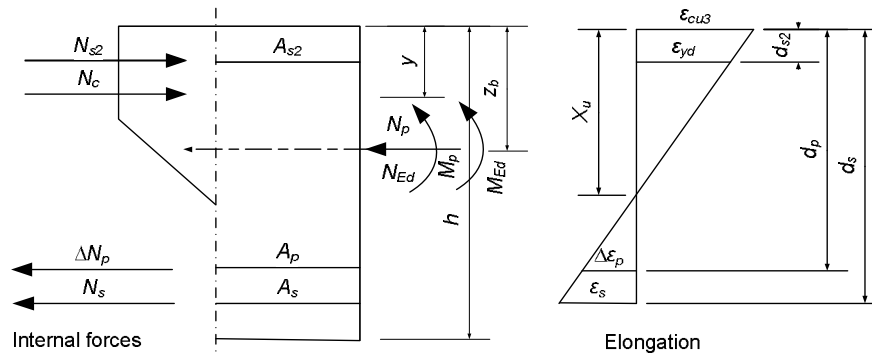


Figure 29-2 Forces and strains in concrete

The maximum allowable moment and normal force are:

$$M_{Rd} = (N_p + N_{Ed})(z_b - y) + \sum N_s(d_s - y) + \sum \Delta N_p(d_p - y) \quad (35.3)$$

$$N_{Rd} = N_c + N_{s2} - N_p - \Delta N_p - N_s \quad (35.4)$$

where:	N_p	[N]	= design value for the effective normal compression force as a result of the pre-stressing force
	M_p	[Nm]	= design value for the effective moment force as a result of the pre-stressing force
	N_{Ed}	[N]	= design value of the normal force (excluding pre-stressing force); if the normal force is a tensile force replace $+N_{Ed}$ with $-N_{Ed}$
	N_c	[N]	= design value of the compression resultant = $0,75 \cdot x_u \cdot f_{cd}$
	f_{cd}	[N/m ²]	= design value of concrete compressive strength
	N_s	[N]	= tensile force in the reinforcement steel
	$N_{s,2}$	[N]	= compressive force in the reinforcement steel
	ΔN_p	[N]	= increase of the force in the pre-stressing reinforcement relative to the initial pre-stressing force ($\Delta N_p = A_p \cdot \Delta \sigma_{pu}$)
	A_p	[m ²]	= cross-sectional area of the pre-stressed element
	$\Delta \sigma_{pu}$	[N/m ²]	= increase of the stress in the pre-stressing reinforcement relative to the initial pre-stressing stress
	y	[m]	= distance between the compression stress resultant and the edge with the highest compression = $7/18 x_u$ (for $\leq C50/60$)
	x_u	[m]	= height of the concrete compression zone
	d_s	[m]	= the distance between the tensile reinforcement and the edge with highest compression
	d_{s2}	[m]	= the distance between the reinforcement in the compression zone and the edge with most compression
	d_p	[m]	= the distance between the pre-stressing steel and the edge with most compression
	z_b	[m]	= the distance between the elastic line of gravity and the edge with most compression
	h	[m]	= total height of the structure
	ε_{cu3}	[m]	= ultimate compressive strain in the concrete

When determining x_u one must take into account that: $\varepsilon_{cu3} = 0,0035$.

Furthermore, there are requirements for the maximum value of x_u if the normal force is small ($N_{Ed} < 0,1 \cdot f_{cd} \cdot A_c$) due to the rotation capacity, for this the reader is referred to TGB 1990 (NEN 6720 article 8.1.3).

To calculate the required reinforcement, the requirement should be satisfied that the reinforcement steel must yield before the concrete will fail and the minimum of the reinforcement percentage must be large enough to be sure there will be no brittle failure when cracking of the concrete occurs (*brosse breuk*). If the structure is mainly loaded by a moment force, the required reinforcement steel can easily be calculated with help of Table 29-6. Note that Table 29-6, Table 29-7, Table 29-8 and the flowchart below only apply to reinforced concrete and not for pre-stressed concrete. The flowchart is used to compute the reinforcement percentage needed in a structural member when the bending moment for the ultimate limit state is known.

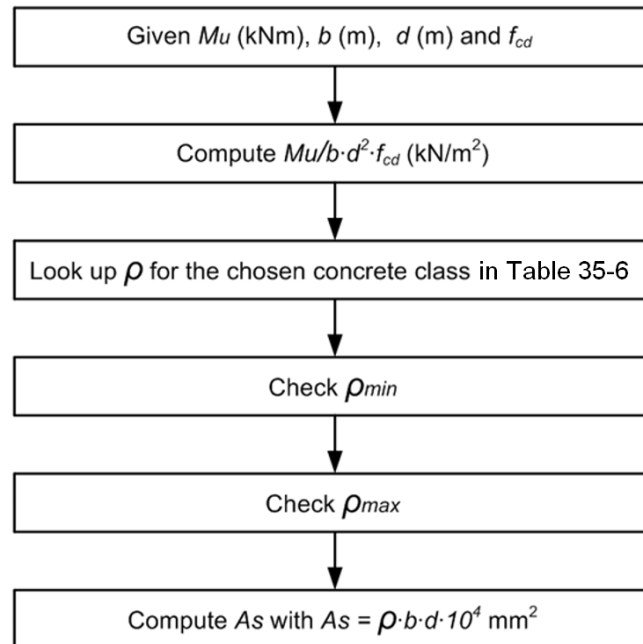


Figure 29-3 Flowchart for the preliminary design of reinforcement using the TGB-tables.

$\frac{M_d}{bd^2 f_{cd}}$	ψ	k_x	k_z	ρ [%]				
				C20/25	C28/35	C35/45	C45/55	C53/65
10	0,010	0,013	0,99	0,03	0,05	0,06	0,08	0,09
20	0,020	0,027	0,99	0,07	0,10	0,13	0,15	0,18
30	0,030	0,240	0,98	0,10	0,15	0,19	0,23	0,27
40	0,041	0,055	0,98	0,14	0,20	0,25	0,31	0,37
50	0,051	0,068	0,97	0,18	0,25	0,32	0,39	0,46
60	0,062	0,083	0,97	0,21	0,30	0,39	0,47	0,56
70	0,073	0,097	0,96	0,25	0,35	0,45	0,55	0,66
80	0,084	0,112	0,96	0,29	0,41	0,52	0,64	0,75
90	0,095	0,127	0,95	0,33	0,46	0,59	0,72	0,85
100	0,106	0,141	0,94	0,37	0,51	0,66	0,81	0,95
110	0,117	0,156	0,94	0,40	0,56	0,73	0,89	1,05
120	0,129	0,172	0,93	0,44	0,62	0,80	0,98	1,16
130	0,140	0,187	0,93	0,48	0,68	0,87	1,06	1,26
140	0,152	0,203	0,92	0,52	0,73	0,94	1,15	1,36
150	0,164	0,219	0,91	0,57	0,79	1,02	1,24	1,47
160	0,176	0,235	0,91	0,61	0,85	1,09	1,34	1,58
170	0,188	0,251	0,90	0,65	0,91	1,17	1,43	1,69
180	0,201	0,268	0,90	0,69	0,97	1,25	1,53	1,80
190	0,214	0,285	0,89	0,74	1,03	1,33	1,62	1,92
200	0,227	0,303	0,88	0,78	1,10	1,41	1,72	2,04
210	0,240	0,320	0,88	0,83	1,16	1,49	1,82	2,16
220	0,253	0,337	0,87	0,87	1,22	1,57	1,92	2,27
230	0,267	0,356	0,86	0,92	1,29	1,66	2,03	2,39
240	0,281	0,375	0,85	0,97	1,35	1,75	2,13	2,52
250	0,295	0,393	0,85	1,02	1,43	1,83	2,24	2,64
260	0,310	0,413	0,84	1,07	1,50	1,93	2,35	2,78
270	0,325	0,433	0,83	1,12	1,57	2,02	2,47	2,91
280	0,340	0,453	0,82	1,17	1,64	2,11	2,58	3,05
290	0,356	0,475	0,81	1,23	1,72	2,21	2,70	3,19
300	0,372	0,496	0,81	1,28	1,80	2,31	2,82	3,34
310	0,388	0,517	0,80	1,34	1,87	2,41	2,94	3,48
320	0,405	0,540	0,79	1,40	1,96	2,51	3,07	3,63

Table 29-6 Reinforcement percentages for rectangular cross-sections, reinforced with B500B, loaded by bending without normal force, With M_u in kNm; b and d in m¹ and f_{cd} in N/mm²

where:

M_u [kNm] = ultimate absorbable bending moment (*breukmoment*)

k [-] = ratio between the strength of concrete and steel $\left(k = \frac{f_{yd}}{f_{cd}} \right)$

f_{yd} [N/mm²] = design yield strength of reinforcement $\left(f_{yd} = \frac{f_{yk}}{\gamma_s} \right)$

f_{cd} [N/mm²] = design value of concrete compressive strength $\left(f_{cd} = \frac{f_{ck}}{\gamma_c} \right)$

ρ [%] = reinforcement percentage

d [m] = total thickness of the concrete member (so, not only the effective width)

b [m] = width of the concrete member, perpendicular to the considered cross-section (so, if forces and moments are per running metre, $b = 1$ m).

ψ [%] = mechanical reinforcement percentage: $\psi = k \cdot \rho$

$$k_x = \frac{x_u}{d} \quad k_z = \frac{z_u}{d}$$

x_u = height of the of the compressive zone (*hoogte drukzone*): $x_u = d \cdot \frac{\rho \cdot k}{0,75}$

z_u = arm of internal leverage (*inwendige hefboomsarm*):

$$z_u = d \cdot (1 - 0,52 \cdot \rho \cdot k) = d - \beta \cdot x_u, \text{ where } \beta = 0,75 \cdot 0,52 = 0,39$$

d [mm] = effective height of the cross-section (*nuttige hoogte*):

$$d = h - (c + \frac{1}{2} \varnothing)$$

h [mm] = height of the cross-section

c [mm] = concrete cover

\varnothing [mm] = bar diameter (*kenmiddellijn*)

A_s [mm²] = total cross-sectional area of the reinforcement

	C20/25	C28/35	C35/45	C45/55
ρ_{min}	0,15	0,18	0,21	0,24

Table 29-7 Minimum reinforcement percentage (ρ_{min}) for B500B.

	C20/25	C28/35	C35/45	C45/55
ρ_{max}	1,38	1,94	2,49	3,05

Table 29-8 Maximum reinforcement percentage (ρ_{max}) for B500B.

To check an existing concrete structural member, the maximum allowable bending moment can be computed using the following equation (see the book *Constructieel Gewapend Beton* of course CTB2220):

$$M_u = A_s \cdot f_{yd} \cdot d \cdot (1 - 0,52 \cdot \rho \cdot k) \text{ and } M_{ed} \leq M_u \quad (35.5)$$

where:

M_{ed} [Nm] = design value for the bending moment in the ultimate limit state

M_u [Nm] = ultimate absorbable bending moment

A_s [m²] = total cross-sectional area of reinforcement

k [-] = ratio between the strength of concrete and steel $\left(k = \frac{f_{yd}}{f_{cd}} \right)$

f_{yd} [N/m²] = design yield strength of reinforcement

f_{cd} [N/m²] = design value of concrete compressive strength

ρ [-] = reinforcement ratio $\left(= \frac{A_s}{b \cdot d} \right)$

b [m] = width of the concrete structure

Automatically the equation can also be used to calculate the necessary reinforcement, when the load is known.

Shear force of concrete elements without shear reinforcement

The design value for the shear resistance $V_{Rd,c}$ **without** shear reinforcement is given by

$$V_{Rd,c} = [C_{RD,c} \cdot k \cdot (100 \cdot \rho_1 \cdot f_{ck})^{1/3} + k_1 \cdot \sigma_{cp}] \cdot b_w \cdot d \quad [N] \quad (35.6)$$

with a minimum of

$$V_{Rd,c} = (v_{min} + k_1 \cdot \sigma_{cp}) \cdot b_w \cdot d \quad [N], \quad (35.7)$$

where f_{ck} [N/mm²] = characteristic compressive cylinder strength of concrete at 28 days in MPa

$$k \quad [-] = 1 + \sqrt{\frac{200}{d}} \leq 2,0 \text{ with } d \text{ in mm}$$

$$\rho_1 \quad [-] = \text{reinforcement ratio for longitudinal reinforcement} = \frac{A_{sl}}{b_w \cdot d} \leq 0,02 ;$$

A_{sl} [mm²] = the area of the tensile reinforcement, which extends more than $(l_{bd} + d)$ beyond the considered section

b_w [mm] = the smallest width of the cross-section in the tensile area

σ_{cp} [N/mm²] = compressive stress in the concrete from axial load or prestressing:

$$\sigma_{cp} = N_{Ed} / A_C < 0,2 \cdot f_{cd}$$

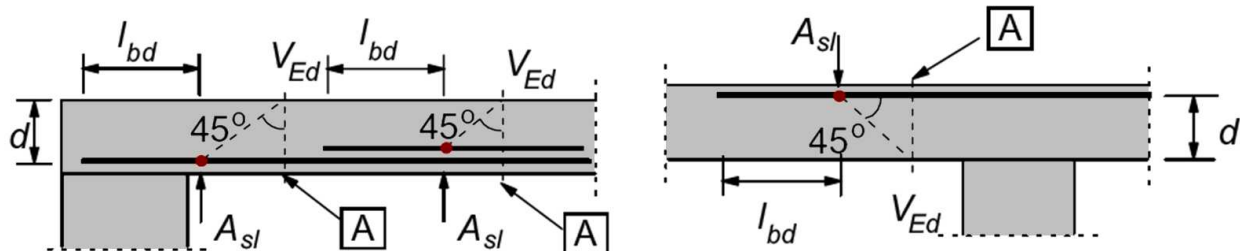
N_{Ed} [N] = the axial force in the cross-section due to loading or prestressing ($N_{Ed} > 0$ for compression)

A_C [mm²] = the area of the concrete cross-section [mm²]

k_1 [-] = a coefficient, in the Netherlands: 0,15

$C_{RD,c}$ [-] = a coefficient, in the Netherlands: $0,18 / \gamma_c = 0,18 / 1,5 = 0,12$

$$v_{min} \quad [-] = 0,035 \cdot k^{3/2} \cdot f_{ck}^{1/2}$$

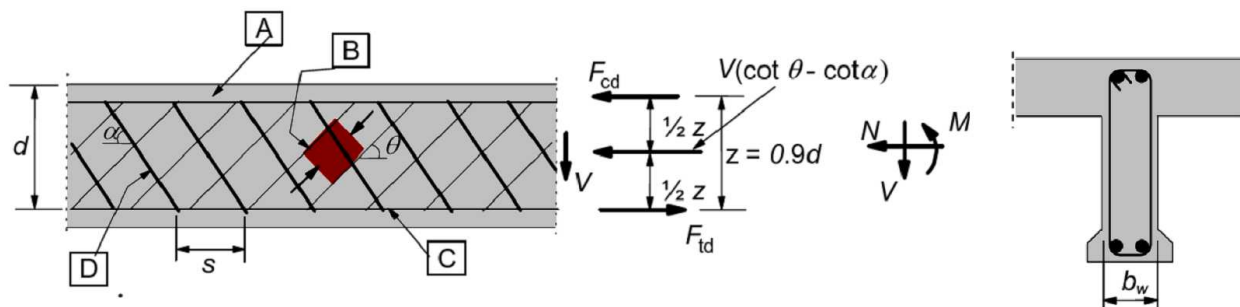


A - section considered

Figure 29-4 Reinforced concrete structural member without shear reinforcement.

Shear force of concrete elements with shear reinforcement

The design of members **with** shear reinforcement is based on a truss model (*vakwerkmodel*), see Figure 29-5.



A - compression chord, **B** - struts, **C** - tensile chord, **D** - shear reinforcement

Figure 29-5 Inclined shear reinforcement

The following notations are shown in Figure 29-5:

- α : angle between shear reinforcement and the beam axis perpendicular to the shear force (measured positive as shown in the figure)
 θ : angle between the concrete compression strut and the beam axis perpendicular to the shear force
 F_{td} : design value of the tensile force in the longitudinal reinforcement
 F_{cd} : design value of the concrete compression force in the direction of the longitudinal member axis.
 b_w : the smallest width of the cross-section in the tensile area
 z : arm of internal leverage, for a member with constant depth, corresponding to the bending moment in the element under consideration. In the shear analysis of reinforced concrete without axial force, the approximate value $z = 0,9 \cdot d$ may normally be used.

The angle θ should be limited. The recommended upper and lower limits are: $21,8^\circ \leq \theta \leq 45^\circ$.

Vertical shear reinforcement

For members with vertical shear reinforcement, the shear resistance, V_{Rd} is the smaller value of :

$$V_{Rd,s} = \frac{A_{sw}}{s} \cdot z \cdot f_{ywd} \cdot \cot \theta \quad (\text{stirrups governing}) \quad (35.8)$$

where:

A_{sw} = the cross-sectional area of the shear reinforcement (be aware that the reinforcement crosses the cross-sectional area of the concrete element twice).

s = the spacing of the stirrups

f_{ywd} = the design yield strength of the shear reinforcement

and:

$$V_{Rd,max} = \frac{\alpha_{cw} b_w z \cdot v_1 \cdot f_{cd}}{\cot \theta + \tan \theta} \quad (\text{concrete compressive struts governing}) \quad (35.9)$$

where:

v_1 = strength reduction factor for concrete cracked in shear. Recommended is that $v_1 = v$

$$\text{and } v = 0,6 \left(1 - \frac{f_{ck}}{250} \right)$$

α_{cw} = coefficient taking account of the state of the stress in the compression chord. The recommended value of α_{cw} is as follows:

- 1 for non pre-stressed structures
- $(1 + \sigma_{cp} / f_{cd})$ for $0 < \sigma_{cp} \leq 0,25 \cdot f_{cd}$
- 1,25 for $0,25 \cdot f_{cd} < \sigma_{cp} \leq 0,5 \cdot f_{cd}$
- $2,5 \cdot (1 - \sigma_{cp} / f_{cd})$ for $0,5 \cdot f_{cd} < \sigma_{cp} \leq 1,0 \cdot f_{cd}$

σ_{cp} = the mean compressive stress, measured positive, in the concrete due to the design axial force. This should be obtained by averaging it over the concrete section taking account of the reinforcement. The value of σ_{cp} need not be calculated at a distance less than $0,5 \cdot d \cdot \cot \theta$ from the edge of the support.

The maximum effective cross-sectional area of the shear reinforcement, $A_{sw,max}$ for $\cot \theta = 1$ is given by:

$$\frac{A_{sw,max} \cdot f_{ywd}}{b_w \cdot s} \leq \frac{1}{2} \cdot \alpha_{cw} \cdot v_1 \cdot f_{cd} \quad (35.10)$$

Inclined shear reinforcement

For members with inclined shear reinforcement (*schuine dwarskrachtwapening*), the shear resistance is the smaller value of:

$$V_{Rd,s} = \frac{A_{sw}}{s} \cdot z \cdot f_{ywd} \cdot (\cot \theta + \cot \alpha) \cdot \sin \alpha \quad (\text{stirrups governing}) \quad (35.11)$$

and

$$V_{Rd,max} = \frac{\alpha_{cw} \cdot b_w \cdot z \cdot v_1 \cdot f_{cd} \cdot (\cot \theta + \cot \alpha)}{1 + \cot^2 \theta} \quad (\text{concrete compressive struts governing}) \quad (35.12)$$

The maximum effective shear reinforcement, $A_{sw,max}$ for $\cot \theta = 1$ follows from:

$$\frac{A_{sw,max} \cdot f_{ywd}}{b_w \cdot s} \leq \frac{\frac{1}{2} \cdot \alpha_{cw} \cdot v_1 \cdot f_{cd}}{\sin \alpha} \quad (35.13)$$

Note

In the walls of many hydraulic structures, there are large areas in which the shear force has reached its maximum while the bending moment is zero. In this case pure tension is found in the concrete wall, which needs special attention.

29.5 Stiffness of the concrete structure

For statically indeterminate structures, the stiffness (EI) of the elements used in the calculations has considerable influence, not only on the resulting deformation and displacements, but on the flow of forces through the structure (global force effect) and the resulting internal forces in each individual member (local force effect) as well. Figure 29-6 illustrates this effect for a U-shaped cross section on a pile foundation. The correct stiffness has to be used in hand or computer calculations to find the governing (internal) load distributions M , N and V .

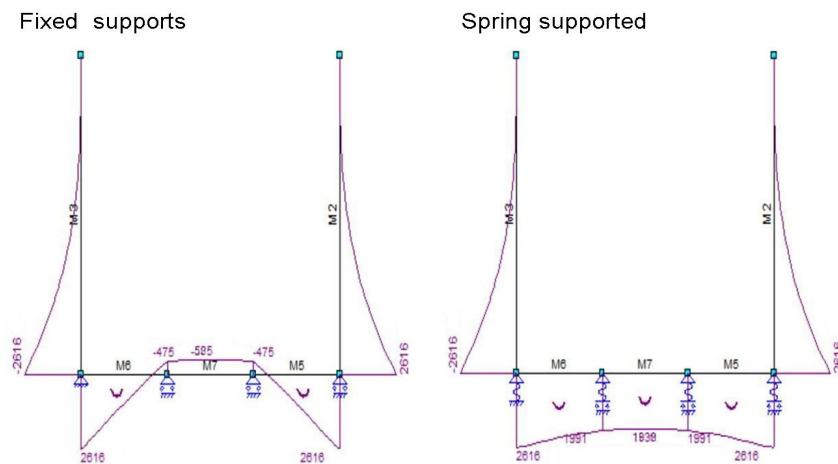


Figure 29-6 Influence of foundation stiffness on force distribution in the structure

Unfortunately, the stiffness of a reinforced concrete section or element changes depending on crack development. There is a significant difference in bending stiffness between the non-cracked and the cracked concrete cross-section. After occurrence of the first cracks, further loading will go hand in hand with a decreasing stiffness of the concrete. This is easily demonstrated by a $M-\kappa$ diagram, here κ is curvature (*kromming*), see Figure 29-7.

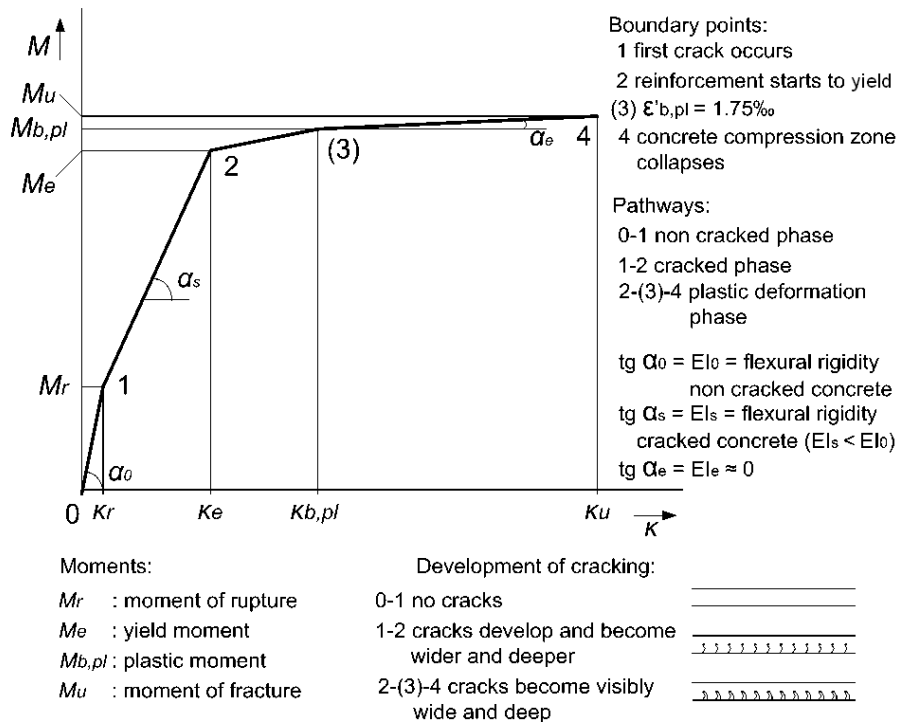


Figure 29-7 M-k-diagram

The bending stiffness of a concrete section, having to resist a certain M, is equal to the tangent of the line in the M-κ-diagram:

$$EI_x = \tan \alpha_x = \frac{M_x}{\kappa_x} \quad \text{and} \quad \kappa_x = \frac{M_x}{EI_x} \tag{35.14}$$

So, for a certain bending moment the intersection with the line in the M-κ-diagram has to be determined first to find the value of the curvature on the x-axis. Finally, the tangent of the line connecting the origin with the intersection point can be found, using the equation above and hence the bending stiffness corresponding to that moment.

To construct a M-κ-diagram, all the M-κ combinations have to be computed. The curvature κ can be determined as follows:

$$\kappa = \frac{\epsilon'_b + \epsilon_s}{d} \tag{35.15}$$

To find the correct stiffness of the whole structure the M-κ-diagram has to be constructed for every different concrete section, for each type of concrete and reinforcement percentage (ρ). This is a lot of work, often too much work for the level of precision required. In the following subsections first an approximation of concrete stiffness will be presented, then development of the M-κ-diagram will be further explained for detailed calculations.

First design calculations with concrete EI estimate

For uncracked cross-sections the bending stiffness of concrete EI_0 can be estimated/computed as follows:

$$EI_0 = E'_b \cdot I \tag{35.16}$$

where:

$$E'_b = 22250 + 250 \cdot f_{ck} \quad \text{for } 15 \leq f_{ck} \leq 65 \text{ (NEN6720)}$$

$$E'_b = 35900 + 40 \cdot f_{ck} \quad \text{for } 65 \leq f_{ck} \leq 105 \text{ (CUR 97)}$$

$$I = \frac{1}{12} \cdot b \cdot h^3 \quad \text{for rectangular cross-sections}$$

For cracked cross-sections the bending stiffness EI_g can be computed as follows:

$$EI_g = 0,5 \cdot E_s \cdot A_s \cdot h^2 \tag{35.17}$$

where:

- E_s [N/m²] = Youngs' modulus of steel
- A_s [m²] = area of the reinforcement steel present in the cross-sectional area of the beam
- f_{ck} [N/m²] = characteristic compressive strength
- b [m] = width of the cross-section
- h [m] = height of the cross-section

(source: 'construieren in gewapend beton' - part 2, Kamerling 1978)

More detailed calculation of concrete stiffness with M-K diagram

In this subsection the critical points of pure bending, i.e., bending moment M without normal force N , will be explained using stress-strain diagrams (*spanning-rek diagrammen*) in the end leading to the M- κ diagram, see Figure 29-7.

Non-cracked beam (*ongescheurde balk*)

At the instant that the concrete tensile strength f_{ctd} is reached, the deformation diagram and stress diagram look like depicted in Figure 29-8. The bending moment equals the moment of rupture M_r (*scheurmoment*) and the concrete is just not cracked. In this stage the concrete's compressive strength is still very small because the mean value of the axial tensile strength of concrete f_{ctm} is much smaller than the design value of the concrete compressive strength f_{cb} , so that $\epsilon'_b \ll 1,75\%$.

Cracked beam

When the load only increases a little the tensile zone in the concrete will crack and the tensile forces will be concentrated in the existing reinforcement. The centroid (*neutrale lijn*) displaces in upward direction. The load can be increased further until the reinforcement reaches its yield stress f_{yd} . The corresponding deformation and stress diagrams are depicted in Figure 29-9. The concrete is cracked so it does not have a tensile strength any longer. The deformation of the concrete at the compression side of the beam (ϵ'_b) is still smaller than 1,75%. The corresponding bending moment is the yield moment (*vloeimoment*). At this point the deformation of the steel changes from elastic to plastic.

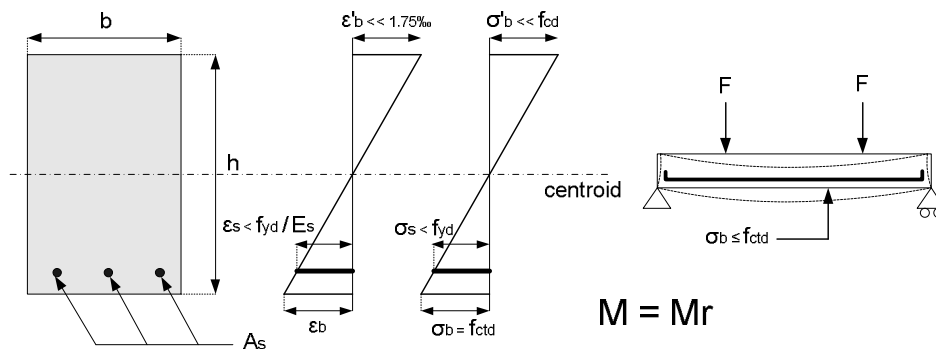


Figure 29-8 Deformation and stress diagram for a non-cracked beam

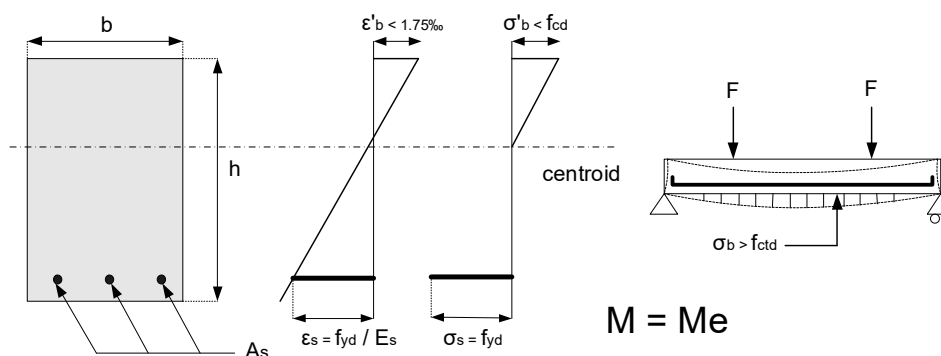


Figure 29-9 Deformation and stress diagram for a cracked beam

Compression strain in concrete (*betonstuik*)

When the load on the beam is increased further, at a certain moment the deformation of the concrete at the compression side of the beam will reach the value of 1,75‰ in the extreme pressure fibre (*uiterste drukvezel*). At the moment the compression strain of 1,75‰ is reached and the corresponding bending moment is equal to the plastic moment $M_{b,pl}$. The corresponding deformation and stress diagrams are depicted in Figure 29-10.

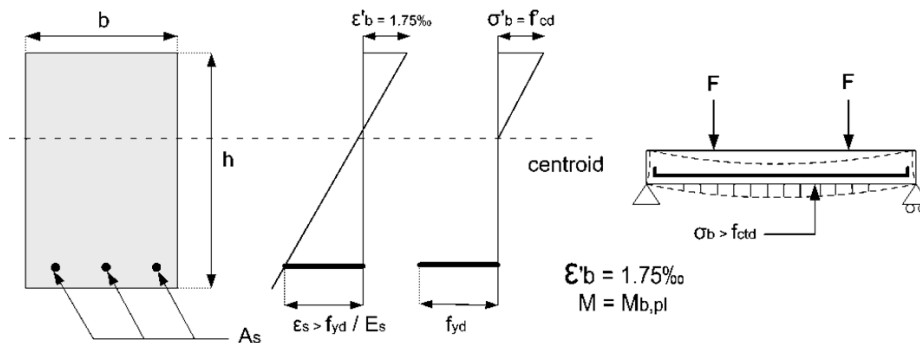


Figure 29-10 Deformation and stress diagram when the compression strain in the concrete has reached a value of 1,75‰.

When the load on the beam increases even further, the compression strain in the concrete will reach eventually a value of 3,50‰ in the extreme pressure fibre. If the beam reaches its point of collapse, the corresponding bending moment is the moment of fracture M_u (*breukmoment*). The corresponding deformation and stress diagrams are shown in Figure 29-11.

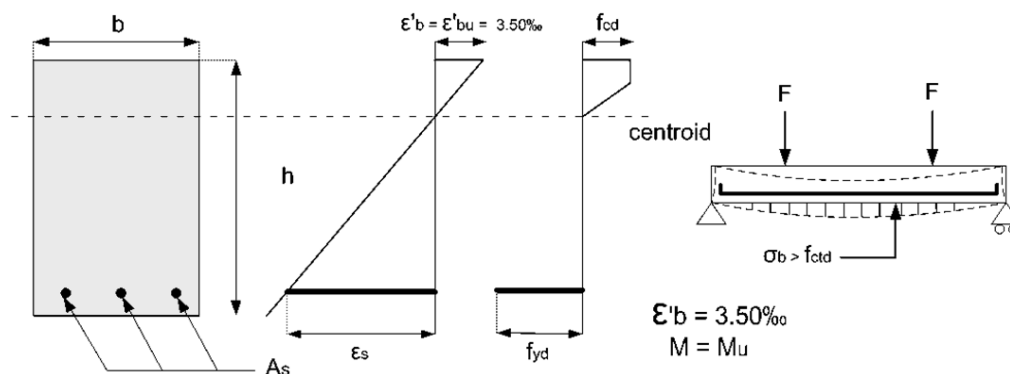


Figure 29-11 Deformation and stress diagram when the compression strain in the concrete has reached a value of 3,50‰.

29.6 Concrete cover (Eurocode 2 method)

The concrete cover on the outer reinforcement bar of a structure protects the reinforcement against external influences, such as rain water, soil, corrosive liquids or fumes or the like, which can lead to corrosion of the reinforcement. Reinforcement bars could oxidise if the concrete cover is too thin or insufficiently dense. This will lead to a reduction of the bar diameter and hence to a decrease of the force that the reinforcement can resist. Since rust has a larger volume than the original steel, there is a probability that the concrete cover is pushed off the reinforcement. This will lead to further corrosion and a further decrease of the strength. It is obvious that the reinforcement in an aggressive environment requires a thicker concrete cover than in a dry environment. The thickness of the concrete cover therefore depends on the environment in which the concrete structure is located. The environment characteristics are expressed via an exposure classification, see Table 29-9.

Besides the type of exposure, the required concrete cover depends on the design life time of the structure, concrete quality, the geometry of the structural member and the quality control of concrete manufacturing, which is indicated by the 'structural class'. The standard 'structural class' is S4, but may be adjusted as indicated in Table 29-10.

Exposure classification			
Class	Corrosion induced by	Class	measure of humidity
X0	no risk		very dry
XC	carbonation	XC1	dry or persistently wet
		XC2	wet, seldom dry
		XC3	moderate humidity
		XC4	alternating wet and dry
XD	chlorides (excl. seawater)	XD1	moderate humidity
		XD2	wet, seldom dry
		XD3	alternating wet and dry
XS	seawater	XS1	exposed to salt in the air, no direct contact with seawater
		XS2	persistently submerged
		XS3	tidal-, splash- and spray-zone
XF	freeze/thaw attack	XF1	not fully saturated with water, without de-icing salt
		XF2	not fully saturated with water, with de-icing salt
		XF3	fully saturated with water, without de-icing salt
		XF4	fully saturated with water, with de-icing salt
XA	chemical attack	XA1	weakly aggressive chemical environment
		XA2	moderately aggressive chemical environment
		XA3	highly aggressive chemical environment

Notation: XC1 X stands for exposure; the letter indicates process that causes the corrosion and the number indicates the humidity

Table 29-9 Exposure classification of the environment in which the structure is situated (Eurocode 2)

Criterion	Structural Class						
	Exposure Class according to Table 4.1 (Eurocode 2)						
	X0	X1	XC2/XC3	XC4	XD1	XD2 / XS1	XD3 / XS2 / XS3
Design life time 100 year	increase class by 2	increase class by 2	increase class by 2	increase class by 2	increase class by 2	increase class by 2	increase class by 2
Strength Class ^{1) 2)}	≥ C30/37 reduce class by 1	≥ C30/37 reduce class by 1	≥ C35/45 reduce class by 1	≥ C40/50 reduce class by 1	≥ C40/50 reduce class by 1	≥ C40/50 reduce class by 1	≥ C45/55 reduce class by 1
slab geometry (position of reinforcement not affected by construction process)	reduce class by 1	reduce class by 1	reduce class by 1	reduce class by 1	reduce class by 1	reduce class by 1	reduce class by 1
Ensured quality control of concrete manufacturing	reduce class by 1	reduce class by 1	reduce class by 1	reduce class by 1	reduce class by 1	reduce class by 1	reduce class by 1

Table 29-10 Modification of the standard structural class S4 (design life time of 50 years), depending on the design life time, strength, geometry and quality control of concrete manufacturing (Eurocode 2, Table 4.4N).

Note: values in national codes can deviate from this table.

According to Eurocode 2, the nominal concrete cover c_{nom} is determined by the minimum cover required for durability or for bond (*aanhechting*), and a construction tolerance:

$$c_{nom} = c_{min} + \Delta c_{dev} \quad (35.18)$$

The minimum cover c_{min} is the highest value of:

- $c_{min,dur}$, the minimum cover because of durability, see Table 29-11.
- $c_{min,b}$, the minimum cover because of bond:
 - $c_{min,b} > \varnothing_{bar}$, or:
 - $c_{min,b} > \varnothing_{bar} + 5 \text{ mm}$ if the largest grain size is 32 mm
- 10 mm

The margin for construction tolerances Δc_{dev} in the Netherlands usually is 5 mm.

Environmental Requirement for $c_{min,dur}$ (mm)							
Structural Class	Exposure Class according to Table 4.1 (Eurocode 2)						
	X0	XC1	XC2 / XC3	XC4	XD1 / XS1	XD2 / XS2	XD3 / XS3
S1	10	10	10	15	20	25	30
S2	10	10	15	20	25	30	35
S3	10	10	20	25	30	35	40
S4	10	15	25	30	35	40	45
S5	15	20	30	35	40	45	50
S6	20	25	35	40	45	50	55

Table 29-11 Minimum concrete cover on reinforcement steel, related to durability (Eurocode 2, Table 4.4N)

Note: values in national codes can deviate from this table.

For pre-stressed steel, higher values of the minimum required cover apply, see Table 4.5N in Eurocode 2.

For finished concrete surfaces (*nabewerkte betonoppervlakken*), the minimum cover c_{min} should be increased with 5 mm. For concrete floors on uneven surfaces (like work floors), $c_{nom} \geq c_{min,dur} + 10$ mm, but for concrete floors directly cast on the ground surface, $c_{nom} \geq c_{min,dur} + 50$ mm.

For hydraulic structures, a nominal concrete cover of 50 mm is not unusual.

29.7 Crack width

Theory

A characteristic of concrete elements that are exposed to tensile and bending stresses is the presence of cracks (*scheuren*). Cracks will develop if the tensile strength of concrete is exceeded.



Figure 29-12 Cracks in a reinforced concrete beam subjected to tensile forces

Cracks are necessary for the well-functioning of reinforced concrete, but they should not become too large, because that would affect the concrete cover. The concrete cover protects the reinforcement steel against aggressive substances, such as groundwater and salts, but if this protection is not sufficient, corrosion of the reinforcement steel will be the result. The volume of corroded steel is larger than of the original steel and can push off the concrete cover, after which the steel is directly exposed to the aggressive substances. Furthermore, corroded steel is less capable of resisting tensile forces, because of a decreased effective cross-sectional area. Therefore, a minimum concrete cover and maximum crack width are required.

For the calculation of the crack width of reinforced or pre-stressed concrete elements due to *short-term* loading, two stages can be distinguished:

1. The crack formation stage: The number of cracks increases while the strain increases. The width of the newly formed cracks increases, until a maximum is reached just before a new crack is formed. If the strain increases further, the tensile force N does not exceed the cracking force N_{cr} . The maximum crack width can be calculated with:

$$w_{max} = \frac{1}{4} \frac{f_{ctm} d}{\tau_{bm} \rho E_s} \sigma_{sr} \quad (35.19)$$

where:

w_{max}	[mm]	= maximum crack width
f_{ctm}	[N/mm ²]	= mean tensile strength of concrete, according to Table 29-1
d	[mm]	= diameter of the reinforcement bars
τ_{bm}	[N/mm ²]	= bond strength (<i>hechtsterkte</i>) $\approx 2,0 f_{ctm}$
ρ	[-]	= reinforcement ratio = $A_{steel} / A_{concrete}$
E_s	[N/mm ²]	= Youngs' modulus of steel
σ_{sr}	[N/mm ²]	= maximum tensile stress in the steel bar (in the crack)

2. The stabilised cracking stage, where a crack pattern has fully developed. New cracks will not develop when the strain increases, but the width of existing cracks will increase. The maximum crack width depends on the steel stress in the crack and can be calculated with:

$$w_{\max} = \frac{1}{2} \frac{f_{ctm} d}{\tau_{bm} \rho E_s} (\sigma_s - 0,5 \sigma_{sr}) \quad (35.20)$$

where:

σ_s [N/mm²] = tensile stress in the steel bar
other symbols: see above.

Causes of *long-term* crack development are:

1. Shrinkage of the concrete, which is usual during the hardening process of concrete. During the crack development stage, concrete shrinkage does not lead to larger crack widths, because of the development of additional cracks (the external force cannot exceed the cracking load). However, in the stabilised crack stage, no new cracks are formed and the width of existing cracks will increase. The crack width caused by load and shrinkage can be calculated with:

$$w_{\max} = \frac{1}{2} \frac{f_{ctm} d}{\tau_{bm} \rho E_s} (\sigma_s - 0,5 \sigma_{sr} + \varepsilon_{cs} E_s) \quad (35.21)$$

where:

σ_s [N/mm²] = steel stress in a crack under external tensile load
 ε_{sc} [-] = shrinkage of the concrete (no steel-concrete bond assumed)
other symbols: see above.

2. Long-term constant or varying loads, that reduce the bond stress. During the crack development stage, the reduced bond strength results in an increase of the transfer length of 25% and thereby 25% increase of the crack width. Equation (35.19) can be used to calculate this crack width, but now $\tau_{bm} = 1,6 f_{ctm}$.

For the stabilised crack stage, the bond stress decreases and therefore also the influence of the concrete in between the cracks. It can be assumed that this reduction is about 40%. This can be taken into account by replacing the coefficient 0,5 in Equation (35.21) by 0,3.

In the theory above, it was assumed that the tensile stresses are uniformly distributed over the entire concrete cross-section. In many cases, however, only a part of the concrete cross-section effectively transfers tensile forces to the reinforcement bars (Figure 29-13).

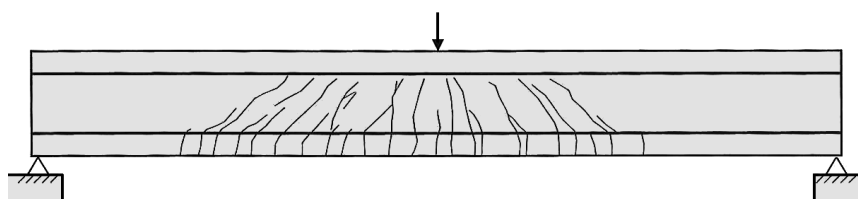


Figure 29-13 Wide cracks in a reinforced concrete beam under extreme loading

The effective tensile areas are indicated in Figure 29-14 for three types of cross-sections. The effective height is $2,5(h-d)$ for beams, $(h-x)/3$ for slabs and $h/2$ for elements subjected to tensile forces.

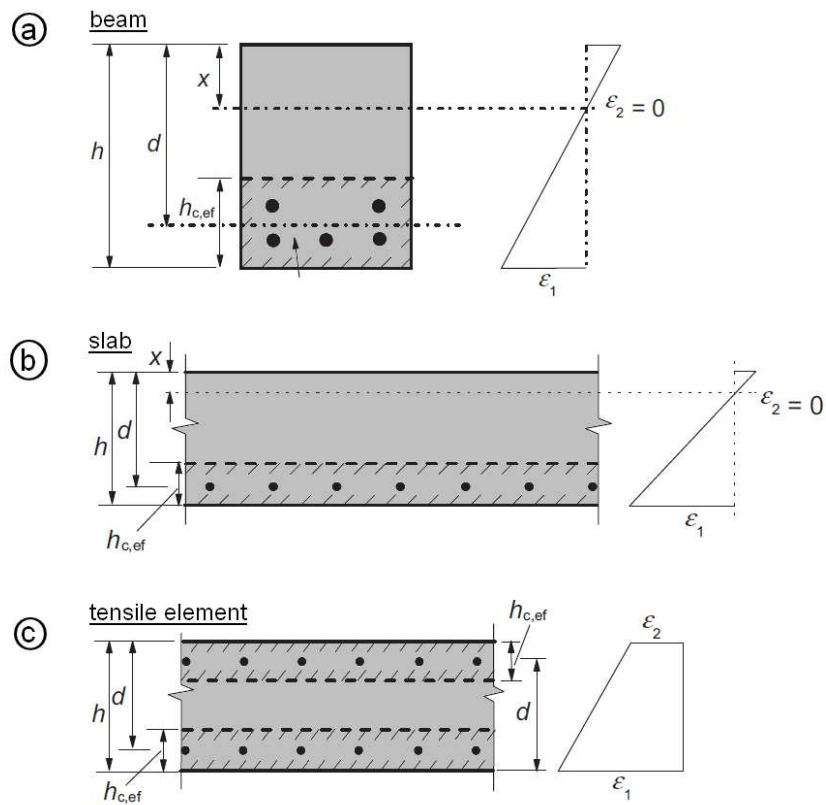


Figure 29-14 Effective tensile area

If one dimension of the cross-section of the concrete element is much larger than the other, the distribution of the tensile stresses in the concrete is not uniform, see Figure 29-15a. As a result, the crack does not proceed over the full width of the element. Such a cross-section can only crack, if the force introduced by the reinforcement is uniformly spread over the width of the element (Figure 29-15b). Only a few cracks reach the outer surface of the concrete element. If the reinforcement would be concentrated near the surface of an element, many cracks with small widths will occur at the surface, but wide cracks occur in the middle (Figure 29-15c).

A similar phenomenon occurs in elements in bending (Figure 29-15d). The main reinforcement limits the crack widths over an area close to the reinforcement and the relatively small cracks at the bottom join higher in the element and develop into wide cracks, if there is no additional reinforcement over the height of the element.

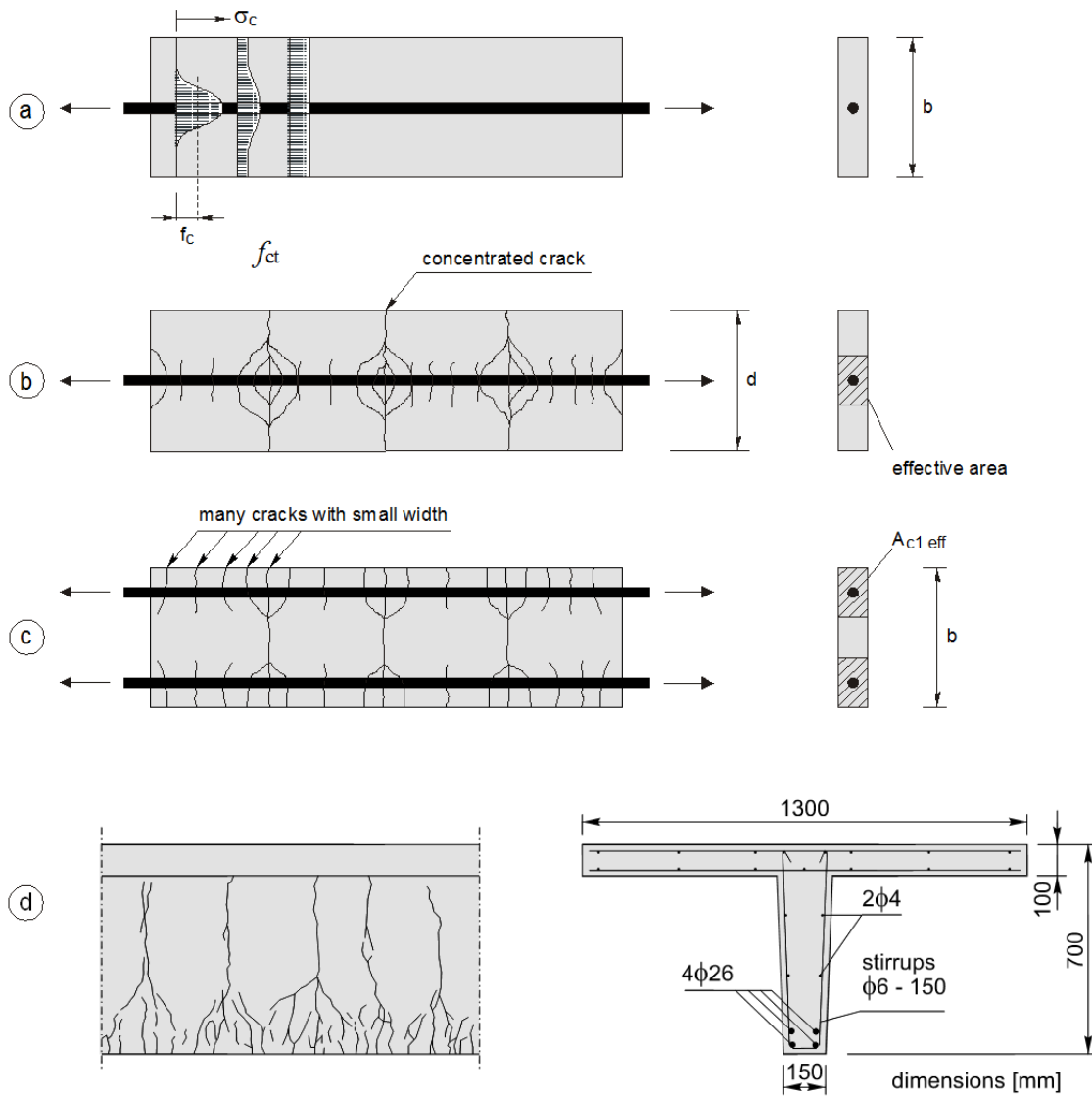


Figure 29-15 Crack behaviour of elements with a high width / transfer length ratio or a concentrated reinforcement

The strain in beams decreases from the bottom, where the highest tensile stresses occur, in upward direction. Therefore, also the crack width decreases in that direction and it is not needed to extend the reinforcement to the neutral axis (Figure 29-16).

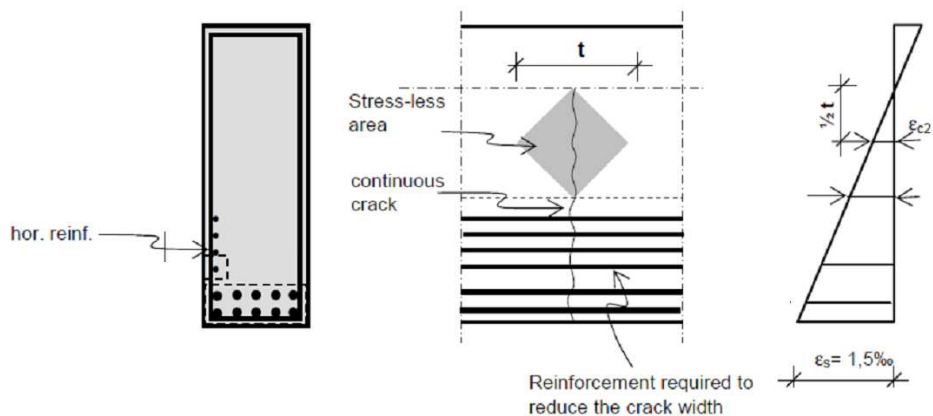


Figure 29-16 Stressless area in a concrete beam above the reinforced area

The crack width follows from the crack spacing that occurs even without reinforcing steel present. It can be assumed that the crack spacing is about equal to the height of the unreinforced area (t in Figure 29-16). The maximum crack width occurs about halfway this area:

$$w_{\max} = t \varepsilon_{c2} \quad (35.22)$$

where the fictitious concrete strain halfway down the unreinforced area is: $\varepsilon_{c2} = \frac{\varepsilon_s}{2} \frac{t}{(d-x)}$

The expression for w_{\max} then becomes: $w_{\max} = \frac{1}{2} t^2 \frac{\varepsilon_s}{(d-x)}$ (35.23)

Figure 29-17 shows graph that can be used to determine the area where reinforcement should be applied. Additional crack distributing reinforcement is only required for relatively high beams. For smaller beams it is sufficient to verify only the crack width in the main tensile tie.

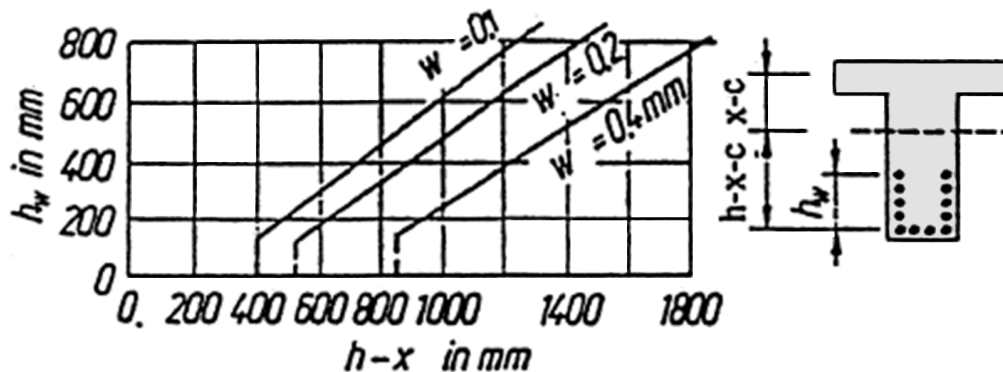


Figure 29-17 Part of the web where crack width limiting reinforcement should be provided to avoid the occurrence of large cracks (Jungwirth, 1985)

It appears that in high beams, crack width limiting reinforcement is required over a certain height. This does not automatically imply that in the remaining parts no reinforcement is needed. In general, a practical minimum reinforcement should always be applied. Summarising one may conclude that the following reinforcement is to be provided:

- Horizontal reinforcement $\varnothing 10 - 100$ mm as crack width limiting reinforcement
- Other parts: horizontal reinforcement $\varnothing 10 - 300$ mm.
- Vertical reinforcement, for instance also $\varnothing 10 - 300$ mm.

Crack width design (Eurocode 2)

For the design of new structures, it is not necessary to calculate the crack widths. The procedure is to design the reinforcement of the structural member in such a way, that the crack width will not exceed the maximum allowable value. So, for designs, the maximum crack width w_{\max} is given.

Crack widths are usually restricted to values between 0,1 and 0,4 mm to avoid unacceptable damage to the concrete cover. The maximum value depends on the type of steel (reinforced or pre-stressed), the durability of the structure and aesthetics. Table 29-12 specifies the maximum values for the maximum crack width, as recommended by the general Eurocode 2. Maximum crack widths can deviate from these recommended values per country!

Exposure Class	Reinforced members and prestressed members with unbonded tendons	Prestressed members with bonded tendons
	Quasi-permanent load combination	Frequent load combination
X0, XC1	0,4 ¹	0,2
XC2, XC3, XC4	0,3	0,2 ²
XD1, XD2, XS1, XS2, XS3		Decompression
<p>Note 1: For X0, XC1 exposure classes, crack width has no influence on durability and this limit is set to guarantee acceptable appearance. In the absence of appearance conditions this limit may be relaxed.</p> <p>Note 2: For these exposure classes, in addition, decompression should be checked under the quasi-permanent combination of loads.</p>		

Table 29-12 Recommended values for the maximum crack width (Eurocode 2, 2011)

Notice that the values vary per country, see the national annexes to Eurocode 2!

In general, the following steps can be followed:

1. calculate the maximum moment M_{max} (with a moment diagram (*momentenlijn*))
2. choose concrete class, steel quality, exposure class (*milieuklasse*)
3. calculate the required reinforcement area per cross-section, $A_{s,req}$
4. choose reinforcement bars / lay-out, and therewith, the provide reinforcement area $A_{s,prov}$
5. calculate the stress in the reinforcement bars σ_s according to:

$$\sigma_s = \frac{M_{freq}}{M_{Ed}} \cdot \frac{A_{s,req}}{A_{s,prov}} \cdot f_{yd}$$

where: M_{freq} [kNm] = bending moment in SLS
 M_{Ed} [kNm] = bending moment in ULS
 $A_{s,req}$ [mm²] = required reinforcement area
 $A_{s,prov}$ [mm²] = provided reinforcement area
 f_{yd} [N/mm²] = design value of the yield strength of the reinforcement steel

6. find the maximum allowed crack width in Table 29-12
7. find the maximum bar diameter in Table 29-13
8. find the maximum distance between the bars in Table 29-13

steel stress (N/mm ²)	max. bar diameter (mm)			max. distance between bars		
	$w_{max} = 0,4$ mm	$w_{max} = 0,3$ mm	$w_{max} = 0,2$ mm	$w_{max} = 0,4$ mm	$w_{max} = 0,3$ mm	$w_{max} = 0,2$ mm
160	40	32	25	300	300	200
200	32	25	16	300	250	150
240	20	16	12	250	200	100
280	16	12	8	200	150	50
320	12	10	6	150	100	-
360	10	8	5	100	50	-

Table 29-13 Maximum bar diameter and maximum distance between reinforcement bars

The value for f_{yd} in the equation for the steel stress σ_s is the design value of the yield strength of the reinforcement steel, which is the characteristic yield strength f_{yk} (Table 29-3), divided by a material factor (1,35 for example). The bending moment in ULS conditions can be about 1,5 (or maybe even 2) times more than during SLS conditions. The reinforcement diameters obtained with help of Table 29-12 and Table 29-13 can still be smaller than the diameters commonly used in hydraulic engineering (32 or 40 mm). These larger diameters are usually obtained by a more detailed crack width control calculation (rather than using the table), which is not required for this course.

Crack width calculation (Eurocode 2)

For the structural verification of existing structures, it should be checked whether the actual calculated crack widths exceed the maximum allowed values (Table 29-12).

A general equation for calculating the crack width, taking the effects described above into account, is:

$$w_{\max} = \frac{1}{2} \frac{f_{ctm} d}{\tau_{bm} \rho E_s} (\sigma_s - \alpha \sigma_{sr} + \beta \varepsilon_{cs} E_s) \quad (35.24)$$

where:

w_{\max}	[mm]	= maximum crack width
f_{ctm}	[N/mm ²]	= mean tensile strength of concrete
d	[mm]	= diameter of the reinforcement bars
τ_{bm}	[N/mm ²]	= bond strength (<i>hechtsterkte</i>), see Table 29-14
ρ	[-]	= reinforcement ratio = $A_{steel} / A_{concrete}$
E_s	[N/mm ²]	= Youngs' modulus of steel
σ_s	[N/mm ²]	= tensile stress in the steel bar
σ_{sr}	[N/mm ²]	= maximum tensile stress in the steel bar (in the crack):

$$\sigma_{sr} = \frac{f_{ctm}}{\rho} (1 + \alpha_e \rho), \text{ where } \alpha_e = E_s / E_c \quad (35.25)$$

ε_{sc}	[-]	= shrinkage of the concrete (no steel-concrete bond assumed)
α, β	[-]	= coefficients, see Table 29-14

	crack formation stage	stabilized cracking stage
short term loading	$\alpha = 0,5 (0,6)$ $\beta = 0$ $\tau_{bm} = 2,0 f_{ctm}$	$\alpha = 0,5 (0,6)$ $\beta = 0$ $\tau_{bm} = 2,0 f_{ctm}$
long term or dynamic loading	$\alpha = 0,5 (0,6)$ $\beta = 0$ $\tau_{bm} = 1,6 f_{ctm}$	$\alpha = 0,3 (0,4)$ $\beta = 1$ $\tau_{bm} = 2,0 f_{ctm}$

Table 29-14 values for the coefficients α , β and τ_{bm} . The values in brackets are recalibrated values, according to Eurocode 2

In the Eurocode2, Equation (35.24) appears in a different form:

$$w_{\max} = s_{r,\max} \frac{\sigma_s - k_t \frac{f_{ct,eff}}{\rho_{p,eff}} (1 + \alpha_e \rho_{p,eff} + \varepsilon_{cs} E_s)}{E_s} \quad (35.26)$$

where:

$s_{r,\max}$ [mm] = maximum crack spacing:

$$s_{r,\max} = k_3 c + k_1 k_2 k_4 \frac{\emptyset}{\rho_{p,eff}}$$

c [mm] = concrete cover to the longitudinal reinforcement

k_1 [-] = bond stress coefficient:
 $k_1 = 0,8$ for high bond (ribbed) bars
 $k_1 = 1,6$ for bars with an effectively plain surface

k_2 [-] = coefficient for the distribution of the strain over the height of the concrete area:
 $k_2 = 0,5$ for bending; $k_2 = 1,0$ for pure tension

k_3 [-] = coefficient; usually recommended: $k_3 = 3,4$

k_4 [-] = coefficient; usually recommended: $k_4 = 0,425$

k_t [-] = load duration coefficient: $k_t = 0,6$ (short-term loading) or $0,4$ (long-term loading)

$f_{ct,eff}$ [N/mm²] = mean value of the concrete tensile strength of the concrete at the time when the crack may first be expected to occur:
 $f_{ct,eff} = f_{ctm}$ or lower

($f_{ctm}(t)$, if cracking is expected earlier than at a concrete age of 28 days)

α_e [-] = ratio between Youngs' moduli of steel and concrete: E_s / E_c

ρ_{pf} [-] = effective reinforcement ratio of the tensile element:

$$\rho_{pf} = \frac{A_s}{A_{c,eff}}$$
 A_s [mm²] = total area of steel in a concrete element cross-section
 $A_{c,eff}$ [mm²] = effective tensile area of a concrete element:

$$A_{c,eff} = h_{eff} b$$
 b [mm] = width of the concrete element
 h_{eff} [mm] = effective height of the virtual tensile element:
 the smallest value of $2,5(h-d)$, $(h-x)/3$ and $h/2$, according to Figure 29-14.

ε_{sc} [-] = shrinkage of the concrete (no steel-concrete bond assumed)
 E_s [N/mm²] = Youngs' modulus of steel

The total shrinkage of the concrete ε_{sc} consists of two components: dehydration shrinkage and autogenous shrinkage. The dehydration shrinkage is a function of the migration of water through the hardened concrete (related to the humidity of the air) and therefore develops gradually. Autogenous shrinkage takes place during the hardening of the concrete, mainly during the first days after casting and is a linear function of the concrete quality. After a long duration, the effect of autogenous shrinkage is much smaller than the effect of dehydration shrinkage. For not too high concrete qualities and outdoor concrete elements (80% humidity), the total shrinkage ε_{sc} is in the order of magnitude of $0,20 \cdot 10^{-3}$, which could be used for preliminary designs. For more detailed designs, the equations and tables of Eurocode 2, article 3.1.4 can be used.

29.8 Strut & tie modelling

Theory

Reinforced concrete members are usually designed to resist shear and bending stresses, based on the assumption that strains vary linearly over a section. The mechanical behaviour of a beam is commonly determined by the assumption that plane sections remain plane (Bernoulli's hypothesis) and that a linear strain distribution can be assumed for all loading stages. The internal state of stress can be derived from the equilibrium of forces at a cross-section as described in Section 29.4, hence the name 'sectional methods'. For deep beams (*hogewandliggers*), however, these assumptions are not valid, because the shear strains are non-linearly distributed. The non-linearity is caused by abrupt changes in geometry or by concentrations of loading. Examples of deep beams are beams on two supports with a small height-to-length ratio, and a bottom plate of a shallow pier foundation. Figure 29-18 shows the difference between a 'normal' and a deep beam.

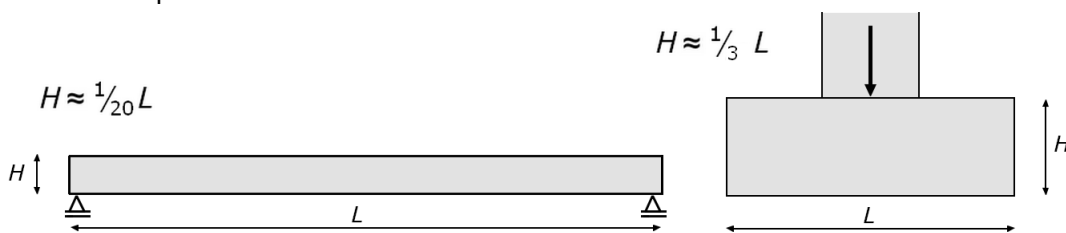


Figure 29-18 A typical 'normal' beam (left) and a typical deep beam (right)

The effects of the specific application of loading on a structure will dissipate or smooth out within regions that are sufficiently far away from the point of application of the load (Saint-Venant's principle). Usually, the distance where the way of load application influences the internal stress situation is one member depth d , see Figure 29-19.

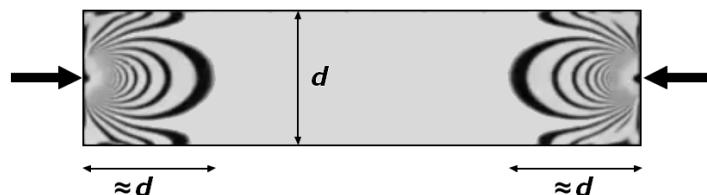


Figure 29-19 Saint-Venant's principle illustrated on a beam loaded with compression forces

In Figure 29-20, the shear span (which is the distance between the applied load and the support) is indicated with a and the depth (actually, the distance between from extreme compression fibre to the centre of the longitudinal tension reinforcement) with d .

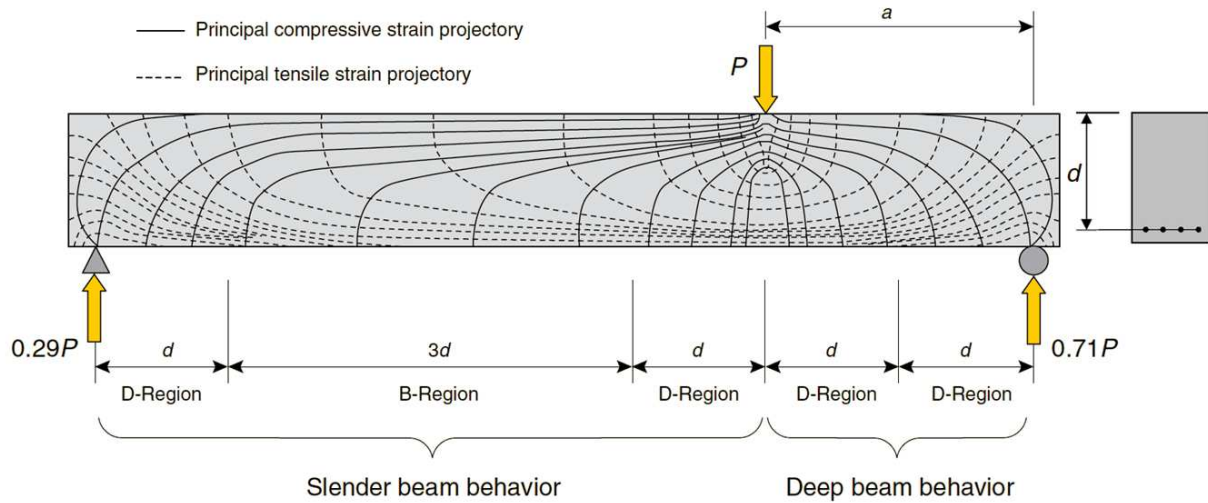


Figure 29-20 Strain distribution in the deep and slender portion of a beam (Tuchscherer et.al. 2011)

The figure shows the two types of regions that can be distinguished depending on the shear span to depth ratio a/d :

- 'B regions' are well understood and can be determined according to sectional methods (B stands for Beam or Bernoulli).
- 'D regions' indicate the regions of discontinuity (D stands for Discontinuity or Disturbed). Deep beams are a typical example of D regions, where the shear span is less than twice the depth. For D regions, the load transfer is assumed to follow an arch action mechanism and the strain distribution across the section is nonlinear.

Where sectional methods cannot be used, the strut & tie model (*staafwerkmodel*) is a useful method for hand calculations. Detailed design of complex structures, such as caissons, locks or bridge piers, often requires a finite element approach. The strut & tie model is a rational approach to represent the structures by a simplified truss model. However, there is no single or unique strut & tie model that can be generally applied, so there is a possibility of less efficient or even wrong strut & tie schematisations. Fortunately, there are techniques and rules that help the designer develop a model to correctly schematise the structure. If the principles for a lower-bound solution are satisfied, it can be assumed that the resulting design is safe.

The strut & tie model provides a conceptual framework, where the stress paths in a structure are schematised as a system of struts, ties and nodes, like a virtual truss. The ties are tension bars in the truss and consist of reinforcement bars. The struts are compression bars and are formed in parts of the concrete in the deep beam. The nodes, connecting the ties and the struts, are the locations where the reinforcement bars are anchored in the concrete (Figure 29-21).

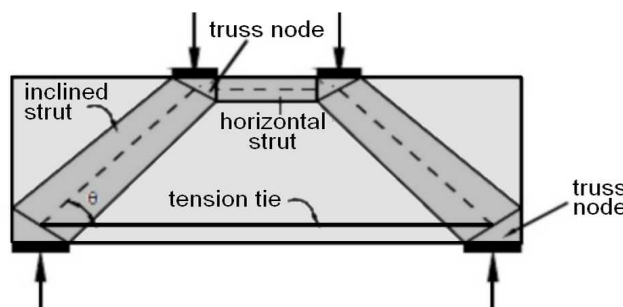


Figure 29-21 Typical strut & tie model for a deep beam

Struts

There are multiple types of struts, of which the three basic compositions are: the prism, the fan and the bottle composition (Figure 29-22). The prism is a strut with a constant width, the fan is a composition with a number of struts with varying inclination that converge to, or diverge from, a single node. The bottle is somewhat alike the fan type, but there is only one strut that converges or diverges.

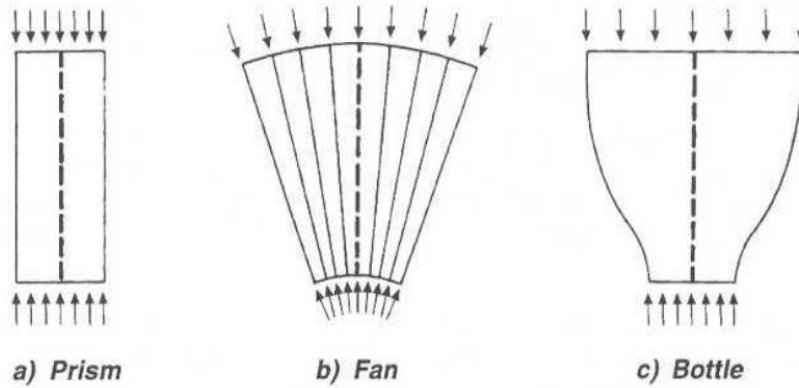


Figure 29-22 Types of struts

Ties

Tension ties include all kinds of reinforcement bars. A critical part in setting up the strut & tie modelling is providing sufficient anchorage for the reinforcement. If this is not provided, anchorage failure is likely to occur and the structure will fail at a load smaller than the design load.

Nodes

At the locations where ties and struts intersect, they are connected via nodes. The loads are redirected at the nodes into other components of the strut & tie model. There are four types of nodes in a 2D-plane: CCC, CCT, CTT and TTT, in which 'C' stands for compression and 'T' stands for tension. So, for instance, in a CCC node, three compression components converge (Figure 29-23).

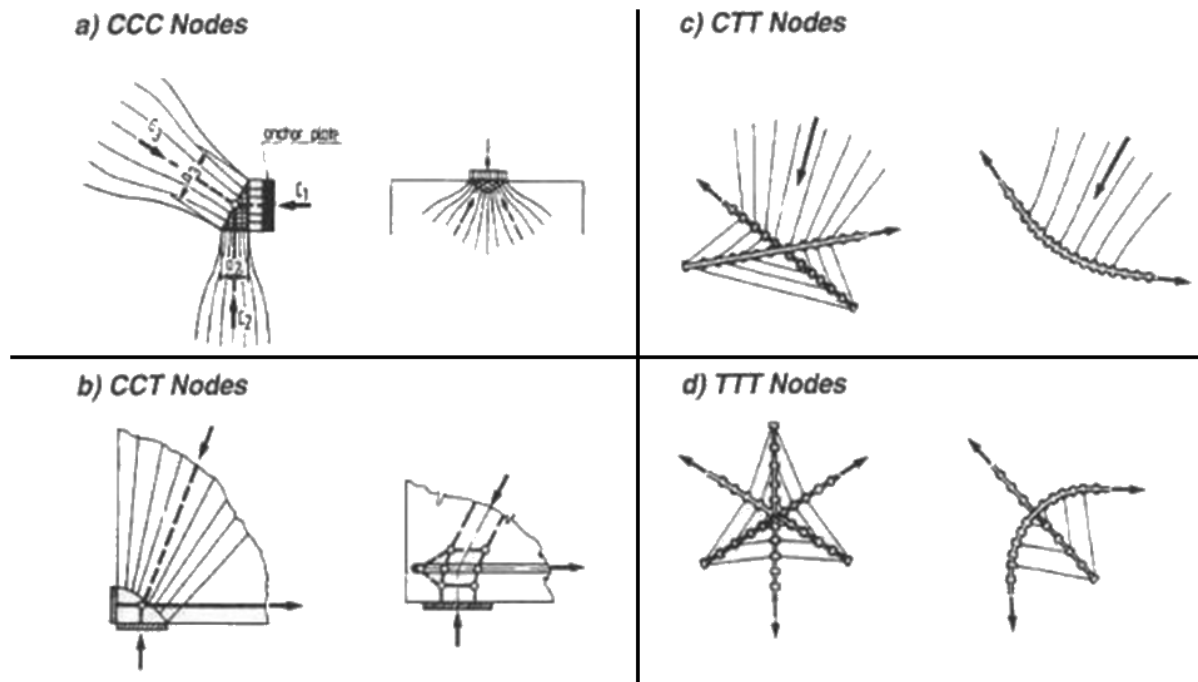


Figure 29-23 Node types (Schlaich et al, 1987)

Design

For the design of a deep structural component with strut & tie modelling, the next steps can be followed (modified from Williams et al, 2012):

Step 1. Define critical load cases and determine the magnitude of the acting loads

The loads acting on the structural component should be determined for each critical load case. The strut & tie model should be analysed for each critical load case, and, if needed, the geometry of the model should be modified. These modifications comprise:

- Replacing a moment acting on the structural component by a couple of forces, since moments cannot be applied to a truss model;
- Concentrated loads at a very short distance from each other can be resolved together as a simplification;
- A distributed load must be divided into a set of point loads that act at the nodes of the strut & tie

model.

This step is often carried out simultaneously with the development of the strut & tie model (step 5).

The loads acting on the boundaries of the D-regions are determined. These loads are relevant for defining the geometry of the component and for determining the forces to be carried by the struts and ties.

Step 2. Distinguish B- and D-regions

Step 2 in the design strut & tie process consists of dividing the structural element into B- and D-regions. In general, D-regions extend to a distance equal to the member depth d from the applied load or support. A region of a structural member is therefore assumed to be dominated by nonlinear behaviour, if the shear span, a , is between 1 and about 2 or 2,5 times the member depth d (see Figure 29-20). These regions are D-regions. The other regions can be assumed to be B-regions, which can be designed using the sectional design approach (Section 29.4). If only a small part of the structural component is a B-region, the entire component can be designed using strut & tie modelling. see Figure 29-24 for an example.

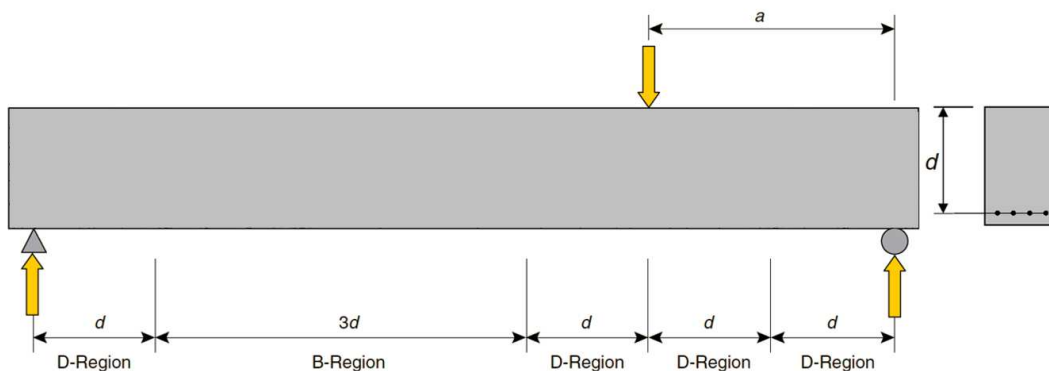


Figure 29-24 linear stress distribution at the interface of a B- and D-region (modified from Tuchscherer et.al, 2011)

Step 3 Determine the required concrete cover

Determine the required concrete cover on the reinforcement bars according to Section 29.6. The concrete cover is needed to calculate the effective depth in the following step.

Step 4. Determine an initial geometry of the strut & tie model

Several strut & tie models can be created for the structural component under the considered load case. The design of a strut & tie model can be considered conservative, if there is an equilibrium with external forces and sufficient deformation capacity to allow the distribution of forces along the paths enforced by the model. A better alignment of the strut & tie model with the flow of forces within the structural element will result in a lower likelihood of cracking. The struts will generally transfer compression forces with less deformation than the reinforcement in tension. The ties represent the steel reinforcement within the structure and should thus be placed where tensile stresses occur.

The model that features the fewest and shortest ties is typically the most efficient and realistic. Loads are mainly resisted by the strongest and stiffest parts of a structural component. The loads will therefore be distributed along the strongest and stiffest paths within that component, which, as a result, minimizes the deformations. In the correct model of Figure 29-25, the forces will naturally flow along the paths, because it has fewer ties and closely matches the flow of forces.

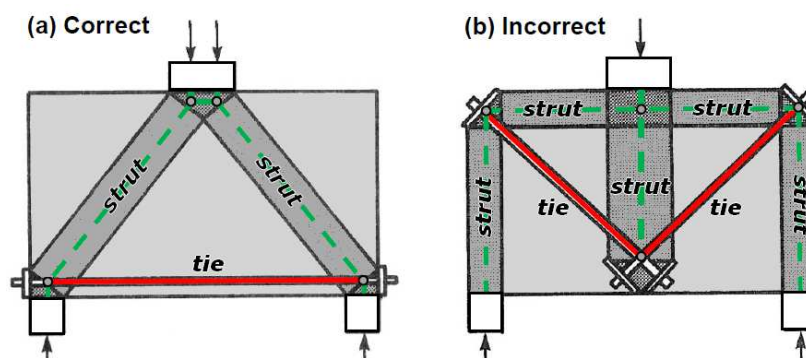


Figure 29-25 A correct and an incorrect strut & tie model (modified from Williams et al, 2012)

The angle between a strut and a tie entering the same node should not be less than about 25° , because otherwise tensile and compression stresses would occur within the same vicinity of the node, which is undesired and unrealistic. The model should therefore include the least number of truss panels while satisfying the 25° rule. The model at the right side of Figure 29-26 is therefore less efficient than the model at the left side.

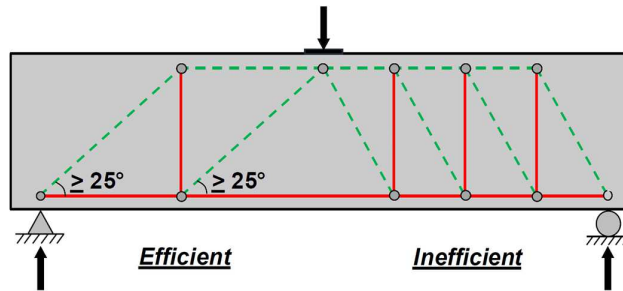


Figure 29-26 An efficient and an inefficient strut & tie model (modified from Williams et al, 2012)

A logical procedure to create a strut & tie geometry appears to be:

1. Assume nodes where the loads apply and where the structural element is supported. If the element is evenly supported by soil, you are flexible to create them where needed when connecting the nodes:
2. Connect the nodes with lines that represent the load paths through the element (= the virtual truss). The nodes should be connected such, that:
 - a. they transfer the forces to the supports in a natural way
 - b. the angle between the load paths is preferably 45° , but anyway between 25 and 65°
 - c. a vertical load should not be vertically transferred to a support
 - d. short and few ties are preferred over long and many ties

It can require some puzzling before an efficient virtual truss has been created. If needed, additional nodes can be created at locations where there are no external loads.

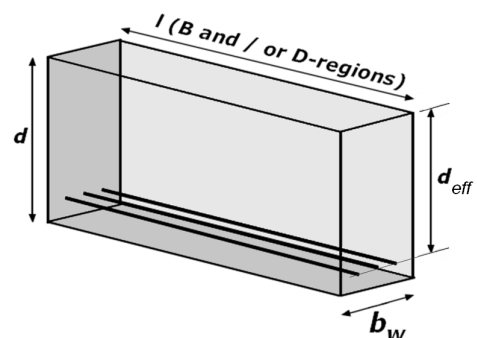
Step 5. Check the shear force capacity of the structural component

To initially determine the dimensions of the structural component, the geometry of the member can be chosen in a manner that reduces the risk of diagonal crack formation. This can be accomplished by predicting the likelihood that diagonal cracks will form within the D-regions of an in-service beam. For beams, the estimated load at which diagonal cracks begin to form, V_{cr} , appears to be related to the shear span - effective depth ratio a/d and the effective shear area $d \cdot b_w$. The properties a , b_w and d should be chosen in such a way, that the actual shear force, to be determined with a shear force diagram (*dwarskrachtenlijn*), should not exceed the critical shear stress V_{cr} :

$$V_{actual} < V_{cr} = \left[6,5 - 3 \frac{a}{d_{eff}} \right] \sqrt{f_{ck}} b_w d_{eff}$$

where:

V_{actual} [N]	=	actual shear force
V_{cr} [N]	=	critical shear force
a [mm]	=	shear span
d_{eff} [mm]	=	effective depth
f_{ck} [N/mm ²]	=	compressive strength of the concrete
b_w [mm]	=	width of the structural web



If the actual shear force is larger than V_{cr} , several measures may be taken:

- increase of the effective shear area, $d \cdot b_w$
- decrease of the ratio a/d
- increase of the compressive strength of the concrete
- apply additional distributed crack control reinforcement

The first three measures are usually the most effective.

Step 6. Determine the forces in the struts and the ties

It is preferable that the truss model is statically determinate, because it will only require equilibrium to calculate the forces in each member. Figure 29-27 shows the steps to determine the forces in the struts and ties.

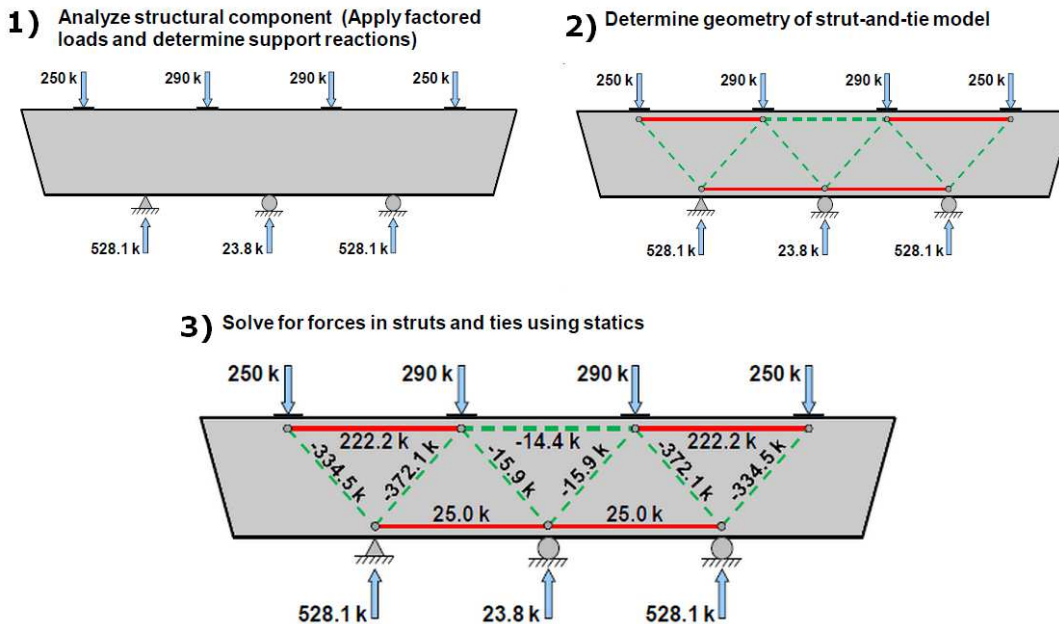


Figure 29-27 Procedure to determine the forces in a strut & tie model (modified from Williams et al, 2012)

Step 7. Proportion the ties

The strength of each tie in the model should be sufficient to resist the acting forces. Ignoring the use of partial safety factors, the required cross-sectional area of the reinforcement bars can be calculated according to:

$$\frac{F_{tie}}{A_{tie}} \geq f_y \Rightarrow A_{tie} \geq \frac{F_{tie}}{f_y}$$

This applies if the centroid of the bars coincides with the position of the tie in the model.

Step 8. Perform strut strength check near the nodes

The actual compression stresses follow the paths of the struts but spread further away from the nodes, resulting in bottle-shaped struts (Figure 29-28).

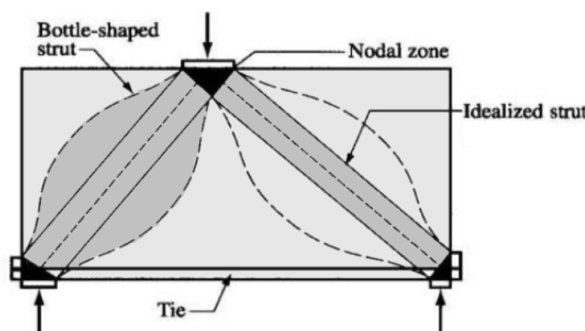


Figure 29-28 Actual shape of a strut (left) vs the idealised shape (right)

Nodes are therefore the highest stressed regions and each node should be checked to ensure that it can resist the imposed forces without crushing the concrete. The width of the path, or strut, is mainly determined by the dimensions of the bearing plate (the contact surface of the load application) and the angle of the strut. Furthermore, it matters whether the node is proportioned in a hydrostatic, or non-hydrostatic way (Figure 29-29). Hydrostatic nodes are proportioned in a manner that causes the stresses applied to each face to be equal. Non-hydrostatic nodes are proportioned based on the origin of the applied stress. This proportioning allows the geometry of the nodes to closely correspond to the actual

stress concentrations at the nodes. As the use of hydrostatic nodes sometimes result in unrealistic nodal geometries and impractical reinforcement layouts, non-hydrostatic nodes are preferred in design.

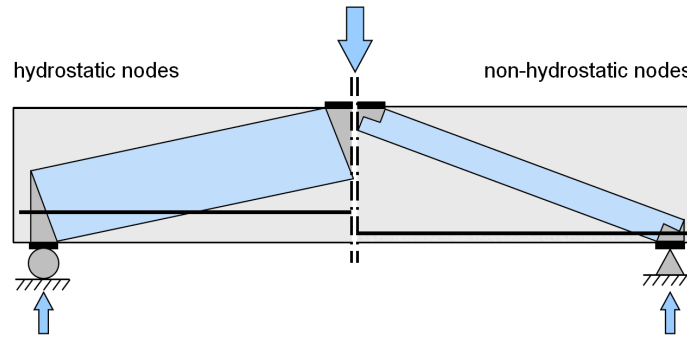


Figure 29-29 Two types of nodes: hydrostatic (left) and non-hydrostatic (right)

The actual compression stress in a strut should not exceed the compressive strength of the concrete. This implies:

$$\sigma_{strut,max} < f_{ck}$$

where f_{ck} [Pa] = compression cylinder strength of concrete (material property)
 $\sigma_{strut,max}$ [Pa] = highest value of the compression stress in the strut under consideration

The compression stress $\sigma_{strut,max}$ can be computed by dividing the strut force, as determined in step 6, by the cross-sectional area of the strut. The cross-sectional area can be calculated as:

$$A_{strut} = w_s \cdot h_s$$

where: w_s , [mm] = strut width (usually the width of the concrete element)
 h_s [mm] = strut height, which differs per node type (Figure 29-30):

For CCT nodes: $h_s = l_b \sin \theta + w_t \cos \theta$

For CCC nodes: $h_s = l_b \sin \theta + a \cos \theta$

l_b [m] = length of the bearing plate, or the part of the bearing plate that can be assigned to the strut under consideration

θ [°] = angle of the strut with the plane perpendicular to the main load direction

w_t [m] = length of the back face of a CCT node (usually twice the distance from the bottom of the beam to the centroid of the longitudinal reinforcement bars)

a [m] = length of the back face of a CCC node

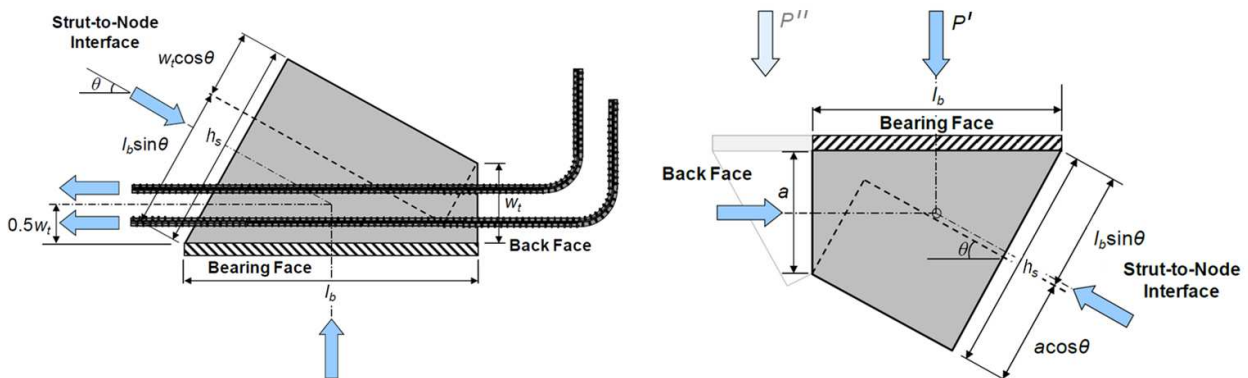


Figure 29-30 Geometry of a CCT node (left) and a CCC node (right) (modified from Williams et al, 2012)

CTT nodes do not have a clearly defined geometry, because the diagonal strut entering the node is able to disperse, or smear, over a large volume of concrete (Figure 29-31). Smeared nodes can therefore be considered as not critical and a check of concrete stresses in these nodes is not necessary, at least not for preliminary designs.

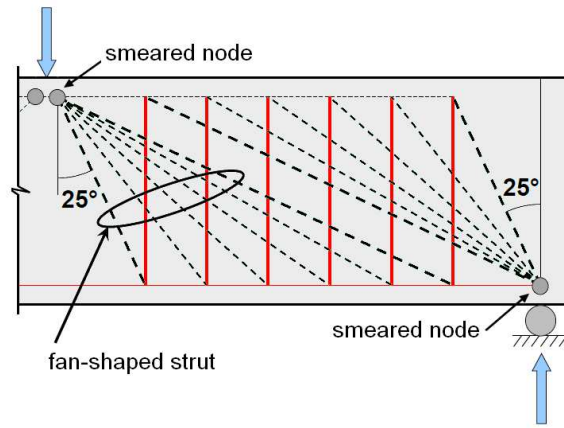


Figure 29-31 'Smearred' CTT nodes (modified from Williams et al, 2012)

Step 9. Proportion the crack control reinforcement

Crack reinforcement should be provided to restrain cracks in the concrete caused by the transverse tension that crosses diagonal bottle-shaped struts (see Figure 29-32), except for slabs and footings.

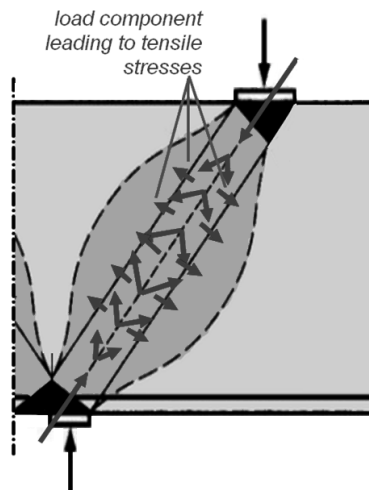


Figure 29-32 Tensile stresses in a bottle-shaped truss, causing cracks

0,3% reinforcement must be provided in each orthogonal direction to restrict crack widths. This percentage is based upon tests performed by Bircher et al (2009). In equation form, the requirement is:

$$\frac{A_v}{b_w s_v} > 0,003 \quad \text{and} \quad \frac{A_h}{b_w s_h} > 0,003$$

where:

- A_v [m²] = total area of horizontal crack control reinforcement within spacing s_v
- A_h [m²] = total area of vertical crack control reinforcement within spacing s_h
- b_w [m] = width of the web of the structural member
- s_v [m] = spacing of vertical crack control reinforcement
- s_h [m] = spacing of horizontal crack control reinforcement

See Figure 29-33 for an explanation of the variables.

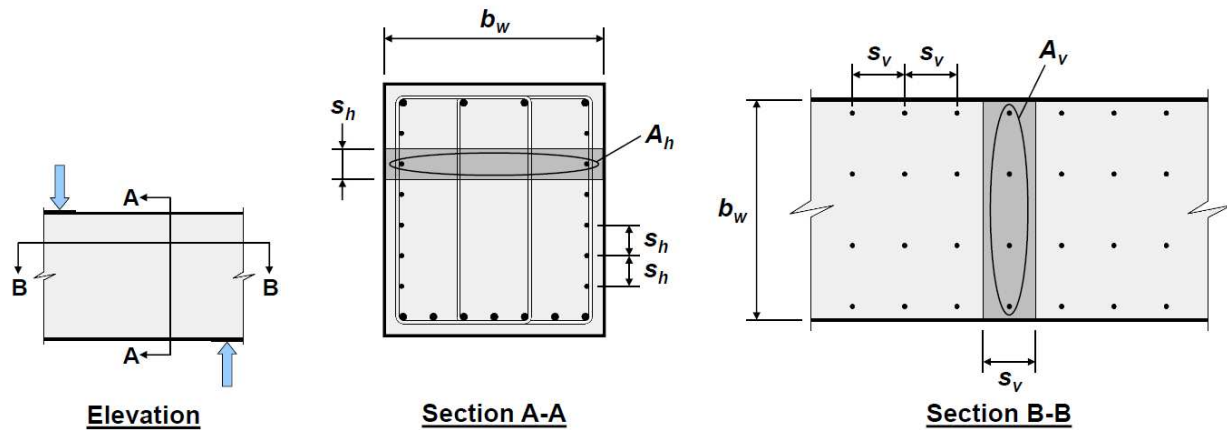


Figure 29-33 Illustration of the variables in the crack control reinforcement requirements (modified from Williams et al, 2012)

Step 10. Provide the necessary anchorage for the ties

The ties must be properly anchored to ensure that the structure can achieve the stress distribution assumed by the strut & tie model. The yield strength of the reinforcement should therefore be developed at the point where the centroid of the bars exits the extended nodal zone, as indicated in Figure 29-34. This implies that the critical section for the development of the tie is taken at the location where the centroid of the bars intersects the edge of the diagonal strut. The available length should be larger than the required development length.

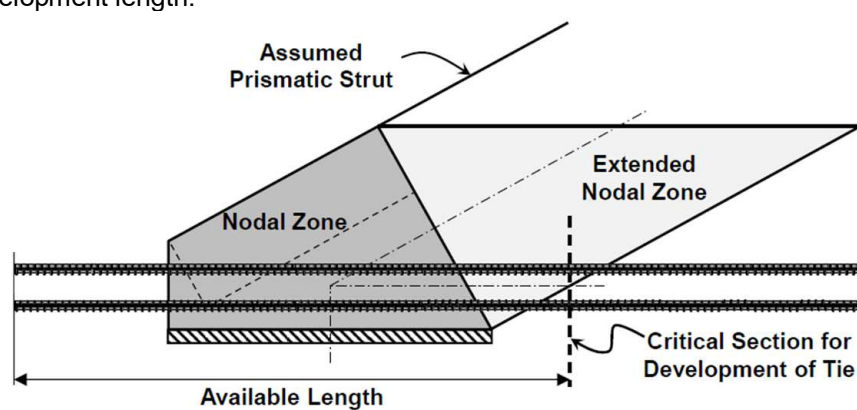


Figure 29-34 Available development length of ties (Williams et al, 2012)

29.9 Literature

Braam, C.R. and Legendijk, P. (2011). Constructieer. Gewapend beton deel 2. Aeneas / Cement & Betoncentrum, Boxtel / 's-Hertogenbosch.

Jungwirth, D. (1985). Begrenzung der Ribreite im Stahlbeton- und Spannbetonbau aus der Sicht der Praxis. Beton- und Stahlbau 7/1985, pp 137-178 & 8/1985, pp. 204-208.

Eurocode 2: "Design of concrete structures", various parts and national annex, Nederlands Normalisatie instituut.

NEN 6008: "Steel for the reinforcement of concrete", July 2008, Nederlands Normalisatie instituut.

NEN_EN 10080: "Steel for the reinforcement of concrete – Weldable Reinforcing steel - General", June 2005, Nederlands Normalisatie instituut

NEN-EN 10138 Draft: "Prestressing steels, various parts, Nederlands Normalisatie instituut.

Sagel, R. and A.J. van Dongen, Constructieer: Gewapend beton, December 2004, ENCI media, 's-Hertogenbosch.

Williams, C., Deschenes, D. and Bayrak, O. (2012). Strut-and-tie design examples for bridges: final report. Center for Transportation Research at the University of Texas at Austin.

30. Steel

major revision: February 2011

Steel is a frequently used material for particularly moveable parts of hydraulic structures and for temporary structures. A well-known example of a temporary structure is the building pit, where the sheet pile wall, the struts and the wales consist of steel elements. Steel structural elements for building pits are dealt with in Chapters 37 and 38 in part III of this Manual. The present chapter deals with the characteristics of steel and the most important calculation checks for beams, according to European standard EN 1993-1-1. More detailed information can be found in the books "(over)spannend staal", and the lecture notes of CTB2220 ("Beton- en staalconstructies"). Reinforcement steel to be used in concrete structures is dealt with in Section 29.2 of this Manual. For an example calculation of struts and wales in a cofferdam, see part III, Chapter 38.

30.1 General

Characteristics of steel

The most common types of construction steel are S235 and S355. For the most important properties, see Table 30-1.

material property ↓ / steel quality →	S235	S275	S355
yield stress f_y at 20 °C [N/mm ²]	235	275	355
tensile strength f_u [N/mm ²]	360	430	510
Young's modulus	$E = 210\,000$ N/mm ²		
Shear modulus (<i>glijdingsmodulus</i>)	$G = \frac{E}{2(1+\nu)} \approx 81\,000$ N/mm ²		
Poisson's ratio in elastic stage	$\nu = 0,3$		
Coefficient of linear thermal expansion	$\alpha = 12 \cdot 10^{-6}$ per °C (for $T \leq 100$ °C)		

Table 30-1 Steel characteristics for S235, S275 and S355

In this chapter, the partial material factors γ_M should be applied to the various characteristic values of resistance as follows:

- Resistance of cross-sections for all classes: $\gamma_{M0} = 1,0$
- Resistance of members to instability assessed by member checks: $\gamma_{M1} = 1,0$
- Resistance of cross-sections in tension to fracture: $\gamma_{M2} = 1,25$
- Resistance of various joints, see EN 1993-1-8

Ultimate limit state (ULS)

The following aspects should be checked in the ultimate limit state (ULS):

- Exceedance of the yield stress caused by tension, compression, bending, shear and torsion
- Global buckling (of bars, beams or columns) (*knik*)
- Lateral buckling (of beams, columns) (*kip*)
- Local (plate) buckling (*plooi*)
- Fatigue

Serviceability limit state (SLS)

For the serviceability limit state the following should explicitly be checked:

- Deformation / deflection (also plays a significant role for second order effects in ULS)

First or second order analysis?

The internal forces and moments may generally be determined using either:

- First-order analysis, using the initial geometry of the structure or
- Second-order analysis, which also takes into account the influences of the deformation of the structure.

First order analysis may be used for the structure if the increase of the relevant internal forces or moments or any other change of the structural behaviour caused by deformations can be neglected. This condition may be assumed to be fulfilled, if the following criterion is satisfied:

$$\alpha_{cr} = \frac{F_{cr}}{F_{Ed}} \geq 10 \quad \text{for elastic analysis}$$

$$\alpha_{cr} = \frac{F_{cr}}{F_{Ed}} \geq 15 \quad \text{for plastic analysis}$$

Where:

α_{cr} [-] = amplification factor to further increase the design load that will result in elastic instability in a global mode

F_{Ed} [kN] = design force acting on the structure

F_{cr} [kN] = elastic buckling force for global instability mode based on initial elastic

$$\text{stiffnesses: } F_{cr} = \frac{\pi^2 EI}{\ell^2}$$

For single storey frames on the basis of elastic global analysis, second order sway effects due to vertical loads may be calculated by increasing the horizontal loads H_{Ed} (e.g. wind) and equivalent loads V_{Ed} due to imperfections and other possible sway effects according to first order theory by a factor:

$$\frac{1}{1 - \frac{1}{\alpha_{cr}}}$$

Classification of cross-sections

Calculation methods for structural elements need to be appropriate with respect to the deformation characteristics of the profile (mostly dependent on the width/thickness-ratio). The plastic theory, for instance, should only be used if the profile is able to sufficiently deform in a plastic way. For the sake of convenience, standards (like the old NEN 6770 - *TGB staal*, and Eurocode 3) make use of classifications to indicate what calculation methods have to be used. This classification is useful to determine the extent to which the resistance and rotation capacity of cross-sections is limited by its local buckling resistance.

Four classes of cross-sections are defined, as follows (see also Table 30-2):

- Class 1: plastic cross-sections which can form a plastic hinge with the rotation capacity of plastic analysis without reduction of the resistance. Plastic theory may be used for the calculation of cross-sections and determination of the load distribution.
- Class 2: compact cross-sections (*gedrongen doorsneden*) which can develop their plastic moment resistance, but have limited rotation capacity because of local buckling. Plastic theory may only be used for the calculation of cross-sections.
- Class 3: semi-compact cross-sections in which the stress in the extreme compression fibre of the steel member assuming an elastic distribution of stresses can reach the yield strength, but local buckling is liable to prevent development of the plastic moment resistance. Elastic theory should be used for both cross-section calculations and load distribution determination. No buckling calculation is required.
- Class 4: slender cross-sections where local buckling will occur before yield stress occurs in one or more parts of the cross-section. Elastic theory should be used for both cross-section calculations and load distribution determination. Buckling calculation is required.

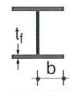
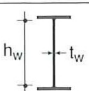
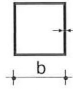
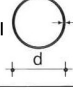
type of plate	type of load	class 1 (plastic)	class 2 (semi-plastic)	class 3 (elastic)
flange rolled I-profile 	pressure	$b/t_f \leq 10$ all HE-profiles	$b/t_f \leq 11$	$b/t_f \leq 15$
web rolled I-profile 	bending pressure	$h_w/t_w \leq 72$ $h_w/t_w \leq 33$	$h_w/t_w \leq 83$ $h_w/t_w \leq 38$	$h_w/t_w \leq 124$ $h_w/t_w \leq 42$
walls rolled square tube 	pressure	$b/t \leq 33$	$b/t \leq 38$	$b/t \leq 42$
wall cylindrical tube 	pressure or bending	$d/t \leq 50$	$d/t \leq 70$	$d/t \leq 90$

Table 30-2 Cross-section classes for steel profiles (S235) (from: (over)spannend staal Construeren A).

30.2 Strength

Possible internal forces in a cross-section are:

- tension
- compression
- bending moment
- shear
- torsion
- combination of bending moment and shear
- combination of bending moment and axial force

Tension

The design value of the tension force N_{Ed} at each cross-section shall be smaller than the design tension

resistance (*maximaal toelaatbare trekkracht*) $N_{t,Rd}$: $\frac{N_{Ed}}{N_{t,Rd}} \leq 1,0$

For sections with holes the design tension resistance $N_{t,Rd}$ shall be the smallest value of:

a) the design plastic resistance of the gross cross-section $N_{pl,Rd} = \frac{A \cdot f_y}{\gamma_{M0}}$

b) the design ultimate resistance of the net cross-section at holes for fasteners $N_{u,Rd} = \frac{0,9 \cdot A_{net} \cdot f_u}{\gamma_{M2}}$

Compression

The design value of the compression force N_{Ed} at each cross-section shall satisfy: $\frac{N_{Ed}}{N_{c,Rd}} \leq 1,0$

The design compression resistance (*maximaal toelaatbare drukkracht*) of the cross-section for uniform compression $N_{c,Rd}$ shall be determined as follows:

$$N_{c,Rd} = \frac{A \cdot f_y}{\gamma_{M0}} \quad \text{for class 1, 2 or 3 cross-sections}$$

$$N_{c,Rd} = \frac{A_{eff} \cdot f_y}{\gamma_{M0}} \quad \text{for class 4 cross-sections}$$

Bending moment

The design value of the bending moment M_{Ed} at each cross-section should satisfy: $\frac{M_{Ed}}{M_{c,Rd}} \leq 1,0$

The design resistance for bending around one principal axis of a cross-section is determined as follows:

$$M_{c,Rd} = M_{pl,Rd} = \frac{W_{pl} \cdot f_y}{\gamma_{M0}} \quad \text{for class 1 or 2 cross sections}$$

$$M_{c,Rd} = M_{el,Rd} = \frac{W_{el,min} \cdot f_y}{\gamma_{M0}} \quad \text{for class 3 cross sections}$$

$$M_{c,Rd} = \frac{W_{eff,min} \cdot f_y}{\gamma_{M0}} \quad \text{for class 4 cross sections}$$

Where $W_{el,min}$ and $W_{eff,min}$ correspond to the fibre with the maximum elastic stress.

Shear

The design value of the shear force V_{Ed} at each cross-section should satisfy $\frac{V_{Ed}}{V_{c,Rd}} \leq 1,0$

Where $V_{c,Rd}$ is the design shear resistance (*maximaal opneembare dwarskracht*).

For plastic design $V_{c,Rd}$ is the design plastic shear resistance $V_{pl,Rd}$. In absence of torsion the design plastic shear resistance is given by:

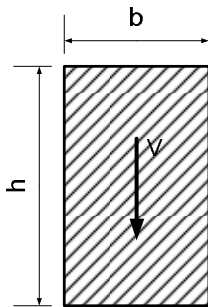
$$V_{pl,Rd} = \frac{A_v (f_y / \sqrt{3})}{\gamma_{M0}} \quad \text{Where } A_v \text{ is the shear area [mm}^2\text{].}$$

For verification of the design elastic shear resistance $V_{c,Rd}$ the following criterion for a critical point of the cross-section may be used unless the buckling verification in Section 5 of EN 1993-1-5 is applicable:

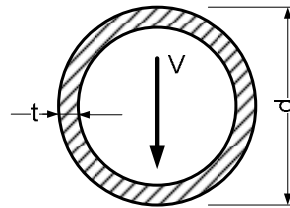
$$\frac{\tau_{Ed}}{f_y / (\sqrt{3} \gamma_{M0})} \leq 1,0 \quad \text{Where } \tau_{Ed} \text{ may be obtained from: } \tau_{Ed} = \frac{V_{Ed} \cdot S}{I \cdot t}$$

Where:

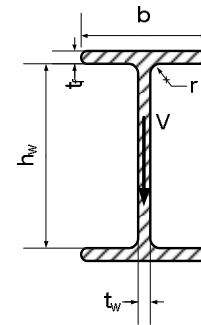
V_{Ed}	[N]	=	design value of the shear force
S	[mm ³]	=	first moment of area (<i>statisch moment</i>) with respect to the centroidal axis of the portion of the cross-section between the point where shear has to be considered and the boundary of the cross-section.
I	[mm ⁴]	=	second moment of area (<i>traagheidsmoment</i>) of the entire cross-section.
t	[mm]	=	thickness at the considered point



$$\tau_{Ed} = \frac{V_{Ed}}{b \cdot h}$$



$$\tau_{Ed} = \frac{V_{Ed}}{\frac{1}{2} \cdot \pi \cdot d \cdot t - \frac{1}{4} \cdot \pi \cdot t^2}$$



$$\tau_{Ed} = \frac{V_{Ed}}{t_w \cdot h_w}$$

Torsion

For members subject to torsion for which distortional deformations may be disregarded, the design value of the torsional moment T_{Ed} at each cross-section should satisfy: $\frac{T_{Ed}}{T_{Rd}} \leq 1,0$

Where T_{Rd} is the design torsional resistance (*torsiemomentweerstand*) of the cross-section.

The total torsional moment T_{Ed} at any cross-section should be considered as the sum of two internal effects: $T_{Ed} = T_{t,Ed} + T_{w,Ed}$

Where $T_{t,Ed}$ is the internal St. Venant torsion (*inwendige St. Venantse wringing*)

$T_{w,Ed}$ is the internal warping torsion (*inwendige wringing met verhinderde welving*)

The following stresses due to torsion should be taken into account:

- the shear stresses $\tau_{t,Ed}$ due to St. Venant torsion $T_{t,Ed}$
- the direct stresses $\sigma_{w,Ed}$ due to the bi-moment B_{Ed} and shear stresses $\tau_{w,Ed}$ due to warping torsion $T_{w,Ed}$.

The above method is prescribed in Eurocode 3 (NEN-EN 1993), which is meant for use in mechanical engineering. For this course, it will go too far for detailing this. For checks on torsion, the calculation method mentioned in TGB1990 (Technische Grondslagen voor Bouwconstructies 1990) may be used in the Netherlands (the way of calculation differs per country).

Combination of bending and shear

Where shear force is present, its effect on the moment resistance (*maximaal opneembare moment*) should be taken into account, except if the shear force is less than half the plastic shear resistance (in which case it may be neglected). Otherwise, the reduced moment resistance calculated using a reduced yield strength should be taken as the design resistance of the cross-section: $(1 - \rho) \cdot f_y$ for the shear area, where:

$$\rho = \left(\frac{2 \cdot V_{Ed}}{V_{pl,Rd}} - 1 \right)^2 \quad \text{and} \quad V_{pl,Rd} = \frac{A_v \cdot (f_y / \sqrt{3})}{\gamma_{M0}}$$

in which A_v = shear area (slide plane) and γ_{M0} = partial factor for cross-sections for the resistance to instability (in most cases $\gamma_{M0} = 1,0$).

If also torsion is present, ρ should be obtained from $\rho = \left(\frac{2 \cdot V_{Ed}}{V_{pl,T,Rd}} - 1 \right)^2$, but should be taken 0 if

$V_{Ed} \leq 0,5 \cdot V_{pl,T,Rd}$, where $V_{pl,T,Rd}$ depends on the profile shape (see NEN-EN 1993-1-1, article 6.2.7).

Combination of bending and axial force

For class 1 and 2 cross-sections, the following criterion should be satisfied: $M_{Ed} \leq M_{N,Rd}$

Where $M_{N,Rd}$ is the design plastic moment resistance reduced due to the axial force N_{Ed} .

For a rectangular solid section without fastener holes $M_{N,Rd}$ should be taken as:

$$M_{N,Rd} = M_{pl,Rd} \left[1 - \left(N_{Ed} / N_{pl,Rd} \right)^2 \right]$$

For double symmetrical I- and H-sections or other flanges sections, the effect of the axial force on the plastic moment resistance around the y-y axis does not have to be taken into account if both the following criteria are satisfied:

$$N_{Ed} \leq 0,25 \cdot N_{pl,Rd} \quad \text{and} \quad N_{Ed} \leq \frac{0,5 \cdot h_w \cdot t_w \cdot f_y}{\gamma_{M0}}$$

The effect of the axial force on the plastic moment resistance around the z-z axis may be neglected if:

$$N_{Ed} \leq \frac{h_w \cdot t_w \cdot f_y}{\gamma_{M0}}$$

For bi-axial bending the following criterion may be used:

$$\left[\frac{M_{y,Ed}}{M_{N,y,Rd}} \right]^\alpha + \left[\frac{M_{z,Ed}}{M_{N,z,Rd}} \right]^\beta \leq 1,0$$

in which α and β are constants, which may conservatively be assumed to be 1, otherwise as follows:

- I- and H-sections: $\alpha = 2$ and $\beta = 5 \cdot n$ but $\beta \geq 1$
- Circular hollow sections: $\alpha = 2$ and $\beta = 2$
- Rectangular hollow sections: $\alpha = \beta = \frac{1,66}{1 - 1,13 \cdot n^2}$ but α and $\beta \leq 6$

Where $n = N_{Ed} / N_{pl,Rd}$

In absence of shear force, **for Class 3 cross-sections** the maximum longitudinal stress $\sigma_{x,Ed}$ should satisfy the criterion: $\sigma_{x,Ed} \leq \frac{f_y}{\gamma_{M0}}$, where $\sigma_{x,Ed}$ is the design value of the local longitudinal stress due to moment and axial force taking account of relevant fastener holes (*boutgaten*).

In absence of shear force, **for Class 4 cross-sections** the maximum longitudinal stress $\sigma_{x,Ed}$ calculated using the effective cross-sections should satisfy the criterion: $\sigma_{x,Ed} \leq \frac{f_y}{\gamma_{M0}}$, where $\sigma_{x,Ed}$ is the design value of the local longitudinal stress due to moment and axial force taking account of fastener holes, which are relevant here. The following criterion should be met:

$$\frac{N_{Ed}}{A_{eff} \cdot f_y / \gamma_{M0}} + \frac{M_{y,Ed} + N_{Ed} \cdot e_{Ny}}{W_{eff,y,min} \cdot f_y / \gamma_{M0}} + \frac{M_{z,Ed} + N_{Ed} \cdot e_{Nz}}{W_{eff,z,min} \cdot f_y / \gamma_{M0}} \leq 1,0$$

where:

A_{eff}	[mm ²]	=	effective area of the cross-section when subjected to uniform compression
$W_{eff,min}$	[mm ³]	=	effective section modulus (corresponding to the fibre with the maximum elastic stress) of the cross-section when subjected only to moment about the relevant axis
e_N	[mm]	=	shift of the relevant centroidal axis when the cross-section is subjected to compression only

Combination of bending, shear and axial force

Provided that the design value of the shear force V_{Ed} does not exceed 50% of the design plastic shear resistance $V_{pl,Rd}$, no reduction of the resistance defined for bending and axial force need be made, except where shear buckling reduces the section resistance, see EN 1993-1-5.

Where V_{Ed} exceeds 50% of $V_{pl,Rd}$ the design resistance of the cross-section to combinations of moment and axial force should be calculated using a reduced yield strength:

$$(1 - \rho) \cdot f_y \text{ for the shear area where } \rho = \left(\frac{2 \cdot V_{Ed}}{V_{pl,Rd}} - 1 \right)^2.$$

30.3 Stability (buckling)

Buckling (*knik*) is a failure mechanism that occurs due to a normal force acting on a beam (or other structural element). Lateral buckling (*kip*) occurs if there is a shear force acting in the element. Both are displacements in the direction perpendicular to the load direction. Dependent on the forces, this failure mechanism must be checked.

Buckling resistance

A structural part under compression should be verified against buckling as follows: $\frac{N_{Ed}}{N_{b,Rd}} \leq 1,0$

Where:

N_{Ed}	[kN]	=	the design value of the compression force
$N_{b,Rd}$	[kN]	=	the design buckling resistance of the compression member

For structural members with non-symmetric class 4 sections the additional moment ΔM_{Ed} due to the eccentricity of the centroidal axis of the effective section should be taken into account.

The design buckling resistance of a compression member should be taken as:

$$N_{b,Rd} = \frac{\chi \cdot A \cdot f_y}{\gamma_{M1}} \quad \text{for class 1, 2 and 3 cross-sections}$$

$$N_{b,Rd} = \frac{\chi \cdot A_{eff} \cdot f_y}{\gamma_{M1}} \quad \text{for class 4 cross-sections}$$

Where χ is the reduction factor for the relevant buckling mode, to be taken from Figure 30-1.

Buckling curves

For axial compression in members the value of χ for the appropriate non-dimensional slenderness $\bar{\lambda}$ should be determined using the relevant buckling curve.

$$\bar{\lambda} = \sqrt{\frac{A \cdot f_y}{N_{cr}}} \quad \text{for class 1, 2 and 3 cross-sections}$$

$$\bar{\lambda} = \sqrt{\frac{A_{eff} \cdot f_y}{N_{cr}}} \quad \text{for class 4 cross-sections}$$

N_{cr} is the elastic critical force for the relevant buckling mode based on the gross cross-sectional properties. $N_{cr} = F_{cr} = \pi^2 EI / l^2$ for classes 1, 2, and 3.

The appropriate buckling curve should be obtained from Table 30-3. Values of the reduction factor χ for the appropriate non-dimensional slenderness $\bar{\lambda}$ may be obtained from Figure 30-1.

For slenderness $\bar{\lambda} \leq 0,2$ or for $\frac{N_{Ed}}{N_{cr}} \leq 0,04$ the buckling effects may be ignored and only cross-sectional checks apply.

Table 6.2: Selection of buckling curve for a cross-section

Cross section	Limits	Buckling about axis	Buckling curve		
			S 235 S 275 S 355 S 420	S 460	
Rolled sections 	$h/b > 1,2$	y-y z-z	$t_f \leq 40$ mm	a b	a ₀ a ₀
			$40 \text{ mm} < t_f \leq 100$	b c	a a
	$h/b \leq 1,2$	y-y z-z	$t_f \leq 100$ mm	b c	a a
			$t_f > 100$ mm	d d	c c
Welded I-sections 	$t_f \leq 40$ mm	y-y z-z	b c	b c	
	$t_f > 40$ mm	y-y z-z	c d	c d	
Hollow sections 	hot finished	any	a	a ₀	
	cold formed	any	c	c	
Welded box sections 	generally (except as below)	any	b	b	
	thick welds: $a > 0,5t_f$ $b/t_f < 30$ $h/t_w < 30$	any	c	c	
U-, T- and solid sections 		any	c	c	
L-sections 		any	b	b	

Table 30-3 Buckling curves for various cross-sections.

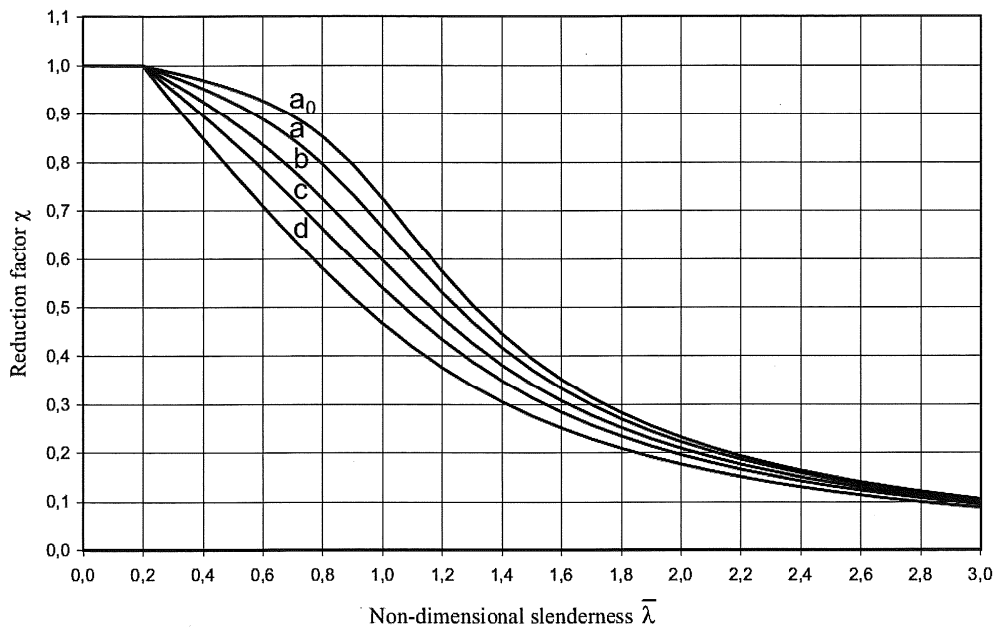


Figure 30-1 Relation between the reduction factor χ and the non-dimensional slenderness (from: NEN-EN 1993-1-1)
 Note: in the older standard NEN 6770, χ is indicated with ω_{buc} (buckling factor) and $\bar{\lambda}$ with λ_{rel} (relative slenderness).

Slenderness for flexural buckling (buigingsknik)

The non-dimensional slenderness $\bar{\lambda}$ is given by

$$\bar{\lambda} = \sqrt{\frac{A \cdot f_y}{N_{cr}}} = \frac{L_{cr}}{i} \frac{1}{\lambda_1} \quad \text{for class 1, 2 and 3 cross-sections}$$

$$\bar{\lambda} = \sqrt{\frac{A_{eff} \cdot f_y}{N_{cr}}} = \frac{L_{cr}}{i} \sqrt{\frac{A_{eff}}{A}} \quad \text{for class 4 cross-sections,}$$

Where: L_{cr} [m] = buckling length in the buckling plane considered (= l_{ef} in Figure 30-2)
 i [m] = radius of gyration around the relevant axis, determined using the moment of inertia
 and the area of the cross-section = $\sqrt{\frac{I}{A}}$

$$\lambda_1 [-] = \pi \cdot \sqrt{\frac{E}{f_y}} = 93,9 \cdot \varepsilon$$

$$\varepsilon [-] = \sqrt{\frac{235}{f_y}}$$

a		$l_{ef} = l_{sys}$
b		$l_{ef} = \frac{l_{sys}}{2}$
c		$l_{ef} = \frac{l_{sys}}{\sqrt{2}}$

Figure 30-2 Effective buckling length.

Uniform members in bending

Buckling resistance (kipweerstand)

A laterally unrestrained member subject to major axis bending should be verified against lateral torsional buckling as follows:

$$\frac{M_{Ed}}{M_{b,Rd}} \leq 1,0$$

Where M_{Ed} [Nm] = design value of the moment
 $M_{b,Rd}$ [Nm] = design buckling resistance moment

The design buckling resistance moment of a laterally unrestrained beam should be taken as:

$$M_{b,Rd} = \chi_{LT} \cdot W_y \cdot \frac{f_y}{\gamma_{M1}}$$

Where:

W_y [m³] = the appropriate section modulus as follows:
 $W_y = W_{pl,y}$ for class 1 or 2 cross-sections
 $W_y = W_{el,y}$ for class 3 cross-sections
 $W_y = W_{eff,y}$ for Class 4 cross-sections

χ_{LT} [-] = the reduction factor for lateral-torsional buckling

Lateral torsional buckling curves (*kipkrommen*)

For determining the value of the reduction factor χ_{LT} the curve of Figure 30-1 can be used, and

$$\bar{\lambda}_{LT} = \sqrt{\frac{W_y \cdot f_y}{M_{cr}}},$$

in which M_{cr} is the elastic critical moment where a beam not only bends about the strong axis (= normal buckling), but also under certain load about the weak axis, in combination with a rotation around the longitudinal axis. The elastic critical moment depends on gross cross-sectional properties and takes into account the loading conditions, the real moment distribution and the lateral restraints. The exact way of calculating of M_{cr} can be found in the National Annex to Eurocode 3 (NEN-EN 1993-1-1).

Recommended values for lateral buckling curves for cross-sections can be found in Table 30-4.

cross-section	Limits	Buckling curve
rolled I-sections	$h/b \leq 2$	a
	$h/b > 2$	b
welt I-sections	$h/b \leq 2$	c
	$h/b > 2$	d
other cross-sections	-	d

Table 30-4 buckling curves per cross-section

30.4 Welded connections

The most often used type of weld in steel structures and especially temporary steel structures, is the fillet weld (*hoeklas*). This is the only type of weld discussed here, based on the general weld calculations.

Three types of connections in the building pit example have to be designed:

1. Pipe strut – long waling (Figure 30-3)
2. Short waling – long waling (4 corners of the building pit) (Figure 30-4)
3. H-beam strut – waling (struts shoring the wales in the corners with an angle of 45°).

These connections can be chosen to be designed as rigid connections or hinges. Especially for a temporary structure such as a building pit, rigid connections are an appropriate choice for all 3 types of connections, but most of the time hinges are preferred. The welds will have to transfer normal forces, shear and bending moments, but the span moments will mostly be smaller. The connection can be strengthened with extra steel plates or stiffeners (*schotjes, kopplaat*).

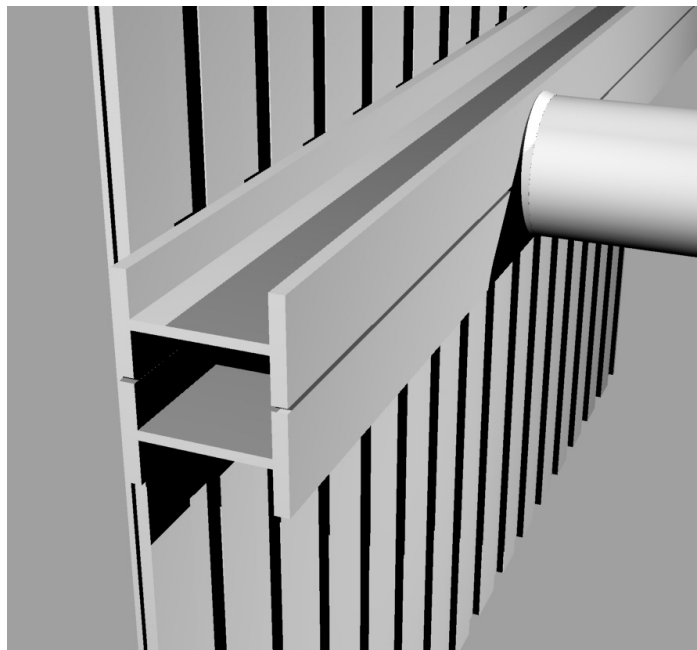


Figure 30-3 Welded connection of pipe strut and waling. The picture on the left (cofferdam near Sebastiaansbrug in Delft, 2007) shows a wale consisting of single H-profile, whereas the drawing on the right depicts the more common case of a double profile.

The theory that is stated in this section applies only to weldable structural steel with a material thickness larger or equal to 4 mm. For welds on thinner material the reader is referred to EN 1993-1-3. Also the mechanical properties, such as the yield strength (f_y); ultimate tensile strength (f_u); etc., of the weld material should be equivalent or better than the parent material, this ensures that the weld is at least as strong as the materials welded together.

Fillet welds may be used for connecting parts where the fusion faces form an angle between 60° and 120°. Fillet welds finishing at the ends or sides of parts that are connected should continue, full-size, around the corner for a distance of at least twice the leg length of the weld; unless access or the configuration of the joint renders this impracticable. Since a fillet weld is roughly rectangular in cross-section the leg length is defined as the length along the base material, or in other words the length of the sides of the triangle that make an angle of 90° (see Figure 30-4). Note that the length of the leg can also be unequal, which, however, is not common practice.

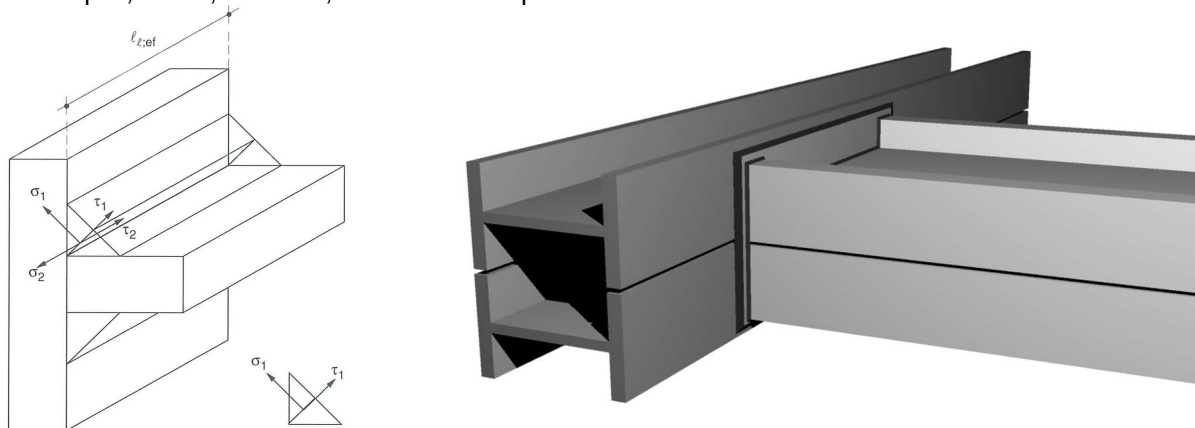


Figure 30-4 Connection between two walings, with front plate ($\sigma_1 = \sigma_{\perp}$ and $\sigma_2 = \sigma_{\parallel}$)

Normal forces in the structural members will either act parallel or rectangular to the weld. They cause a stress in the direction parallel or rectangular to the weld, σ_{\parallel} or σ_{\perp} respectively. The bending moments on a rigid welded connection also cause stresses in these directions.

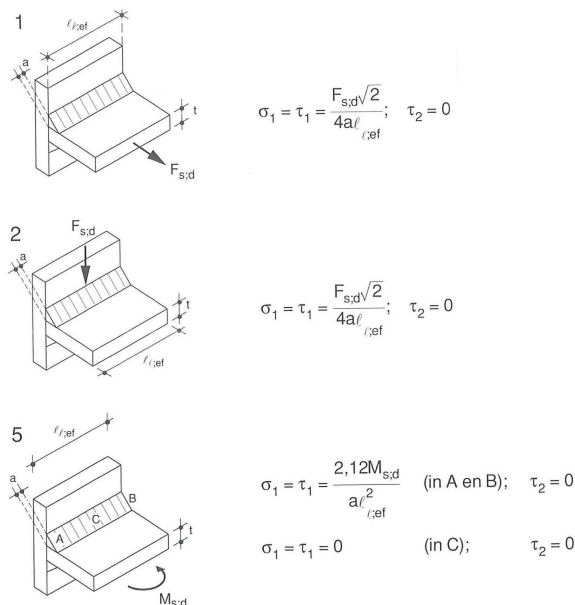


Figure 30-5: Standard cases 1, 2 and 5 of a normal force and shear force in a connected member. (Overspannend staal- Construeren A)

Figure 30-5 shows three basic standard cases of fillet welds connecting rectangular members with one weld per side; l_{ef} is the effective length of the member, a is the throat thickness.

1. Normal force in connected member

$$\sigma_{\perp} = \tau_{\perp} = \frac{F_d \cdot \sqrt{2}}{4 \cdot a \cdot l_{eff}} ; \tau_{\parallel} = 0$$

2. Shear force or load in connected member, perpendicular to the weld length

$$\sigma_{\perp} = \tau_{\perp} = \frac{\sqrt{2} \cdot F_d}{4 \cdot a \cdot l_{eff}} ; \tau_{\parallel} = 0$$

5. A bending moment on the connected member

A concentrated load on the member is modelled as a concentrated load plus a bending moment on the connection. The stresses resulting from the bending moment alone are:

In points A and B:
$$\sigma_{\perp} = \tau_{\perp} = \frac{3 \cdot M_{S;d}}{\sqrt{2} \cdot a \cdot l_{eff}^2} ; \tau_{\parallel} = 0$$

In point C:
$$\sigma_{\perp} = \tau_{\perp} = 0 ; \tau_{\parallel} = 0$$

According to European standard EN 1993-1-8 the design resistance of a fillet weld can be determined using either the directional method or the simplified method, which will be discussed in the remainder of this section. Important notions are the effective length (l_{eff}) and the effective throat thickness (a) of the weld.

The effective length of a fillet weld should be taken as the length over which the fillet is full-size. This may be taken as the overall length of the weld reduced by twice the effective throat thickness. Provided that the weld is full-size throughout its length including starts and terminations, no reduction in effective length need be made for either the start or the termination of the weld. Note: a fillet weld with an effective length less than 30 mm or less than 6 times its throat thickness, whichever is larger, should not be designed to carry load.

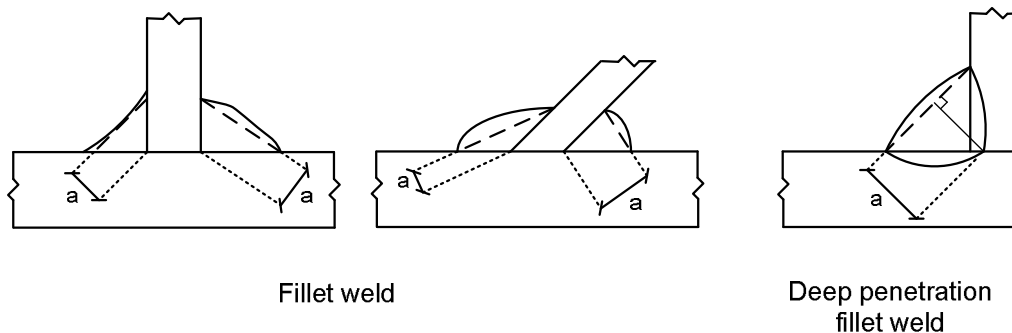


Figure 30-6 Throat thickness of a (deep penetration) fillet weld.

The effective throat thickness of a weld should be taken as the height of the largest triangle (with equal or unequal legs) that can be inscribed within the fusion faces and the weld surface, measured perpendicular to the outer side of this triangle, see Figure 30-6. The effective throat thickness of a fillet weld should not be less than 3 mm for practical reasons. In determining the design resistance of a deep penetration fillet weld, one may take its additional throat thickness into account, provided that preliminary tests show that the required penetration can be achieved consistently.

Directional method

In the directional method, the forces transmitted by a unit length of weld are resolved into components parallel and transverse to the longitudinal axis of the weld and normal and transverse to the plane of its throat (a). The design throat area (A_w) should be taken as $A_w = \sum a \cdot l_{eff}$ and should be assumed concentrated in the root of the weld.

An uniform distribution of stress is assumed on the throat section of the weld, leading to normal and shear stresses as shown in Figure 30-7.

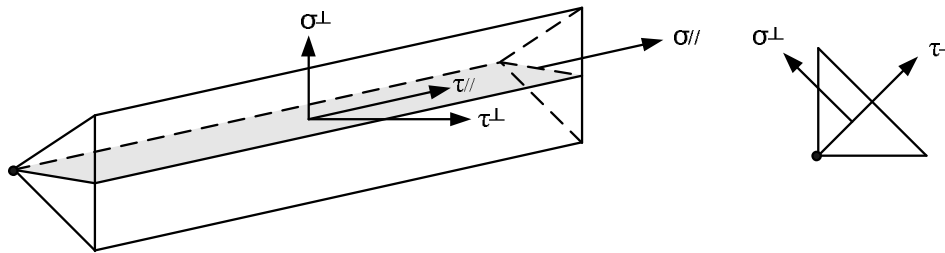


Figure 30-7 stresses on the throat section of a fillet weld.

where:

σ_{\perp}	[N/mm ²]	=	normal stress perpendicular to the throat
$\sigma_{//}$	[N/mm ²]	=	normal stress parallel to the axis of the weld
τ_{\perp}	[N/mm ²]	=	shear stress (in the plane of the throat) perpendicular to the axis of the weld
$\tau_{//}$	[N/mm ²]	=	shear stress (in the plane of the throat) parallel to the axis of the weld

The design resistance of the filled weld is sufficient if the following equations are both satisfied:

$$\sigma_d = \sqrt{\sigma_{\perp}^2 + 3(\tau_{\perp}^2 + \tau_{//}^2)} \leq \frac{f_u}{\beta_w \cdot \gamma_{M2}} \quad \text{and} \quad \sigma_{\perp} \leq \frac{0,9 \cdot f_u}{\gamma_{M2}}$$

where:

f_u	[N/mm ²]	=	nominal tension strength of the weaker part joined
β_w	[-]	=	appropriate correlation factor taken from Table 30-5
γ_{M2}	[-]	=	partial factor for the tensile strength ($\gamma_{M2} = 1,25$)

Using these criteria, the throat thickness of the weld can be determined. As stated before, the practical minimum amounts to 3 mm. Note that the stress parallel to the axis, $\sigma_{//}$, is not considered when verifying the design resistance of the weld.

When welds connect parts with two different material strengths, the weld should be designed using the properties of the material with the lower strength grade.

Steel grade	Tensile stress	Correlation factor
S235	360 N/mm ²	0,80
S275	275 N/mm ²	0,85
S355	360 N/mm ²	0,90
S420	360 N/mm ²	1,00
S460	360 N/mm ²	1,00

Table 30-5 correlation factor for fillet welds

Simplified method

Alternatively, the design resistance of a fillet weld may be assumed to be adequate if, at every point along its length, the resultant of all the forces per unit length transmitted by the weld satisfy the following criterion:

$$F_{w,Ed} \leq F_{w,Rd}$$

Where:

$F_{w,Ed}$	[N/mm]	=	design value of the weld force per unit length
$F_{w,Rd}$	[N/mm]	=	design weld resistance per unit length

Independent of the orientation of the weld throat plane to the applied force, the design resistance per unit length should be determined from:

$$F_{w,Rd} = f_{vw,d} \cdot a \quad \text{where} \quad f_{vw,d} = \frac{f_u}{\sqrt{3} \cdot \beta_w \cdot \gamma_{M2}}$$

Where:

$f_{vw,d}$	[N/mm ²]	=	design shear strength of the weld
------------	----------------------	---	-----------------------------------

NB. The deformations of temporary structures, such as, struts are not often checked. They could be estimated using the deformation diagrams (*vergeet-me-nietjes*) from structural mechanics and then checked against the requirements.

30.5 Bolt connections

Bolts are used to connect two or more structural components in a steel structure. They are a form of threaded fasteners which have a male thread and preformed matching female thread, such as nuts.

In a tension joint, the bolt and the clamped components of the joint transfer an applied tension load through the joint by way of the clamped components by a proper balance of joint and bolt stiffness. In a shear type of joint, the applied load is transferred in shear of the bolt shank (*steel*) and relies on the shear strength of the bolt. Tension loads on shear joints are only incidental.

The partial safety factor γ_M for the tensile strength of bolts (*bouten*) is $\gamma_{M2} = 1,25$. The partial safety factor for the preload of high strength bolts is $\gamma_{M7} = 1,1$. Detailed information about connections made by bolts can be found in EN 1993-1-8. The rules in this standard are valid for the bolt classes given in Table 30-6.

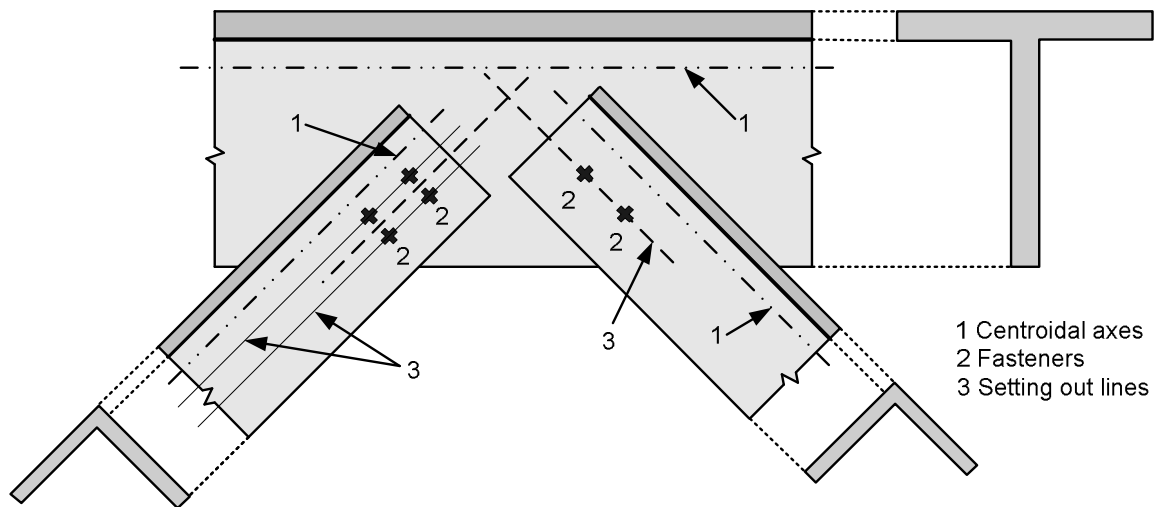


Figure 30-6 Two angular sections (*hoekprofiel*) are bolted to a T-profile

The yield strength f_{yb} and the ultimate tensile strength f_{ub} for bolt classes 4.6, 4.8, 5.6, 5.8, 6.8, 8.8 and 10.9 are given in Table 30-6. These values should be adopted as characteristic values in design calculations.

Bolt class	4.6	4.8	5.6	5.8	6.8	8.8	10.9
f_{yb} (N/mm ²)	240	320	300	400	480	640	900
f_{ub} (N/mm ²)	400	400	500	500	600	800	1000

Table 30-6 Bolt classes (Nominal values of the yield strength and the ultimate tensile strength for bolts.)



Figure 30-7 Cofferdam for the construction of the metro line in Thessaloniki, with bolt connections struts-wales (August 2009)

Categories of bolted connections**Shear connections**

Bolted connections loaded in shear should be designed as one of the following categories:

- Category A : Bearing type
In this category bolts from class 4.6 up to and including class 10.9 should be used. No preloading and special provisions for contact surfaces are required. The design ultimate shear load should not exceed the design shear resistance, nor the design bearing resistance.
- Category B : Slip-resistant at serviceability limit state
In this category preloaded bolts from classes 8.8 and 10.9 should be used. Slip should not occur at the serviceability limit state. The design serviceability shear load should not exceed the design slip resistance. The ultimate shear load should not exceed the design shear resistance, nor the design bearing resistance.
- Category C : Slip-resistant at ultimate limit state
In this category preloaded bolts from classes 8.8 and 10.9 should be used. Slip should not occur at the ultimate limit state. The design ultimate shear load should not exceed the design slip resistance, nor the design bearing resistance. In addition, for a connection in tension, the design plastic resistance of the net cross-section at bolt holes should be checked at the ultimate limit state.

Tension connections

Bolted connections loaded in tension should be designed as one of the following categories:

- Category D : Non-preloaded
In this category bolts from class 4.6 up to and including class 10.9 should be used. No preloading is required. This category should not be used where the connections are frequently subjected to variations of tensile loading. However, they may be used in connections designed to resist normal wind loads.
- Category E : Preloaded
In this category preloaded bolts from classes 8.8 and 10.9 with controlled tightening in conformity with 1.2.7 Reference Standards: Group 7 should be used.

Positioning of holes for bolts (and rivets)

Minimum and maximum spacing and end and edge distances for bolts (*bouten*) and rivets (*klinknagels*) are given in Table 30-7.

Distances and spacings, see figure 26-10	Minimum	Maximum ^{1) 2) 3)}		
		Structures made from steels conforming to EN 10025 except steels conforming to EN 10025-5		Structures made from steels conforming to EN 10025-5
		Steel exposed to the weather or other corrosive influences	Steel not exposed to the weather or other corrosive influences	Steel used unprotected
End distance e_1	$1,2 d_0$	$4t + 40$ mm		The larger of $8t$ or 125 mm
Edge distance e_2	$1,2 d_0$	$4t + 40$ mm		The larger of $8t$ or 125 mm
Distance e_3 in slotted holes	$1,5 d_0$ ⁴⁾			
Distance e_4 in slotted holes	$1,5 d_0$ ⁴⁾			
Spacing p_1	$2,2 d_0$	The smaller of $14t$ or 200 mm	The smaller of $14t$ or 200 mm	The smaller of $14t_{min}$ or 175 mm
Spacing $p_{1,0}$		The smaller of $14t$ or 200 mm		
Spacing $p_{1,i}$		The smaller of $28t$ or 400 mm		
Spacing p_2 ⁵⁾	$2,4 d_0$	The smaller of $14t$ or 200 mm	The smaller of $14t$ or 200 mm	The smaller of $14t_{min}$ or 175 mm

¹⁾ Maximum values for spacing, edge and end distances are unlimited, except for the following cases:
- for compression members in order to avoid local buckling and to prevent corrosion in exposed members and;
- for exposed tension members to prevent erosion.
²⁾ The local buckling resistance of the plate in compression between the fasteners should be calculated according to EN 1993-1-1 using $0,6 p_1$ as buckling length. Local buckling between the fasteners need not to be checked if p_1 / t is smaller than 9ϵ . The edge distance should not exceed the local buckling requirements for an outstand element in the compression members, see EN 1993-1-1. The end distance is not affected by this requirement.
³⁾ t is the thickness of the thinner outer connected part.
⁴⁾ The dimensional limits for slotted holes are given in 1.2.7 Reference Standards: Group 7.
⁵⁾ For staggered rows of fasteners a minimum line spacing of $p_2 = 1,2 d_0$ may be used, provided that the minimum distance, L , between any two fasteners is greater or equal than $2.4 d_0$, see figure 26-10 b).

Table 30-7 Minimum and maximum spacing, end and edge distances of bolts

where:

- e_1 [mm] = the end distance from the centre of a fastener hole to the adjacent end of any part, measured in the direction of load transfer
 e_2 [mm] = the edge distance from the centre of a fastener hole to the adjacent edge of any part, measured at right angles to the direction of load transfer
 e_3 [mm] = the distance from the axis of a slotted hole to the adjacent end or edge of any part
 e_4 [mm] = the distance from the centre of the end radius of a slotted hole to the adjacent end or edge of any part
 p_1 [mm] = the spacing between centres of fasteners in a line in the direction of load transfer
 $p_{1,0}$ [mm] = the spacing between centres of fasteners in an outer line in the direction of load transfer
 $p_{1,i}$ [mm] = the spacing between centres of fasteners in an inner line in the direction of load transfer
 p_2 [mm] = the spacing measured perpendicular to the load transfer direction between adjacent lines of fasteners
 d_0 [mm] = the hole diameter for a bolt, a rivet or a pin

The difference between edges and ends is shown in Figure 30-8.

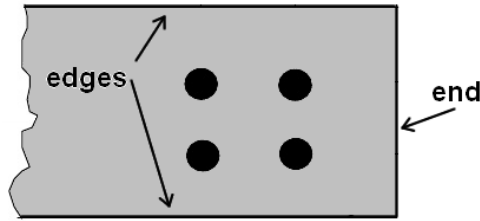
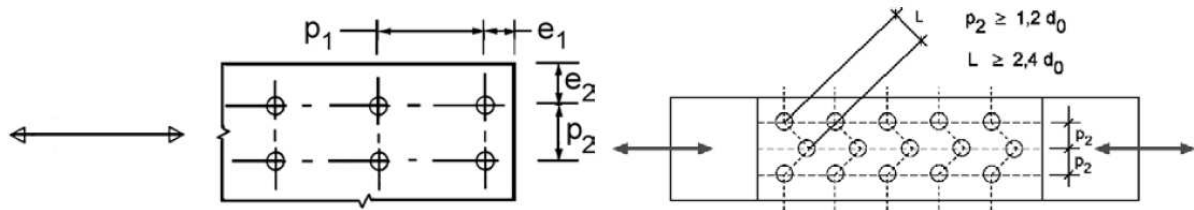


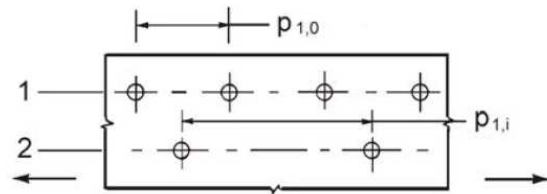
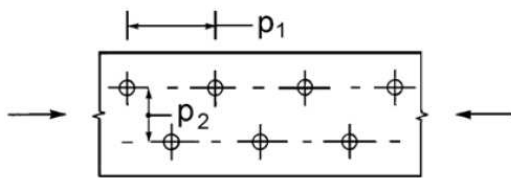
Figure 30-8 Explanatory sketch of 'ends' and 'edges'



Staggered Rows of fasteners

a) Symbols for spacing of fasteners

b) Symbols for staggered spacing



$p_1 \leq 14 t$ and ≤ 200 mm $p_2 \leq 14 t$ and ≤ 200 mm

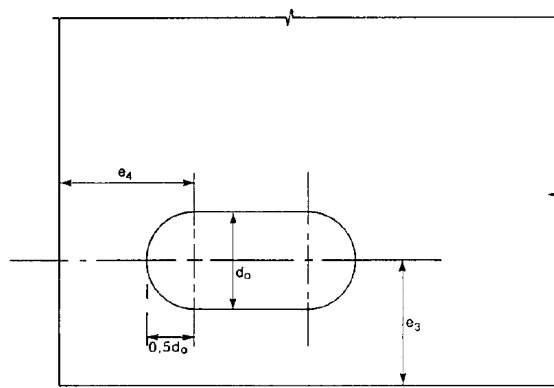
$p_{1,0} \leq 14 t$ and ≤ 200 mm $p_{1,i} \leq 28 t$ and ≤ 400 mm

1 outer row

2 inner row

c) Staggered spacing in compression members

d) Staggered spacing in tension members



e) End and edge distances for slotted holes

Figure 30-9 Symbols for end and edge distances and spacing of fasteners

Design resistance of individual fasteners

The design resistance for an individual fastener subjected to shear and/or tension is given in Table 30-8. For preloaded bolts the design preload, $F_{p,Cd}$, to be used in design calculations is:

$$F_{p,Cd} = 0,7 \cdot f_{ub} \cdot A_s / \gamma_{M7}$$

where:

$F_{p,Cd}$ [N]	=	design preload
f_{ub} [N/mm ²]	=	ultimate tensile strength
A_s [mm ²]	=	tensile stress area of the bolt
γ_{M7} [-]	=	partial factor for preload of high strength bolts ($\gamma_{M7} = 1,1$)

In single lap joints with only one bolt row, the bolts should be provided with washers (*ringen*) under both the head and the nut (*moer*). The design bearing resistance (*stuikweerstand*) for each bolt should be limited to:

$$F_{b,Rd} \leq 0,7 \cdot f_u \cdot d \cdot t / \gamma_{M2}$$

where:

$F_{b,Rd}$ [N]	=	design bearing resistance
f_u [N/mm ²]	=	tensile stress
d [mm]	=	nominal bolt diameter
t [mm]	=	thickness of the thinner outer connected part
γ_{M2} [-]	=	partial factor for the tensile strength ($\gamma_{M2} = 1,25$)

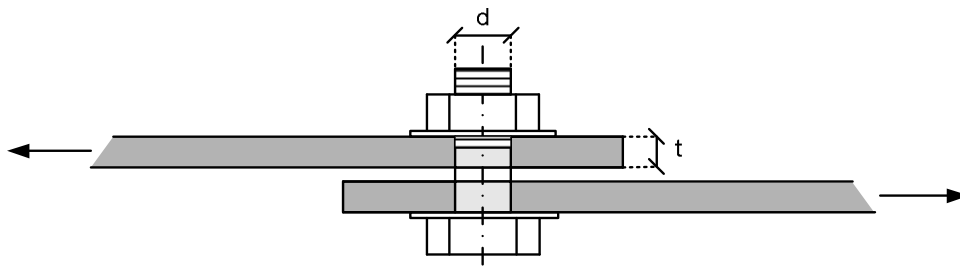


Figure 30-10 Single lap joint with one row of bolts

Failure mode	Bolts	Rivets
Shear resistance per shear plane	$F_{v,Rd} = \frac{\alpha_v \cdot f_{ub} \cdot A}{\gamma_{M2}}$ <ul style="list-style-type: none"> - where the shear plane passes through the threaded portion of the bolt (A is the tensile stress area of the bolt A_s) <ul style="list-style-type: none"> - for classes 4.6, 5.6, 8.8: $\alpha_v = 0.6$ - for classes 4.8, 5.8, 6.8 and 10.9: $\alpha_v = 0.5$ - where the shear plane passes through the unthreaded portion of the bolt (A is the gross cross-section of the bolt): $\alpha_v = 0.6$ 	$F_{v,Rd} = \frac{0.6 \cdot f_{ur} \cdot A_0}{\gamma_{M2}}$
Bearing resistance ^{1) 2) 3)}	$F_{b,Rd} = \frac{k_1 \cdot \alpha_b \cdot f_u \cdot d \cdot t}{\gamma_{M2}}$ <ul style="list-style-type: none"> - where α_b is the smallest of α_d; $\frac{f_{ub}}{f_u}$ or 1,0 - in the direction of load transfer: <ul style="list-style-type: none"> - for end bolts: $\alpha_d = \frac{e_1}{3 \cdot d_0}$; for inner bolts: $\alpha_d = \frac{p_1}{3 \cdot d_0} - \frac{1}{4}$ - perpendicular to the direction of load transfer: <ul style="list-style-type: none"> - for edge bolts: k_1 is the smallest of $2.8 \cdot \frac{e_2}{d_0} - 1.7$ or 2,5 - for inner bolts: k_1 is the smallest of $1.4 \cdot \frac{p_2}{d_0} - 1.7$ or 2,5 	
Tension resistance ²⁾	$F_{t,Rd} = \frac{k_2 \cdot f_{ub} \cdot A_s}{\gamma_{M2}}$ <p>where $k_2 = 0.63$ for countersunk bolt, otherwise $k_2 = 0.9$</p>	$F_{t,Rd} = \frac{0.6 \cdot f_{ur} \cdot A_0}{\gamma_{M2}}$
Punching shear resistance	$B_{p,Rd} = \frac{0.6 \cdot \pi \cdot d_m \cdot t_p \cdot f_u}{\gamma_{M2}}$	No check needed
Combined shear and tension	$\frac{F_{v,Ed}}{F_{v,Rd}} + \frac{F_{t,Ed}}{1.4 \cdot F_{t,Rd}} \leq 1.0$	
¹⁾ The bearing resistance $F_{b,Rd}$ for bolts <ul style="list-style-type: none"> - in oversized holes is 0,8 times the bearing resistance for bolts in normal holes. - in slotted holes, where the longitudinal axis of the slotted hole is perpendicular to the direction of the force transfer, is 0,6 times the bearing resistance for bolts in round, normal holes. ²⁾ For countersunk bolt: <ul style="list-style-type: none"> - the bearing resistance $F_{b,Rd}$ should be based on the plate thickness t equal to the thickness of the connected plate minus half the depth of the countersinking. - for the determination of the tension resistance $F_{t,Rd}$ the angle and depth of countersinking should conform with 1.2.4 Reference Standards: Group 4, otherwise the tension resistance $F_{t,Rd}$ should be adjusted accordingly. ³⁾ When the load on a bolt is not parallel to the edge, the bearing resistance may be verified separately for the bolt load components parallel and normal to the end.		

Table 30-8 Design resistance for individual fasteners subjected to shear and/or tension

where:

F_{v,R_d}	[N]	= the design shear resistance per bolt
F_{b,R_d}	[N]	= the design bearing resistance per bolt
F_{t,R_d}	[N]	= the design tension resistance per bolt
F_{v,E_d}	[N]	= the design shear force per bolt for the ultimate limit state
F_{t,E_d}	[N]	= the design tensile force per bolt for the ultimate limit state
B_{p,R_d}	[N]	= the design punching shear resistance of the bolt head and the nut
f_u	[N/mm ²]	= tensile stress
f_{ub}	[N/mm ²]	= ultimate tensile strength
f_{ur}	[N/mm ²]	= the specified ultimate tensile strength of the rivet
α_v	[-]	= factor defined in the table
α_d	[-]	= factor defined in the table
α_b	[-]	= factor defined in the table
A	[mm ²]	= the gross cross-section area of bolt
A_s	[mm ²]	= the tensile stress area of the bolt
A_0	[mm ²]	= the area of the rivet hole
γ_{M2}	[-]	= partial factor for the tensile strength ($\gamma_{M2} = 1,25$)
t_p	[mm]	= the thickness of a plate
k_1	[-]	= factor defined in the table
k_2	[-]	= factor defined in the table
e_1	[mm]	= the end distance from the centre of a fastener hole to the adjacent end of any part, measured in the direction of load transfer
e_2	[mm]	= the edge distance from the centre of a fastener hole to the adjacent edge of any part, measured at right angles to the direction of load transfer
p_1	[mm]	= the spacing between centres of fasteners in a line in the direction of load transfer
p_2	[mm]	= the spacing measured perpendicular to the load transfer direction between adjacent lines of fasteners
d_m	[mm]	= the mean of the across points and across flats dimensions of the bolt head or the nut, whichever is smaller
d_0	[mm]	= the hole diameter for a bolt, a rivet or a pin

Group of fasteners

The design resistance of a group of fasteners may be taken as the sum of the design bearing resistances F_{b,R_d} of the individual fasteners, provided that the design shear resistance F_{v,R_d} of each individual fastener is greater than or equal to the design bearing resistance F_{b,R_d} . Otherwise, the design resistance of a group of fasteners should be taken as the number of fasteners multiplied by the smallest design resistance of any of the individual fasteners.

30.6 Fatigue of welds

This section presents an introduction to the phenomenon of fatigue of welds. Of all structural members, welds are, in general for hydraulic structures, the most vulnerable to fatigue. Reference is made to the lecture notes of CIE5126 on fatigue and NEN-EN 1993-1-9 "Fatigue".

Fatigue is the progressive and localized structural damage that occurs when a material is subjected to cyclic loading. Final failure occurs in regions of tensile stress, if the reduced governing cross-section of the structural member becomes insufficient to bear the repetitive peak load without rupture. Fatigue is a major threat for structures under dynamic loads, such as bridges, cranes and offshore structures, where the live load presents a high portion of the total load. This is mostly the case in steel structures, where the dead weight is relatively low compared to the total load. Fatigue mainly leads to static failure by rupture (cracking) or buckling.

For a simple check, follow these design steps:

1. Locate the stress areas in the structure
2. Locate geometrical stress concentrations in the structure
3. Determine the fatigue strength
4. Determine the dynamic loads resulting in fatigue
5. Define the number of cycles n , using a cycle counting method
6. Check if damage will occur ($D_d = \sum (n_i / N_i) \leq 1$) (Miner's summation)

Ad 1/2. Design simple structural details. Start checking fatigue in critical sections, such as welds, connections, changes in structural member and high live load/dead load ratio etc.

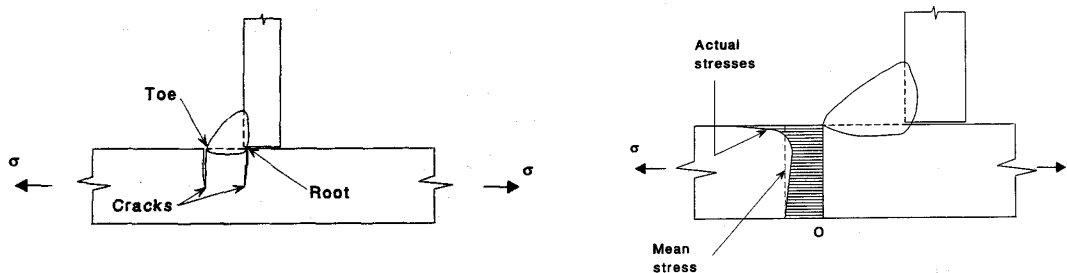


Figure 30-12: Discontinuities, stress peaks and cracks at the toe of a fillet weld

Ad3. Fatigue strength

The fatigue strength of a weld component is defined as the stress range ($\Delta\sigma_R$) between the minimum and maximum stress in the cycle which would cause failure of the structural member when fluctuating with a constant amplitude for a specified number of cycles (N_R). The number of cycles to failure N_R is known as the endurance or fatigue life.

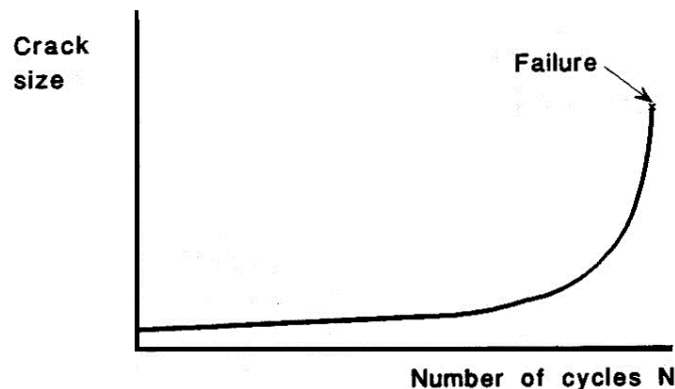


Figure 30-13: Typical crack growth curve

$$N_R = \frac{d}{\Delta\sigma_R^m} \quad \text{or} \quad \log N_R = \log d - m \cdot \log \Delta\sigma_R$$

where:

- m = slope of the fatigue strength curve (3 for most welded details)
- d = design weld strength parameter, or the fatigue detail category coefficient, dependent on the stress range, see Table 30-9.

Detail Category $\Delta\sigma_c$ [N/mm ²]	d		m [-]
160	7,962	10^{12}	3
140	5,636	10^{12}	3
125	3,990	10^{12}	3
112	2,825	10^{12}	3
100	2,000	10^{12}	3
90	1,416	10^{12}	3
80	1,002	10^{12}	3
71	0,710	10^{12}	3
63	0,502	10^{12}	3
56	0,356	10^{12}	3
50	0,252	10^{12}	3
45	0,178	10^{12}	3
40	0,126	10^{12}	3
36	0,089	10^{12}	3

Table 30-9 Classification table

$\Delta\sigma_c$ is the characteristic value for the weld-class applied, and represents the value for the stress range that is exceeded 10^7 times during the lifetime of the structure (see Figure 30-11).

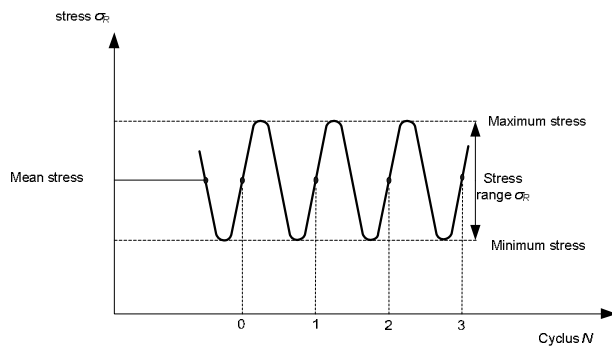


Figure 30-11: Constant amplitude stress history

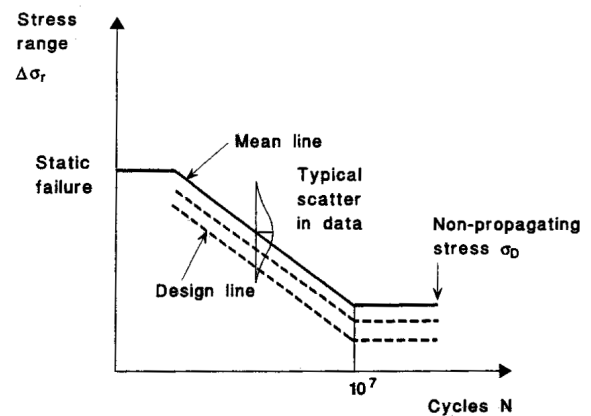


Figure 30-12: Typical S-N curve for constant amplitude tests

Beyond 5-10 million cycles, the stress range is generally too small to allow crack propagation under constant amplitude loading. Beneath this limit stress range cracks will not grow. The force fluctuation shall be calculated using the elasticity theory. No plastic redistribution is permitted because that would decrease the safety margin of the design.

Ad. 6 Calculation of damage.

The load spectrum is often simplified into a limited number of bands, see Figure 30-13. The damage per band is defined as n / N , where n is the number of cycles in the band and N is the endurance belonging to that stress range.

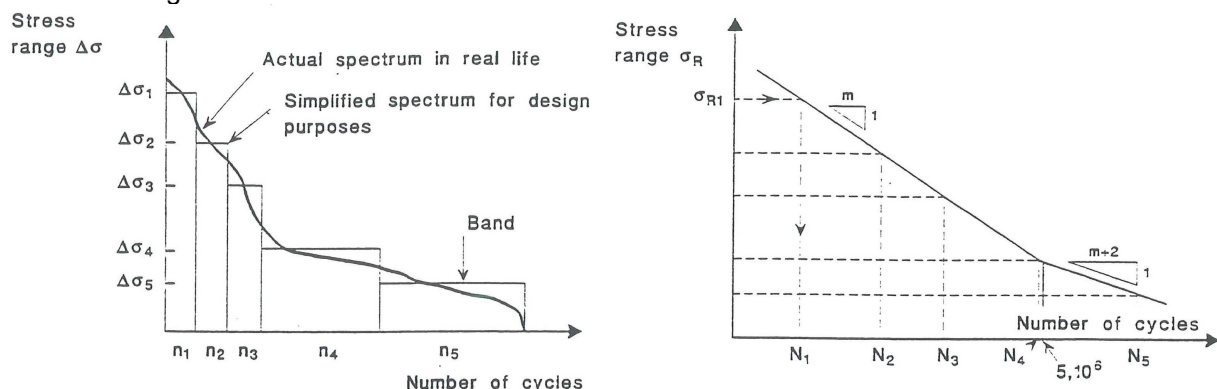


Figure 30-13 Simplification of stress spectrum and determination of endurance for each band (from lecture notes CT5126)

The damage during the design life (D_d) as a result of all stress bands should not exceed unity:

$$D_d = \sum \frac{n_i}{N_i} \leq 1$$

In the design, the following aspects should be taken into account:

- Fatigue depends on the whole service loading sequence, not just one extreme load event.
- Fatigue is very sensitive to the geometry of details. Details should be simple and smoothness of the stress path should be ensured.
- In well steel structures, fatigue cracks will almost certainly start to grow from welds, because
 - most welding processes leave minute metallurgical discontinuities from which cracks may grow (peak stresses at discontinuity).
 - At the toes of butt welds, sharp changes of direction often occur. Discontinuities at these points cause local stress concentrations, therefore cracks will grow faster.
- Fatigue requires more accurate prediction of elastic stress.
- A structure designed on fatigue makes more demands on workmanship and inspection.
- The static design safety margins are not sufficient for fatigue, therefore during the conceptual design should be checked whether fatigue is likely to be critical.
- Check areas of high live load/dead load ratios first on fatigue.

30.7 Literature

Nederlands Normalisatie instituut, Eurocode 3: "Design of steel structures – Part 1-1: General rules for buildings" (NEN-EN 1993-1-1), januari 2006, Nederlands Normalisatie instituut.

Nederlands Normalisatie instituut, Eurocode 3: "Design of steel structures – Part 1-8: Design of joints" (NEN-EN 1993-1-8), januari 2006, Nederlands Normalisatie instituut.

Nederlands Normalisatie instituut, Eurocode 3: "Design of steel structures – Part 1-9: Fatigue" (NEN-EN 1993-1-9), januari 2006, Nederlands Normalisatie instituut.

Manual Hydraulic Structures

Part III: temporary and permanent structures

31. Stability of structures on shallow foundations

New chapter: February 2011; updated February 2015; 'Piping' section slightly improved in 2016 and 2019
'Scour protection' improved in 2018, 2019

A foundation is denominated 'shallow', if the structure is supported by a soil stratum near the ground surface. Shallow foundations are usually applied on non-compressible soils (sand) and can consist of pad footings (*poeren*), rafts/strips (*stroken*), or slabs (*platen*). For large structures, like most hydraulic structures, slab foundations are usual, where a part or the whole slab area is used to transfer forces to the subsoil. Frost edges (*vorstranden*) should reach as deep as the frost-free level.

Shallow foundations are usually less expensive than deep foundations, and also easier to construct. Therefore, it is advised to first check whether a shallow foundation would suffice. The bearing capacity of the shallow soil stratum should suffice and the deformations (settlement) should be acceptable, possibly after soil improvement (*grondverbetering*) by replacing soft layers with sand, or by dewatering (*bemaling*). Potential uplift of the entire structure should be checked as well for this purpose. If a shallow foundation would not suffice, a deep foundation is required.

In addition, hydraulic structures have to be stable and not get into motion due to loads. This implies that there has to be a horizontal, vertical and rotational stability:

$$\begin{aligned}\Sigma H_{total} &= 0 \\ \Sigma V_{total} &= 0 \\ \Sigma M_{total} &= 0,\end{aligned}$$

where:

$$\begin{aligned}\Sigma H_{total} \text{ [kN]} &= \text{total of the horizontal components of the solliciting and resisting forces} \\ \Sigma V_{total} \text{ [kN]} &= \text{total of the vertical components of the solliciting and resisting forces} \\ \Sigma M_{total} \text{ [kNm]} &= \text{total of the moment caused by the solliciting and resisting forces}\end{aligned}$$

Another threat to the stability is groundwater flow under the structure, which can lead to internal erosion or undermining of the structure if sediment particles are moved away with the flow. External erosion, i.e., erosion in front of a structure, can also lead to collapse. These five criteria are elaborated in this chapter.

31.1 Horizontal stability

The total of the horizontal forces acting on a hydraulic structure based on a shallow foundation will be transferred to the subsoil (Figure 31-1). The friction force of the subsoil should resist the resulting total acting horizontal force, otherwise it will slide aside. This friction force is determined by the total of the forces solliciting (acting) on the structure in vertical direction (or the total of the vertical components of the forces, ΣV), multiplied by a dimensionless friction coefficient f . The friction force should not be less than the total of acting horizontal forces (ΣH), to prevent the structure from sliding aside. In equation form:

$$\Sigma H < f \cdot \Sigma V \quad (31.1)$$

The self-weight of the structure and buoyant forces should be included in ΣV .

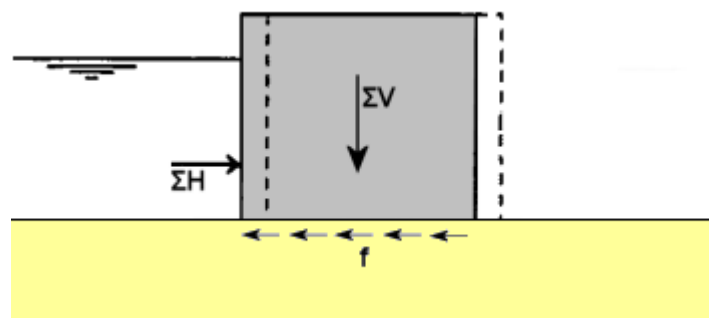


Figure 31-1 Slip-off principle sketch

Depending on the failure mechanism, more specifically the position and alignment of the slip surface, a certain type of friction develops. Potential critical slip planes are:

1. friction between structure and subsoil: $f = \tan(\delta)$, with δ = friction angle between structure and subsoil. If δ is unknown, it can be approximated: $\delta \approx \frac{2}{3} \varphi$ (φ is angle of internal friction of the subsoil). The friction coefficient for concrete-rubble is about 0,5; in case of a rubble bed: 0,6 (Dutch Deltaworks). Values for cast concrete on soil are given in Table 31-1.
2. Internal friction of the subsoil: $f = \tan(\varphi)$, with φ is the angle of internal friction of the subsoil.
3. A deeper soil layer with a low sliding resistance.

Interface Materials	Friction Coefficient, f
Mass concrete on the following foundation materials:	
Clean sound rock	0.70
Clean gravel, gravel--sand mixtures, coarse sand	0.55 to 0.60
Clean fine to medium sand, silty medium to coarse sand, silty or clayey gravel	0.45 to 0.55
Clean fine sand, silty or clayey fine to medium sand	0.35 to 0.45
Fine sandy silt, nonplastic silt	0.30 to 0.35
Very stiff and hard residual or preconsolidated clay	0.40 to 0.50
Medium stiff and stiff clay and silty clay	0.30 to 0.35

Table 31-1 Friction coefficient for cast concrete on soil [USACE Technical Letters]

31.2 Rotational stability

Between the soil and the structure only compression stresses can develop. For the stability of shallow founded structures, tensile stresses should not be taken into account for force equilibrium. Especially the adhesive and cohesive properties of sand are very poor, so in general, tensile stress cannot be provided by the subsoil. Therefore, it is usually stipulated that the soil stresses necessary for rotational stability may only be compressive (so, no tensile stresses allowed). This is the case if the resulting action force intersects the core of the structure. The core is defined as the area extending to 1/6 of the structure width on both sides of the middle of the structure (point K). In equation form:

$$e_R = \frac{\sum M}{\sum V} \leq \frac{1}{6} b \tag{31.2}$$

- where: e_R [m] = distance from the middle of the structure (K) to the intersection point of the resulting force and the bottom line of the structure
- $\sum V$ [N] = total of the acting vertical forces (or vertical components)
- $\sum M$ [Nm] = total of the acting moments, preferably around point K, halfway the width
- b [m] = width of the structure

See Figure 31-2 for an illustration.

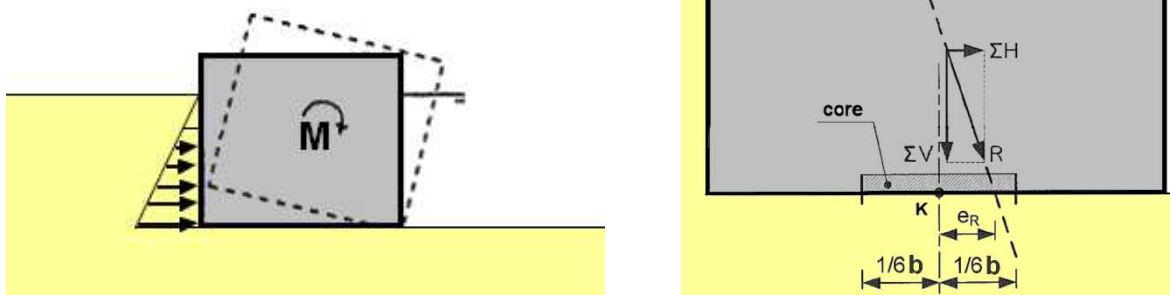


Figure 31-2 The action line of the resulting force should intersect the core of the structure. The rotation depicted on the left side is very unusual. In reality, if there is a maximum load acting in just one point (the corner), the soil under the corner will immediately collapse. The adjoining soil will then start bearing the load.

If, however, the action line of the resulting force is located outside the core of the structure, only part of the soil below the structure will contribute to the bearing, see Figure 31-3. In that case, the no-tensile criterion is not met. It actually can occur that even in this case the maximum occurring soil stress is not exceeded and the situation is not really problematic.

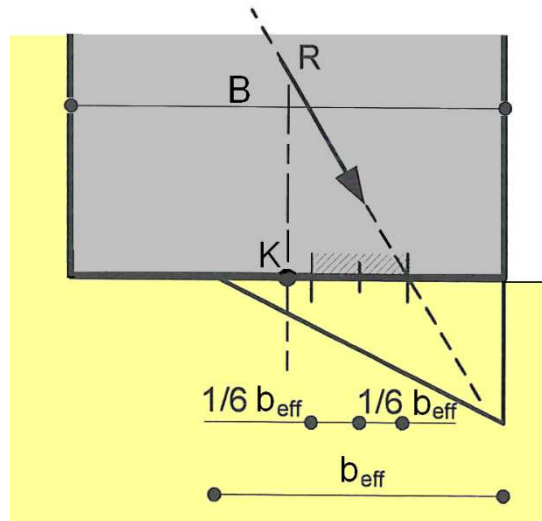


Figure 31-3 Action line of resultant force does not intersect to core of the structure

31.3 Vertical stability

The vertical stability of shallow-founded structures can be subdivided into bearing capacity and settlements.

Bearing capacity

The vertical effective soil stress, required to resist the acting loads ($\sigma_{k,max}$), should not exceed the maximum bearing capacity of the soil (p'_{max}), otherwise the soil will collapse:

$$\sigma_{k,max} < p'_{max} \quad (31.3)$$

The maximum acting load on the soil can be calculated with:

$$\sigma_{k,max} = \frac{F}{A} + \frac{M}{W} = \frac{\sum V}{b \cdot \ell} + \frac{\sum M}{\frac{1}{6} \ell b^2} \quad (31.4)$$

where: $\sum V$ [N] = total of the acting vertical forces (or vertical components)
 A [m²] = area of the bottom plate
 W [m³] = section modulus of the contact area of the bottom plate
 b [m] = width of the structural element
 ℓ [m] = length of the structural element
 $\sum M$ [kNm] = total of the acting moments, preferably around point K, halfway the width

The bearing capacity p'_{max} can be calculated according the Brinch Hansen method for determining the maximum bearing capacity of a foundation. This method takes into account the influence of cohesion, surcharge including soil coverage and capacity of the soil below the foundation, see Section 26.2 of this Manual (Part II).

As a rule of thumb (instead of the Brinch Hansen calculation), the bearing capacity of densely packed sand is often assumed to be 400 kN/m² (= 0,4 N/mm²), in accordance with the Dutch Handboek Funderingen (CUR, 2010).

The minimum acting load on the soil can be calculated with:

$$\sigma_{k,min} = \frac{F}{A} - \frac{M}{W} = \frac{\sum V}{b \cdot \ell} - \frac{\sum M}{\frac{1}{6} \ell b^2} \quad (31.5)$$

Because soil cannot or barely cope with tensile forces, $\sigma_{k,min} > 0$ (31.6)

Settlements

The soil under structures will settle because of compaction due to the added weight on top of them. See Chapter 28 for an explanation.

31.4 Piping (internal backward erosion)

Theory

A difference in water level (the 'hydraulic gradient') across a hydraulic structure or dike can cause a flow of groundwater in permeable soil under or besides that structure. The phenomenon of groundwater pouring out of the soil is called 'seepage'. The consequences of seepage are usually not severe, because the quantity of seepage water mostly does not lead to a flood, but only to an amount of excess water that can usually be dealt with by the lower water system. The flow under the structure can best be described by a flow net as in Figure 31-4 (left), where a piping screen (= 'seepage screen'), usually a sheetpile wall, has been installed under the structure.

If the flow velocity is sufficiently high, sediment particles will start extruding from permeable soil at the land side of the structure. This internal erosion leads to the formation of cavities or channels in the subsoil: the so-called pipes. Little sand boils (*zandmeevoerende wellen*) appear where the water flows out at ground level. The pipes can grow until they reach the water side of the dike or structure, undermining its foundation, which can lead to collapse or sliding of the dike body. Hence the name 'piping' (*zanduitspoeling*). Pipes need a so-called roof (a cohesive layer or a hard structure) that prevents immediate collapse of the pipes. This effect causes the piping paths to follow the geometry of the structure, so they are usually orientated horizontally or vertically and do not follow the lines of the original flow net, see Figure 31-4 (right).

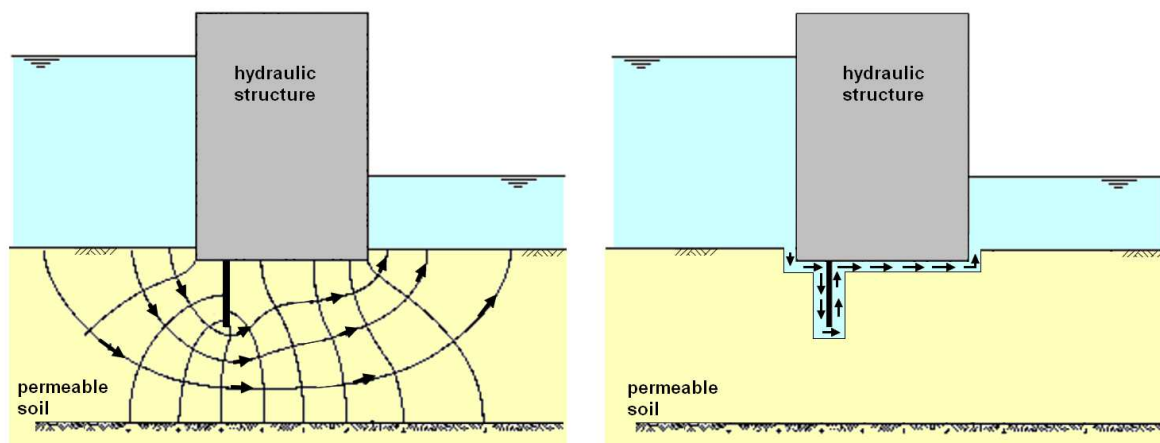


Figure 31-4 Piping: Initial flow pattern under the structure (left) and final piping path (right)

There are two types of internal backward erosion:

- Piping (*onderloopsheid*) is the formation of erosion pipes *under* a structure.
- Outflanking (*achterloopsheid*) is the formation of erosion pipes *around* (besides) a structure.

It is important to realise that two basic conditions have to be met before piping can occur:

1. The duration of the water level difference has to be sufficiently long to complete the process of pipe formation. This is the reason why piping under normal Dutch sea dikes has not yet been observed: water levels along the coast highly depend on tidal fluctuations and the duration of a storm is usually not longer than approximately 24 hours with a peak of about 2 hours. However, for hard structures along the coast, piping measures are usually included in the design.
2. Sand particles must have a possibility to extrude. So, if the ground level at the side of the lower water level is relatively high, piping becomes unlikely, just like in case of a closed and sufficiently strong surface, like an underwater concrete floor in a building pit. Before erosion can start, rupture of the top layer should occur. In case of low-permeable cohesive soil or a filter layer this phenomenon is called *uplift*; for sand (aquifer material) the term *heave* is used.

Piping under *pile-founded* structures is very critical, because the subsoil can easily settle a bit while the pile-founded structure remains at its place (because of its foundation in a deep, stable ground layer). This results in an open space under the structure, where the water can flow without significant hindrance and very likely cause internal erosion.

Design

Empirical formulas based on research describe the critical situations in which piping can occur. The most well-known are the Bligh and Lane formulas. According to these formulas there is a limit state with a critical ratio between the differential head and the seepage distance. More recent research has confirmed this. For the results of this research and the design rules that have been derived from it, one is referred to Sellmeijer, 1988 (only for standard dikes, not for structures with seepage screens). It should be realised that the Bligh and Lane formulas are inaccurate and that they should only be used for a first impression about potential piping problems.

W.G. Bligh was among the first to find a formula for a safe seepage distance. He studied several structures like small weirs, dams and barrages, mainly in the USA, India and France. Based on his observations, he developed a 'critical average gradient model' which determines the critical ratio between head difference and seepage length. Bligh mainly considered horizontal seepage paths.

E.W. Lane extended Bligh's theory based on an investigation of more than 200 masonry dams. Lane distinguished between horizontal and vertical seepage paths. He found that vertical paths offer a three times higher resistance against piping than horizontal paths, mainly due to the fact that vertical pipes tend to collapse due to gravity, thereby blocking the pipe. In Lane's formula, pipes with a slope angle of 45° or larger are treated as vertical, slopes at less than 45° are considered horizontal.

A sketch with horizontal and vertical seepage distances under a structure is shown in Figure 31-5.

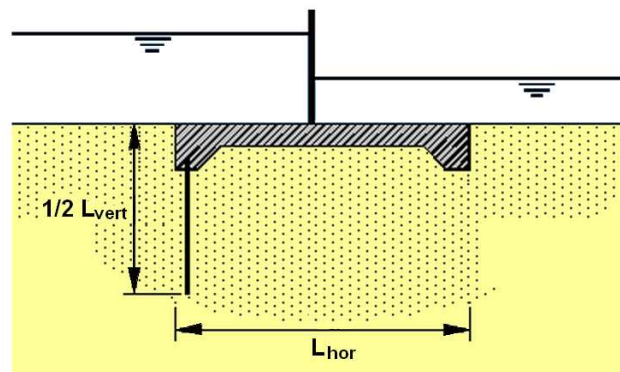


Figure 31-5 Horizontal and vertical seepage paths

Bligh assumes $L = \sum L_{vert} + \sum L_{hor}$ and Lane assumes $L = \sum L_{vert} + \sum \frac{1}{3} L_{hor}$. On ground of Lane's assumption, the soil constants also undergo changes compared to Bligh's constants (see Table 31-2). It should be noticed that for pile-founded structures, L_{hor} should not be included in the total seepage length L , unless it is certain that the soil volume below the structure cannot settle (as it would lead to interspace between the soil and the structure).

Piping method:	Bligh	Lane
requirement:	$L \geq \gamma \cdot C_B \cdot \Delta H$	$L \geq \gamma \cdot C_L \cdot \Delta H$
used seepage length	$L = \sum L_{vert} + \sum L_{hor}$	$L = \sum L_{vert} + \sum \frac{1}{3} L_{hor}$
Soil type ↓ constant →	C_B	C_L
very fine sand or silt	-	8,5
fine sand or silt	18	-
fine sand (micr.)	18	7
fine sand (quartz)	15	7
middle fine sand	-	6
coarse sand	12	5
fine gravel	9	4
middle fine gravel	-	3,5
course gravel	-	3
very coarse gravel	4	-
weak clay	-	-
normal clay	-	2
stiff clay	-	1,8

Table 31-2 Safe seepage distance for piping (TAW report Piping Check for River Dikes, 1994)

where: L [m] = total seepage distance, which is the distance through the soil where the water flow is impeded by the soil structure¹
 C_B [-] = Bligh's constant, depends on soil type
 C_L [-] = Lane's constant, depends on soil type
 ΔH [m] = differential head across structure
 γ [-] = safety factor (1,5)
 i_{max} [-] = maximum (allowed) hydraulic gradient = $\Delta H / L$

In the Dutch design practice, both methods are being applied for conceptual designs. For a first check on piping under dikes, Bligh's method is most suitable, whereas Lanes' method should be used to estimate whether piping will occur under water retaining structures with seepage screens or other vertical piping paths..

Hans Sellmeijer more recently (1988) developed a mathematical model to describe piping. The design rules resulting from this model lead to more favourable dimensions for the required horizontal piping line, compared to Bligh's method. Sellmeijers original model, however, is not applicable for vertical piping lines and is only suitable for the dimensioning of dikes. That is why he formulated additional design rules for the dimensioning of heave (*hydraulische grondbreuk*) behind seepage screens. These new design rules can be used if the piping criterion of Lane doesn't suffice.

According to Sellmeijer, a piping channel becomes critical if its length exceeds half of the seepage length. If this occurs, the piping channel will progressively increase until failure. The observation of sand boils therefore does not immediately imply failure, but it is not very well possible to determine how safe the structure then still is.

The critical water level difference can be computed with an empirical equation (Sellmeijer, 2011):

$$\Delta H = F_1 F_2 F_3 L > 0$$

$$F_1 = \eta \left(\frac{\gamma_s}{\gamma_w} - 1 \right) \tan \theta$$

$$F_2 = \frac{d_{70m}}{\sqrt[3]{\frac{\nu k L}{g}}} \left(\frac{d_{70}}{d_{70m}} \right)^{0,4} \quad (31.7)$$

$$F_3 = 0,91 \cdot (D/L)^{\frac{0,28}{(D/L)^{2,8}-1} + 0,04}$$

where:

L [m] = (horizontal) seepage length
 γ_s [kN/m³] = specific weight of sand particles (for sand 26,5 kN/m³)
 γ_w [kN/m³] = specific weight of water
 θ_R [°] = bedding angle
 D [m] = thickness of the aquifer (sand layer)
 η [-] = drag factor coefficient
 d_{70} [m] = 70% fractile of the grain size distribution
 d_{70m} [m] = reference value of d_{70}
 ν [m²/s] = kinematic viscosity
 k [m/s] = specific conductivity
 g [m²/s] = gravitational acceleration

This method can only be used if sufficient specific soil parameters are known.

¹ The horizontal distance under *pile-founded* structures should not be included in the horizontal seepage distance L_{hor} .

Effect of piping screens on water pressure under a structure

The water pressure in front and behind a hydraulic structure depends on the water depth on both sides. It linearly changes along the length of the seepage path directly under the structure, see Figure 31-6a. The same applies, if there is a piping screen under the structure. The presence of the screen causes a discontinuity in the upward pressure under the structure at the location of the screen, see Figure 31-6b. The piping screen is preferably placed at the side of the structure with the highest water level, as it then maximally reduces the vertical pressures, thus reducing the uplift force.

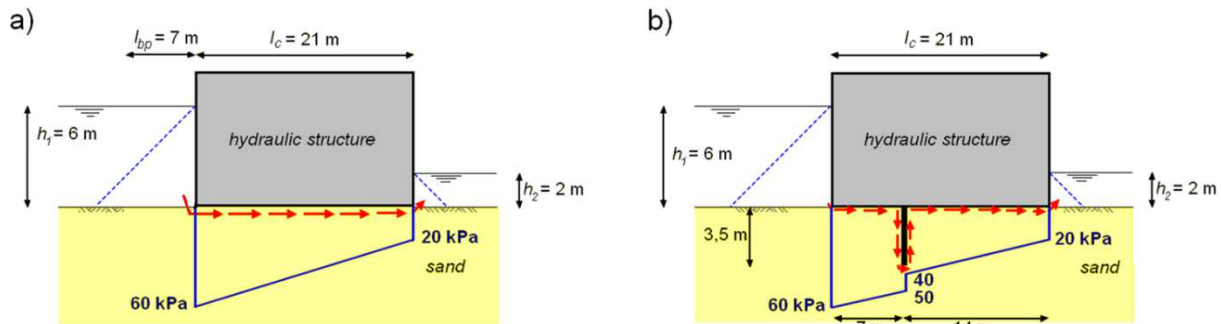


Figure 31-6 Water pressure under a structure a) without a piping screen and b) including a piping screen

Measures to prevent piping

If a structure does not meet requirements for piping, the following solutions could be considered:

1. apply a piping berm (consisting of clay) at the inner side of a dike
2. use (longer) sheet piling upstream as a screen against seepage
3. apply grout columns upstream to make the soil impermeable and cohesive
4. insert a diagonal protective textile in the soil in front of a structure
5. insert a filter structure downstream
6. install gravel piles (*grindpalen*) to lower hydraulic head at the inner side of a dike
7. (temporarily) increase the downstream water level (for instance in the ditch behind the dike)
8. apply a clay core (*kleikist*) in the aquifer as an impermeable blocking system
9. as an emergency measure: sandbagging around a sand boil (*opkisten*)

Notes

1. The full and one third part of respectively the vertical and horizontal piping paths may only be taken into account if the following conditions are satisfied:
 - The building material must be in direct contact with undisturbed soil
 - The walls must be closed and must have a water-tight connection with the rest of the structure
2. The first condition means that if a structure has a pile foundation, which may allow settlements that create a split between the structure and the soil, the seepage path along the bottom slab may not be counted, unless extra measures are taken to seal the split.
3. One should not only consider under-seepage, but must also take backward seepage into account. Cut-off walls to prevent this are obviously placed in the same plane as the normal cut-off walls to prevent under-seepage. Furthermore, these walls are extended sideways beyond the loose ground of the building site.
4. It is very important to compact the soil around the structure so it erodes less easily.

31.5 Scour protection

The presence of a hydraulic structure along or in the water usually affects the flow current and the waves. This leads to a change of the motion of water particles near that structure, which can lead to scour of the bed in front of it. A gradual dislocation of a sill or geotechnical instability of the structure can be the result. Scour can be prevented by applying granular filters, geotextile, or and more or less impermeable layers like asphalt². This section first explains when scour can be expected, followed by the basic design principles of (geometrically closed) granular filters. More information on bed protection can be found in the lecture notes on 'Bed, bank and shore protection' (Schiereck & Verhagen, 2016).

Scour of sand beds, caused by waves

The interaction of waves with a structure can lead to a scour hole that could threaten the stability of the structure (Figure 31-7).

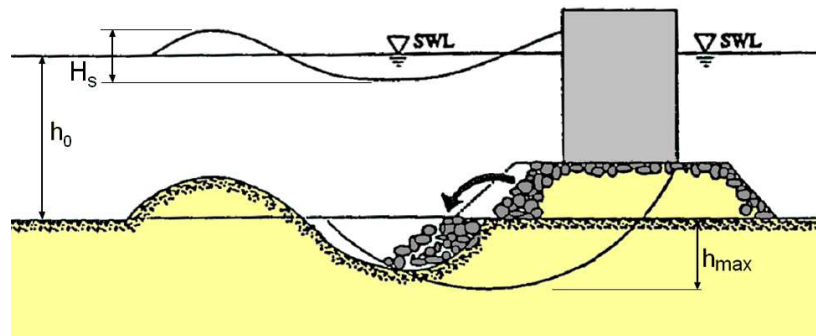


Figure 31-7 Bottom scour induced by waves in front of a breakwater

If no information is available, only for preliminary designs, the maximum wave-induced scouring depth h_{max} in front of structures with vertical walls may be assumed to be equal to the height of the maximum unbroken wave, which cannot become more than 0,5 to 0,7 times the original water depth h_0 , which could occur under the worst conditions (Shore Protection Manual, 1984):

$$h_{max} = H_{max} \leq 0,7 \cdot h_0 \quad (31.8)$$

Xie (1981) proposed a simple equation for scour near vertical or steeply sloping impermeable structures, related to the wave height, water depth and wave length:

$$h_{max} = 0,4 \cdot H \left(\sinh \left(\frac{2 \cdot \pi \cdot h_0}{L_{wave}} \right) \right)^{-1,35} \quad (31.9)$$

The equation is based on experiments on both fine and coarse sediments with regular waves.

Scour of sand beds, caused by current

Bed protection prevents structural damage by water currents near hydraulic structures. Turbulence can cause scour holes at the end of the scour protection, if the amounts of sediment transported over the protection are small (Figure 31-8).

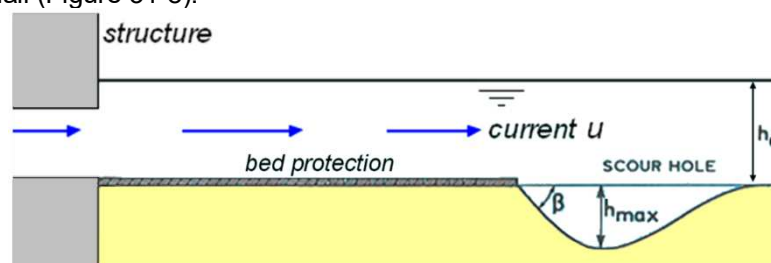


Figure 31-8 Scour due to current

The angle of the upper slope of the scour hole, β , is usually considerably less steep than the natural slope of sediment under water. Usual values for β are between 18° and 26° .

² To prevent scour at both sides of a closure dam, much research on the required length of a bed protection has been carried out during the execution of the Deltaworks in the Netherlands (Huis in 't Veld, 1987, § 2.4.9).

The maximum depth of the scour hole at a given moment can be calculated with the formula of Herman Breusers of Deltares (1991), but the method requires much information, which is difficult to obtain. A simplification can be achieved by calculating the equilibrium depth of the scour hole, while assuming that there is no sand coming from upstream (clear water scour). In that case the maximum (= equilibrium) scour depth h_{max} is given by:

$$h_{max} = \frac{0,5 \cdot \alpha \cdot \bar{u} - u_{cr}}{u_{cr}} \cdot h_0 \quad \text{for } 0,5 \cdot \alpha \cdot \bar{u} - u_{cr} > 0 \quad (31.10)$$

where:

h_{max}	[m]	= maximum depth of the scour hole (= equilibrium depth)
h_0	[m]	= initial water depth
\bar{u}	[m/s]	= depth-averaged flow velocity at the end of the scour protection
u_{cr}	[m/s]	= critical velocity regarding begin of motion of sand particles
α	[-]	= turbulence coefficient, depending on the upstream disturbance. The value of α is in the order of 3.

The critical velocity u_{cr} for the initiation of sand transport under uniform flow can be calculated with the Shields equation:

$$u_{cr} = C \sqrt{\Theta_{cr} \cdot \Delta \cdot D_{50}} \quad (31.11)$$

where:

D_{50}	[m]	= mass-median nominal diameter of sand particles at the end of the scour protection
C	[$\sqrt{m/s}$]	= Chézy coefficient ³
Θ_{cr}	[-]	= Shields (stability) parameter (= τ_*), the dimensionless critical shear stress:

$$\Theta_{cr} = \frac{\tau_{cr}}{g \cdot \Delta \cdot D_{50}} \quad (31.12)$$

Δ	[-]	= relative density: $\Delta = \frac{\rho_s - \rho_w}{\rho_w}$ (usually about 1,65 for fresh and 1,59 for sea water)
----------	-----	---

The Chézy coefficient can be calculated with:

$$C = 18 \cdot \log \left(\frac{12 \cdot R}{k_r} \right) \quad (31.13)$$

where:

k_r	[m]	= equivalent bed roughness: $k_r \approx 2 D_{n50}$ for narrowly graded gravel and rock ($D_{n50} \approx 0,85 \cdot D_{50}$) $k_r \approx 3 D_{n90} \approx 6 D_{n50}$ for widely graded gravel and rock $k_r \approx 10$ to 50 cm for sand, which is the height of the bed form (ripples or flow channels) $k_r \approx 5$ cm for the bed form of river beds consisting of clay (ripples or flow channels)
R	[m]	= hydraulic radius of the flow channel at the end of the scour protection: $R = \text{wet area} / \text{wet circumference of the flow channel}$ $R \approx h_0$ for wide channels

The Shields parameter depends on the dimensionless grain diameter: $d_* = D_{50} \cdot 3 \sqrt{\frac{\Delta \cdot g}{\nu^2}}$, where ν is the kinematic viscosity [m^2/s]. Figure 31-9 shows the relation between the Shields parameter Θ_{cr} and the dimensionless grain diameter d_* (lower horizontal axis). For normal circumstances (temperature, density), the value of Θ_{cr} can be directly related to D_{50} (upper horizontal axis).

³ If this equation is used to calculate the critical velocity for the initiation of rock, for example to determine the stability of a bed protection, D_{n50} should be used in stead of D_{50} .

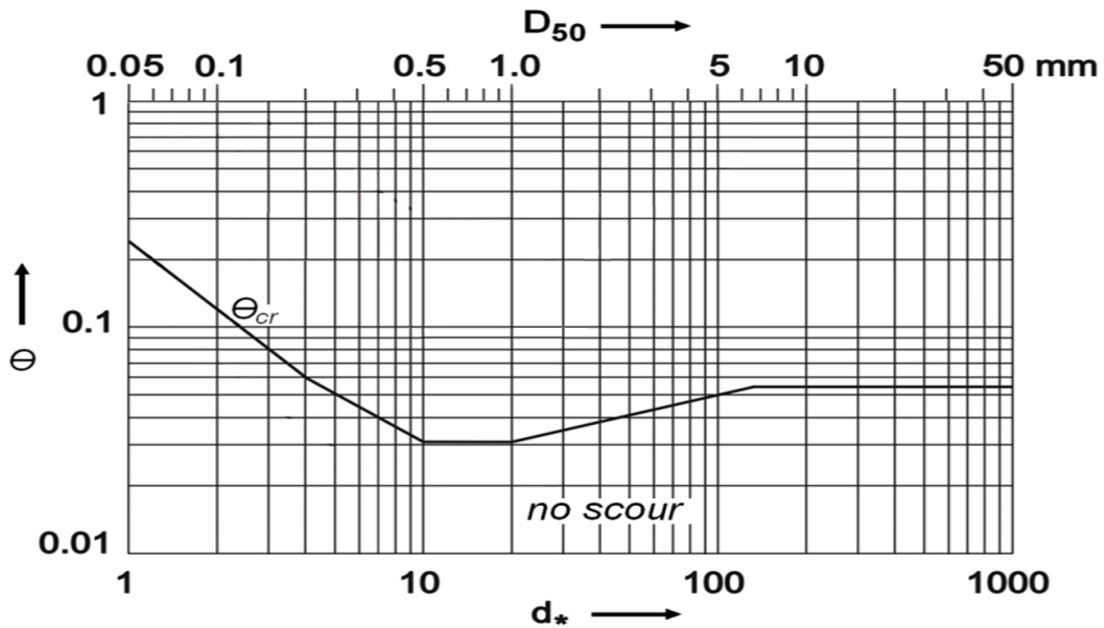


Figure 31-9 Relation between the Shields parameter and d_* or D_{50} for determining the scour depth of sand beds under usual conditions (after Schiereck & Verhagen, 2016)

Scour of sand beds caused by a plunging jet

Scour of sand beds, caused by plunging, free falling jets, can be a relevant failure mechanism for the gates of locks and cut-offs (*coupures*) (Figure 31-10). The jet that hits the water surface with an impulse that is proportional to the product of the discharge and the velocity of the jet. The jet propagates into the lower water body and will reach the bed with a reduced velocity (and impulse). There it can lead to erosion of the bed particles or rock. Eddies originate in front of and behind the jet and circulate the eroded particles, part of which is consequently transported by the current in the downstream direction.

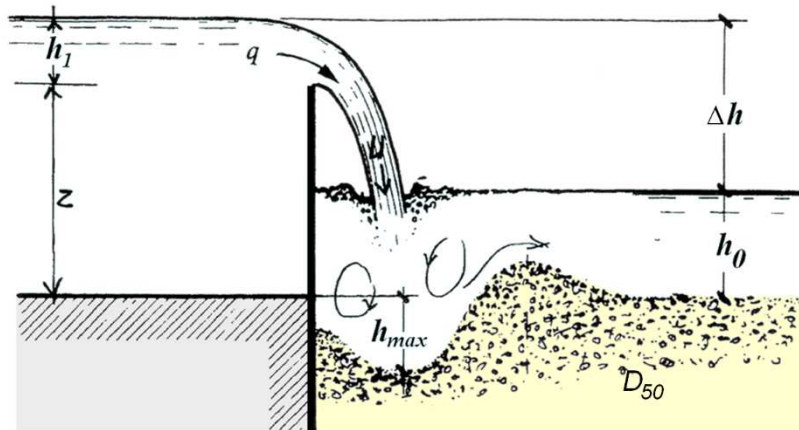


Figure 31-10 Scour caused by a plunging jet (WTI, 2015)

The maximum scour depth due to plunging jets according to WTI 2017 (Achtergrondrapport toetsspoor Hoogte II - Bepaling kritiek overslag-/overloopdebiet, 2015) can be calculated with:

$$h_{max} = 0,4 \cdot q^{0,6} \cdot \Delta h^{0,4} \cdot D_{50}^{-0,3} - 0,5 \cdot h_0 \tag{31.14}$$

where:

- h_{max} [m] = maximum scour depth
- q [m³/s/m] = specific discharge per m width
- Δh [m] = water level difference
- h [m] = water depth downstream
- D_{50} [m] = median nominal particle diameter

There is no equation for the erosion of clay or sand-clay mixtures due to plunging jets. However, the maximum scour depth for these bed materials will be less than for sand with the same D_{50} .

Scour of sand behind piles and piers, caused by waves and currents

The scouring process around vertical piles and piers is mainly caused by:

- local disturbance of the flow field (local scour)
- local reduction of cross-section (contraction scour)

Other general relevant scour effects are:

- general degradation effects (downstream of weirs, reservoir dams, etc)
- bend scour; deeper part of cross-section in outer bend area (variability in river planform)
- confluence scour; deeper parts of cross-section downstream of confluence
- thalweg variations (deepest point of cross-section may shift in lateral direction)
- bed-form variations

The flow pattern around a cylindrical pipe is shown in Figure 31-11.

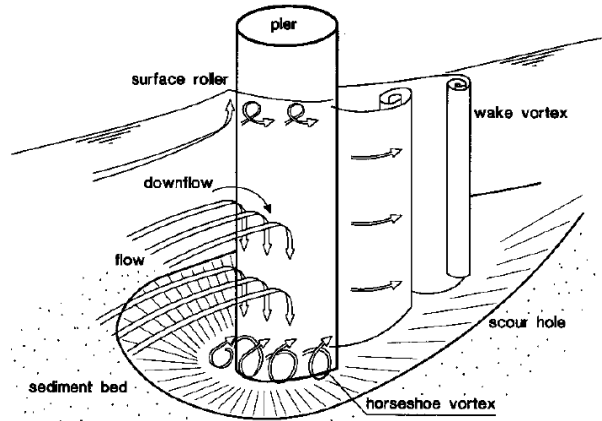


Figure 31-11 Scour pattern behind a pile or pier (Melville, 1988)

Several researchers have studied the scour development behind cylindrical piers and piles. Based on their data, Van Rijn (2013) proposes the following equation for the scour hole depth:

$$h_{max} = 0,35 \cdot D_{pile} \left(\frac{D_{pile}}{h_0} \right)^{0,2} \cdot V_{par} \quad (31.15)$$

where:

- h_{max} [m] = scour hole depth
 D_{pile} [m] = pile diameter
 h_0 [m] = water depth

V_{par} [-] = dimensionless velocity parameter: $V_{par} = \frac{\sqrt{u_c^2 + (0,7 \cdot u_w)^2}}{u_{cr}}$ (31.16)

- u_c [m/s] = near-bed peak orbital velocity due to storm
 u_w [m/s] = maximum flow velocity upstream due to tide and wind
 u_{cr} [m/s] = critical velocity for initiation of motion:
 $u_{cr} = 0,35$ m/s for 100-300 μm ; 0,4 m/s for 400 μm and 0,5 m/s for 600 μm

Scour of cohesive beds, caused by current

Cohesive forces cause a distinct increase of the soil resistance against erosion compared to homogeneous sand beds. The amount of erosion mainly depends on the type of fine minerals, biological activity at the bed and the rate of consolidation of the soil. A sand bed with small amounts of silts and clays already shows a considerably increased resistance against erosion and old compact clay soils are even highly resistant against erosion. There are two main ways of clay erosion: erosion of (many) single particles and chunk erosion (*kluiterosie*).

Based on tests performed at Delft Hydraulics (1989) on bed samples from the North Sea with particle sizes of $100 \mu\text{m} < D_{50} < 200 \mu\text{m}$, and mud-silt percentages of 2 to 20%, the critical bed shear stress $\tau_{cr,c}$ was related to the critical bed shear stress for sand according to Shields, $\tau_{cr,sand}$, and the percentage of fines (mud or silt) smaller than $50 \mu\text{m}$, p_s (Van Rijn, 1993, §4.1.2):

$$\tau_{cr,c} = \rho_s^{0,5} \cdot \tau_{cr,sand} \quad (31.17)$$

Similarly, it can be stated that

$$\Theta_{cr,c} = \rho_s^{0,5} \cdot \Theta_{cr} \quad (31.18)$$

where Θ_{cr} is the critical Shields parameter of sandy beds as indicated in Figure 31-9. Be aware that this equation only applies to homogeneous soil layers and not to chunk-type erosion.

Thus, the procedure to find out whether a mixed sand-clay bed will scour is:

- Determine the percentage (not the fraction) of fines (ρ_s)
- Calculate the Shields parameter for this clayey bed ($\Theta_{cr,c}$) with Equation (31.18)
- Draw a new line in the graph of Figure 31-9, and determine the $\Theta_{cr,c}$ for median diameter D_{50} of the sand-clay mixture. This value will be slightly less than the D_{50} of the sand fraction in the mixture.
- Calculate the critical velocity with Equation (31.11). Also here, use the D_{50} of the sand-clay mixture.
- Calculate the maximum scour depth with Equation (31.10)
- Calculate the required length of the scour protection with Equation (31.25).

For erosion of soils with more than 20% cohesive materials and especially for chunk-type erosion of cohesive beds, still no design formulas are available.

Bed protection

The sediment particles of the bed protection should be sufficiently large to avoid erosion. The D_{50} of these particles can be estimated with help of the adapted Shields Equation (31.19) for uniform flow:

$$D_{50} > \frac{\bar{u}^2}{\Theta_{cr} \cdot \Delta \cdot C^2} \cdot \frac{K_v^2}{K_s} \quad (31.19)$$

where:

\bar{u} [m/s] = depth-averaged flow velocity on the scour protection
 Θ_{cr} [-] = Shields (stability) parameter for no motion: $\Theta_{cr} = 0,03$ (so, don't use Figure 31-9!)

Δ [-] = relative density: $\Delta = \frac{\rho_s - \rho_w}{\rho_w}$ (usually $\Delta \approx 1,65$)

C [$\sqrt{m/s}$] = Chézy coefficient of the top filter layer

K_v [-] = factor for non-uniform (deceleration) flow = 1 to 2 ($\approx 1,5$)

K_s [-] = reduction factor for a slope perpendicular to the flow direction:

$$K_s = \sqrt{1 - \frac{\sin^2 \alpha}{\sin^2 \varphi}} \quad (31.20)$$

where α = the bed slope angle and φ = the angle of internal friction.

Extrusion of particles of underlying layers through the pores of the bed protection should be prevented. This can be accomplished by granular filters, or with help of geotextile (Figure 31-12).

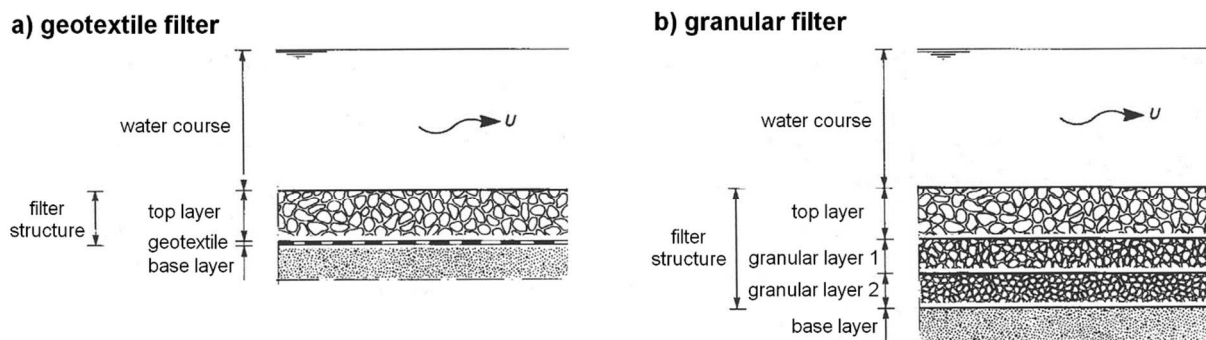


Figure 31-12 Definition filter structures

Granular filters can be divided in geometrically open and closed filters. Geometrically open filters allow loss of filter material (sediment particles) if the load becomes higher than a critical value. To establish a stable

open filter, a critical filter gradient has to be determined, which requires detailed information on the loading gradients. In geometrically closed filters, the grain sizes are chosen in such a way, that they cannot move in the filter. Classical closed-filter rules have already been developed by Karl von Terzaghi in the 1930s.

In general, there are three types of geometrically closed filters, viz.:

- granular filter
- asphalt concrete
- geotextile

The granular filter type is the most commonly used and in the following paragraphs the design of geometrically closed filters is explained.

A geometrically closed granular filter should be designed in such a way, that grains in the basic layer cannot pass the holes of the filter. The holes in the granular filter consist of the pores in the grain packet that are interconnected by small pore channels. If the diameter of the pore channels D_c is smaller than the diameter of the governing grains of the basic layer D_b , no transport can take place, irrespective of the value of the water level slope, the direction and type (stationary or not) of the flow⁴.

The governing grain size of the base layer (the lower layer) is about D_{85} . If grains with the governing diameter cannot be transported, smaller grains can be transported neither. A layer is therefore considered geometrically closed, if

$$\frac{D_{f15}}{D_{b85}} < 5 \quad (31.21)$$

This only applies if the sieve curve of the basic material does not differ too much from the curve of the filter material. If a layer is widely graded, internal instability can occur. In that case, the small grains can be transported through the channels of the big ones. Internal stability can be expected, if

$$\frac{D_{60}}{D_{10}} < 10 \quad (31.22)$$

which should also be the case for a filter layer.

To avoid overpressure perpendicular to the separating layer, the filter layer should be more permeable for water than the basic layer. In general, smaller grain diameters imply smaller permeability. In graded layers principally small grains of about D_{15} determine the permeability. During the lifetime of the structure, the diameters of the pore channels can decrease because of siltation with material from the basic layer, or because of deterioration (*verwering*). It is difficult to check up on this effect and eventual repairs are practically nearly impossible. Therefore, an extra requirement for permeability should be met:

$$\frac{D_{f15}}{D_{b15}} > 5 \quad (31.23)$$

For geotextile filters, similar rules apply. A geotextile is considered to be tight, if the larger fraction of the grains of the basic layer cannot pass the characteristic pores of the geotextile:

$$O_{90} < D_{b90}, \text{ which is very strict, and usually: } O_{90} < 2D_{b90}$$

where O_{90} = the diameter of the fraction of which 90 weight-percentage remains on the geotextile after 10 minutes of sieving (so it is not an indication for the pore size distribution!)

If the basic material has a wide gradation ($D_{b60}/D_{b10} > 10$), D_{b90} in the equation can be replaced with D_{b50} .

⁴ D_{xx} is the size of the holes in a sieve, through which passes xx percent by weight of the material, see Dutch standard NEN 2560.

To avoid overpressure in upward vertical direction (possibly leading to uplift), the filter should be more permeable than the basic material. In this case the permeability coefficient of the geotextile should be more than the permeability coefficient of the basic layer:

$$k_{ng} > \gamma \cdot k_b \quad (31.24)$$

where:

- k_{ng} [m/s] = permeability coefficient of the geotextile
 γ [-] = safety coefficient, dependent on the composition of the basic material:
 $\gamma = 2,5$ for a uniform grain distribution,
 $\gamma = 10$ for a highly graded material ($D_{60}/D_{10} > 10$)
 k_b [m/s] = permeability coefficient of the basic layer

The permeability can be determined with help of a straightforward test, using a glass tube filled with soil, connected with two reservoirs of water - see the book on 'Soil Mechanics' by Verruijt/Van Baars, Section 8.1.

The required length of the bed protection is determined by the depth and the slope of the scour hole h_{max} near the structure (Figure 31-13).

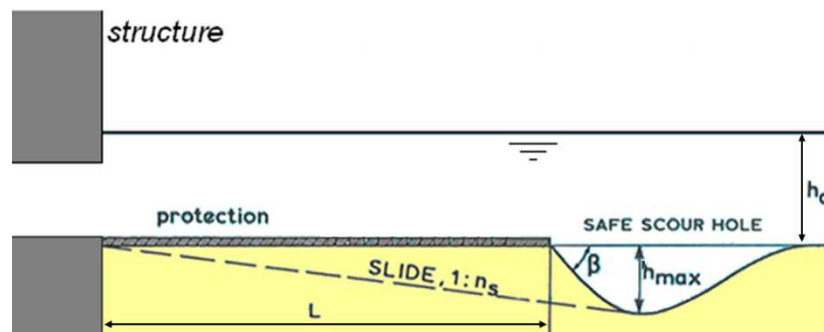


Figure 31-13 The required length of a bed protection near a structure

If the scour hole would become too deep, a critical slope $1:n_s$ will be exceeded, in which case sliding is probable to occur. For normal packed sand this will result in normal sliding, but for loosely packed sand this may lead to liquefaction (*zettingsvloeiing*). The values of n_s can vary very much, but for tentative designs, $n_s \approx 6$ can be assumed for densely packed, or cohesive material, and $n_s \approx 15$ for loosely packed material.

The length of the scour protection should be such, that the sliding plane does not reach the structure, to prevent its undermining. For a first estimate, the required length can be calculated with:

$$L \geq \gamma \cdot n_s \cdot h_{max} \quad (31.25)$$

where:

- γ [-] = safety factor ($> 1,0$)
 $1:n_s$ [-] = average slope of the slide plane
 h_{max} [m] = maximum scour depth

31.6 Literature

- Bligh, W.G. (1915). *Submerged weirs founded on sand*. In: Dams and weirs.
- Breusers, H.N.C. and Raudkivi, A.J. (1991). *Scouring*. Balkema, Rotterdam.
- Calle, E.O.F. and Weijers, J.B. (1994) *Technisch rapport voor controle op het mechanisme van piping bij rivierdijken*. Grondmechanica Delft.
- Hoffmans, G.J.C.M. and Verheij, H.J. (1997). *Scour manual*. Balkema, Rotterdam.
- Huis in 't Veld, J.C. (1987). *Closure of tidal basins*, Delft University press, ISBN 90-6275-287-X.
- Kanning, W. (2013) *The weakest link. Spatial variability in the piping failure mechanism of dikes*. PhD-thesis Delft University of Technology.
- Lane, E.W. (1935). *Security from under-seepage. Masonry dams on earth foundations*. Transactions American Society of Civil Engineers, no. 100.
- Rijn, L.C. van (1993). *Principles of sediment transport in rivers, estuaries and coastal seas. Part 1*. Aqua publications, Amsterdam.
- Schiereck, G.J. & Verhagen, H.J. (2016). *Introduction to Bed, Bank and Shore Protection*, VSSD, ISBN ISBN 978-90-407-1683-6.
- Schweckendiek, T. (2014). *On reducing piping uncertainties. A Bayesian decision approach*. PhD-thesis Delft University of Technology.
- Sellmeijer, J.B. (1988) On the mechanism of piping under impervious structures. PhD-thesis Delft University of Technology.
- Weijers, J.B.A. & Sellmeijer, J.B. (1993). A new model to deal with the piping mechanism. In: Filters in Geotechnical and Hydraulic Engineering.
- WTI 2017 (B. van Bree) (2015). *Achtergrondrapport toetspoot Hoogte II - Bepaling kritiek overslag-/overloopdebiet*. Deltares, Delft.

32. Pile foundations: Compression piles

Section on piles types added in 2019, pile plan added in 2022

32.1 Pile types

Before considering pile foundations, it should be checked whether a shallow foundation would be feasible regarding:

- bearing capacity of the soil to resist the self-weight of the structure and its loads (Chapter 26)
- settlements of the subsoil under the structure (Chapter 28)
- the stability of the shallow-founded structure (Chapter 31)

A shallow foundation is generally (but not always!) easier to construct and less expensive than a pile foundation. If a shallow foundation does not have sufficient bearing capacity, soil improvement can be considered in the form of a replacement of compressive layers by sand. However, if the soil improvement reaches to a level under the groundwater table (1 m or more), it generally becomes too expensive. In cases where a shallow foundation is not feasible, piles should be used (or in a few special cases, pneumatic caissons).

An overview of pile types is presented in Figure 32-1. All the displayed pile types are soil displacing (*grondverdringend*), except for the screwed soil replacing piles (*grondverwijderend*).

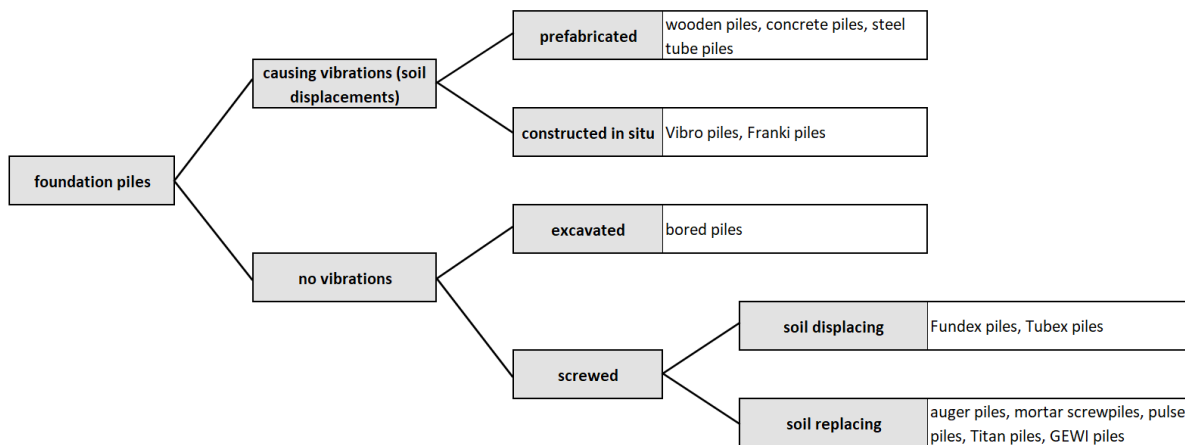


Figure 32-1 Overview of foundation pile types. Only the most common types are included.

There are different installation methods that all have their advantages and disadvantages: driving/drilling (*heien*), pulsing (*drukken*), boring (*boren*), screwing (*schroeven*), vibrating (*trillen*). The choice for installation method and pile type is usually made by the contractor. There are too many pile types to make a simple decision tree. If possible, the least expensive and simplest to install prefab & pre-stressed concrete piles shall be used (these piles are also suitable for tension). However, if no noise or no vibrations are allowed, other pile types should be considered. This is also the case if the cone resistance of the soil is too high for proper driving (especially in gravel layers). The choice for a suitable pile type mainly depends on the following considerations.

Consideration 1: Disturbance of the surrounding soil

A first consideration for selecting pile types is disturbance for the surrounding soil. The installation of piles can lead to undesired or not permitted shock waves and vibrations in the soil. Within a radius of $8D$ (D = pile diameter), the installation of soil displacing piles can lead to excess water pressures (*wateroverspanning*) that can temporarily decrease the bearing capacity of the existing piles. All types of screwed piles result in a release of water pressures (*ontspanning*) within a radius of $4D$ to $6D$. To not influence the bearing capacity of existing piles, the influence sphere of screwed piles should not intersect the soil cylinders around the existing piles (radius $2D$) that contribute to their bearing capacity.

Consideration 2: Disturbance of surrounding buildings and structures

The second consideration usually is whether driving (*heien*) of the piles is permitted, because driven piles have several advantages. Driven piles can be selected if the vibrations or shock waves (under the ground surface) and noise (through the air, above the ground surface) caused by the pile driving are acceptable to the surroundings.

Several of the main advantages of driven piles are:

- the blows of driven piles can be counted ('*kalenderen*') to verify whether the soil layer composition is according to the design conditions
- the soil around the piles is displaced (*verdrongen*), leading to an increase of the bearing capacity
- the pile shaft is relatively insensitive to lateral soil pressures and insensitive for groundwater flow.

Driving piles at a distance of more than 2 m from adjacent buildings or structures usually does not lead to structural damage, but vibrations can cause nuisance and (minor) cracks. If vibrations cannot cause big problems, prefab piles or in situ created piles can be used. If vibrations are expected to cause problems, other pile types should be chosen, like screwed piles, Fundex and Tubex piles, auger piles (*avegaarpalen*), screw-injection piles, etc.

A noise sleeve (*geluidsmantel*) can be used to reduce noise levels with max. 5 dB(A).

Consideration 3: Construction site and transport

The available space, work height, accessibility and obstacles can influence the suitability of certain pile types. For instance, if there is a limited work height, only small equipment can be used, which often leads to a choice for steel tube piles or segment piles. (Horizontal) transport of prefabricated piles restricts their slenderness (= length-diameter ratio) to 80 (like driveability requirements). Because of accessibility reasons for transport over road, the length of prefabricated piles in inner cities can usually not be more than 25 m.

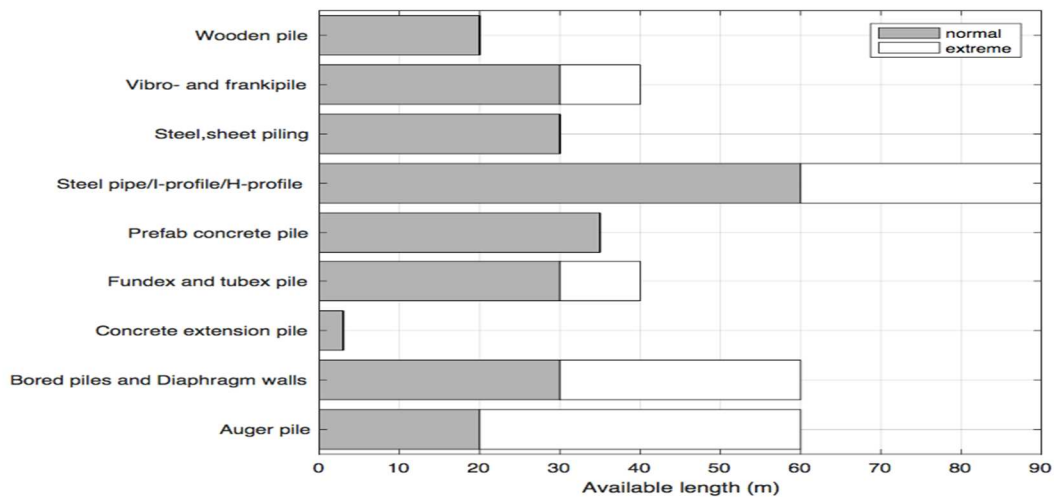


Figure 32-2 Indication of available pile lengths (consult the information of manufacturers for exact data)

Consideration 4: Pile installation equipment

The length of all driven piles is restricted by the piling rig (*heistelling*), more specifically by the length of the guiding system (*makelaar*). The maximum length of a guiding system is about 40 m, of which 5 m is needed for the driving block (*heiblok*), which restricts the length of driven piles to 35 m. Furthermore, not all equipment is suitable for installing piles under inclinations and the force of driving hammers should not damage the pile heads. A universal piling rig for prefab piles is shown in Figure 32-3 to give an impression of its dimensions. The driveability (*heikbaarheid*) of prefabricated piles poses further restrictions to the length of the piles: usually, the slenderness (= length-diameter ratio) should not be larger than 80. An overview of possible lengths per pile type is shown in Figure 32-2.

Consideration 5: Type and magnitude of loading

The suitability for resisting compression forces, tensile forces or both varies per pile type. This also applies to the resistance against bending moments. An overview of all load conditions during the life time of a structure can be helpful to determine which of these load types can occur. If there are only tensile forces, anchor piles can be considered. Several other piles that are suitable for tension are: prefabricated concrete piles, Tubex piles, screwed grout piles and bored piles.

The magnitude of the pile load not only depends on the self-weight and external loads of the superstructure, but also on the distance between the piles (determined by the pile grid). The pile load should be resisted by the surrounding soil (bearing capacity) and by the material properties of the pile itself (strength).

A balance should be found between creating sufficient bearing capacity (by increasing the length of the piles to achieve sufficient tip resistance or increasing the diameter of the piles to achieve sufficient shaft resistance) and reducing the load per pile (by reducing the centre-to-centre distance between the piles).

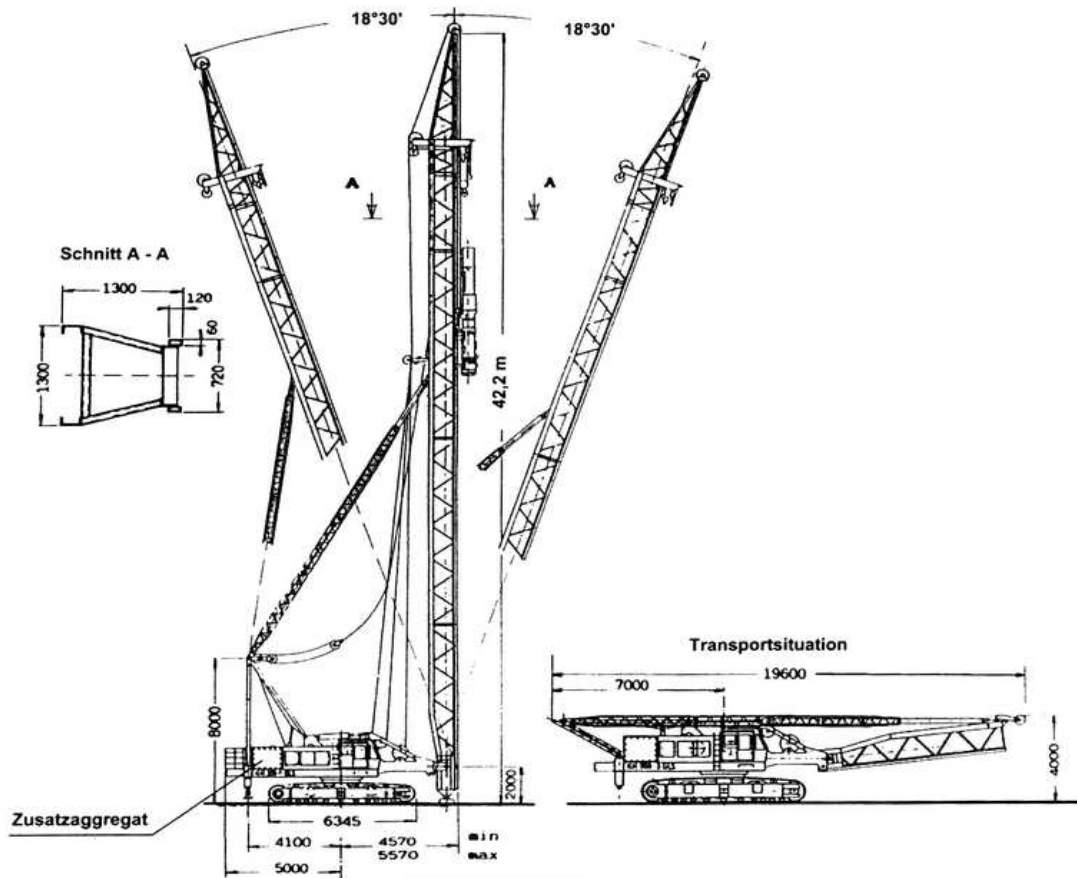


Figure 32-3 A universal piling rig for prefabricated concrete piles (Handbuch der Ramm- Vibrations- und Einpresstechnik, 2012)

The required strength of the piles is determined by the magnitude of its loading, see Figure 32-4 for the strengths of a few common pile types.

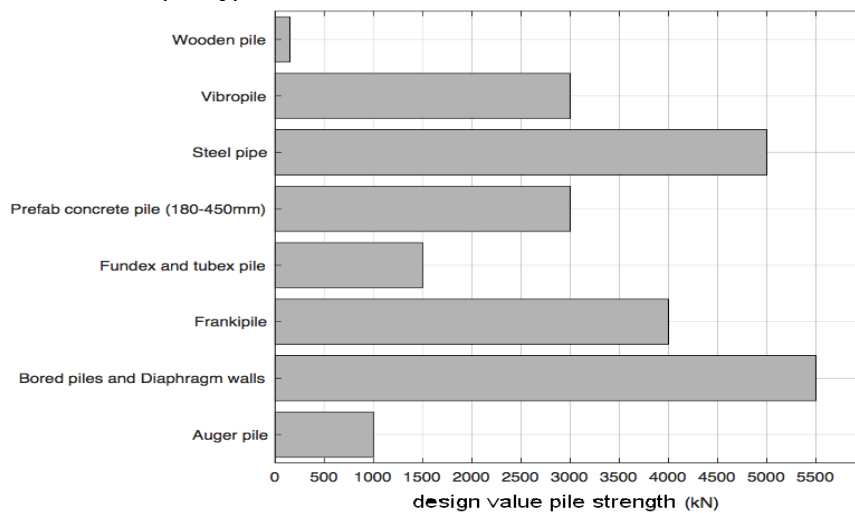


Figure 32-4 Indicative design values for the pile strength (consult the information of manufacturers for exact data)
Notice that the soil bearing capacity is governing in most cases

Consideration 6: Soil composition

The soil composition determines the magnitude of the tip resistance and the shaft friction. In addition, the driveability (*heilbaarheid*) is highly dependent on the soil type. For a pile foundation on a gravel layer, the driveability is a problem, next to the porosity which complicates grout injection. However, screwed injection piles (*mortelschroefpalen*) can be used in gravel. For gravel-sand layers, bored piles (with bentonite injection) can be used with some precautions during construction.

Consideration 7: Suitability to resist tensile forces

If foundation piles need to resist tension forces as well, to prevent uplift in a certain construction or use stage, they should be suitable for that purpose.

32.2 Bearing capacity of compression piles, general theory

The ultimate resistance of a compression pile is determined by the strength of the pile and the bearing capacity of the pile-soil system. The strength of compression piles is determined by the characteristics of the material and shape of the piles (mainly the compressive strength). The strength per pile type can be obtained from the manufacturers of these piles. The strength of prefabricated pre-stressed concrete piles depends on the concrete quality, steel reinforcement and length of the piles and varies from about 500 kN to about 4000 kN. Critical loading can occur during transport and installation (during hoisting (*inhijzen*) or driving (*heien*)), prior to loading by the completed structure.

The bearing capacity of compression piles is determined by both the tip bearing capacity and the shaft bearing capacity:

$$F_{r,max} = F_{r,max;tip} + F_{r,max;shaft} > \Sigma V + G_{pile}$$

where:

$$F_{r,max;tip} = A_{tip} \cdot p_{r,max;tip}$$

and:

$$F_{r,max;shaft} = O_{p,avg} \int_0^{\Delta L} p_{r,max;shaft} dz$$

in which:

$F_{r,max}$	[kN]	= bearing capacity of the pile
$F_{r,max;tip}$	[kN]	= maximum tip resistance force
$F_{r,max;shaft}$	[kN]	= maximum shaft friction force
A_{tip}	[m ²]	= surface area of the tip of the pile
$p_{r,max;tip}$	[kN/m ²]	= maximum tip resistance according to a cone penetration test
$O_{p,avg}$	[m ²]	= average circumference of the pile shaft
ΔL	[m]	= length of the pile
$p_{r,max;shaft}$	[kN/m ²]	= maximum pile shaft friction according to a cone penetration test

Notes

- In case prefab piles with enlarged feet are used, ΔL may not be larger than the height of the enlarged foot H (see Figure 32-4).
- The maximum tip resistance should be limited to 15 MPa

32.3 Preliminary design: Pile resistance according to Prandtl and Meyerhof

If not cone penetration test results are known for the project location, for preliminary designs, the analytical methods of Prandtl and Meyerhof could be used to determine the pile resistance. Both Prandtl and Meyerhof assume a slip plane with a certain shape next to the foot of the pile. To determine the shaft bearing capacity one can simply total the maximum shear forces along the pile's surface.

Prandtl

The maximum tip resistance can be determined analogously to the bearing capacity of a shallow foundation, which is based on a slip plane according to Prandtl. This entails simply using the 2-dimensional solution for 3-dimensional collapse (conservative) and simply disregarding the shear strength, not the weight, of the soil above the foundation plane (conservative).

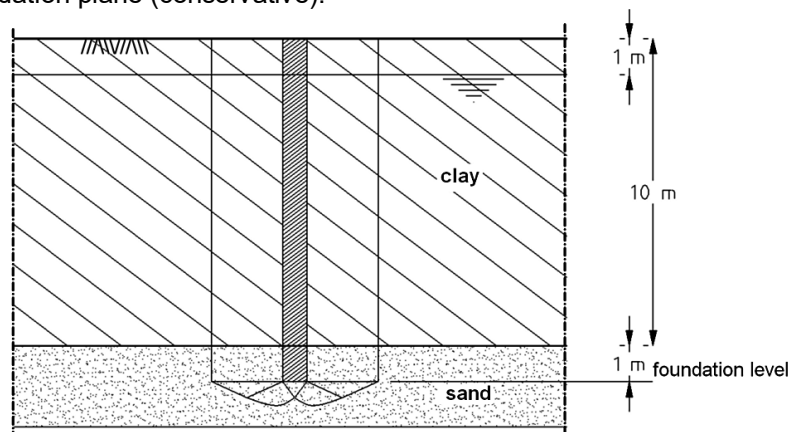


Figure 32-1 Slip planes under a pile according to Prandtl

In this case $p_{r,max;tip}$ can be approached using $\sigma'_{max;d}$ according to Part II, Section 26.2. For pile calculations, the term $0,5 \gamma'_{e;d} B_{ef} N_{\gamma} s_{\gamma}$ is negligible relative to $\sigma'_{v;z;o;d} N_q s_q$. Therefore, the tip resistance can most simply be calculated using:

$$p_{r,max;tip} = \sigma'_{v;z;o;d} N_q s_q$$

Meyerhof

Contrary to Prandtl, Meyerhof assumes that the slip plane developed below and beside the foundations, continues to above the foundation level. According to Meyerhof, one can differentiate between three basic cases, see Figure 32.3.

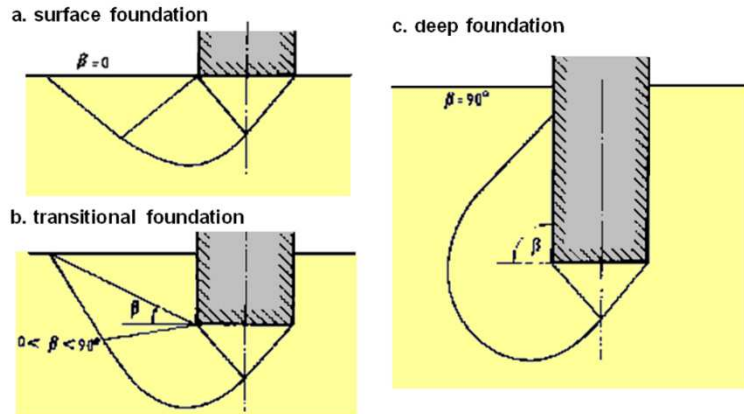


Figure 32-2 Basic cases according to Meyerhof

In his collapse analysis, besides normal stresses, Meyerhof also takes into account the shear stresses that could develop along the top of the slip plane and along the vertical part of the foundation element. This means Meyerhof's factors for the limit bearing capacity, especially in the case of high ϕ values and relatively deep foundations are larger than Prandtl's. This leads to a more favourable, more economical design. The figure below shows the difference between Meyerhof and Prandtl for a foundation pile.

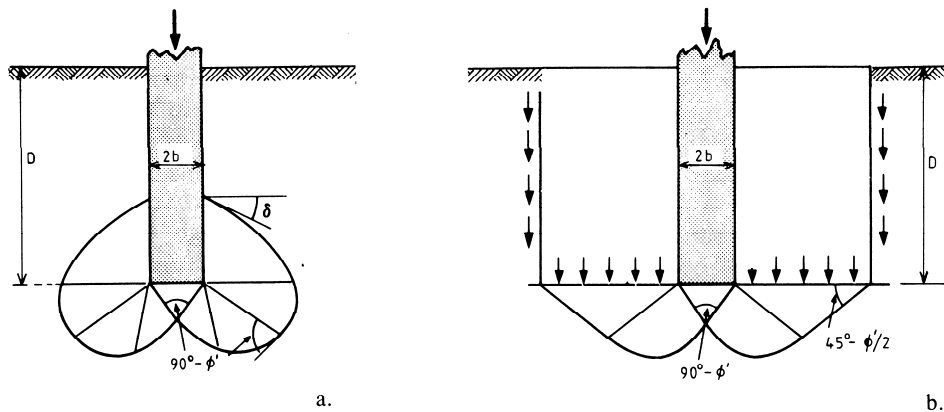


Figure 32-3 Slip planes according to Meyerhof (a) and Prandtl (b)

Figure 32-3 shows that according to Meyerhof, the ground properties above the foundation plane are also of importance when slip planes occur.

Shaft bearing capacity

A simple method to estimate the shaft bearing capacity is to find the cumulative shear stress of all ground layers along the pile:

$$F_{shaft} = O_s \int (\sigma'_v \cdot K \cdot \tan \delta + c') dz$$

In the case of soil displacing piles (prefab driving piles) the ground is tensed horizontally, which means: $K \geq K_0$. In the case of drilled piles, one should assume $K \leq K_0$.

32.4 Bearing capacity, method Koppejan

In the Netherlands, the bearing capacity of a pile is usually determined with soundings (Cone Penetration Tests). A sounding can be perceived as a model test, loading a compression pile beyond the state of collapse. Theoretically sounding entails determining the maximum tip resistance at every level in the ground. Because the size of the slip plane below and beside the pile or sounding cone depends on the dimensions of the foundation area, the cone resistance cannot be directly interpreted as the maximum tip resistance of a pile. Generally, one assumes the slip plane continues to some 0,7 times the pile diameter below the pile and up to approximately 8 times the diameter above the foundation (Figure 32-5).

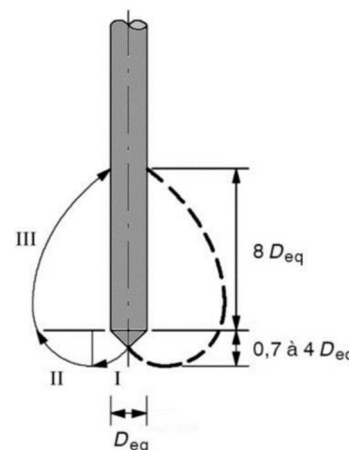


Figure 32-5 Definition of slip planes

The Koppejan method was adopted in the Dutch standard NEN 6743 and more recently in NEN 9997-1 that complies to the Eurocode on Geotechnology.

Maximum tip resistance

In this case the maximum tip resistance can be derived from the sounding using:

$$p_{r,max;tip} = \frac{1}{2} \alpha_p \beta s \left(\frac{q_{c;I;avg} + q_{c;II;avg}}{2} + q_{c;III;avg} \right)$$

in which:

- $q_{c;I;avg}$ [MPa] = the average value of the cone resistances $q_{c;z;corr}$ along section I, from the level of the tip of the pile to a level that is 0,7 D_{eq} to 4 D_{eq} deeper. D_{eq} is the equivalent pile tip diameter (see below). The bottom of section I must be selected between these boundaries, so that $p_{r,max;tip}$ is minimal;
- $q_{c;II;avg}$ [MPa] = the average value of the cone resistances $q_{c;z;corr}$ along section II, from the bottom of section I to the level of the tip of the pile; the value of the cone resistance to be used in this calculation may never exceed that of a lower level;
- $q_{c;III;avg}$ [MPa] = the average value of the cone resistances $q_{c;z;corr}$ along section III, which runs up from the pile tip level to a level of 8 D_{eq} above the pile tip; like for section II, the value used for the cone resistance may never exceed that of a lower level, starting with the value of cone resistance at the top of section II.

In the case of auger piles (*avegaarpalen*), this section must start with a cone resistance equal to or less than 2 MPa, unless the sounding took place within 1 metre of the side of the pile after the pile was placed in the ground;

- D_{eq} [m] = equivalent pile tip diameter:

$$\text{Round pile: } D_{eq} = D$$

$$\text{Square/rectangular pile: } D_{eq} = \sqrt{\frac{4}{\pi}} a \sqrt{b/a}$$

a = width of pile, shortest side

b = width of pile, longest side (with $a \leq b \leq 1,5a$)

- α_p [-] = pile class factor according to Table 32-1, according to NEN 9997-1 since 2017.
- β [-] = factor that takes into account the influence of the shape of the foot of the pile, determined using Figure 32-4 and Figure 32-5;
- s [-] = factor that takes the shape of the cross-section of the foot of the pile into account, see Figure 32-6.

pile class / type	α_p
<ul style="list-style-type: none"> soil displacing placement methods <ul style="list-style-type: none"> - driven piles - driven piles, formed in the soil - screwed piles, formed in the ground - prefabricated screwed piles piles with little soil displacement, such as steel profiles and open steel tubes piles made with soil replacement <ul style="list-style-type: none"> - auger piles - drilled piles - pulsated piles 	0,70 0,70 0,63 0,56 0,70 0,56 0,35 0,35

Table 32-1 Values of the pile class factor α_p

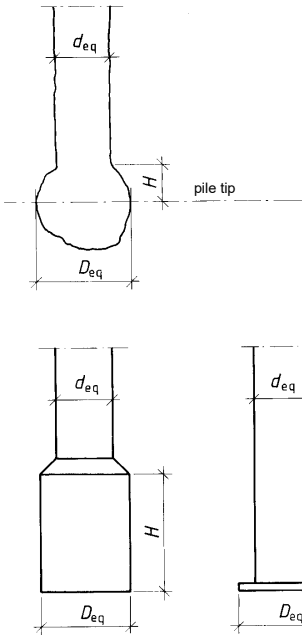


Figure 32-4 Shape of the pile footing

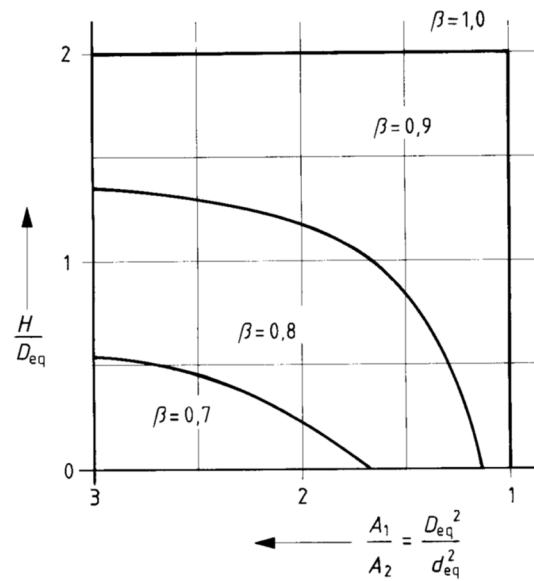


Figure 32-5 Factor for the shape of the pile footing β

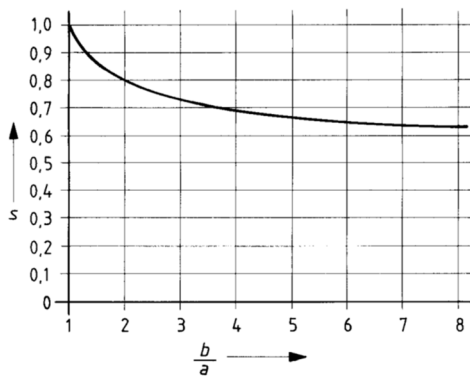
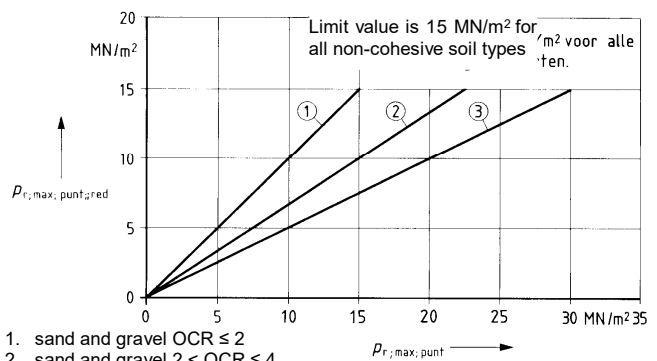


Figure 32-6 Values of the pile footing shape factor s



1. sand and gravel $OCR \leq 2$
2. sand and gravel $2 < OCR \leq 4$
3. sand and gravel $OCR > 4$

OCR = degree of overconsolidation

③ zand en grind $OCR > 4$

OCR = overconsolidatiegraad

Figure 32-7 Value of the maximum tip resistance in sand and gravel

Maximum pile shaft friction

The maximum pile shaft friction derived from the sounding is:

$$p_{r,max;shaft;z} = \alpha_s q_{c;z;a}$$

in which:

- $p_{r,max;shaft;z}$ [MPa] = maximum pile shaft friction at depth z ;
 α_s [-] = factor that takes into account the influence of the method of pile installation. Table 32-2 applies for fine to coarse sand. An additional reduction factor of 0,75 applies for extremely coarse sand. For gravel this reduction factor is 0,50. For clay, silt or peat, Table 32-3 should be used.
 $q_{c;z;a}$ [MPa] = cone resistance, whereby the peaks in the sounding diagram with values larger than 15 MN/m² are removed if these values occur over sections of at least 1 metre and otherwise at values of 12 MN/m².

Pile class / type	α_s
<ul style="list-style-type: none"> ground displacing placement methods: <ul style="list-style-type: none"> - driven smooth prefab concrete pile and steel tube pile with closed tip - pile made in the soil, whereby the concrete column presses directly onto the ground and the tube was driven back out of the ground - in the case of a tube removed by vibration - tapered wooden pile - screwed piles with grout injection or grout mix - without grout piles with little ground displacement <ul style="list-style-type: none"> - steel profiles piles made with ground replacement <ul style="list-style-type: none"> - auger piles - drilled piles - pulsated piles 	<p>0,010</p> <p>0,0014</p> <p>0,0012</p> <p>0,0012</p> <p>0,009</p> <p>0,006</p> <p>0,0075</p> <p>0,006</p> <p>0,006</p> <p>0,005</p>

Table 32-2 Maximum values of α_s in sand and in sand containing gravel

ground type	relative depth z/D	α_s
clay/silt : $q_c \leq 1\text{Mpa}$	$5 < z/D < 20$	0,025
clay /silt : $q_c \geq 1\text{Mpa}$	$z/D \geq 20$	0,055
clay /silt : $q_c > 1\text{Mpa}$	not applicable	0,035
peat	not applicable	0

Table 32-3 Values of α_s for clay, silt or peat

Notes

- The shaft friction factor is in fact the same as the friction value of a CPT-sounding test as mentioned in Part II, Chapter 25 'Soil properties'. The only difference is that for α_s one does not use an average, but for safety's sake, a lower limit value.
- In the case of peat, one assumes no frictional strength because it is not certain that the shear stress doesn't relax to zero due to the creep of the peat.

Maximum negative shaft friction

The effective bearing capacity of the pile is not only determined by the shaft bearing capacity and the tip bearing capacity, but also by the negative shaft friction (*negatieve kleeft*), which influences the bearing capacity unfavourably. Settling soil layers can hang onto the pile, causing a downward shaft friction force. The negative shaft friction depends on the contact area of the shaft, the horizontal soil pressure and the friction coefficient:

$$F_{s,nk} = O_s \sum h \cdot \sigma'_{v,avg} \cdot K_0 \cdot \tan \delta$$

where:

- $F_{s,nk}$ [N] = negative shaft friction
 O_s [m] = circumference of the pile
 h [m] = height of the soil layer that 'hangs' on the pile
 $\sigma'_{v,avg}$ [kPa] = average vertical effective soil stress, per soil layer
 K_0 [-] = neutral soil pressure coefficient
 $\tan \delta$ [-] = friction between soil and concrete

Notes

- For groups of piles the following applies: The negative shaft friction per pile can never be larger than the total weight of the settling ground divided by the number of piles. The weight of the weak ground per pile is therefore an upper limit for the calculation of the negative shaft friction ($\gamma_{m;g} = 1,0$!).
- In ULS, the pile will fail, meaning that it displaces downward. This implies that negative shaft friction will be overruled and should therefore not be taken into account.

32.5 Stiffness

As a rule of thumb, calculation programmes often use a pile length of 2ℓ instead of ℓ . This provides a fairly good estimate of the stiffness of the pile and the soil together.

It is more accurate to divide the pile settlement into two parts:

1. The shortening of the pile
2. The settlement of the tip of the pile

The calculation method for the pile settlement under a load has been normalised (see NEN 6743) and needs to be calculated according to this norm for the final design. The principle of this norm is described briefly below.

Pile shortening

The shortening of the pile $\Delta\ell$ can be estimated using:

$$\sigma = E\varepsilon$$

with:

$$\sigma = \frac{F}{A} \quad \text{and} \quad \varepsilon = \frac{\Delta\ell}{\ell}$$

in which:

$$F \quad [\text{kN}] = \text{load on the pile}$$

$$\ell \quad [\text{m}] = \text{representative pile length}$$

The representative pile length is shorter than the true pile length because the load on the pile is already partly absorbed by the shaft friction, which reduces the compression stress and therefore also the strain in the pile. See the following table for the Youngs' moduli of several pile materials.

Material	<i>E</i> -value
Concrete	$20 \cdot 10^6 \text{ kN/m}^2$
Steel	$200 \cdot 10^6 \text{ kN/m}^2$
Wood	$15 \cdot 10^6 \text{ kN/m}^2$

Table 32-1 Youngs' moduli

Pile tip settlement

For a preliminary design one can assume a rough estimate of the pile tip settlement.

The settlement of the pile tip largely depends on the proportion between the true pile load and the maximum acceptable load on the pile. Due to the coefficients of safety, there is a ratio of about 1,5 between these two. In this case the tip settlement of a ground displacing pile (prefab concrete) is:

$$w_{tip} \approx 2\% \text{ to } 3\% \cdot D_{eq}$$

The tip settlement of drilled and auger piles is roughly twice as large because the ground has not been compressed as for driven prefab concrete piles, but has even been made looser by the drilling. A temporary excavation (deep building site excavation or drill tunnel) near the pile tip will cause relaxation of the soil, a drop of the value of q_c and a serious increase of the pile tip settlement.

For a more accurate description, refer to: NEN 6743 "Berekeningsmethoden voor funderingen op palen, drukpalen" (Calculation methods for foundations on piles, compression piles).

32.6 Pile plan

After the calculation of the required number of piles and their positions, a pile plan has to be made for the actual installation of the piles. The position of all piles should be clearly indicated, including the centre-to-centre distances, see Figure 32-6. Notice the grid lines, the North orientation and the pile properties.

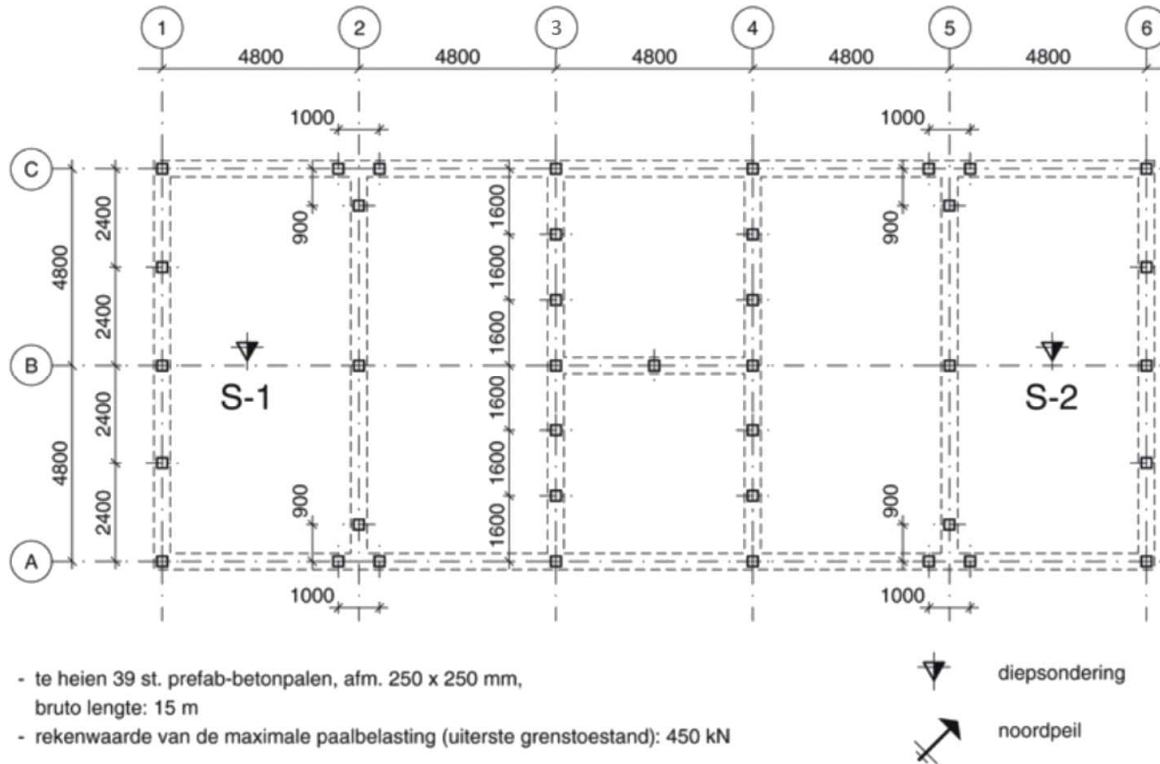


Figure 32-6 Example of a basic pile plan

Figure 32-7 shows an example of a pile plan for a combination of vertical and raking piles.

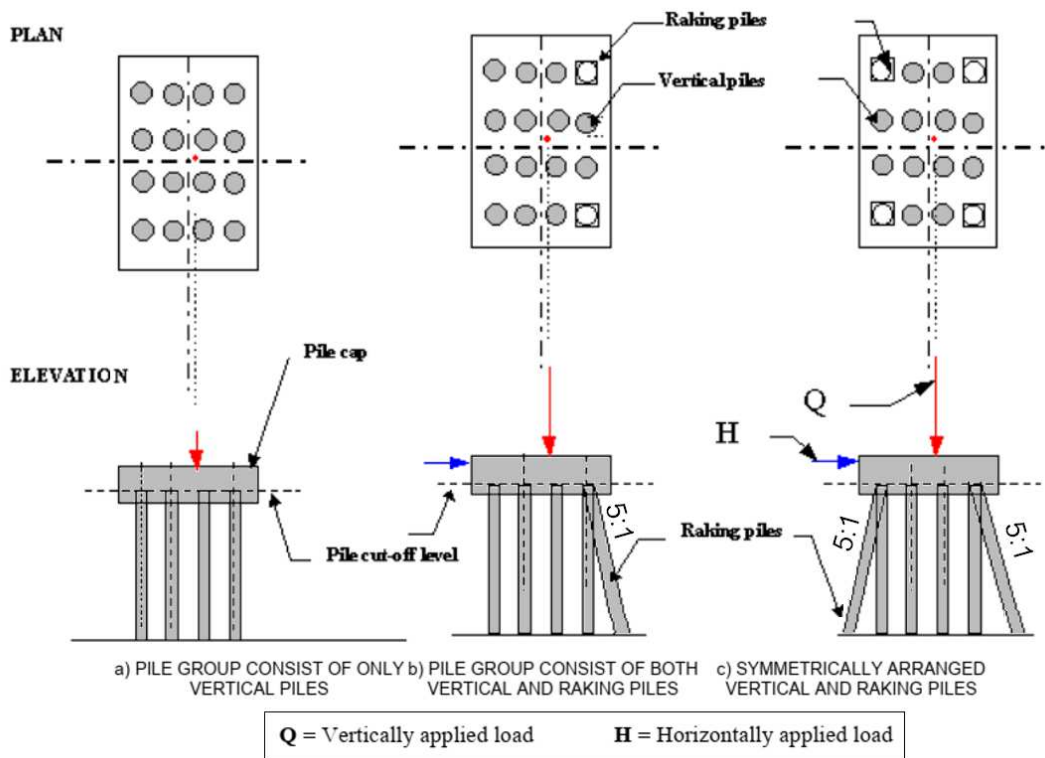


Figure 32-7 Example of a pile plan with raking piles

33. Pile foundations: Tension piles

Major revision: February 2011

In some cases, resulting loads will cause structures to lift, if the present piles are not able to bear the tension forces. For quay walls founded on piles and similar structures, a number of piles will normally be subjected to tension forces where the soil pressure exerts a horizontal force on the structure. Other examples of structures that may need tension piles are the access ramps of tunnels, parts of infrastructure like a railroad that are situated partially deeper than the surrounding ground water level, pump cellars etc. In such cases one needs to compute the maximum admissible tension force, which is the subject of this chapter.

A foundation pile that is subjected to a tension force generates shear stresses along the shaft. Since the tip is not loaded, tip resistance should not be taken into account when calculating the strength. Note that during the construction phase a tension pile can be exposed to compression forces (due to the lowering of the ground water table by well-pointing (*bronbemaling*)). In other cases, e.g., a lock chamber (*sluiskolk*), well-pointing results in the opposite situation. When the chamber is in use, a compression load is exerted on the piles. The same chamber, when it is in maintenance and therefore empty, can be subjected to a buoyancy force under its floor, causing a tensile load on the foundation piles. To determine the shaft friction, it seems logical to use the friction chart (*wrijvingsgrafiek*) of a sounding. This, however, is not possible without restrictions since the friction as a result of tension is less than the friction due to compression, see Figure 33-1. This reduction of the shear stress is a result of the fact that in case of compression the vertical soil pressure increases around the mantle of the sounding pipe which leads to an increased shaft friction, while in case of tension the vertical soil pressure decreases.

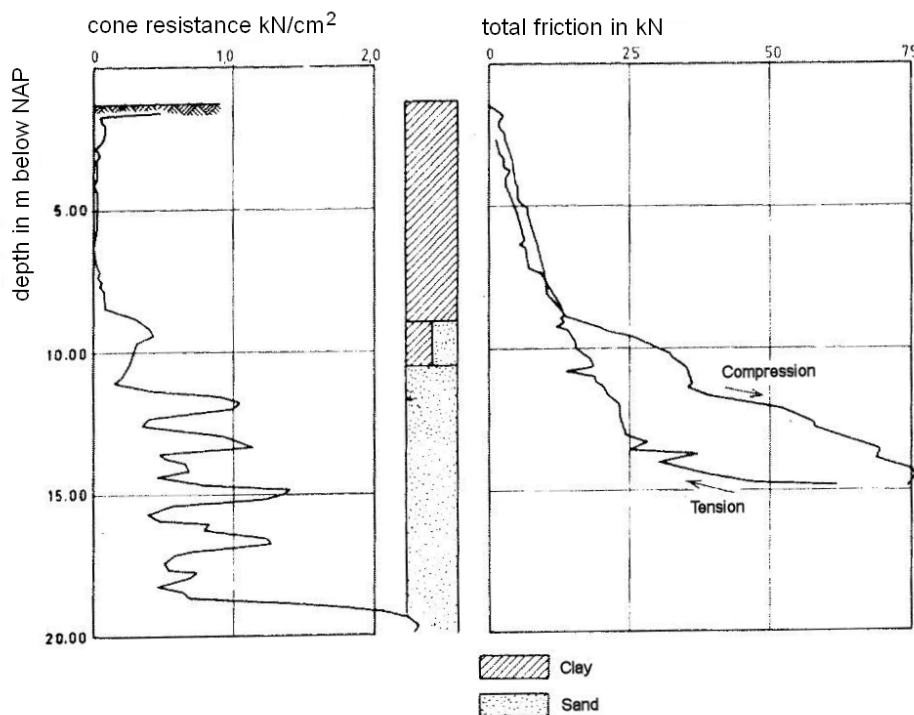


Figure 33-1 Friction chart of a sounding illustrating the difference between pressing and pulling of the sounding pipe.

As can be seen in the figure above there is not much difference in the clay layer, but there is a significant difference visible in the sand layer.

33.1 Bearing capacity of tension piles: comparison with compression piles

The pile resistance calculation of tension piles resembles that of compression piles. For the bearing capacity of the pile-soil system, however, there are some differences that should be kept in mind:

1. Tension piles only generate bearing capacity as a result of shaft friction, not tip resistance;
2. Tension piles have smaller coefficients for shaft friction than compression piles;
3. Tension piles are most commonly used in excavated construction sites to withstand the buoyancy force underneath the structure after construction. As a result of the excavation of the construction site, the soil pressure is reduced due to a weight reduction. Hence the effective soil pressure is also reduced and thus the value of q_c and the friction force on the pile are reduced;
4. Due to the tensile force exerted by the tension piles, the vertical effective soil pressure is reduced and as a result also the value of q_c , see Figure 33-1;
5. Not only should a single pile be tested for possible slip, but also a group of piles should be tested as the piles may influence each other in an unfavourable way. If the piles are placed in a group, the zones from which each pile receives its strength may overlap thus reducing the strength of each pile. This is checked with the clump weight (*kluitgewicht*) criterion, which states that the tensile force of a pile can never be larger than the weight of the soil that is, on average, present between the piles, see also Figure 33-2;
6. The safety factors used in the computation are larger than in case of compression piles. This is a result of the fact that inaccuracies in determining the shaft friction are larger than when determining the tip resistance. These inaccuracies are enhanced further as a result of the effect described in statement 4;
7. The dead-weight of the pile, usually the underwater weight, has a positive effect on the strength of the tension pile.

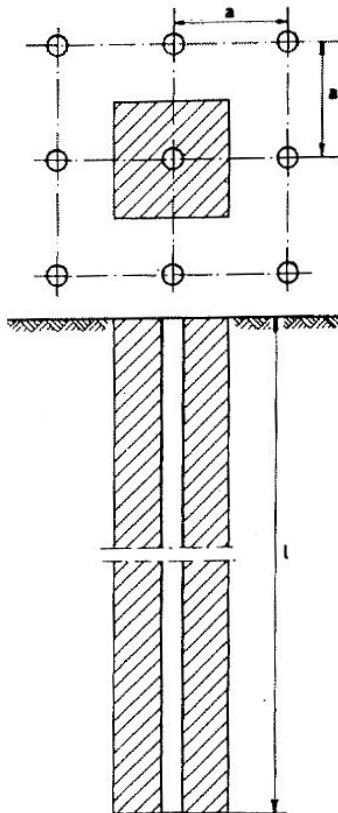


Figure 33-2 Maximum occurring friction in pile groups

As a result of statements 1-6 the tensile capacity of a pile is much less than the compression capacity of a pile. No standards exist for the computation of tension piles. Usually, the rules according to the CUR-report 2001-4 "Design rules for tension piles" are used, but they are disputable.

Particularly for very large tension forces grout anchors are used instead of tension piles. For this the reader is referred to Section 39.5. In the remainder of this chapter the method for computing the strength of a single tensile pile is described, after which the method for checking the clump criterion is explained in order to establish whether a group of piles is stable or not.

33.2 Bearing capacity: cone resistance method

For the computation of the strength of a tension pile many influences have to be taken into account. For instance, the reduction of the shaft friction due to reduction of the vertical effective soil pressure as a result of the exerted tensile force and the excavation works. This leads to a complex computation method. Hence, in general, the strength of tension piles is computed using a computer programme that determines the maximum shaft friction of the pile. For a first estimate of the strength of tension piles, the cone resistance method, can be used, or other methods like the slip method and the method according to Begemann. This Section explains the cone resistance method as applied in the Netherlands, also known as the q_c -method, as described in CUR report 2001-4 and Eurocode 7 (NEN 9997-1+C1). The most important reason for choosing the q_c -method is that it does not include the soil-pressure-coefficient (K) and the angle of internal friction (φ) of the soil, since these parameters are difficult to determine.

The maximum tensile force that a pile can resist without slipping is computed with the following equation:

$$F_{r,tension,d} = O_{p,mean} \cdot \int_{z=0}^L \alpha_t \cdot f_1 \cdot f_2 \cdot q_{c,z,d} dz \quad (33.1)$$

where:

$F_{r,tension,d}$	[kN]	=	design value for the tensile strength of the pile-soil combination
α_t	[-]	=	pile class factor (<i>paalklassefactor</i>)
$O_{p,mean}$	[m]	=	average circumference of the pile shaft
L	[m]	=	length over which shaft friction is computed
z	[m]	=	depth
f_1	[-]	=	pile installation factor at depth z ($f_1 \geq 1$)
f_2	[-]	=	cone resistance reduction factor at depth z ($f_2 \leq 1$)
$q_{c,z,d}$	[kN/m ²]	=	design value of the cone resistance at depth z

The parameters are explained below.

Cone resistance

The design value for the cone resistance is determined per soil layer, using the following equation:

$$q_{c,z,d} = \frac{q_{c,z,rep}}{\gamma_{m,b,4} \cdot \gamma_{m,var,qc}} \quad \text{where } q_{c,z,rep} = \frac{q_{c,z,a}}{\xi} \quad (33.2)$$

where:

$q_{c,z,d}$	[MN/m ²]	=	design value for the cone resistance at depth z
$q_{c,z,rep}$	[MN/m ²]	=	representative value for the cone resistance at depth z
$q_{c,z,a}$	[MN/m ²]	=	value of the cone resistance at depth z in the sounding
ξ	[-]	=	correlation factor, depending on the number of performed soundings, the number of piles and the stiffness of the structure (see Table 33-1)
$\gamma_{m,b,4}$	[-]	=	resistance factor for tension piles (= 1,35)
$\gamma_{m,var,qc}$	[-]	=	factor for variable loads (see Figure 33-4)

If the cone resistance in the sounding exceeds 12 MPa, the value of 12 MPa should be used for $q_{c,z,max}$, unless the layer for which the cone resistance exceeds 12 MPa is at least one meter thick. In that case the cone resistance of the sounding can be used with a maximum of 15 MPa.

Cone resistance after excavation or in case of over-consolidation

If an excavation takes place after the soundings were made or if there is over-consolidation of the soil, the design value for the cone resistance has to be corrected for the reduction in cone resistance that is caused by these processes. In case of an excavation this is done as follows:

Piles driven after excavation or with a high vibration level:

$$q_{c,z,exca,max} = q_{c,z,max} \cdot \frac{\sigma'_{v,z,exca}}{\sigma'_{v,z,0}} \leq 12 \text{ or } 15 \text{ MPa} \quad (33.3)$$

where:

$q_{c,z,exca,max}$	[MN/m ²]	=	corrected cone resistance at depth z after excavation
$q_{c,z,max}$	[MN/m ²]	=	value of the cone resistance at depth z in the sounding
$\sigma'_{v,z,exca}$	[kN/m ²]	=	vertical effective soil pressure at depth z after excavation
$\sigma'_{v,z,0}$	[kN/m ²]	=	vertical effective soil pressure at depth z before excavation

- Piles driven before excavation or with very low vibration level:

$$q_{c,z,exca,max} = q_{c,z,max} \cdot \sqrt{\frac{\sigma'_{v,z,exca}}{\sigma'_{v,z,0}}} \leq 12 \text{ or } 15 \text{ MPa} \tag{33.4}$$

If the corrected cone resistance is computed with equations (33.3) and (33.4), equation (33.2) should be used to determine the design value of the cone resistance at depth z by replacing $q_{c,z,max}$ with $q_{c,z,exca,max}$.

- In case of over consolidated soil and the piles are driven using vibrations the cone resistance is corrected using the following equations:

$$q_{c,z,nc,max} = q_{c,z,max} \cdot \sqrt{\frac{1}{OCR}} \leq 12 \text{ or } 15 \text{ MPa} \tag{33.5}$$

where:

- $q_{c,z,nc,max}$ [MN/m²] = cone resistance at depth z corrected for over consolidation
- $q_{c,z,max}$ [MN/m²] = value of the cone resistance at depth z in the sounding
- OCR [-] = factor expressing the degree of over-consolidation

Again, the design value of the cone resistance at depth z is computed using equation (33.2), now replacing $q_{c,z,max}$ with $q_{c,z,nc,max}$.

Material factor for variable loads (γ_m)

Alternating loading, meaning alternately a compression force and a tensile force or a large tensile force and a small tensile force, on a structure leads often to the normative loading situation. In Figure 33-3 the test results of a tensile test (*trekproef*) with alternating loading are shown. As one can see, the effect of the alternating loading is that the pile head will rise when a large tensile force is exerted and will lower again when the tensile force is reduced. Alternating loading, however, will cause a gradually rise of the pile head, which is called creep. Tension piles are very sensitive for creep, which is therefore the most common short-coming of this type of piles.

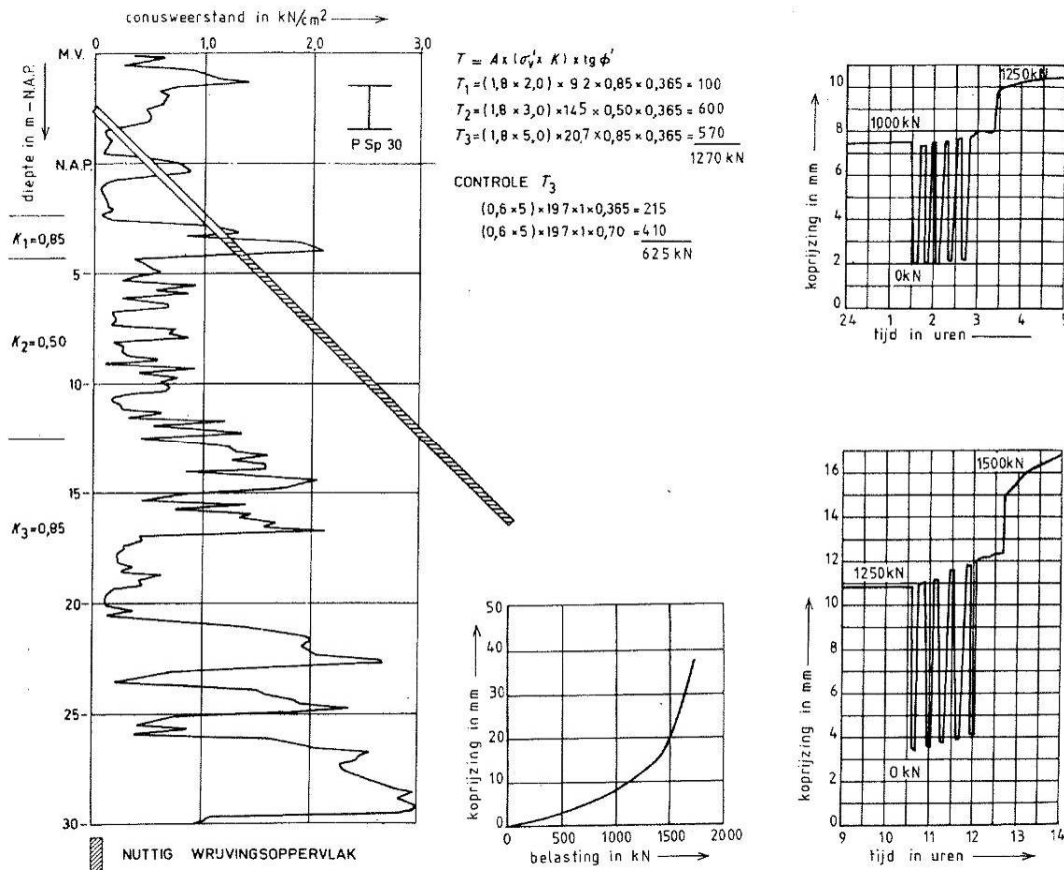


Figure 33-3 Results of a test load on a prefabricated concrete pile (tension)

The effects of alternating loading are taken into account with the material factor for variable loads, which is a function of the maximum and minimum force exerted on the tension pile, see the figure below. In case of tension the force has a positive value; in case of compression the force is assumed to be negative. The maximum value of the material factor for variable loads is 1,5.

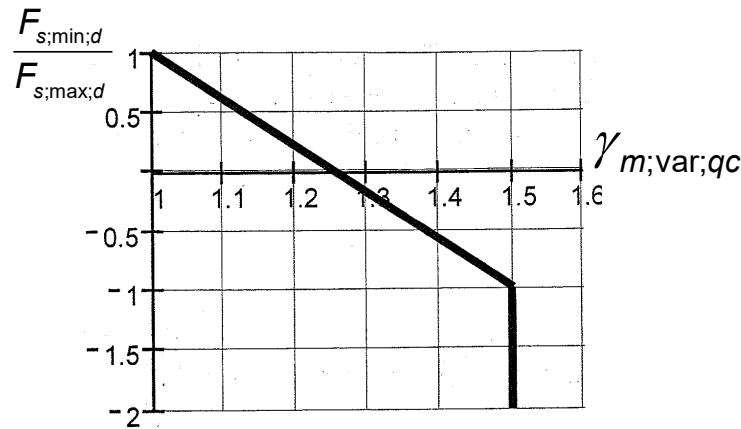


Figure 33-4 Factor for variable loads

The corresponding equation reads:

$$\gamma_{m,var;q_c} = 1,0 + 0,25 \cdot \frac{F_{s,max;d} - F_{s,min;d}}{F_{s,max;d}} \quad \text{where } \gamma_{m,var;q_c} \leq 1,5 \quad (33.6)$$

where:

$\gamma_{m,var;q_c}$	[-]	= material factor for variable loads
$F_{s,max;d}$	[kN]	= maximum design value of the exerted force
$F_{s,min;d}$	[kN]	= minimum design value of the exerted force

Influence of the number of soundings and installed piles

The influence of the number of performed soundings, the number of installed piles and the stiffness of the construction is expressed by the factor ξ . Table 33-1 is used to determine this factor.

m	n						
	1	2	3	4	5	10	>10
1 or 2	1,39	1,32	1,30	1,28	1,28	1,27	1,25
> 3	1,29	1,21	1,18	1,16	1,15	1,15	1,13

Table 33-1 Values for the correlation factor ξ . This table applies to both compression and tension piles!

where:

m	[-]	= number of piles installed underneath a structure
n	[-]	= number of performed Standard Penetration Tests (SPT)

Pile installation factor (f_1)

When piles are driven into the ground the soil is compressed under the tip and along the shaft. As a result, the soil becomes stiffer, hence the cone resistance increases. The stiffening of the soil is taken into account via the pile installation factor (f_1).

$$q_{c,z,1} = f_1 \cdot q_{c,z,d} \quad (33.7)$$

where:

$q_{c,z,1}$	[MN/m ²]	= corrected design value for the cone resistance after pile installation
q	[MN/m ²]	= design value for the cone resistance before pile installation
f_1	[-]	= pile installation factor

Notice that equation (33.7) already is integrated in equation (33.1).

The pile installation factor can be computed as follows:

$$f_1 = e^{3 \cdot \Delta R_e} \quad \text{where} \quad \Delta R_e = \frac{\sum_1^n \Delta e}{(e_{\max} - e_{\min})} \quad (33.8)$$

$$\text{and} \quad \sum_1^n \Delta e = -\frac{r-6}{5,5} \cdot \frac{1+e_0}{50} \quad \text{and} \quad R_e = 0,34 \cdot \ln \left(\frac{q_{c,z}}{61 \cdot (\sigma'_{v,z,0})^{0,71}} \right) \quad (33.9), (33.10)$$

where:

f_1	[-]	=	pile installation factor
R_e	[-]	=	initial value of the relative density of the soil
ΔR_e	[-]	=	increase of the relative density of the soil as a result of pile installation
Δe	[-]	=	decrease of the void ratio within a radius of $6 D_{eq}$ of the pile ⁵
e_{\max}	[-]	=	maximum void ratio of the soil (0,80 in NL)
e_{\min}	[-]	=	minimum void ratio of the soil (0,40 in NL)
e_0	[-]	=	initial void ratio of the soil
n	[-]	=	number of piles within a radius of $6 D_{eq}$
r	[-]	=	distance, expressed in D_{eq} , from an arbitrary pile to the pile that is regarded ⁶
$q_{c,z}$	[kN/m ²]	=	initial value of for the cone resistance
$\sigma'_{v,z,0}$	[kN/m ²]	=	initial value of the effective stress at depth z

In Figure 33-5 the relative density of soil is given as a function of the cone resistance for different effective stresses. The influence area of a pile with respect to the increase of the relative density is a cylindrical area with a maximum radius of $6 D_{eq}$.

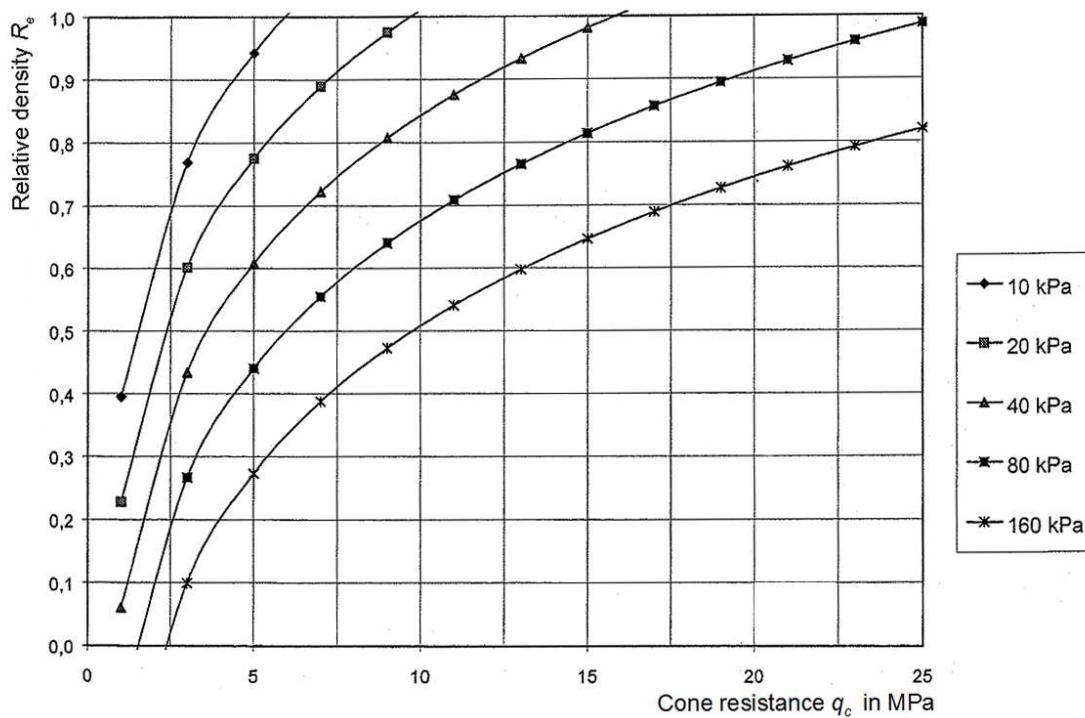


Figure 33-5 Relative density as a function of the cone resistance for different effective stresses.

If one uses a pile installation factor that is larger than one, one should perform standard penetration tests after installation to check whether the effective soil pressure indeed has increased or not. In the latter case it is not allowed to use a value larger than 1,0 for the pile installation factor. In practice, it is inconvenient to change the design during construction, therefore f_1 is assumed to be 1,0 in most cases.

⁵ $D_{eq} = 1,13 \cdot D_{\square}$, so for a pile 400x400 mm $D_{eq} = 1,13 \times 400 = 452$ mm.

⁶ When $r > 6$, the pile will not be affected by the other pile(s), therefore the maximum value for $r = 6$. This parameter, in combination with equation (33.9), enables to distinguish between centre piles, edge piles and corner piles.

In the following cases, the pile installation factor is always 1,0:

- For single piles;
- In clay layers;
- If soil investigations are performed after the installation of the pile(s) with ground-displacing installing methods.

Cone resistance reduction factor (f_2)

The tensile load on a pile group reduces the effective soil pressure in the soil layers from which a single pile receives its tensile strength. Since for piles placed in a group these zones may overlap, the strength of each pile is thus reduced even more. This reduction is taken into account by applying a reduction factor f_2 to the cone resistance. In case of a single pile the reduction factor f_2 has a value of 1,0. The value of the cone resistance reduction factor is always 1,0 for clay, in sand the value may become less than 1,0.

The reduction of the effective soil pressure is taken into account by dividing the soil along the length of the pile into layers of for example 0,5 m thick. The factor f_2 is subsequently computed per layer using the following equation:

$$f_{2,i} = \frac{-M_i + \sqrt{M_i^2 + (2 \cdot \sigma'_{v,z,d,0,i} + \gamma'_{d,i} \cdot d_i) \cdot \left(2 \cdot \sigma'_{v,z,d,0,i} + \gamma'_{d,i} \cdot d_i - 2 \cdot \sum_{n=0}^{i-1} T_{d,n} \right)}}{2 \cdot \sigma'_{v,z,d,0,i} + \gamma'_{d,i} \cdot d_i} \quad (33.11)$$

$$\text{With: } M_i = \frac{f_{1,i} \cdot O_{p,i} \cdot \alpha_t \cdot q_{c,z,d,i} \cdot 1000 \cdot d_i}{A} \quad \text{and} \quad T_{d,i} = M_i \cdot f_{2,i} \quad (33.12), (33.13)$$

Where:

$f_{2,i}$	[-]	= cone resistance reduction factor for layer i
M_i	[kN/m ²]	= reduction of the vertical effective soil pressure in layer i
$\sigma'_{v,z,d,0,i}$	[kN/m ²]	= vertical effective soil pressure on top of layer i
$\gamma'_{d,i}$	[kN/m ³]	= design value of the effective volumetric weight of the soil in layer i
d_i	[m]	= thickness of layer i
$T_{d,i}$	[kN/m ²]	= maximum possible friction between the pile and the soil
$f_{1,i}$	[-]	= pile installation factor for layer i
$O_{p,i}$	[m]	= average circumference of the pile in layer i
α_t	[-]	= pile class factor as indicated in Table 33-2 or Table 33-3
$q_{c,z,d,i}$	[MN/m ²]	= average cone resistance in layer i
A	[m ²]	= influence surface area of the pile

The vertical effective soil pressure can be computed using the design value of the volumetric mass of the soil:

$$\sigma'_{v,z,d,0,i} = \sum_{n=0}^{i-1} \gamma'_{d,n} \cdot d_n \quad \text{Above the water table: } \gamma'_d = \frac{\gamma}{\gamma_{m,g}} \quad (33.14)$$

$$\text{Beneath the water table: } \gamma'_d = \frac{\gamma}{\gamma_{m,g}} - \gamma_{water}$$

Where:

$\sigma'_{v,z,d,0,i}$	[kN/m ²]	= vertical effective soil pressure on top of layer i
$\gamma'_{d,i}$	[kN/m ³]	= design value of the effective volumetric weight of the soil in layer i
d_i	[m]	= thickness of layer i
$\gamma_{m,g}$	[-]	= material factor for the weight of the soil
γ_w	[kN/m ³]	= volumetric weight of water

The material factor for the weight of the soil ($\gamma_{m,g}$) is to be taken 1,0 if the weight of the soil works favourable on the pile's maximum admissible tension force and 1,1 if the weight of the soil works unfavourable on the pile's maximum admissible tension force. As a result the material factor for the weight of the soil will be 1,0 from ground level to the excavation level and 1,1 beneath the excavation level.

Effective friction area of the pile shaft ($O_{p,mean}$)

If a tensile force is exerted on a foundation pile, deformation of the soil occurs (in the direction of the pile axis), causing a friction force along the pile shaft. The magnitude of this friction force depends, among other things, on the amount of deformation. The deformation process depends on the soil type, e.g. small deformations in sand and large deformations in clay. Since the soil structure consists of several layers with a different deformation process not all layers contribute to the useful friction area of the pile shaft. In Figure 33-3 the useful friction area is shaded.

When determining the useful friction area of the pile shaft one should keep the following aspects in mind:

1. As long as the subsoil consists of relative homogeneous sand, the circumference of the pile shaft over the whole length of the pile is considered to be part of the useful friction area;
2. If the upper layers consist of clay or peat with a relative homogeneous sand layer beneath these layers, only the contact surface area pile/sand is considered to be the useful friction area;
3. If the subsoil consists of two (or more) qualitatively different types of sand (density and composition) the whole contact surface area pile/sand is regarded as useful friction area. However one should also account for the fact that:
 - when the deformation is too small in the qualitatively poorer sand layer(s) only part of the shear stresses will develop;
 - when the deformation is too large in the qualitatively good sand layer(s) only the residual shear stresses will occur (12 or 15 MPa);
4. When in a certain section of the subsoil (thin) clay layers occur one should account for the consequences of possible consolidation (as a result of the driving or the occurrence of a tensile force), such as relaxation or the deformation of the sand layers.

Pile class factor (α_t)

The influence of the installation process on the shaft friction resistance is taken into account with the pile class factor (α_t). The magnitude of the pile class factor depends on the roughness of the shaft and the installing method. In Table 33-2 the pile class factors are given for piles driven in sand and sand containing gravel. For other pile types, reference is made to Table 7d of Eurocode 7 (NEN9997-1+C1).

Pile class/type	α_t
Ground displacing installing methods:	
- driven smooth prefab concrete pile and steel tube pile with closed tip ¹⁾	0,007
- pile made in the soil, whereby the concrete column directly presses onto the ground and the tube is driven back (<i>teruggeheid</i>) out of the soil ²⁾	0,012
- ditto, in case the tube is removed by vibration	0,010
- tapered wooden pile	0,012
Screwed piles:	
- with grout injection or mixing	0,009
Piles with little ground displacement:	
- driven steel profiles	0,004
Soil removing piles:	
- drilled piles (and auger piles)	0,0045
¹⁾ The base of a tube pile with a closed tip shall not exceed 10 mm beyond the tube protruding.	
²⁾ For this type of pile the diameter of the base may in principle be 30-50 mm larger than the outside diameter of the casing.	

Table 33-2 Maximum values for the pile class factor in sand and sand containing gravel (CUR 2001-4)

The contribution of cohesive layers to the shaft friction resistance is much smaller. Table 33-3 shows the pile class factors for piles in cohesive layers. As a conservative value for clay, $\alpha_t = 0$ can be assumed. It should be noticed that the water pressure in cohesive layers needs some time to adjust after soil displacement. This implies that the shaft resistance in clay needs some time to develop after installation.

For piles that predominantly derive their tensile bearing capacity from sand layers, the contribution of clay/silt layers may be taken into account as well. In these cases, the values for α_t in Table 33-3 should be reduced with 50% to account for the difference in the stress-strain behaviour of sand and cohesive soils.

Soil type	Relative depth z/D_{eq}	α_t ³⁾
Clay/silt: $q_c \leq 1$ Mpa	$0 < z/D_{eq} < 20$	0,02
Clay/silt: $q_c \leq 1$ Mpa	$z/D_{eq} > 20$	0,025
Clay/silt: $q_c > 1$ Mpa	not applicable	0,025

³⁾ In the case that piles derive their tensile resistance for most part from sand layers, only half of the values for α_t may be taken into account! This is because of the difference in stress-strain behaviour of sand and clay/silt.

Table 33-3 Maximum values for the pile class factor in clay/silt

33.3 Bearing capacity: clump criterion

Not only should one check whether the tension pile will fail due to sliding and whether it can be pulled "clean" out of the ground. One should also verify if a pile, including the surrounding soil, cannot be pulled out of the ground. This is achieved by verifying that the clump criterion is met. The clump criterion implies that the tensile force on a pile can never be larger than the weight of the pile plus the clump of ground around a pile. For a group of piles, the average weight of the ground situated around a pile between the other piles should be used.

The clump criterion is computed using the following equation:

$$F_{clump} = F_{r,tension,max,d} = (V_{cone} + V_{cylinder} - V_{pile}) \cdot \gamma'_{d,soil} + V_{pile} \cdot \gamma'_{d,concrete} \quad (33.15)$$

where:

F_{clump}	[kN]	= maximum tensile force the soil can absorb
$F_{r,tension,max,d}$	[kN]	= maximum tensile force the soil can absorb
V_{cone}	[m ³]	= volume of the conical soil volume at the tip of the pile
$V_{cylinder}$	[m ³]	= volume of the schematically cylinder-shaped soil volume near the pile tip, below the conical part
V_{pile}	[m ³]	= volume of the pile (the part under the ground surface)
$\gamma'_{d,soil}$	[kN/m ³]	= design value for the effective specific weight of the soil
$\gamma'_{d,concrete}$	[kN/m ³]	= design value for the underwater weight of the pile

Since the soil can absorb a tensile load only once, it is not allowed for the zones to overlap. The maximum influence area of a pile is a cylindrical area with a radius of $3 D_{eq}$.

In order to be able to determine the volumes of the cone and cylinder in Equation (33.15), the top angle should be known. This angle depends on the pile type and the position of a pile within the pile group. As a result of the influence of other piles the top angle of piles within a group will be larger than for piles along the edge of the group, see also Table 33-4. This means that the shape of the clump around the pile is asymmetric for edge piles, at the outer edge the top angle is smaller and therefore the volume of the clump is larger than at the inner side of the edge pile due to the influence of the other piles (larger top angle).

Pile type	Half top angle of piles within a group or the inner side of edge piles [°]	Half top angle of the outer side of edge piles [°]
Ground displacing installing methods	45	30
Piles with little ground displacement	$2/3 \varphi'$	$1/2 \varphi'$
Soil removing piles	$2/3 \varphi'$	$1/2 \varphi'$

(φ' = angle of internal friction of the soil at the pile tip)

Table 33-4 Top angle used for determining the clump volume

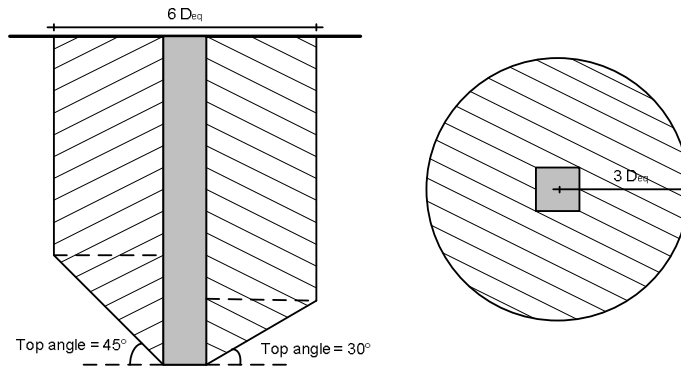


Figure 33-6 Clump volume of tension piles

As said, clumps around piles cannot overlap, so if the centre-to-centre distance of the piles is less than the maximum clump diameter $6 D_{eq}$ (Figure 33-7), the clumps will be smaller than a cylinder around the pile with diameter $6 D_{eq}$. Therefore, the shape of these clumps will actually be less round (partly straight planes). The clump will even be completely box-shaped if the centre-to-centre distance is small enough ($< 6/\sqrt{2} \cdot D_{eq}$). In this last case, the part of the clump at the tip of the pile has a truncated pyramid shape.

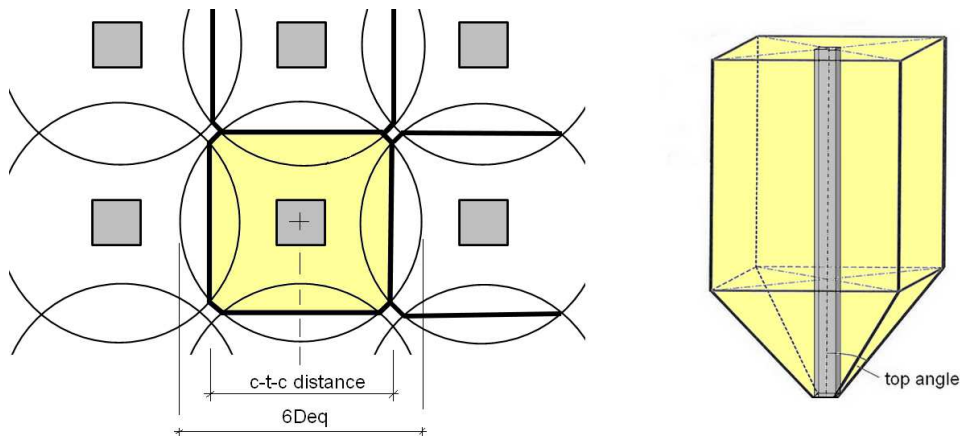


Figure 33-7 Different clump shape for dense pile groups

Self-weight of the pile

Since the self-weight of a tension pile is working favourably for its strength it may be taken into account as follows:

$$W_{pile,d} = V_{pile} \cdot \gamma'_{pile,d} \quad \text{where} \quad \gamma'_{pile,d} = \frac{\gamma_{pile}}{\gamma_{m,g}} - \gamma_{water} \tag{33.16}$$

Where:

- $W_{pile,d}$ [kN] = design value of the pile's self-weight
- V_{pile} [m³] = pile volume (see Appendix D for the volumes of cones and pyramids)
- $\gamma'_{pile,d}$ [kN/m³] = design value for the effective volumetric weight of the pile
- γ_{pile} [kN/m³] = volumetric weight of the pile
- $\gamma_{m,g}$ [-] = material factor for the pile weight (1,1)
- γ_{water} [kN/m³] = volumetric weight of water

The design value for the dead weight of the pile can be added to the maximum design value for the tensile force of the soil computed according to Equation (33.1).

33.4 Edge piles

Particularly around an open access road to a tunnel, edge piles sometimes have larger tensile loads than the other piles. In this case, to determine the tensile load capacity, one must take into account:

- Limited reduction of the sounding resistance along the edge of the excavated building site due to the excavations.
- Group action based on the average pile tensile forces in a cross-section and thus not based on the tension in the edge piles themselves.
- Possible horizontal forces in sheet piling next to the pile.

33.5 Stiffness

This manual does not go into the description of the stiffness/flexural behaviour of tension piles. If grout anchors are used, they must be stressed after they have been placed, so that the subsoil does not float on the groundwater but builds up effective soil pressure and thereby responds more stiffly.

33.6 Literature

Civieltechnisch Centrum Uitvoering Research en regelgeving, *Cur-rapport 2001-4: "Ontwerpregels voor trekpalen"*, Gouda, juni 2001, Curnet.

Keverling Buisman, A.S., *Grondmechanica*, Delft, 1944, Waltman.

Verruijt, A., revised by S. van Baars, *Soil Mechanics*, Delft, 2005, VSSD.

34. Pile foundations: Laterally loaded piles

improved: February 2016

34.1 Introduction

The forces on the foundation of buildings predominantly work in vertical direction. Therefore, in general, the use of only vertical foundation piles will suffice for buildings. Hydraulic structures, on the contrary, frequently have to resist considerable horizontal (= lateral) forces, besides the vertical forces. Think of horizontal soil and water pressures behind a soil retaining structure, mooring and berthing forces on a jetty or quay wall, etc. A deep foundation with only vertical piles is generally not suited to for resisting the large horizontal forces and the overturning moment accompanying these forces. Therefore, the deep foundation of a hydraulic structure is often a combination of vertical piles and piles driven under an angle to the vertical. These piles are called 'raking piles' or 'batter piles' (*schoorpalen*).

Irrespective of the type of structure and the type of pile, vertical or batter, the horizontal load has to be transferred into deeper soil layers where enough horizontal bearing capacity can be provided (see the following section). In addition, the strength of the piles should be able to resist the shear forces. The shear strength can be calculated with help of Chapter 29 for reinforced concrete piles and Chapter 30 for steel pipes. As a rule of thumb, for the purpose of conceptual designs, a shear capacity of 100 kN could be used for prefabricated concrete foundation piles, which in most cases is very conservative.

34.2 Blum: pile theory

A commonly used method to compute the required embedded depth (*inheidiepte*) needed to provide enough passive soil resistance to lateral loads, is Blum's method (*Die Bautechnik*, Heft 5, 1932). Blum used the following assumptions for his theory:

- 1) the embedded part of the foundation pile is regarded as an elastically supported beam;
- 2) the soil response is perfectly plastic;
- 3) the soil reaction on the deeper part of the pile is substituted by a concentrated force known as the *Ersatzkraft* (R_3), see Figure 34-2;
- 4) for stiffness considerations the pile is thought to have a fixed support at the depth were the concentrated force R_3 is acting on the pile.

Ad 2: It is assumed that the elastic range of the soil is extremely small. As soon as there is a displacement (u) the soil response is either immediately at its maximum (passive, $\sigma_{h,max}$) or minimum (active, $\sigma_{h,min}$). Hence the stiffness of the soil is assumed to be very large. It is to be expected that the displacements as a result of the load will be somewhat underestimated (see Figure 44 1).

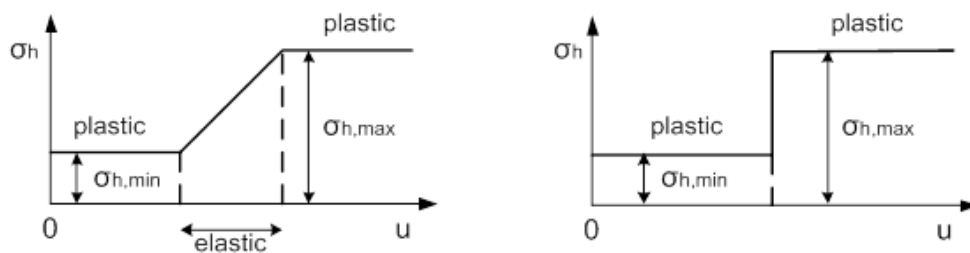


Figure 34-1 On the left: elasto-plastic soil response. On the right: perfectly plastic soil response.

Ad 3: The basic idea is that the pile is displaced towards the right by the applied force, except at the lower end where a displacement towards the left occurs because the pile rotates around a point somewhere above its deepest point. The soil reaction towards the left is replaced by the concentrated force (R_3) generally known as *Ersatzkraft* (German for substitute force), see Figure 34-2.

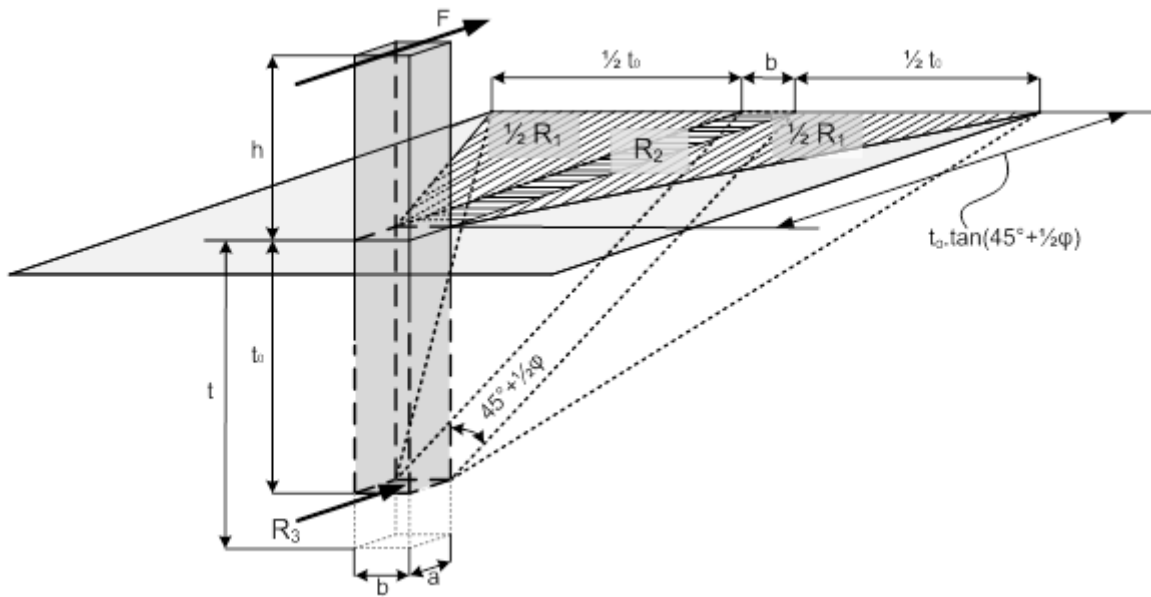


Figure 34-2 Schematic representation of the shearing soil wedge behind a laterally loaded pile.

where:

F	[kN]	=	load
R_1	[kN]	=	resultant force of the soil wedges on both sides next to the soil wedge directly behind the pile (two half pyramids)
R_2	[kN]	=	resultant force of the soil wedge directly behind the pile (a triangle with width b)
R_3	[kN]	=	substitute force ('Ersatzkraft')
a	[m]	=	width of the pile in the direction of the load
b	[m]	=	width of the pile perpendicular to the load
h	[m]	=	length of the unsupported part of the pile
t_0	[m]	=	theoretical embedded depth
t	[m]	=	practical embedded depth $t = 1,2 \cdot t_0$
φ	[°]	=	angle of internal friction

Strength

The maximum load the soil wedge behind the pile is able to resist can be computed by taking the sum of the moments at depth t_0 below bed level, in this way the concentrated force R_3 does not enter into the equations (see Figure 34-3).

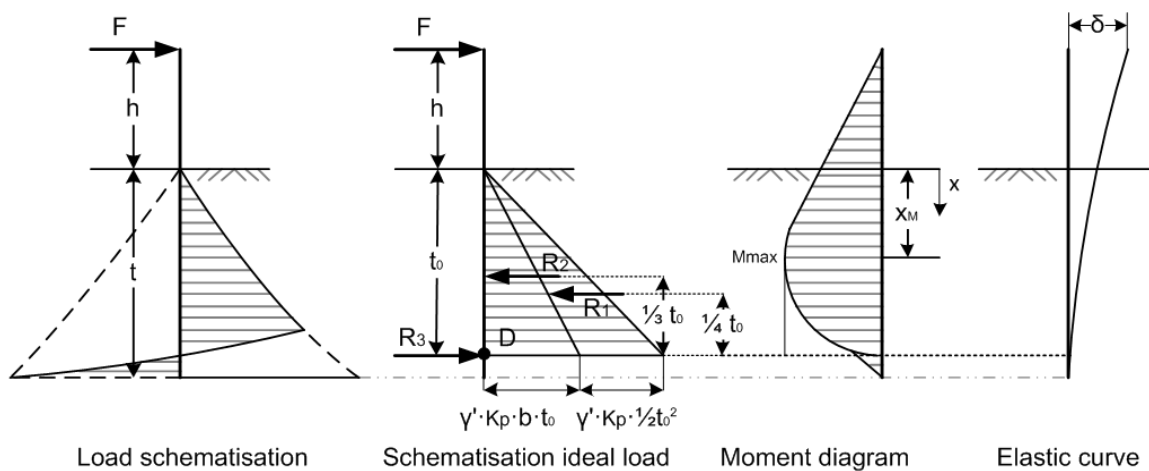


Figure 34-3 Blum's schematization

$$\begin{aligned}
\sum M_D &= 0 \\
-F_{\max} \cdot (t_0 + h) + R_1 \cdot \frac{1}{4} \cdot t_0 + R_2 \cdot \frac{1}{3} \cdot t_0 &= 0 \\
F_{\max} \cdot (t_0 + h) &= \left(\frac{1}{6} \cdot \gamma' \cdot K_p \cdot t_0^3\right) \cdot \frac{1}{4} \cdot t_0 + \left(\frac{1}{2} \cdot \gamma' \cdot K_p \cdot b \cdot t_0^2\right) \cdot \frac{1}{3} \cdot t_0 \\
F_{\max} \cdot (t_0 + h) &= \frac{1}{24} \cdot \gamma' \cdot K_p \cdot t_0^4 + \frac{1}{6} \cdot \gamma' \cdot K_p \cdot b \cdot t_0^3 \\
\Rightarrow F_{\max} &= \gamma' \cdot K_p \cdot \frac{t_0^3}{24} \cdot \frac{t_0 + 4 \cdot b}{t_0 + h}
\end{aligned} \tag{34-1}$$

where:

F_{\max}	[kN]	= maximum load that can be resisted
R_1	[kN]	= resulting force of soil at either side of the pile
R_2	[kN]	= resulting force of soil directly behind the pile
b	[m]	= width of the pile perpendicular to the load
h	[m]	= length of the unsupported part of the pile
t_0	[m]	= theoretical embedded depth
K_p	[-]	= passive soil pressure coefficient
γ'	[kN/m ³]	= effective volumetric weight ($\gamma_s - \gamma_w$)
δ	[°]	= (pile) wall friction; generally $\delta = -\frac{2}{3}\varphi$

$$K_{p,h,\sigma} = \frac{\cos^2(\varphi - \alpha)}{\cos^2(\alpha) \left(1 - \sqrt{\frac{\sin(\varphi - \delta)\sin(\varphi + \beta)}{\cos(\alpha - \delta)\cos(\alpha + \beta)}}\right)^2} \quad \text{with } \alpha = \beta = 0$$

Because all (shear) forces are known, the moment diagram can be determined using the following equation:

$$M_x = F \cdot (h + x) - \gamma' \cdot K_p \cdot (x + 4 \cdot b) \cdot \frac{x^3}{24} \tag{34-2}$$

where:

M_x	[kNm]	= moment at depth x
F	[kN]	= load
x	[m]	= distance below bed level

The maximum moment M_{\max} occurs at depth X_m , where $\frac{\delta M}{\delta x} = 0$. This depth can be found by solving the following equation iteratively:

$$x_M^2 \cdot (x_M + 3 \cdot b) = \frac{t_0^3}{4} \cdot \frac{t_0 + 4 \cdot b}{t_0 + h} \tag{34-3}$$

Notes

1. The soil resistance only depends on the angle of internal friction and the volumetric weight of the soil. Almost always the effective (submerged) weight of the soil has to be used in combination with $\delta = -\frac{2}{3}\varphi$, to calculate the K_p , and arrive at the lateral bearing capacity.

2. In case of an impact load (stootbelasting) the load duration is short; in cohesive soils there is quite a possibility that the groundwater does not have time to flow out of the soil wedge behind the foundation pile or flow into the soil in front of the pile. For that reason, Blum proposes to use the volumetric weight of saturated soil (γ_s), however in combination with $\delta = 0$ to calculate the K_p .

3. For the strength considerations in the above, the position of the fixed support of the pile is at a distance X_M below ground level.

Stiffness

A vertical pile, fixed in the soil, will bend if it is loaded perpendicular to its axis. The displacement of the part of the pile embedded in soil causes a passive resisting force. The bending moment diagram of, according to Blum's strength considerations, shows a curved line, see Figure 34-4. The pile could also be modelled as a cantilever beam with concentrated horizontal load. For this last schematization, the bending moment diagram and the formula for the maximum displacement are well-known:

$$\delta = \frac{F \cdot L_i^3}{3EI} \quad (34-4)$$

where: δ [m] = maximum displacement
 F [N] = concentrated horizontal load
 L_i [m] = not-supported part of the pile ($= h + 0,65 \cdot t$)
 EI [Nm⁻¹] = bending stiffness of the pile

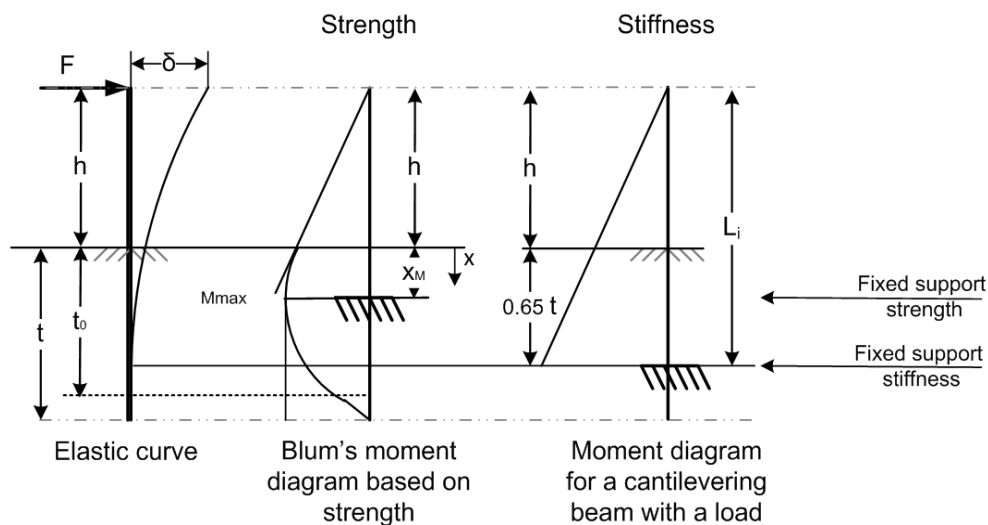


Figure 34-4 Moment diagrams for laterally loaded piles

Equating the static moments of both moment diagrams, Blum found the following expression for the displacement of the pile head as a result of a lateral load F :

$$\delta = \frac{F \cdot (h + 0,65 \cdot t)^3}{3EI} \quad (34-5)$$

where:

δ [m] = displacement of the pile head
 F [N] = load
 h [m] = length of the unsupported part
 t [m] = practical embedded depth
 E [N/m²] = Young's modulus of the pile material
 I [m⁴] = moment of inertia of the pile
 L_i [m] = not-supported length of the pile $h + 0,65 \cdot t$

Hence, the overall pile stiffness, the spring stiffness k of the pile, which includes a contribution of both soil and pile material, when the maximum load is acting, can be estimated as follows:

$$k_{pile} = \frac{F_{max}}{\delta} = \frac{3EI}{(h + 0,65 \cdot t)^3} \quad [\text{N/m}] \quad (34-6)$$

As long as the soil can be schematized as one layer, Blum's schematization results in a reasonable approximation of the maximum absorbable lateral load on a foundation pile. However when the soil profile consists of multiple layers, then the displacements better be analysed using a finite element model or an elasto-plastic spring model. In the latter case the foundation pile will be schematized as a beam on an elastic bed. For subgrade moduli (k -values) of the soil (*beddingsconstanten van grond*) the reader is referred to Section 27.5 of this Manual.

34.3 Literature

Blum, H., *Wirtschaftliche Dalbenformen und deren Berechnung*. Die Bautechnik, Heft 5, 1932.

Houthandel v/h G. Alberts Lzn. & Co., *Het ontwerpen, berekenen en vergelijken van ducdalven in tropisch hout en staal*, Middelburg, september 1957.

Veen, van der, C., Horvat, E., Kooperen, van, S.H., *Grondmechanica met beginselen van de funderingstechniek*, Waltman, Delft, oktober 1981.

Verruijt, A., *Laterally loaded pile*, March 29, 1999.

35. Pile foundations: Pile groups

The previous chapters gave calculation methods for the determination of the pile load. The choice of method depends on the schematisation of the structure. Figure 35-1 is a flow chart to determine which calculation method to use. It is always possible to use a method shown to the right of the calculation method selected with the flow chart.

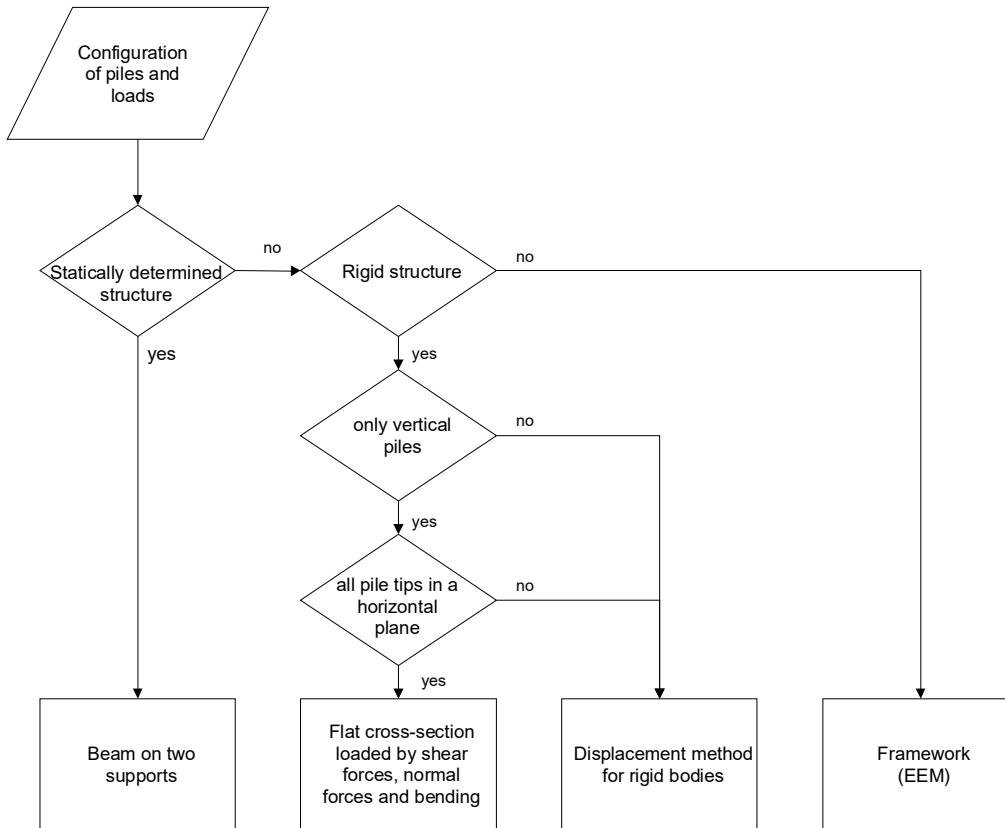


Figure 35-1 Flow chart for the determination of a calculation method

A common problem in structural hydraulic engineering is a group of horizontally loaded piles.

36. Stability of floating structures

Minor revision: February 2011, additional clarifications: February 2015

To ensure that floating elements do not undesirably move or rotate, they should be statically and dynamically stable. The stability of a floating element depends on forces and moments, and the shape of the element.

36.1 Static stability

Equilibrium of vertical forces

Vertical forces establish an equilibrium if the buoyant force (*opwaartse kracht*) equals the weight of the floating body (including all ballast). For a floating body, this buoyant force has the same magnitude as the weight of the displaced volume of fluid (Archimedes' principle: a floating body displaces its own weight of fluid).

A vertical equilibrium is usually reached if the element is floating, or if it is resting on the bottom of the water body. If there is no equilibrium, a completely immersed element will move upward or downward until an equilibrium state is reached. An element will move upward if the buoyancy is more than the total weight of the element. Then, at a certain moment, the part of the element rising out of the water will result in a decrease of the buoyant force in such an amount that this buoyant force equals the weight of the element. It then stops moving upward. An element, conversely, will sink if the weight of the element exceeds the buoyant force, until it reaches the bottom. The bottom will resist the downward directed force and will stop the element moving down.

Equilibrium of moments

For the design of large-scale prefabricated elements, vessels and dredging equipment, not just the weight is of importance. There must also be an assurance that the elements do not tilt in an unacceptable degree during the floating transport or the immersing procedure. Tilting can be initiated by the mooring forces, wave motions, and inlet of water during immersion, etc. Elements must therefore be designed or equipped in such a way that a rotation, caused by external factors, is corrected by a righting moment that will return the element to its original position.

If the sum of moments around the point of rotation (= point of gravity) equals zero, the element will not incline to tilt. This principle is illustrated in Figure 36-1, where equilibrium is not reached yet. It will tilt in such a way that an equilibrium will be reached.

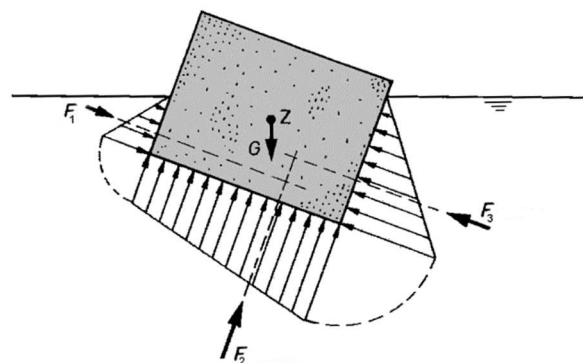


Figure 36-1 Forces acting on a floating element (Nortier, 1991)

Static stability - metacentric height

A check of the equilibrium of moments (previous paragraph) is sufficient if an element is floating in still water. In reality, however, this is rarely the case. This is why also the 'sensitivity to tilting' has to be taken into account. A measure for the resistance to tilting is given by the 'metacentric height'. The principle is illustrated in Figure 36-2. The left side depicts the cross-section of a floating element (like a caisson). On the right side the same element is showed in tilted position. The rotation angle is φ .

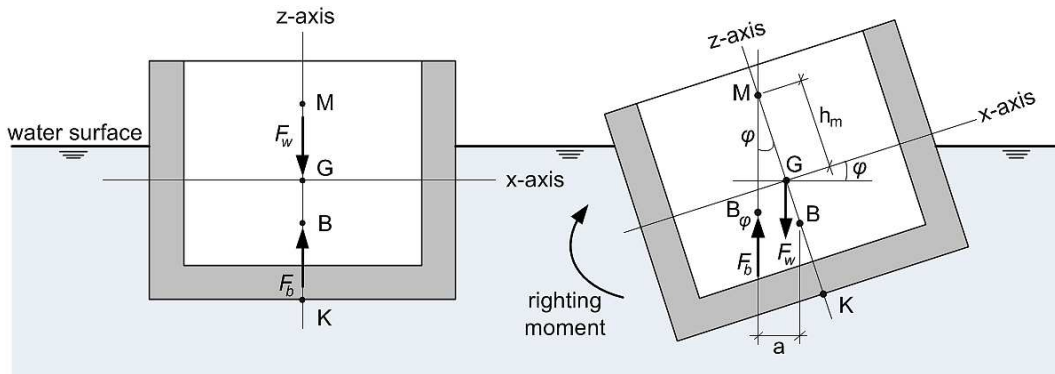


Figure 36-2 Floating element

Indicated are three points, which are of importance in the evaluation of the stability:

- B is the centre of buoyancy (*drukingspunt*), the point of application of the buoyant force F_b in state of equilibrium (the state in which the axis of symmetry of the element is vertical). B is therefore the centre of gravity of the displaced water. In a rectangular container (caisson), B is found halfway between the water surface and the bottom of the element. In tilted position the centre of buoyancy shifts to a new position because the geometry of the displaced volume has changed. The shifted centre of buoyancy is indicated with B_φ and the horizontal shift is a [m].
- G is the centre of gravity (*zwaartepunt*) of the element. If the element is filled with a layer of gravel or water for the benefit of the immersing procedure (not shown in Figure 36-2), this weight should also be taken into account when calculating G. Not only will this ballast lower the centre of gravity, it will also increase the draught and will therefore raise B relative to the bottom. If the element heels over, the centre of gravity generally remains fixed with respect to the element because it just depends upon the position of the element's weight and ballast. The centre of gravity at the same time is the rotation point.
- M is the metacentre; the point of intersection of the axis of symmetry, the z-axis, and the action line of the buoyant force in tilted position. For small rotations ($\varphi < 10^\circ$) the metacentre is a fixed point (see lecture notes OE4652, 'Floating Structures' for a proof). The determination of point M is explained below.

For static stability, rotation of the element should be compensated by a righting moment caused by the buoyant force and the weight of the element. This is the case if M is located over G: the line segment \overline{GM} , also known as the metacentric height h_m , must be positive.

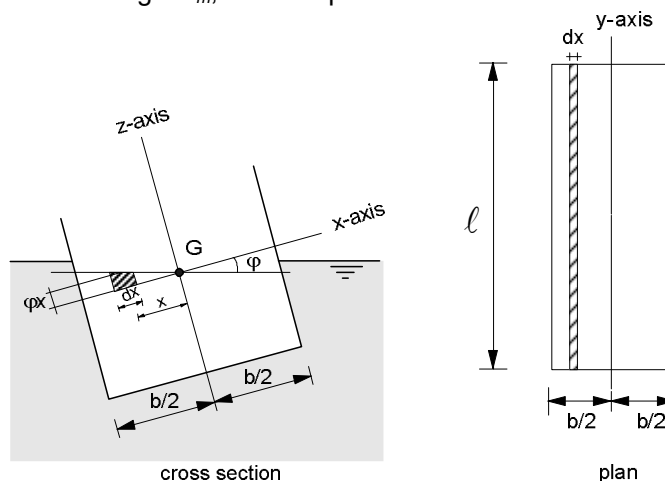


Figure 36-3 Tilted element

Figure 36-3 shows an element with a rotation φ . The part dx , which has been forced under water by the rotation, experiences a buoyant force:

$$dF_b = \varphi x dx \ell \rho_w g \quad (36.1)$$

in which ρ_w is the volumetric mass of water. This equation is only valid for rotations smaller than 10° in which case $\tan \varphi \approx \varphi$ [rad]!

Relative to G this gives a moment $dM = x dF_b = \varphi x^2 dx \ell \rho g$.

Over the entire width this means a righting (corrective) moment of: $M = \int_{x=-\frac{1}{2}b}^{+\frac{1}{2}b} \varphi x^2 dx \ell \rho g$, which could

$$\text{be rewritten as } M = \varphi \rho g \int_{x=-\frac{1}{2}b}^{+\frac{1}{2}b} x^2 \ell dx \quad (36.2)$$

Because $\int_{x=-\frac{1}{2}b}^{+\frac{1}{2}b} x^2 \ell dx$ represents the area moment of inertia (a.k.a. 'second moment of area') relative to the y-axis, I_{yy} , the expression for the moment can be formulated as:

$$M = \varphi \rho g I_{yy}, \text{ in which } I_{yy} = \frac{1}{12} \ell b^3. \quad (36.3)$$

The point of application of the buoyant force (F_b) in a state of rest, is the centre of buoyancy B. A rotation φ leads to a translation of the line of action of F_b over a distance a (see Figure 36-2). $M = F_b \cdot a$, so:

$$a = \frac{M}{F_b} = \frac{\varphi \rho g I_{yy}}{\rho g V} = \frac{\varphi I_{yy}}{V_{dw}} \quad (36.4)$$

In this equation, V_{dw} is the volume of the immersed part of the element (= the volume of the displaced water).

$$\text{Because } \sin \varphi = \frac{a}{\overline{BM}}, \overline{BM} = \frac{a}{\sin \varphi} \approx \frac{a}{\varphi} \quad (36.5)$$

$$\text{So, } \overline{BM} \approx \frac{I_{yy}}{V_{dw}} \quad (36.6)$$

For small rotations ($\varphi < 10^\circ$) the metacentre is a fixed point, but \overline{BM} increases because the position of B will go down. In case of considerable rotations, the metacentre displaces upward and sideways in the opposite direction in which the ship has rolled and is no longer situated directly above the centre of gravity. If M is positioned above G, a righting moment $F_b h_m \varphi = \rho g V_{dw} h_m \varphi$ is created, which tries to return the element to its stable position.

For small seagoing vessels a metacentric height h_m of at least 0,46 m is required. A ship with a small metacentric height will be "tender" - have a long roll period. A low metacentric height increases the risk of a ship capsizing in rough weather and more likely to develop "synchronized rolling". It also puts the vessel at risk of potential for large angles of heel if the cargo or ballast shifts. If a ship with low h_m is damaged and partially flooded, the metacentric height will be reduced further and will make it even less stable.

For large ships h_m should be at least 1,1 m, but not too large because in that case the vessel will be too 'stiff': it will snap back upright too quickly after a wave or wind gust has passed, which will cause heavy stresses in the structural parts of the vessel, maybe shifting of the cargo and not unlikely sea sickness of the persons on board.

The requirements for caissons and tunnel elements are less tight: 0,5 m suffices for h_m . If M is positioned below G, the element is unstable and will tilt.

Check design static stability

The check of the static stability (in this case also known as the outset stability, because only small rotations of the element are investigated) is made up of the following steps:

- Calculate the weight F_w and the position of the gravity centre G of the floating element with reference to K (\overline{KG}). K is the intersection of the z-axis with the bottom line of the element. In general,

$$\overline{KG} = \frac{\sum V_i \cdot e_i \cdot \gamma_i}{\sum V_i \cdot \gamma_i}, \quad (36.7)$$

where V_i [m³] = volume of element i
 γ_i [kN/m³] = specific weight of element i
 e_i [m] = distance between gravity centre of element i and reference level (which is a horizontal plane through point K)

- Calculate the draught d of the element.
- Locate the centre of buoyancy B and calculate its position above the bottom of the element. This distance is \overline{KB} . In case of rectangular elements, $\overline{KB} = \frac{1}{2}d$.
- Determine the shape of the area at the fluid surface and compute the smallest area moment of inertia I for that shape (this is the most unstable). For rectangular elements: $I_{yy} = \frac{1}{12} \cdot \ell \cdot b^3$.
- Compute the volume of the displaced water V_{dw} .
- Compute $\overline{BM} = \frac{I_{yy}}{V_{dw}}$
- Calculate $h_m = \overline{GM} = \overline{KB} + \overline{BM} - \overline{KG}$
- Theoretically, if $h_m > 0$, the body is stable. In practice, $h_m > 0,50$ m is recommended. If $h_m < 0,50$, additional measures are required.

Besides the static stability, the dynamic stability (the oscillation) must also be checked. This will be explained later in this chapter.

Measures for unstable elements

If the element is unstable, the design should be altered or additional measures have to be taken.

Examples of design alterations are:

- widening of the element, thereby increasing the area moment of inertia I (usually the floor thickness will increase too, because of strength requirements).
- making the floor of the element heavier. This lowers G and increases the draught (if the transport route allows for this), which raises B relative to the bottom of the element. Unfortunately, V also increases, which decreases \overline{BM} , but the other effects dominate, so the stability is increased.

Examples of additional measures are:

- adding ballast to the element (below the point of gravity) during transport.
- the use of stabilising pontoons or vessels (see
- Figure 36-4a), which increases I_{yy} .
- linking two elements during the floating transport (see
- Figure 36-4b), which increases I_{yy} . Before the elements are disconnected at their destination, extra ballast must be applied to ensure the stability of the individual elements.

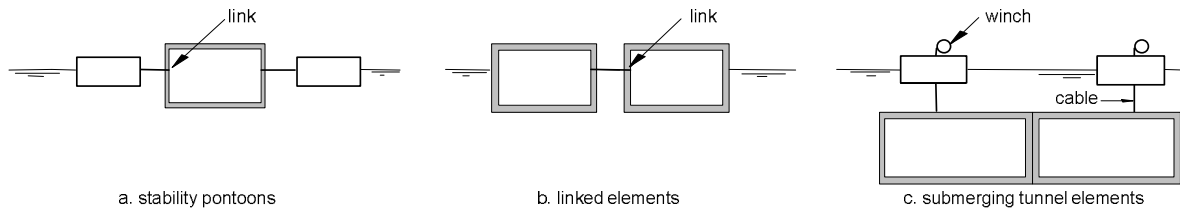


Figure 36-4 Stabilizing measures

If the required stability is achieved, one can opt to alter the design or use additional measures. Of course, combinations of both are also possible.

Stability during immersion

Floating tunnel elements generally owe their stability to their large area moment of inertia. Once the elements have been given extra ballast, they immerse under water and no longer have a plane intersected by the waterline. The area moment of inertia is then zero. Stability is then only achieved if B is positioned above G. However, the elements are lowered on four cables using winches placed on four pontoons (see Figure 36-4c). This way, the elements are lowered accurately and in a controlled fashion. The element and the four pontoons together act as one system, which, around the pontoons, does have a plane that is intersected by the waterline and thus has an area moment of inertia. By positioning the pontoons as closely to the corners of the element as possible, large moments of inertia arise, both in the transverse direction and alongside the element.

Water ballast in the immersing process (free surface effect)

The use of water as ballast to immerse elements is attractive because it is a fast method and filling up with water can be simply accomplished by opening the valves (mostly placed in or just above the floor).

If a closed element (i.e., with a roof) is completely filled with water, it acts in effect as a solid mass. This means that its weight can be regarded as being concentrated at its centre of gravity. If the element is only partly filled, or completely but not having a roof, the water surface is free to move and therefore possesses inertia. This causes a destabilising effect for the element, which can also be observed from Figure 36-5a. Due to the rotation, the depth of the ballast water increases on the left and reduces on the right. This results in a moment that amplifies the rotation. If the inner space of the element is partitioned, as is shown in Figure 36-5b, the moment driven by the ballast water decreases.

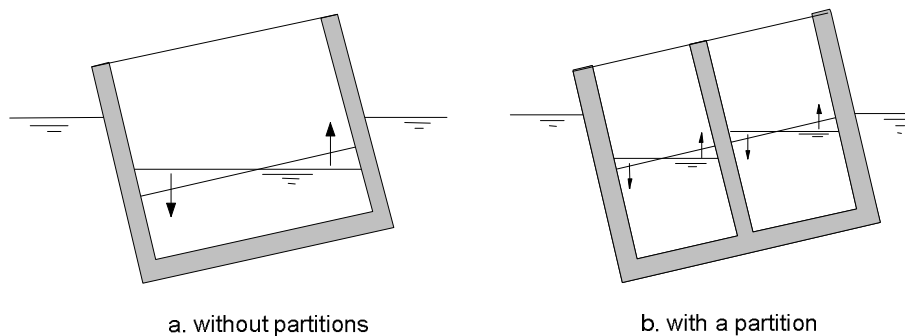


Figure 36-5 Water ballast

The unfavourable influence of the ballast water on the stability can be discounted by defining I as:

$$I_{yy} = I_{caisson} - \sum I_{comp,i} \tag{36.8}$$

in which:

- $I_{caisson}$ [m⁴] = area moment of inertia of the plane intersected by the waterline if there would be no water in the caisson
- I_{comp} [m⁴] = area moment of inertia of the ballast water area relative to the gravity centre line of the compartment concerned

It should be noticed that Steiners theorem (*verschuivingsregel van Steiner*) is not applicable here. This can be explained with help of a somewhat different approach to the free surface effect (just another explanation of the same phenomenon):

The centre of gravity of a compartment filled with a fluid will shift if the caisson (including the compartment) is tilted. It shifts towards the lowest side of the compartment (moving away from the bottom of the caisson). The shift of the gravity centre of the compartment in horizontal direction, similar to equation (36.4) that expresses the shift of the centre of buoyancy, is:

$$\overline{gg'} = \frac{I_{comp}}{V_{comp}} \cdot \varphi \quad (36.9)$$

where:

$$\begin{aligned} I_{comp} \quad [m^4] &= \text{area moment of inertia of a compartment relative to its own axis through} \\ &\quad \text{the water surface in the compartment} \\ V_{comp} \quad [m^3] &= \text{volume of water in the compartment} \\ \varphi \quad [\text{radians}] &= \text{rotation angle} \end{aligned}$$

If the density of the liquid in the compartment differs from the water outside the caisson, this should be taken into account according to:

$$\overline{gg'} = \frac{\rho_{comp}}{\rho_{outside\ water}} \cdot \frac{I_{comp}}{V_{dw}} \cdot \varphi \quad (36.10)$$

The shift of the gravity centre of the compartment results in a shift in the gravity centre of the entire caisson. This shift of the gravity centre of the entire caisson in horizontal direction is:

$$\overline{GG'} = \frac{\overline{gg'} \cdot V_{comp}}{V_{dw}} = \frac{\left(\frac{I_{comp}}{V_{comp}} \cdot \varphi \right) \cdot V_{comp}}{V_{dw}} = \frac{I_{comp}}{V_{dw}} \cdot \varphi \quad (36.11)$$

where:

$$\begin{aligned} \overline{gg'} \quad [m] &= \text{horizontal shift of the gravity centre of the compartment} \\ V_{comp} \quad [m^3] &= \text{volume of the water in the compartment} \\ V_{dw} \quad [m^3] &= \text{total volume of 'outside water' displaced by the caisson} \\ \varphi \quad [\text{radians}] &= \text{rotation angle} \end{aligned}$$

This corresponds to a rise of the gravity centre of the caisson of $\overline{GG''}$ (in z-direction):

$$\overline{GG''} = \frac{\overline{GG'}}{\varphi} = \frac{I_{comp}}{V_{dw}} \cdot \frac{\varphi}{\varphi} = \frac{I_{comp}}{V_{dw}}, \quad (36.12)$$

which is also called the 'free surface correction'.

For multiple compartments, the free surface corrections for the separate compartment have to be added up to find the total free surface correction.

The rise of the gravity centre could be expressed as a decrease of the value of \overline{BM} :

$$\overline{BM'} = \overline{BM} - \overline{GG''} = \frac{I_{caisson}}{V_{dw}} - \sum \frac{I_{comp,i}}{V_{dw}} = \frac{I_{caisson} - \sum I_{comp,i}}{V_{dw}}, \quad (36.13)$$

so actually the shift of the caisson gravity centre can be expressed as a decrease of the area moment of inertia:

$$I_{yy} = I_{caisson} - \sum I_{comp,i}, \text{ indeed without applying Steiners theorem. Q.E.D.}$$

Not only in transverse direction, as treated above, but particularly lengthways is the creation of compartments beneficial for the stability!

The partitions, which incidentally won't always be used and not for every type of prefab element, also have

the following advantages:

- Smaller spans (and so smaller moments and shear forces) of outer walls, floor and if present, roof.
- Realization of a better flow of forces. Concentrated loads (*puntlasten*) like shipping and crane wheel loads can be resisted more easily.
- Correcting the tilt (trimming) during the immersing process, by letting more (or less) water into one compartment than into the other.

Notes

- Water is let into ballast tanks during the immersion of tunnel elements. These tanks are of limited sizes, in order to keep I_{comp} as small as possible.
- Working without tanks: letting water straight into the elements, immediately leads to tilting, especially lengthways.
- Rainwater tanks used by farmers are often used as ballast tanks. These tanks are easy to fix and remove and are also relatively inexpensive.
- The mentioned stability problems do not occur if sand or gravel is used as ballast material, provided that the material is spread evenly (so there is no unnecessary tilt) and that a coincidental unwanted tilt does not lead to the sliding of the ballast material.

36.2 Dynamic stability

Not only the static stability but also the dynamic stability should be checked. If an element is transported over water, it will be affected by waves or swell (*deining*). This can cause the element to swing (*slingeren*), which can cause problems with respect to navigability and clearance (*kielspeling*).

Swing

If the dimensions (length or width) of a floating element are too small compared to the length of the waves or swell, the element will start swinging on the waves (*rolling* or *pitching*). If there is only a limited clearance beneath the the floating element, it is likely to hit the river or estuary bed and get stuck or damaged, see Figure 36-6. This is especially relevant for caissons for closure dams that have to be towed through rivers or estuaries (with limited depth) to their final destination.

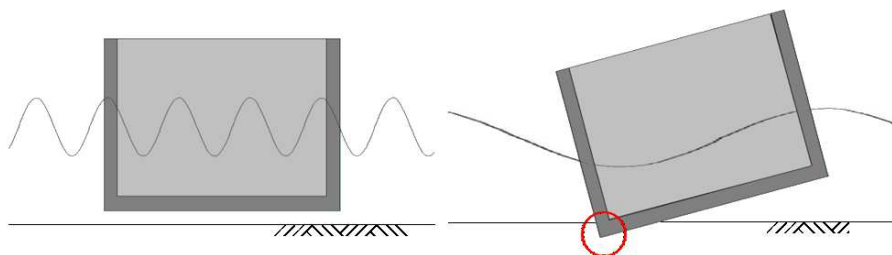


Figure 36-6 Too much rolling / pitching will lead to hitting the bed

The following rule of thumb is being used in engineering practice:

$$L_w < 0,7 \cdot \ell_e \quad \text{or} \quad L_w < 0,7 \cdot b_e$$

where:

L_w [m] = wave length

ℓ_e [m] = length of the floating element

b_e [m] = width of the element

(use ℓ_e or b_e dependent on the direction of the waves relative to the caisson)

If this condition does not apply, problems due to swinging of the element can be expected.

Natural oscillation

Worse than just swaying on the waves or on the swell is the movement of an element if the period of the water movements comes close to the natural oscillation period (*eigenperiode*) of the element. In order to prevent this, one must ensure that the natural oscillation period of the element differs significantly larger from that of the waves or swell. For example, long swell was a problem for the transport of caissons in the bay of South Africa. If the natural oscillation period could be a problem and adjustments of the design or additional measures do not offer a solution, or are too expensive, the transportation and positioning at the final location should be postponed until favourable wave conditions come back. This can, however, lead to serious delays and thus larger costs. Therefore, one should conduct a cost optimisation: on the one hand the costs of additional measures and/or design alterations, on the other hand the costs of possible delays.

Ignoring the hydrodynamic mass (the additional water mass) and damping, the natural oscillation period T_0 can be calculated by considering the angular acceleration and the righting moment of the floating body. For small rotational angles, the body can be assumed to oscillate around its metacentre. The angular acceleration by definition is:

$$\alpha(t) = -\frac{d\omega}{dt} = -\frac{d^2\varphi}{dt^2} \quad [\text{rad/s}^2] \quad (36.14)$$

where:

$$\begin{aligned} \omega \quad [\text{m/s}] &= \text{angular velocity} \\ \varphi \quad [\text{rad}] &= \text{rotation after time } t \\ t \quad [\text{s}] &= \text{time} \end{aligned}$$

The direction of the angular acceleration $\alpha(t)$ is towards the equilibrium position, hence the minus sign. The mass moment of inertia (so not the second moment of area, also called the area moment of inertia!) of the floating body about the centre of gravity is:

$$I_G = \frac{G}{g} j^2 \quad [\text{kg m}^2] \quad (36.15)$$

where:

$$\begin{aligned} G \quad [\text{N}] &= \text{weight of the floating body} \\ g \quad [\text{m/s}^2] &= \text{gravity acceleration} \\ j \quad [\text{m}] &= \text{radius of gyration about the horizontal axis through the gravity centre} \\ &\quad (\text{sometimes indicated with } i) \end{aligned}$$

The radius of gyration (*polaire traagheidsstraal*) j can be found according to:

$$j = \sqrt{\frac{I_{\text{polar}}}{A}}, \quad (36.16)$$

where A is the area of concrete in a vertical cross-section.

The polar moment of inertia I_{polar} is a measure for accelerated rotation and should in this case be considered around the y-axis:

$$I_{\text{polar}} = \int_A r^2 dA = I_{xx} + I_{zz}, \quad (36.17)$$

where I_{xx} = rectangular moment of inertia respective to the z-axis, and I_{zz} = rectangular moment of inertia respective to the x-axis, both in relation to the centre of gravity G.

The mass moment of inertia of the body about the metacentre is:

$$I_M = \frac{G}{g} (j^2 + h_m^2) \quad (36.18)$$

where:

$$h_m \quad [\text{m}] = \text{metacentric height}$$

If the metacentric height is small compared to the radius of gyration, $I_G \approx I_M$. For small angles of rotation, the righting moment equals the mass moment of inertia multiplied with the angular acceleration:

$$M = I \cdot \alpha = G h_m \varphi = I_G \frac{-d^2\varphi}{dt^2} \quad (36.19)$$

After substituting the equation for I_G , it is obtained that:

$$G h_m \varphi = -\frac{G}{g} j^2 \frac{d^2\varphi}{dt^2} \quad (36.20)$$

It can then be deduced that:

$$\frac{d^2\varphi}{dt^2} + \frac{g \cdot h_m \cdot \varphi}{j^2} = 0 \quad (36.21)$$

The solution of an equation in the shape $\frac{d^2y}{dx^2} + a^2y = 0$ is given by $y = A \cdot \sin(ax) + B \cdot \cos(ax)$, so in our case the solution is:

$$\varphi = A \cdot \sin \sqrt{\frac{g \cdot h_m}{j^2}} \cdot t + B \cdot \cos \sqrt{\frac{g \cdot h_m}{j^2}} \cdot t \quad (36.22)$$

If $t = 0$, also $\varphi = 0$ and therefore $B = 0$, it follows from equation (36.22) that:

$$A \cdot \sin \left(\frac{g \cdot h_m}{j^2} \right) \cdot t = 0 \quad (36.23)$$

If still $\varphi = 0$, and $t = \frac{1}{2}T_0$ (where T_0 is the period of a complete oscillation), this can be rewritten as:

$$A \cdot \sin \left(\frac{g \cdot h_m}{j^2} \right) \cdot \frac{T_0}{2} = 0 \quad (36.24)$$

Since $A \neq 0$, this is only true if:

$$\sin \left(\frac{g \cdot h_m}{j^2} \right) \cdot \frac{T_0}{2} = 0 \quad (36.25)$$

The simplest solution of this equation is:

$$\sqrt{\frac{g \cdot h_m}{j^2}} \cdot \frac{T_0}{2} = \pi \quad (36.26)$$

from which the expression for the natural oscillation period can be found:

$$T_0 = \frac{2 \pi j}{\sqrt{g \cdot h_m}} \quad (36.27)$$

If the natural oscillation frequency is much larger than the wave or swell frequency, the element is dynamically stable for oscillations (rotation). Short-term forecasts (a few days ahead) of wave characteristics can for many locations be found on the internet, for instance www.windfinder.com, or <https://waterinfo.rws.nl> (the last one only for the Dutch North Sea).

A large natural oscillation period is gained by a large polar inertia radius. A large metacentric height, however advantageous for the static stability, decreases the natural oscillation period.

The same type of calculation has to be carried out for dynamic stability for pitching (vertical translation instead of rotation), but this calculation method is not discussed here. A good example of pitching is the rolled-up mat that was used for the Oosterschelde storm surge barrier. This floating roll weighed 9000 tonnes and moved 0,60 m up and down in calm seas ($H = 0,20$ m and $T = 9$ s). Pitching can also be a problem for dredging vessels, because the cutter can hit the seabed.

36.3 Literature

- Barltop, N.D.P. et al: *Floating Structures: a guide for design and analysis*. Centre for Marine and Petroleum Technology (CMPT), 1998.
- Eugene A. Avallone and Theodore Baumeister, eds.: *Mark's Standard Handbook for Mechanical Engineers*. McGraw-Hill, New York, 1996.
- J.J.M. Journée and W.W. Massie: *Offshore Hydromechanics*. Lecture notes OE4620. Delft University of Technology. August 2001. Chapter 2.
- Robert L. Mott: *Applied Fluid Mechanics*. Pearson, Prentice Hall, 2006. Chapter 5
- I.W. Nortier and P. de Koning: *Toegepaste Vloeistofmechanica. Hydraulica voor Waterbouwkundigen*. 7th edition. Stam Techniek, Houten, 1991. Section 2.5
- H.J. Pursey. *Merchant Ship Stability*. 4th edition. Brown, Son & Ferguson, Glasgow, 1969.
- <http://www.golfklimaat.nl>, Rijkswaterstaat, accessed: July 2007.
- http://www.codecogs.com/library/engineering/fluid_mechanics/floating_bodies, accessed: August 213.

37. Retaining structures

(major revision: 2011, improved and extended: 2014; sheet pile design improved in 2019)

A soil retaining wall is a structure intended to resist lateral (= horizontal) soil pressure. Retaining walls are needed if the required slope of the surface exceeds the angle of repose (*hoek van natuurlijk talud*) of the soil. If this maximum angle to the horizontal is exceeded, the soil will start sliding if not hindered by a wall. Retaining walls are also applied if water has to be retained.

There are mainly three types of soil retaining structures (Figure 37-1):

1. Gravity walls (*gewichtconstructies*)
 - including L- walls, standard caissons, reinforced earth (*terre armée*), often masonry (*metselwerk*) or (reinforced) concrete;
2. Sheet pile walls (*damwanden*)
 - cantilever (*onverankerd*) or anchored (*verankerd*), including combi-walls (*combiwanden*), mostly steel profiles, sometimes pre-stressed concrete sheetpiles (*spanwanden*);
3. Diaphragm walls (also called slurry walls; *diepwanden*), in reinforced concrete.

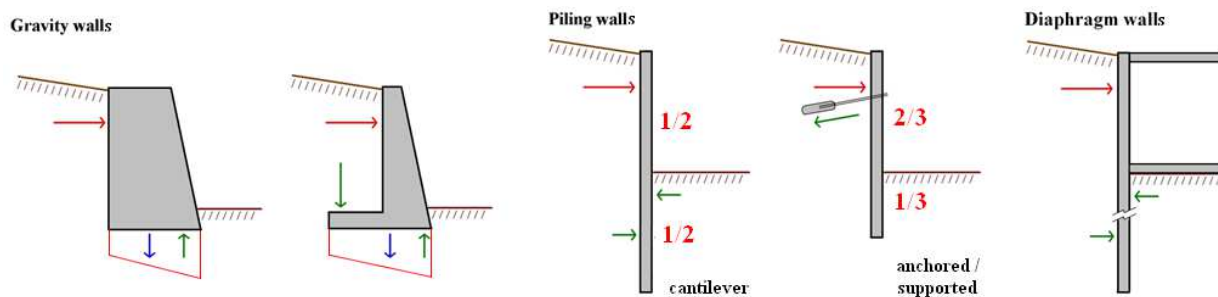


Figure 37-1 Five types of soil retaining walls (from: Wikimedia Commons, modified)

The following sections elaborate on the most interesting of these types. The designs of all these types have in common that:

- The structure and the soil body as a whole should be stable
- The retaining wall is sufficiently embedded in the soil
- The wall elements are able to resist the load (especially the largest occurring bending moments)

37.1 Gravity walls

Gravity walls derive their stability from a combination of their shape and mass. They typically have a shallow foundation and their stability can be calculated according to Chapter 31 'Stability of structures on shallow foundations'. For strength calculations, normal force, shear force and moment diagrams (*normaalkrachten-, dwarskrachten- en momentenlijnen*) can be used to find the stresses occurring in the wall material, which have to be resisted by the material properties.

If the displacements are not known, it cannot be judged whether the magnitude of the displacements are acceptable. In that case, it is better to not allow displacements and to use neutral soil stresses, which leads to conservative designs. The neutral soil pressure coefficient can be estimated using the formula proposed by Jáký: $K_0 \approx 1 - \sin \varphi \cdot \sqrt{OCR}$, where φ is the angle of internal friction of the soil, and OCR the Over Consolidation Ratio. If the friction angle is very small, e.g., for soft clays, the neutral soil pressure coefficient is close to 1. The neutral soil pressure coefficient of sand varies from about 0,5 to about 0,7 (see also Section 18.2).

37.2 Sheet piling

General characteristics

The least expensive soil retaining wall is usually made of steel sheet piling, particularly if it is only needed temporarily (excavated building site) and can be reclaimed. Sheet pile walls are generally used in soft soils and tight spaces. They are usually made of steel and can be installed one by one, or more usual in pairs. The sheet piles are connected by special joints or interlocks, see Figure 37-3. If installed in pairs, two sheets are connected before installation by tack welds (*hechtlassen*) or by continuous filled welds (*hoeklassen*) along the joints (or interlocks, *sloten*). Another method to join two sheets to make pairs, is by pinching (*vastknijpen*) the joints.

Sheet piles can also be made of pre-stressed concrete (*spanwanden*), wood or synthetic materials. Installation into the soil can be done by driving (*heien*), vibrating (*trillen*) or pressing-in (*drukken*) (Figure 37-2).



Figure 37-2 Driving a sheet pile
(<http://www.hjfoundation.com/Services/Sheet-Piling/>)







LARSSEN section Interlock design conforming to DIN EN 10248-2 and E 67 of EAU 2004	
LARSSEN 43, 430 Interlock design conforming to DIN EN 10248-2 and E 67 of EAU 2004	
HOESCH section (finger-and-socket interlock) Interlock design conforming to DIN EN 10248-2 and E 67 of EAU 2004	
PEINE interlock steel/ PEINE sheet piling Interlock design conforming to DIN EN 10248-2 and E 67 of EAU 2004	
UNION straight-web section Interlock design conforming to DIN EN 10248-2 and E 67 of EAU 2004	
KL lightweight section Interlock design conforming to DIN EN 10249-2	

Figure 37-3 Various joint types
(ThyssenKrupp sheet piling handbook)

There are two main profile types of sheet piles: U-profiles (like the 'Larssen' profiles) and Z-profiles (like the 'Hoesch' profiles). Two U-profiles together are not symmetrical which leads to oblique deflection when subjected to load. This reduces the strength and stiffness of these profiles by tenths. Z-profiles don't have this problem. If the heaviest sheet pile profile is insufficient regarding strength or stiffness, one should choose a combi-wall. It is least expensive to use steel quality S235. If this meets the demands for stiffness but not for strength, it is advisable to opt for steel with a higher yield stress rather than for heavier profiles. The AZ-type profiles from ArcelorMittal are relatively stiff.

Appendix C gives the properties for the most common sheet pile profiles in the Netherlands.

Notes

- See <http://www.tk-steelcom.com.au/documents/sheetpile-handbook-full.pdf> for details of many Hoesch and Larssen profiles, connections and combinations. ArcelorMittal profiles can be found on: <http://sheetpiling.arcelormittal.com/>
- Sheet pile walls do not only need a strength and stiffness design, but also a vibrating or driving design.

Calculation of sheet pile walls: general principles

Differences in the horizontal soil pressures in front of and behind a sheetpile wall, cause it to deform and displace. Deformations occur due to the relatively low stiffness of the sheetpiles. Displacements can consist of a rotational movement of the entire wall about a deep point, and, to a lesser extent, of a translational movement. These movements cause deformations of the soil, resulting in an active soil state where the wall moves away from the soil, and a passive state where the wall moves towards the soil (see Section 18.2.2). The embedded depth (t), the part of the wall under excavation level where it has soil at both its sides, should suffice to provide a balance in horizontal pressures and forces, as well as a moment equilibrium to prevent overturning of the wall.

If vertical stresses or forces act on the wall, e.g., the vertical component of an inclined anchor rod, or a vertical line load coming from a top structure, the friction along the wall should be high enough to prevent subsidence of the wall. The toe resistance of the wall helps to resist vertical loads as well, but this effect is relatively very small.

This Manual explains the basics of the calculation of the required length and profile of the sheetpile elements with help of classical methods. These methods are suitable for hand calculations, hence very suitable for educational purposes, though the number of soil layers should not be more than two or three (a simplification of the real situation might be needed). The results of the classical methods are not very precise, but could be used for preliminary designs. The classical methods assume soil coming into motion because of the deflection or translation of a sheetpile wall in case of unequal loading. These methods assume that soil wedges (*grondwigger*) will start moving along straight slip planes (*glijvlakken*), if the system reaches its limit state, see Figure 37-4.

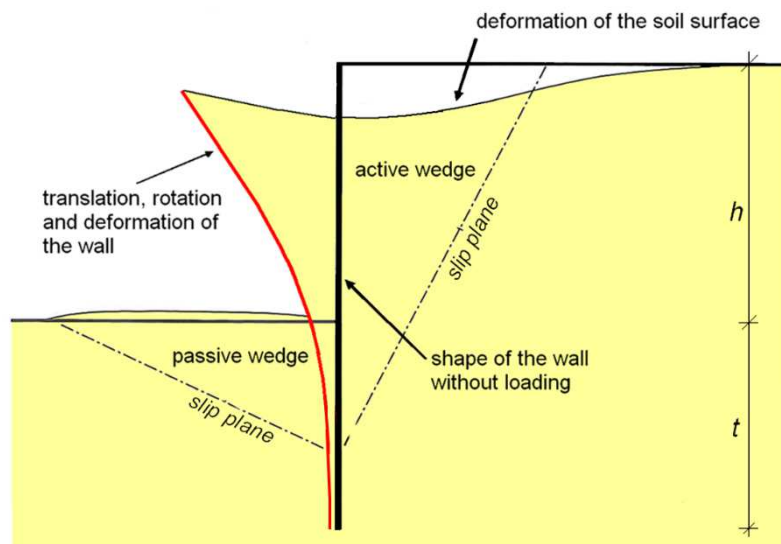


Figure 37-4 Soil wedges and deformation of a sheet pile wall due to loading (very much exaggerated)

Hermann Blum proposed to simplify sheetpile wall calculations by assuming that the local displacement of sheet pile walls would result in immediate yielding of the soil at both the active and passive side, instead of the real gradual development of shear stresses in the soil⁷. This means that soil deformations are assumed to be maximum. At the active side, minimum soil stresses will occur and at the passive side maximum soil stresses (Figure 37-5). As a result, it is assumed that no elastic soil deformation occurs. This is of course a simplification of the real situation, just as the assumption that the active and passive wedge have straight slip planes. The consequence is that these methods are not suitable to calculate the deformations of sheet pile walls.

⁷ Active and passive soil pressures are explained in Section 18.2 of this Manual.

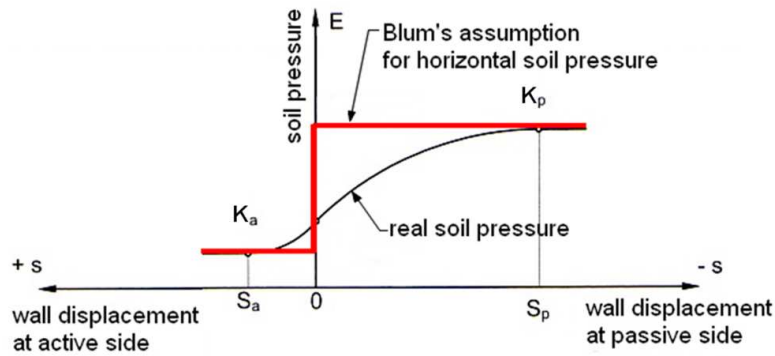


Figure 37-5 Blum's assumption regarding horizontal soil pressure

Next to the stability check of the active and passive slip planes, the stability of deep slip planes should be checked as well, because larger soil bodies with slip planes below the active and passive wedges could be mobilised as well. The stability of these soil bodies can be checked with help of the methods of Krantz, who assumed a straight slip plane, and Bishop, who assumed a circular slip plane (see Figure 37-6 and Section 0).

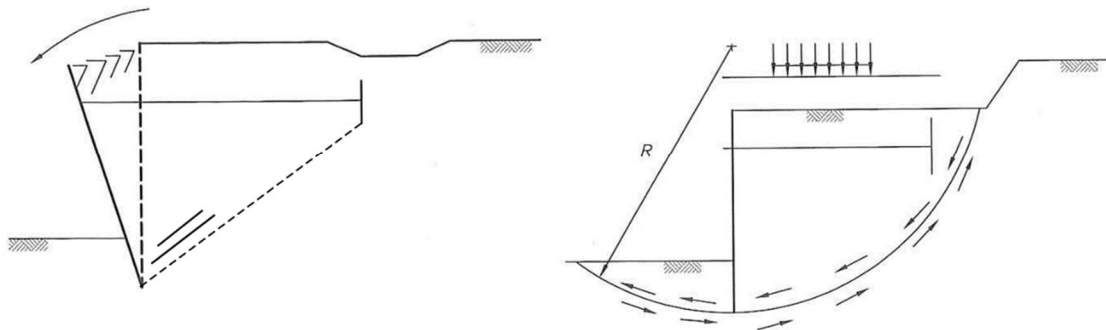


Figure 37-6 Deep slip planes: a straight plane (left) and a circular plane (right)

Other points of attention regarding the stability of sheet pile walls are piping and scour, which could potentially lead to collapse of the wall (see sections 31.4 and 31.5 for the calculation methods).

A general point of attention for sheetpile wall calculations is the schematisation of water pressures. Usually, the water levels on both sides of a sheetpile wall are not equal. The water level of the surface water in a harbour or river often differs from the ground water table at the other side of the wall. When assuming that the water pressure increases linearly with the depth, according to $\sigma_w = \gamma_w \cdot z$ (where γ_w is the specific weight of water and z is the depth below ground surface), this would lead to different water pressures at the left and right side of the toe of the wall, as in case of an infinitely deep wall, see the thick lines in Figure 37-7, where $\sigma_{w,p} = h_1 \cdot \gamma_w$ and $\sigma_{w,a} = h_2 \cdot \gamma_w$.

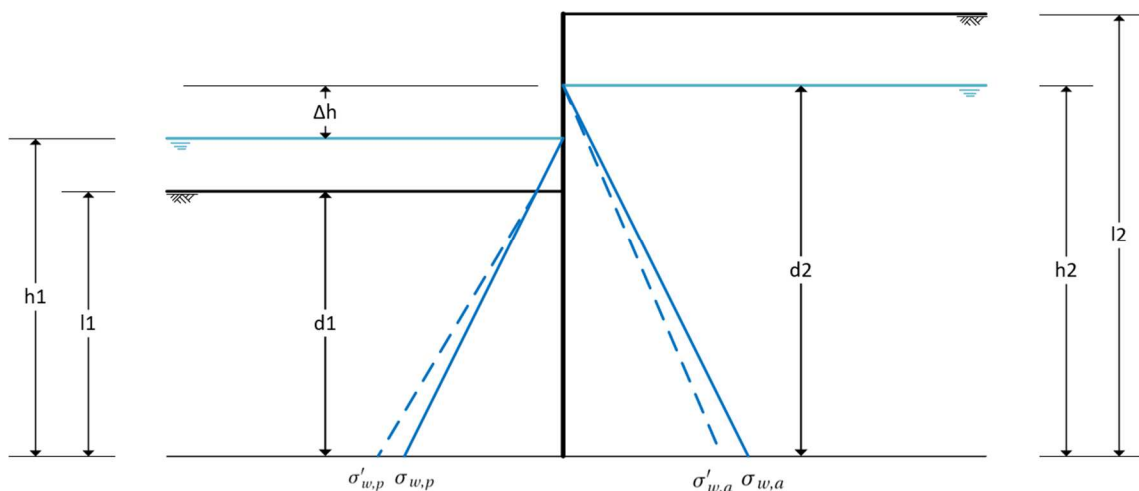


Figure 37-7 Hydrostatic pressures. Thick line: in case of no free flow of water; dashed line: after redistribution of unequal stresses (Ronckers, 2021)

In reality, this situation cannot exist. In sand, immediately after excavation and lowering the water level in the construction pit, groundwater will start flowing, which leads to levelling of the water pressures on both sides of the toe. The D-Sheet Piling User Manual (Deltares, 2017) proposes an approximation method for the water pressures acting on the wall, which could be used for preliminary designs. It proposes the following water pressures at the toe of sheetpile wall:

$$\sigma'_{w,p} = h_1 \gamma_w + \frac{0,7 \cdot \Delta h}{d_1 + \sqrt{d_1 d_2}} \cdot h_1 \cdot \gamma_w \quad \text{and} \quad \sigma'_{w,a} = h_2 \gamma_w - \frac{0,7 \cdot \Delta h}{d_2 + \sqrt{d_1 d_2}} \cdot h_2 \cdot \gamma_w,$$

where d_1 and d_2 are the thicknesses of the wet soil layers above the toe of the sheetpile wall, i.e. $d_1 = \min(h_1, l_1)$ in which h_1 and h_2 are the water levels and l_1 and l_2 are the soil levels above the toe.

A more accurate method to determine the real water pressures uses the theory of potential flow (flow nets), for which reference is made to Section 4.6.3 of CUR 166.

The situation in cohesive soils (clay) is different from sandy soils. Initially, the water pressure on the excavated side at the toe will be the same as in the original situation, thus the same as the water pressure at the active side: $\sigma_{w,p} = \sigma_{w,a} = h_2 \cdot \gamma_w$, and it linearly decreases to zero when going up towards the bottom level of the construction pit.

The following sections explain 'classical' methods to calculate the length and profile of sheet pile walls. These simple methods can be used for analytical (hand)calculations as a first rough estimate. They are all schematised in such a way that the internal moments and shear forces at the top and the toe of the wall are equal to zero. Elastoplastic and finite element methods can be used for more detailed dimensioning of sheet pile walls.

Calculation of cantilever sheet pile walls

A sheetpile wall that is not supported by anchors or struts, just only embedded in the soil, mechanically acts as a cantilever (*uitkragende ligger*). The pressure of the soil at the active side leads to a tendency of the wall to move towards the passive side. This movement consists of a translation effect (because of an imbalance of horizontal forces) and a rotational effect (because of an imbalance of moments). Because of the flexibility of the wall, the sheet piles will deform as well. Figure 37-4 shows the deformations of a cantilever sheet pile wall in a rather extreme extent (failure state).

An increase of the height to be retained, and accordingly an increase in acting loads (until a certain depth), results in rapidly increasing deformations and an increasing claim on the bending capacity of the structure. Cantilever sheetpile walls are therefore usually not used as permanent structures. For temporary structures, like most building pits, they can only be used in the case of relatively low retaining heights. Otherwise, the profiles would become too big and too long, hence too expensive compared to supported sheetpile walls.

Schematisation of cantilever sheetpile walls according to Blum

As a result of the forces acting on the sheet pile wall and the assumption that the sheet piles are infinitely stiff, the sheet pile wall inclines to turn around point D, see Figure 37-8A. Accordingly, a clamping load (*inklembelasting*) will develop under point D, which resists the turning of the wall (Figure 37-8B). In this schematisation, if the wall goes deeper than point D to reach a clay layer as way of preventing seepage from aside, the active and passive soil wedges don't go deeper than that point (Figure 37-8C).

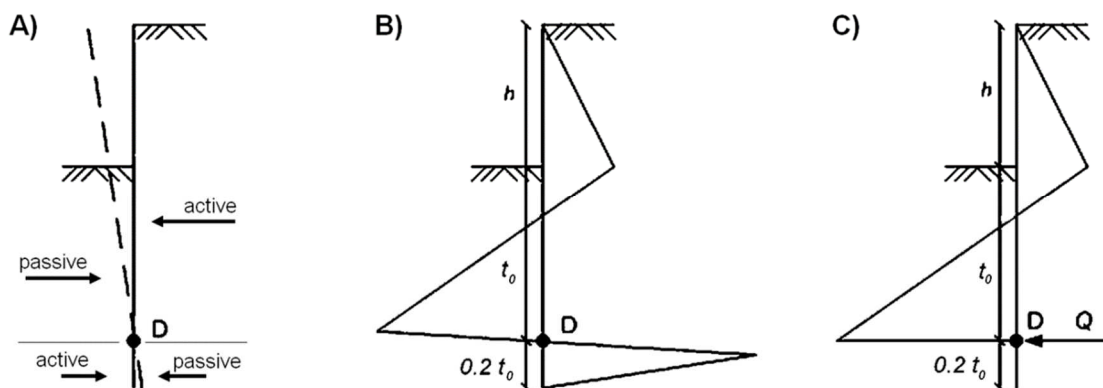


Figure 37-8 A) sheetpile with rotation point; B) 'real' resulting soil pressure diagram; C) simplified resulting pressure diagram

To calculate the required embedded depth of the wall, the real pressure diagram is simplified to a schematised diagram as shown in Figure 37-8C. Blum proposed to replace the clamping load under point D by a concentrated load (*Ersatzkraft*, or substitute force Q) acting through point D. In addition, the fixed end is replaced by a free support at point D (hence, $M = 0$ at point D). The theoretical embedded depth can then be calculated considering an equilibrium of moments about point D. Since the passive pressure at the front side of the wall is underestimated in this schematisation, the deviation is corrected by increasing the computed theoretical embedded depth (t_0) by a factor α (1,20). This is done in such a way that the needed shear force, Q , in point D can be delivered ($Q = F_{p,h} - F_{a,h}$). Notice that the magnitude of the field moment is not influenced by this schematisation.

The increment factor α that is used to increase the theoretical embedded depth t_0 , varies between 1,20 and 1,60, depending on the water level difference. Table 37-1 gives an overview of the various values for this factor α .




wall type	 small water head difference	 big water head difference	 very big water head difference or only water pressure
cantilever	1,20	1,30	1,40 - 1,60

Table 37-1 Increment factor α for the embedded depth of cantilever sheetpile walls (from: Hoesch Spundwand-Handbuch 1980)

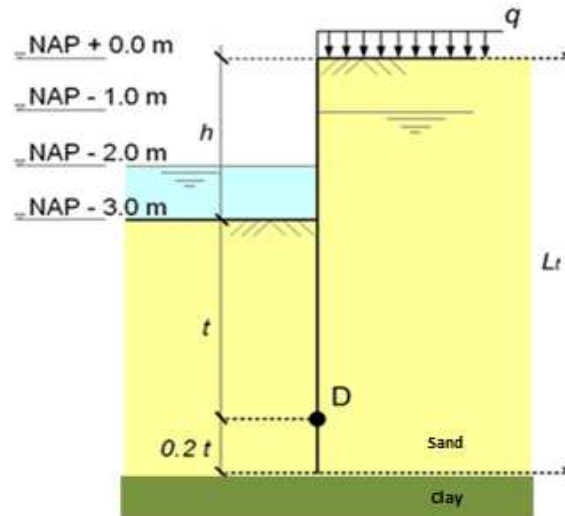
Calculation method of the length (depth) and the profile of a cantilever sheet pile wall:

- Step 1. Determine the governing load situation regarding water levels, surcharge and other external loads;
- Step 2. Calculate and draw the vertical soil stresses and the (ground) water pressures;
- Step 3. Calculate the horizontal loads stresses at the active and passive side as a function of the theoretical embedded depth (*inheidiepte*) t_0 .
- Step 4. Calculate the embedded depth t_0 considering an equilibrium of moments around the theoretical pile tip, point D.
- Step 5. Calculate the substitute force Q considering the equilibrium of horizontal forces.
- Step 6. Calculate and draw the shear force and the moment diagrams.
- Step 7. Determine the maximum moment in the sheetpile wall and calculate the minimum required section modulus ($W_{eff,y}$).
- Step 8. Multiply the theoretical embedded depth t_0 with the increment factor α , as given in Table 37-1 to determine the real required length ($t = \alpha \cdot t_0$).
- Step 9. Choose a suitable sheetpile profile from the product specifications of the manufacturer.

Notice that the presence of water at the passive side of the sheet pile wall works favourable for the strength of the sheet pile wall. Therefore, one shall either assume a certain safe (= guaranteed!) water level at the passive side of the sheet pile, or assume that no water is present at all above the excavation level.

Elaborated example: Calculation of a cantilever sheet pile wall

For dividing two areas a cantilever sheet pile needs to be placed. It is yet unknown what profile and depth is required for this cantilever sheet pile. In the following figure the situation previously mentioned is visualized.

**Parameters**

Variable	Value and unit
surcharge at the surface q	22 [kN/m ²]
specific weight of dry sand (γ_d)	18 [kN/m ³]
specific weight of saturated sand (γ_s)	20 [kN/m ³]
specific weight of water (γ_w)	10 [kN/m ³]
angle of internal friction of the sand (φ):	30 [°]
cohesion of the sand (c):	0 [kN/m ²]
wall friction for a smooth wall (δ):	0 [°]

Ground and water levels are indicated in the figure. Assume that the toe of the sheet pile wall touches a clay layer, preventing groundwater flow (so the water pressure is hydrostatic).

Asked

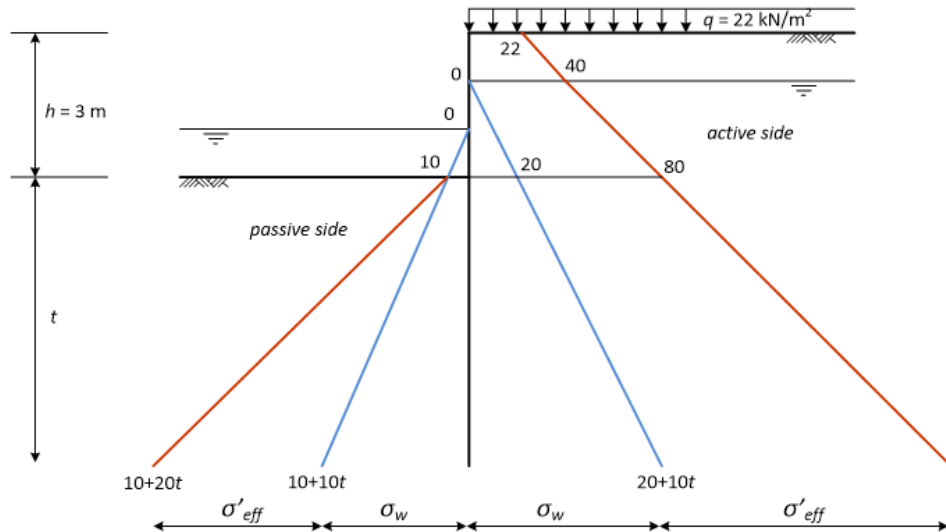
Compute the required length and profile of the sheet piles. Do not use safety factors for this example.

Step 1. Calculate the horizontal loads at the active and passive side

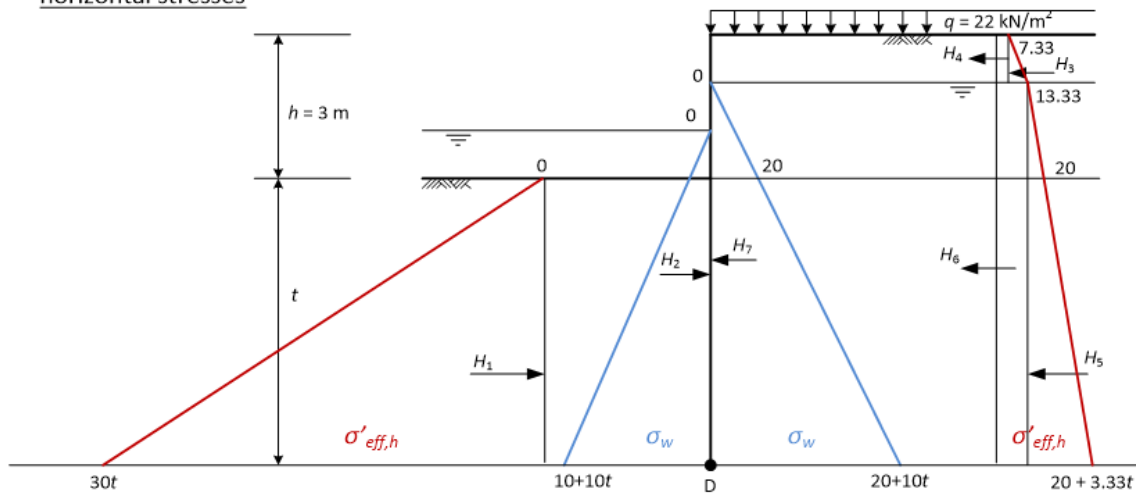
First, the vertical stresses should be calculated. This is done for the water and the soil separately. Then the horizontal stresses acting on the wall are calculated. The horizontal water stresses are equal to the vertical water stresses (Law of Pascal) and the horizontal effective stress is found by multiplying the vertical effective stress with the active and passive soil coefficients. This is shown in the following figure. For $\varphi = 30^\circ$, $K_a = 0,33$ and $K_p = 3,0$ (see Section 18.2 for the equations).

Notice that the water pressure at the toe of the wall at the active side differs from the water pressure at the passive side. This is only possible because of the assumption that there is an impermeable clay layer at the toe of the wall. In reality, this can initially be the case, but some levelling will take place after some time because of seepage and it is more likely that the water pressure at both sides will become the same at the toe level. The real water pressure in sand can be determined by constructing flow nets.

vertical stresses



horizontal stresses



Step 2. Calculate the embedded depth t considering an equilibrium of moments around point D.

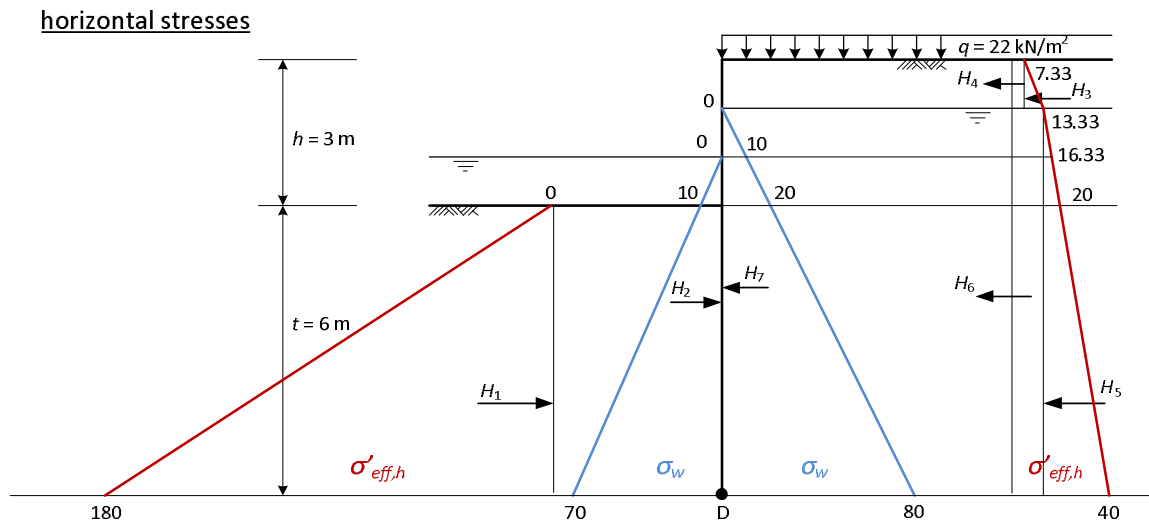
The embedded depth is calculated in the following table. First the resulting horizontal forces are calculated, then the arm from point D to the work lines of these forces is determined. The resulting moment about point D is a third-degree equation with one variable.

force [kN/m]	arm [m]	moment [kNm/m]
$H_1 = \frac{1}{2} \cdot 30t \cdot t =$	$\frac{1}{3}t$	$-5t^3$
$H_2 = \frac{1}{2} \cdot (10 + 10t)(1 + t) =$	$\frac{1}{3}(t + 1)$	$-1\frac{2}{3} - 5t - 5t^2 - 1\frac{2}{3}t^3$
$H_3 = \frac{1}{2} \cdot (13\frac{1}{3} - 7\frac{1}{3}) \cdot 1 =$	$t + 2\frac{1}{3}$	$7 + 3t$
$H_4 = 7\frac{1}{3} \cdot 1 =$	$t + 2\frac{1}{2}$	$18\frac{1}{3} + 7\frac{1}{3}t$
$H_5 = \frac{1}{2} \cdot (20 + 3\frac{1}{3}t - 13\frac{1}{3}) \cdot (t + 2) =$	$\frac{1}{3}(t + 2)$	$4\frac{4}{9} + 6\frac{2}{3}t + 3\frac{1}{3}t^2 + 5\frac{5}{9}t^3$
$H_6 = 13\frac{1}{3} \cdot (t + 2) =$	$\frac{1}{2}(t + 2)$	$26\frac{2}{3} + 26\frac{2}{3}t + 6\frac{2}{3}t^2$
$H_7 = \frac{1}{2} \cdot (20 + 10t) \cdot (t + 2) =$	$\frac{1}{3}(t + 2)$	$13\frac{1}{3} + 20t + 10t^2 + 1\frac{2}{3}t^3$
$\Sigma H - Q =$	$58\frac{2}{3} + 30t - 13\frac{1}{3}t^2$	$\Sigma M_D = 68\frac{1}{9} + 58\frac{2}{3}t + 15t^2 - 4\frac{4}{9}t^3$

$$\Sigma M_D = 0 \rightarrow 68\frac{1}{9} + 58\frac{2}{3}t + 15t^2 - 4\frac{4}{9}t^3 = 0 \rightarrow t = 6,00 \text{ m}$$

The substitute force Q then is $58\frac{2}{3} + 30 \cdot 6 - 13\frac{1}{3} \cdot 6^2 = 241,33 \text{ kN/m}$.

Mistakes are easily made, so it would be wise to check the calculation until now. This is done by redrawing the horizontal stress figure, but now with 6,00 substituted for t (directly in the graph). All partial horizontal forces and arms can now be directly calculated, without making use of the variable t . The sum of moments about D should still be zero.



$$\begin{aligned}
 M_1 &= -0.5 \cdot 180 \cdot 6 \cdot 6/3 = & -1080,00 \\
 M_2 &= -0.5 \cdot 70 \cdot 7 \cdot 7/3 = & -571,67 \\
 M_3 &= 0.5 \cdot (13.33-7.33) \cdot 1 \cdot 8.33 = & +25,00 \\
 M_4 &= 7.33 \cdot 1 \cdot 8.5 = & +62,33 \\
 M_5 &= 0.5 \cdot (40-13.33) \cdot 8 \cdot 8/3 = & +284,44 \\
 M_6 &= 13.33 \cdot 8 \cdot 8/2 = & +426,67 \\
 M_7 &= 0.5 \cdot 80 \cdot 8 \cdot 8/3 = & +853,33 \\
 \hline
 \Sigma M &= & 0,10 \approx 0 \\
 &\rightarrow \text{Check OK!}
 \end{aligned}$$

Step 3. Calculate the maximum moment and the required section modulus

The resulting stress diagram is drawn first, which is used to draw the shear force diagram (*dwarskrachtenlijn*) in order to find the moment diagram (*momentenlijn*). The maximum moment in the sheetpile wall can be found with help of this moment diagram.

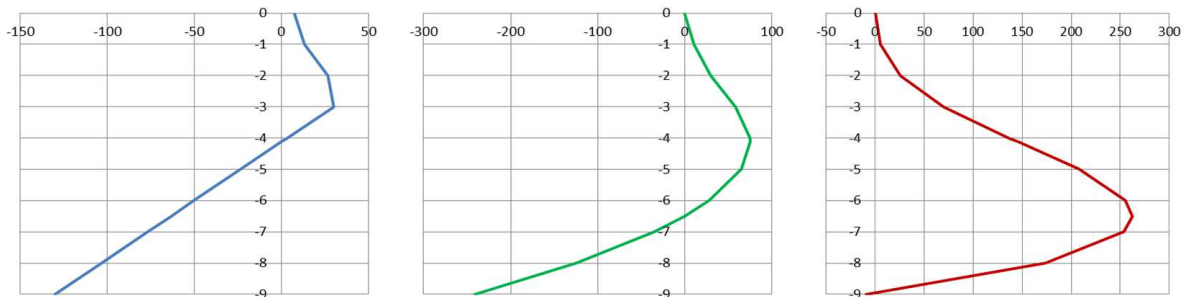
So, first the resulting stress diagram is drawn. This can be easily accomplished using the figure above. The resulting horizontal stress can be found by just summarizing the horizontal soil stresses and the water pressures on both sides (active and passive) for every depth. For instance, at 1,00 m below the soil surface (right side), the total horizontal stress is $0 + 13,33 = 13,33 \text{ kN/m}^2$. One metre lower, it is $10 + 16,33 = 26,33 \text{ kN/m}^2$. Three metre below ground surface, the total horizontal stress is $20 + 20 - 10 = 30 \text{ kN/m}^2$.

The shear force diagram, calculated in the same table, can be found by integrating the equation for total horizontal stress. This means that the area below the stress diagram equals the difference in the shear force diagram. At ground level, the shear force diagram starts with a value of 0 kN/m (because of Blums' schematisation), so, for instance at 1 metre below ground level, the value of the shear force diagram is $0 + (7,33 + 13,33)/2 \cdot 1,0 = 10,33 \text{ kN/m}$. This can be calculated for every slice of soil of 1,0 m. This has done a bit more precise to find the maximum shear force: this occurs where the total stress equals zero, which is at 4,125 m below ground level. An extra check here is that the shear force found at the toe of the wall (9 m below ground surface) should be the same as the value found for the substitute force Q , which luckily is the case.

The moment diagram can be found now by integrating the shear force diagram. The area below the shear force diagram is the change in moment diagram. Also here $M = 0$ at ground level, so from there the M -line can be calculated downward. At 9 m below ground level, M should be 0, which is almost the case (small rounding-off error). The maximum moment appears where $S = 0$, at 6,505 m below ground level.

The resulting horizontal stresses, the shear forces and the moments are presented in the following table and graphs.

height	hor. stress	S-diagram	M-diagram
0,000	7,33	0,00	000
-1,000	13,33	10,33	5,17
-2,000	26,67	30,33	25,50
-3,000	30,00	58,67	70,00
-4,000	3,33	75,33	137,00
-4,125	0,00	75,54	146,43
-5,000	-23,33	65,33	208,06
-6,000	-50,00	28,67	255,06
-6,505	-63,47	0,02	262,30
-7,000	-76,67	-34,67	253,73
-8,000	-103,33	-124,67	174,06
-9,000	-130,00	-241,33	-8,94



Resulting horizontal stresses [kN/m²], S-diagram [kN/m] and M-diagram [kNm/m]

The maximum moment in the sheetpile wall appears to be 262 kNm/m at a depth of 6,505 m below ground surface.

For those who like to solve this analytically, this is demonstrated here. There are four linear parts in the resulting horizontal stress development:

$$\begin{aligned}
 0 \leq z < 1,0: & \quad \sigma_{\text{hor, res}}(z) = 7^{1/3} + 6 \cdot z \\
 1,0 \leq z < 2,0: & \quad \sigma_{\text{hor, res}}(z) = 13^{1/3} + 13^{1/3} \cdot (z-1) = 13^{1/3} \cdot z \\
 2,0 \leq z < 3,0: & \quad \sigma_{\text{hor, res}}(z) = 26^{2/3} + 3^{1/3} \cdot (z-2) = 20 + 3^{1/3} \cdot z \\
 3,0 \leq z < 9,0: & \quad \sigma_{\text{hor, res}}(z) = 30 - 26^{2/3} \cdot (z-3) = 110 - 26^{2/3} \cdot z
 \end{aligned}$$

Where z is the depth below ground level in [m].

The values for S can be found by integrating $\sigma_{\text{hor, res}}(z)$: $S(z) = \int \sigma_{\text{hor, res}}(z) dz$:

$$\begin{aligned}
 0 \leq z < 1,0: & \quad S(z) = \int (7^{1/3} + 6 \cdot z) dz = 7^{1/3} \cdot z + 3 \cdot z^2 \\
 1,0 \leq z < 2,0: & \quad S(z) = \int (13^{1/3} \cdot z) dz = 3^{2/3} + 6^{2/3} \cdot z^2 \\
 2,0 \leq z < 3,0: & \quad S(z) = \int (20 + 3^{1/3} \cdot z) dz = -16^{1/3} + 20 \cdot z + 1^{2/3} \cdot z^2 \\
 3,0 \leq z < 9,0: & \quad S(z) = \int (110 - 26^{2/3} \cdot z) dz = -151^{1/3} + 110 \cdot z - 13^{1/3} \cdot z^2
 \end{aligned}$$

(The integral constants can be found by considering the highest level per range, for which the value of S is known, starting with $S = 0$ at ground level.)

The same recipe can now be followed to find the expressions for $M(z) = \int S(z) dz$:

$$\begin{aligned}
 0 \leq z < 1,0: & \quad M(z) = \int (7^{1/3} \cdot z + 3 \cdot z^2) dz = 3^{2/3} \cdot z^2 + z^3 \\
 1,0 \leq z < 2,0: & \quad M(z) = \int (3^{2/3} + 6^{2/3} \cdot z^2) dz = -0,61 + 1,833 \cdot z^2 + 2,22 \cdot z^3 \\
 2,0 \leq z < 3,0: & \quad M(z) = \int (-16^{1/3} + 20 \cdot z + 1^{2/3} \cdot z^2) dz = 12,72 - 16^{1/3} \cdot z + 10 \cdot z^2 + 0,556 \cdot z^3 \\
 3,0 \leq z < 9,0: & \quad M(z) = \int (-151^{1/3} + 110 \cdot z - 13^{1/3} \cdot z^2) dz = 147,72 - 151^{1/3} \cdot z + 55 \cdot z^2 - 4^{4/9} \cdot z^3
 \end{aligned}$$

The thus found values for M are slightly more accurate than those mentioned in the table above, which is caused by the rather rough subdivision in slices of 1 m thick in the numerical calculation above. The analytically calculated maximum moment, however, is still about 262 kNm/m.

The section modulus of the sheet pile wall required to resist the maximum bending stresses is:
 = 1115 cm³/m (for steel quality S235)

Step 4. Choose a suitable sheetpile profile from the product specifications

20% should be added to t to compensate for the simplified schematisation: $L_t = 1,20 \cdot t = 7,20$ m.

A profile with a sufficient section modulus is Larssen 603, for which $W_{eff,y} = 1200 \text{ cm}^3/\text{m} > 1115 \text{ cm}^3/\text{m}$ (see Appendix H of this Manual).

Calculation of horizontally supported sheet pile walls

If the design of a cantilever sheetpile wall does not suffice, horizontal supports can be applied as alternative to large or long profiles. The most common types of supports are struts (Chapter 38) and anchors (Chapter 39).

The mechanical schematisation of the supported sheet pile structure as a beam on two supports, or on a support and a (partly) fixed end, is a simplification of reality, but acceptable for a first conceptual design as it leads to conservative designs if the right safety factors are used. Figure 37-9 shows different, schematisations of the toe of the piled wall. If the wall has insufficient embedded depth, it will move towards the passive side (a), but this translation of the lower support point will be prevented if the embedded depth increases (b). The sheet pile wall could be more or less considered as a beam on two supports. If the wall becomes longer, a partly fixed end originates (c), which transforms into a fully fixed end at a certain depth, where the deflection angle is zero (d). A further increase of the embedded depth does not lead to a change of the position of the fixed support and is needless.

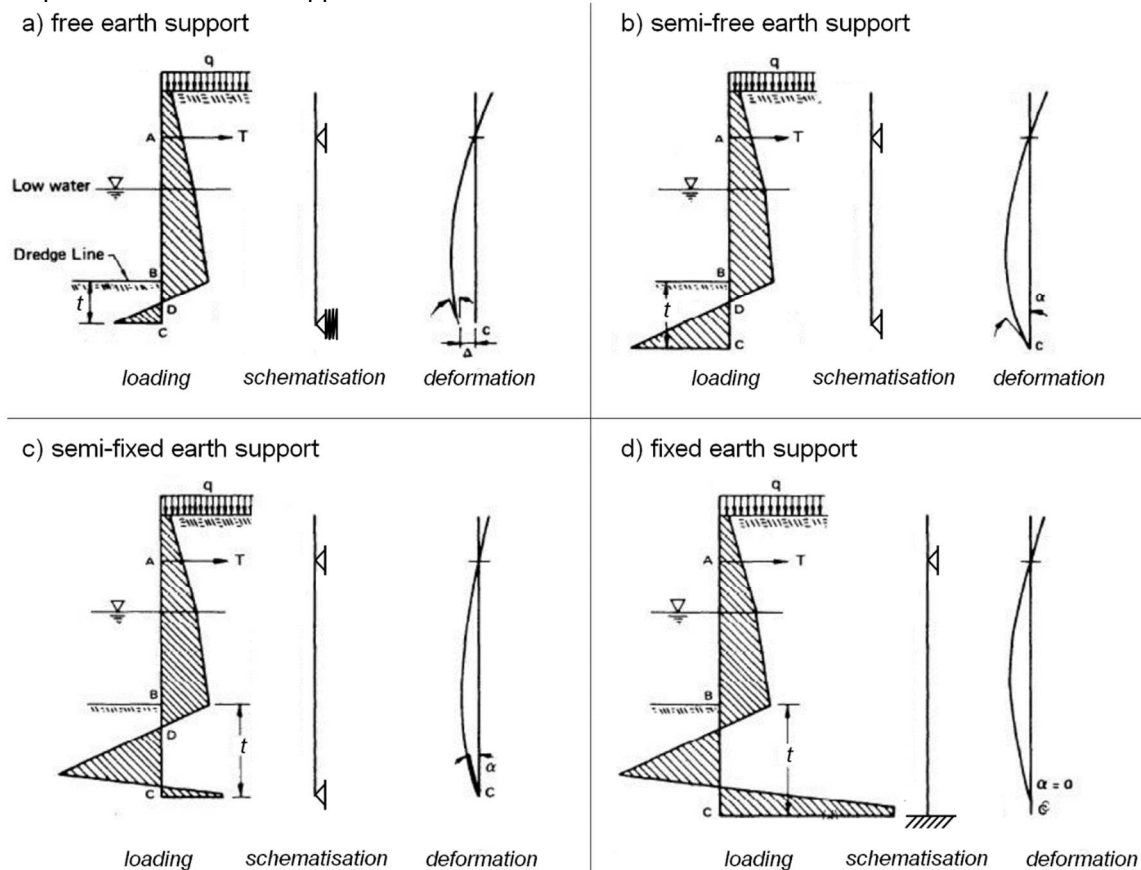


Figure 37-9 Effect of the embedded depth on the pressure distribution and the deflection

The first schematisation (a) is commonly called the free earth support schematisation. The passive stresses in front of the wall are insufficient to prevent lateral movement and rotations in point C. The next schematisations show the effect of increasing the embedded depth. In cases (b) and (c) the passive stresses pressure has increased enough to prevent lateral deflection at point C; however, rotation still occurs. In case (d) passive pressures have sufficiently developed on both sides of the wall to prevent both lateral deflection and rotation at C. This schematisation is commonly called the fixed earth support schematisation, because point C is essentially fixed.

For the free earth support schematisation (a), the soil at the lower part of the piles is incapable of inducing effective resistance, so that it would not result in negative bending moments. The passive pressures in front of the sheet piles are insufficient to prevent lateral movement and rotations at the lower end of the piling.

No passive resistance is developed on the backside of the wall below the line of excavation.

For the fixed earth support schematisation, the piling is driven deep enough so that the soil under the line of excavation provides the required resistance against deformations and rotations. In other words: the lower end of piling is essentially fixed.

Free and fixed earth schematisations are mutually independent; their results should not be mixed. Sheet pile walls designed with free earth schematisations tend to be shorter and have a higher moment of inertia against bending stresses than fixed earth schematisations, while the latter tend to be longer with a lower moment of inertia.

The following two subsections explain the free and fixed schematisations in more detail.

1. Free earth support schematisation of supported sheet pile walls (American method)

The wall is schematised as a beam on two free supports and it is assumed that the anchor provides the necessary resistance of the sheet pile (Figure 37-9b). Free earth methods result in a statically determinate structure, but that structure is only stable under certain load conditions, namely 1) the sum of the distributed loads equals to the anchored load and 2) the passive earth pressure resistance below the excavation line is sufficiently large to prevent overturning. Generally, the first criterion governs, with the resultant horizontal support force being a result of the calculations.

Calculation steps of the embedded depth and anchor force per running metre:

- Step 1. Determine the governing load situation regarding water levels, surcharge and other external loads;
- Step 2. Calculate and draw the vertical soil stresses and the (ground) water pressures;
- Step 3. Calculate the horizontal loads stresses at the active and passive side as a function of the theoretical embedded depth (*inheidiepte*) t_0 .
- Step 4: Compute the equilibrium of moments around the anchor point $\sum M_E = 0$ in order to determine the embedded depth t_0 .
- Step 5: Compute the support force T from the horizontal equilibrium $\sum H = 0$.
- Step 6: Determine the maximum moment in the sheetpile wall and calculate the minimum required section modulus ($W_{eff,y}$).
- Step 7: Choose an appropriate sheet pile profile and length from the manufacturer's information ($t = t_0$).

To increase the safety of the structure, often either a larger maximum bending moment is assumed than computed, or the passive ground pressure is reduced by using a conservative value for K_p .

2. Fixed earth support schematisation of supported sheet pile walls (European, or Blum's method)

With the fixed earth schematisation, the wall has two supports: a simple support at the anchor and a fixed support at the toe. The system is therefore statically indeterminate, forcing the designer to consider system deflections. This would become very elaborative for hand calculations, which is the reason why Blum proposed to replace the fixed end of the toe of the wall by a free support plus a substitute force. The loads on the sheet pile wall are schematized as shown on the right-hand side of Figure 37-10.

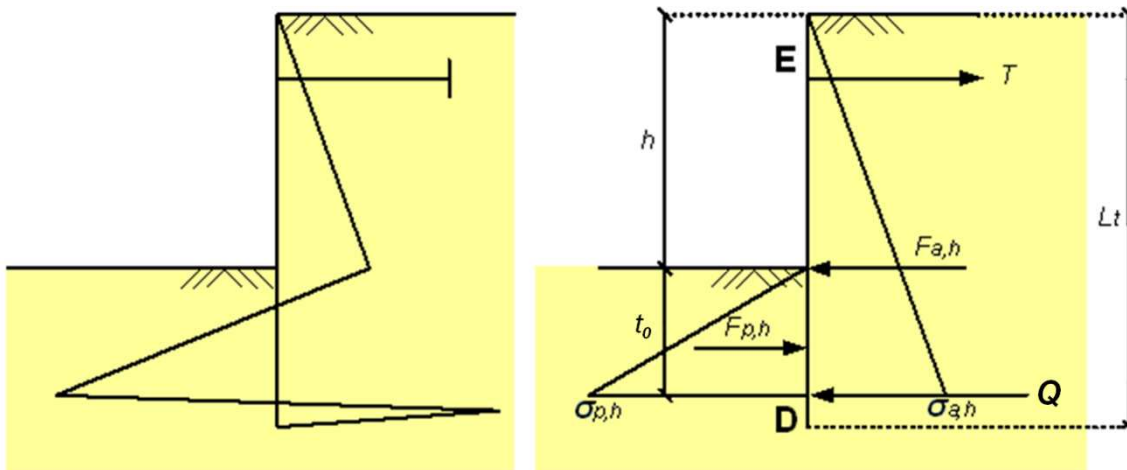


Figure 37-10 left: 'real' situation; right: Blum's schematisation.

The substitute force R (= *Ersatzkraft*) in the above schematisation is equivalent to the horizontal soil pressure at the lower part of the right-hand side of the sheet pile wall. Furthermore, it is assumed that the bending moment at the toe of the sheet pile is zero, but a shear force (of the magnitude Q) is allowed. To ensure that this shear force can develop, the actual length of the sheet piles should be longer than the sum of the retaining height and the embedded depth. Usually, the computed embedded depth is increased by 20%, similar to the cantilever method (see Table 37-2 for the exact values of this increment factor).



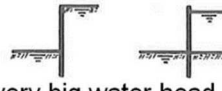
wall type	 small water head difference	 big water head difference	 very big water head difference or only water pressure
anchored and fixed toe	1,10	1,15	1,20 - 1,30
anchored and toe free supported	1,05	1,10	1,15 - 1,20

Table 37-2 Increment factor α for the embedded depth of supported sheetpile walls (from: Hoesch Spundwand-Handbuch 1980)

The computation of the main sheetpile characteristics of supported sheet pile walls differs from cantilever sheetpile walls, because now there are not two, but three unknown parameters: the embedded depth (d), the anchor force (T) and the substitute force (R). They can be solved by considering the displacement at the anchor point, in addition to the horizontal equilibrium of forces, and the moment equilibrium. The displacement of the sheetpile wall at the anchor point is prevented by the anchors, so it equals zero.

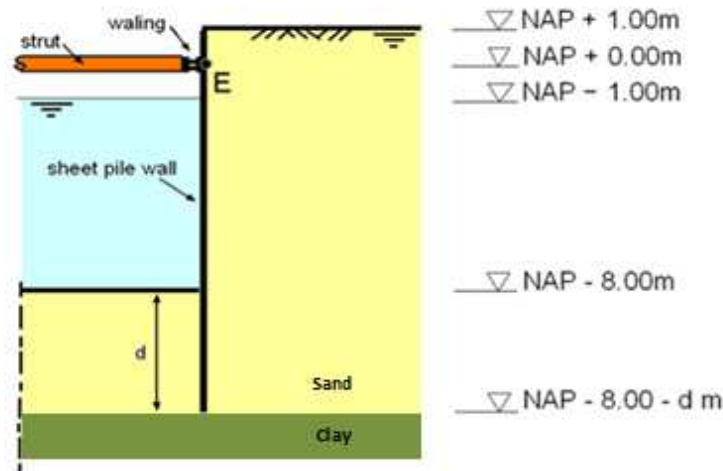
Compared to the free earth schematisation for supported sheetpile walls, Blums' schematisation will mostly lead to somewhat longer sheetpiles, but the required profiles will be lighter and the displacements will be less. Hence the advantages of Blum's method, a lighter profile and smaller displacements, comes at the expense of a longer sheet pile wall.

The calculation of the embedded depth, anchor force and substitute force per running metre thus consists of the following steps:

- Step 1. Determine the governing load situation regarding water levels, surcharge and other external loads;
- Step 2. Calculate and draw the vertical soil stresses and the (ground) water pressures;
- Step 3. Calculate the horizontal loads stresses at the active and passive side as a function of the theoretical embedded depth (*inheidiepte*) t_0 .
- Step 4: Compute the theoretical embedded depth (d) using the condition that the horizontal displacement at the level of the anchor (point E) must be zero.
- Step 5: Compute the equilibrium of moments around the toe of the sheet pile (point D) in order to determine the anchor force (T).
- Step 6: Compute the substitute force (Q), from the horizontal equilibrium $\sum H = 0$.
- Step 7: Determine the maximum moment in the sheetpile wall and calculate the minimum required section modulus ($W_{eff,y}$).
- Step 8. Multiply the theoretical embedded depth with the increment factor α given in Table 37-2 to determine the real required length.
- Step 9. Choose a suitable sheetpile profile from the product specifications of the manufacturer.

Elaborated example: Calculation of a horizontally supported sheet pile wall calculation with the free earth support method

In the Figure, an overview is given of a sheet pile wall in homogeneous wet sand.



Parameters

Variable	Value and Unit
Specific weight of saturated sand (γ_s)	20 [kN/m ³]
Angle of internal friction of the sand (ϕ):	30 [°]
Cohesion of the sand (c):	0 [kN/m ²]
Wall friction for a smooth wall (δ):	0 [°]

Water and ground levels are indicated in the figure as well as the height of the strut. Assume that the toe of the sheet pile wall touches a clay layer, preventing groundwater flow (so the water pressure is hydrostatic).

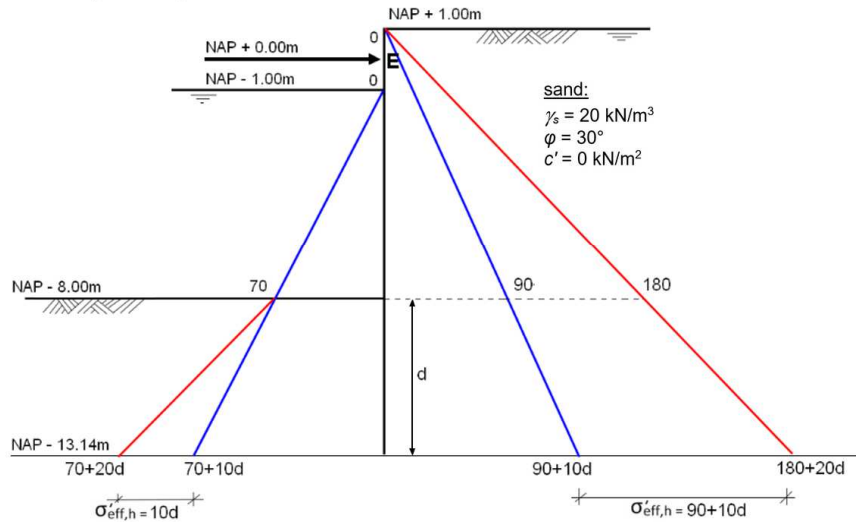
Question

Calculate what sheetpile profile is needed to resist the loads in the given load situation, using the free earth support schematisation. Choose a Hoesch profile with steel quality S235. There is no surcharge to be taken into account. Also the use of safety coefficients is refrained of in this example.

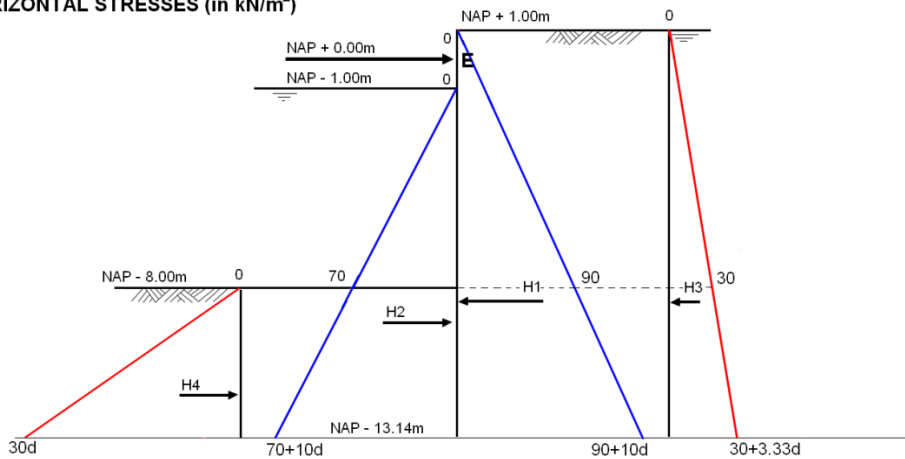
Step 1. Calculate the embedded depth of the sheetpile wall

The first step is to calculate the embedded depth d of the sheet pile wall, by considering the equilibrium of moments around the anchor point (NAP + 0.00m). The vertical stresses are indicated below. The values at the lower/lowest levels are expressed as a function of d . The total soil stress and the water pressure are separately drawn, in order to be able to calculate the effective stress. The horizontal effective stresses are calculated by multiplying the effective vertical soil stresses with $K_a = 0,33$ (active side) and $K_p = 3,0$ (passive side). A value of $\gamma_s = 20$ kN/m³ has been used everywhere, because the soil is wet on both sides in this (simplified) situation. *Also notice that the water stresses at the toe of the wall differ at the passive and active side, which is only possible because of the assumption that the toe of the wall touches an impermeable clay layer (see the previous example calculation for an explanation).*

VERTICAL STRESSES (in kN/m²)



HORIZONTAL STRESSES (in kN/m²)



force:

$$\begin{aligned}
 H1 &= \frac{1}{2}(90+10d) \cdot (9+d) = 405 + 90d + 5d^2 \\
 H2 &= \frac{1}{2}(70+10d) \cdot (7+d) = 245 + 70d + 5d^2 \\
 H3 &= \frac{1}{2}(30+3.33d) \cdot (9+d) = 135 + 30d + 1.67d^2 \\
 H4 &= \frac{1}{2}(30d) = 15d^2
 \end{aligned}$$

arm:

$$\begin{aligned}
 a1 &= 5 + \frac{2}{3}d \\
 a2 &= 5\frac{2}{3} + \frac{2}{3}d \\
 a3 &= 5 + \frac{2}{3}d \\
 a4 &= 8 + \frac{2}{3}d
 \end{aligned}$$

moment:

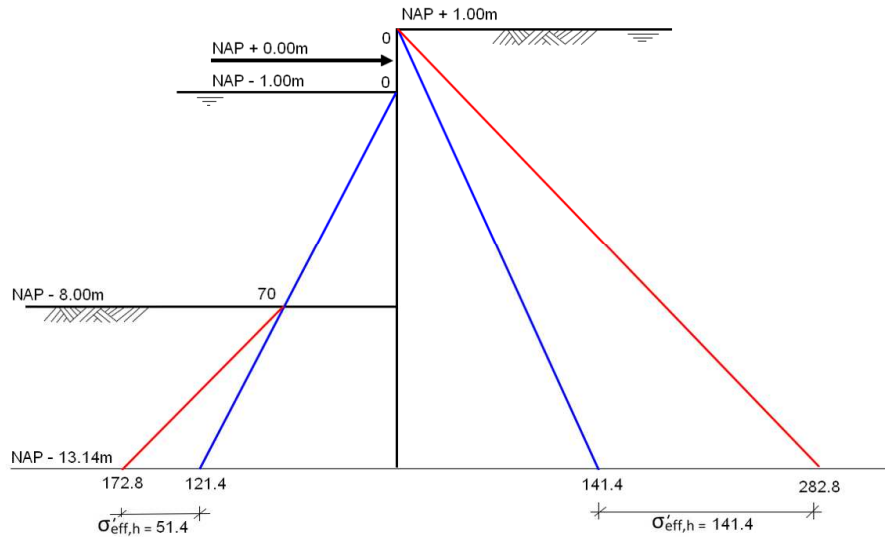
$M1_E = H1 \cdot a_1 =$	2025	+ 720 d	+ 85 d ²	+ 3,33 d ³
$M2_E = H2 \cdot a_2 =$	- 1388	- 560,3 d	- 75 d ²	- 3,33 d ³
$M3_E = H3 \cdot a_3 =$	675	+240 d	+ 28,33 d ²	+1,11 d ³
$M4_E = H4 \cdot a_4 =$			-120 d ²	-10 d ³
$\Sigma M =$	1312	+399,67 d	- 81,67 d ²	-8,89 d ³

Equilibrium $\Sigma M = 0$ is established for $d = 5,14$ m.

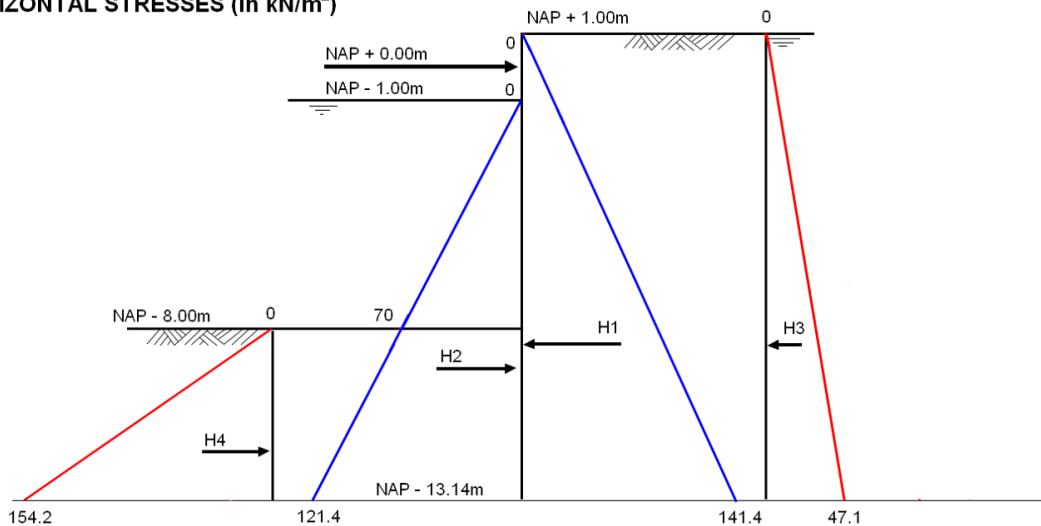
Step 2. Calculate the required strut force.

The stresses for $d = 5,14$ m are indicated below.

VERTICAL STRESSES (in kN/m²)



HORIZONTAL STRESSES (in kN/m²)



Resulting horizontal forces:

Water:

$$H1 = 141,4/2 \times 14,14 = 999,7 \text{ kN/m'}$$

$$H2 = 121,4/2 \times 12,14 = 736,4 \text{ kN/m'}$$

Soil:

$$H3 = 47,3/2 \times 14,14 = 333,2 \text{ kN/m'}$$

$$H4 = 154,2/2 \times 5,14 = 396,3 \text{ kN/m'}$$

$$\Sigma H = 0 \rightarrow H_{strut} = H1 - H2 + H3 - H4 = 200 \text{ kN/m' } (\rightarrow)$$

Step 3. Calculate the required section modulus $W_{eff,y}$, choose a sheetpile profile:

The diagram of the resulting horizontal stresses can be found by summarizing the horizontal water pressures and horizontal effective soil stresses as in the previous figure.

The shear force diagram is found by calculating the area under the resulting horizontal stresses diagram. The area of every slice equals the change in the shear stress diagram. (In other words: the shear stress is obtained by integrating the function for the resulting horizontal stresses). In the chosen schematisation, the shear stress diagram starts with 0 kN (per m') at the soil surface.

The moment diagram is found by calculating the area under the shear stress diagram. The area per slice of the shear stress diagram equals the change in the moment diagram. The moment diagram starts with 0 kNm (per m') at the soil surface.

The M-diagram reaches its highest value where the value of the S-diagram is zero. This zero point can be calculated with the equation below (valid for $2 < h < 9$ m and only for the situation in this example):

$$\frac{1}{2} \cdot \gamma_w (h-2)^2 + F_{strut} - \frac{1}{2} \gamma_w \cdot h^2 - \frac{1}{2} K_a \cdot h^2 \cdot (\gamma_{s,w} - \gamma_w) = 0 \rightarrow h = 6,95 \text{ m below ground level}$$

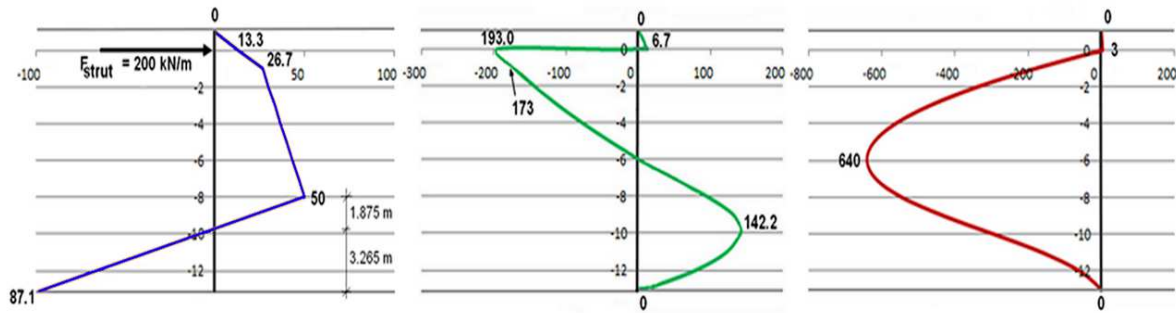
The point of zero shear force can also be found numerically by subdividing the soil into slices of 1 m and calculating the areas below the resulting horizontal stress diagram, which equals the change in the S-diagram line (which starts with $S = 0$ at ground level). For instance, the total horizontal stress on the wall at NAP (1 m below ground level) is $1,00 \cdot K_a (\gamma_{s,w} - \gamma_w) + 1,00 \gamma_w = 13,33 \text{ kN/m}^2$. The value of the shear force in the wall at that point is $\frac{1}{2} \cdot 13,3 \cdot 1,00 = 6,67 \text{ kN/m}$ (= the area below the resulting stress diagram over the highest 1 m). Because of the strut force, the shear force diagram then jumps to $6,67 - 200 = -193,33 \text{ kN/m}$. The shear diagram then follows a line to NAP - 5,95 m, where the shear stress is zero, then further to the right where it reaches a new (local) maximum and then it bends back because of the increasing passive stresses. This is a second degree function.

The moment diagram, a third degree function, can now be found by calculating the areas below the shear force diagram. These areas equal the changes in the moment diagram line. At ground level, $M = 0$ because of the schematisation (free support). For the upper 1 m, this area is $6,67 / 2 = 3,33 \text{ kNm/m}$.

The values of the σ_h , S- and M-diagrams are presented in the table below. This has been elaborated for slices of 1.00 m to obtain a rather precise result, see the following table and graphs.

depth level [m]	horizontal stress [kN/m]	S-diagram [kN/m]	M-diagram [kNm/m]
NAP + 1	0,00	0,00	0,00
NAP + 0	13,33	6,67	3,33
NAP + 0	13,33	-193,03	3,33
NAP - 1	26,67	-173,03	-179,70
NAP - 2	30,00	-144,70	-338,57
NAP - 3	33,33	-113,03	-467,43
NAP - 4	36,67	-78,03	-562,97
NAP - 5	40,00	-39,70	-621,83
NAP - 5.95	43,17	-0,20	-640,78
NAP - 6	43,33	1,97	-640,70
NAP - 7	46,67	46,97	-616,23
NAP - 8	50,00	95,30	-545,10
NAP - 9	23,33	131,97	-431,47
NAP - 9.875	0,00	142,17	-311,53
NAP - 10	-3,33	141,97	-293,77
NAP - 11	-30,00	123,22	-161,18
NAP - 12	-56,67	79,88	-59,63
NAP - 13	-83,33	12,00	-0,75
13.14	-87,07	0,00	0,00

σ_h , S- and M-diagram



Resulting horizontal stress, shear force and moment diagrams

The maximum moment appears to be 641 kNm/m, at NAP - 5,95 m.

The required section modulus (*weerstandsmoment*) of the sheetpile profile then is:

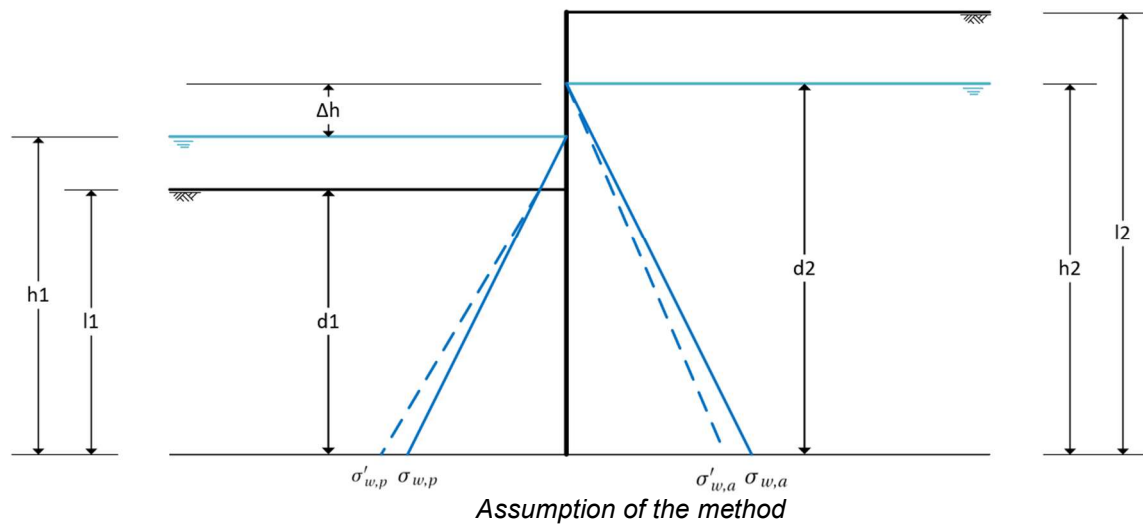
$$W = \frac{M_{\max}}{f_{y,d}} = \frac{641 \cdot 10^6}{235} = 2728 \cdot 10^3 \text{ mm}^3/\text{m} = 2728 \text{ cm}^3/\text{m}$$

Step 4: choose an appropriate sheet pile profile

According to the specifications of the manufacturer (Appendix H), profile Hoesch 215 has a section modulus of 3150 cm³/m, which is a bit more than strictly required.

Alternative situation: no impermeable clay layer at the toe

If there is no clay layer present at the toe of the sheet pile wall, the groundwater is free to flow underneath it. Practically this means that the water pressure distribution is not hydrostatic anymore. This is visualised in the figure below, where the solid lines indicate the hydrostatic water pressure distribution, and the dashed lines indicate the resulting water pressure distribution due to groundwater flow. Note that the open water on the passive side is not affected.



The D-Sheet Piling User Manual (Deltares, 2017) proposes an approximation method for the water pressures acting on the wall, which could be used for preliminary designs. It proposes the following water pressures at the toe of sheetpile wall:

$$\sigma'_{w,p} = h_1 \gamma_w + \frac{0,7 \cdot \Delta h}{d_1 + \sqrt{d_1 d_2}} \cdot h_1 \cdot \gamma_w \quad \text{and} \quad \sigma'_{w,a} = h_2 \gamma_w - \frac{0,7 \cdot \Delta h}{d_2 + \sqrt{d_1 d_2}} \cdot h_2 \cdot \gamma_w,$$

where d_1 and d_2 are the thicknesses of the wet soil layers above the toe of the sheetpile wall, i.e. $d_1 = \min(h_1, l_1)$ in which h_1 and h_2 are the water levels and l_1 and l_2 are the soil levels above the toe.

However, this method can only be applied as a correction after the calculation has been performed, and does not give an easy way to find the water pressure at every depth. In order to do this the equation can be rewritten such that an effective specific weight of groundwater can replace the normal specific weight of water:

$$\gamma'_{w,p} = \gamma_w \left(1 + \frac{0,7 \cdot \Delta h}{d_1 + \sqrt{d_1 d_2}} \right) \quad \text{and} \quad \gamma'_{w,a} = \gamma_w \left(1 - \frac{0,7 \cdot \Delta h}{d_2 + \sqrt{d_1 d_2}} \right)$$

The only problem left is that d_1 and d_2 depend on the embedded depth which is still unknown. To work around this, an estimate of the embedded depth can be made using rules of thumb. Note that this estimate should only be used for the determination of $\gamma'_{w,p}$ and $\gamma'_{w,a}$ but nothing else. Some rules of thumb that can be used are as follows:

$$t_{\text{est}} = \frac{1}{2} \left(L + \frac{q}{20} + \Delta h \right) \quad \text{for horizontally supported sheet piles (free earth support)}$$

$$t_{\text{est}} = \frac{3}{4} \left(L + \frac{q}{20} + \Delta h \right) \quad \text{for horizontally supported sheet piles (fixed earth support)}$$

$$t_{\text{est}} = \frac{5}{4} \left(L + \frac{q}{20} + \Delta h \right) \quad \text{for sheet piles without horizontal support}$$

In these rules of thumb L is the retaining height [m] and q is the surcharge on top of the active side [kN/m²].

Be aware that an overestimation of the embedded depth leads to a smaller correction (closer to the hydrostatic situation), whereas an underestimation of the embedded depth leads to larger corrections than are realistic. When in doubt, it is better to take a slightly larger estimation for the embedded depth than taking a smaller one.

Note: in the following section this question is worked out for the alternative situation, but only step 1 is shown since this is the only step that is inherently different.

Step 1. Calculate the embedded depth of the sheetpile wall

For the free earth support schematization the following rule of thumb gives an estimation for the embedded depth:

$$t_{\text{est}} = \frac{1}{2} \left(L + \frac{q}{20} + \Delta h \right) = \frac{1}{2} \left(9,0 + \frac{0}{20} + 2 \right) = 5,5 \text{ m}$$

With this the thicknesses of the wet soil layers d_1 and d_2 can be found:

$$d_1 = \min(h_1, l_1) = \min(t_{\text{est}} + 7,0; t_{\text{est}}) = 12,5 \text{ m}$$

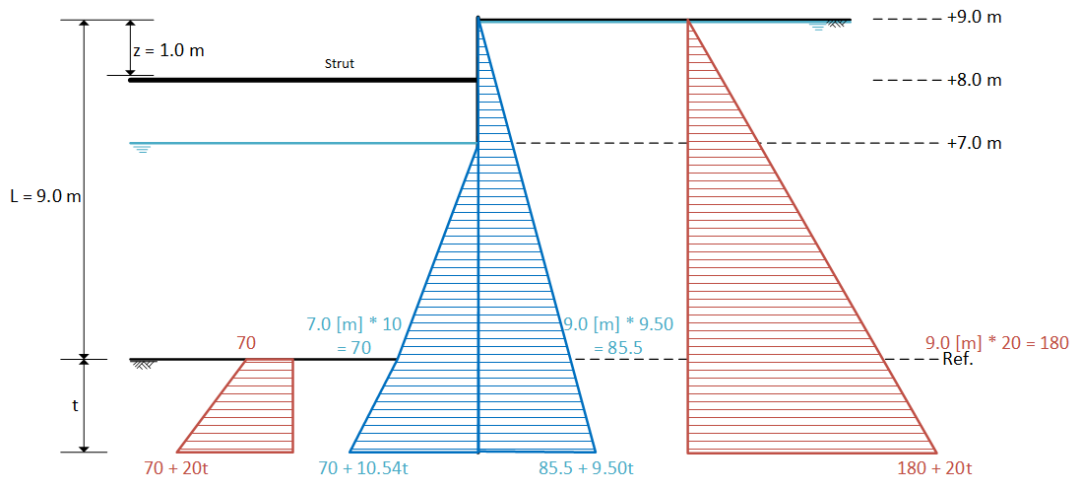
$$d_2 = \min(h_2, l_2) = \min(t_{\text{est}} + 9,0; t_{\text{est}} + 9,0) = 14,5 \text{ m}$$

Now the effective specific weights can easily be calculated:

$$\gamma'_{w,p} = \gamma_w \left(1 + \frac{0,7 \cdot \Delta h}{d_1 + \sqrt{d_1 d_2}} \right) = 10 \left(1 + \frac{0,7 \cdot 2,0}{12,5 + \sqrt{12,5 \cdot 14,5}} \right) = 10,54 \quad \text{kN/m}^3$$

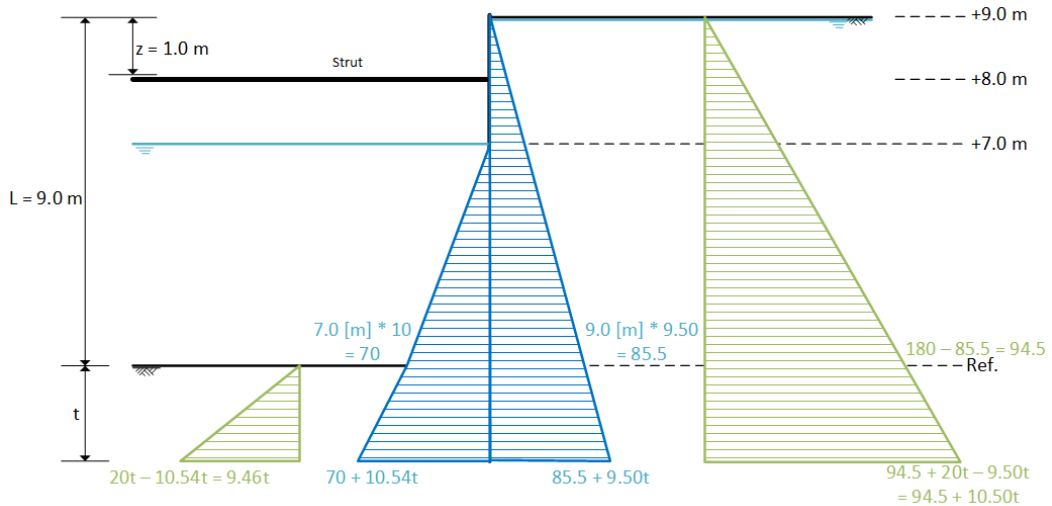
$$\gamma'_{w,a} = \gamma_w \left(1 - \frac{0,7 \cdot \Delta h}{d_2 + \sqrt{d_1 d_2}} \right) = 10 \left(1 - \frac{0,7 \cdot 2,0}{14,5 + \sqrt{12,5 \cdot 14,5}} \right) = 9,50 \quad \text{kN/m}^3$$

The vertical stresses are calculated in the figure below. Especially pay attention to which specific weight for water is used at each location.



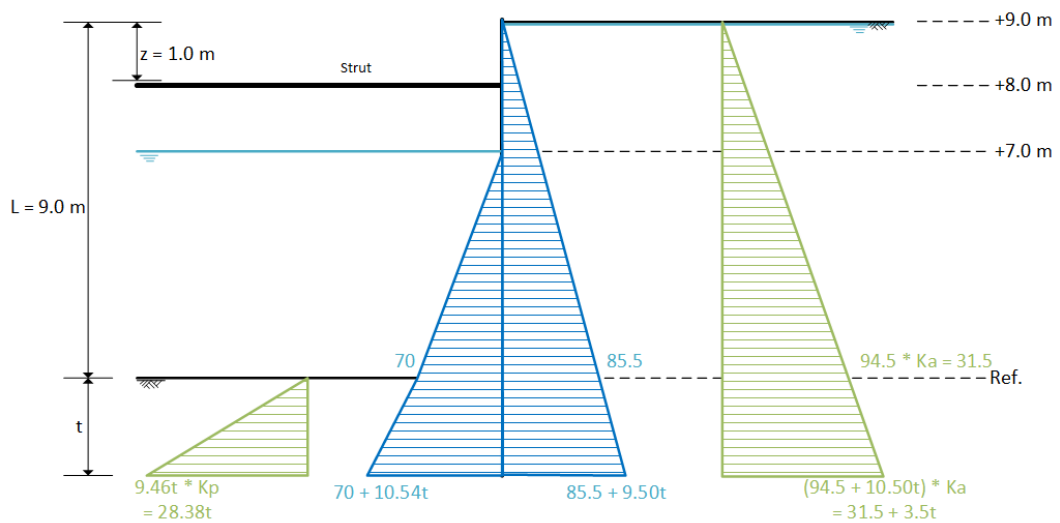
Vertical stresses: water pressures (blue) and total stresses (red)

Next, this diagram can be converted to show the effective vertical stresses and water pressures:



Vertical stresses: water pressures (blue) and effective stresses (green)

Then this diagram can be converted to the horizontal stress diagram:



Horizontal stresses: water pressures (blue) and soil stresses (green)

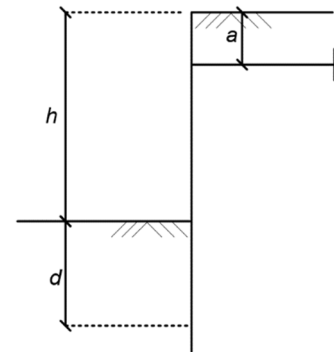
From this point onwards the problem is very similar to the original situation with a clay layer, the only difference being that the bend in the water pressure from the left at reference level. This introduces a few extra forces in the the moment equilibrium equation, but because the next steps remain the same they are not further shown here.

Calculation of a horizontally supported sheet pile wall calculation with the fixed earth support method

The situation and soil profile for this example are extremely simplified to avoid too complex computation, see the following figure: It is assumed that the sheet pile wall is placed in homogeneous dry sand. There is no surface water and no ground water.

Parameters

Variable	Value and unit
active soil pressure coefficient (K_a)	$\frac{1}{3}$ [-]
passive soil pressure coefficient (K_p)	3 [-]
specific weight of dry sand (γ_d)	18 [kN/m ³]
retaining height (h)	6 [m]
depth of the anchor below ground level (a)	1 [m]
cohesion (c)	0 [°]
wall friction for a smooth wall (δ)	0 [°]



Asked

Calculate required section modulus and length of the sheet pile wall using the fixed earth support schematisation and choose a suitable Larssen profile with steel quality S235.

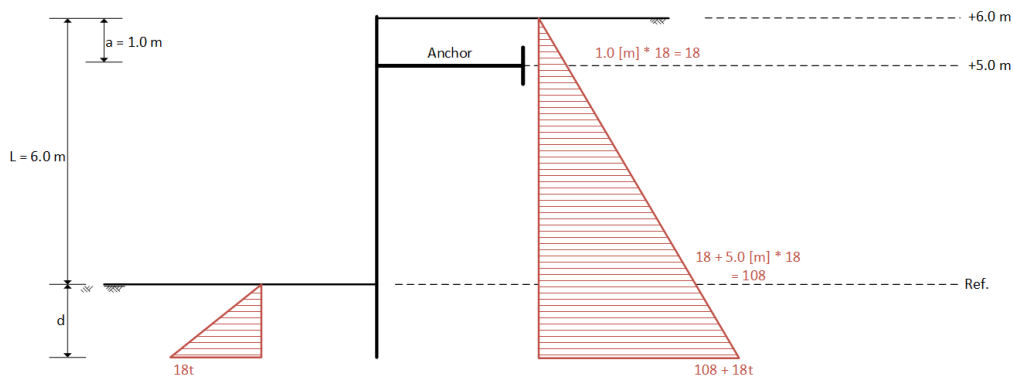
Note: For the first half of this example, two alternative workings are given. Method A places the anchor force at the real level, which is of course more accurate but can much work. Method B places the anchor force at the ground level (only in calculation, not in reality), which is less accurate but reduces several terms from the calculations and is easier to perform by hand.

Method A:

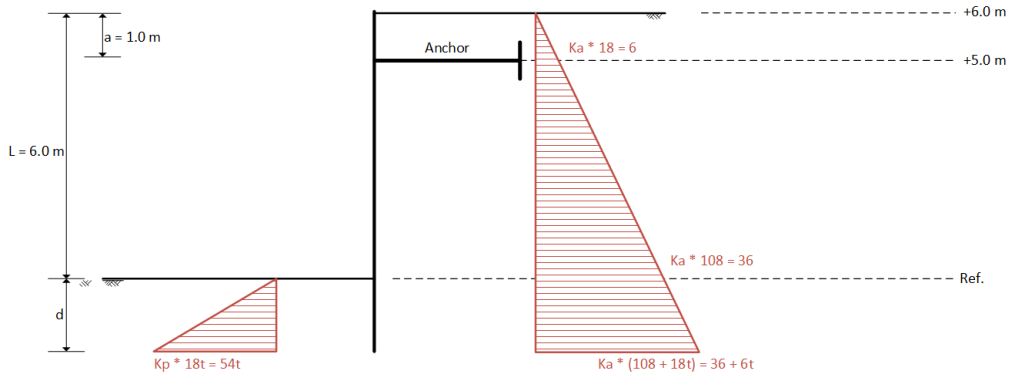
Step 1. Compute the embedded depth (d), total length of the sheet piles (L_t) and anchor force (T) per m¹

Step 1.1. Find an expression for the horizontal displacement at the anchor level

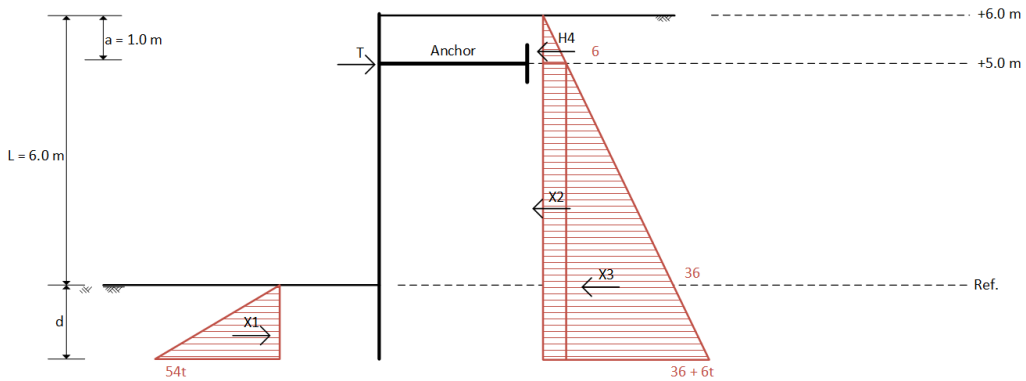
Vertical stress



Horizontal stress



Horizontal forces

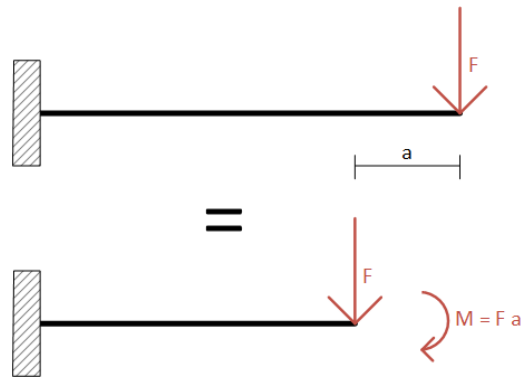


One of the boundary conditions in this approach is that the sum of all displacements at the anchor point must be zero, since the anchor is fixed in place. To derive an expression for this, the horizontal stresses need to be divided into several standard load cases, for example equivalent point loads. The deflections as a result of each load are given in the table below.

Force	Value [kN/m']	Arm (a) [m]	Direct deflection [m]	Additional deflection (kwispeleffect) [m]
T	T	d + 5,0	$\frac{T \cdot (a_T)^3}{3 \cdot EI}$	0

Load	Load (q) [kN/m/m']	Length (l) [m]	Direct deflection [m]	Additional deflection (kwispeleffect) [m]
X1	54 d	d	$\frac{q_1 \cdot (l_1)^4}{30 \cdot EI}$	$(d + 5,0) \cdot \frac{q_1 \cdot (l_1)^3}{24 \cdot EI}$
X2	- 6	d + 5,0	$\frac{q_2 \cdot (l_2)^4}{8 \cdot EI}$	0
X3	-(30 + 6d)	d + 5,0	$\frac{q_3 \cdot (l_3)^4}{30 \cdot EI}$	0

The force H4 has to be taken separately, because it works above the point of interest (the anchorpoint). The resulting deflection from this force consists of two components: the pointload as if it works at the anchor point, and an additional moment that is introduced by moving the pointload. See the image below.



Force	Value [kN/m']	Deflection pointload [m]	Moment [kNm/m']	Deflection moment [m]
H4	$-\left(\frac{1}{2} \cdot 1,0 \cdot 6\right) = -3$	$\frac{H_4 \cdot (a_4)^3}{3 \cdot EI}$	$0,33 \cdot H_4 = -1$	$\frac{M_4 \cdot (d + 5,0)^2}{2 \cdot EI}$

The sum of all displacements at the anchor- or strut level needs to be zero:

$$\sum u = u_1 + u_2 + u_3 + u_4 + u_T = 0$$

Filling in all the derived components:

$$\sum u = \frac{q_1 \cdot (l_1)^4}{30 \cdot EI} + (d + 5,0) \cdot \frac{q_1 \cdot (l_1)^3}{24 \cdot EI} + \frac{q_2 \cdot (l_2)^4}{8 \cdot EI} + \frac{q_3 \cdot (l_3)^4}{30 \cdot EI} + \frac{H_4 \cdot (a_4)^3}{3 \cdot EI} + \frac{M_4 \cdot (t + 5,0)^2}{2 \cdot EI} + \frac{T \cdot (a_T)^3}{3 \cdot EI} = 0$$

Filling in values for the forces, loads, moments, arms and lengths

$$\sum u = \frac{54d \cdot (d)^4}{30 \cdot EI} + (d + 5,0) \cdot \frac{54d \cdot (d)^3}{24 \cdot EI} - \frac{6 \cdot (d + 5,0)^4}{8 \cdot EI} - \frac{(30 + 6d) \cdot (d + 5,0)^4}{30 \cdot EI} - \frac{3 \cdot (d + 5,0)^3}{3 \cdot EI} - \frac{1 \cdot (d + 5,0)^2}{2 \cdot EI} + \frac{T \cdot (d + 5,0)^3}{3 \cdot EI} = 0$$

The expression can be simplified removing the denominators:

$$\sum u = 1,8 \cdot d \cdot (d)^4 + (d + 5,0) \cdot 2,25d \cdot (d)^3 - 0,75(d + 5,0)^4 - \frac{1}{30}(30 + 6d) \cdot (d + 5,0)^4 - (d + 5,0)^3 - 0,5(d + 5,0)^2 + \frac{1}{3}T \cdot (d + 5,0)^3 = 0$$

Next the expression can be simplified:

$$\begin{aligned} \sum u &= 1,8d^5 + (d + 5,0) \cdot 2,25d^4 - \\ &0,75(d + 5,0)^4 - \\ &(1 + 0,2d) \cdot (d + 5,0)^4 - \\ &(d + 5,0)^3 - 0,5(d + 5,0)^2 + \\ &\frac{1}{3}T \cdot (d + 5,0)^3 = 0 \end{aligned}$$

Lastly, the expression can be written in the following form with help from software:

$$\sum u = 3.85d^5 + 5.5d^4 - 66d^3 - 378d^2 - 1080d - 1231.25 + \frac{1}{3}T \cdot (d + 5.0)^3 = 0$$

Step 1.2. Find an expression for the sum of moments around the toe of the wall

The second boundary condition in this approach is that the sum of moments around the toe of the sheet pile wall must be equal to zero. The following table uses the same subdivision as used in the deflection formula, but uses forces instead of loads.

Force	Value [kN/m']	Arm (a) [m]
H1	$\frac{1}{2}d \cdot 54d = 27d^2$	$\frac{1}{3}d$
H2	$-(6 \cdot (d + 5.0)) = -(6d + 30)$	$(d + 5.0) / 2$
H3	$-\left(\frac{1}{2} \cdot (d + 5.0) \cdot ((6d + 36) - 6)\right)$ $= -(3d^2 + 30d + 75)$	$(d + 5.0) / 3$
T	T	d + 5.0

Using this the moment equilibrium equation can be derived as follows:

$$\begin{aligned} \sum M &= M_1 + M_2 + M_3 + M_4 + M_T = \\ 27d^2 \cdot \frac{1}{3}d - (6d + 30) \cdot \left(\frac{1}{2}d + 2.5\right) - (3d^2 + 30d + 75) \cdot \left(\frac{1}{3}d + 1.67\right) - 3 \cdot (d + 5) + \frac{1}{3} \cdot 1.0 + T \cdot (d + 5.0) &= \\ 9d^3 - (3d^2 + 30d + 75) - (d^3 + 15d^2 + 75d + 125) - (3d + 16) + T \cdot (d + 5.0) &= \\ 8d^3 - 18d^2 - 108d - 216 + T \cdot (d + 5.0) &= 0 \end{aligned}$$

Step 1.3. Find the required depth (d) and anchor force (T) per m¹

Now the two derived expressions can be combined to find the values for the embedded depth t_0 and anchor force T . First the moment equilibrium expression is rewritten for T .

$$\begin{aligned} \sum M &= 8d^3 - 18d^2 - 108d - 216 + T \cdot (d + 5.0) = 0 \\ T &= \frac{-8d^3 + 18d^2 + 108d + 216}{(d + 5.0)} \end{aligned}$$

This expression for T can then be substituted into the expression for the zero displacement condition.

$$\sum u = 3.85d^5 + 5.5d^4 - 66d^3 - 378d^2 - 1080d - 1231.25 + \frac{1}{3} \left(\frac{-8d^3 + 18d^2 + 108d + 216}{(d + 5.0)} \right) \cdot (d + 5.0)^3 = 0$$

Solving these expressions results in the following values:

$$\begin{aligned} d_0 &\approx 4.41 \text{ m} \\ T &\approx 37.76 \text{ kN/m} \end{aligned}$$

As was already mentioned earlier, it is common practice to increase the embedded depth by 20% to some safety within the structure. The total length of the sheet piles then becomes:

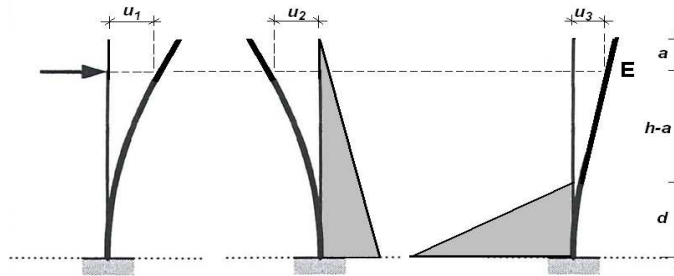
$L_t = h + 1.2d_0 = 6.00 + 1.2 \cdot 4.41 \approx 11.29 \text{ m}$. According to the manufacturers of sheet pile elements, their delivered length can deviate +/- 0.20 m from the ordered length, so choose an overall-length of at least 11.49 m.

Note: as can be seen this approach is a bit more time-consuming and sensitive to mistakes. Especially when water levels need to be taken into account as well the number of terms can become quite high. Because of this engineers sometimes assume the anchor to be placed at the ground level since this reduces the number of terms in the expression for horizontal displacement. However, be aware that this makes the outcome less reliable, and in typical situations this trick underestimates the loads on the sheet pile wall.

Method B:

Step 1.1. Compute the anchor force (T) per m^1

For the computation of the horizontal displacement at the top of the sheet pile wall (which must be zero), the contribution of the three types of loading can best be considered separately, see figure below: $u_1 - u_2 + u_3 = 0$. The displacements are computed using the theory of bending beams, from applied mechanics. For the calculation of the displacements, the toe of the wall is assumed to be fixed in the soil.



The first loading case is the anchor force (T), which leads to a horizontal displacement at the anchor point of:

$$u_1 = \frac{T \cdot (h+d-a)^3}{3 \cdot EI}$$

(See the standard deflection formulas (*vergeet-me-nietjes*) as given in Appendix D of this Manual)

The loading as a result of the active soil pressure results in a horizontal displacement at the anchor point of:

$$u_2 = -\frac{q \cdot (h+d-a)^4}{30 \cdot EI} = -\frac{K_a \cdot \gamma_d \cdot (h+d-a)^5}{30 \cdot EI} \text{ (by approximation!)}$$

The loading as a result of the passive soil pressure results in a horizontal displacement at the anchor point of:

$$u_3 = \frac{q \cdot d^4}{30 \cdot EI} + \frac{q \cdot d^3}{24 \cdot EI} \cdot (h-a) = \frac{K_p \cdot \gamma_d \cdot d^5}{30 \cdot EI} + \frac{K_p \cdot \gamma_d \cdot d^4 \cdot (h-a)}{24 \cdot EI}$$

The first term in this expression of u_3 indicates the displacement at the top of the passive load, the second term is the additional displacement of the wall above the top of the load (*kwispeleffect*).

The sum of these three displacements should be zero at the anchor point.

The computation for this simple example can be solved with some tricks. First, u_1 is rewritten as:

$$u_1 = \frac{T \cdot (h+d-a)^3}{3 \cdot EI} = \frac{T \cdot (h+d-a) \cdot (h+d-a)^2}{3 \cdot EI}$$

Then the displacements u_1 , u_2 and u_3 are multiplied with $\frac{EI}{K_p \cdot \gamma_d}$, so that, because $u_1 + u_2 + u_3 = 0$, also

$$(u_1 + u_2 + u_3) \cdot \frac{EI}{K_p \cdot \gamma_d} = 0.$$

The following 'trick' is to substitute $T \cdot (h+d-a) = \frac{1}{6} \cdot K_a \cdot \gamma_d \cdot (h+d)^3 - \frac{1}{6} \cdot K_p \cdot \gamma_d \cdot d^3$ in the expression for u_1 (which follows from an equilibrium of moments about the toe of the sheet pile). This results in the following equation:

$$(u_1 + u_2 + u_3) \cdot \frac{EI}{K_p \cdot \gamma_d} =$$

$$= \frac{K_a}{K_p} \cdot \frac{(h+d)^3 (h+d-a)^2}{18} - \frac{d^3 (h+d-a)^2}{18} - \frac{K_a}{K_p} \cdot \frac{(h+d-a)^5}{30} + \frac{d^5}{30} + \frac{d^4 (h-a)}{24} = 0$$

Because all variables are known except for d , this equation can be solved by substituting the other symbols with their values:

$$\frac{(6+d)^3 \cdot (5+d)^2}{162} - \frac{d^3 \cdot (5+d)^2}{18} - \frac{(5+d)^5}{270} + \frac{d^5}{30} + \frac{5 \cdot d^4}{24} = 0$$

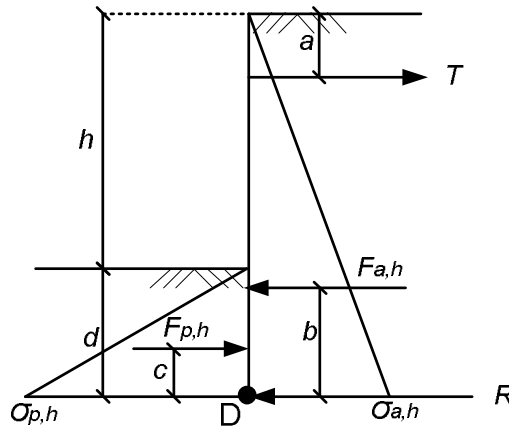
It can now be iteratively computed that this equation is valid for $d = 4,94$ m.

As was already mentioned earlier it is common practice to increase the embedded depth by 20% in order to provide some safety within the structure. The total length of the sheet piles then becomes:

$L_t = h + 1,2d = 6,00 + 1,2 \cdot 4,94 \approx 12$ m. According to the manufacturers of sheet pile elements, their delivered length can deviate $\pm 0,20$ m from the ordered length, so choose an overall-length of at least 12,20 m.

Step 2. Compute the anchor force (T) per m^1

$$\sum M_D = 0 \rightarrow -F_{a,h} \cdot \frac{1}{3} \cdot (h+d) + F_{p,h} \cdot \frac{1}{3} \cdot d + T \cdot (h+d-a) = 0$$



$$\sigma_{p,h} = K_p \cdot \sigma_{p,eff,v} + \sigma_w = K_p \cdot \gamma_d \cdot d + 0$$

$$\sigma_{a,h} = K_a \cdot \sigma_{a,eff,v} + \sigma_w = K_a \cdot \gamma_d \cdot (h+d) + 0$$

$$F_{a,h} = \frac{1}{2} \cdot K_a \cdot \gamma_d \cdot (h+d)^2 \quad \text{and} \quad F_{p,h} = \frac{1}{2} \cdot K_p \cdot \gamma_d \cdot d^2$$

$$b = \frac{1}{3} \cdot (h+d) \quad \text{and} \quad c = \frac{1}{3} \cdot d$$

$$\sum M_D = 0 \Rightarrow -F_{a,h} \cdot \frac{1}{3} \cdot (h+d) + F_{p,h} \cdot \frac{1}{3} \cdot d + T \cdot (h+d-a) = 0$$

$$\Leftrightarrow T \cdot (h+d-a) = \frac{1}{6} \cdot K_a \cdot \gamma_d \cdot (h+d)^3 - \frac{1}{6} \cdot K_p \cdot \gamma_d \cdot d^3$$

$$\Leftrightarrow T = \frac{\frac{1}{6} \cdot K_a \cdot \gamma_d \cdot (h+d)^3 - \frac{1}{6} \cdot K_p \cdot \gamma_d \cdot d^3}{(h+d-a)} = \frac{\frac{1}{6} \cdot \frac{1}{3} \cdot 18 \cdot (6+4,94)^3 - \frac{1}{6} \cdot 3 \cdot 18 \cdot 4,94^3}{(6+4,94-1)} = 22,54 \text{ kN/m}$$

Methods A & B converge here, but the numerical values of method B are used:Step 3. Compute the substitute force (R) per m¹

$$\sum H = 0 \Rightarrow -F_{a,h} + F_{p,h} + T - R = 0$$

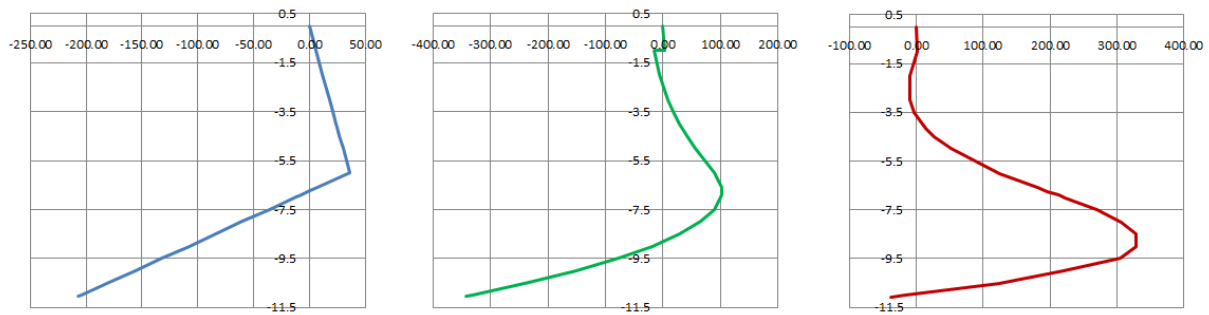
$$\Leftrightarrow R = -F_{a,h} + F_{p,h} + T$$

$$\Leftrightarrow R = -\frac{1}{2} \cdot K_a \cdot \gamma_d \cdot (h + d)^2 + \frac{1}{2} \cdot K_p \cdot \gamma_d \cdot d^2 + T$$

$$\Leftrightarrow R = -\frac{1}{2} \cdot \frac{1}{3} \cdot 18 \cdot (6 + 4,94)^2 + \frac{1}{2} \cdot 3 \cdot 18 \cdot 4,94^2 + 22,54 = -359,05 + 658,90 + 22,54 = 322,39 \text{ kN/m}$$

Step 4. Compute the required section modulus ($W_{eff,y}$)

The required section modulus can be found when the maximum bending moment in the wall and the yield stress of the steel are known. The yield stress is a material property which should be guaranteed by the manufacturer of the sheet piles (depending on the steel quality). The maximum bending moment can be computed with help of the diagrams of horizontal stress, the shear force diagram and moment diagram. The way of drawing these diagrams has been explained in the previous two examples, so only the result is presented in the following figure.



The maximum moment occurs where the shear force is zero. This is at 8,80 m below the ground surface, where $M_{max} = 329 \text{ kNm/m}$.

To check the calculation, two things can be done now:

1. Check if the value of the shear force diagram at $d + h = 11,06 \text{ m}$ below soil surface equals the substitute force found in step 3 of the calculation.
2. Check if the value of the moment diagram is zero (or about zero) at $d + h = 11,06 \text{ m}$ below soil surface.

Step 5. Choose a suitable profile.

The required section modulus (*weerstandsmoment*) of the sheetpile profile then is:

$$W = \frac{M_{max}}{f_{y,d}} = \frac{329 \cdot 10^6}{235} = 1400 \cdot 10^3 \text{ mm}^3/\text{m} = 1400 \text{ cm}^3/\text{m}$$

A Larssen 704 profile ($W_y = 1600 \text{ cm}^3/\text{m}$) will suffice (see Appendix H). Again, no factors of safety were used in this example!

Regards the relatively low anchor force, it is in a real design worthwhile to try whether a cantilever sheetpile wall would suffice here. Maybe the length and profile would increase, but it would save the costs (and trouble) of making anchors or a support framework.

Governing loading condition for building pits with underwater concrete floors

At first sight, there are usually two load cases that could be governing for the design of sheetpile walls for building pits. The first case is the construction phase where the struts or anchors have been installed, excavation has taken place until the bottom of the underwater concrete floor (which has not yet been cast) and there is still water in the building pit. The second potentially governing load case concerns a pumped-dry building pit with a cast and hardened under-water concrete floor and struts or anchors. Figure 37-11 shows both load cases.

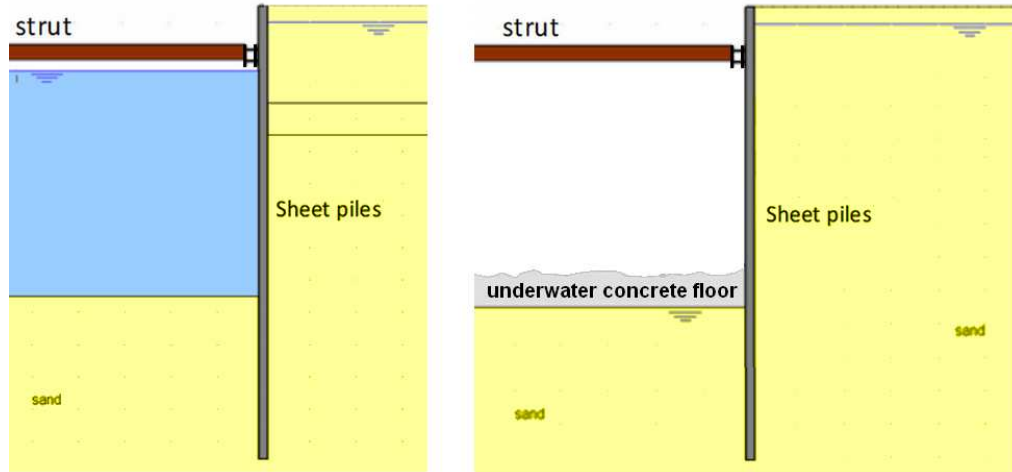


Figure 37-11 Two potentially governing load cases for sheetpile wall stability

It can be reasoned that the first case is governing for overall stability of the wall, because some wall depth under the building pit bottom is needed to provide sufficient clamping. In the second case, no wall depth under the underwater concrete floor is required, because both horizontal supports provide rotational stability. However, for the strut force and the maximum bending moment in the sheetpile wall, it is less obvious what case would be governing, because the water pressure in the first case is replaced by a horizontal force by the underwater concrete floor, but the effect of this on the strut force and the maximum moment is not obvious in quantitative terms.

This first case can be solved with the 'classical methods' as described in this chapter, because the mechanical schematisation considered in these classical methods is a statically determined system. In the second case, there are multiple horizontal supports, because next to the struts or anchors, the underwater concrete floor acts as an extra horizontal support. It can therefore not easily be solved by a hand calculation because there are too many variables compared to the number of equations.

De Bruin (2018) therefore did a series of computer simulations for his BSc-thesis, from which it appeared that in the second case, the horizontal forces in the upper supports become higher than in the schematisation used in the first case. This also applies to the maximum moments in the wall. The support force can become up to 40% higher and the maximum moment 30% higher than in the 'classical load case' as explained above. This can be used as a rule of thumb for conceptual designs that use hand calculations.

Vertically loaded sheetpile walls

Sheetpile walls can be exposed to vertical forces, originating from:

- self-weight of the sheetpile elements
- vertical component of resulting soil force (active + passive)
- vertical components of inclined anchors
- surcharge or vertical forces from superstructures, usually transferred via a coping beam (*kesp*)
- possible other vertical forces acting on the wall

These forces have to be transferred to subsoil, which should have sufficient bearing capacity.

The bearing capacity of the subsoil consists of two components:

- bearing capacity of the tip of the sheetpile elements
- bearing capacity of the wall friction of the sheetpile elements

According to CUR-publication 166 'Quay Walls', the calculation of the vertical bearing capacity can be done in analogy to the method for compression piles (see also Chapter 32 of this Manual):

$$F_{r, max} = F_{r, max, tip} + F_{r, max, wall}$$

and:

$$F_{r, max, tip} = A_{tip} \cdot p_{r, max, tip}$$

$$F_{r, max, wall} = 2 \cdot A_{wall} \cdot \int p_{r, max, wall} dz$$

where:

$F_{r, max, tip}$	[kN/m']	= bearing capacity of the tip
$F_{r, max, wall}$	[kN/m']	= shaft friction capacity
A_{tip}	[m ² /m]	= cross-sectional area of the sheet pile wall
A_{wall}	[m ² /m]	= wall area (one side of the wall)
$p_{r, max, tip}$	[kN/m ²]	= maximum tip resistance
$p_{r, max, wall}$	[kN/m ²]	= maximum wall friction

For the estimation of the maximum tip resistance $p_{r, max, tip}$ and the maximum wall friction $p_{r, max, wall}$, reference is made to section 32.4.

The max. vertical force that can be resisted by wall friction is:

$$F_{v, max} = F_h \cdot \tan(\delta),$$

where δ represents the angle of wall friction (*wandwrijvingshoek*). This angle can be determined with help of tests on soil samples (direct shear stress test), but these tests are often difficult to carry out and the result is anyhow not very reliable. Therefore, δ is often related to the angle of internal friction (φ') and also the coarseness of the soil. Eurocode 7 restricts δ to $2/3 \varphi'$ (for steel or concrete sheet piles in sand or gravel) and to φ' for concrete cast in soil.

Based on long experience, Rijkswaterstaat found the following values for the angle of wall friction:

- for gravel with $D_{50} > 8$ mm:	$\delta = 0^\circ$
- for coarse sand with $D_{50} > 2$ mm:	$\delta = 1/3 \varphi'$
- for sand with $D_{50} < 2$ mm:	$\delta = 2/3 \varphi'$
- for loam	$\delta = 1/2 \varphi'$
- for clay	$\delta = 1/3 \varphi'$

The direction of the wall friction respective to the wall is downward at the active side and upward at the passive side. In case of an external load on the sheetpile wall, these directions can reverse.

For the calculation of the tip resistance of sheet pile walls, the following parameters should be used:

$\alpha_p = 1,0$; $\beta = 1,0$; $s = 0,62$. The tip cross-sectional area can be computed with $D_{eq} = \sqrt{\frac{4}{\pi} A_{tip}}$.

If the average vertical load does not exceed 12,5 kN/m², the vertical bearing capacity can be calculated separate from the horizontal equilibrium check. Otherwise, an interaction calculation should be carried out of vertical and horizontal forces. Usually, finite element or spring models are used for these cases.

Note

- An eccentric vertical load will introduce a second order moment the wall, which should be taken into account.
- Vertically loaded sheetpiles can be susceptible to buckling (*knik*), so this should be verified during the design (see Section 30.3 of this Manual).

37.3 Combi-walls

Combi-walls (*combiwanden*) are walls that consist of a combination of different elements, for instance sheet piles and steel pipe piles. Usually a combi-wall section, see Figure 37-12, consists of two pipe piles with two to three Z-shaped sheet piles or one U-shaped sheet pile in between (The most commonly used configuration has two Z-sheet piles in between). The pipe piles are fitted with interlocks, thus providing a soil and water tight connection between the sheet piles and the pipe piles. The pipe piles have a far larger flexural rigidity (EI) than the sheet piles and hence give the structure strength and stiffness. The sheet piles provide a watertight seal in between two pipe piles.



Figure 37-12 Cross-section, side-view and welded interlock of a combi-wall

An overview of combi-wall types is given in Figure 37-13.

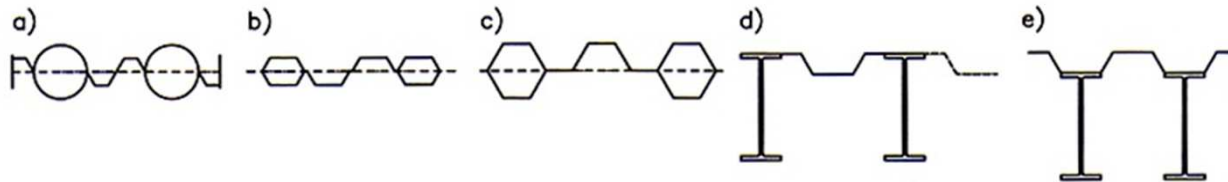


Figure 37-13 Types of combi-walls (from: Grundwerke in Beispielen)

The disadvantages of combi-walls are that the pipe piles make the wall much more expensive and that removing the pipe piles leaves a large hole, because the ground usually stays stuck within the tube (especially in cohesive ground layers).

Combi-walls are generally used for deep excavations. However, as a result of the use of the pipe piles they can withstand larger loads than conventional sheet pile structures. Examples of the application of combi-walls are: underground car parks, quay walls and tunnel entrances. In quay walls the toe of sheet piles are often placed less deep than pipe piles. The customary external diameter of the steel pipe piles lies between about 800 and 2000 mm, the customary wall thickness lies between 10 and 20 mm.

As stated before, combi-walls have a far larger flexural rigidity. A combi-wall $\text{Ø } 1620 \text{ mm} \times 19 \text{ mm} + 2 \text{ PU20}$ has an EI equal to $2,28 \cdot 10^6 \text{ kNm}^2/\text{m}$. That is almost 10 times as stiff as an AZ48! In this case the flexural rigidity of the PU20 sheet piling is almost negligible compared with that of the tubular pile.

It is easy to calculate the bending stiffness (EI) of tubular piles. After all, for tubular profiles:

$$I_y = I_z = \frac{\pi(D^4 - d^4)}{64}$$

where: I [m⁴/m] = area moment of inertia
 D [m] = outer diameter pipe pile
 t [m] = thickness tube wall = $(D - d)$
 d [m] = inner diameter pipe pile = $D - 2t$

For the Youngs' modulus one can use: $E_{steel} = 2,1 \cdot 10^5 \text{ N/mm}^2 (= 2,1 \cdot 10^8 \text{ kN/m}^2)$.

The bending stiffness (flexural rigidity) EI per metre combi-wall therefore mainly depends on the type of pipe pile and on the collective width of sheet piling between these tubular piles. The area moment of inertia (I) of a sheet pile profiles can be found in Table H-1, Table H-2, Table H-3 or in the manufacturers' fact sheet.

Note. Combi-walls have to be checked for local buckling of the pile shaft.

37.4 Diaphragm walls

The scarcity of space, especially in urban areas, has in recent years led to an increasing demand for underground structures. The required depth of these structures has increased over the years, and also stringent requirements regarding noise and vibration nuisance are imposed during construction. Furthermore, often nearby adjacent properties are situated close to the building site, as a result of which the retaining walls should be very stiff in order to keep the deformation of the wall small. All in all, diaphragm walls, also called slurry walls, (*diepwanden*) have become an indispensable alternative.

Especially for diaphragm walls the relationship between design and construction is important. Critical parts of the design and construction process are:

- the design of the reinforcement cage (good concrete flow ability and hence a large enough mesh width);
- control of the properties of both the concrete and bentonite;
- the process of de-sanding or exchanging the bentonite;
- the cleaning of the joints, if necessary;
- the process of casting the concrete.

Design

In this section only the basic outline of the design rules regarding diaphragm walls are treated. For more detailed information the reader is referred to the Handbook Sheetpile Structures (CUR 166, in Dutch), the Handbook Quay Walls (CUR 211, in English). CUR-report 76 gives design rules for diaphragm walls (in Dutch).

Strength

In essence, the strength that a diaphragm wall needs, is computed in a similar way as for sheet pile walls computations using Blum's method, see Section 37.2 of this Manual. However, there are some differences. First of all, the bending stiffness (EI) is rather different. As shown in the following computation the bending stiffness of a diaphragm wall is much larger than that of a very stiff sheet pile profile.

As a result of the large bending stiffness of the diaphragm wall, the deformation at the top of the wall is very small, resulting in an equally very small deformation of the soil behind the wall. The horizontal passive soil pressure should therefore be calculated with a passive soil coefficient (K_p) with an angle of internal friction of maximum $\frac{2}{3}\varphi \leq 20^\circ$.

Another major difference with the computation of a sheet pile wall according to Blum's method is that after the initial computation, using Blum's method, the diaphragm wall has to be computed again using a simple spring model, e.g., D-Sheetpiling. This is necessary because Blum's method gives a good initial estimation of the strength needed, but for a final design the computation with a simple spring model is necessary in order to establish the real occurring bending moments and shear forces, as these are slightly underestimated by Blum's method (in case of a diaphragm wall). Usually, the diaphragm wall will turn out to be somewhat longer and heavier. The computed horizontal force and moment are used to determine the amount of reinforcement steel needed.

An additional benefit of using a computer model is that curved sliding planes can be used, which gives a more accurate representation of reality. For a hand calculation this is too complicated, so straight sliding planes are used then. This, however, leads to an overestimated strength, which is compensated by a reduction of the wall friction angle (δ). According to NEN 6740, table 4, the following values for the wall friction should be used in diaphragm computations:

Curved sliding planes: - in sand and clay: $\delta = \frac{1}{2} \varphi$
 - in peat: $\delta = 0$

Straight sliding planes: - in sand and clay: $\delta = \frac{2}{3} \varphi$
 - in peat: $\delta = 0$

(where φ = the angle of internal friction)

Reinforcement and concrete cover

See Chapter 29 for the computation regarding the required reinforcement.

As a result of the way in which a diaphragm wall is constructed, several essential additional requirements have to be met with respect to the reinforcement cage:

- 1) due to the long panel length (6-8 m), usually two reinforcement cages are placed alongside (in top view). Since the forces are mostly directed perpendicular to the wall the cages are usually not coupled width-wise;
- 2) due to the large depth the reinforcement cages consist of parts of transportable lengths which are coupled on site before or during the lifting;
- 3) stiffness of the reinforcement cages is of minor importance because they are suspended vertically. Nevertheless, they should be stiff enough in order to be able to be transported and to prevent lasting deformations during the placement. Usually welded cages are used, instead of twined cages (*gevlochten korven*);
- 4) the flow ability of the reinforcement cage has to meet high standards since the support fluid has to be displaced during the placement and because the concrete has to be poured continuously over a large height;
- 5) the concrete cover has to be at least 75 mm under normal conditions and at least 100 mm in case of weak soil layers, such as peat and clay;
- 6) the free space between the reinforcement cage and the grout float of the previous section must be at least 100 mm, but preferred is 200 mm. The distance between the bottom of the wall and the reinforcement cage must be at least 200 mm;
- 7) the minimum centre to centre distance between horizontal reinforcement bars amounts 200 mm, between vertical bars this distance is 100 mm;
- 8) the minimum distance between reinforcement cages within one panel must be at least 200 mm, but preferred is 400 mm.

The concrete used for diaphragm walls is usually C20/25 or C30/37 and the exposure classification is XC4, alternating wet and dry (see also Chapter 29 of this Manual). Additional requirements are:

- a high resistance against segregation (*ontmenging*);
- a good consistency (plastic behaviour) and maintaining sufficient consistency;
- a good coherence;
- certain self-compacting properties.

Deformation

Both failure of the soil- and/or water retaining function of a diaphragm wall and the deformation of the wall are likely to lead to settlements of the soil behind the diaphragm wall. In order to prevent damage, the allowable deformations of the diaphragm wall and/or the adjacent land are limited. These limits are defined as an allowable combination of settlement, relative rotation (β) and horizontal displacement (ϵ_h) that adjacent structures may undergo. In appendix H of NEN-EN 1997-1 recommendations are stated for the limit values for the deformation of normal, conventional structures. For many structures a maximum relative rotation of 1:500 is acceptable in order to prevent the occurrence of the serviceability limit state. The ultimate limit state occurs around a relative rotation of 1:150, see Table 37-3. The ratios mentioned apply to the sagging mode, see Figure 37-14. For a hogging mode (edge settling is larger than the part in between) the ratios mentioned should be halved.

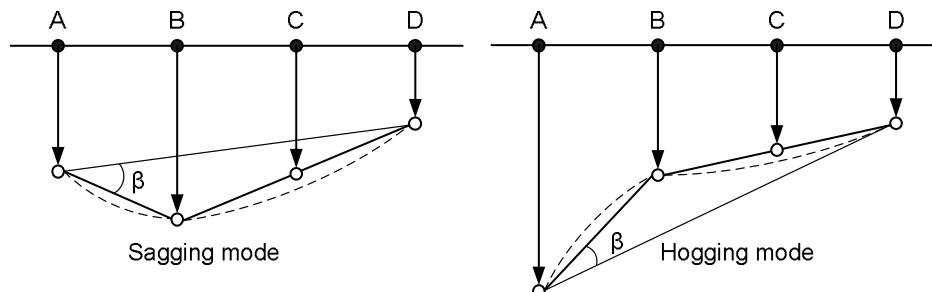


Figure 37-14 Structural deformation

Furthermore, it is stated in the NEN-EN 1997-1 that for separate foundations under normal conditions a total settlement of maximum 50 mm is allowable. A larger settlement may be allowable provided that the relative rotation is limited and no problems with house connections and public utilities (*nutsvoorzieningen*) come into play.

Table 37-3 is suitable for newly constructed structures. For an older structure, that is likely to have already undergone a differential settlement, stricter rules must be applied, for example, an allowable rotation that is 1.5 times smaller than otherwise (1:500 instead of 1:300).

Qualification	Limit state	Limit relative rotation (β)	
		Framing (<i>skeletbouw</i>)	Masonry
Architectonic damage (cracks up to 5 mm)	SLS	1:300 (general) 1:600 (skyscrapers) 1:1000 (warehouse)	1:600 (downward direction) 1:1200 (upward direction)
Structural damage (cracks 15-25 mm)	ULS	1:150	1:300 (downward direction) 1:600 (upward direction)
Collapse	ULS	1:75	1:150 (downward direction) 1:300 (upward direction)

Table 37-3 Allowable limits for the relative rotation

In Figure 37-15 damage thresholds related to a combination of the relative rotation and the horizontal displacement are presented. In this figure, the relative rotation is the result of the differential settlement due to the self-weight of the structure and the horizontal displacements represent the influence of the nearby excavation.

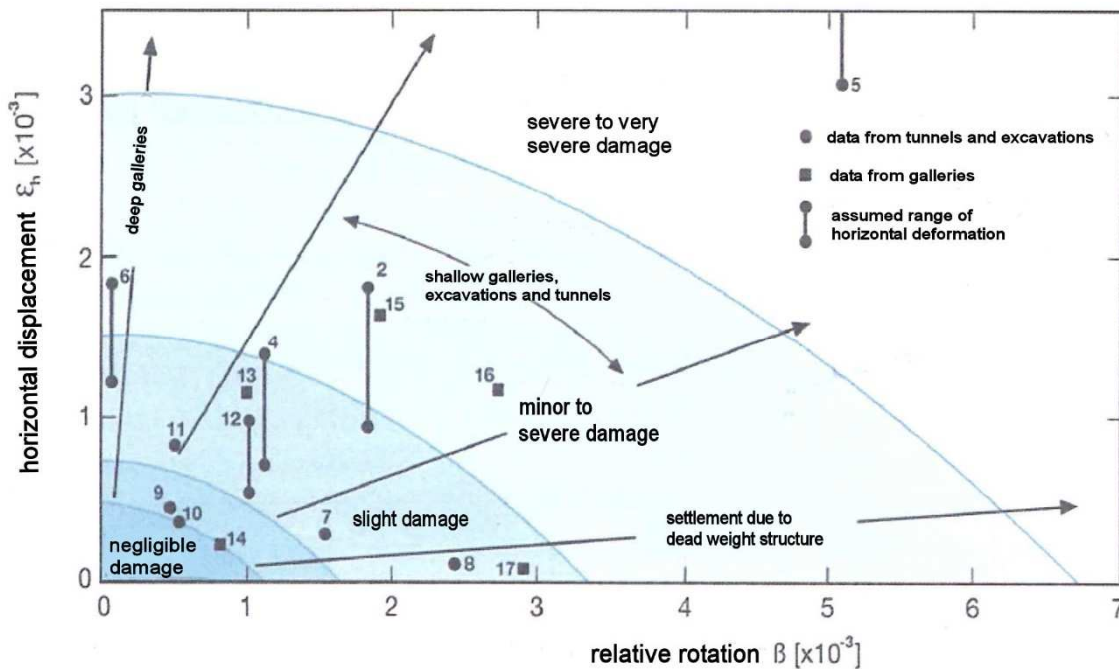


Figure 37-15 Damage thresholds of diaphragm walls

Limits for the horizontal displacement in the subsoil at the location of pile foundations are not found in literature. However, during the design of the Willems railroad tunnel in Rotterdam a maximum horizontal displacement equal to 1/6 of the shaft diameter was allowed as a safe limit for prefabricated concrete piles. This limit value is related to the fact that in the case of a centric load on the pile no tensile stress occurs in the pile shaft as a result of eccentricity. For wooden foundation piles a horizontal displacement of 0,10 m was considered allowable.

Water-tightness

In many cases diaphragm walls are used to enable dry excavation in a deep building pit. Often the lowest point of the wall is situated in an impermeable soil layer, but also underwater concrete can be used to close off the bottom of the building pit.

The under normal circumstances occurring amount of leakage water depends on the following environmental factors:

- permeability of the soil layers behind the diaphragm wall;
- water pressure present in these layers;
- quality of the diaphragm wall and the joints.

To be able to relate the usage of an underground space to the allowable amount of leakage water, a classification is desired. A possible classification based on Austrian guidelines is presented in Table 37-4.

Classification	Description	Quantification water locking ability	Functionality
1	completely dry	-	specific goods storage
2	relatively dry	damp stains acceptable up to 1‰ of the visible surface. Water trails up to 0,20 m	spaces for public use, storage
3	slightly damp	damp stains acceptable up to 1‰ of the visible surface. A few water trails are permitted	garages, infrastructural projects
4	damp	Maximum leakage per spot or per m ¹ joint 0,2 l/h; and the average amount per m ² wall 0,01 l/h	garages, infrastructural projects with additional measures
5	wet	Maximum leakage per spot or per m ¹ joint 2 l/h; and the average amount per m ² wall 1 l/h	-

Table 37-4 Classification regarding the amount of allowable leakage water.

Taking into account a high-water table, which is customary in the western part of The Netherlands, and excavation depths for which the usage of a diaphragm wall is realistic, generally speaking the water pressure against the wall is 10 metre water column or more. For a situation where aquifers are present behind the diaphragm wall it turns out that in practise only structures belonging to classes 4 and 5 are feasible. In case of water pressures exceeding 15 metre water column only class 5 structures are feasible. The consequence of these findings is that usually a front wall (*voorzetwand*) must be constructed in front of the diaphragm wall.

Construction

The construction stages of diaphragm walls are illustrated in Figure 37-16. First, the trench is excavated in panels with help of guiding beams and special rectangular diggers (stages 1 and 2). A standard panel has a width of 0,6 to 1,5 m and a length of 2,8 to 8,0 m. The depth can amount up to 30 m. As a rule of thumb, the minimum dimensions of the guide walls have a height of 1,00 m and a width of 0,20 m. These guide wall dimensions are governed by the horizontal load (soil and equipment) and the changing fluid level in the trench during the excavation. The fluid level is not allowed to drop regularly beneath the guide walls as the fluid motion will erode the soil underneath the walls.

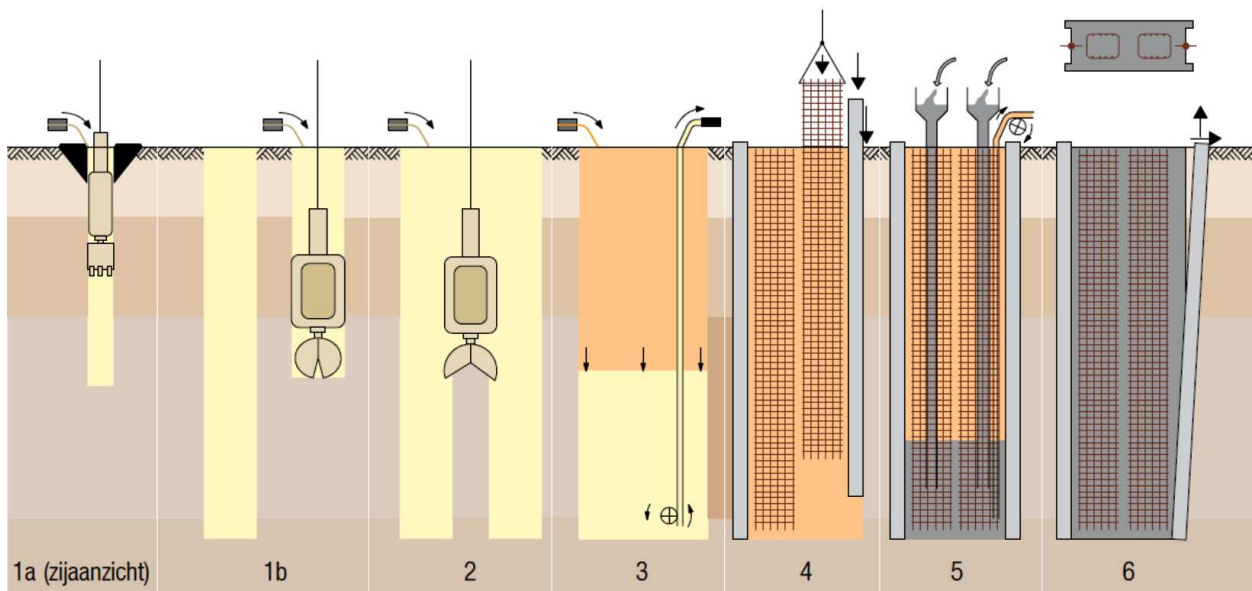


Figure 37-16 Construction stages of a diaphragm wall (from: <http://www.wtcb.be>)

The trench is filled with a support fluid (mostly bentonite) already during excavation to avoid collapse of the soil walls. So, the excavation takes place in the support fluid. The support fluid becomes mixed with soil falling down from the wall, therefore it is replaced by clean bentonite (stage 3) before the joints and the reinforcement cages are positioned (stage 4). Synthetic joint ribbons (*voegbanden*) are integrated in these joints so that they can be cast-in in the concrete.

Subsequently, concrete is cast with help of cast tubes (*stortbuizen*) (stage 5). Since the density of concrete is larger than that of the bentonite mixture and because the concrete mixture is pumped in the trench near the bottom, the bentonite mixture “floats” on top of the concrete and the surplus can be collected for re-use. There is some mixing, hence the upper 1 to 2 m concrete is of poor quality and must be removed (and eventually replaced) afterwards. Finally, the joints are removed, but the cast-in joint ribbons remain at their place so that they form a water-tight connection between the panels (stage 6).

Leakage of the joints

If the diaphragm wall appears to contain soil or bentonite lumps adjacent to the joints, this will most probably lead to leakage. This can be repaired by attaching steel plates to the inside of the diaphragm walls and injecting PUR-foam behind the plates in the arisen gap. If the flow of the soil-water mixture through the gap is too strong to use this repair method, the gap can otherwise be blocked with a 'dam' consisting of clay or sand with a clay core, after which the soil behind the diaphragm wall is frozen by freeze lances. After the flow is stopped the temporary dam is removed and again steel plates are positioned over the weak spots. When this is done, the freeze lances can be removed.

Trench stability

If no special measures are taken during excavation of a deep trench, it is very likely that the walls of the trench will collapse. In the case of diaphragm walls the trench is filled with a support fluid, usually a bentonite mixture, to enhance the stability of the trench walls.

One distinguishes between micro instability and macro instability of the trench walls, see Figure 37-17.

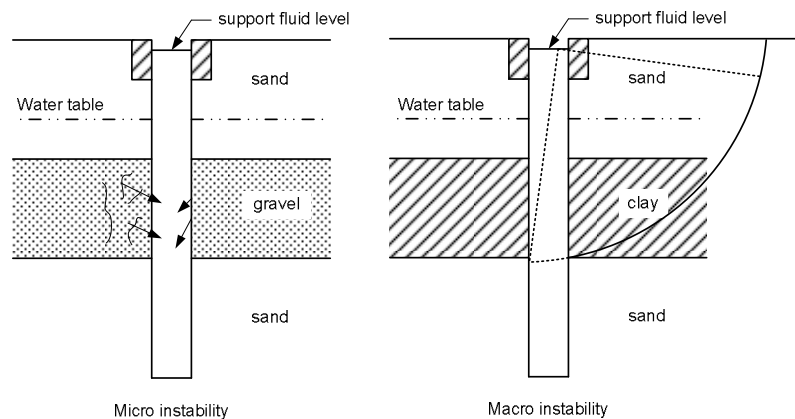


Figure 37-17 Micro and macro instability of trench walls

Micro-instability is a failure mechanism that only occurs in non-cohesive soils. It occurs when individual grains situated at the edge of the trench lose their stability and fall into the trench. Also the collapse of small sections of the trench walls is regarded as micro instability. The presence of support fluid in the trench can prevent micro instability. This will work if the support fluid does not move any more, in which case it will have a certain shear strength. The fluid that has infiltrated the grain skeleton of the soil will then stabilize the grains at the edge of the trench wall.

This yield stress (*bezwijkspanning*) can be computed as follows:

$$\tau_f \geq \frac{d_{10} \cdot \gamma'}{\tan(\varphi)},$$

where:

τ_f	[kN/m ²]	=	yield stress
d_{10}	[m]	=	grain diameter of the 10% fraction from the sieve curve of the soil
γ'	[kN/m ³]	=	effective volumetric weight of the support fluid
φ	[°]	=	angle of internal friction of the soil

Note that the grain size is a very important parameter in determining the micro instability of a trench wall. In case the grain diameter is smaller than 0,2 mm or the layer thickness of the coarse material is smaller than 0.5 m micro instability can be disregarded.

Macro instability is failure due to the sliding of a large soil section. In order to prevent this failure mechanism, the fluid pressure within the trench must be larger than the water pressure in the surrounding soil. This

overpressure, however, does not have to be very large: According to DIN 4126 the hydrostatic bentonite mixture pressure must be 1.05 times larger than the hydrostatic water pressure at all depths. NEN-EN 1538 prescribes that the level of support fluid must be at least 1 m above the rise (*stijghoogte*) of the ground water in the layer under consideration. In general, one strives to choose the support fluid level 2 m above the highest rise. Macro instability is often checked with a finite element model (FEM), important for the computations is the fluctuating support fluid level as a result of the digging process (which may lead to erosion of the trench walls).

One should also be aware of the dynamic effects in the neighbouring area that can influence the trench stability, for example strong vibrations caused by the hammering down of piles or sheet piles.

Sequence of work and panel width

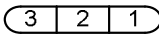
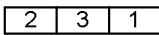
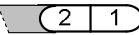
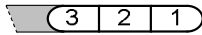
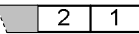
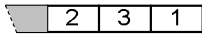
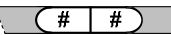
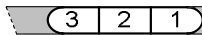
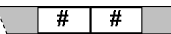
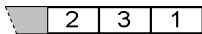
From an economical point of view, it is recommended to make the panel width as large as possible. An additional advantage resulting from this is that the number of joints is as small as possible. It should nevertheless be kept in mind that in most cases trench stability and impact on the surroundings are the governing factors.

Important for the sequence in which the panels are dug are the shape of the panel, the type of joint (round or flat) between successive panels and the type of panel under construction.

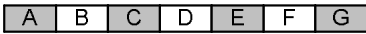
One can distinguish the following panel types:

- start panels: do not connect to already constructed panels;
- follow up panels: connect to an existing panel at one side;
- end panels: connect to existing panels at both sides.

In the following table the different sequences of work are presented.

Panel type	Joint type	1 movement	2 movements	3 movements
Start	round	yes	no	yes 
	flat	yes	no	yes 
Follow	round	no	yes 	yes 
	flat	yes	yes 	yes 
End	round	yes	yes 	yes 
	flat	no	yes 	yes 

sequence not relevant



3 movement sequence: between 2 start panels a end panel is constructed. So the sequence of work becomes: first A-C-E-G and then B-D-F

Table 37-5 applicability panel types and sequence of work

Usually one-movement panels (*eengangspanelen*) are only constructed in special situations, e.g. to limit the settlements of adjoining structures (higher trench stability!), or for logistic reasons (limitation of the amount of concrete needed to construct a panel, so less change on disruption of the pouring process) and as heavy foundation piles.

Types of joints between successive panels:

- joint pipe (*voegbuizen*);
- flat grout floats (*voegplanken*);
- permanent grout floats;
- cascade joint.

37.5 Literature

- Blum, H. *Einspannungsverhältnisse bei Bohlwerken*, 1931, Technische Hochschule Braunschweig.
- Blum, H. *Beitrag zur Berechnung von Bohlwerken*. Die Bautechnik, 27 Jahrgang Heft 2 Februar 1950.
- Blum, H. *Beitrag zur Berechnung von Bohlwerken unter Berücksichtigung der Wandverformung, insbesondere bei mit der Tiefe linear zunehmender Widerstandsziffer*. Berlin, 1951. Verlag von Wilhelm Ernst & Sohn.
- Bruin, A. de. *Schematisering van een onderwaterbetonvloer in een bouwkuip*. BSc-thesis Delft University of Technology, 2018.
- Civieltechnisch Centrum Uitvoering Research en regelgeving (CUR), *CUR-publicatie 166: "Damwand-constructies"*, 5^e druk, Gouda, 2008, CUR.
- Civieltechnisch Centrum Uitvoering Research en regelgeving (CUR), *CUR/COB-rapport 231: "Handboek diepwanden – Ontwerp en uitvoering"*, 1^e druk, Gouda, 2010, CURNET.
- Civieltechnisch Centrum Uitvoering Research en regelgeving (CUR), *CUR-publicatie 211: "Handboek kademuren"*, Gouda, september 2005, Stichting CUR.
- Deltares. *D-Sheet Piling Design of diaphragm and sheet pile walls User Manual*. Delft, 2017.
- Nederlands Normalisatie instituut, *Eurocode 3: "Design of steel structures – Part 1-1: General rules for buildings" (NEN-EN 1993-1-1)*, januari 2006, Nederlands Normalisatie instituut.
- Nederlands Normalisatie instituut, *Eurocode 7: "Geotechnical design – Part 1: General rules" (NEN-EN 1997-1)*, maart 2005, Nederlands Normalisatie instituut.
- Rowe, P.W., 1952. Anchored Sheet Pile Walls, PICE, Vol. 1, part 1, pp. 27-70.
- Simpson, B, and Powrie, W. *Embedded retaining walls: theory, practice and understanding*. Perspective lecture 15th International Conference on Soil Mechanics and Geotechnical Engineering. Istanbul, 2001.
- Vanhoutte, B. and Verstrynghe, F. *Ontwerpmethodes voor damwandconstructies*. MSc thesis Katholieke Hogeschool Vives Noord. Oostende, 2007.
- Verruijt, A., revised by S. van Baars, *Soil Mechanics*, Delft, 2005, VSSD.

Websites:

- http://www.spoorzonedelft.nl/Het_project/Heden/Bouwtechniek_2
<http://www.thyssenkrupp-bautechnik.com/products/sheet-piles/>
<http://sheetpiling.arcelormittal.com/>

38. Construction pits: Struts and wales

major revision : February 2011

Sheet pile walls are often horizontally supported by struts (*stempels*) or anchors. The advantage of a support is that the embedded length of sheet piling doesn't need to be as long (less passive soil pressure) and heavy (smaller moment) compared to an unsupported wall, which saves money. Another advantage is that there is less settlement of the ground level behind the sheet piling. The disadvantages of supports are the higher costs and the possibility of obstruction during construction works.

As a rule, excavations of a couple of metres are carried out without supports, unless settlements behind the sheet piling are unacceptable, for example for buildings. Deeper excavations are normally spoken carried out with supports. Building site excavations can be supported in front of the sheet piling with struts. Support behind the sheet piling is possible by using anchors. The forces of the strut or anchor are usually not transferred to the sheet piling directly, but via wales (horizontal beams).

For the dimensioning of struts, see the following section; for wales see Section 38.2 "Wales" and for anchors see Chapter 39 "Anchors".

38.1 Struts

Struts consist of steel profiles that can absorb axial compression forces (strut forces). These forces cause stress in the steel, which should not exceed the compression strength of the steel to avoid failure. Another possible way of failure is buckling. Buckling is possible both in the vertical and horizontal plane, therefore it should be resisted in both planes. That is the reason why circular pipes are often used for large spans and loads. For smaller spans and loads usually H-profiles are applied because they are less expensive and still sufficient against buckling.

So, struts should be checked on both strength and stability, which concerns their ultimate limit state (ULS). In theory, the deflection in the serviceability limit state (SLS) should also be checked, but experience has learned that this normally spoken is not necessary for the design of struts.

Strength check

The dominant load in struts is caused by the normal (axial) compression force in horizontal direction. The stress σ_c due to the combination of axial force and bending moments in two directions should not exceed the yield stress (*vloeispanning*) of the steel: $\sigma_n + \sigma_b < f_y$.

The required unity check thus is as follows:

$$\frac{N_{Ed}}{A_{eff} \cdot f_y / \gamma_{M0}} + \frac{M_{y,Ed}}{W_{eff,y,min} \cdot f_y / \gamma_{M0}} + \frac{M_{z,Ed}}{W_{eff,z,min} \cdot f_y / \gamma_{M0}} \leq 1,0 \quad \text{where: } N_{Ed} = 1,5 \cdot N_{Rk}; \quad M_{i,Ed} = 1,5 \cdot M_{i,Rk}$$

If the design shear force (V_{Ed}) exceeds 50% of the plastic shear force ($V_{pl,Rd}$), the cross-sectional design resistance to combinations of moment and axial force should be calculated using a reduced yield strength:

$$f_{red} = (1 - \rho) \cdot f_y$$

for the shear area where $\rho = \left(\frac{2 \cdot V_{Ed}}{V_{pl,Rd}} - 1 \right)^2$ and where: $V_{pl,Rd} = \frac{A_v (f_y / \sqrt{3})}{\gamma_{M0}}$

The required unity check for the shear force is $\frac{\tau_{Ed}}{f_y / (\sqrt{3} \gamma_{M0})} \leq 1,0$ and the local shear stress (τ_{Ed}) may be

obtained from: $\tau_{Ed} = \frac{V_{Ed} \cdot S}{t \cdot l} = \frac{0,9 \cdot V_{Ed}}{t_w \cdot h}$.

where:

$M_{y;Ed}$	[Nmm]	= design value for the bending moment in the strut about the y-y axis
$M_{z;Ed}$	[Nmm]	= design value for the bending moment in the strut about the z-z axis
F_{Ed}	[N]	= design force of the load
A_{eff}	[mm ²]	= effective cross-sectional area of the member
For a cylindrical profile: $A_{eff} = \frac{\pi}{4} \cdot D^2 - \frac{\pi}{4} \cdot (D - 2 \cdot t)^2$		
D	[mm]	= diameter of the cylindrical profile
t	[mm]	= steel thickness
f_y	[N/mm ²]	= yield strength
γ_{MO}	[-]	= partial safety factor for resistance of cross-sections ($\gamma_{MO} = 1,00$)
$W_{eff;y,min}$	[mm ³]	= minimum section modulus (moment of resistance) in y-y direction
$W_{eff;z,min}$	[mm ³]	= minimum section modulus (moment of resistance) in z-z direction
A_v	[mm ²]	= projected shear area (for a cylindrical profile $A_v = A_{eff}$)
S	[mm ⁴]	= first moment of area

For calculating the moment of inertia I of cylindrical profiles see Section 37.3 "Combi-walls".

The moment in a strut is caused by:

- a uniformly distributed load q , consisting of the self-weight of the strut and dropped sand laying on the strut (design value of 1 kN/m', according to CUR166);
- a concentrated load $F_{Ed,grab}$ (design value of 10 kN, according to CUR166) from a grab (*grijper*) that accidentally hits the strut in the middle;
- a second order moment introduced by the initial bending of the strut and the normal force⁸.

The maximum moment in the strut in y-direction can therefore be computed with:

$$M_{y,Ed} = \frac{1}{8} q \cdot \ell^2 + \frac{1}{4} F_{Ed,grab} \cdot \ell + N_{Ed} \cdot e_{Ny} \quad (\text{The struts are considered to be hinge-supported.})$$

where:

N_{Ed}	[N]	= design value of the compression force in the wale
e_{Ny}	[mm]	= eccentricity of the axial force in y-y direction:

$$e_{N;y} = \frac{5}{384} \cdot \frac{q \cdot \ell^4}{EI} + \frac{1}{48} \cdot \frac{F_{Ed} \cdot \ell^3}{EI}$$

q	[N/mm]	= uniformly distributed load
E	[N/mm ²]	= Youngs' modulus ($E = 2,1 \cdot 10^5$)
I	[mm ⁴]	= moment of area of the profile
ℓ	[mm]	= length of the strut

Stability check

A strut is considered to be stable if the stress caused by normal force (σ_n) and bending moment (σ_b), including a second order effect introduced by initial bending of the strut, does not exceed the yield stress of the steel:

$$(\sigma_n + \sigma_b) \cdot \left(\frac{1}{1 - \frac{1}{\alpha_{cr}}} \right) \leq f_{y,d} \quad \text{where} \quad \alpha_{cr} = \frac{F_{cr}}{F_{Ed}} \quad \text{and} \quad F_{cr} = \frac{\pi^2 EI}{\ell^2}$$

F_{cr} is the elastic critical buckling load (Euler force) for a global instability mode based on initial elastic stiffnesses and the design buckling load F_{Ed} .

⁸ Additional forces caused by temperature changes should be included in the value of the normal force.

It should also be checked that $\frac{N_{Ed}}{N_{b,Rd}} \leq 1,0$ (unity check)

where:

N_{Ed} [N] = design value of the compression force in the strut
 $N_{b,Rd}$ [N] = design value for the buckling resistance of the compression member:

$$N_{b,Rd} = \frac{\chi \cdot A \cdot f_y}{\gamma_{M1}}$$

χ [-] = buckling factor (formerly indicated with ω_{buc})
 A [mm²] = cross-sectional area of the member
 f_y [N/mm²] = yield stress
 γ_{M1} [-] = partial safety factor for resistance to instability ($\gamma_{M1} = 1,00$)

The buckling factor χ is a measure for the sensibility for buckling instability, and is dependent on the relative slenderness $\bar{\lambda}$ of the profile. The relationship between the relative slenderness of a profile and its buckling factor is given by the instability curve (see the graph or the equation in part II, Section 30.3). For closed, hot formed tubular profiles, instability curve *a* is valid.

The relative slenderness is defined by: $\bar{\lambda} = \sqrt{\frac{A \cdot f_y}{N_{cr}}} = \frac{L_{cr}}{i} \frac{1}{\lambda_1}$,

Where:

$\bar{\lambda}$ [-] = relative slenderness
 N_{cr} [N] = critical Euler load
 L_{cr} [mm] = the buckling length in the buckling plane considered
 i [mm] = radius of inertia

λ_E [-] = Euler slenderness = $\lambda_1 = \pi \cdot \sqrt{\frac{E}{f_y}} = 93,9 \cdot \varepsilon$

ε [-] = strain

A third unity check deals with the ultimate limit state for the combination of flexural and lateral buckling (*knik en kip*):

$$\frac{N_{Ed}}{\chi \cdot N_{Rk} / \gamma_{M1}} + \frac{M_{y,Ed}}{\chi_{LT} \cdot M_{y,Rk} / \gamma_{M1}} \leq 1,0$$

Where:

N_{Ed} [N] = design value for the compression force
 N_{Rk} [N] = characteristic value for resistance to compression for the critical cross-section
 $N_{Rk} = A \cdot f_y$
 $M_{y,Ed}$ [Nmm] = design value for the bending moment in the strut about the y-y axis
 $M_{y,Rk}$ [Nmm] = characteristic value of resistance to bending moments about the y-y axis
 χ [-] = reduction factor (= buckling factor) (see Figure 36-1)
 χ_{LT} [-] = lateral-torsional reduction factor (see Section 36.3)

It is not necessary to check a cylindrical pipe strut on lateral buckling (*kippen*), because all the axes are equally strong. Therefore, the strut will sooner fail on vertical deformation than on lateral buckling. H-profiles should be checked separately on lateral buckling.

Notes

- The strut (and also the sheet piling!) should be checked for fluctuating temperature loads during day and night.
- The construction site should be checked for strut failure, especially the zip effect, resulting from a strut being knocked out of position by a digger or crane.

38.2 Wales

If the wales (*gordingen*) of a cofferdam are supported by struts, they usually exist of two H-beams placed against the wall, with the webs (*lijven*) horizontal, and the flanges (*flenzen*) one under the other. If the wales are supported by anchors, sometimes two U-profiles are used that are positioned opposite each other, with the end of the anchor in between.

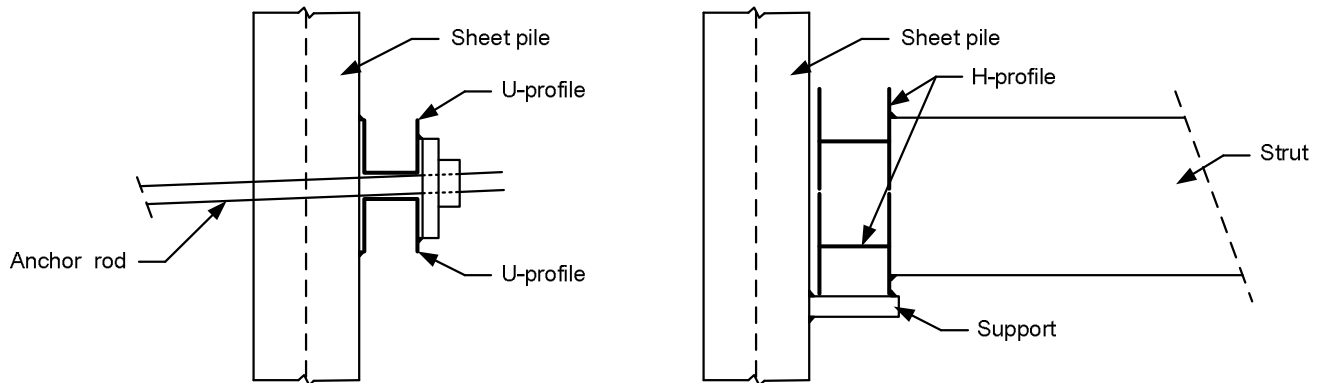


Figure 38-1: wales supported by anchors (left) and wales supported by struts (right).

The collar section of the H-beam will be the governing section of the entire cross-section. The combination of the normal, bending and shear stresses will be at its maximum here.

The stress due to the normal force F is $\sigma_n = \frac{F}{A}$, and is equally spread over the entire cross-section.

Stress caused by the bending moment can be calculated according to $\sigma_b = \frac{M}{W}$. The occurring bending moment is resisted mainly by the flanges. For a beam on two supports, the maximum moment in a bending beam is: $M = \frac{1}{8}q \cdot \ell^2$ and for a beam on multiple supports: $M = \frac{1}{12}q \cdot \ell^2$. Furthermore, the maximum moment at the end of a beam on multiple supports is set in between these two values: $M \approx \frac{1}{10}q \cdot \ell^2$. This is a good estimate for the moment working on the wales in the corners of a building pit. The design of wales is therefore based on this moment.

Since it is assumed that the anchor force F_{anchor} is evenly spread across the sheet pile wall via the wales, the following applies: $q = \frac{F_{\text{anchor}}}{\ell}$. In which ℓ is the distance between the anchors. The maximum bending

moment in the wale is therefore: $M \approx \frac{1}{10} \cdot F_{\text{anchor}} \cdot \ell$

The maximum shear stress is located at the centre of the cross-section of the H-profile and thus mainly born by the web of the H-beam. Again, the unity check is:

$$\frac{\tau_{Ed}}{f_y / (\sqrt{3} \cdot \gamma_{M0})} \leq 1,0 \quad \text{where } \tau_{Ed} \text{ may be obtained from: } \tau_{Ed} = \frac{V_{Ed} \cdot S}{t \cdot l} = \frac{0,9 \cdot V_{Ed}}{t_w \cdot h},$$

where:

τ_{Ed}	[Nmm ²]	= local shear stress
t_w	[mm]	= nominal web thickness
h	[mm]	= height of the web

The combined stress at the collar section as a result of both the bending moment and shear force is determined from the stress distribution over the cross-section. Where the design shear force (V_{Ed}) exceeds 50% of the plastic shear force ($V_{pl,Rd}$), the design resistance of the cross-section to combinations of moment and axial force should be calculated using a reduced yield strength $f_{red} = (1 - \rho) \cdot f_y$ for the shear area, where

$$\rho = \left(\frac{2 \cdot V_{Ed}}{V_{pl,Rd}} - 1 \right)^2$$

The required unity check for the ultimate limit state is as follows:

$$\frac{N_{Ed}}{A_{eff} \cdot f_y / \gamma_{M0}} + \frac{M_{y,Ed}}{W_{eff,y,min} \cdot f_y / \gamma_{M0}} + \frac{M_{z,Ed}}{W_{eff,z,min} \cdot f_y / \gamma_{M0}} \leq 1,0$$

Where:

$M_{y,Ed}$	[Nmm]	=	design value for the bending moment in the wale about the y-y axis
$M_{z,Ed}$	[Nmm]	=	design value for the bending moment in the wale about the z-z axis
A_{eff}	[mm ²]	=	effective cross-sectional area of the member
f_y	[N/mm ²]	=	yield strength
γ_{M0}	[-]	=	partial safety factor for resistance of cross-sections ($\gamma_{M0} = 1,00$)
$W_{eff,y,min}$	[mm ³]	=	minimum section modulus (moment of resistance) in y-y direction
$W_{eff,z,min}$	[mm ³]	=	minimum section modulus (moment of resistance) in z-z direction
A_v	[mm ²]	=	projected shear area (for a cylindrical profile $A_v = A_{eff}$)

The wales, being beams on many supports (the struts), and being evenly supported by the sheet piling, do not have to be checked on stability (buckling).

38.3 Literature

Nederlands Normalisatie instituut, *Eurocode 3: "Design of steel structures – Part 1-1: General rules for buildings"* (NEN-EN 1993-1-1), januari 2006, Nederlands Normalisatie instituut.

Nederlands Normalisatie instituut, *Eurocode 3: "Design of steel structures – Part 1-5: Piling"* (NEN-EN 1993-1-5), februari 2008, Nederlands Normalisatie instituut.

39. Construction pits: Anchors

extended: 2023

39.1 General

There are two ways for horizontal supporting soil retaining walls. Struts, in combination with wales, are usually preferred because they can be re-used. If struts are not possible, ground anchors can be used. The most important anchor types are:

1. Tieback anchors (*legankers*)
2. Screw anchors (*schroefankers*)
3. Screw grout anchors (*schroefinjectiepalen*)
4. Grout anchors (*groutankers*)
5. Anchor piles (*ankerpalen*)

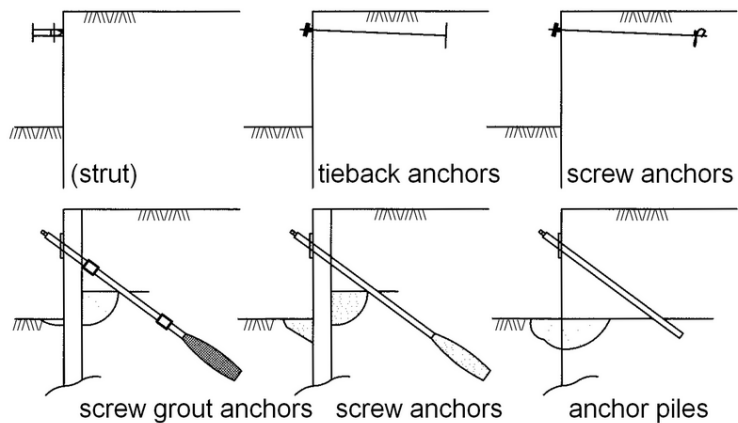


Figure 39-1 Types of horizontal supports

See Figure 39-1 for an overview.

For all types of anchor structures, the bearing capacity is extremely dependent on constructional aspects and soil properties. To eliminate anchors with a small bearing capacity in an early stage, each anchor has to be tested before it is connected to the retaining structure. The magnitude of the test load should be about the design load of the anchor force ($F_{s;A;d}$).

39.2 Tieback anchors

When regarding limit states in determining the ultimate resistance of anchor walls, one normally assumes straight slip planes according to Coulomb. These slip planes are shown schematically in Figure 39-2, along with the horizontal soil pressures working directly onto the both sides of the anchor wall. Generally, one assumes slip planes that extend unto ground level. This situation corresponds with an anchor wall that extends till ground level. However, this assumption only applies to anchor walls with a ratio of $\frac{h}{h_1} \leq 1,5$ since in such situations the ground above the anchor wall will slide in the same way as if the wall would extend all the way up to ground level. In other words, the anchor wall is fully embedded.

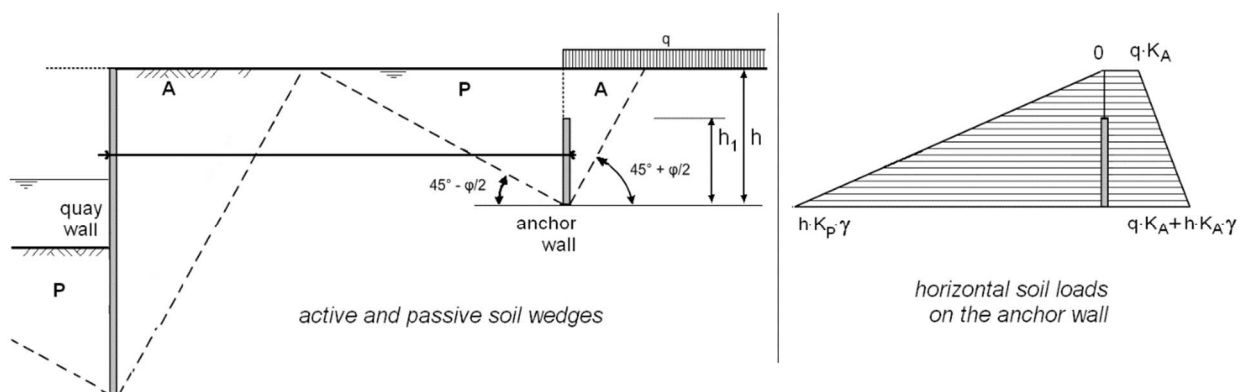


Figure 39-2 Unfavourable location of surcharge next to an anchor wall

Using Coulomb's theory and assuming that the anchor wall consists of steel rods connected to steel plates, the maximum anchor force can be computed as follows:

$$F_{A;max;d} = K_p \cdot \frac{1}{2} \cdot \gamma' \cdot h^2 \cdot a - K_a \cdot \frac{1}{2} \cdot \gamma' \cdot h^2 \cdot a = (K_p - K_a) \cdot \frac{1}{2} \cdot \gamma' \cdot h^2 \cdot a$$

where:

$F_{A;max;d}$	[kN]	=	maximum anchor force the anchor wall can resist
K_p	[-]	=	passive soil pressure coefficient
K_a	[-]	=	active soil pressure coefficient
γ'	[kN/m ³]	=	effective volumetric weight of the soil (= γ_d or $\gamma_s - \gamma_w$)
h	[m]	=	depth of the bottom tip of the anchor wall below ground surface
a	[m]	=	centre-to-centre distance between the tie rods, with $a \leq a_{max}$
a_{max}	[m]	=	maximum centre to centre distance allowed between tie rods

If there is a variable external load (q) at ground level, see Figure 39-2, the most unfavourable situation is the presence of the load above the active slip plane of the anchor wall and the absence of the external load above the passive slip plane. The maximum anchor force is now computed as:

$$F_{A;max;d} = K_p \cdot \frac{1}{2} \cdot \gamma' \cdot h^2 \cdot a - K_a \cdot \frac{1}{2} \cdot \gamma' \cdot h^2 \cdot a - K_a \cdot q_d \cdot h \cdot a = (K_p - K_a) \cdot \frac{1}{2} \cdot \gamma' \cdot h^2 \cdot a - K_a \cdot q_d \cdot h \cdot a$$

where:

q_d	[kN/m ²]	=	design value of the external load
-------	----------------------	---	-----------------------------------

The design value for the maximum anchor force ($F_{S;d}$) is determined as follows:

$$F_{S;A;d} = 1,1 \cdot F_{A;max;d}$$

Separated anchor boards

In engineering practice, a sheet pile wall is often anchored by a series of individual anchor boards spaced at certain distances, instead of by a continuous anchor wall. When regarding these anchor boards, the maximum anchor force can be computed in the same way as for a continuous anchor wall as long as the distance between the tie rods is not too large. The maximum distance between tie rods can be expressed as:

$$a_{max} = h_1 (\beta + \alpha - 1),$$

where:

a_{max}	[m]	=	maximum centre to centre distance allowed between tie rods
h_1	[m]	=	height of the anchor board
α	[-]	=	ratio between the height and width of the anchor board: b/h_1
β	[-]	=	Buchholz's factor, according to Figure 39-3.

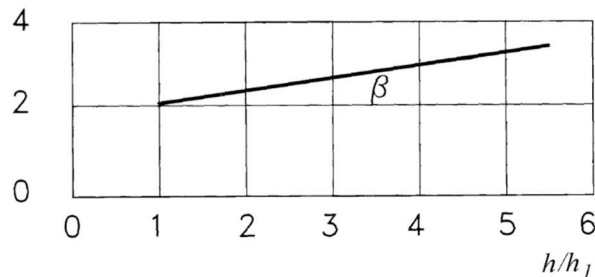


Figure 39-3 Buchholz's factor

If the centre-to-centre distance turns out to be larger than a_{max} then a_{max} is considered to be the total width of the ground slice that slips.

As a rule, the advantage of anchor walls or anchor boards is that they are cheaper than other anchor systems. The disadvantage is that one must have sufficient space to dig trenches for the tie rods and to be able to drive the walls or boards into the ground.

Strength of a tie rod

The design calculation of a sheet pile wall results in an anchor force per running meter (Section 37.2), which has to be converted into an anchor force, F_A , per anchor. The design value used for the tensile force in a tie rod ($F_{s;A;st;d}$) is found by increasing the design anchor force with an additional load factor:

$$F_{s;A;st;d} = F_{A;max;d} = \gamma_{f,b} \cdot F_{A;max} \quad \text{with: } \gamma_{f,b} = 1,25$$

Where:

$F_{s;A;st;d}$ [kN]	=	design value for the tensile force in the tie rod
$F_{A;max;d}$ [kN]	=	design value of the maximum anchor force
$F_{A;max}$ [kN]	=	maximum anchor force that can be resisted
$\gamma_{f,b}$ [-]	=	load factor

The minimum cross-section of the tie rod is calculated using the maximum calculated force in the tie rod, $F_{A;max;d}$, according to:

$$F_{A;max;d} = \frac{A_s \cdot f_u}{\gamma_{m,a}} \quad \text{with: } \gamma_{m,a} = 1,4$$

Where:

$F_{A;max;d}$ [kN]	=	design value of the maximum anchor force
A_s [m ²]	=	cross-section of the tie rod
f_u [kPa]	=	tensile strength of steel (see Table 36-1, where f_u is in N/mm ²)
$\gamma_{m,a}$ [-]	=	partial material factor

Overall stability

One can distinguish three failure types for an anchored sheet pile wall:

- along a deep sliding plane;
- along a circular sliding plane;
- as a result of bursting of the bottom of the excavation pit, during construction of the anchor wall

See Figure 39-4.

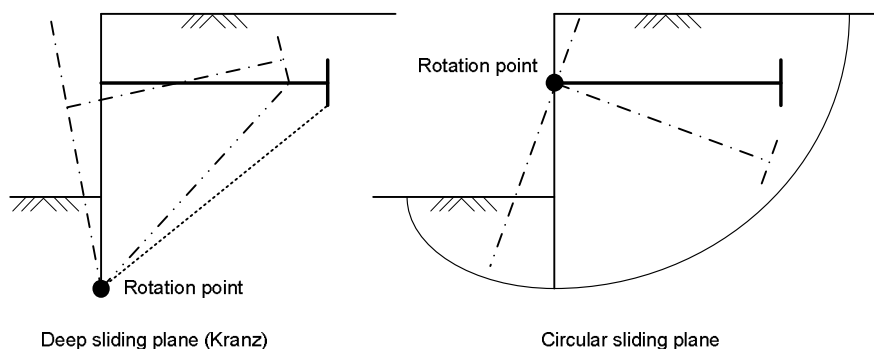


Figure 39-4 sliding planes

In the remainder of this section only the first failure mechanism will be discussed in detail, since checking for a circular slip plane is only required in specific circumstances such as short anchors and a small sheet pile length. Bursting of the bottom of an excavation pit occurs if the water pressure under an impermeable layer becomes too large compared to the layer thickness of the impermeable layer. This phenomenon is also known as 'heave' (*hydraulische grondbreuk*).

In case one keeps the areas of influence of the anchor boards, or other tension elements, and the sheet piling strictly separated, it is very unlikely that the whole structure consisting of sheet piling, anchor plates and soil will slide. The areas of influence are shown in Figure 39-5. As a rule of thumb there should always be a distance of at least 1 meter between the straight sliding planes at ground level (This is added safety!). If the distance between the sheet pile wall and the anchor becomes too small, the areas of influence intersect, see dashed lines in the figure below. This results in higher pressures at the active side of the retaining structure (here sheet pile wall), while the resistance of the anchor is reduced, or in other words: the pressures at the passive side are lowered.

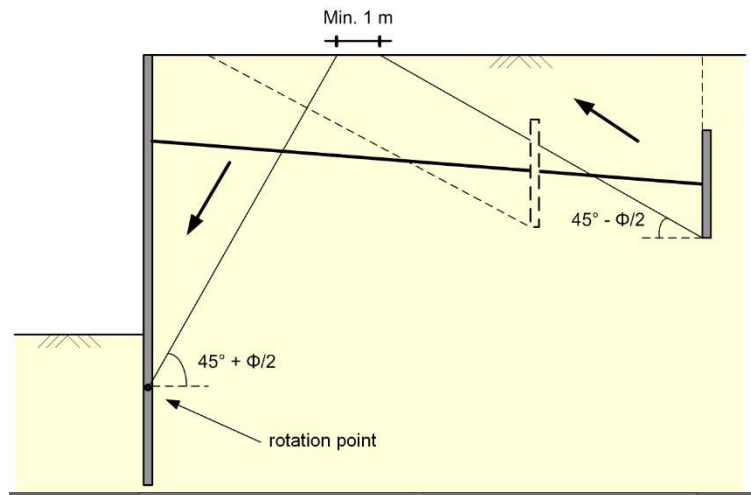


Figure 39-5 Areas of influence using straight slip planes.

Using the method of Kranz, one can compute the required minimum distance between the anchor and the sheet pile wall. If this distance is too short, a straight sliding plane will occur approximately between the point where the shear force in the sheet piling is zero and the bottom of the anchor plate. More specific, for free supported sheet piles and anchor screens the sliding plane will occur between the bottom of the sheet pile wall and the bottom of the anchor structure. For clamped sheet pile walls and anchor screens, the sliding plane will occur between the lowest zero point of the shear force in the sheet pile wall and the bottom of the anchor structure.

To prove that the total stability is sufficient one should demonstrate that the design value of the maximum anchor force can be supported by the soil retained between the sheet pile walls and the anchor structure. This is done by considering the balance of the soil body enclosed by ground level, the vertical planes just behind the sheet pile wall and just in front of the anchor structure and the assumed deep sliding plane, see Figure 39-6.

All the forces working directly on this soil body have to be taken into account when using this method. Forces working directly onto the retaining structure are already accounted for in the computation of the design value for the maximum anchor force. For example; if a bollard is situated in the ground behind the sheet pile wall, this force is working directly on the soil body regarded with Kranz's method. Thus, it has to be accounted for. However, if the bollard is connected to the sheet pile wall it has already been taken into account when computing the design value for the maximum anchor force. Therefore, it is not considered in the Kranz method.

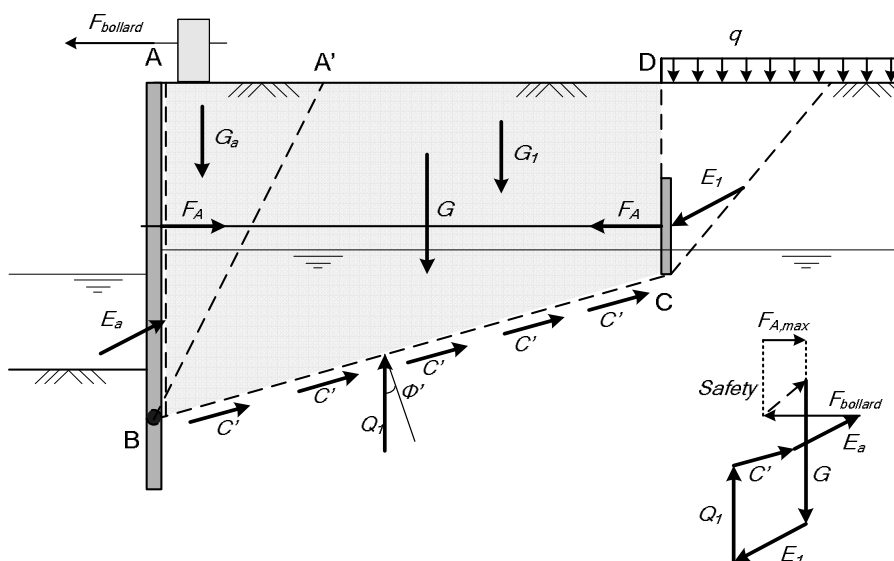


Figure 39-6 Computational scheme according to Kranz.

On the soil body ABCD (light shaded area in Figure 39-6) the following forces are working, which should balance each other:

G	[kN]	=	weight of the soil body ABCD
E_a	[kN]	=	force exerted on AB by the sliding active soil mass in case of failure. This force can be deduced from the active pressure on the sheet piling and the soil mass G_a of the soil body AA' B working on the active sliding plane A'B.
E_1	[kN]	=	soil pressure exerted on the vertical through the anchor structure. In this force also the presence of a possible external load (q) should be included.
Q_1	[kN]	=	force exerted on the plane BC, that in case of failure makes an angle (φ') with the normal on this plane.
F_A	[kN]	=	anchor force exerted on the soil body by the anchor structure, as computed in the sheet pile computation.
$F_{bollard}$	[kN]	=	bollard force, if present.
c'	[kN]	=	friction force as a result of cohesion, if present. This force works in the direction of plane AB.
φ'	[°]	=	angle of internal friction

In case the above forces do not balance each other, the soil body ABCD will slide along plane BC. As a result, the direction of force Q_1 is determined and the force polygon (*krachtenveelhoek*) can be drawn for the chosen distance between the sheet piling and the anchor structure, see Figure 39-6. Or one can determine the maximum allowable anchor force analytically.

Note that the presence of a horizontal groundwater table behind the sheet piling only affects the weight of the soil masses; there is no resulting horizontal water pressure. Water pressure as a result of a head difference is already included via the computed maximum anchor force as computed in the sheet pile computation. In case of a curved groundwater table behind the sheet piling one should include the influence of this curved groundwater table by including a resulting horizontal force caused by the difference in water pressure over the length of the anchor, see Figure 39-7.

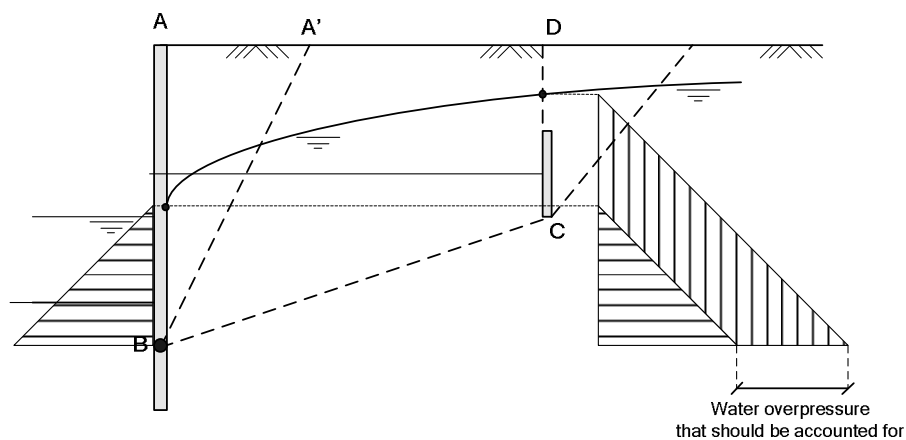


Figure 39-7 Influence of a curved groundwater table.

If after computation the maximum allowable anchor force is too large, one can either increase the length of the anchor bar or increase the length of the sheet piles.

39.3 Screw anchors

Screw anchors consist of a steel tie rod with a diameter of approximately 30 mm width and at the end a steel screw blade of approximately 250 to 500 mm that is welded to the tie rod. Only a small excavation behind the sheet piling is necessary to install the anchors. The anchors are installed using a vibrating drill. This type of anchors can be installed horizontally or at an angle. The maximum capacity is attained when the anchors are installed at a depth of approximately 12 times the diameter of the screw blade. When the depth over blade diameter ratio is increased further, the capacity of the anchor hardly increases. In case the depth over blade diameter ratio is smaller than 5, the capacity of the anchor will reduce rapidly. In general, the bearing capacity of a screw anchor is rather small (< 75 kN), therefore they are mainly used for campsheets (*beschoeiingen*).

The way in which the ground around a screw anchor will fail depends both on the installation depth of the anchor and on the angle of the tie rod relative to horizontal.

If the depth over diameter ratio of a screw anchor is smaller than 5 ($H/D \leq 5$), the anchor is considered to be shallow. This implies that the sliding planes reach unto ground level, see the upper anchor in Figure 39-8. In case of a deep anchor ($H/D > 5$), the collapse pattern of the soil largely resembles that of the pattern around the tip of a compression pile, see the lower anchor in Figure 39-8.

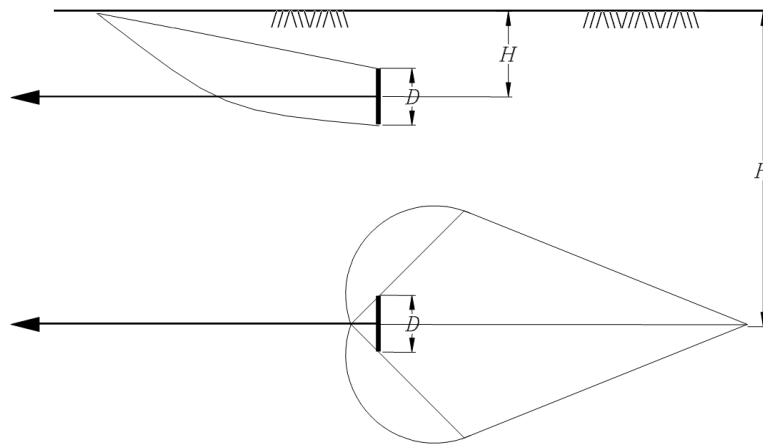


Figure 39-8 Sliding planes around an anchor blade during failure

Hergarden (1983) researched the grip force of the anchor. For deep screw anchors in sandy soils, he found a relationship between the anchor force and the cone resistance in the area of influence of the anchor. This relationship reads as follows for sand:

$$F_{r,A;scr,min} = 0,4 \cdot A \cdot q_{c,avg} \geq F_{s,A;d}$$

where:

$F_{r,A;scr,min}$	[kN]	=	minimum grip force of the screw anchor
$F_{s,A;d}$	[kN]	=	design value for the maximum anchor force the screw anchor can resist
A	[m ²]	=	area of the anchor blade
$q_{c,avg}$	[kPa]	=	average cone resistance in the area of influence ($3 \cdot D$ above and beneath the anchor's axis)

In cohesive soils the relationship reads:

$$F_{r,A;scr;d} = 10 \cdot C_{u;d} \cdot A \geq F_{s,A;d}$$

where:

$F_{r,A;scr;d}$	[kN]	=	design grip force of the screw anchor
$F_{s,A;d}$	[kN]	=	design value for the maximum anchor force the screw anchor can resist
$C_{u;d}$	[kPa]	=	design value for the undrained cohesion of the soil
A	[m ²]	=	area of the anchor blade

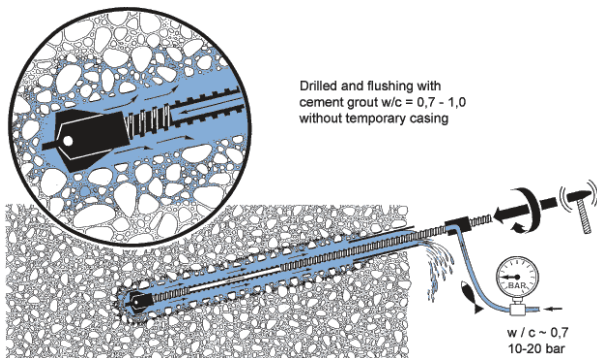
39.4 Screw grout anchors

An anchor type derived from the grout anchor is the screw grout anchor, e.g., the *Leeuwanker*. This anchor type consists of a thick-walled tube with a spiral drill head welded onto the end. The grout body is formed by injecting grout through the drill head while installing the anchor. Compared to the grout anchors mentioned above the grout body is formed under relatively low pressure. The thick-walled pipe is made of normal quality steel, which means that the maximum allowable stresses in the tube are a lot less than for the high-quality steel rods or wires in the grout anchors. The screw grout anchor, however, is a lot stiffer than the grout anchor.

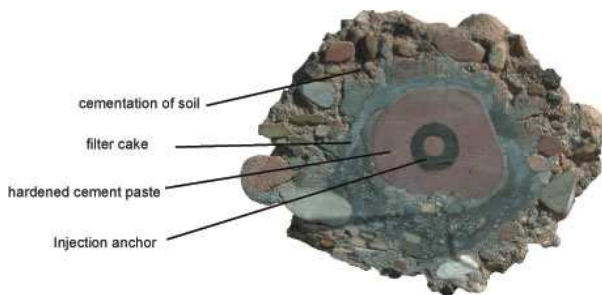
Another subtype of grout anchor that is often used nowadays is the self-drilling grout anchor, e.g. titan and jetmix anchors. The main advantage compared to the other grout anchors is that the system is cheaper to install (less laborious), but still has a large bearing capacity (1500-2000 kN). This anchor consists of a tube with thread (*schroefdraad*) and a drill head. These threads are formed much like the ribs on a reinforcement bar and result in a higher bond with the grout body compared to standard drill steel. During installation the drill head is moved back and forth while at the meantime grout is being injected. In this way the soil is removed from the drill hole and replaced by the grout mixture. This results in a drill hole with a diameter between 150 and 200 mm. After reaching the planned position of the grout anchor, the grout pressure is

increased and the drilling is continued until the thus created grout anchor has reached its required length. Note that the drill hole widens after increasing the pressure (Figure 39-9). After installation, the grout anchor serves as a draw bar (*trekelement*).

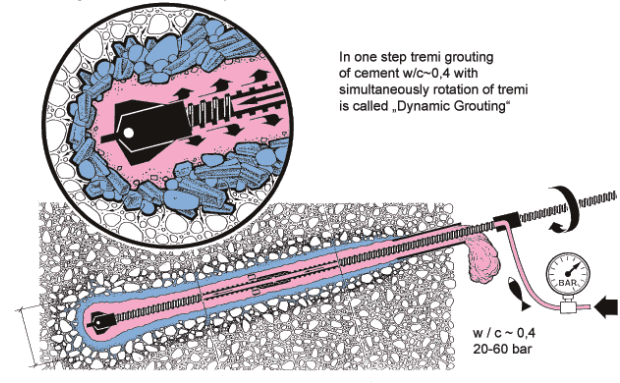
Drilling the drill hole



Cross-section of anchor body



Creating the anchor body



Drill tube



Figure 39-9 Installation of self-drilling grout anchor. (<http://www.ischebeck.de>)

Screw grout anchors closely resemble auger piles (*avegaarpalen*), since no soil displacement occurs during construction of the pile. The minimum grip force and hence maximum anchoring force of the anchor can be determined using:

$$F_{r,A,gr,min} = \alpha_t \cdot q_{c,gem} \cdot O \cdot L_A \geq F_{s,A,d}$$

where:

- $F_{r,A,gr,min}$ [kN] = minimum grip force of the screw grout anchor
- $F_{s,A,d}$ [kN] = design value for the maximum anchor force the screw grout anchor can resist
- α_t [-] = pile class factor ($\alpha_t = 0,011$)
- $q_{c,gem}$ [kPa] = average cone resistance along the embedded part of the anchor
- O [m] = average circumference of the embedded part of the anchor
- L_A [m] = length of the embedded part of the anchor

Again all anchors should be tested with a load equal to the design value for the maximum anchor force. This may lead to a lower safety factor, which in return leads to fewer anchors.

39.5 Grout anchors

A grout anchor consists of a steel anchor rod or a bunch of pre-stressed cables, and a cylindrical body of cement grout, created in the soil (Figure 39-10).

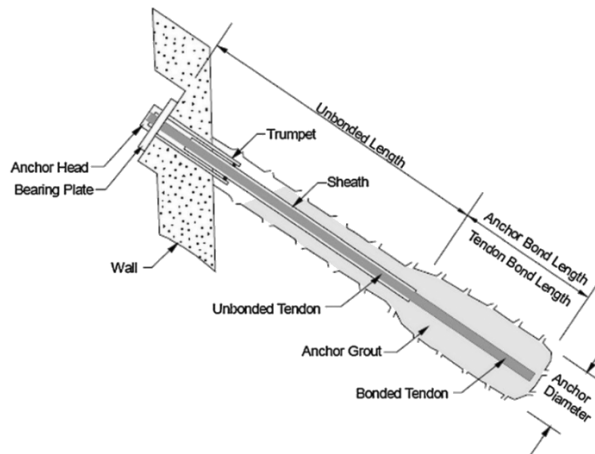


Figure 39-10 Schematic drawing of a grout anchor (Özhan and Guler, 2017)

The grout body usually has a length between 4 and 20 m and a diameter between 110 and 200 mm, depending on the diameter of the drill pipe. The anchor is connected to the sheet piling by means of a steel rod or steel wire that is installed by driving or drilling a hollow drill pipe into the ground (see Figure 39-11, picture 1). Subsequently the steel rod or wire is inserted into the drill pipe (2) and the cement grout is injected under high pressure into the surrounding ground through the drill pipe while pulling back the pipe (3). When a grout body of sufficient length is created, the drill pipe is pulled out completely. When the cement of the grout body has hardened enough, the steel rod or wire is tightened up to 70-90% of the needed anchor force (4), after which the external load is exerted on the sheet piling. As a result of this pre-stressing of the steel rod or wire, most of the elastic strain is removed from the anchor. This limits the horizontal deformations of the soil retaining structure.

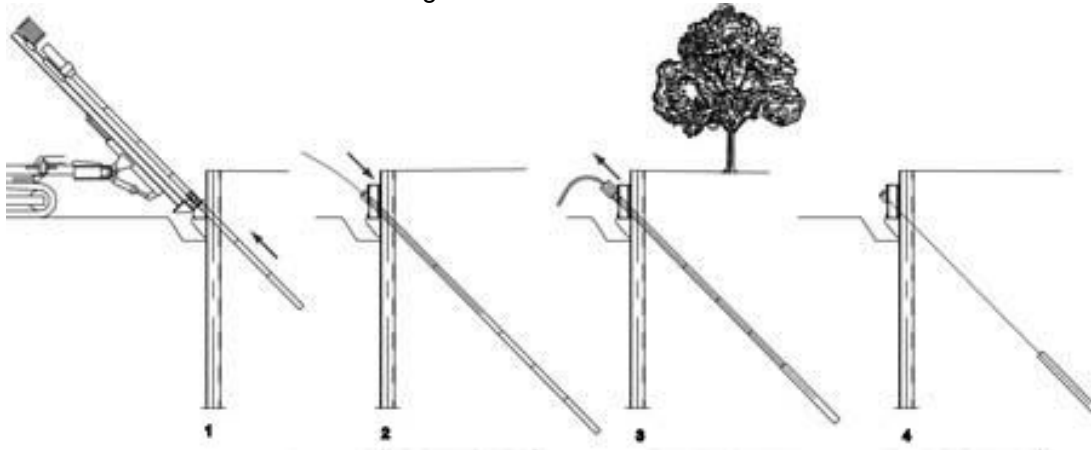


Figure 39-11 Installation of a grout anchor (Funderingstechnieken BAM Infra, 2020)

The way in which the anchors are installed influences their yield strength. Usually, one achieves higher tensile strengths using driven (*geheide*) anchors instead of drilled (*geboorde*) anchors. The anchors are installed under an angle of 25-45° to a depth where a sufficiently strong sand layer is present in order to form the grout body. Since the rods and wires are made of high-quality steel with a relatively high allowable stress, their cross-section can be kept relatively small. Minor damage to a rod can therefore considerably decrease its cross-section area, which has large consequences for the reliability of an anchor. The maximum ultimate bearing capacity is around 3000 kN.

When determining the maximum strength of anchors, one usually assumes the values given in Figure 39-12.

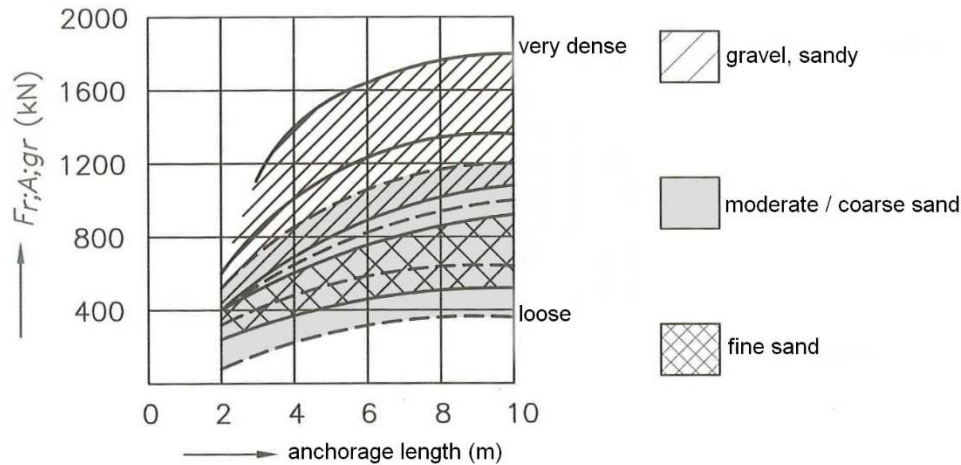


Figure 39-12 Maximum grip force for grout anchors with $D_{anchor} = 100$ to 150 mm and $H \geq 4$ m (CUR 166)

A grout anchor can fail due to various mechanisms:

1. Grout body is pulled out of the ground

The friction capacity of the grout - ground interface should not be exceeded. The capacity cannot precisely be determined and can best be tested in situ. For a first estimation, the resistance can be related to the cone resistance:

$$\tau_{grout/ground} = \frac{F_{r,A;gr;d}}{D_{grout} \cdot \pi \cdot L_{grout}} \leq \tau_{max} \leq 0,3 \text{ N/mm}^2$$

where: $\tau_{grout/ground}$ [N/mm²] = tension stress in the grout-ground interface
 D_{grout} [m] = average diameter of the grout body
 L_{grout} [m] = length of the grout body
 $F_{r,A;gr;d}$ [kN] = design value of the acting anchor force:

$$F_{r,A;gr;d} = \frac{\zeta}{\gamma_{m,b}} \cdot F_{r,A;gr;min}$$

ζ [-] = reduction factor, based on a number of control tests. If all anchors have been tested⁹, $\zeta = 1$, otherwise according to NEN 6743

$\gamma_{m,b}$ [-] = partial material factor ($\gamma_{m,b} = 1,4$, according to NEN6740, but if all anchors have been tested, $\gamma_{m,b} = 1,25$)

$F_{r,A;gr;min}$ [kN] = indication of the minimum actual anchor force
 τ_{max} [N/mm²] = slip resistance of the grout-rod interface:
 $\tau_{max} = 0,02 q_c$.

q_c [N/mm²] = cone resistance of the soil

2. Anchor rod is pulled out of the grout body

It is assumed that the pulling-out criterion of the anchor rod becomes relevant at cone resistances of more than 10 MN/m^2 :

$$\tau_{grout/rod} = \frac{F_{r,A;gr;d}}{D_{rod} \cdot \pi \cdot L_{rod}} \leq \tau_{max}$$

where: $\tau_{grout/rod}$ [N/mm²] = tension stress the anchor grout - rod interface
 $F_{r,A;gr;d}$ [kN] = design value of the acting anchor force (see above)
 D_{rod} [m] = average diameter of the anchor rod
 L_{rod} [m] = length of the anchor rod
 τ_{max} [N/mm²] = slip resistance of the grout-rod interface:
 $\tau_{max} = 1,5$ for smooth rods and $2,2 \text{ N/mm}^2$ for rippled rods.

⁹ Testing all anchors is obligatory for sheetpile walls with safety class II and III, see CUR-report 166.

3. Rupture of the anchor rod

The anchor rod will fail, if its strength is exceeded:

$$1,25 \cdot F_{A,max} \geq F_{r,st;d} = \text{MIN} \left(\frac{F_{r;br;rep}}{1,4}, \frac{F_{r;y;rep}}{1,0} \right)$$

where: $F_{A,max}$ [kN] = maximum anchor action force
 $F_{r,st;d}$ [kN] = design value of the steel resistance force (related to the steel quality)
 $F_{r;br;rep}$ [kN] = representative value of the yield strength of the rod
 $F_{r;y;d}$ [kN] = representative value of the rupture strength of the rod

The rupture strength is usually governing

4. Ground failure

The equilibrium of forces of the anchor-influenced soil body is called the Kranz stability. If the distance between the wall and the grout body is too small, a slip plane will originate from the point straight above the middle of the grout body at ground surface (point D) towards the middle of the grout body (point C) to the rotation point in case of a fixed support, or the lowest point of the wall in case of a free earth support (point B), to the top of the wall (point A). This soil body should be able to resist the design value of the anchor force. See Figure 39-13.

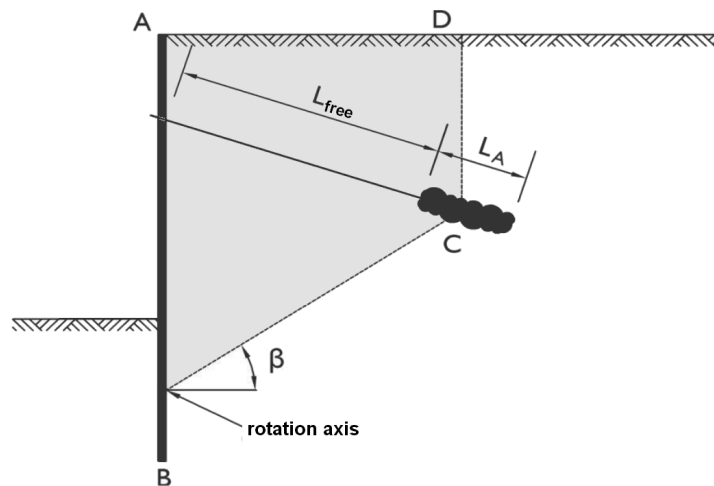


Figure 39-13 Kranz soil body in case of a fixed earth support

The reader is referred to CUR report 166 for information regarding a more detailed design of grout anchors. All anchors have to be subjected to a test load equal to the design load ($F_{s;A;d}$). The test results may lead to a lower safety factor, which in turn leads to the use of fewer anchors. One should be aware that over time the soil pressure, which is temporarily increased as a result of the installation of the grout anchors, will creep back to lower values (this holds in sand too). Since the test loads only have a short duration one tends to find too large values for the maximum anchor force ($F_{A,max}$). Hence one should not simply use the test values found for determining the maximum grout force with Figure 39-12.

39.6 Anchor piles

Anchor piles are used, if very large anchor forces are involved. Like other anchor types, this type transfers the load to the subsoil by means of friction. The presence of sand along the effective length of the pile is required. The effective length of the anchor pile is the part of the pile that is situated outside the active sliding zone behind the sheet piling, see Figure 39-14. Nearly all pile types that are suitable as vertical tension piles are also suitable as anchor piles. The strength of the anchoring pile is determined in the same way as for tension piles and the stability is checked by means of the clump criterion, see Section 33.3 of this manual.

An example of an anchor pile that is often used for heavy quay structures is the MV-pile (*Müller Verpress Pfähle*, which is German for 'Müller grouting piles'). This type of pile consists of a steel H-beam that is coated with cement grout during installation. The cement grout coating can be applied in two ways, first by welding an enlarged foot at the end of the H-beam and second by welding steel strips on the outside of the flanges of the H-beam. In both cases the cement grout fills the cavities that are formed in the ground, thus

forming the coating.

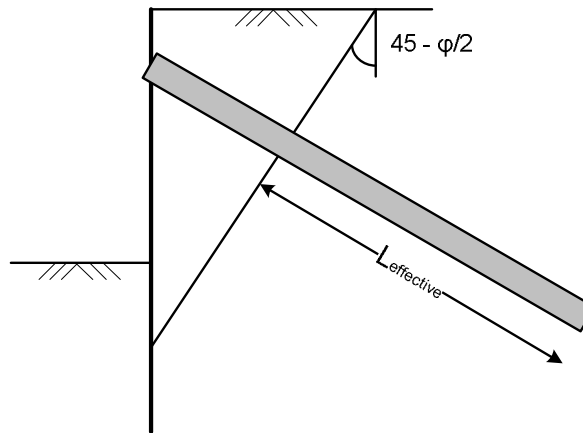


Figure 39-14 Effective length of an anchor pile.

A continuous anchor wall and anchor screens can be used if there is:

- a reasonably strong and stiff top layer and fill.
- sufficient space to install the anchor wall and to excavate in order to install the tie rods.

39.7 Literature

Civieltechnisch Centrum Uitvoering Research en regelgeving (CUR), *CUR-publicatie 166: "Damwand-constructies deel 1"*, 5^e druk, Gouda, 2008, CUR.

Civieltechnisch Centrum Uitvoering Research en regelgeving (CUR), *CUR-publicatie 166: "Damwand-constructies deel 2"*, 5^e druk, Gouda, 2008, CUR.

Webpages:

<http://www.gebr-vanleeuwen.nl>

<http://www.ischebeck.de>

<http://www.jetmix.nl>

40. Construction pits: Underwater concrete floor

40.1 General

Underwater concrete is mostly used to create a watertight floor, usually of a building pit. It takes away the necessity of dewatering, which can lead to considerable cost savings. In addition, the risk of settlements due to groundwater extraction is reduced by using an underwater concrete floor. Underwater concrete can be applied in floors with a maximum slope angle of 6 to 7°.

The composition of underwater concrete is quite similar to normal structural concrete. During application, special attention is paid to the prevention of washing out of the concrete when in contact with water, which could lead to a badly mixed concrete that does not harden sufficiently. In exceptional cases, underwater concrete can be reinforced with steel bars, but this is problematic regarding construction. However, if it is reinforced, it can be considered structural concrete, for which one needs to take larger tolerances concerning the shape, the dimensions and the quality of the concrete into account. Loads on reinforced underwater concrete are usually transmitted by bending and shear forces. Non-reinforced concrete transmits its loads different from reinforced concrete, as non-reinforced concrete cannot take tensile forces. Hence, as a rule, more concrete is required in case of non-reinforced concrete. On the other hand, one does not need to place reinforcement cages under water.

The forces in a non-reinforced underwater concrete floor can be compared to those in masonry arches. Between the floor supports (piles and sheet piling), pressure arches are created, which transmit the loads to the supports.

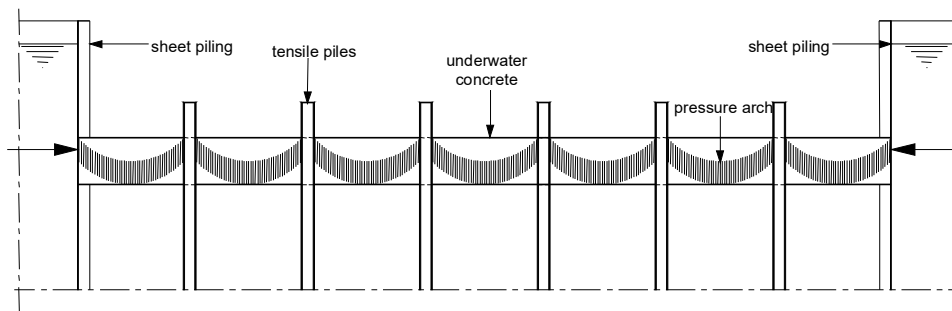


Figure 40-1 Pressure arches in underwater concrete

An arched structure owes its strength to so-called arch thrust. This arch thrust is a horizontal reaction force in the support (see Figure 40-1 and Figure 40-2). The arch thrust makes an equilibrium with the strutting force in the floor, which originates from the sheet piling.

The non-reinforced concrete floor can also be compared with a pre-stressed floor. In this case the strutting forces can be considered pre-stressing forces in the floor. Because the floor is subjected to a compression load, the non-reinforced concrete is able to absorb moments without the presence of tensile stresses.

The non-reinforced concrete floor can therefore be schematised as a number of arches between the supports and as a plate that is pre-stressed in two directions with supports in a number of points and lines.

At the supports, however, the reaction force has to be transmitted by a shear force between the concrete and the pile. If steel piles are used, the concrete is usually well attached to the pile, however, if the shape of the pile encourages the creation of gravel pockets or soil enclosures, one cannot simply depend on the attachment. Clean contact areas are of large importance for a good attachment. If prefab concrete piles are used, the top metres of the sides of those piles are often given ribs to improve the join.

40.2 Limit states

There are three ultimate limit states that apply for an underwater concrete floor:

1. Floatation of the floor
2. Fracture of the floor
3. Fracture of the join between the floor and the tension piles

Floatation of the floor

In the case of this ultimate limit state; one must consider the equilibrium of the floor. The downward forces are:

- the weight of the floor
- the weight of the piles and anchors, plus the attached clump weight (weight of the soil under water that is pulled up by the piles) or the maximum friction along the pile shaft

The upwards forces are:

- the upwards groundwater pressure under the floor
- the effective soil pressure under the floor (loads caused by swell of lower clay and peat layers)

Fracture of the floor

Fracture of the floor is possible when the ultimate bearing capacity of the arch is exceeded. The determination of the ultimate bearing capacity of the arch created in the underwater concrete floor is not simple because the geometry of the arch is not set beforehand. To determine the maximum bearing capacity, one often assumes an arch with a height of 75% of the floor thickness and with a thickness of 10% of the floor thickness. Generally, this limit state is not normative for the thickness of the underwater concrete.

Fracture of the join between the floor and the tension piles

A fracture of the join between the floor and the pile is possible if the maximum acceptable shear stress along the piles is exceeded.

To describe this limit state, one cannot simply use the limit state "Punch" of TGB 1990 for columns punching through floors, because there is no firm attachment to the reinforcement steel. A safe approach is to only consider the transfer of forces from the floor to the pile in the contact areas between the pile and the underwater concrete.

In the case of a steel pile the force from the floor is transferred in the entire contact area, assuming a good attachment of the pile and the concrete. The slide plane in the concrete is assumed to be the smallest envelope around the pile.

In the case of prefab concrete piles, one usually assumes that the shear force in the floor is transferred to the pile along the ribbed sides of the pile.

The limit state involved assumes that the calculation value of the occurring shear force in the mentioned slide planes equals the maximum acceptable shear force in the underwater concrete.

40.3 2-D Arch effect

The shape and height of the pressure arches depend on the type of load and the arch thrust that occur.

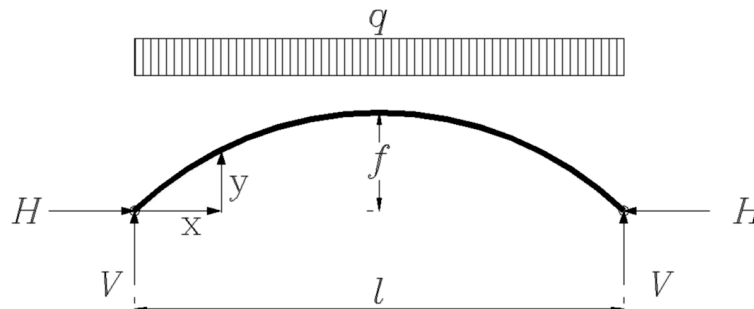


Figure 40-2 Schematisation of a pressure arch

Before we look more closely at the (3-D) arch that is created between the supports, the general distribution of forces in a two-dimensional arch is considered first.

The value of the arch thrust can be found by considering the balance of moments in the centre. The vertical reaction force and the uniform distributed load to the left of the centre cause an anticlockwise moment equal to $1/8 q l^2$. The arch thrust in the left support causes a clockwise moment equal to $H \cdot f$.

The balance of moments leads to:

$$H = \frac{q l^2}{8f} \quad \text{or} \quad f = \frac{q l^2}{8H}$$

The optimum shape of an arch with a uniform distributed load is derived from the balance of moments for every point on the arch:

$$H y = \frac{1}{2} q x (l - x)$$

The position of the median of a pure pressure arch, loaded by an equally distributed load is:

$$y = \frac{qx(l-x)}{2H}$$

For a horizontal non-reinforced concrete beam, in which a uniform distributed load leads to a pressure arch, the height of the arch is determined by the point of application of the horizontal arch thrust and the centroid of the stress diagram in the middle of the beam. The shape of the stress diagram depends on the deformations in the cross-section of the beam and on the δ - ϵ diagram of concrete. Figure 40-3 shows a number of possible stress diagrams.

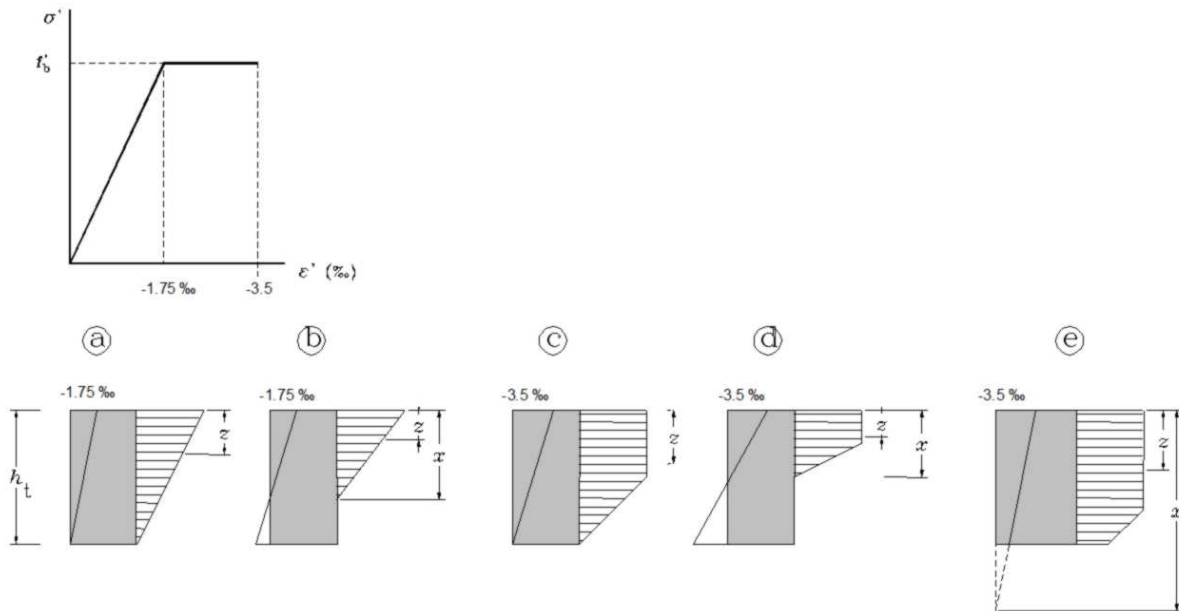


Figure 40-3 Centroid of the pressure arch in concrete, dependent on the deformation

The position of the line of action of the horizontal arch thrust depends, amongst others factors, on the way the pressure is applied to the side of the beam. In this case the position of the line of action depends on the angle of rotation of the plane on which the force acts. For an underwater concrete floor in an excavated building site, this angle of rotation occurs when the wall and floor deflect after the water has been removed from the site.

40.4 3-D Dome effect

The previous section only discussed the arch. In an underwater concrete floor with tension piles, pressure arches will occur between the piles in different directions. Between these pressure arches, the load is also transferred by means of arches. Between four piles the arches will form an inverted dome. Figure 40-4 schematically shows the main load bearing structure, drawn in thick lines.

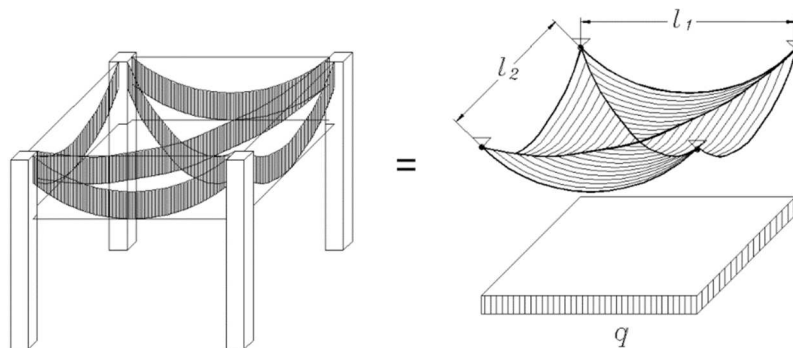


Figure 40-4 Dome effect between four piles

The horizontal arch thrusts on the dome can be calculated by considering the balance of moments around a horizontal axis through the centre of the dome.

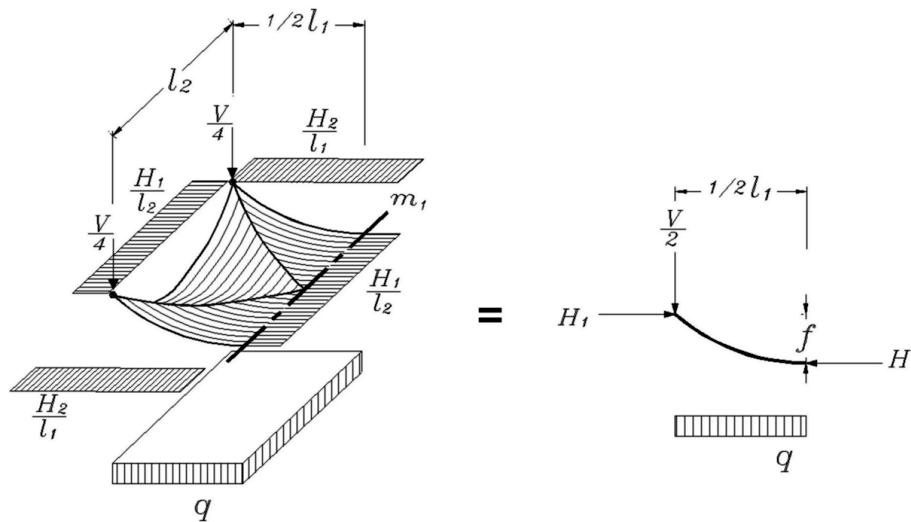


Figure 40-5 Balance of moments around an axis through the centre

The equilibrium leads to: $H_1 = \frac{ql_2 l_1^2}{8f}$ and $H_2 = \frac{ql_1 l_2^2}{8f}$

Consequently: $\frac{H_1}{H_2} = \frac{l_1}{l_2}$

The vertical reaction force is: $\frac{V}{4} = \frac{ql_1 l_2}{4}$

40.5 Transfer of forces to piles

The reaction force that the piles have to provide is transferred from the floor to the pile through the contact area between the floor and pile.

For a clean steel pile, the steel and concrete attach like reinforcement steel attaches to concrete. Next to the pile, the load is transferred to the underwater concrete floor by means of shear stress (see Figure 40-6).

For a smooth prefab concrete pile, the attachment between the underwater concrete and the pile is inferior. For this reason prefab piles usually have ribs along the top few metres, to ensure a certain amount of catch resistance.

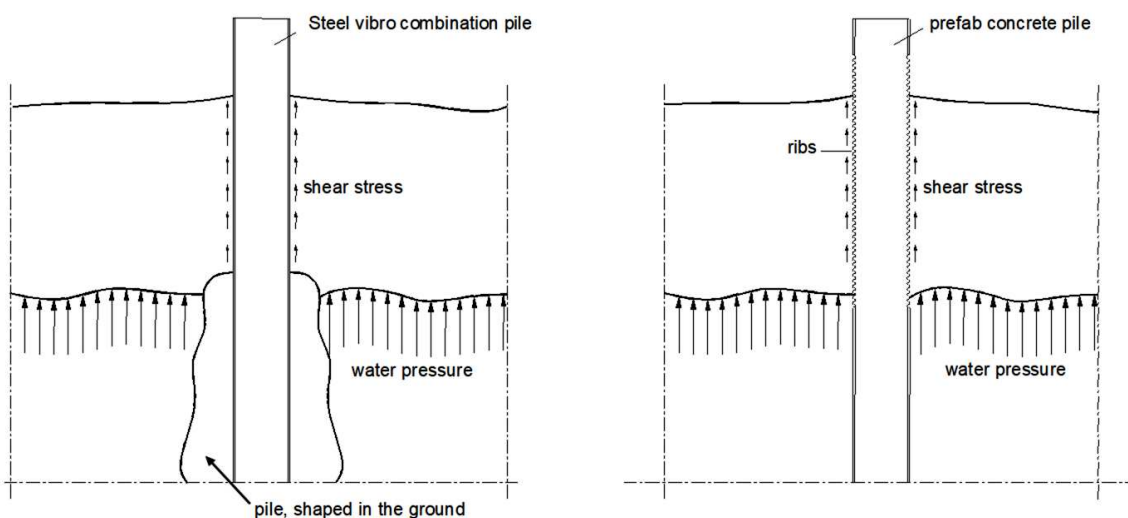


Figure 40-6 Shear stress along a pile shaft

The underwater concrete floor is loaded by the upward water pressure less its own weight. The floor transfers the load to the piles. A test calculation will have to decide whether the thickness determined practically is sufficient.

41. Construction pits: Dewatering

Major revision: February 2008

This chapter first covers dewatering in general. Subsequently, it shows how (theoretical) designs are made. For comprehensibility of the dewatering mechanism, one should distinguish between two types of aquifers (*waterhoudende grondlagen*):

- An "unconfined aquifer" is an underground layer of porous material with a free groundwater level (*niet-afgesloten grondlaag met freatisch water*).
- In a "confined aquifer" the groundwater is trapped between impermeable ground layers (*afgesloten grondlaag met spanningswater*). The water level usually rises above the top of the aquifer, in which case the well is called an artesian well (artesian water, *overspannen water*). Sometimes the water level is below the top of the aquifer (*onderspannen water*).

41.1 General

Dewatering methods

Theoretically two methods of dewatering are possible:

- open dewatering, where drainage trenches along the foot of a slope carry the water to wells. From there the water is removed from the construction site using dirty-water pumps (Figure 41-1). Dewatering in the open is only possible for small water level reductions in impermeable soil types (at most 4 to 5 metres in clay).

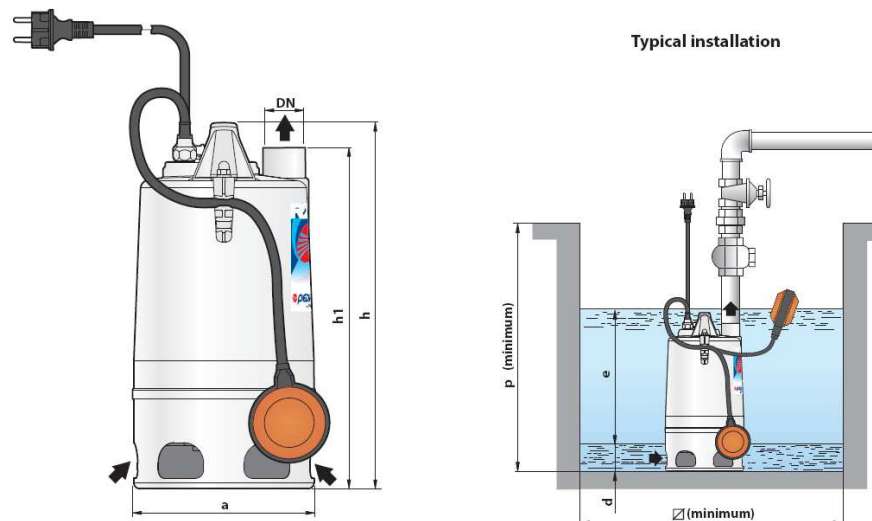


Figure 41-1 Dirty-water pump (from www.pedrollo.co.uk/)

- wellpoint drainage (*bronbemaling*), for which the following systems can be distinguished (see Figure 41-2):
 - vacuum drainage with closed wells, where flexible pipes connect the riser (*stijgbuis*) of every well to a header (= suction pipe, *zuigbuis*). The under-pressure in the header is created using centrifugal or plunger pumps.
 - vacuum drainage with open wells. The system is the same as the vacuum drainage mentioned above, though here each well has a draw pipe (*haalbuis*) suspended in it. The advantage over the system mentioned above is that the water level in the wells can be reduced maximally, provided the draw pipes are long enough.

Because the under-pressure can never be more than atmospheric pressure (1 atm = 101 kPa \approx 10 m column of water), the water level reduction that can be achieved by means of vacuum drainage is rarely more than 5 to 6 metres. Vacuum drainage in deep excavations must therefore be carried out in stages. The method is applicable to a range of soil types, from silty to fine sand sills. The yield per well is approximately 1,5 to 2,0 m³/hour.

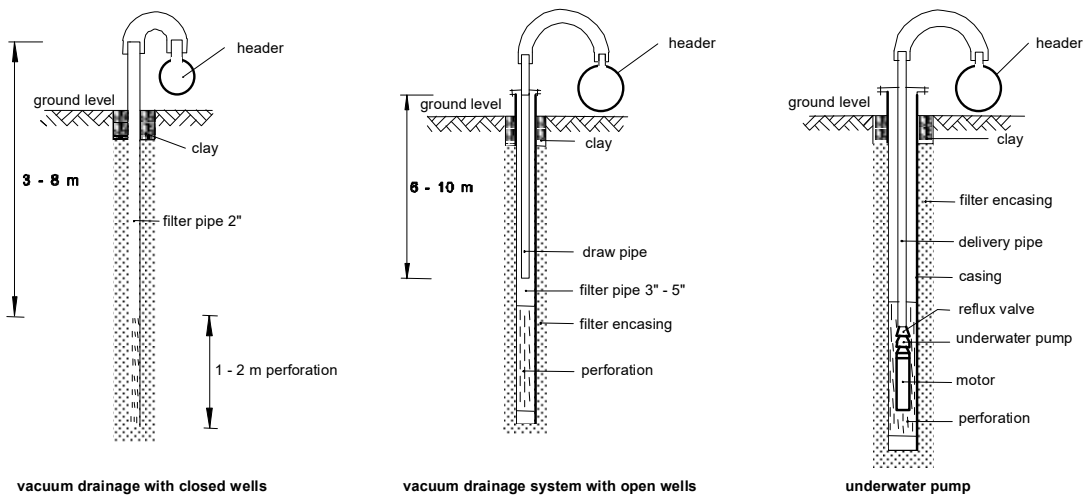


Figure 41-2 Types of wellpoint drainage

- a pumping system with underwater pumps, in which a pump is placed in every well (*perspomp*).

Underwater pumps are suspended in the groundwater and force up the water mainly through compression instead of suction. Thus, the limit of the suction head (*zuighoogte*) is not relevant and large groundwater level reductions can be realised. This makes this type of pump attractive for the construction of hydraulic engineering works. The installation is more reliable than a vacuum drainage system, in which air leaks can lead to problems (air suction in one well can stop the water yield of all other wells connected to the same pump). One must ensure that the pump is suspended at sufficient depth to prevent it from falling dry. Underwater pumps are used in soil types ranging from fine sand to coarse gravel. The capacity of the pumps varies between 5 and 250 m³/hour. In hydraulic engineering pumps with capacities between 40 and 120 m³/hour are usually employed.

Dewatering problems

A pump system (e.g. consisting of wells with underwater pumps) can start to function less efficiently or even fail entirely due to a number of reasons. Causes could include:

- electricity failure (power station, transformer station, cables etc.)
- mechanical or electrical defects of the pump(s)
- breakage, tearing and leakage of the pipes
- blocked pipes (for instance due to iron oxide deposits) and/or filters encasings (*filteromstorting*) and blocked perforations in the casings (see Figure 41-3).
- air in the drainage pipes or suction of air via the pumps. The air can accumulate in high points of a non-level discharge pipe, increasing the resistance.



Figure 41-3 Blocked pipe used during construction of the Haringvliet discharge sluice in the building pit

Reduced efficiency or even failure can have the following consequences:

- in an unconfined aquifer:
the excavation can be partly or entirely flooded, which will lead to a work delay and possibly to damaged equipment, certainly as regards electrical or electronic items.
- in a confined aquifer:
as for an unconfined aquifer, but also bursting open of the bottom of the excavation, in case of an aquitard (*slechtdoorlatende laag*) or impermeable aquifer. This can cause disturbance of the foundation soil of the structure under construction. For an explanation of the bursting open of a clay layer, see CTB2410 (Waterbouwkunde), section 3.7.3 "Opbarsten".

Depending on the extent of the possible damage, measures must be taken such as placing emergency generators, which partially or fully take over the power supply in case of power failure, and double cables on the building site. The examples above are based on the assumption that the building site uses power from the national grid. However, if the building site is in an isolated location, it can be worthwhile to use generators for the daily power supply. In this case one could also consider backup generators.

Depending on the extent of the possible damage and on the duration of the drainage, the following matters will also be necessary:

- regular inspection
- preventive maintenance
- monitoring operations
- emergency procedures for calamities, etc.

Particularly the last two points depend largely on the situation. In small projects stagnation of the drainage needs not be very grave (though disruption of the foundation base is also serious in these projects). However, in large projects it can be beneficial to register certain parameters continuously and to sound alarms and trigger certain procedures automatically when certain limits are exceeded. Limits that could be exceeded are the groundwater level measured in a well (upper limit), and the minimum drainage discharge (lower limit). The alarm can be sounded in a permanently staffed area, in somebody's home, close to the site and with an occupant who is on guard duty outside normal working hours or by phone. Procedures that can be initiated automatically include starting emergency generators if the grid fails.

Trouble for the surroundings

Often a building pit (with slopes and a dewatering system) leads to lower building costs than a coffer dam, even if one includes the possible damage to the surroundings. Disadvantages of the building pit construction method can be the consequences of dewatering on the surroundings and the large use of space (the slopes require a lot more space than is necessary for the completed structure, which can cause problems in built-up areas and if the new structure is to be built next to an existing structure). Very often dewatering causes no damage at all or only limited damage.

In agricultural areas, dewatering dehydrates soil, thereby ruining crops. Nature reserves and recreational areas can also suffer badly from a lowered groundwater level. Sometimes the surface layer will "retain" sufficient amounts of precipitation to counter the effect of the lowered groundwater level. Furthermore, precipitation wells for agriculture and horticulture can dry up.

Another important point is the possible settlement as a result of the temporary lowering of the groundwater level. This causes an increase of the effective soil pressure (see Chapter 21 of part I "Loads, Soil, Groundwater"). In soil types that are susceptible to this, it will lead to compression of the soil and settlement of the ground level, as well as to an increase of negative shaft resistance on piles. If houses or buildings settle evenly across the whole of their foundation, this does not have to result in damages. It can be worse if settlements are uneven for one building. The breaking of unfounded sewer pipes and cables at the point where they connect to a house or building on a pile foundation is not uncommon. Wooden piles can start to decay above groundwater level.

Even settlements of the ground level in agricultural areas are not a problem as long as the water level in the ditches can be adjusted accordingly. In old agricultural areas with considerable differences in ditch levels this adjustment is not always possible, because lowering of the ground level could lead a decrease of the distance between groundwater and ground level, which can result in a permanent reduction of crop productivity (however, if the distance between ground water and ground level was too high, productivity could be increased). Uneven settlements can be a nuisance for sowing and harvesting. Drains can get an unfavourable slope.

In water extraction areas dewatering is usually forbidden, because, as a rule, drainage water is pumped out to open water and is therefore lost. Return pumping can offer a solution: the water pumped out of the site is returned to the ground through injection wells, at some distance from the building site. During the construction of the tunnel under the Dordtse Kil, for example, a large amount of drainage water was supplied directly to the water works. The water was taken from a soil layer that was normally not used for drinking water extraction, but with sufficient quality. The extraction from deeper layers could be reduced during the construction of the tunnel.

Sometimes the water acquired by means of drainage is of bad quality and may not be discharged into open water. Drained water in coastal areas and deep polders can be salty, which could cause open water to become brackish (this was a problem for the construction of the Schiphol tunnel near Amsterdam). In that case separate discharge is required to protect agriculture, horticulture or livestock industry. Moreover, people in the past few years have become aware that groundwater flow (however slow) can lead to unwanted diffusion of harmful substances from toxic waste dumps.

Once again: these problems can occur although they often don't. Possible damages will have to be compensated by the constructor. Good observation (groundwater levels, height measurements, descriptions of buildings and crops) before, during and after dewatering is necessary to identify the damages. Photos can be used to describe houses and buildings. In fact, in the Netherlands this is prescribed: an independent committee makes an estimate of the expected damage. Constructors generally buy off the risk.

41.2 Design

Groundwater can be divided into two types: groundwater in an unconfined aquifer and groundwater in a confined aquifer. In an unconfined aquifer the flow profile equals the piezometric height. The groundwater level is therefore free. In a confined aquifer the flow profile is determined by an impermeable layer. A badly sealed layer that leaks, is called a semi-confined aquifer. The water level can be above or below the top of the aquifer (*overspannen of onderspannen water*).

Unconfined aquifer

A drainage well will affect the phreatic surface in a certain volume of permeable soil around it. The phreatic surface drops gradually until a stationary situation is achieved. In an ideal situation, the affected soil body has a cylindrical shape with radius R , see Figure 41-1. The subsoil is impermeable, in contrary to the soil that surrounds the soil body.

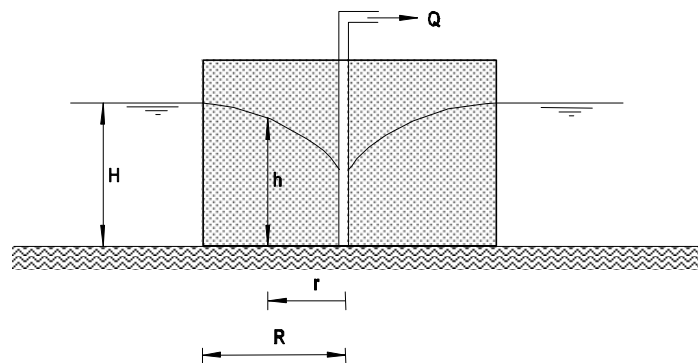


Figure 41-1 Dewatering of groundwater in an unconfined aquifer in a cylindrical soil body

The discharge of the well depends on the slope of the groundwater level and the permeability of the soil, which is expressed in Darcy's law:

$$q = k \cdot i$$

in which:

q	$[\text{m}^3/\text{s}/\text{m}^2 = \text{m}/\text{s}]$	= specific discharge in the soil body
k	$[\text{m}/\text{s}]$	= coefficient of permeability (see Table 41-2)
i	$[-]$	= slope = $\frac{dh}{dr}$

For the total discharge Q , we can write $Q = q \cdot F$ [m^3/s], where F is the circumference area of the soil body:

$$F = \pi \cdot d \cdot h = \pi \cdot 2r \cdot h \quad [\text{m}^2].$$

For the well this means:

$$Q = k \cdot i \cdot F = k \cdot \frac{dh}{dr} \cdot 2\pi r h$$

or

$$2h \, dh = \frac{Q}{\pi k} \frac{dr}{r}, \text{ so:}$$

$$2 \int h \, dh = \frac{Q}{\pi k} \int \frac{1}{r} \, dr,$$

where the solution is: $h^2 = \frac{Q}{\pi k} \ln r + C$

If $r = R$ (and $h = H$) then: $H^2 = \frac{Q}{\pi k} \ln R + C$

If we subtract the equations from one another:

$$H^2 - h^2 = \frac{Q}{\pi k} (\ln R - \ln r) = -\frac{Q}{\pi k} \cdot \ln\left(\frac{r}{R}\right)$$

In practice it is customary to determine the maximum allowable water level first, to avoid that water will enter the building pit. The phreatic water level should be at least 0,50 m below the pit floor. (This applies to all places on the construction site to avoid problems with saturated soil, freezing and the accumulation of rainwater; see Section 4.1 ('Construction Pit') of the general lecture notes of the course "Hydraulic Structures 1"). Knowing this, the value of the acceptable groundwater height h can be affixed. With h , the required total discharge can be calculated if we rewrite the previous equation:

$$Q = -\frac{\pi k (H^2 - h^2)}{\ln\left(\frac{r}{R}\right)}$$

Confined aquifer

Similarly, we can derive the following relation for the groundwater in a confined artesian aquifer, in the permeable layer shown in Figure 41-2:

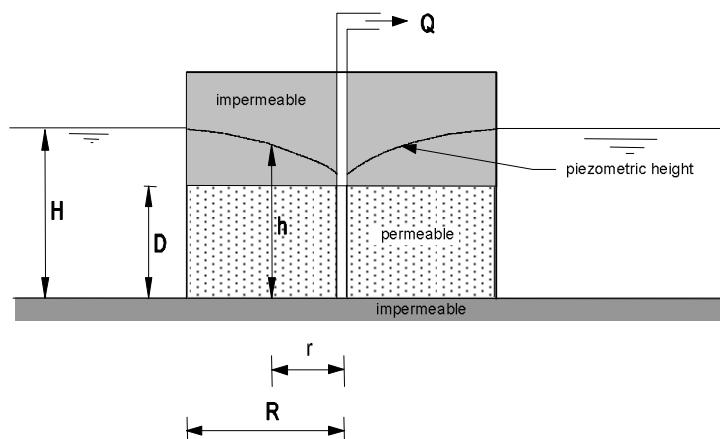


Figure 41-2 Dewatering of confined aquifer in a cylindrical soil body (artesian well)

$$Q = k \cdot 2\pi r \cdot D \cdot \frac{dh}{dr} \rightarrow dh = \frac{Q}{2\pi k r D} dr \rightarrow \int dh = \frac{Q}{2\pi k D} \int \frac{1}{r} dr \rightarrow h = \frac{Q}{2\pi k D} \ln r + C,$$

and also: $H = \frac{Q}{2\pi k D} \ln R + C$

Subtraction yields: $H - h = -\frac{Q}{2\pi k D} \ln\left(\frac{r}{R}\right),$

from which the discharge can be derived: $Q = -\frac{2\pi k D (H - h)}{\ln\left(\frac{r}{R}\right)}$

This equation can be used when the maximum allowed piezometric height h has been determined with respect to the bursting open criterion (an impermeable layer should not burst open because of too high water pressure from the layer underneath).

Semi-confined aquifer

Usually, the sealing layer is not entirely impermeable and the water is in a semi-confined aquifer. Figure 6-14 shows a common profile: two very permeable layers separated by an almost impermeable layer of clay with thickness d . We assume that any withdrawal of water from the bottom layer does not cause a reduction of the groundwater level in the top layer (for instance, this is realised by polder ditches in the top layer). This means that the bottom layer is fed by the top layer through the layer of clay.

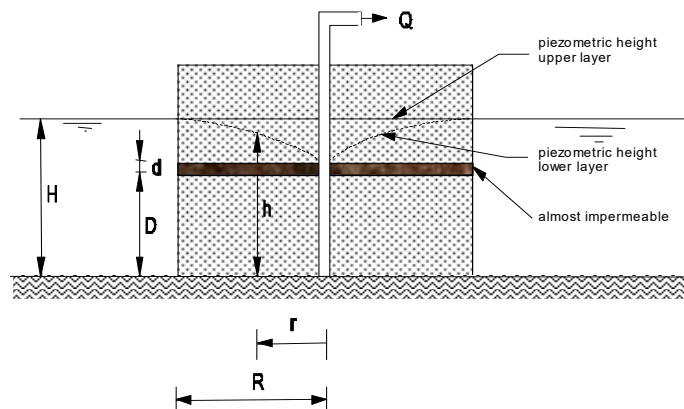


Figure 41-3 Dewatering of semi-confined aquifer in a cylindrical soil body

According to Darcy, this supply q equals

$$q = k' \cdot i = k' \cdot \frac{H - h}{d}$$

per unit of area, in which k' is the vertical coefficient of permeability of the layer of clay. In this situation the following relation can be derived (see also lecture notes *Soil Mechanics* by Verruijt / Van Baars):

$$H - h = -\frac{Q}{2\pi k D} K_0(r/\lambda)$$

in which:

$K_0(r/\lambda)$ = a modified Bessel-function of the first type, order zero.

(see following table, or see lecture notes *Soil Mechanics*; appendix A, or see Abramowitz & Stegun: 'Handbook of mathematical functions').

λ = the leakage factor = $\sqrt{k D C}$ [-]

C = the resistance of the clay layer = $\frac{d}{k'}$ [s] or [d]

r/λ	0,1	0,5	1,0	1,5	2,0	2,5	3,0	4,0
$K_0(r/\lambda)$	2,43	0,92	0,42	0,21	0,11	0,062	0,035	0,011

Table 41-1 Values for the Bessel function

Schematization effects

The formulas above have all been derived for so-called perfect wells, i.e., their filters run along the full height of the layer from which water is extracted. This will not always be the case. In an unconfined aquifer the following applies: If the bottom of the well does not coincide with an impermeable layer the formula for unconfined aquifer is still used, as it has been shown that the water beneath the bottom of the well hardly participates in the flow (i.e., assume that the impermeable layer does not extend beyond the bottom of the well). If the impermeable layer is very deep, Sichardt advises us to increase the calculated discharge by 20%.

The formulas have been derived for a cylindrical volume of soil, not an everyday situation. In reality the excavated site that needs to be dewatered is usually on land. R is understood to be the distance from the well to a point where the groundwater level reduction approaches zero. For small dewatering systems, R is sometimes approximated with Sichardt's empirical formula:

$$R = 3000 (H - h) \sqrt{k} \quad (\text{units in metres and seconds}).$$

For a first rough estimation, the following table gives an overview of order of magnitude of the permeability k , it is certainly is not absolute:

Soil type	k [m/s]
gravel	10^{-2}
coarse sand	10^{-3}
moderately coarse to moderately fine sand	10^{-3} to 10^{-4}
fine sand	10^{-4} to 10^{-5}
clay	10^{-9} to 10^{-11}

Table 41-2 Permeability

For large scale dewatering one uses experience or pump tests. The influence of a "wrong" estimate of R on the discharge calculation is limited by the use of the natural logarithm of r/R .

The formulas are derived for one well in the centre. In practice a number of wells will be placed around the building site. In this case the principle of superposition applies, i.e., the water level reduction in any one point is the sum of the reductions caused by each individual well. In an unconfined aquifer this is not the case, as this requires the superposition of the differences of the squares of H and h .

The formulas are derived for a stationary situation. Other formulas apply for the preceding non-stationary phases. However, dewatering systems are usually designed for the stationary situation, though it is important to start pumping well in time because it takes some time to reach the stationary situation (and the desired situation). Furthermore, the pump system needs to have sufficient overcapacity to deal with precipitation (a greater reduction of the groundwater level than technically necessary can create a buffer for extreme rainfall) and the possible failure of one of the pumps.

Certain parameters, such as the coefficient of permeability k , can be found by carrying out laboratory tests on undisturbed samples. However, they are usually not representative for the extensive area in which the groundwater flow occurs. It is therefore desirable, if not indispensable, to carry out a pump test; a dewatering well surrounded by a number of measuring wells. The pump test can determine parameters such as the coefficient of transmissibility kD (usually in m^2/day) and the leakage factor λ ([m]).

Influence of supply borders

Building sites as a rule are close to waterways (rivers, canals), which are to take on the hydraulic engineering work sometime later. This waterway can act as a supply for the construction pit. The water level in the waterway (H) will not be affected by the dewatering, so the piezometric height at this supply border remains the same. Mathematically this can be approximated by introducing a fictitious "mirror well" (i.e., a supply) on the same distance from the waterway as the construction pit, but on the opposite side of the waterway (see Figure 41-4).

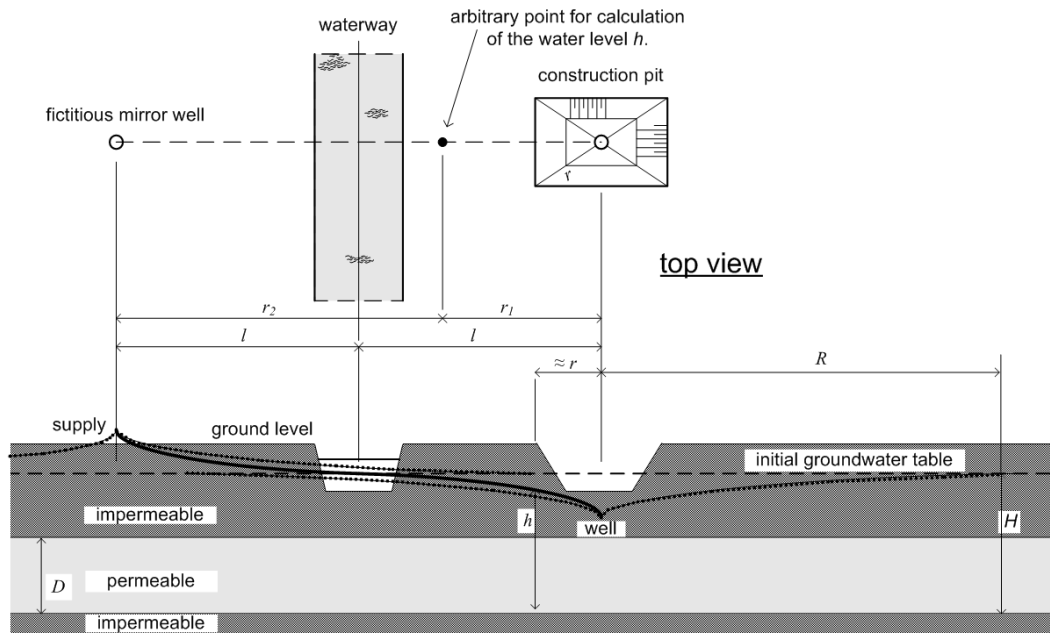


Figure 41-4 Schematisation of the mirror well principle

So, draw a line from the dewatering well perpendicular to the supply border and project an injection well on the opposite side of the border, which injects as much water as the first well discharges, on this line. By making the distances to the border (l) the same, the piezometric height remains the same along the border line (middle of the waterway), provided it is straight, so $(h_2 + h_1)/2 = H$. The reduction of the water level caused by the drainage well is compensated by the injection of water in the other well. With both of these wells one can calculate the water level at any point on the side of the drainage well.

In case of a confined aquifer the following applies to a given point on the line between the well and the fictitious injection well:

$$h = H + \sum_{j=1}^n \frac{Q}{2\pi kD} \ln\left(\frac{r_j}{R}\right) = H + \frac{Q}{2\pi kD} \ln\left(\frac{r_1}{R}\right) - \frac{Q}{2\pi kD} \ln\left(\frac{r_2}{R}\right)$$

(derived from the formula for n wells).

Given that the distance from the drainage well -and hence also from the injection well- to the border is l , and expressing r_1 and r_2 in r ($r_1 = r$ and $r_2 = 2l - r$) this equation reads:

$$h = H + \frac{Q}{2\pi kD} \ln\left(\frac{r}{R}\right) - \frac{Q}{2\pi kD} \ln\left(\frac{2l-r}{R}\right) = H + \frac{Q}{2\pi kD} \ln\left(\frac{r}{2l-R}\right)$$

from which can be derived:

$$H - h = -\frac{Q}{2\pi kD} \left(\ln\frac{r}{R} - \ln\frac{2l-r}{R} \right)$$

For an unconfined aquifer the formula is:

$$H^2 - h^2 = -\frac{Q}{\pi k} \left(\ln\frac{r}{R} - \ln\frac{2l-r}{R} \right)$$

Note that the supply border normally is not perfect. In wide, deep rivers (e.g., the Nieuwe Maas at Pernis near Rotterdam, measuring approximately 600 m by 13 m) the influence of the dewatering system on one side was still detectable on the other side. A layer of silt on the riverbed creates a large entry resistance, which means the river does not qualify as a perfect supplying border: no reduction of the piezometric height at the border as a result of dewatering. In that case the border should really be moved, from the waterway to further inland, on the fictitious injection side. If the river has just been dredged, the layer of silt will have been removed and the river can act as a perfect supplying border.

42. Flood defence design (exceedance probability)

New chapter: 2016, improved: 2018, 2020 and 2023

This chapter explains the design of flood defences according to the exceedance probability approach. The establishment of the target safety level according to this approach is described in the General Lecture Notes Hydraulic Structures (2023), Section 7.6 and Appendix A.

42.1 Flood defence height as the main property

The main property of a flood defence is its height, which should be sufficient to retain design water levels and reduce the discharge of overtopping waves to acceptable quantities (however, for dunes, the volume of sand in a cross-section is crucial to resist a storm). This implies that the flood defence is sufficiently strong and stable to provide structural safety.

The height should be determined with respect to two types of limit states:

- serviceability limit state (SLS): the discharge of overtopping waves or overflow causes unacceptable difficulties, or damage, without collapse of the flood defence structure. Consequences of exceedance of the serviceability limit state are:
 - the amount of water flowing into the hinterland is more than the capacity of the hinter-lying water system, leading to flooding of the polder;
 - pedestrians, vehicles and properties on and directly along the flood defence suffer too much from water passing the flood defence.
- ultimate limit state (ULS): collapse of the flood defence causes flooding of the hinterland, leading to unacceptable consequences. Flood consequences can consist of loss of lives, cultural and natural values and such alike, and economic damage. Collapse can be caused by wave-overtopping or overflow leading to erosion or softening of the inner dike slope, but also by other failure mechanisms, such as sliding-off of soil bodies (macro-instability), erosion of revetment, piping and horizontal shear of the entire embankment.

42.2 Exceedance probability approach in general

In general, the required height of a flood defence is mainly determined by the following two components:

- Design water level (*maatgevende hoogwaterstand* = MHW in Dutch¹⁰)
- Maximum allowable discharge of wave overtopping or overflow, and several other effects.

Figure 42-1 depicts the components that determine the height of a flood defence.

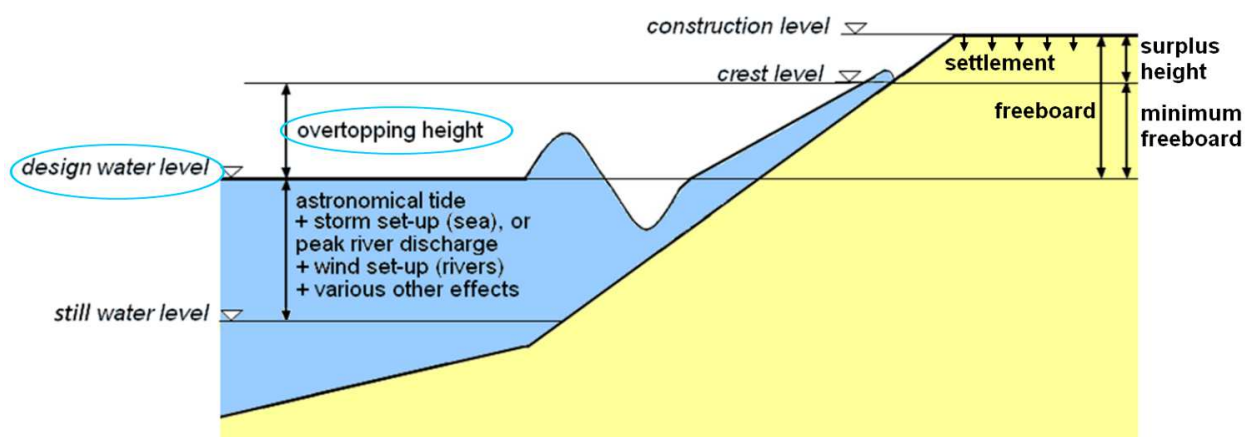


Figure 42-1 Determination of the construction level of a dike

The design water level, which is the water level under governing conditions, is based on the still water level, which occurs if there would be no wind, no waves and no tides.

¹⁰ In English, MHW = mean high water, but that is not the same as the Dutch MHW. This can be rather confusing!

1. The design water level

To find the design water level, several effects should be taken into account, if present at the flood defence location:

- highest astronomical tide, spring tide (*springtij*).
- wind set-up (*opwaaiing*).
- funnel-effect (*trechtereffect*)
- short-term atmospheric depressions (*buistoten*)
- seiches (*staande golven in waterbasins*)
- tidal resonance (*getijresonantie*)
- tidal bores
- tsunamis
- climate change effects:
 - sea level rise
 - increase of river discharges

See Chapter 7 for a description of these effects.

Land subsidence (*bodemdaling*) is another effect that shall be taken into account when estimating the height of a flood defence. It is often included in the term 'relative sea level rise'. Land subsidence is caused by geological processes and gas or oil extraction. It differs from settlement, which is a compaction of the soil.

2. Wave overtopping and other effects

A flood defence should be higher than the design water level to account for waves and uncertainties. The thus obtained height is the 'crest level' of the flood defence. To compensate for settlements, a 'surplus height' should be applied on top of the crest level. This leads to the 'construction height'. The required flood defence height on top of the design water level is called the 'freeboard' (*waakhoogte*).

The effects that have to be included when determining the crest level of a flood defence are:

- **Wave-overtopping height (*overslaghoogte*)**

The height that is required to limit wave overtopping to acceptable amounts (Section 11.2) is called the 'overtopping height.' This mainly applies to coastal defences and flood defences along the lower rivers. For the upper rivers and smaller lakes, where the waves are relatively small, overflow is usually more critical than overtopping. In several coastal areas in the world, tsunami waves should be considered as well.
- **Mathematical surplus heights:**
 - Length effect. The failure probability of a long dike is higher than the failure probability of a short dike because of partial correlation or independence between different cross-sections and/or structural elements. An additional height compensates this effect.
 - Robustness surcharge (*robuustheidstoelage*). For uncertainties regarding changes in the estimation of water levels, changes in prescribed calculation principles and changes in strength criteria, a robustness surcharge is used as compensation (TAW, *TR Ontwerpbelastingen voor het Rivierengebied*, 2007). The aim of adding this surcharge is to cope with potential setbacks during the lifetime of a structure. Two main types of robustness uncertainties can be distinguished:
 - Technical uncertainties:
 - magnitude of discharges
 - modelling uncertainties (water levels and wave parameters)
 - climate change scenario uncertainties
 - statistical uncertainties in load parameters
 - Policy uncertainties

Surplus height

The following surplus heights for geotechnical effects have to be taken into account to find the initial construction level (if applicable):

- **Settlement**

Soil gradually settles because of extra loading, namely by the weight of the dike. This has to be compensated by a surplus height. Compaction can occur in the subsoil (*zetting*) and the embankment itself (*klink*). The rate of compaction depends on the development of the consolidation in time, which indicates how much water has already been expelled. In the Netherlands, mainly two methods are used in engineering practice: Koppejan (modified) and Terzaghi/Bjerrum (Section 28.2). For a very rough first indication for conceptual designs, when no data is available, as a rule of thumb, a value of 10% settlement could be used for clay, or 5% if the clay is carefully applied and densified. For sand, a value of 5% could be used, but if it is well compacted, settlement of sand can be neglected.

- **Earthquake surplus height**

Earthquakes induced by seismic movements and by extraction of natural resources can cause deformation of dikes, next to subsoil subsidence. This could cause additional lowering of the crest by compaction of the dike core, squeezing of softened soil (*zijdelings wegpersen van verweekte grond*), or macro-instability induced by an earthquake (rotational slip of the slope). Usually, advanced calculation methods are used to compute the magnitude of these effects and research is still in progress. These calculation methods are not included in this Manual.

The term 'freeboard' (*waakhoogte*) is not uniformly defined, so the exact definition varies per guideline. The freeboard is more or less defined as the difference between construction level and (local) assessment level (for assessment purposes) or between construction level and design water level (for design purposes). Often, a minimum value of 0,50 m is prescribed for the freeboard. This minimum freeboard usually applies to the crest level, not the construction level!

42.3 Application of the exceedance probability approach in the Netherlands

The main cause of failure of dikes, according to the exceedance probability approach, is breaching caused by too much wave-overtopping or overflow over the dike, which could cause erosion of the inner slope. Given the present knowledge, we may assume that the maximum allowable mean discharge of overtopping waves is 5 litres per second per linear metre of dike (although in present regulations still 1 l/s per metre is used for grass-covered inner slopes).

The basis for dike designs is a given probability of exceedance of a water level at the dike location. This exceedance probability is usually considered over a reference period of one year. The normative exceedance probability is for example 1/10 000 [-] for dike ring areas 13 and 14 (more or less the provinces of North and South Holland). This means that the crest level of the dikes in this area should be determined in such a way, that the dike withstands (extreme) loading conditions that, during a random year, have a probability of exceedance of 1/10 000 [-]. Under higher loading conditions (higher water levels), it is considered acceptable if the flood defence fails.

The thus determined critical water level along coasts and rivers is the **assessment level (*toetspeil*)**, as listed per dike section (*dijkvak*) in the book *Hydraulische Randvoorwaarden* (Hydraulic Boundary Conditions) of *Rijkswaterstaat*. This book is used to assess the reliability of existing flood defences.

1. Normative High Water along the coast

The measurements along the coast include:

- astronomical tides,
- wind set-up, including a possible funnel effect (*trechtereffect*).

These effects are included in the assessment water levels, found after extrapolation of the measurement points.

2. Normative High Water along rivers

The governing water level along river dikes can be based on the design river discharge for the location where it enters the Netherlands (like Lobith for the Rhine) and then making a discharge computation for locations further downstream. The levels in the lower rivers (*benedenrivieren*) are influenced by both river discharge and tidal influences from sea. Control objects like weirs and discharge sluices can influence the water level in lower and upper rivers (*bovenrivieren*), so these effects have to be taken into account as well, as they are not included in the normative high-water levels. Usually, software like Hydra-NL is used to compute the NHW at specific locations.

Governing water levels

Two types of governing water levels (*maatgevende waterstanden*) are distinguished: assessment and design water levels. The difference is explained below.

1. Assessment water levels

For the assessment of hydraulic structures, it should be considered per failure mechanism what conditions are critical. For the bearing capacity of gravity quay walls, for example, a low water level combined with a low ground water table and full variable loads on the quay will be governing. For checking the possibility of uplift of the same quay wall, or critical overtopping volumes, a high-water level will be governing. This and the following section concentrate on high-water levels.

An assessment level (*toetspeil*) is a water level that is governing for the assessment of present flood defences. If a flood defence passes the assessment, it means that it complies with the requirements until at

least the end of the assessment period. In the Netherlands, this period is twelve years at present.

The assessment level of the water along river dikes was determined starting with the governing river discharge for the location where it enters the Netherlands (like Lobith for the Rhine) and then making a discharge computation. Along the North Sea coast, observed extreme water levels were extrapolated until the norm exceedance probability. This is complicated work and interpretation differences can lead to small deviations in the results. To ensure that the same starting points were used, the Ministry of Public Works regularly issued a report with hydraulic boundary conditions (*hydraulische randvoorwaarden*) that have to be taken into account for the assessment of primary flood defences. In the report '*Hydraulische Randvoorwaarden primaire waterkeringen 2006*', assessment levels and significant wave heights are given per dike section (*dijkvak*).

The *Hydraulische Randvoorwaarden 2006* were used for the assessment of primary flood defences. For new assessment rounds, a data base with measurements and software is available to compute these values. The given assessment levels apply to existing flood defences until the end of the concerning 12-year assessment period. Design water levels cover the entire life time of a flood defence, and can be based on the given assessment levels, but have to be adjusted to include effects that change over time, such as sea level rise.

The funnel effect and the effect of wind set-up is included in the measurements of storm levels, and therefore in the extrapolation of storm levels as well. However, there are a few effects that are not included in the water level measurements and therefore neither in the assessment levels:

- local wind set-up¹¹
- wave set-up
- short-term atmospheric depressions
- tidal resonance
- seiches

In addition, several mathematical surplus heights have to be included. The Dutch TAW-guidelines do not prescribe statistical and policy uncertainties, because a useful estimation could not be made. For the Design Toolkit 2014 (*Ontwerpinstrumentarium 2014*) a robustness surcharge of 0,30 m (for rivers) up to 0,70 m (for the Ketelmeer) is recommended to account for modelling uncertainties (Rijkswaterstaat, *Handreiking ontwerpen met overstromingskansen*, 2014). For the new Scheveningen boulevard, the following surcharges were taken into account for a design life time of 100 years: 0,30 m for the length effect, extra wind set-up due to more severe storms: 0,40 m, higher shower oscillations, also caused by more severe storms: 0,10 m. Water Board Rivierenland uses a robustness surcharge of 0,30 m for their primary river dikes (unless a probabilistic model is used for calculation) (TAW, 1999a).

The above mentioned effects should be added to the official assessment levels as given in the *Hydraulische Randvoorwaarden*.

2. Design water levels

Design water levels (*ontwerpwaterstanden*) deviate from assessment levels, because the design life time of these structures (50, 100 years or even more) exceed the assessment period. Temporal effects therefore play a larger role for designs than for assessments.

To transform the assessment levels into design water levels, several additional effects have to be included:

- **Relative sea level rise** should be included in the design of coastal flood defences or lower river stretches (*benedenrivieren*) where the water level is influenced by the tides. Increasing **river discharges**, leading to the elevation of the water surface, should be included in higher river stretches (*bovenrivieren*) that are not influenced by tides, but also in the lower river stretches, where also the effect of sea level rise plays a role.
- **Land subsidence.** The rate of subsidence varies per location in the Netherlands. Outside the Netherlands, the deeper ground layers can also gradually rise, dependent on the geological history of that area. De Lange & Gunnink studied land subsidence in the Netherlands and produced the map as presented in Figure 42-2. Their results should be carefully dealt with, because of the uncertainties of the assumptions.

¹¹ Local wind set-up that is additional to the wind set-up at the measurement location at sea. Local, additional wind set-up can for instance occur in a shallow sea arm.

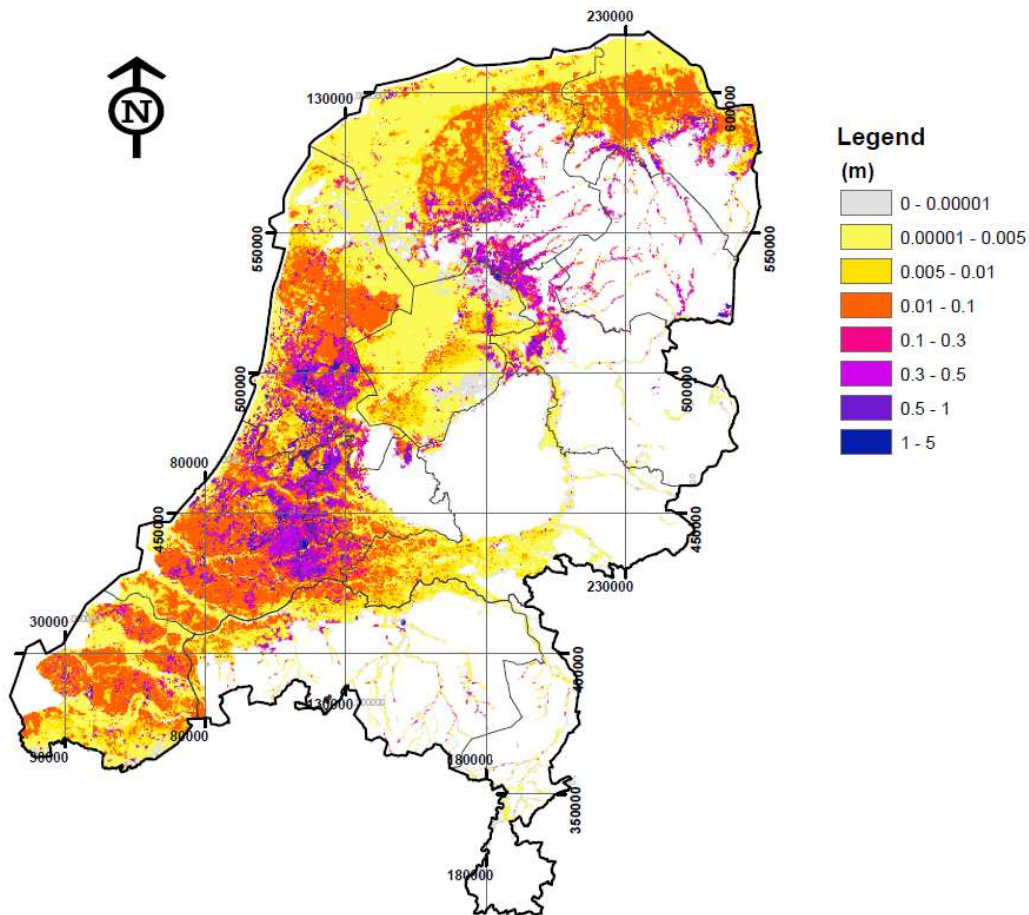


Figure 42-2 Land subsidence between 2011 and 2061 if the climate and ground water table would not change (De Lange & Gunnink, 2011)

Boundary conditions at other locations

The wave height for inland water courses is not given in the book on hydraulic boundary conditions. Therefore, for these locations, you'll have to estimate it yourself using the wind velocity. The governing wind velocity occurs only in very rare cases, so it has probably not been measured yet. In order to nevertheless estimate this wind velocity, measurements that are more frequent can be extrapolated.

All maximum wind velocities of last years can be drawn in a graph on logarithmic scale. It then appears that all points are more or less on a straight line, so extrapolation seems justified. However, detailed studies show that low occurrence frequencies deviate from this line. This is corrected by applying a "Rijkoort-Weibull model". A detailed analysis of this has been carried out by Ilja Smits of the Dutch meteorological institute KNMI. This resulted in Table 42-1 and Figure 42-3.

The strongest winds in the Netherlands come from western directions (to be exact: from directions between 225° and 255° , so on average from 240°). The wind velocities in the exceedance table are maximum values, so related to this wind direction of about 240° . If the governing wind direction at a certain dike section can only come from other directions (for example for the dike bordering the IJsselmeer near Enkhuizen), it would not be realistic to use the value from the exceedance table. Therefore, a reduction of the velocity in the table should be applied. This can be done by constructing an exceedance line per direction for every measuring station, but for this exercise we'll use the correction factors that have been derived for Vlissingen, see Table 42-2. These correction factors are considered representative for all locations in the Netherlands.

	return period of wind velocities (years)									
	10	20	50	100	200	500	1000	2000	5000	10000
LS Texel	28,1	29,8	31,8	33,4	34,9	36,8	38,3	39,7	41,5	42,8
Schiphol	24,9	26,4	28,3	29,8	31,2	33	34,4	35,7	37,4	38,7
De Bilt	21	22,3	24	25,2	26,5	28	29,2	30,3	31,8	33
Soesterberg	21,9	23,5	25,5	26,9	28,4	30,2	31,6	33	34,7	36
Leeuwarden	24	25,5	27,2	28,5	29,7	31,3	32,4	33,5	34,9	35,9
Deelen	24,7	26,5	28,7	30,4	32	34,2	35,8	37,4	39,6	41,2
Eelde	22,6	24,1	26,1	27,5	28,9	30,6	31,9	33	34,7	35,9
Vlissingen	23,2	24,6	26,5	27,8	29,1	30,8	32	33,2	34,7	35,8
Zestienhoven	24	25,5	27,4	28,8	30,1	31,9	33,2	34,5	36,1	37,3
Gilze-Rijen	22,1	23,4	25,1	26,3	27,5	29,1	30,1	31,4	32,8	33,9
Eindhoven	22,4	23,8	25,6	26,9	28,2	29,9	31,1	32,4	34	35,2
Beek	20,5	21,7	23,2	24,2	25,2	26,5	27,5	28,4		30,4

Table 42-1 Wind velocities [m/s] with corresponding return periods per measuring station

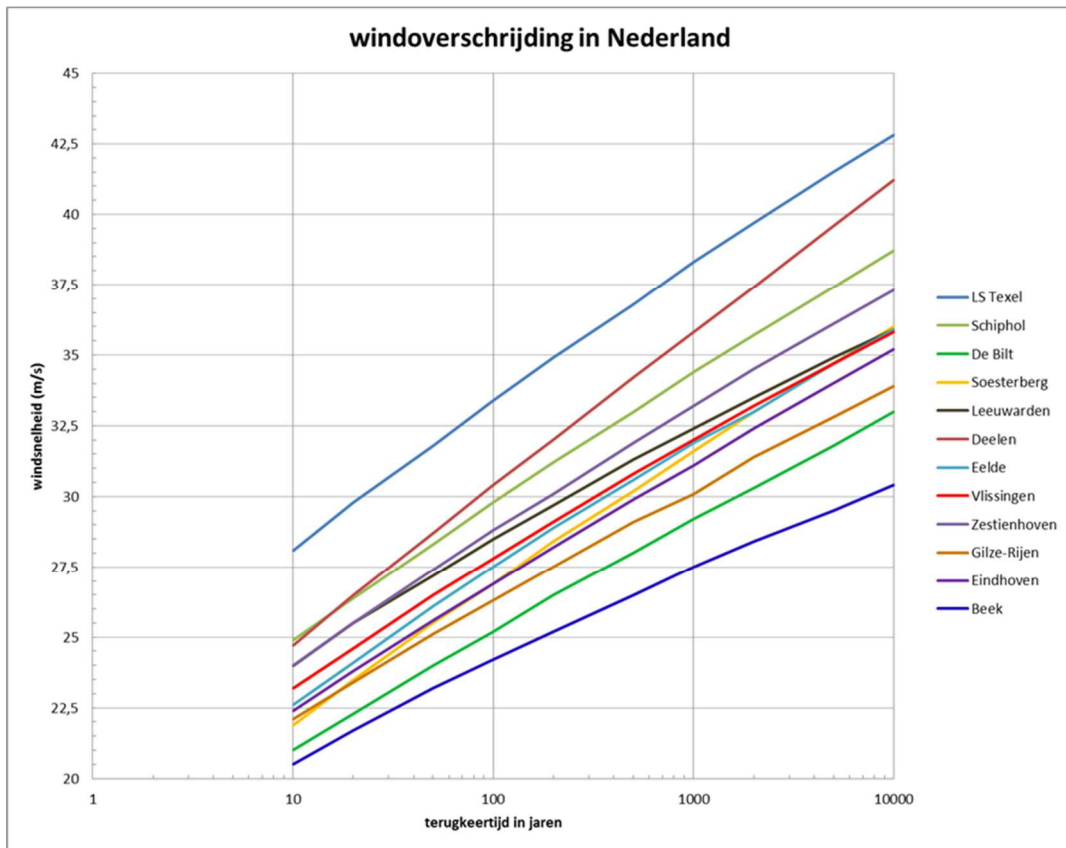


Figure 42-3 Exceedance of wind velocities (Smits, 2001)

direction	correction factor	direction	correction factor
330°	75%	150°	71%
N 360°	69%	Z 180°	81%
030°	64%	210°	90%
060°	66%	240°	100%
O 090°	64%	W 270°	94%
120°	65%	300°	86%

Table 42-2 Correction factors for wind directions

For example: The safety norm for a given dike near De Bilt facing East is $1 \cdot 10^{-4}$. The exceedance line gives an according wind velocity of 33 m/s. The governing wind velocity from directions 60°, 90° and 120° is more or less 21 m/s.

With the thus found design wind velocity, the design wave height can be calculated according to the equations of YOUNG & VERHAGEN (1996), see Section 9.1.1 of this Manual. The required overtopping height can then be calculated according to Section 11.2, taking into account the assessment or design high water level.

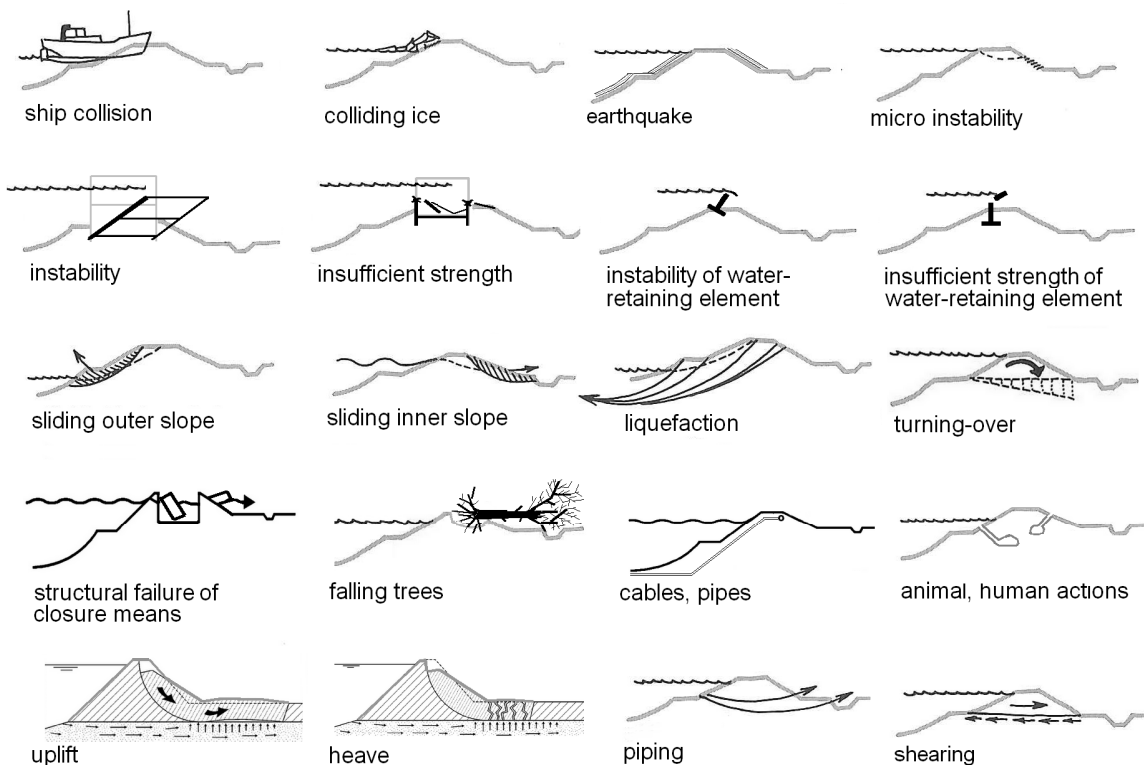
The design velocity can as well be used to calculate the governing wind set-up, according to Section 7.2.

Surplus height

The surplus height on top of the flood defence crest height to compensate for settlements can be calculated according to Chapter 28 of this Manual. The subsoil will subside due to the added weight of a new dike or dike reinforcement (*zetting*), but also due to settlement of the dike body itself (*klink*).

Check of additional failure mechanisms

Once the crest height and construction height have been calculated, several other failure mechanisms shall be checked. The most common failure mechanisms are: overflow/overtopping, uplift/piping, macro instability inner slope, damage to revetment and erosion. For engineering works in dikes: non-closure, piping and structural failure. Figure 42-4 shows a more extensive overview of potential failure mechanisms.



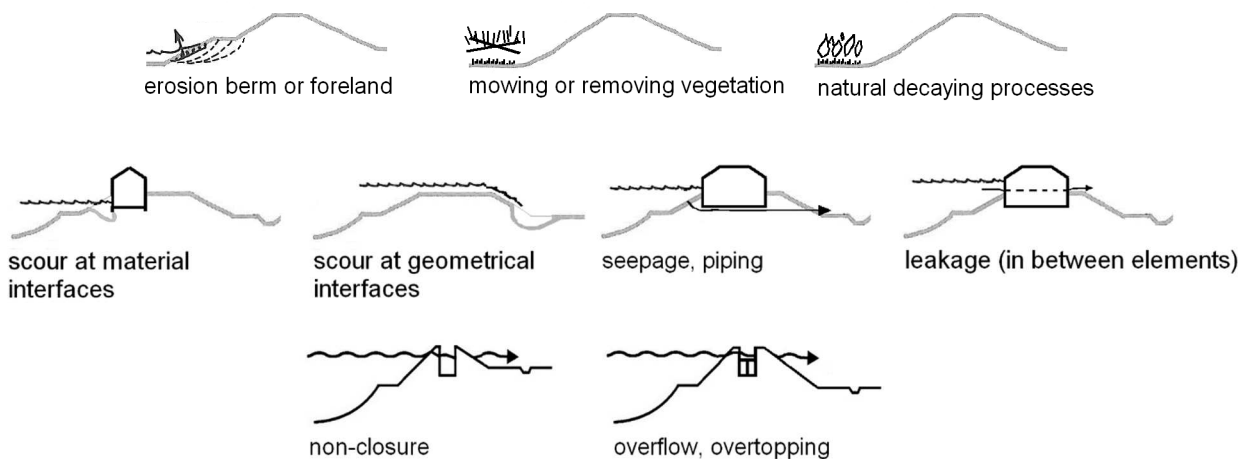


Figure 42-4 Overview of potential failure mechanisms of flood defences

Methods to check these failure mechanisms can mostly be found in this Manual. Additional information can be found in the TU Delft lecture notes on Flood Defences.

Design optimisation

Before you calculate the dike height, you should also consider two additional variables (dike characteristics): the slope angles and a possible outer berm*. Both can reduce wave overtopping, but this requires more material on the outer slope, which could or could not be compensated by a lower dike crest height. If the land price etc. is specified in the spreadsheet, the result of varying the slope angle and applying a berm can be seen by using the sliders. They should be moved in such a way that the optimal dike height is found, given the acceptable risk.

42.4 Literature

- Bottema, M. (2004), Verrassend snelle golfgroei op het IJsselmeer, *Meteorologica*, maart 2004, p. 1519.
- Dantzig, D. van (1956). Economic decision problems for flood prevention. *Econometrica*, 24:276–287.
- Deltacommissie (1960a). Rapport Deltacommissie deel 1. Eindverslag en interimadviezen. Technical report.
- Deltacommissie (1960b). Rapport Deltacommissie deel 2. Bijdragen 1 - Meteorologische en oceanografische aspecten van stormvloed (Report Delta Committee part 2. Contributions 1 - meteorological and oceanographical aspects of storm surges). Technical report.
- Deltacommissie (1960c). Rapport Deltacommissie deel 3. Bijdragen 2 - Beschouwingen over stormvloed en getijbeweging door het Mathematisch Centrum (Report Delta Committee part 3. Contributions 2 - Considerations on storm surges and tidal movements). Technical report.
- Dilingh, D. (2008). Zeespiegelstijging langs de Nederlandse kust. Personal correspondence. Deltares.
- Jonkman, S.N., R.E. Jorissen, T. Schweckendiek and J.P. van den Bos (2021). Flood defences. Lecture notes Delft University of Technology.
- Lange, G. de and J.L. Gunnink (2011). Bodemdalingskaarten. Deltares, TNO.
- Ministerie van Verkeer en Waterstaat (2007). Hydraulische Randvoorwaarden primaire waterkeringen voor de derde toetsronde 2006-2011 (HR 2006). Ministerie van Verkeer en Waterstaat.
- Rijkswaterstaat (2014a). Achtergrondrapport ontwerpinstrumentarium.
- Rijkswaterstaat (2014b). Handreiking ontwerpen met overstromingskansen.
- TAW (1998). Grondslagen voor waterkeren. Balkema uitgevers BV.
- TAW (1985). Leidraad voor het ontwerpen van rivierdijken. Deel 1 - bovenrivierengebied. Staatsuitgeverij 's-Gravenhage.
- TAW (1985). Leidraad voor het ontwerpen van rivierdijken. Deel 2 - benedenrivierengebied. Staatsuitgeverij 's-Gravenhage.
- TAW (1999). Leidraad zee- en meerdijken. Staatsuitgeverij 's-Gravenhage.
- TAW (2003). Leidraad kunstwerken. Rijkswaterstaat, Dienst Weg- en Waterbouwkunde.
- TAW (2007). Technisch Rapport Ontwerpbelastingen voor het Rivierengebied.

43. Flood defences: Gates

There are many different types of closure mechanisms, namely:

- flat gates
- vertical lift gates
- drop gates
- sliding gates
- mitre gates
- single gates
- shutter weirs
- visor dams
- radial gates
- sector gates
- inflatable dams

This chapter, however, only covers the action of forces in the following types:

- flat gates
- mitre gates
- radial gates
- sector gates
- arc

43.1 Flat gates

A flat gate (*vlakke schuif of deur*) transfers the load onto its rabbeted stops. These rabbeted stops can be positioned both on the sides and on the top and bottom. If rabbeted stops are only positioned on the sides, the total load must be transferred horizontally. This horizontal transfer of load can be accomplished using various systems. The flat sluice can, for instance, be equipped with vertical girders that transfer the load a number of horizontal rails, which, in turn, transfer the load to the supports. It is also possible to mainly use rails that transfer the load to the supports in one go. The use of rails and/or vertical girders depends highly on the shape of the gate or sluice and the position of the rabbeted stops.

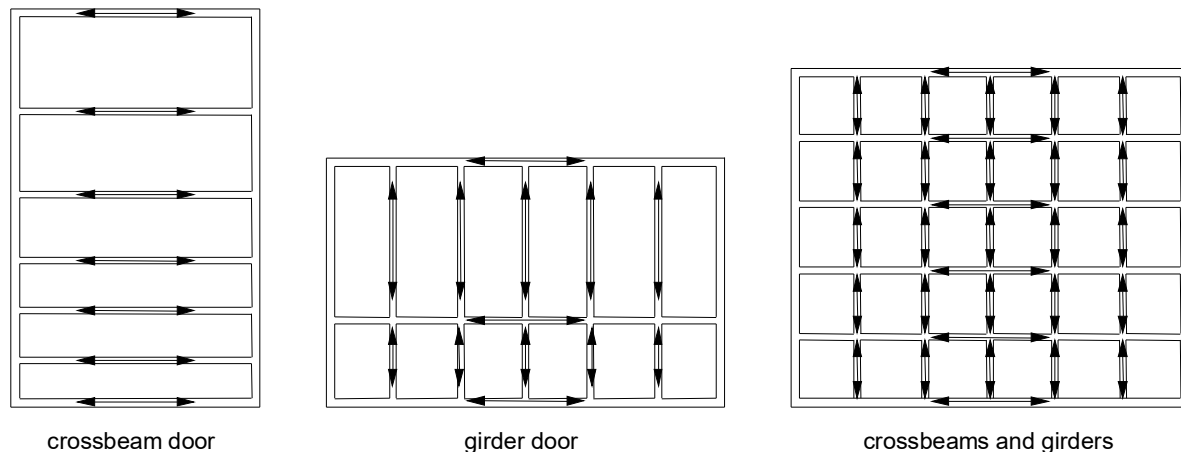


Figure 43-1 Principle support system with rails and girders

The rails and girders can be constructed as a solid web girder, a Vierendeel girder, a box girder or a truss (see also Figure 43-2). For small span girders (= c-c distance of horizontal rails), one can also use a so-called trough girder.

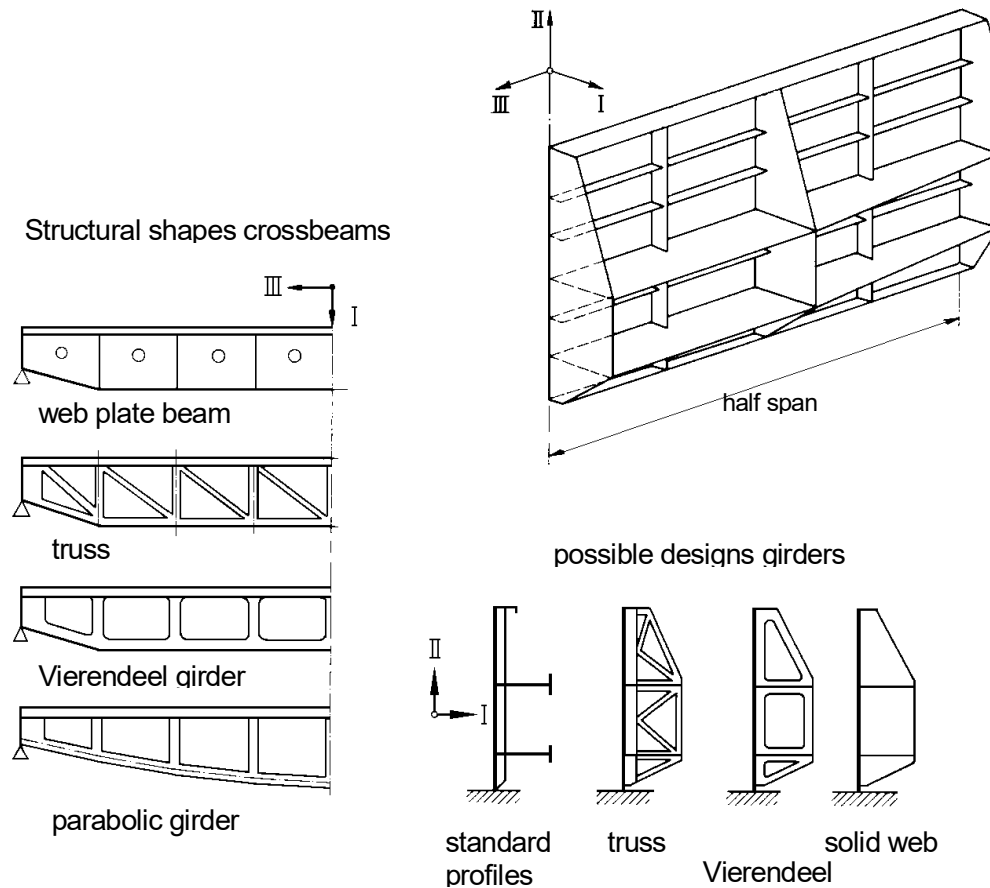


Figure 43-2 Several structural shapes of a gate or sluice on double supports

The vertical girders outside of a gate that rest on the rabbeted stops are known as “posts”.

If the gate also transfers load to a sill and/or an upper rabbeted stop, the use of rails and girders is obvious. The transfer of loads and the forces and moments in the girders and rails of such a gate can be calculated by schematising the structure as a beam grid. In such a calculation the torsional rigidity of the profile must be estimated correctly, because this can have an important effect on the spread of the load. Particularly when applying box girder profiles or plates on two sides, this is of large importance.

An alternative to a gate with rails and girders is a gate with plates on both sides, where the rails and girders are plates that keep the main plates together and create a rigid profile. This structure is used in particular for sliding gates. The forces and moments in such a gate can be calculated using the three-dimensional finite elements method, where the gate is modelled with plates and discs.

A gate with plates on two sides has reasonable to large torsional rigidity. The result of this is that, in the case of hinged supports on the sides and top and/or bottom of the gate, the gate will want to curl inwards and will therefore start to leak. For this reason, such a method of load transfer is avoided or is combined with measures in the bottom rabbeted stops to counter the curling. Such a measure could be to insert a jack in the gate, which fixes the corner of the gate. However, the edges of the structure have to be very stiff to ensure that it is fully waterproof.

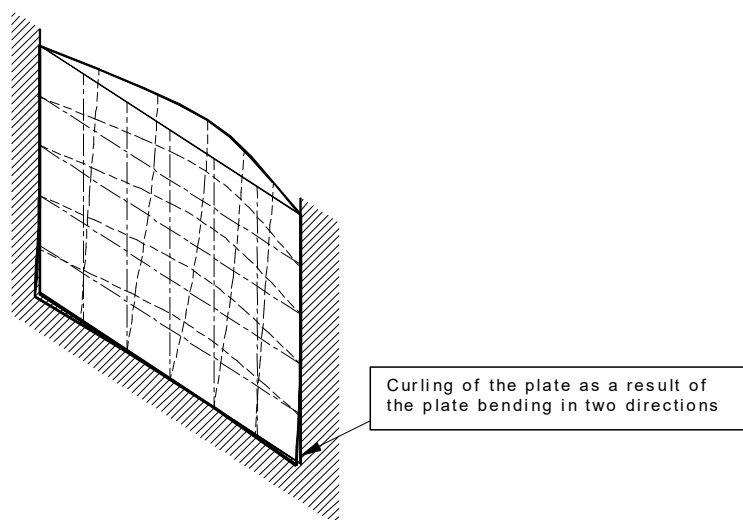


Figure 43-3 Curling of a gate or sluice supported on three sides

The supports of the sluice can be single points or linear. For single point supports it seems obvious that the supports should be positioned at the ends of the rails and girders. For linear supports, the posts need to be sufficiently stiff to be able to spread the load from the girders over the entire rabbeted stop. The same applies for a structure, supported on three or four sides, for the top and bottom rails.

43.2 Mitre gates

In mitre gates the load is transferred to the side rabbeted stops of the gate. The bottom rail is generally not considered as a support, because torsional moments will occur in the gate. Both outer vertical girders of the mitre gate are called posts ("har"s, after the old Dutch word for hinge). The girder nearest the rotational axis is called the rear post, whilst the girder at the loose end of the gate is called the front post. If the gate is closed, the support of both vertical girders can be uniformly distributed or concentrated in two or more points.

For an even spread transfer of the load at the rear post, it is necessary that there is some give in both points of rotation. The lower hinge usually has a little give, because the pivot would otherwise have to be set infinitely accurately, relative to the vertical rabbeted stop strip. The upper hinge needs more give, because, during closure, the gate can be pushed against the rabbeted stop in the sluice wall by the water pressure. If there is no give available in the upper hinge, the reaction forces will have to be supplied by both hinges. In this case, too, a small amount of give is allowed in the bottom hinge in order to be able to lower the pivot socket over the pivot when the gate is put in place.

First, the gate is considered in its closed position, subjected to a load caused by the water pressure, due to the head over the gate. This situation is shown in Figure 43-4. By regarding the mitre gate as a triple hinge truss, symmetry considerations dictate that the forces in the contact point between the front posts have to be in equilibrium i.e., equally large but aimed in opposite directions, perpendicular to the sluice axis.

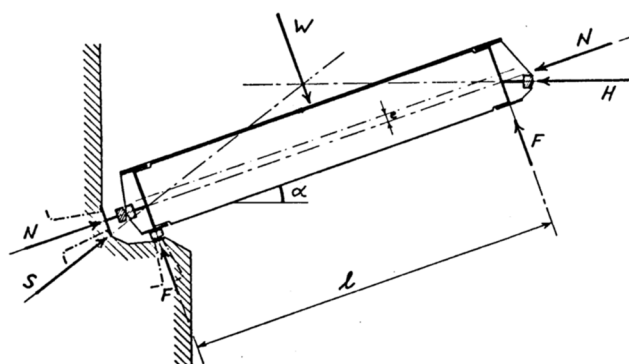


Figure 43-4 Forces and reactions on a closed gate

The reaction force S can be resolved in a force parallel to the gate (N) and a force perpendicular to the gate (F). These reaction forces can be denoted as a function of the resulting force from the water W and the angle α between the gate doors and the sluice axis (see Figure 43-4).

$$S = H = \frac{W}{2 \cdot \sin \alpha}$$

$$F = \frac{1}{2} W$$

$$N = \frac{W}{2 \cdot \tan \alpha}$$

where: S [kN] = reaction force of the sluice head
 H [kN] = force from the other door (perpendicular to the length axis of the sluice or lock)
 W [kN] = resulting hydrostatic force on the door
 α [°] = angle between the gate door and the length axis of the sluice or lock

From the formulas one can deduct that if the angle α is small, the reaction force is very large. This advocates a large angle α . However, if angle α is large, the gate doors become longer and hence the load (W) becomes larger. Furthermore, longer gate doors would mean heavier gate doors as well as longer gate chambers and lock heads. For economic reasons, one often usually chooses a ratio of $\tan \alpha = 1:3$.

The way the reaction forces S and H are provided depends strongly on the choice of supports along the vertical sides. One could opt for a uniformly distributed load transmission or a load transmission with support points.

Uniformly distributed load transfer

As mentioned earlier, a uniformly distributed load transfer, requires a certain amount of give in both hinges. The transfer of load at the lock head then takes place according to the linear loads N and F . Due to structural considerations, one also opts for a uniformly distributed load transfer at the front post, there in the direction of H . In this case, an adjustable gate is selected, in order to approximate a uniformly distributed load as well as possible.

Load transfer via point supports

To transfer the loads via point supports there may not be any give in the top hinge. At the rear post, the hinges provide the reaction forces, which point in the direction of S . Two supports are also made in the front post. It seems obvious to make two heavy horizontal rails between the four supports and to transfer the load on the plates to these rails via girders (girder gate). For the height of these rails, an optimum between the moments in the girders and in the rear post is sought (see Figure 43-5).

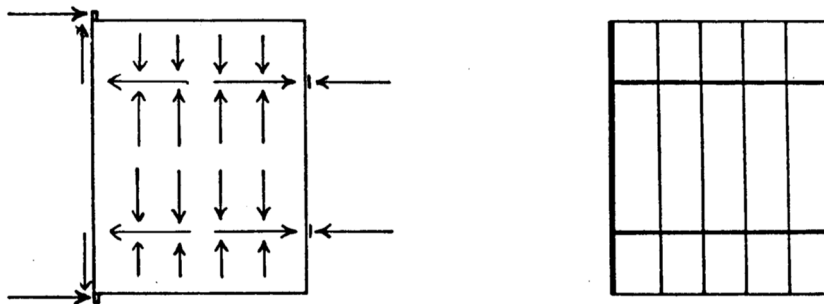


Figure 43-5 Internal transfer of forces in the girder gate

Nowadays, the latter solution is employed often. Setting vertical rabbeted stop plains (for N and F) at the rear post, which has to carry the load as evenly as possible, is very difficult. However, according to the solution given in Figure 43-5 only two points have to be positioned accurately. Moreover, techniques have been developed to equip the top hinge with ball bearings that tolerate barely any give and that can absorb large forces.

Another load situation occurs when the door is open, in which case the hinges only need to be able to take on the self-weight of the gate. The vertical load, the self-weight of the gate, is nearly always taken on by the lower hinge. The moment that is thus created results in a tensile force in the upper hinge and a compression load in the lower hinge (see Figure 43-6).

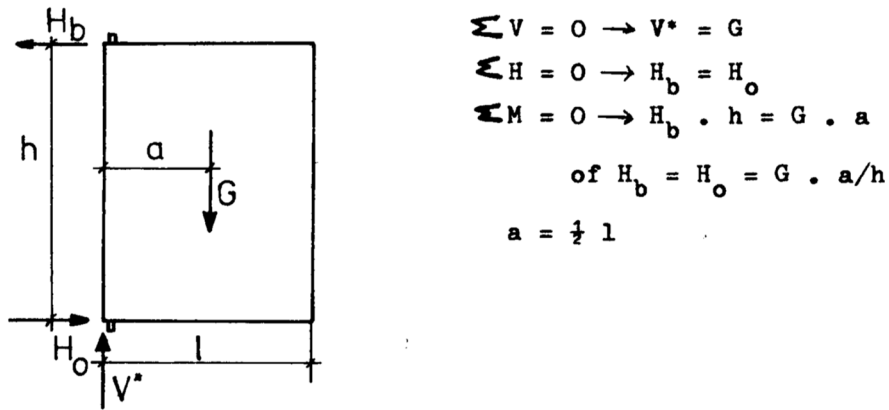


Figure 43-6 Balance of forces for an open gate

As the length of the gate increases, the gate is more and more inclined to start to sag (*zakken*) at the loose end, due to its self-weight, so-called tilting. This problem especially affects wooden adjustable gates. This is because they are not very rigid. Tilting can be avoided by creating rigid triangles. Starting from the hinges one can create a triangle by placing a compression bar.

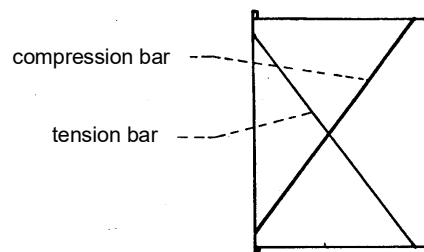


Figure 43-7 Diagonal compression and tension bar

Further structural measures include placing a tension bar and applying planks in the direction of the compression bar.

Steel mitre gates can be made sufficiently structurally stiff, hence the tilting problem is no longer relevant.

43.3 Water pressure on radial gates

See also Chapter 3 of part I of this manual for hydrostatic loads.

One distinguishes between radial lock gates with horizontal and vertical axes.

Radial gate with a horizontal axis

Figure 43-8 gives an example of a radial lock gate with a horizontal axis. The moving parts are not included. Basically, the radial lock gate consists of a gate, which can be built up out of beams and girders with plates on the high-water side, and an arm that transfers the forces on the gate to the hinge. It is important that the curves of the gate correspond to a circle and the hinge is placed in the middle of this circle.

The transfer of the loads on the gate is completely dependent on the type of load. Hence, such the (partially immersed) self-weight of the structure is carried by both the sill and the hinges, but the load caused by the water pressure is taken on entirely by the hinges.

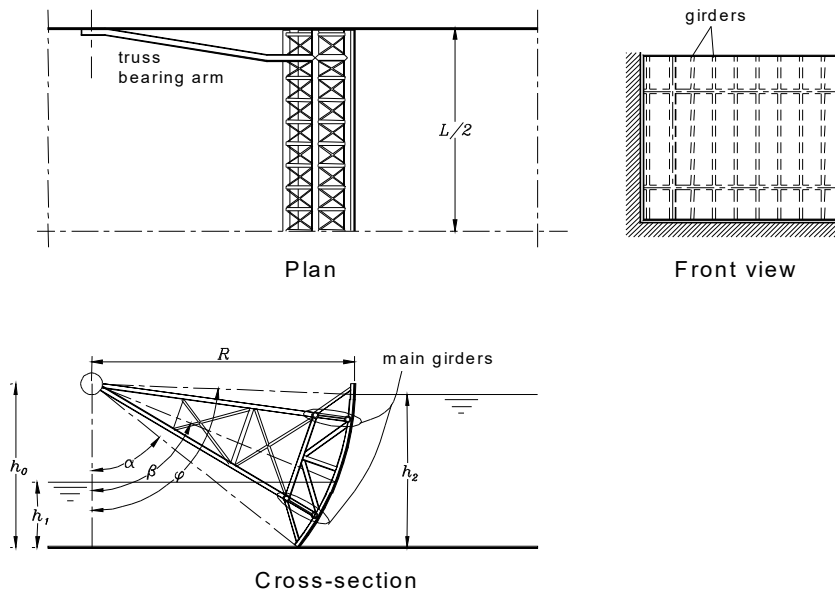


Figure 43-8 Radial gate with a horizontal axis

A special transfer of load to the hinge occurs if the gate is equipped with watertight plates on two sides, or if the rear side of the gate is not circular. Figure 43-9 gives an example of such a gate. The horizontal component of the load remains the same but the vertical component is anomalous and is wholly determined by the lift force of the hatched areas shown in Figure 43-9. In this case, the resultant of the water pressure does not pass through the hinge. However, the resultant can be resolved into a force through the hinge (water pressure, high water side) and a force in another direction (water pressure, low water side). In the calculations it is sometimes also useful to combine the water pressure on the side of the low water level with a part of the self-weight, so this combined load also passes through the gate's hinge.

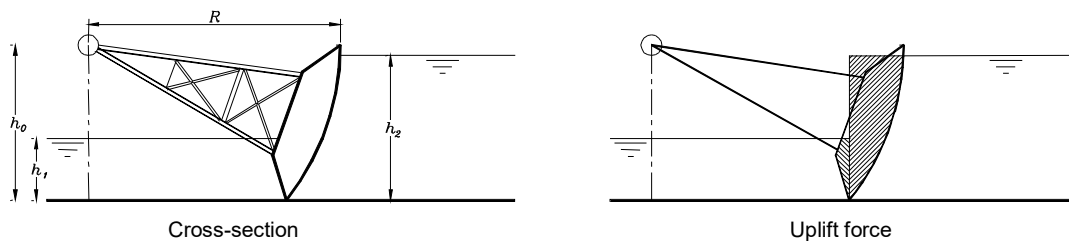


Figure 43-9 Radial gate with water proof plating on both sides

To calculate the load on the gate with the line of action through the hinge, the structure can be schematised as a two-dimensional framework.

Depending on the shape of the arms and the way the arms are attached to the gate, a force parallel to the hinge axis is applied to the hinge, as well as a force perpendicular to its axis. Figure 43-10 shows this for a structure in which the gate is hinged to the truss arms. The line of action of the resultant load on the axis of the hinge passes through two structural hinges. In the case of a small angle between the arms and the perpendicular of the axis and a load perpendicular to the gate, this results in a small force parallel to the axis. The downside of the given structure is that it is not stable for a load parallel to the gate. Such a load can occur if the gate is open and there is a side wind. That is why such a system requires guidance equipment for the gate that offers sufficient lateral support to guarantee stability.

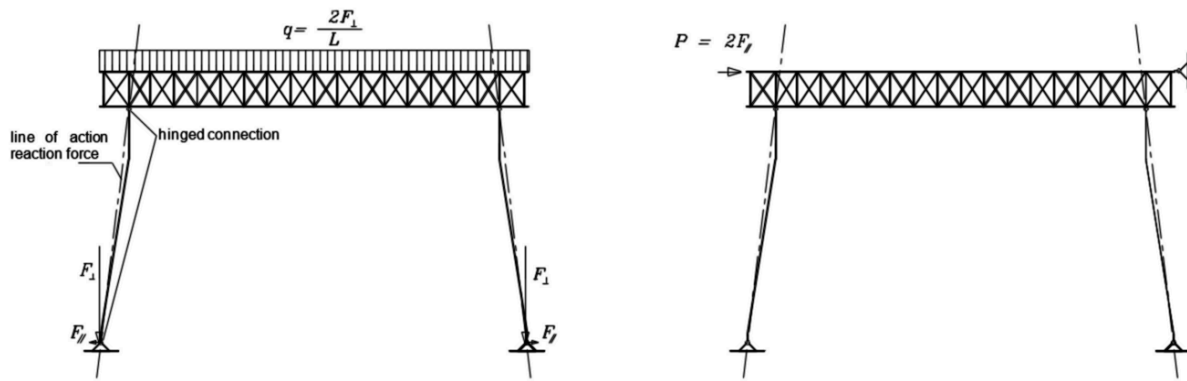


Figure 43-10 Force parallel to the axis of the hinge in the case of hinged arms

If the truss arms are fixed to the gate (not hinged), one creates a stable system in the shape of a portal frame (see Figure 43-11). In this case, for a load q perpendicular to the axis, the force F_{\parallel} parallel to the axis of the hinge will be larger than with hinged arms. This parallel force is caused by the deflection of the radial gate. This generates an outwards rotation of the arms, which is prevented in the hinges.

The relationship between the forces perpendicular and parallel to the axis of the hinge depends on the stiffness of the truss arm and the gate. The stiffer the arms, the larger the load parallel to the axis. The theoretical maximum parallel load caused by a load perpendicular to the wall is:

$$F_{\parallel} = \frac{L}{4R} \cdot F_{\perp}$$

However, this can only occur with infinitely stiff truss arms.

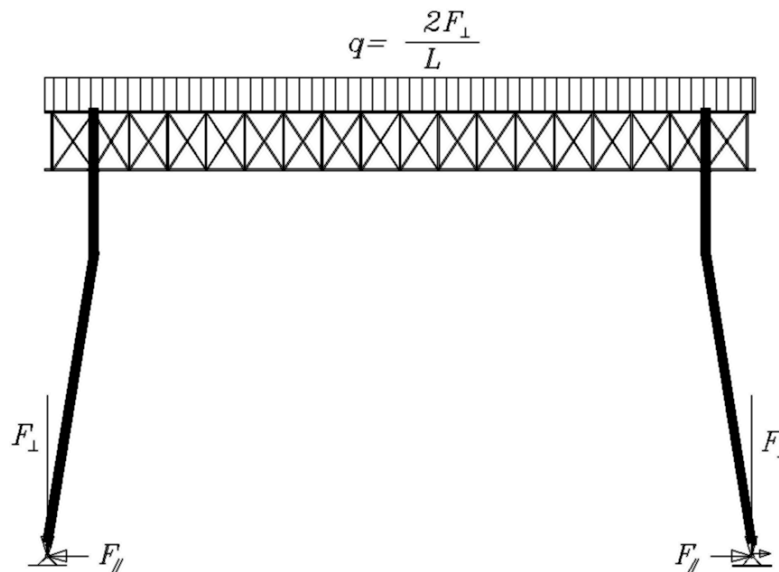


Figure 43-11 Force parallel to the axis of the hinge in the case of fixed arms

Radial gate with a vertical axis

In the case of a radial gate with a vertical axis, the gate is curved in the horizontal plane to an arc with a centre that coincides with the position of the hinge. Thus, the resultant of the water pressure load goes precisely through the hinge in the horizontal plane. The direction of the resultant depends on the lengthwise profile of the gate. This is apparent in Figure 43-12, which shows two different profiles.

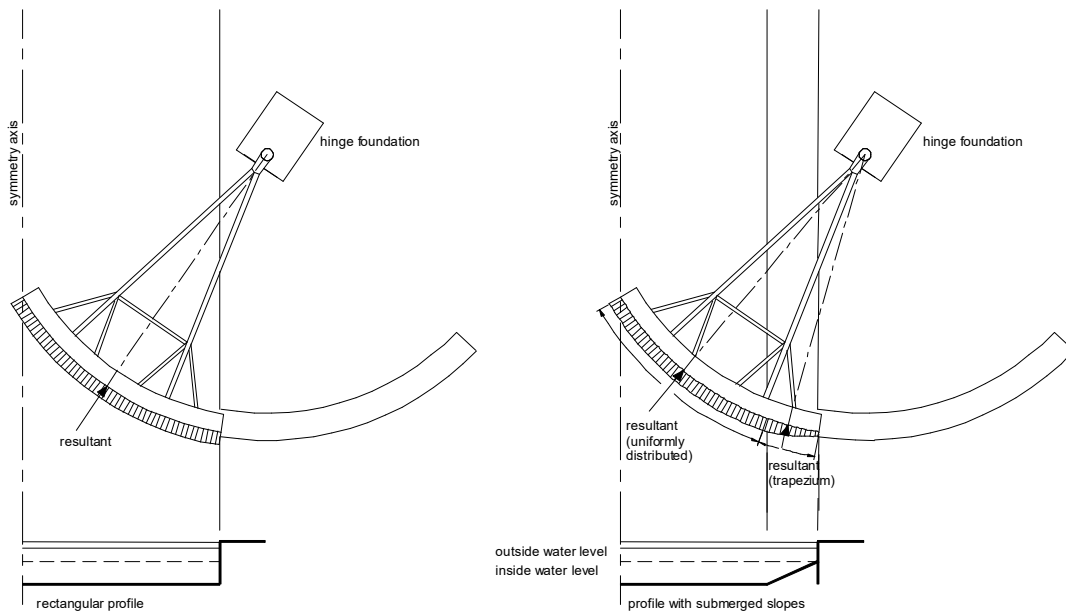


Figure 43-12 Direction of the resultant water pressure on a radial gate with a vertical axis

In the vertical plane, the direction and the position of the resultant of the water pressure depends on the shape of the gate in the vertical cross-section. Figure 43-13 shows a number of possible cross-sections and the forces on the gate per metre. The position of the seal with the bottom is an important detail which determines the size of the upward force.

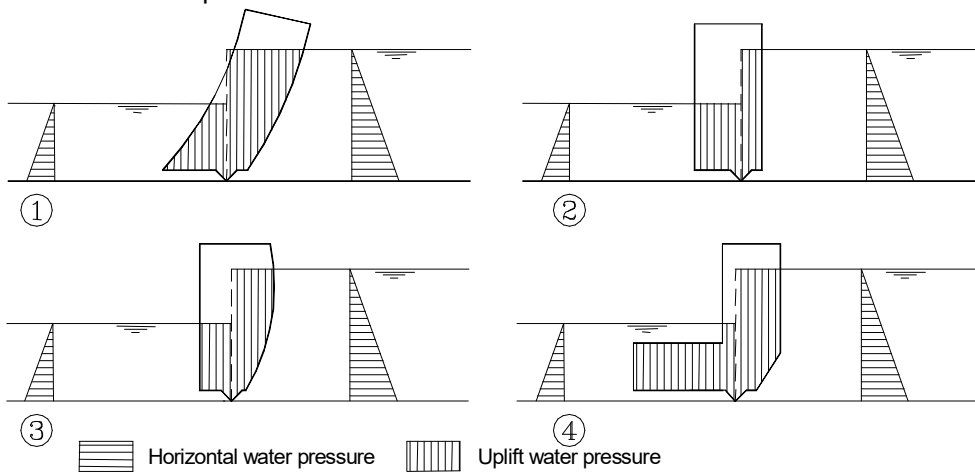


Figure 43-13 Loads dependent on the shape of the gate

A force with a line of action that does not go through the hinge can be replaced with a force through the hinge plus a moment. An example of this is given in Figure 43-14. The moment is taken on by the system as for a beam on two supports.

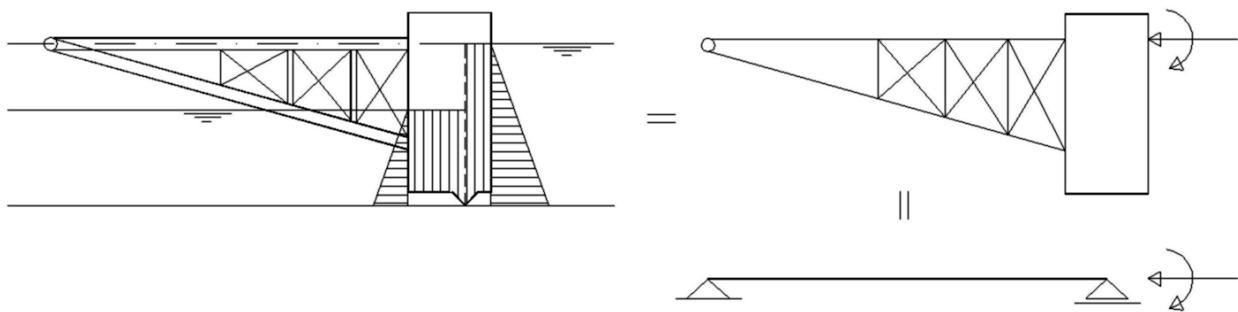


Figure 43-14 Schematisation of the load from the gate on the arms

43.4 Water pressure on sector gates

The sector gate transfers its loads directly to the sill. The line of action of the resultant of the water pressure on the plates on the side of the high-water level goes through the hinge. The water pressure on the plates on the side of the low water level causes a moment relative to the hinge. This moment is in equilibrium with the moment on the hinge as a result of the self-weight of the gate and the possible reaction force created by a rabbeted stop.

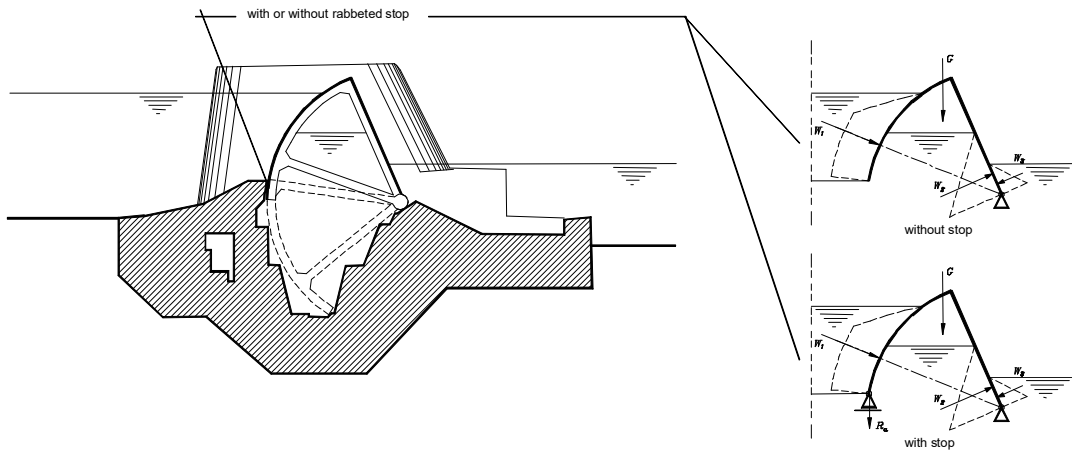


Figure 43-15 Action of forces in a sector gate

If, on the low water side, the gate is not only subject to hydrostatic loads, but also to dynamic loads such as waves, one will always opt to include a rabbeted stop for the gate. The water level in the gate is then kept high enough to ensure that there is always a force present in the rabbeted stop. Waves on the high-water side do not influence the position of the gate, because the resultant water pressure goes through the hinge.

43.5 Water pressure on arcs

Arcs that are subjected to a load on all sides (fluid or gas pressure) do not develop any shear stresses or moments, only normal forces. One can make use of this property to optimise the use of materials. Concrete, for instance, will be used in a compression arc (dam) and steel will be used in a tension arc (visor dam).

The transfer of load in an arc is relatively simple because the direction of the forces in the supports is known; these naturally follow the tangent of the circle. This is shown in Figure 43-16.

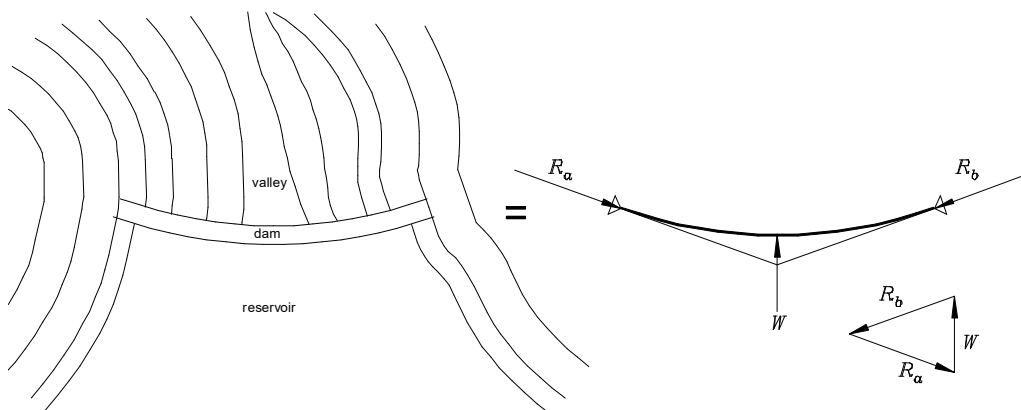


Figure 43-16 Load transfer in a circular arc

Manual Hydraulic Structures

Appendices

A. Dutch translation of Hydraulic Structures keywords

A

abutment	landhoofd
angle of internal friction	hoek van inwendige wrijving
apron	vlonder
aquifer	waterhoudende grondlaag
area moment of inertia	traagheidsmoment

B

backwater curve	stuwkromme
barrier	kering
beam	ligger
bearing	ondersteuning(sconstructie)
bearing capacity	draagvermogen
bentonite	bentoniet
berth	ligplaats
berthing dolphin	meerstoel
blinding	werkvloer
bollard	bolder
bolt	bout
breakwater	golfbreker
bridge clearance	doorvaarthoogte
buckle (to buckle)	knikken
building dock / construction dock	bouwdok
building pit / construction pit	bouwput
bulkhead	slingerschot / scheidingswand
buoyancy	opdrijving
buttress	schoor / steunbeer

C

cable bridge / rope bridge	tuibrug
cantilever	kraagligger / console
capping beam	deksloof
cellular cofferdam	cellenwand
chamber lock	schutsluis
clearance	kielspeling / vrije ruimte
cofferdam	bouwkuip / kistdam
compression stress	drukspanning
confined aquifer	afsgeloten grondlaag met spanningswater
conceptual design	voorlopig ontwerp
construction height	aanleghoogte
construction pit / building pit	bouwput
creep	kruip
crest	kruin
culvert	duiker
cut and cover method	wanden-dakmethode
cut-off	coupure
cut-off screen	kwelscherm (ondoorlatend scherm)
cutting-edge	snijrand

D

dam	stuwdam
deep foundation	paalfundering
density	dichtheid (soortelijke massa)
design value	rekenwaarde
dewatering sluice	uitwateringssluis
diaphragm wall	diepwand
dike section	dijkvak
dike segment	dijktraject
discharge sluice	spuisluis
dissipation chamber	woelbak

dolphin
 dragline
 draught
 drop gate
 dry dock

dukdalf
 sleepgraver (dragline)
 diepgang
 zakdeur
 droogdok

E

effective stress
 embedded depth
 engineering structure
 entry ramp
 equilibrium state
 excavator
 expansion joint

korreldruk
 inheidiepte
 kunstwerk
 toerit (naar tunnel)
 evenwichtssituatie
 graafmachine
 dilatatievoeg

F

falsework
 fascine mattress
 fender
 fetch
 fillet weld
 fixed end
 flange
 flexural rigidity
 flood
 flood defence
 flushing sluice
 footing
 formwork
 freeboard
 frontline waters

steigerwerk / bekisting
 zinkstuk (van rijshout)
 stootblok
 strijklengte
 hoeklas
 inklemming
 flens
 buigstijfheid
 overstroming
 waterkering
 spoelsluis
 fundament
 bekisting
 waakhoogte
 buitenwateren

G

gantry crane
 girder
 gravity floor
 ground level
 ground water table
 guard lock
 guide beam
 guide work
 guiding system (of a pile ridge)

portaalkraan
 draagbalk / steunbalk
 gewichtsvloer
 maaiveld
 grondwaterstand
 keersluis
 geleidebalk
 geleidewerk
 makelaar (van een heistelling)

H

hawser force
 heave
 high water slack
 hinge
 hoist
 hydraulic structure

troskracht
 hydraulische grondbreuk
 hoogwaterkentering
 scharnier
 takel
 waterbouwkundige constructie

I

immersed tunnel
 inclined plane
 inflatable barrier
 influence coefficient
 inland waters
 inundation

afgezonken tunnel
 hellend vlak
 balgkering of schulpkering
 invloedscoëfficiënt
 binnenwateren
 inundatie (opzettelijk veroorzaakte overstroming)

J

jack
 jetty

vijzel
 steiger, golfbreker

L

lay-by berth	wachtplaats
lean concrete	stampbeton
liquefaction	zettingsvloeiing
load-bearing structure	draagconstructie
lock chamber	schutkolk
lock head	sluishoofd
low water slack	ebkentering

M

masonry	metselwerk
mitre gate	puntdeur
modulus of subgrade reaction	beddingsconstante
mole	havenhoofd
moment diagram	momentenlijn
mooring facility	aanlegvoorziening
mooring force	aanlegkracht
mooring post	meerpaal
mould	mal

N

natural oscillation period	eigenperiode
navigation lock	schutsluis
navigation width	doorvaartbreedte
neap tide	doodtij
normal force diagram	normaalkrachtenlijn
nut	moer

O

overtopping	(golf)overslag
-------------	----------------

P

pad footing	poer
pier	pijler
pile	paal
pile ridge	heistelling
pillar	pilaar
piping	zanduitspoeling, pijpvorming
pivot	taats
plunger	zuiger
point of fixity	inklemmingspunt
prop	stempel
pulley	katrol
pumping station	gemaal

Q

quay	kade
quay wall	kademuur
quoin	wig

R

radial gate	segmentdeur
raft foundation	strookfundering
raised outer portion of a dike crest	tuielkade
raking pile	schoorpaal
recess	uitsparing, inkassing
reference crest level	dijktafelhoogte, kruinhoogte
reinforcement	wapening
reinforcement bar yard	wapeningsvlechterij
reliability index	betrouwbaarheidsindex
roller bearing	roloplegging
roller gate	roldeur

S

scour	ontgronding, wegspoeling
screed /to screed	afweerkmachine / afreien, afwerken
screw	schroef
screw thread	schroefdraad
screwed pile	schroefpaal
section modulus	weerstandsmoment
sector gate	sectordeur
seepage	onderloopsheid, achterloopsheid
seepage screen	kwelscherm
self-weight	eigen gewicht
settlement	zetting
settling	klink
shallow foundation	fundering op staal
shear force	dwarskracht
shear force diagram	dwarskrachtenlijn
sheet pile wall	damwand
ship-lift	scheepslift
shop floor	werkvloer
shovel	laadschop
shutter	schuif / schot
shutter weir	klepkering / klepstuw
sill	dorpel, drempel
sill beam	dorpelbalk, drempelbalk
slab foundation	plaatfundering
slackening structure	remmingwerk
slack water	kentering / doottij
sliding gate	roldeur
sliding surface	glijvlak / schuifvlak
sluice caisson	doorlaatcaisson
slurry wall	diepwand
spalling force	spatkracht
span	overspanning
specific gravity	relatieve dichtheid
specific weight	soortelijk gewicht
stiffener	verstijvingsbalk / verstijver / versterkingsrib
stop lock	spuisluis
stop log	schotbalk
storm surge	stormvloed
storm-surge barrier	stormvloedkering
strip foundation	strookfundering
strut	stempel / schoor(balk)
subsidence	daling (bijv. van bodem, of pneumatisch caisson)
surcharge	bovenbelasting
suspension bridge	hangbrug / kettingbrug
sway	slingering
swell	deining
swivel	wartel / oogbout

T

tender	aanbesteding
tensile stress	trekspanning
tidal divide	wantij
tie rod / tie bar	trekstang, ankerstaaf
timber	balk / hout
toe berm	plasberm / kreukelberm (bij een dijk)
tow boat	sleepboot
trestle	aanloopsteiger
truss	spant, ligger
tug boat	sleepboot
tunnel entrance ring dike	kanteldijk
turnbuckle	spanschroef

B. Units and conventions

Units

The world's most widely used system of physical units, both in everyday commerce and in science, is the International System of Units (abbreviated SI from the French "Système International d'unités"). A notable exception is the United States of America, which still uses many old units in addition to SI. The SI-standard is maintained by the Bureau International des Poids et Mesures in Sèvres, France. The seven SI base units are presented in Table B-43-1.

quantity		unit	
name	symbol	name	symbol
length	l	metre	m
mass	m	kilogram	kg
time	t	second	s
electric current	I	ampere	A
thermodynamic temperature	T	kelvin	K
amount of substance	n	mole	mol
luminous intensity	I_v	candela	cd

Table B-43-1 base units

Base units can be put together to derive units of measurement for other quantities. Some have been given names. Table B-43-2 gives an overview of derived SI units relevant for hydraulic engineering.

quantity		unit		
name	symbol	name	non-SI units (generally used)	SI base units
acceleration	a	metre per second squared		$m\ s^{-2}$
angle	α, β, \dots	radian	rad	1
angular velocity	ω	radian per second	rad / s	s^{-1}
area	A	square metre		m^2
area moment of inertia	I	metre to the fourth power		m^4
axial rigidity	EA	newton per metre	$N\ m^{-1}$	$kg\ s^{-2}$
bending stiffness	EI	newton per square metre	$N\ m^2$	$kg\ m^{-1}\ s^{-2}$
density	ρ	kilogram per cubic metre		$kg\ m^{-3}$
dynamic viscosity	η	pascal second	$Pa\ s\ (N\ s / m^2)$	$kg\ m^{-1}\ s^{-1}$
energy, work, heat	W	joule	$J\ (N\ m)$	$kg\ m^2\ s^{-2}$
first moment of area	S	cubic metre		m^3
force, weight	F, G	newton	N	$kg\ m\ s^{-2}$
frequency	f	hertz	Hz	s^{-1}
impulse, momentum	p	newton second	$N\ s$	$kg\ m\ s^{-1}$
kinematic viscosity	ν	square metre per second		$m^2\ s^{-1}$
moment of force, torque	M	newton metre	$N\ m$	$kg\ m^2\ s^{-2}$
section modulus	W	cubic metre		m^3
power	P	watt	$W\ (J / s)$	$kg\ m^2\ s^{-3}$
pressure, stress	σ	pascal	$Pa\ (N / m^2)$	$kg\ m^{-1}\ s^{-2}$
speed, velocity	v	metre per second		$m\ s^{-1}$
specific weight	γ	newton per cubic metre	N / m^3	$kg\ m^{-2}\ s^{-2}$
volume	V	cubic metre		m^3
wave number	k	reciprocal metre		m^{-1}
Young's modulus	E	newton per square metre	$N\ m^{-2}$	$kg\ m^{-1}\ s^{-2}$

Table B-43-2 Selection of derived SI-units

The 'area moment of inertia', or 'second moment of area' in hydraulic engineering is mostly referred to as 'moment of inertia'. In some literature, the 'section modulus' is indicated as the 'moment of resistance'. The 'bending stiffness' is also known as 'flexural rigidity'. The 'Young's modulus' is also known as 'modulus of elasticity', 'elastic modulus' or 'tensile modulus'.

Depending on age and place, many non-SI units are in use. The most important non-SI units still in use are presented in Table B-43-3. Extensive lists with conversion factors can be found on internet, see for example

<http://www.unc.edu/~rowlett/units/>.

quantity		unit		
name	symbol	name	symbol	relation to SI-units
area	<i>A</i>	are	a	= 100 m ²
energy	<i>W</i>	kilocalorie	Cal, kcal	= 4,1868 kJ
energy	<i>W</i>	kilowatt-hour	kWh	= 3,6 MJ
force	<i>F</i>	ton / tonnes (force)	tnf	= 1000 kgf ≈ 9,81 kN
force	<i>F</i>	pound	lb (lbf)	≈ 4,448 N
length	<i>L</i>	mile	mi	≈ 1609 m
length	<i>L</i>	nautical mile	nmi, NM	= 1852 m
length	<i>L</i>	yard	yd	= 0,9144 m
length	<i>L</i>	foot (international)	ft	= 0,3048 m
length	<i>L</i>	inch	in (")	= 0,0254 m
mass	<i>m</i>	slug	slug (lb-s ² /ft)	= 14,59 kg
mass	<i>m</i>	ton / tonnes (mass)	t	= 1000 kg
power	<i>P</i>	horsepower (metric)	hp	≈ 735,499 W
pressure	<i>σ</i>	atmosphere	atm	= 101 325 Pa
pressure	<i>σ</i>	bar	bar	= 10 ⁵ Pa
speed, velocity	<i>v</i>	knot (international)	kn (kt)	= 0,514 m s ⁻¹ (= 1 nmi/h)
temperature	<i>T</i>	degree Celsius	°C	= <i>T_K</i> - 273.15
temperature	<i>T</i>	degree Fahrenheit	°F	= <i>T_K</i> × 1.8 - 459.67
volume	<i>V</i>	litre	l or L	= 1 dm ³ = 0.001 m ³
volume	<i>V</i>	gallon (imperial)	gal	≈ 4,546 × 10 ⁻³ m ³
volume	<i>V</i>	gallon (USA)	gal	≈ 3,785 × 10 ⁻³ m ³

Table B-43-3 Non-SI units

Prefixes may be added to units to produce a multiple of the original unit. All multiples are integer powers of ten. See Table B-43-4 for an overview of the most used prefixes.

name	symbol	factor
peta-	P	10 ¹⁵
tera-	T	10 ¹²
giga-	G	10 ⁹
mega-	M	10 ⁶
kilo-	k	10 ³
hecto-	h	10 ²
deca-	da	10 ¹
deci-	d	10 ⁻¹
cent-	c	10 ⁻²
milli-	m	10 ⁻³
micro-	μ	10 ⁻⁶
nano-	n	10 ⁻⁹
pico-	p	10 ⁻¹²
femto-	f	10 ⁻¹⁵

Table B-43-4 SI-prefixes

For direct conversion of °C to °F and v.v., next formulae apply:

$$T_C = (T_F - 32)/1,8$$

$$T_F = 1,8 T_C + 32$$

Besides the related quantities of density and specific weight, in some anglo-saxon literature 'specific gravity'

(sg) is used. This is defined as: $sg = \frac{\gamma_{\text{specific material}}}{\gamma_{\text{water, 4}^\circ\text{C}}} = \frac{\rho_{\text{specific material}}}{\rho_{\text{water, 4}^\circ\text{C}}} [-]$.

Conventions for the notation of units and numbers

In design practise, and also in this Manual, stresses and material properties are expressed in N/mm², only values for soundings are in MPa. Forces are generally expressed in kN.

The decimal mark and the thousands separator in numbers are written in the style that is used in most of Europe: a comma is used as decimal delimiter, and a blank space is used as digit grouping delimiter (for reading comfort). So, for example, one million newton with a precision of two decimals is written as 1 000 000,00 N.

Many authorities recommend that in scientific notation, when numbers are represented using powers of ten, the exponent of the 10 should be a multiple of 3. So, for example, $1,234 \cdot 10^4$ should be written as $12,34 \cdot 10^3$.

C. Trigonometric, cyclometric and hyperbolic functions

Chapter added: February 2017

Trigonometric functions

The trigonometric functions are functions of an angle. They are commonly defined as ratios of two sides of a right triangle containing the angle, and can equivalently be defined as the lengths of various line segments from a unit circle (which has a radius of 1).

$$\sin \alpha = \frac{\text{opposite}}{\text{hypotenuse}} = \cos\left(\frac{\pi}{2} - \alpha\right) = \frac{1}{\csc \alpha}$$

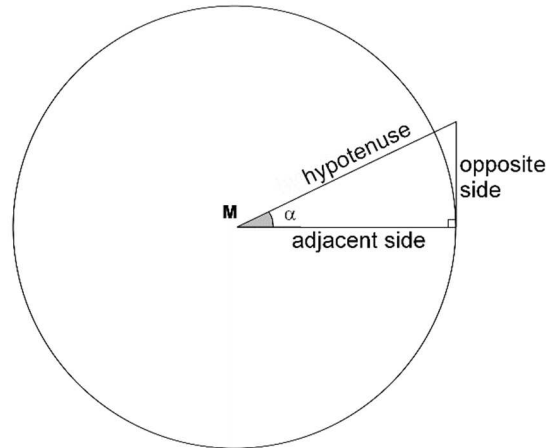
$$\cos \alpha = \frac{\text{adjacent}}{\text{hypotenuse}} = \sin\left(\frac{\pi}{2} - \alpha\right) = \frac{1}{\sec \alpha}$$

$$\tan \alpha = \frac{\text{opposite}}{\text{adjacent}} = \frac{\sin \alpha}{\cos \alpha} = \cot\left(\frac{\pi}{2} - \alpha\right) = \frac{1}{\cot \alpha}$$

$$\cot \alpha = \frac{\text{adjacent}}{\text{opposite}} = \frac{\cos \alpha}{\sin \alpha} = \tan\left(\frac{\pi}{2} - \alpha\right) = \frac{1}{\tan \alpha}$$

$$\sec \alpha = \frac{\text{hypotenuse}}{\text{adjacent}} = \csc\left(\frac{\pi}{2} - \alpha\right) = \frac{1}{\cos \alpha}$$

$$\csc \alpha = \frac{\text{hypotenuse}}{\text{opposite}} = \sec\left(\frac{\pi}{2} - \alpha\right) = \frac{1}{\sin \alpha}$$



(These equations apply to angles in radians. For angles in degrees: replace $\frac{\pi}{2}$ by 90°)

Cyclometric, or reverse trigonometric functions

Cyclometric functions are the inverse functions of the trigonometric functions.

So, if $x = \sin(\alpha)$, $\alpha = \arcsin(x)$. In an analogous way, $\arccos(x)$, $\arctan(x)$, $\text{arccot}(x)$, $\text{arcsec}(x)$ and $\text{arccsc}(x)$ can be defined.

Hyperbolic functions

Hyperbolic functions are analogues of the ordinary trigonometric functions. They are related to hyperboles and often occur in the solutions of many linear differential equations. A ray through the origin intersects the hyperbole $x^2 - y^2 = 1$ in point $(\cosh(A), \sinh(A))$, where the hyperbole angle A equals the area enclosed by the ray, the ray mirrored by the x -axis and the hyperbole. The hyperbolic functions may be defined in terms of the legs of a right triangle covering this sector.

The hyperbolic functions can be expressed as exponential functions:

$$\sinh(x) = \frac{e^x - e^{-x}}{2}$$

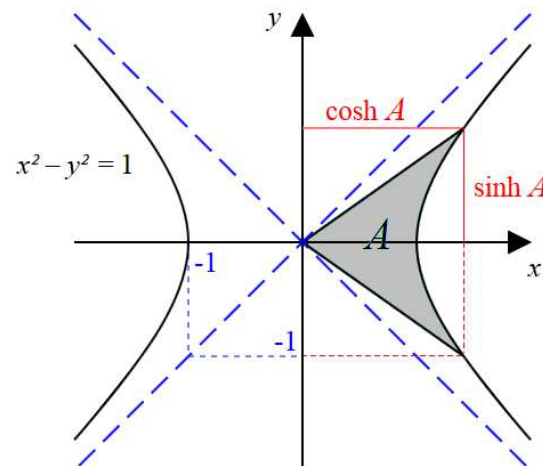
$$\cosh(x) = \frac{e^x + e^{-x}}{2}$$

$$\tanh(x) = \frac{\sinh(x)}{\cosh(x)} = \frac{e^x - e^{-x}}{e^x + e^{-x}}$$

$$\coth(x) = \frac{1}{\tanh(x)} = \frac{e^x + e^{-x}}{e^x - e^{-x}}$$

$$\text{sech}(x) = \frac{1}{\cosh(x)} = \frac{2}{e^x + e^{-x}}$$

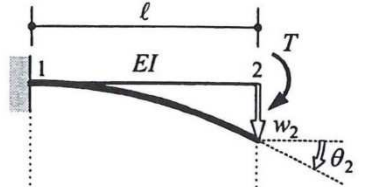
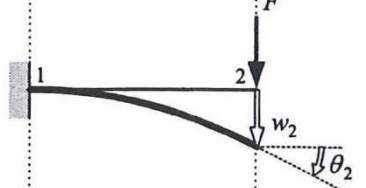
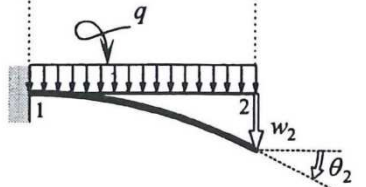
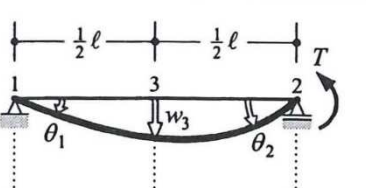
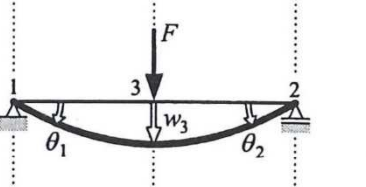
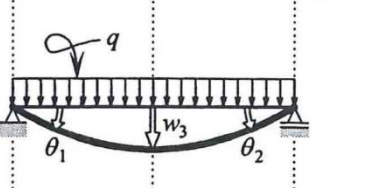
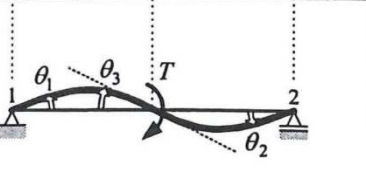
$$\text{csch}(x) = \frac{1}{\sinh(x)} = \frac{2}{e^x - e^{-x}}$$



D. Structural Mechanics

Moment and deflection formulas

The 'moment and deflection formulas' (*vergeetmenietjes*) consist of a set of equations of rotation angles and deflections for standard load situations on supported and fixed beams.

(1)		$\theta_2 = \frac{Tl}{EI}; \quad w_2 = \frac{Tl^2}{2EI}$
(2)		$\theta_2 = \frac{Fl^2}{2EI}; \quad w_2 = \frac{Fl^3}{3EI}$
(3)		$\theta_2 = \frac{ql^3}{6EI}; \quad w_2 = \frac{ql^4}{8EI}$
(4)		$\theta_1 = \frac{1}{6} \frac{Tl}{EI}; \quad \theta_2 = \frac{1}{3} \frac{Tl}{EI}; \quad w_3 = \frac{1}{16} \frac{Tl^2}{EI}$
(5)		$\theta_1 = \theta_2 = \frac{1}{16} \frac{Fl^2}{EI}; \quad w_3 = \frac{1}{48} \frac{Fl^3}{EI}$
(6)		$\theta_1 = \theta_2 = \frac{1}{24} \frac{ql^3}{EI}; \quad w_3 = \frac{5}{384} \frac{ql^4}{EI}$
(a)		$\theta_1 = \theta_2 = \frac{1}{24} \frac{Tl}{EI}; \quad \theta_3 = \frac{1}{12} \frac{Tl}{EI}; \quad w_3 = 0$

cantilevering beam

simply supported beam (statically determinate)

statically indeterminate beam
(one fixed end and one simple support)

(7)		$\theta_2 = \frac{1 T l}{4 EI}; \quad w_3 = \frac{1 T l^2}{32 EI}$ $M_1 = \frac{1}{2} T; \quad V_1 = V_2 = \frac{3 T}{2 l}$
(8)		$\theta_2 = \frac{1 F l^2}{32 EI}; \quad w_3 = \frac{7 F l^3}{768 EI}$ $M_1 = \frac{3}{16} F l; \quad V_1 = \frac{11}{16} F; \quad V_2 = \frac{5}{16} F$
(9)		$\theta_2 = \frac{1 q l^3}{48 EI}; \quad w_3 = \frac{1 q l^4}{192 EI}$ $M_1 = \frac{1}{8} q l^2; \quad V_1 = \frac{5}{8} q l; \quad V_2 = \frac{3}{8} q l$
statically indeterminate beam (two fixed ends)		
(10)		$w_3 = \frac{1 F l^3}{192 EI}$ $M_1 = M_2 = \frac{1}{8} F l; \quad V_1 = V_2 = \frac{1}{2} F$
(11)		$w_3 = \frac{1 q l^4}{384 EI}$ $M_1 = M_2 = \frac{1}{12} q l^2; \quad V_1 = V_2 = \frac{1}{2} q l$
(b)		$\theta_3 = \frac{1 T l}{16 EI}; \quad w_3 = 0$ $M_1 = M_2 = \frac{1}{4} T; \quad V_1 = V_2 = \frac{3 T}{2 l}$

Some formulae for prismatic beams with bending stiffness EI .

T , F and q represent the load by a couple, force and uniformly distributed load respectively.

M_i and V_i represent the bending moment and shear force on the end i of the beam, due to the support reactions.

(c)		$\theta_1 = \frac{Fab(\ell + b)}{6EI\ell} = \frac{F\ell^2}{6EI} \left(2\frac{a}{\ell} - 3\frac{a^2}{\ell^2} + \frac{a^3}{\ell^3} \right)$ $\theta_2 = \frac{Fab(\ell + a)}{6EI\ell} = \frac{F\ell^2}{6EI} \left(\frac{a}{\ell} - \frac{a^3}{\ell^3} \right)$
(d)		$M_1 = \frac{Fb(\ell^2 - b^2)}{2\ell^2} = F\ell \left(\frac{a}{\ell} - \frac{3}{2}\frac{a^2}{\ell^2} + \frac{1}{2}\frac{a^3}{\ell^3} \right)$ $V_1 = \frac{Fb(3\ell^2 - b^2)}{2\ell^3} = F \left(1 - \frac{3}{2}\frac{a^2}{\ell^2} + \frac{1}{2}\frac{a^3}{\ell^3} \right)$ $V_2 = \frac{Fa^2(3\ell - a)}{2\ell^3} = F \left(\frac{3}{2}\frac{a^2}{\ell^2} - \frac{1}{2}\frac{a^3}{\ell^3} \right)$ $\theta_2 = \frac{Fa^2b}{4EI\ell} = \frac{F\ell^2}{4EI} \left(\frac{a^2}{\ell^2} - \frac{a^3}{\ell^3} \right)$
(e)		$M_1 = \frac{Fb^2}{\ell^2} = F\ell \left(\frac{a}{\ell} - 2\frac{a^2}{\ell^2} + \frac{a^3}{\ell^3} \right)$ $V_1 = \frac{Fb^2(\ell + 2a)}{\ell^3} = F \left(1 - 3\frac{a^2}{\ell^2} + 2\frac{a^3}{\ell^3} \right)$ $M_2 = \frac{Fa^2b}{\ell^2} = F\ell \left(\frac{a^2}{\ell^2} - \frac{a^3}{\ell^3} \right)$ $V_2 = \frac{Fa^2(\ell + 2b)}{\ell^3} = F\ell \left(3\frac{a^2}{\ell^2} - 2\frac{a^3}{\ell^3} \right)$
(f)		$M_1 = \frac{3EI}{\ell^2} w^0; \quad V_1 = V_2 = \frac{3EI}{\ell^3} w^0$ $\theta_2 = \frac{3}{2} \frac{w^0}{\ell}$ $\theta_3 = \frac{9}{8} \frac{w^0}{\ell}; \quad w_3 = \frac{5}{16} w^0$
(g)		$M_1 = M_2 = \frac{6EI}{\ell^2} w^0; \quad V_1 = V_2 = \frac{12EI}{\ell^3} w^0$ $\theta_3 = \frac{3}{2} \frac{w^0}{\ell}; \quad w_3 = \frac{1}{2} w^0$

support reactions and rotations at the beam ends

displacements

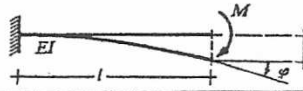
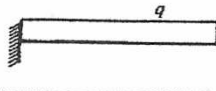

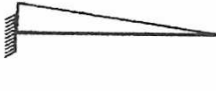
Table D-1 Moment and deflection formulas (from: Hartsuijker / Welleman: Engineering Mechanics, Volume 2)

	$A_{\text{vert}} = \frac{11}{16} F$ $B_{\text{vert}} = \frac{5}{16} F$	$M_A = \frac{3}{16} Fl$ $\varphi_B = \frac{Fl^2}{32EI}$	$\delta_C = \frac{7Fl^3}{768EI}$
	$A_{\text{vert}} = \frac{F \cdot b(3l^2 - b^2)}{2l^3}$ $B_{\text{vert}} = \frac{F \cdot a^2(2l + b)}{2l^3}$	$M_A = \frac{F \cdot b \cdot (l^2 - b^2)}{2l^2}$ $\varphi_B = \frac{Fa^2b}{4lEI}$	$a \leq b \quad \delta_C = \frac{F \cdot a^2 \cdot (9b - 2a)}{96EI}$ $a \geq b \quad \delta_C = \frac{F \cdot b \cdot (3l^2 - 5b^2)}{96EI}$
	$A_{\text{vert}} = \frac{4}{10} ql$ $B_{\text{vert}} = \frac{1}{10} ql$	$M_A = \frac{1}{15} ql^2$ $\varphi_B = \frac{ql^3}{120EI}$	$\delta_C = \frac{9ql^4}{3840EI}$
	$A_{\text{vert}} = \frac{5}{8} ql$ $B_{\text{vert}} = \frac{3}{8} ql$	$M_A = \frac{1}{8} ql^2$ $\varphi_B = \frac{ql^3}{48EI}$	$\delta_C = \frac{ql^4}{192EI}$
	$A_{\text{vert}} = \frac{21}{64} ql$ $B_{\text{vert}} = \frac{11}{64} ql$	$M_A = \frac{5}{64} ql^2$ $\varphi_B = \frac{5ql^3}{384EI}$	$\delta_C = \frac{ql^4}{290EI}$
	$A_{\text{vert}} = \frac{q(5l^3 - 4al^2 - 2a^2l + a^3)}{8l^2}$ $B_{\text{vert}} = q(l - a) - A_{\text{vert}}$	$M_A = \frac{q(l^3 - 2a^2l + a^2)}{8l}$ $\varphi_B = \frac{q(l^3 - 2a^2l + a^3)}{48EI}$	$\delta_C = \frac{q(10l^4 - 10a^2l^2 - 15a^3l + 16a^4)}{1920EI}$
	$A_{\text{vert}} = \frac{3M(l^2 - b^2)}{2l^3} \uparrow$ $B_{\text{vert}} = \frac{3M(l^2 - b^2)}{2l^3} \downarrow$	$M_A = \frac{M(3b^2 - l^2)}{2l^2} \zeta$ $\varphi_B = \frac{M \cdot a(a - 2b)}{4lEI}$	$a \leq b \quad \delta_C = \frac{M \cdot a \cdot (6b - 5a)}{32EI} \uparrow$ $a \geq b \quad \delta_C = \frac{M(l^2 - 5b^2)}{32EI} \downarrow$
	$A_{\text{vert}} = \frac{3}{2} \frac{M}{l} \uparrow$ $B_{\text{vert}} = \frac{3}{2} \frac{M}{l} \downarrow$	$M_A = \frac{1}{2} M \zeta$ $\varphi_B = \frac{Ml}{4EI}$	$\delta_C = \frac{Ml^2}{32EI}$
	$A_{\text{vert}} = \frac{3EI\delta}{l^3} \downarrow$ $B_{\text{vert}} = \frac{3EI\delta}{l^3} \uparrow$	$M_A = \frac{3EI\delta}{l^2} \zeta$ $\varphi_B = \frac{3}{2} \frac{\delta}{l}$	$\delta_C = \frac{5}{16} \delta \uparrow$

Table D-2 Singular statically indeterminate beams (Ir.E.O.E van Rotterdam: Sterkteleer 2 toegepaste mechanica)

	$A_{\text{vert}} = \frac{1}{2} F \uparrow$ $B_{\text{vert}} = \frac{1}{2} F \uparrow$	$M_A = \frac{1}{8} Fl \curvearrowright$ $M_B = \frac{1}{8} Fl \curvearrowleft$	$\delta_C = \frac{Fl^3}{192EI} \downarrow$
	$A_{\text{vert}} = \frac{Fb^2(3a + b)}{l^3}$ $B_{\text{vert}} = \frac{Fa^2(a + 3b)}{l^3}$	$M_A = \frac{Fab^2}{l^2}$ $M_B = \frac{Fa^2b}{l^2}$	$a \leq b$ $\delta_C = \frac{Fa^2(3b - a)}{48EI}$
	$A_{\text{vert}} = \frac{7}{20} ql$ $B_{\text{vert}} = \frac{3}{20} ql$	$M_A = \frac{1}{20} ql^2$ $M_B = \frac{1}{30} ql^2$	$\delta_C = \frac{ql^4}{768EI}$
	$A_{\text{vert}} = \frac{1}{2} ql$ $B_{\text{vert}} = \frac{1}{2} ql$	$M_A = \frac{1}{12} ql^2$ $M_B = \frac{1}{12} ql^2$	$\delta_C = \frac{ql^4}{384EI}$
	$A_{\text{vert}} = \frac{1}{4} ql$ $B_{\text{vert}} = \frac{1}{4} ql$	$M_A = \frac{5}{96} ql^2$ $M_B = \frac{5}{96} ql^2$	$\delta_C = \frac{7ql^4}{3840EI}$
	$A_{\text{vert}} = \frac{q(l - a)}{2}$ $B_{\text{vert}} = \frac{q(l - a)}{2}$	$M_A = \frac{q(l^3 - 2a^2l + a^3)}{12l}$ $M_B = \frac{q(l^3 - 2a^2l + a^3)}{12l}$	$\delta_C = \frac{q(5l^4 - 20a^3l + 16a^4)}{1920EI}$
	$A_{\text{vert}} = \frac{6Mab}{l^3} \uparrow$ $B_{\text{vert}} = \frac{6Mab}{l^3} \downarrow$	$M_A = \frac{Mb(b - 2a)}{l^2} \curvearrowright$ $M_B = \frac{Ma(2b - a)}{l^2} \curvearrowleft$	$\delta_C = \frac{Ma(b - a)}{8EI} \uparrow$
	$A_{\text{vert}} = \frac{12EI\delta}{l^3} \downarrow$ $B_{\text{vert}} = \frac{12EI\delta}{l^3} \uparrow$	$M_A = \frac{6EI\delta}{l^2} \curvearrowright$ $M_B = \frac{6EI\delta}{l^2} \curvearrowleft$	$\delta_C = \frac{1}{2} \delta \uparrow$

Table D-3 Twofold statically indeterminate beams (Van Rotterdam: Sterkteleer 2 toegepaste mechanica)
(Point C is in the middle of the beam)

	$\varphi = \frac{Ml}{EI}$	$\delta = \frac{Ml^2}{2EI}$		$\varphi = \frac{ql^3}{6EI}$	$\delta = \frac{ql^4}{8EI}$
	$\varphi = \frac{Fl^2}{2EI}$	$\delta = \frac{Fl^3}{3EI}$		$\varphi = \frac{ql^3}{24EI}$	$\delta = \frac{ql^4}{30EI}$

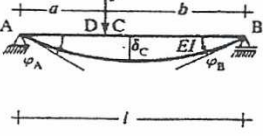
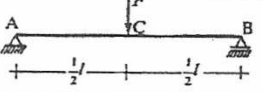
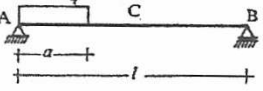
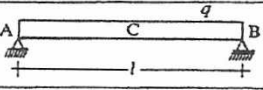
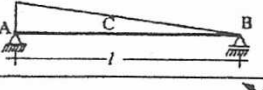
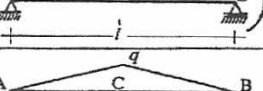
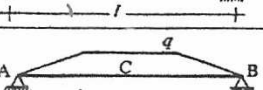
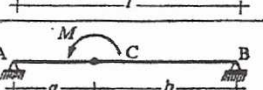
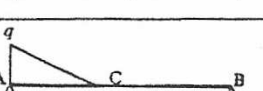
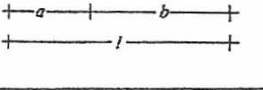
	$\varphi_A = \frac{Fab(l+b)}{6EI}$	$\varphi_B = \frac{Fab(l+a)}{6EI}$	$\delta_D = \frac{Fa^2b^2}{3EI}$
			als $a \leq b$ $\delta_C \approx \delta_{max} = \frac{Fa(3l^2 - 4a^2)}{48EI}$
	$\varphi_A = \varphi_B = \frac{Fl^2}{16EI}$		$\delta_C = \delta_{max} = \frac{Fl^3}{48EI}$
	$\varphi_A = \frac{qa^2(2l-a)^2}{24EI}$	$\varphi_B = \frac{qa^2(2l^2-a^2)}{24EI}$	als $a \leq \frac{1}{2}l$ $\delta_C \approx \delta_{max} = \frac{qa^2(3l^2-2a^2)}{96EI}$
	$\varphi_A = \varphi_B = \frac{ql^3}{24EI}$		$\delta_C = \delta_{max} = \frac{5ql^4}{384EI}$
	$\varphi_A = \frac{ql^3}{45EI}$	$\varphi_B = \frac{7 \cdot ql^3}{360EI}$	$\delta_C = \delta_{max} = \frac{1}{2} \cdot \frac{5ql^4}{384EI}$
	$\varphi_A = \frac{Ml}{6EI}$	$\varphi_B = \frac{Ml}{3EI}$	$\delta_C \approx \delta_{max} = \frac{Ml^2}{16EI}$
	$\varphi_A = \varphi_B = \frac{5ql^3}{192EI}$		$\delta_C = \delta_{max} = \frac{ql^4}{120EI}$
	$\varphi_A = \varphi_B = \frac{q(l^3 - 2a^2l + a^3)}{24EI}$		$\delta_C = \delta_{max} = \frac{q(25l^4 - 40a^2l^2 + 16a^4)}{1920EI}$
	als $a \leq b$ $\varphi_A = \frac{M(l^2 - 3b^2)}{6EI}$	als $a \leq b$ $\varphi_B = \frac{M(3a^2 - l^2)}{6EI}$	als $a \leq b$ $\varphi_C = \frac{M(4a^2 - l^2)}{16EI}$
	$\varphi_A = \frac{qa^2(20l^2 - 15al + 3a^2)}{360EI}$ $\varphi_B = \frac{qa^2(10l^2 - 3a^2)}{360EI}$		$\delta_C = \delta_{max} = \frac{q}{aEI} \left(\frac{5(a-b)l^4}{768} + \frac{b^3(5l^2 - 2b^2)}{480} \right)$

Table D-4 Statically determinate beams (Van Rotterdam: Sterkteleer 2 toegepaste mechanica)
(Point C is in the middle of the beam)

Second moments of area and properties of plane figures

Figure	Area, coordinates centroid C	Second moments of area	
		centroidal	other
	<p>Rectangle</p> $A = bh$ $\bar{y}_C = \frac{1}{2}b$ $\bar{z}_C = \frac{1}{2}h$	$I_{yy} = \frac{1}{12}b^3h$ $I_{zz} = \frac{1}{12}bh^3$ $I_{yz} = 0$	$I_{\bar{y}\bar{y}} = \frac{1}{3}b^3h$ $I_{\bar{z}\bar{z}} = \frac{1}{3}bh^3$ $I_{\bar{y}\bar{z}} = \frac{1}{4}b^2h^2$
	<p>Parallelogram</p> $A = bh$ $\bar{y}_C = \frac{1}{2}(a+b)$ $\bar{z}_C = \frac{1}{2}h$	$I_{yy} = \frac{1}{12}(a^2 + b^2)bh$ $I_{zz} = \frac{1}{12}bh^3$ $I_{yz} = \frac{1}{12}abh^2$	$I_{\bar{z}\bar{z}} = \frac{1}{3}bh^3$
	<p>Triangle</p> $A = \frac{1}{2}bh$ $\bar{y}_C = \frac{1}{3}(2a-b)$ $\bar{z}_C = \frac{2}{3}h$	$I_{yy} = \frac{1}{36}(a^2 - ab + b^2)bh$ $I_{zz} = \frac{1}{36}bh^3$ $I_{yz} = \frac{1}{72}(2a-b)bh^2$	$I_{\bar{z}\bar{z}} = \frac{1}{4}bh^3$ $I_{\bar{y}\bar{z}} = \frac{1}{8}(2a-b)bh^2$ $I_{\bar{y}\bar{y}} = \frac{1}{12}bh^3$
	<p>Trapezium</p> $A = \frac{1}{2}(a+b)h$ $\bar{z}_C = \frac{1}{3}\frac{a+2b}{a+b}h$	$I_{zz} = \frac{1}{36}\frac{a^2 + 4ab + b^2}{a+b}h^3$	$I_{\bar{z}\bar{z}} = \frac{1}{12}(a+3b)h^3$ $I_{\bar{y}\bar{y}} = \frac{1}{12}(3a+b)h^3$
	<p>Circle</p> $A = \pi R^2$	$I_{yy} = I_{zz} = \frac{1}{4}\pi R^4$ $I_{yz} = 0$ $I_p = \frac{1}{2}\pi R^4$	$I_{\bar{y}\bar{y}} = I_{\bar{z}\bar{z}} = \frac{5}{4}\pi R^4$ $I_{\bar{y}\bar{z}} = \pi R^4$

Figure	Area, coordinates centroid C	Second moments of area	
		centroidal	other
	<p>Thick-walled ring</p> $A = \pi(R_e^2 - R_i^2)$	$I_{yy} = I_{zz} = \frac{1}{4}\pi(R_e^4 - R_i^4)$ $I_{yz} = 0$ $I_p = \frac{1}{2}\pi(R_e^4 - R_i^4)$	
	<p>Thin-walled ring</p> $A = 2\pi R t$	$I_{yy} = I_{zz} = \pi R^3 t$ $I_{yz} = 0$ $I_p = 2\pi R^3 t$	$I_{\bar{y}\bar{y}} = I_{\bar{z}\bar{z}} = 3\pi R^3 t$
	<p>Semicircle</p> $A = \frac{1}{2}\pi R^2$ $\bar{y}_C = 0$ $\bar{z}_C = \frac{4}{3\pi}R = 0.424R$	$I_{yy} = \frac{1}{8}\pi R^4 = 0.393R^4$ $I_{zz} = (\frac{\pi}{8} - \frac{8}{9\pi})R^4 = 0.110R^4$ $I_{yz} = 0$	$I_{\bar{y}\bar{y}} = I_{\bar{z}\bar{z}} = \frac{1}{8}\pi R^4$ $I_{\bar{y}\bar{z}} = 0$
	<p>Semicircular ring</p> $A = \pi R t$ $\bar{y}_C = 0$ $\bar{z}_C = \frac{2}{\pi}R = 0.637R$	$I_{yy} = \frac{1}{2}\pi R^3 t$ $I_{zz} = (\frac{\pi}{2} - \frac{4}{\pi})R^3 t = 0.298R^3 t$ $I_{yz} = 0$	$I_{\bar{y}\bar{y}} = I_{\bar{z}\bar{z}} = \frac{1}{2}\pi R^3 t$ $I_{\bar{y}\bar{z}} = 0$

Table D-5 Second moments of area

Note

The notation for the second moments of area (= moments of inertia) used in this Manual complies to the notation used in the BSc-courses on structural mechanics at Delft University of Technology. This notation is different from international literature. If, for example, the x-axis is horizontal and the y-axis vertical, the notations are as follows: In this Manual: $I_{yy} = \int y^2 dA$ and in often, in other literature: $I_x = \int y^2 dA$. To put it in other words: $I_{yy} \neq I_y$. This could lead to confusion, so be aware of this.

properties of 2D shapes to be used for the moment-area theorems

(1)		<p>rectangle: $y = h$ $A = bh$ $x_C = \frac{1}{2}b$</p>
(2)		<p>triangle: $y = h \left\{ 1 - \frac{x}{b} \right\}$ $A = \frac{1}{2}bh$ $x_C = \frac{1}{3}b$</p>
(3)		<p>parabola: $y = h \left\{ 1 - \frac{x}{b} \right\}^2$ $A = \frac{1}{3}bh$ $x_C = \frac{1}{4}b$</p>
(4)		<p>parabola: $y = h \left\{ 1 - \left(\frac{x}{b} \right)^2 \right\}$ $A = \frac{2}{3}bh$ $x_C = \frac{3}{8}b$</p>
(5)		<p>parabola: $A = \frac{2}{3}bh$ $x_C = \frac{1}{2}b$</p>
(6)		<p>trapezium: $y = h_1 + (h_2 - h_1) \frac{x}{b}$ $A = \frac{1}{2}b(h_1 + h_2)$ $x_C = \frac{1}{3}b \frac{h_1 + 2h_2}{h_1 + h_2}$</p>

Table D-6 Properties of plane shapes


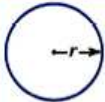
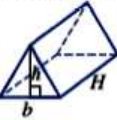

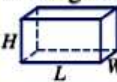
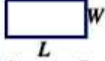
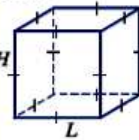
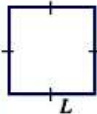


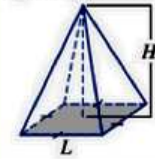
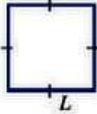
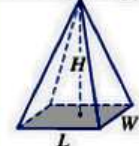
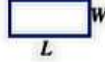


Shape	Cross-sectional shape	Volume
Cylinder 	 Area = πr^2	$V = \text{area of a circle} \times \text{height}$ $= \pi r^2 \times H$
Triangular prism 	 Area = $\frac{1}{2} bh$	$V = \text{area of a triangle} \times \text{height}$ $= \frac{1}{2} bh \times H$ <i>Note:</i> Lowercase h represents the height of the triangle.
Rectangular prism 	 Area = $L \times W$	$V = \text{area of a rectangle} \times \text{height}$ $= L \times W \times H$
Cube 	 Area = L^2	$V = \text{area of a square} \times \text{height}$ $= L^2 \times H$ $= L^2 \times L$ $= L^3$ (since in a square, $H = L$)
Cone 		$V = \frac{1}{3} \times \text{area of a circle} \times \text{height}$ $V = \frac{1}{3} \pi r^2 \times H$
Square pyramid 		$V = \frac{1}{3} \times \text{area of a square} \times \text{height}$ $V = \frac{1}{3} L^2 \times H$
Rectangular pyramid 		$V = \frac{1}{3} \times \text{area of a rectangle} \times \text{height}$ $= \frac{1}{3} L \times W \times H$
sphere. 	 Area = πr^2	$V = \frac{4}{3} \pi r^3$ r is the radius of the sphere.

Table D-7 Properties of 3D-objects (from: <http://cshsyear10maths.global2.vic.edu.au/>)

E. Natural oscillation frequencies

Natural frequencies of structures with a uniform and homogeneous section can be calculated according to $f_n = \omega_n / 2\pi$ [Hz].

The angular velocity is $\omega_n = C \sqrt{\frac{EI}{\mu L^4}}$ [rad/s],

where:

- E [N/m²] = Youngs modulus (*elasticiteitsmodulus*)
- L [m] = length of the beam/girder
- I [m⁴] = moment of inertia (*traagheidsmoment*)
- μ [kg/m] = mass per running metre beam
- C [m] = coefficient according to Table E-1

		$n = 1$	$n = 2$	$n = 3$	$n = 4$	$n = 5$
clamped	free	 $C = 3.52$	 $C = 22.4$	 $C = 61.7$	 $C = 121.0$	 $C = 200.0$
simply supported	simply supported	 $C = 9.87$	 $C = 39.5$	 $C = 88.9$	 $C = 158.0$	 $C = 247.0$
clamped	clamped	 $C = 22.4$	 $C = 61.7$	 $C = 121.0$	 $C = 200.0$	 $C = 296.0$
free	free	 $C = 22.4$	 $C = 61.7$	 $C = 121.0$	 $C = 200.0$	 $C = 298.0$
clamped	simply supported	 $C = 15.4$	 $C = 50.0$	 $C = 104.0$	 $C = 178.0$	 $C = 272.0$
simply supported	free	 $C = 15.4$	 $C = 50.0$	 $C = 104.0$	 $C = 178.0$	 $C = 272.0$

Table E-1 Natural frequency (eigen frequency) f_n and principal modes of vibration (patterns of motion).

The position of the nodes is indicated by their distance to the support on the left

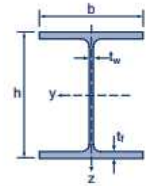
F. Properties of steel H and I profiles

breedflensbalken, HEA

leveringsvoorwaarden: NEN-EN 10025-1 en -2

toleranties: NEN-EN 10034; DIN 1025/3

max. handelslengte: 28 m

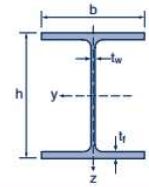


profiel nr.	G_8 kg/m	A mm ²	h mm	b mm	t_w mm	t_f mm	A_L m ² /m	I_y x10 ⁴ mm ⁴	$W_{y,el}$ x10 ³ mm ³	I_z x10 ⁴ mm ⁴	$W_{z,el}$ x10 ³ mm ³
100	17,0	2124	96	100	5	8	0,561	349	72,8	134	26,8
120	20,3	2534	114	120	5	8	0,677	606	106	231	38,5
140	25,1	3142	133	140	5,5	8,5	0,794	1033	155	389	55,6
160	31,0	3877	152	160	6	9	0,906	1673	220	616	76,9
180	36,2	4525	171	180	6	9,5	1,02	2510	294	925	103
200	43,1	5383	190	200	6,5	10	1,14	3692	389	1336	134
220	51,5	6434	210	220	7	11	1,26	5410	515	1955	178
240	61,5	7684	230	240	7,5	12	1,37	7763	675	2769	231
260	69,5	8682	250	260	7,5	12,5	1,48	10455	836	3668	282
280	77,8	9726	270	280	8	13	1,60	13673	1013	4763	340
300	90,0	11253	290	300	8,5	14	1,72	18263	1260	6310	421
320	99,5	12437	310	300	9	15,5	1,76	22929	1479	6985	466
340	107	13347	330	300	9,5	16,5	1,79	27693	1678	7436	496
360	114	14276	350	300	10	17,5	1,83	33090	1891	7887	526
400	127	15989	390	300	11	19	1,91	45069	2311	8564	571
450	142	17803	440	300	11,5	21	2,01	63722	2896	9465	631
500	158	19754	490	300	12	23	2,11	86975	3550	10367	691
550	169	21176	540	300	12,5	24	2,21	111932	4146	10819	721
600	181	22646	590	300	13	25	2,31	141208	4787	11271	751
650	193	24164	640	300	13,5	26	2,41	175178	5474	11724	782
700	208	26048	690	300	14,5	27	2,50	215301	6241	12179	812
800	229	28583	790	300	15	28	2,70	303443	7682	12639	843
900	256	32053	890	300	16	30	2,90	422075	9485	13547	903
1000	277	34685	990	300	16,5	31	3,10	553846	11189	14004	934

Table F-1 Broad-flanged beams HEA (staaltabellen.nl)

breedflensbalken, HEB

leveringsvoorwaarden: NEN-EN 10025-1 en -2
 toleranties: NEN-EN 10034; DIN 1025/2
 max. handelslengte: 28 m

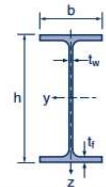


profiel nr.	G _g kg/m	A mm ²	h mm	b mm	t _w mm	t _f mm	A _L m ² /m	I _y x10 ⁴ mm ⁴	W _{y,el} x10 ³ mm ³	I _z x10 ⁴ mm ⁴	W _{z,el} x10 ³ mm ³
100	20,8	2604	100	100	6	10	0,567	450	89,9	167	33,5
120	27,2	3401	120	120	6,5	11	0,686	864	144	318	52,9
140	34,4	4296	140	140	7	12	0,805	1509	216	550	78,5
160	43,4	5425	160	160	8	13	0,918	2492	312	889	111
180	52,2	6525	180	180	8,5	14	1,04	3831	426	1363	151
200	62,5	7808	200	200	9	15	1,15	5696	570	2003	200
220	72,8	9104	220	220	9,5	16	1,27	8091	736	2843	258
240	84,8	10599	240	240	10	17	1,38	11259	938	3923	327
260	94,8	11844	260	260	10	17,5	1,50	14919	1148	5135	395
280	105	13136	280	280	10,5	18	1,62	19270	1376	6595	471
300	119	14908	300	300	11	19	1,73	25166	1678	8563	571
320	129	16134	320	300	11,5	20,5	1,77	30824	1926	9239	616
340	137	17090	340	300	12	21,5	1,81	36656	2156	9690	646
360	145	18063	360	300	12,5	22,5	1,85	43193	2400	10141	676
400	158	19778	400	300	13,5	24	1,93	57681	2884	10819	721
450	174	21798	450	300	14	26	2,03	79888	3551	11721	781
500	191	23864	500	300	14,5	28	2,12	107176	4287	12624	842
550	203	25406	550	300	15	29	2,22	136691	4971	13077	872
600	216	26996	600	300	15,5	30	2,32	171041	5701	13530	902
650	229	28634	650	300	16	31	2,42	210616	6480	13984	932
700	245	30638	700	300	17	32	2,52	256888	7340	14441	963
800	267	33418	800	300	17,5	33	2,71	359084	8977	14904	994
900	297	37128	900	300	18,5	35	2,91	494065	10979	15816	1054
1000	320	40005	1000	300	19	36	3,11	644748	12895	16276	1085

Table F-2 Broad-flanged beams HEB (staaltabellen.nl)

profielbalken, IPE

leveringsvoorwaarden: NEN-EN 10025-1 en -2
 toleranties: NEN-EN 10034; DIN 1025/5
 max. handelslengte: 28 m



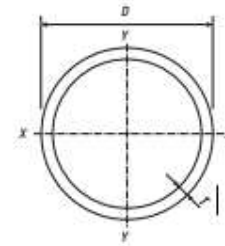
profiel nr.	G _g kg/m	A mm ²	h mm	b mm	t _w mm	t _f mm	A _L m ² /m	I _y x10 ⁴ mm ⁴	W _{y,el} x10 ³ mm ³	I _z x10 ⁴ mm ⁴	W _{z,el} x10 ³ mm ³
80	6,11	764	80	46	3,8	5,2	0,328	80,1	20,0	8,49	3,69
100	8,26	1032	100	55	4,1	5,7	0,400	171	34,2	15,9	5,79
120	10,6	1321	120	64	4,4	6,3	0,475	318	53,0	27,7	8,65
140	13,1	1643	140	73	4,7	6,9	0,551	541	77,3	44,9	12,3
160	16,1	2009	160	82	5	7,4	0,623	869	109	68,3	16,7
180	19,2	2395	180	91	5,3	8	0,698	1317	146	101	22,2
200	22,8	2848	200	100	5,6	8,5	0,768	1943	194	142	28,5
220	26,7	3337	220	110	5,9	9,2	0,848	2772	252	205	37,3
240	31,3	3912	240	120	6,2	9,8	0,922	3892	324	284	47,3
270	36,8	4595	270	135	6,6	10,2	1,04	5790	429	420	62,2
300	43,0	5381	300	150	7,1	10,7	1,16	8356	557	604	80,5
330	50,1	6261	330	160	7,5	11,5	1,25	11767	713	788	98,5
360	58,2	7273	360	170	8	12,7	1,35	16266	904	1043	123
400	67,6	8446	400	180	8,6	13,5	1,47	23128	1156	1318	146
450	79,1	9882	450	190	9,4	14,6	1,61	33743	1500	1676	176
500	92,4	11552	500	200	10,2	16	1,74	48199	1928	2142	214
550	108	13442	550	210	11,1	17,2	1,88	67117	2441	2668	254

Table F-3 Profile beams IPE (staaltabellen.nl)

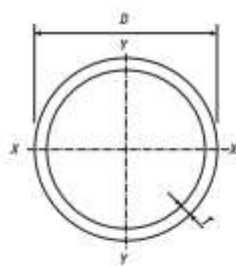
G. Properties of steel pipes

2.1 Buisprofielen, warmvervaardigd, rond

- D - Buitenmiddellijn
- T - Dikte
- M - Massa per lengte-eenheid
- A - Oppervlakte van de dwarsdoorsnede
- I - Axiaal kwadratisch oppervlaktemoment
- i - Traagheidsstraal
- W_{el} - Elastisch weerstandsmoment
- A_s - Uitwendige oppervlakte per meter lengte



D mm	T mm	M kg/m	A cm ²	I cm ⁴	i cm	W_{el} cm ³	A_s m ² /m
508,0	16,0	194	247	74909	17,4	2949	1,60
508,0	20,0	241	307	91428	17,3	3600	1,60
508,0	25,0	298	379	110918	17,1	4367	1,60
508,0	30,0	354	451	129173	16,9	5086	1,60
508,0	40,0	462	588	162188	16,6	6385	1,60
508,0	50,0	565	719	190885	16,3	7515	1,60
610,0	6,0	89,4	114	51924	21,4	1702	1,92
610,0	6,3	93,8	119	54439	21,3	1785	1,92
610,0	8,0	119	151	68551	21,3	2248	1,92
610,0	10,0	148	188	84847	21,2	2782	1,92
610,0	12,0	177	225	100814	21,1	3305	1,92
610,0	12,5	184	235	104755	21,1	3435	1,92
610,0	16,0	234	299	131781	21,0	4321	1,92
610,0	20,0	291	371	161490	20,9	5295	1,92
610,0	25,0	361	459	196906	20,7	6456	1,92
610,0	30,0	429	547	230476	20,5	7557	1,92
610,0	40,0	562	716	292333	20,2	9585	1,92
610,0	50,0	691	880	347570	19,9	11396	1,92
711,0	6,0	104	133	82568	24,9	2323	2,23
711,0	6,3	109	139	86586	24,9	2436	2,23
711,0	8,0	139	177	109162	24,9	3071	2,23
711,0	10,0	173	220	135301	24,8	3806	2,23
711,0	12,0	207	264	160991	24,7	4529	2,23
711,0	12,5	215	274	167343	24,7	4707	2,23
711,0	16,0	274	349	211040	24,6	5936	2,23
711,0	20,0	341	434	259351	24,4	7295	2,23
711,0	25,0	423	539	317357	24,3	8927	2,23
711,0	30,0	504	642	372790	24,1	10486	2,23
711,0	40,0	662	843	476242	23,8	13396	2,23
711,0	50,0	815	1038	570312	23,4	16043	2,23
711,0	60,0	963	1227	655583	23,1	18441	2,23
762,0	6,0	112	143	101813	26,7	2672	2,39
762,0	6,3	117	150	106777	26,7	2803	2,39
762,0	8,0	149	190	134683	26,7	3535	2,39
762,0	10,0	185	236	167028	26,6	4384	2,39
762,0	12,0	222	283	198855	26,5	5219	2,39
762,0	12,5	231	294	206731	26,5	5426	2,39
762,0	16,0	294	375	260973	26,4	6850	2,39
762,0	20,0	366	466	321083	26,2	8427	2,39



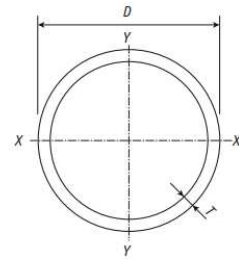
2.1 Buisprofielen, warmvervaardigd, rond

- D - Buitenmiddellijn
 T - Dikte
 M - Massa per lengte-eenheid
 A - Oppervlakte van de dwarsdoorsnede
 I - Axiaal kwadratisch oppervlaktmoment
 i - Traagheidsstraal
 W_{el} - Elastisch weerstandsmoment
 A_s - Uitwendige oppervlakte per meter lengte

D mm	T mm	M kg/m	A cm ²	I cm ⁴	i cm	W_{el} cm ³	A_s m ² /m
762,0	30,0	542	690	462853	25,9	12148	2,39
762,0	40,0	712	907	593011	25,6	15565	2,39
762,0	50,0	878	1118	712207	25,2	18693	2,39
813,0	8,0	159	202	163901	28,5	4032	2,55
813,0	10,0	198	252	203364	28,4	5003	2,55
813,0	12,0	237	302	242235	28,3	5959	2,55
813,0	12,5	247	314	251860	28,3	6196	2,55
813,0	16,0	314	401	318222	28,2	7828	2,55
813,0	20,0	391	498	391909	28,0	9641	2,55
813,0	25,0	486	619	480856	27,9	11829	2,55
813,0	30,0	579	738	566374	27,7	13933	2,55
914,0	8,0	179	228	233651	32,0	5113	2,87
914,0	10,0	223	284	290147	32,0	6349	2,87
914,0	12,0	267	340	345890	31,9	7569	2,87
914,0	12,5	278	354	359708	31,9	7871	2,87
914,0	16,0	354	451	455142	31,8	9959	2,87
914,0	20,0	441	562	561461	31,6	12286	2,87
914,0	25,0	548	698	690317	31,4	15105	2,87
914,0	30,0	654	833	814775	31,3	17829	2,87
1016,0	8,0	199	253	321780	35,6	6334	3,19
1016,0	10,0	248	316	399850	35,6	7871	3,19
1016,0	12,0	297	378	476985	35,5	9389	3,19
1016,0	12,5	309	394	496123	35,5	9766	3,19
1016,0	16,0	395	503	628479	35,4	12372	3,19
1016,0	20,0	491	626	776324	35,2	15282	3,19
1016,0	25,0	611	778	956086	35,0	18821	3,19
1016,0	30,0	729	929	1130352	34,9	22251	3,19
1067,0	10,0	261	332	463792	37,4	8693	3,35
1067,0	12,0	312	398	553420	37,3	10373	3,35
1067,0	12,5	325	414	575666	37,3	10790	3,35
1067,0	16,0	415	528	729606	37,2	13676	3,35
1067,0	20,0	516	658	901755	37,0	16903	3,35
1067,0	25,0	642	818	1111355	36,9	20831	3,35
1067,0	30,0	767	977	1314864	36,7	24646	3,35
1168,0	10,0	286	364	609843	40,9	10443	3,67
1168,0	12,0	342	436	728050	40,9	12467	3,67

2.1 Buisprofielen, warmvervaardigd, rond

- D = Buitenmiddellijn
 T = Dikte
 M = Massa per lengte-eenheid
 A = Oppervlakte van de dwarsdoorsnede
 I = Axiaal kwadratisch oppervlaktemoment
 i = Traagheidsstraal
 W_{el} = Elastisch weerstandsmoment
 A_s = Uitwendige oppervlakte per meter lengte



D mm	T mm	M kg/m	A cm ²	I cm ⁴	i cm	W_{el} cm ³	A_s m ² /m
1168,0	20,0	566	721	1188632	40,6	20353	3,67
1168,0	25,0	705	898	1466717	40,4	25115	3,67
1219,0	10,0	298	380	694014	42,7	11387	3,83
1219,0	12,0	357	455	828716	42,7	13597	3,83
1219,0	12,5	372	474	862181	42,7	14146	3,83
1219,0	16,0	475	605	1094091	42,5	17951	3,83
1219,0	20,0	591	753	1354155	42,4	22217	3,83
1219,0	25,0	736	938	1671873	42,2	27430	3,83

Table G-1 Properties of hot-rolled (*warmvervaardigde*) steel tubular pipes (MCB Buizenboek 2006)

H. Properties of sheetpile elements

HOESCH sections (Finger-and-socket interlock)

	Section modulus		Weight		Second moment of inertia	Section width	Wall height	Back thickness	Web thickness
	W_y				I_y	b	h	t	s
	cm ³ /m	cm ³ /	kg/m ²	kg/m	cm ⁴ /m	mm	mm	mm	mm
	Wall	Single pile	Wall	Single pile	Wall	mm	mm	mm	mm
HOESCH 1105	1100	633	101.0	58.1	14300	575	260	8.8	8.8
HOESCH 1205	1140	655	107.0	61.5	14820	575	260	9.5	9.5
HOESCH 1205 K	1200	690	112.5	64.7	15600	575	260	10.2	10.2
HOESCH 1255	1250	719	118.0	67.9	16250	575	260	10.8	10.8
HOESCH 1605	1600	920	107.0	61.5	28000	575	350	9.2	8.1
HOESCH 1705	1720	989	116.0	66.7	30100	575	350	10.0	9.0
HOESCH 1705 K	1700	978	117.0	67.3	29750	575	350	9.5	9.5
HOESCH 1805	1800	1035	125.0	71.9	31500	575	350	10.8	9.9
HOESCH 2305	2320	1334	142.3	81.8	40600	575	350	11.5	8.4
HOESCH 2405	2400	1380	148.0	85.1	42000	575	350	12.1	9.0
HOESCH 2505	2480	1426	152.0	87.4	43400	575	350	12.5	9.5
HOESCH 2555 K	2540	1460	155.0	89.1	44450	575	350	12.8	10.0
HOESCH 2555	2550	1466	158.0	90.9	44625	575	350	13.0	10.0
HOESCH 2605	2600	1495	162.3	93.3	45500	575	350	13.3	10.3
HOESCH 2506 ¹⁾	2500	1688	143.0	96.5	55000	675	440	12.6	11.2
HOESCH 2606 ¹⁾	2600	1754	150.0	101.3	57200	675	440	13.2	12.0
HOESCH 2706 ¹⁾	2700	1823	157.5	106.3	59400	675	440	13.9	12.9
HOESCH 3406	3420	2308	166.1	112.1	82940	675	485	13.5	10.8
HOESCH 3506	3500	2363	171.7	115.9	84880	675	485	14.0	11.4
HOESCH 3606	3600	2370	177.0	119.5	87300	675	485	14.5	12.0
HOESCH 3706	3700	2497	183.9	124.1	89730	675	485	15.1	12.7
HOESCH 3806	3780	2498	188.5	127.2	91665	675	485	15.5	13.2

¹⁾ Rolling/delivery on request only.

Lengths from 30 m to 36 m on request.

The basis for billing is the weight of the single pile (kg/m).

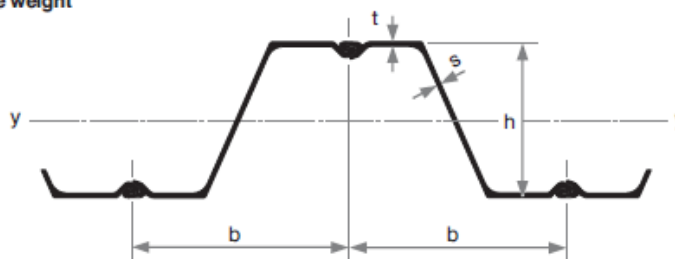
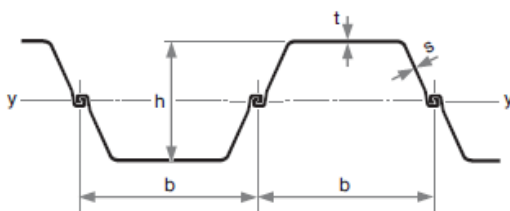


Table H-1 Sheetpile profiles, Hoesch type (from: Sheet piling handbook)

LARSSEN sections

	Section modulus		Weight		Second moment of inertia	Section width	Wall height	Back thickness	Web thickness
	$W_y^{1)}$				I_y	b	h	t	s
	cm ³ /m	cm ³ /Single pile	kg/m ²	kg/m	cm ⁴ /m	mm	mm	mm	mm
	Wall	Single pile	Wall	Single pile	Wall	mm	mm	mm	mm
LARSSEN 755	2000	580	127.5	95.6	45000	750	450	11.7	10.0
LARSSEN 703	1210	414	96.4	67.5	24200	700	400	9.5	8.0
LARSSEN 703 K	1300	426	103.0	72.1	25950	700	400	10.0	9.0
LARSSEN 703 10/10 ³⁾	1340	437	108.0	75.6	26800	700	400	10.0	10.0
LARSSEN 704	1600	529	115.0	80.5	35200	700	440	10.2	9.5
LARSSEN 600	510	109	94.0	56.4	3840	600	150	9.5	9.5
LARSSEN 600 K	540	123	99.0	59.4	4050	600	150	10.0	10.0
LARSSEN 601	745	251	77.2	46.3	11520	600	310	7.5	6.4
LARSSEN 602	830	265	89.0	53.4	12870	600	310	8.2	8.0
LARSSEN 603	1200	330	108.0	64.8	18600	600	310	9.7	8.2
LARSSEN 603 K	1240	340	113.5	68.1	19220	600	310	10.0	9.0
LARSSEN 603 10/10 ³⁾	1260	350	116.0	69.6	19530	600	310	10.0	10.0
LARSSEN 604	1620	425	124.2	74.5	30710	600	380	10.5	9.0
LARSSEN 605	2020	520	139.2	83.5	42370	600	420	12.5	9.0
LARSSEN 605 K	2030	549	144.5	86.7	42550	600	420	12.2	10.0
LARSSEN 606 n	2500	605	157.0	94.2	54375	600	435	14.4	9.2
LARSSEN 607 n	3200	649	190.0	114.0	72320	600	452	19.0	10.6
LARSSEN 22 10/10 ³⁾	1300	369	130.0	65.0	22100	500	340	10.0	10.0
LARSSEN 23	2000	527	155.0	77.5	42000	500	420	11.5	10.0
LARSSEN 24	2500	547	175.0	87.5	52500	500	420	15.6	10.0
LARSSEN 24/12	2550	560	185.4	92.7	53610	500	420	15.6	12.0
LARSSEN 25	3040	562	206.0	103.0	63840	500	420	20.0	11.5
LARSSEN 43	1660	483	166.0	83.0	34900	500	420	12.0	12.0
LARSSEN 430	6450	—	234.5 ²⁾	83.0	241800	708 ⁴⁾	750	12.0	12.0

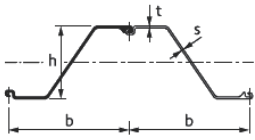


- 1) The section modulus values may only be used in static computations if at least every second interlock in the wall is cramped to adsorb shear forces.
- 2) Wall assembly fabricated from LARSSEN 43 sections. Where quad pile assemblies are supplied, allowance must be made for the weight of the weld seams and reinforcements.
- 3) Rolling/delivery on request only.
- 4) With the use of quadruple piles
W = 1416 mm

Lengths from 30 m to 36 m on request. The basis for billing is the weight of the single pile (kg/m).

Table H-2 Sheetpile profiles, Larssen type (from Sheet piling handbook)

ArcelorMittal sections



	Width	Height	Thickness		Mass		Moment of inertia cm ⁴ /m	Elastic section modulus cm ³ /m
	b mm	h mm	t mm	s mm	single pile kg/m	wall kg/m ²		
AZ[®]-700 & AZ[®]-770								
AZ 12-770	770	344	8.5	8.5	72.6	94.3	21 430	1 245
AZ 13-770	770	344	9.0	9.0	76.1	98.8	22 360	1 300
AZ 14-770	770	345	9.5	9.5	79.5	103.2	23 300	1 355
AZ 14-770-10/10	770	345	10.0	10.0	82.9	107.7	24 240	1 405
AZ 12-700	700	314	8.5	8.5	67.7	96.7	18 880	1 205
AZ 13-700	700	315	9.5	9.5	74.0	105.7	20 540	1 305
AZ 13-700-10/10	700	316	10.0	10.0	77.2	110.2	21 370	1 355
AZ 14-700	700	316	10.5	10.5	80.3	114.7	22 190	1 405
AZ 17-700	700	420	8.5	8.5	73.1	104.4	36 230	1 730
AZ 18-700	700	420	9.0	9.0	76.5	109.3	37 800	1 800
AZ 19-700	700	421	9.5	9.5	80.0	114.3	39 380	1 870
AZ 20-700	700	421	10.0	10.0	83.5	119.3	40 960	1 945
AZ 24-700	700	459	11.2	11.2	95.7	136.7	55 820	2 430
AZ 26-700	700	460	12.2	12.2	102.9	146.9	59 720	2 600
AZ 28-700	700	461	13.2	13.2	110.0	157.2	63 620	2 760
AZ 24-700N	700	459	12.5	9.0	89.7	128.2	55 890	2 435
AZ 26-700N	700	460	13.5	10.0	96.9	138.5	59 790	2 600
AZ 28-700N	700	461	14.5	11.0	104.1	148.7	63 700	2 765
AZ 36-700N	700	499	15.0	11.2	118.6	169.5	89 610	3 590
AZ 38-700N	700	500	16.0	12.2	126.4	180.6	94 840	3 795
AZ 40-700N	700	501	17.0	13.2	134.2	191.7	100 080	3 995
AZ 42-700N	700	499	18.0	14.0	142.1	203.1	104 930	4 205
AZ 44-700N	700	500	19.0	15.0	149.9	214.2	110 150	4 405
AZ 46-700N	700	501	20.0	16.0	157.7	225.3	115 370	4 605
AZ[®]								
AZ 18	630	380	9.5	9.5	74.4	118.1	34 200	1 800
AZ 18-10/10	630	381	10.0	10.0	77.8	123.4	35 540	1 870
AZ 26	630	427	13.0	12.2	97.8	155.2	55 510	2 600
AZ 46	580	481	18.0	14.0	132.6	228.6	110 450	4 595
AZ 48	580	482	19.0	15.0	139.6	240.6	115 670	4 800
AZ 50	580	483	20.0	16.0	146.7	252.9	121 060	5 015

Table H-3 Sheetpile profiles, ArcelorMittal AZ type (from: ArcelorMittal brochure Z-profiles 2013-2)

I. Mechanical schematisations of connections



	hinge connection 	stiff connection 
middenkolom-ligger		
eindkolom-ligger		
doorg. kolom-ligger		
kolomvoet		
ligger-ligger		
ligger-wand		

Table I-1 Various types of connections and their mechanical schematisation (Infomap Constructieer, 2006)

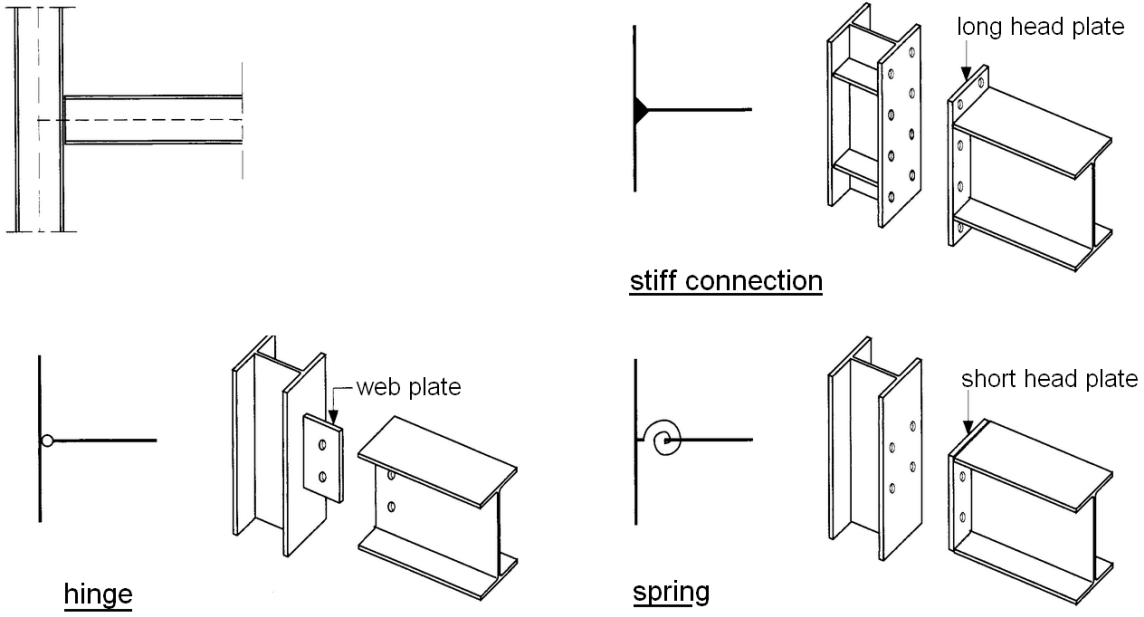


Table I-2 Various types of connections and their mechanical schematisation ((Over)spannend staal)